TETRAPOD WATER-LAND TRANSITION: RECONSTRUCTING SOFT TISSUE ANATOMY AND FUNCTION

EDITED BY: Julia L. Molnar, Rui Diogo, Ingmar Werneburg and Catherine Anne Boisvert

PUBLISHED IN: Frontiers in Ecology and Evolution

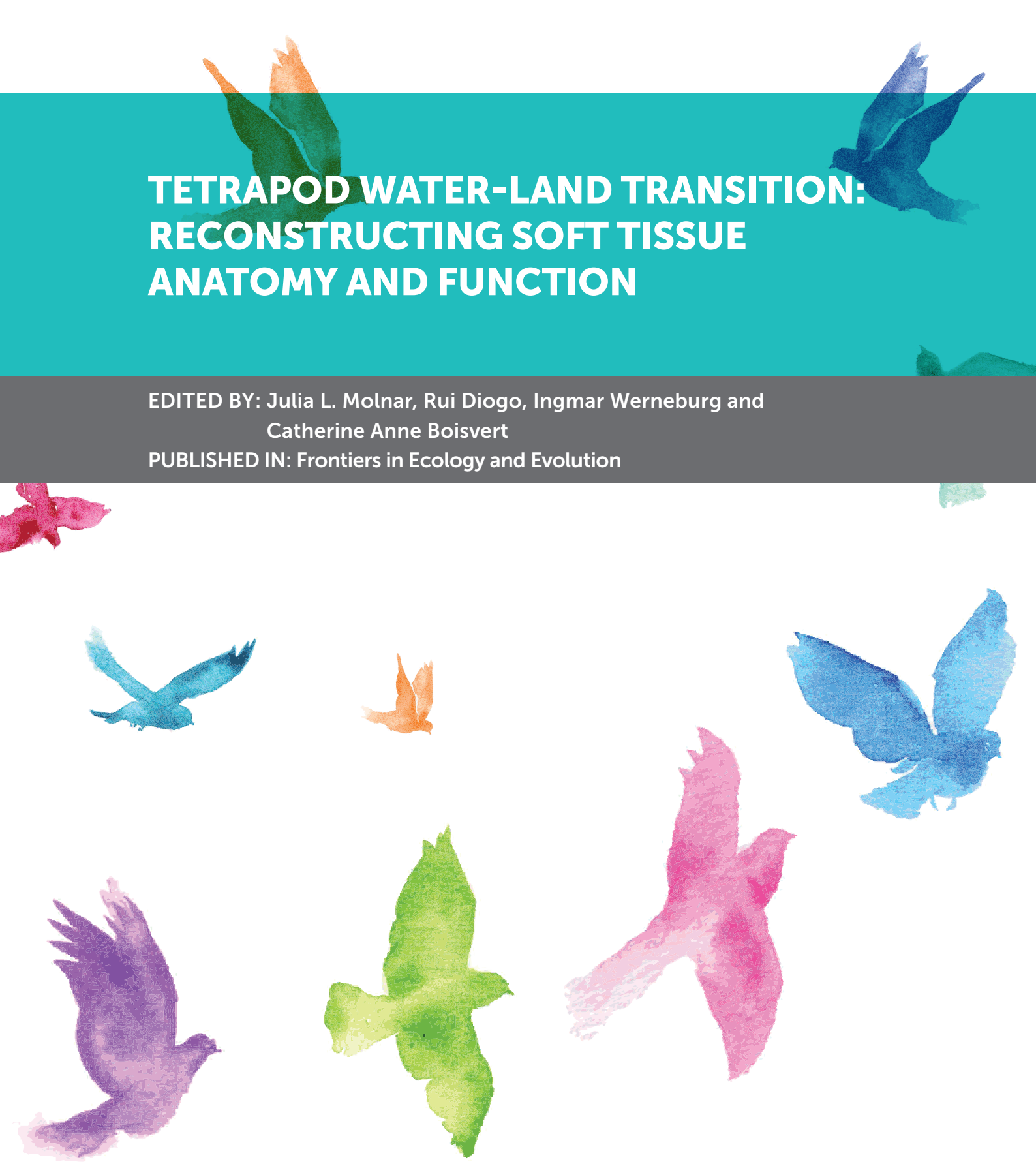

frontiers Research Topics

ISSN 1664-8714
ISBN 978-2-88976-787-8
DOI 10.3389/978-2-88976-787-8

About Frontiers

Frontiers is more than just an open-access publisher of scholarly articles: it is a pioneering approach to the world of academia, radically improving the way scholarly research is managed. The grand vision of Frontiers is a world where all people have an equal opportunity to seek, share and generate knowledge. Frontiers provides immediate and permanent online open access to all its publications, but this alone is not enough to realize our grand goals.

Frontiers Journal Series

The Frontiers Journal Series is a multi-tier and interdisciplinary set of open-access, online journals, promising a paradigm shift from the current review, selection and dissemination processes in academic publishing. All Frontiers journals are driven by researchers for researchers; therefore, they constitute a service to the scholarly community. At the same time, the Frontiers Journal Series operates on a revolutionary invention, the tiered publishing system, initially addressing specific communities of scholars, and gradually climbing up to broader public understanding, thus serving the interests of the lay society, too.

Dedication to Quality

Each Frontiers article is a landmark of the highest quality, thanks to genuinely collaborative interactions between authors and review editors, who include some of the world's best academicians. Research must be certified by peers before entering a stream of knowledge that may eventually reach the public - and shape society; therefore, Frontiers only applies the most rigorous and unbiased reviews.
Frontiers revolutionizes research publishing by freely delivering the most outstanding research, evaluated with no bias from both the academic and social point of view. By applying the most advanced information technologies, Frontiers is catapulting scholarly publishing into a new generation.

What are Frontiers Research Topics?

Frontiers Research Topics are very popular trademarks of the Frontiers Journals Series: they are collections of at least ten articles, all centered on a particular subject. With their unique mix of varied contributions from Original Research to Review Articles, Frontiers Research Topics unify the most influential researchers, the latest key findings and historical advances in a hot research area! Find out more on how to host your own Frontiers Research Topic or contribute to one as an author by contacting the Frontiers Editorial Office: frontiersin.org/about/contact

TETRAPOD WATER-LAND TRANSITION: RECONSTRUCTING SOFT TISSUE ANATOMY AND FUNCTION

Topic Editors:
Julia L. Molnar, New York Institute of Technology, United States
Rui Diogo, Howard University, United States
Ingmar Werneburg, University of Tübingen, Germany
Catherine Anne Boisvert, Curtin University, Australia

Citation: Molnar, J. L., Diogo, R., Werneburg, I., Boisvert, C. A., eds. (2022). Tetrapod Water-Land Transition: Reconstructing Soft Tissue Anatomy and Function. Lausanne: Frontiers Media SA. doi: 10.3389/978-2-88976-787-8

Table of Contents

frontiers | Frontiers in Ecology and Evolution

TYPE Editorial
PUBLISHED 19 July 2022
DOI 10.3389/fevo.2022.968979

OPEN ACCESS

EDITED BY
Bruce S. Lieberman,
University of Kansas, United States

REVIEWED BY
Kenneth Angielczyk,
Field Museum of Natural History,
United States

*CORRESPONDENCE
Julia L. Molnar
julia.molnar@nyit.edu

SPECIALTY SECTION
This article was submitted to Paleontology,
a section of the journal
Frontiers in Ecology and Evolution

RECEIVED 14 June 2022
ACCEPTED 05 July 2022
PUBLISHED 19 July 2022

CITATION
Molnar JL, Diogo R, Boisvert CA and Werneburg I (2022) Editorial: Tetrapod water-land transition: Reconstructing soft tissue anatomy and function.
Front. Ecol. Evol. 10:968979.
doi: 10.3389/fevo.2022.968979

Editorial: Tetrapod water-land transition: Reconstructing soft tissue anatomy and function

Julia L. Molnar[1]*, Rui Diogo[2], Catherine A. Boisvert[3,4] and Ingmar Werneburg[5,6]

[1]Department of Anatomy, College of Osteopathic Medicine, New York Institute of Technology, Old Westbury, NY, United States, [2]Department of Anatomy, Howard University, Washington, DC, United States, [3]School of Molecular and Life Sciences, Curtin University, Perth, WA, Australia, [4]Curtin Health Innovation Research Institute, Curtin University, Perth, WA, Australia, [5]Senckenberg Centre for Human Evolution and Palaeoenvironment and der Eberhard Karls Universität Tübingen, Tübingen, Germany, [6]Fachbereich Geowissenschaften, Eberhard Karls Universität Tübingen, Tübingen, Germany

KEYWORDS

amniote, fin-limb transition, soft tissue reconstruction, terrestriality, tetrapod

Editorial on the Research Topic
Tetrapod Water-Land Transition: Reconstructing Soft Tissue Anatomy and Function

Thanks to new methods of modeling and analysis, we are discovering much more about movement, sensation, and feeding in animals that span the tetrapod water-land transition and the origin of amniotes. As investigations of function in extinct animals become more complex and rigorous, the need to take soft tissues into account becomes more pressing. For example, biomechanical simulations of locomotion in early tetrapods rely on assumptions about their muscles and cartilages that come from living animals. Thus, the drive to learn more about our ancient relatives leads us to ask new questions about the relationships between hard and soft tissues over development and evolution. How did early land vertebrates transition from aquatic to terrestrial feeding? How did muscle anatomy and development change during the transformation from fins to limbs in tetrapods and with the loss of metamorphosis in amniotes? In this Research Topic, researchers approach these questions using fossils, biomechanical models, observation of living animals, and new imaging modalities that allow us to view embryonic development and adult anatomy in unprecedented detail.

Historical perspective

Soft tissue reconstructions often are subject to scientific biases, which carry direct repercussions for scientific illustrators, educators, and children who will become the next generation of scientists. Campbell et al. A; Campbell et al. B brought together a team from diverse disciplines, ethnic and cultural backgrounds, and career stages to examine current examples of racism, Western-centrism and sexism within not only biological and

anthropological works, but also in prominent natural history museums. The theme of current and historical approaches to soft tissue anatomy is further developed by Pears et al., who examined the ontogeny and morphology of the pelvic musculature in chondrichthyans using a combination of modern and historical methods. Nano-CT imaging and 3D-reconstructions were used to describe development in a growth series of elephant shark embryos, while historical descriptions from the 19th century and traditional dissection methods were used to re-describe the adult anatomy. The latter paper is a fine example of how historical data can be synthesized with new observations obtained from state-of-the-art imaging methods to advance our understanding in exciting new ways.

Locomotion with fins and limbs

Improvements in imaging techniques have allowed non-destructive analysis of increasingly small specimens, both with and without contrast, which is important when utilizing rare material from endangered species. Hirasawa et al. imaged embryos of the Australian lungfish to understand the evolution of pectoral musculature and increases in number and size of appendicular muscles across the fish-to-tetrapod transition. They hypothesized that the mesenchyme needed to develop the innervation of the pectoral limb in tetrapods is absent in fish, and that the cleithrum forms a barrier to its migration along the body wall. Thus, the gradual reduction of the cleithrum in tetrapodomorph fishes may have opened the door for increased complexity of appendicular muscles. Such increase in complexity is beautifully illustrated by the comparative dissection of the coelacanth and alligator by Mansuit and Herrel, which documents an increase in appendicular muscle mass in tetrapods and larger superficial muscles compared to sarcopterygian fishes. The combination of state-of-the-art imaging of development in extant fishes with meticulous examination of museum specimens provides much needed granularity in soft tissue evolution underlying the major locomotor shifts of the fish-to-tetrapod transition.

The parallel transition from water to land in the ontogeny of extant amphibians has prompted many researchers to use amphibians as models for early tetrapods. Molnar measured articular cartilage in various salamanders and found that, regardless of size, aquatic salamanders have much thicker cartilage caps on their limb bones than terrestrial salamanders. This finding is important because the extant phylogenetic bracket (Witmer, 1995) of stem tetrapods includes animals that vary wildly in skeletal cartilage, such as lungfish, amphibians, and amniotes. Greater accuracy in estimating soft tissue dimensions will improve biomechanical models of locomotion in stem tetrapods. Abdala et al. provided an ontogenetic perspective, co-opting geographical mapping technology to quantify changes in relative size and location of tissues over pelvic development in frogs and chickens. As frogs metamorphose from tadpoles, their girdles grow much faster than those of chickens and rotate laterally, paralleling evolutionary changes that took place during the tetrapod water-land transition.

As tetrapods became independent of bodies of water for reproduction, they developed more effective and efficient terrestrial locomotion. Zwafing et al. tested the hypothesis that stem amniotes used a more erect posture by adding muscles to an existing kinematic and dynamic model of locomotion in the Permian tetrapod *Orobates* (Nyakatura et al., 2019), a fossil close to the origin of amniotes. A semi-erect, crocodile-like posture in *Orobates* produced optimal muscle strains. However, multiple postures fell within the range of reasonable muscle strains, emphasizing the great difficulty of reconstructing behavior in extinct animals.

Cranial and feeding systems

In their study of ontogenetic changes of the aquatic food uptake mode in a newt, Natchev et al. illustrate the integration of locomotion with feeding systems. Feeding mode in younger larvae was dramatically different from pre-metamorphic larvae and adults, hinting that control of the feeding apparatus is integrated with activity of the locomotor system. These changes may be triggered by formation of functional limbs during late larval development, a finding with broad implications for the evolution and physiological integration of the locomotor and feeding systems across the water-land transition.

In addition to feeding, terrestrialization in tetrapods required many other ecological adaptations, such as air-breathing. Stem tetrapods such as *Acanthostega* relied partially on a spiracle for air-breathing. The spiracle derives from an embryonic hyomandibular pouch, which is thought to have been present as a fully formed gill in early jawed vertebrates (Gegenbaur, 1872). Gai et al. demonstrated the presence of a spiracular gill in the galeaspid *Shuyu,* the sister group to osteostracans + gnathostomes, and found that the spiracle retained a respiratory function across the fish-tetrapod transition even as the morphology of the hyomandibula (stapes) transformed into the tetrapod middle ear. Thus, this manuscript brings together exceptionally preserved fossils and new advances in phylogenetics to answer a long-standing evolutionary question. Working in another region of the skull, Clement et al. investigated the complex relationship between the brain and endocast (the cavity which houses the brain) in extant amphibians. In addition to producing detailed reconstructions of brain morphology that can be used for future interpretation of fossils, they show the importance of ecology when using an extant phylogenetic bracket, given that brain size can vary between 1 and 78% of the endocast volume.

As the amniote lineage became independent from an aquatic milieu and acquired a cleidoic egg, the larval stage was lost. Freed from the constraint of larval feeding (Werneburg, 2019), cranial bones and jaw musculature evolved new ontogenetic pathways. The most obvious changes relate to the formation and diversity of the temporal skull region, including number of temporal openings (Abel and Werneburg, 2021). In two studies presented herein, the Late Permian reptile *Captorhinus aguti* was used to represent ancestral amniotes. The complexity of skull sutures was studied to infer the degree of cranial kinesis, and weakly sutured regions of the skull were identified as potential locations for evolution of temporal openings (Abel et al.). Taking *C. aguti* as a template, Werneburg and Abel simulated temporal openings inside the anapsid skull using the Anatomical Network approach (Werneburg et al., 2019; Sookias et al., 2020). The authors show that evolution of the temporal skull region is most clearly understood in the context of feeding adaptations to hard or soft food items. Nevertheless, also other factors such as skull dimensions, neck posture, and phylogenetic constraints must be considered to permit a balanced discussion on the origin and meaning of temporal skull openings.

In this Research Topic, an exceptional group of international scientists discussed recent developments in vertebrate terrestrialization. Using modern analytical and conceptual frameworks, they defined new avenues for future research in vertebrate locomotion, feeding, and cranial anatomy. The challenges are not trivial: for animals on both sides of the water-land transition, reconstructing soft tissues based on extant relatives is difficult because of the great morphological gap between fish and tetrapods. Even in relatively conservative regions such as the braincase, factors other than phylogeny are important, such as ecology, habits, and lifestyle. In these cases, a better understanding of structure-function relationships in extant taxa can help to constrain reconstructions. In the case of evolutionary novelties such as the tetrapod limb, developmental and genetic approaches may be needed to supplement morphological comparisons. Yet, despite its difficulties, incorporating soft tissues into fossil reconstructions has many benefits, from testing and refining fossil-based locomotor hypotheses to predicting the consequences of changes in skull morphology for feeding. In addition, newly developed approaches to soft tissue reconstruction can complement historical methods and promote a more accurate, less biased understanding of evolution, whether it be in more recent or ancient human ancestors.

Author contributions

All authors listed have made a substantial, direct, and intellectual contribution to the work and approved it for publication.

Funding

IW was funded by DFG-grant WE 5440/6-1.

Acknowledgments

We thank all authors for their inspiring contributions. Moreover, we are grateful to the Journal Manager Ewan Bodenham for his support.

Conflict of interest

The authors declare that the research was conducted in the absence of any commercial or financial relationships that could be construed as a potential conflict of interest.

Publisher's note

References

Abel, P., and Werneburg, I. (2021). Morphology of the temporal skull region in tetrapods: research history, functional explanations, and a comprehensive new classification scheme. *Biol. Rev.* 96, 2229–2257. doi: 10.1111/brv.12751

Gegenbaur, C. (1872). Untersuchungen zur Vergleichenden Anatomie der Wirbeltiere. 3: Das Kopfskelett der Selachier. Leipzig: Engelmann.

Nyakatura, J. A., Melo, K., Horvat, T., Karakasiliotis, K., Allen, V. R., Andikfar, A., et al. (2019). Reverse-engineering the locomotion of a stem amniote. *Nature.* 565, 351–55. doi: 10.1038/s41586-018-0851-2

Sookias, R., Dilkes, S., Sobral, G., Smith, R., Wolvaardt, F. P., Arcucci, A. B., et al. (2020). The craniomandibular anatomy of the early archosauriform *Euparkeria capensis* and the dawn of the archosaur skull. *Royal Society Open Science.* 7, 200116. doi: 10.1098/rsos.200116

Werneburg, I. (2019). Morphofunctional categories and ontogenetic origin of temporal skull openings in amniotes. *Front. Earth Sci.* 7, 1–7, doi: 10.3389/feart.2019.00013

Werneburg, I., Esteve-Altava, B., Bruno, J., Torres Ladeira, M., and Diogo, R. (2019). Unique skull network complexity of *Tyrannosaurus rex* among land vertebrates. *Scientific Rep.* 9, 14. doi: 10.1038/s41598-018-37976-8

Witmer, L. M. (1995). "The extant phylogenetic bracket and the importance of reconstructing soft tissues in fossils," in *Functional Morphology in Vertebrate Paleontology*. Cambridge, Mass: Cambridge University Press. p 19–33

frontiers in Ecology and Evolution

REVIEW
published: 26 February 2021
doi: 10.3389/fevo.2021.639048

Visual Depictions of Our Evolutionary Past: A Broad Case Study Concerning the Need for Quantitative Methods of Soft Tissue Reconstruction and Art-Science Collaborations

Ryan M. Campbell[1]†, Gabriel Vinas[2†], Maciej Henneberg[1,3†] and Rui Diogo[4†]*

[1] Department of Anatomy & Pathology, University of Adelaide, Adelaide, SA, Australia, [2] Department of Sculpture, Arizona State University, Tempe, AZ, United States, [3] Institute of Evolutionary Medicine, University of Zurich, Zurich, Switzerland, [4] Department of Anatomy, Howard University, Washington, DC, United States

Flip through scientific textbooks illustrating ideas about human evolution or visit any number of museums of natural history and you will notice an abundance of reconstructions attempting to depict the appearance of ancient hominins. Spend some time comparing reconstructions of the same specimen and notice an obvious fact: hominin reconstructions vary in appearance considerably. In this review, we summarize existing methods of reconstruction to analyze this variability. It is argued that variability between hominin reconstructions is likely the result of unreliable reconstruction methods and misinterpretation of available evidence. We also discuss the risk of disseminating erroneous ideas about human evolution through the use of unscientific reconstructions in museums and publications. The role an artist plays is also analyzed and criticized given how the aforementioned reconstructions have become readily accepted to line the halls of even the most trusted institutions. In conclusion, improved reconstruction methods hold promise for the prediction of hominin soft tissues, as well as for disseminating current scientific understandings of human evolution in the future.

Keywords: artistic license, facial approximation, hominid, hominin, hard tissue, soft tissue

OPEN ACCESS

Edited by:
Stefano Dominici,
University of Florence, Italy

Reviewed by:
David O. Lordkipanidze,
Georgian National Museum, Georgia
Lorenzo Rook,
University of Florence, Italy
Dawid Adam Iurino,
Sapienza University of Rome, Italy

****Correspondence:***
Ryan M. Campbell
ryan.campbell@adelaide.edu.au

†ORCID:
Ryan M. Campbell
orcid.org/0000-0003-2630-1701
Gabriel Vinas
orcid.org/0000-0003-3374-3460
Maciej Henneberg
orcid.org/0000-0003-1941-2286
Rui Diogo
orcid.org/0000-0002-9008-1910

Specialty section:
This article was submitted to Paleontology, a section of the journal Frontiers in Ecology and Evolution

Received: *08 December 2020*
Accepted: *25 January 2021*
Published: *26 February 2021*

Citation:
Campbell RM, Vinas G, Henneberg M and Diogo R (2021) Visual Depictions of Our Evolutionary Past: A Broad Case Study Concerning the Need for Quantitative Methods of Soft Tissue Reconstruction and Art-Science Collaborations. Front. Ecol. Evol. 9:639048. doi: 10.3389/fevo.2021.639048

INTRODUCTION: WHY STUDY AND RECONSTRUCT MUSCLES?

At a time in which we are increasingly exposed to acclaims about new powerful genetic tools in the media and academia, one may wonder as to why we would focus on muscle reconstructions at all in this introductory paper of this special issue. This is particularly the case since genetic tools are now being used in studies that have been typically done with anatomical tools in the past, such as

those concerning phylogenetic reconstructions. Actually, molecular tools are now being used to undertake facial reconstructions, an area that was exclusive to anatomy until very recently. In September 2019, newspapers across the globe reported with astonishment that a new method based on DNA information recovered from the remains of extinct individuals known as the Denisovans enabled scientists to give them a face. Namely, those scientists gleaned anatomical clues from ancient genomes to put together a rough composite portrait of a young female that lived at Denisova Cave in Siberia 75,000 years ago (Gokhman et al., 2019), despite the fact that only small fragments of bones and teeth of Denisovans were found and their skeletal anatomy has not been documented. We will obviously not discuss here the details of that paper and its artistic repercussions, nor the way in which it affected the way Denisovans are perceived by the broader public, although we will briefly refer below to some other similar studies. Rather, the point is that, if we have all these new tools, including eventual facial reconstructions in the future, are anatomical fossil reconstructions destined to become unimportant? The answer is that this is not at all the case; as will be seen in the present paper, and in this special issue as a whole, it is in fact the opposite. There has been a renewed interest in such reconstructions, using new methods and expanding them to tissues other than skeletal ones, such soft tissues like muscles, arteries, veins, and nerves, making them more complete and comprehensive than ever before. This special issue is, in itself, the proof of that, as it would have been difficult to do a whole issue with so many papers from top scholars completely dedicated to muscle reconstructions a few decades ago. In fact, this new interest in fossil muscle reconstructions is part of a resurgence of the study of comparative anatomy *per se*—the now re-awoken "sleeping beauty", to paraphrase Virginia Abdala—which was in great part a by-product of the rise of Evo-Devo in the past decades (Diogo, 2018).

Some years ago, one of us, with Bernard Wood (Diogo and Wood, 2013), published a paper summarizing why the study of muscles continues to be extremely important for not only Evo-Devo, but also for evolutionary biology, anatomical sciences, biological/physical anthropology, and many other fields. As noted in that paper, a major reason why molecular tools have not yet completely eclipsed anatomical ones in studies of evolutionary relationships is that it is still not possible to recover DNA for most of the millions of species that became extinct much before the time that Denovisans did. For instance, no DNA has been recovered for the fossil taxa that are the central focus of this special issue; those representing the transitions from fishes and early tetrapods. Therefore, phylogenetic works of such groups have been traditionally done mainly with bones but are also increasingly using soft tissues—particularly muscles as will be seen in this issue. One of the reasons for this is, as noted in that paper, studies by us and various other authors on the whole osteichthyan clade (bony "fish" plus tetrapods), and on specific groups such as our own (primates), have shown that although osteological structures often provide more potential characters for phylogenetic analyses, myological characters tend to be more useful for inferring the phylogenetic relationships among higher clades.

Indeed, this seems to apply even to fossil taxa such as non-avian dinosaurs (e.g., Dilkes, 2000). This therefore illustrates how crucial it is to undertake accurate muscle reconstructions of fossils, to not only understand their functional morphology, and biology as a whole—bones do *not* move without muscles—but to also learn more about their evolutionary relationships, history, and adaptations. This is moreover crucial, as will be discussed below, for science dissemination and the way the broader public perceives those fossil taxa, such as early tetrapods, dinosaurs, and even the closest extinct relatives of the human lineage. We are thus living in a fascinating time in which instead of a decrease of interest in muscles, there is an exponential interest in developing new tools and ways to reconstruct them more accurately in fossil taxa, and in displaying them artistically in the web, dissemination books, popular movies and documentaries, and museum fossil displays. Due to the particular interest in the reconstructions of fossils of our human lineage for all these types of media, their artistic repercussions, and the way they influence the public perception and narratives built around them—including, unfortunately, racist and misogynistic ones, as shown in Moser's (1996) book *Ancestral images: the iconography of human origins*—in this introductory paper we will focus on our own lineage. The idea is to show that the focus of this issue, muscle reconstructions, has not only scientific repercussions, but also societal and artistic implications. As will be shown in sections below, such reconstructions involve major complexities and difficulties, but also bring fascinating new opportunities.

Over the last century, there has been a huge interest in reconstructing the face of members of our human lineage that lived many thousands, or even some millions, of years ago. However, most of these are based on unfalsifiable ad hoc stories that have little or no empirical evidence. For instance, it has been said that the prognathic faces of *Australopithecus* were more similar to our closest living relatives, the great apes (chimpanzees, gorillas, and orangutans), than to anatomically modern humans. Based on this observed similarity, some have assumed that the soft tissues covering their faces would also have been more similar to those of apes than to those of *Homo sapiens* (Aiello and Dean, 1990; Gurche, 2013). This kind of rhetoric, which is largely untestable, is frequently deployed in the process of reconstructing Plio-Pleistocene hominins (N.B., in this paper hominins means all humans since we split from common ancestors with separately evolving lineages). It is based on a kind of interpretation called retrodiction, which is an intuitive method for predicting the past based on present observations of natural phenomena. It is based on Charles Lyell's uniformitarian principle underlying evolutionary science. But how reliable is retrodiction? Could not this rhetoric be questioned? Here, we review the practice of hominin reconstruction from a scientific perspective and address some of its broader implications. Specifically, we begin by presenting some of the earliest examples of hominin reconstruction followed by a review of the current methods used. We then show where future research holds promise for improving existing methods and producing scientifically accurate reconstructions, followed by a discussion of our own view on the ethical and societal implications of artistic interpretations of hominins. Our aim is to identify areas where fresh research

is needed, which can be applied to other non-human or non-primate taxa.

Our fascination with hominin reconstructions—and the basis for this review—stems chiefly from the work carried out by two of us (RC and GV) over the last 6 years attempting to reproduce 3D reconstructions of extinct hominins often using the muscle data that have been recently made available for apes by another co-author (RD) and his colleagues. Although many 2D reconstructions of hominins exists, which are arguably just as important as 3D reconstructions, we will focus mainly on 3D reconstructions as these are the ones that we have spent the most time trying to replicate. It is hoped that including our own reconstructions in this review will help to expose the limitations of existing methods and to substantiate our claim that the practice is lacking a robust scientific and empirical foundation. As we shall show, many of the questions regarding the appearance of Plio-Pleistocene hominins are yet to be answered and most, if not all, reconstructions are based on methods that are irreplicable. This once again highlights the difficulties and complexities of muscle reconstructions but also the enormous opportunities that we now have to make progress in the area of muscle, facial, and whole-body reconstructions.

A BRIEF HISTORY OF HOMININ FACIAL RECONSTRUCTION

The earliest reconstructions of hominins were carried out in the late nineteenth and early twentieth centuries by artists and scientists in the form of both 2D and 3D portraits as well as whole-body reconstructions, produced soon after the discovery of various fossils. As very few hominin fossils have ever been found—it is, after all, a well-known fact that there are more active physical anthropologists today than there are hominin finds—it is relatively easy to compare reconstructions of the same individual. As we shall show, there are only a handful of well-preserved skulls suitable for reconstruction, which not only makes it easy to compare appearances between reconstructions of the same individuals produced by separate practitioners, but also highlights the role of how individually constructed knowledge about human evolution can affect their results. We would like to be transparent with the reader and admit that this section is by no means a complete list of all the reconstructions that have ever been produced, however, it does include the most well-recognized practitioners and reconstructions that are featured in scholarly publications, scientific textbooks, and on display at institutions of international repute.

The best documented 3D hominin reconstructions based on scientific methods were produced by the Russian anthropologist and archeologist Mikhail Gerasimov (Gerasimov, 1971). Gerasimov is especially renowned for his contributions to the field of forensic facial reconstruction—now more commonly referred to as facial approximation—which is the process of reproducing a likeness that can assist in identifying an individual from a skull found in a forensic context. In his published work, Gerasimov used his forensic methods—for a review of these methods, see Ullrich and Stephan (2016)—to reconstruct two Australopithecines as well as various members of the genus *Homo*. The best known 3D reconstructions of hominins today are produced by John Gurche (Balter, 2009; Gurche, 2013). Gurche has allegedly reconstructed over fifteen hominin individuals that are featured in the Smithsonian National Museum of Natural History in Washington, D.C. These reconstructions include *Sahelanthropus tchadensis*, *Australopithecus afarensis*, *Australopithecus africanus,* and *Paranthropus boisei*. Gurche has also reconstructed individuals from the genus *Homo*, including *Homo erectus, Homo heidelbergensis*, a Neandertal, and LB1 (Balter, 2009; Gurche, 2013). Other well-known practitioners of 3D reconstruction include Élizabeth Daynès, Gary Sawyer, Viktor Deak, Philippe Froesch, and Adrie and Alfons Kennis (Balter, 2009).

Is it important to note here that not all reconstructions of hominins have been produced in 3D since 2D reconstructions are arguably more numerous and thus any review would be incomplete without acknowledging them. In general, 2D reconstructions appear to conform less to the scientific approach and more to artistic intuition but this fact does not weaken their power of influence on public perceptions about human evolution and are therefore relevant to this review. Zdeněk Burian is one of the most celebrated 2D paleoartists in physical anthropology and produced a number of illustrations of hominins depicted in their ancestral environments (Jelínek, 1975). Jay Matternes also produced 2D reconstructions. One of these illustrations is of an individual of *Australopithecus afarensis* and is regarded by world-renowned paleoanthropologist Donald Johanson—who was consulted during the production of this reconstruction—as one of the "finest representations of this species" (Johanson, 1981). With respect to Burian, little is known regarding how the soft tissues were extrapolated from the fragmentary fossils upon which his reconstructions were based. Here we can only assume that these illustrations were reconstructed intuitively. In contrast to Burian, Matternes provides a full description of his methods. The reconstruction, he says, was made over an image of a composite reconstruction of an *Australopithecus afarensis* skull (Kimbel et al., 1984; Kimbel and White, 1988). The masticatory muscles and muscles of expression were constructed over the skull first, then existing methods for approximating the other features of the face were borrowed from the facial approximation literature, including mouth width determination, locating the eyeballs within the eye sockets, as well as deciding on the ear morphology, flexure wrinkles, and hirsuteness (Johanson, 1981).

Anyone attempting to reconstruct a hominin ought to be aware of the aforementioned practitioners and their influence on the current state of the practice. Scientists like Gerasimov and artists like Burian were some of the first to attempt to produce a hominin face from skeletal remains. Their results have functioned as hypotheses for the facial appearances of their subjects and while not all of these hypotheses may appear equally valid to the reader, we would like to propose that in the absence of a well-established systematic approach for reconstructing hominin soft tissues, these works provide valuable insights into each practitioners' methodology. However, although these works have helped immensely in encouraging interest in human evolution, the methods employed by the aforementioned practitioners

remain largely unchanged today. Gerasimov's methods have seen no improvement in their application to hominins and Burian's artistic intuition has been replicated by other artists, such as the paleoartist Mauricio Antón, with varying results.

THE PROBLEM OF VARIABILITY

Differences among hominin reconstructions were first systematically documented in a pivotal study by Karen Anderson, in which 860 hominin reconstructions were assessed from 55 museum displays across Europe and Australia. Inconsistencies between reconstructions of the same individual were found in both their surface appearances and body proportions (Anderson, 2011). To make matters worse, most hominin reconstructions were found to be presented without any rigorous empirical justifications. Despite this, and to the surprise of the authors, the same reconstructions are commonly cited in the scientific literature and presented in scientific textbooks on human evolution (Jelínek, 1975; Balter, 2009; Jablonski, 2013; Roberts, 2018). So severe are the differences between reconstructions of the same individual that it is almost as though the practitioners had never encountered another hominin reconstruction before commencing their own. From a scientific point of view, there are only two ways of explaining an error of this magnitude: either (1) the reconstructions are purely artistic interpretations based on individually constructed knowledge about human evolution, which can vary between practitioners and ultimately results in variability, and/or (2) the practitioners were using unreliable reconstruction methods. Why such varying reconstructions continue to be used in the dissemination of science when such reconstructions have never been formally verified is disconcerting to us because the quality of knowledge perpetuated by their use is clearly inconsistent. To make matters worse, consider the reconstruction of Lucy presented at the "Answers in Genesis" ministry's Creation Museum in Petersburg, Kentucky. While Lucy was indeed a primate, the decision to reconstruct this specimen as a knuckle-walker is an obvious error. However, the argument of variability put forward by the Creation Museum is a valid one that has, as of yet, not been addressed by the scientific community.

To the knowledge of the authors, Gerasimov is the only practitioner to express doubt about the use of his methods for reconstructing the faces of ancient hominins. He acknowledged from the outset that there was an inherent risk in interpolating soft tissue depth data collected from orangutans into his reconstruction of the *Australopithecus africanus* specimen Sts 5 (Gerasimov, 1971). In contrast, Gurche is on record saying that he developed his method for reconstructing hominins from personal research carrying out dissections of extant apes and modern humans (Gurche, 2013), but this research has never been formally verified nor published in any scientific literature. Regarding Élizabeth Daynès, Gary Sawyer, Viktor Deak, and Adrie and Alfons Kennis, none of these practitioners have ever published any details regarding their methods or justifying their results. Thus, at present it is evident that hominin reconstruction is a practice lacking a robust scientific and empirical foundation.

METHODS AND TECHNIQUES USED FOR RECONSTRUCTING HOMININS

To explore the question of why the aforementioned variability has and is still occurring, we will evaluate the evidence and methods available to practitioners of hominin reconstruction. As stated in the Introduction, to aid in our review we will present the various reconstructions performed by RC and GV over the last 6 years as case studies to (1) exemplify the quality of evidence that is available in each case and (2) to show what existing methods were employed in each case to explore their strengths and weaknesses.

Reconstructing Hard Tissues

The production of hominin reconstructions is interconnected with the discovery of fossils. This is not surprising since the internal skeleton serves as the basis for all of the external soft tissues. The vast majority of hominin fossils are represented by skulls, which are well-connected sets of bones that are usually preserved together, although often distorted or missing mandibles, unlike postcranial remains that consist of many separate bones that can become easily scattered in the environment (Suzuki and Takai, 1970; Sartono, 1972; Brown et al., 1985; Suwa et al., 2009; Berger et al., 2010; Kimbel and Rak, 2010; Laird et al., 2017). Postcranial fossils, by comparison, are exceptionally fragmented. Large portions of these fossils are poorly represented and/or were never recovered. Therefore, before the soft tissues for any hominin can be considered, the osteological material must first be reconstructed.

Methods for the reconstruction of hominin crania have been, and are still being, developed (Kimbel et al., 1984; Kimbel and White, 1988; Zollikofer et al., 2005; Gunz et al., 2009; Suwa et al., 2009; Kimbel and Rak, 2010; Benazzi et al., 2011; Amano et al., 2015; Brassey et al., 2018). In 1984, Kimbel, White, and Johanson reconstructed a male *Australopithecus afarensis* skull. The skull was a composite reconstruction that incorporated the skeletal elements from 12 different supposedly male fossil specimens found from sediments at A.L. 200-1a and one specimen found at A.L. 333/333w. This skull was later revised after the discovery of further fossil evidence (Kimbel and White, 1988). Similarly, in 1996, Tattersal and Sawyer revised Weidernreich and Swan's 1937 reconstruction of the skull of *Homo erectus* from a collection of casts from Zhoukoudian, China (Tattersall and Sawyer, 1996). This reconstruction was different from the Weidenreich and Swann skull, which was reconstructed as a female, whereas Tattersal and Sawyer reconstructed the skull as a male (Tattersall and Sawyer, 1996). To the knowledge of the authors, these are two of the only physical reconstructions of hominin skulls that have had their initial reconstruction and subsequent revision formally published. What this means for all other reconstructions of hominin skulls is unclear.

Reconstructions of hominin skulls facilitated by computer software are becoming increasingly popular (Gunz et al., 2009; Benazzi et al., 2011; Gunz and Mitteroecker, 2013; Kikuchi and Ogihara, 2013; Amano et al., 2015; Senck et al., 2015; Mounier and Mirazón Lahr, 2016). Gunz et al. (2009) produced virtual reconstructions of three hominin skulls from CT scans

of the original specimens. These were the Taung child skull, the adult specimen of *Australopithecus africanus* Sts 5 (Broom, 1947), and a skull of the *Homo erectus* juvenile specimen KNM-WT 15000 (Brown et al., 1985). For the Sts 5 specimen, CT scans were combined with geometric morphometric methods to produce a complete skull. Landmarks were applied to a modern human cranium for the purpose of extracting coordinates and to produce a reference surface. The surface of the original Sts 5 cranium was then warped to match those coordinates taken from the modern human reference. This method goes beyond the reassembly of missing fragments like a jigsaw puzzle, such as those mentioned previously, as the entire fossil is replaced with a warped model of the modern human reference cranium. In other words, no fragments belonging to the original fossil are preserved in the result. For this reason, the method has received criticism (Senck et al., 2015). Accuracy of the method hinges on the correct use of reference surfaces. Interspecies and intraspecies reference surfaces can produce different results. Senck et al. (2015) concluded that it is possible to reconstruct hominin crania using reference surfaces but only if the morphometry of the subject being reconstructed is similar, or if bilateral symmetry can be exploited.

When we reconstructed the Taung child's skull in 2017, we used traditional molding and casting methods to produce a duplicate cast made directly from the first-order cast of the original specimen that was gifted to MH in 1995, rather than commercially available products—such as those from Bone Clones, Inc.—which are not exact copies of the original fossils themselves. The Taung fossil required very little restoration since its preserved parts provided enough anatomical constraints, such as occlusion and articulation, which meant that very few assumptions were needed to obtain complete anatomical information. However, in our reconstruction of Lucy's skull shown in **Figure 1C**, the reconstruction process was not as straightforward. Lucy, being the adult female specimen of *Australopithecus afarensis* and one of the most complete Pliocene hominin fossil skeletons ever found, has been subject to the facial reconstruction procedure more so than any other fossil hominin. By attempting to reconstruct Lucy's skull ourselves, we found that this specimen is a poor candidate for the facial reconstruction procedure because most of Lucy's cranial bones are missing. Lucy's mandible (**Figure 1B**) is relatively well-preserved and as such formed the basis for our reconstruction, but the cranium had to be digitally interpolated from the previously discussed composite male skull shown in **Figure 1A** (Kimbel et al., 1984; Kimbel and White, 1988). While doing so we discovered that the male cranium is much larger and does not articulate with the mandible well, so we scaled the cranium uniformly on all axes to fit Lucy's mandible based on bilateral symmetry and parabolic curve alignment of the upper and lower dental arches. The method we employed can be described as a "best-fit" approach and we do *not* by any means present our own reconstruction of Lucy's skull as the definitive version of this individual. However, it does show how each practitioner is required to model their own skull or borrow commercially available products that have never been formally verified.

What can be inferred from the methods involved in the reconstruction of hominin skulls is that separate methods are likely to produce varying results, especially in the case of Lucy. There is one other fact that needs to be acknowledged here. Since Lucy was discovered, other skulls have been found. So well-preserved are these skulls that almost no osteological reconstruction is necessary. The skulls belonging to individuals attributed to *Homo naledi* (LES1), *Australopithecus sediba* (MH1), and *Homo floresiensis* (LB1) are just a few specimens that are ideal candidates for the facial reconstruction procedure (Brown et al., 2004; Berger et al., 2010; Laird et al., 2017). Despite these new discoveries, and to our surprise, there are still

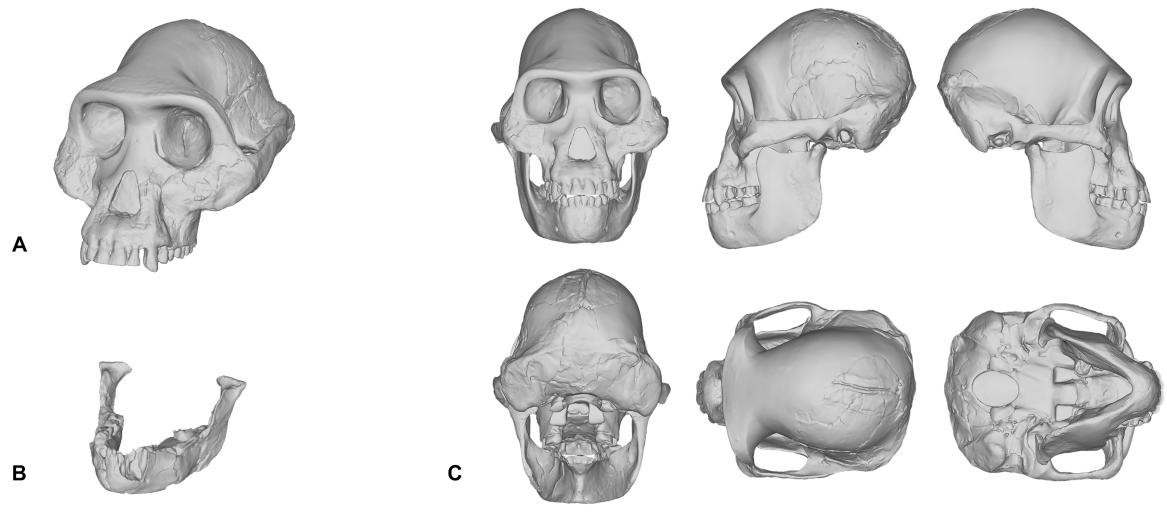

FIGURE 1 | Digital model of the *Australopithecus afarensis* composite male cranium reconstructed in Kimbel et al. (1984) and Kimbel and White (1988) **(A)**. Mandible belonging to the A.L. 288-1 (Lucy) partial skeleton **(B)**. Reconstruction of Lucy's skull that was produced by scaling the male cranium to fit the A.L. 288-1 mandible **(C)**.

facial reconstructions of Lucy being performed today. For these reasons, we would like to encourage practitioners to perform facial reconstructions on well-preserved fossils first before attempting to reconstruct those that are heavily fragmented.

Since this special issue is about more than just reconstructions of the skull and face, we feel that it is essential to include the various attempts at reconstructing hominin post-cranial skeletons in this review. However, an extensive survey of the scientific literature revealed that there is only one peer-reviewed article including a reconstruction of a complete hominin postcranial skeleton. The skeleton was reconstructed in a recent study exploring the use of a volumetric technique for estimating the body mass of hominins, in which a complete virtual 3D model was reconstructed for, yet again, Lucy (Brassey et al., 2018). However, in this case the subject is a logical choice since Lucy's post-cranial skeleton is exceptionally preserved. In this reconstruction, scans were made from casts of the original fossil bones and then virtual reproductions were articulated in computer software. 3D modeling techniques, such as mirroring and sculpting, were then used to reproduce existing parts of the skeleton. Additional hominin fossils were used for the completion of missing parts, including, but not limited to, an *Australopithecus sediba* (UW88-38) right clavicle and the *Homo habilis* specimen OH-8. Scans were also made from these elements and the virtual reproductions were then scaled to fit the partial skeleton. The thorax morphology was reconstructed using an iterative, geometric morphometric technique based upon a sample of both *Homo sapiens* and *Pan troglodytes*. The resulting 3D model of Lucy's skeleton was used in our reconstruction of Lucy's face and body (**Figure 2**). Putting the soft tissues aside for the moment to focus on the skeleton alone, we are not confident that the 3D model reconstructed in Brassey et al. (2018) is a true representation of Lucy's anatomy. The decision to reconstruct Lucy as an upright, free-standing hominin fully capable of erect bipedalism is well supported; it is indicated by the anatomy of the A.L. 288-1 fossil, the discovery of earlier and more numerous fossils attributed to *Australopithecus afarensis*, and the footprints from the Laetoli Beds of northern Tanzania (Leakey and Hay, 1979; Leakey, 1981; Johanson et al., 1982; Kimbel et al., 1984; Aiello and Dean, 1990). The footprints, for example, demonstrate that at the time of the *Australopithecus* there existed upright, free-standing hominins fully capable of walking bipedally and, therefore, Lucy has been reconstructed in such a way as to make this functionally possible. However, we agree with Brassey et al. (2018) in that the reconstruction is incorrect but only to the extent that the addition of skeletal elements from other specimens—belonging to separate species—will inevitably produce error, and how could it not? One could never confidently extrapolate the missing bones from an anatomically modern human with those belonging to a chimpanzee, so why would the talus from the *Homo habilis* specimen OH-8 be a suitable substitute for the talus of *Australopithecus afarensis*? We would also like to add that the ribcage is highly speculative. It is currently held that anatomically modern humans and hylobatids (gibbons and siamangs) share a barrel-shaped ribcage, whereas the great apes share a funnel-shaped rib cage. However, hypotheses about the shape of the *Australopithecus* rib cage vary and a consensus is yet to be reached on whether *Australopithecus* were markedly different from great apes and more similar to modern humans, or if the *Australopithecus* rib cage was more comparable to extant intermediates, such as hylobatids and orangutans (Bastir et al., 2017). Furthermore, the general stance of the skeleton is also potentially in error in part due to the ilium of the pelvis seeming to be angled in a position not seen in any extant hominin, much less a hominid. This horizontal position of the pelvis makes Lucy's stature shorter since the acetabula are raised upward and forward. Thus, similar to what has been previously discussed regarding hominin skulls, variability among post-cranial soft tissues is not just the result of differences in the shaping of the external appearances, it also appears to be the result of differences in the anthropometrics and arrangement of the underlying post-cranial skeletons.

FIGURE 2 | An intuitive reconstruction of Lucy's soft tissues (without hair and pigment) produced in 2018 and reconstructed over the digitally reconstructed A.L. 288-1 skeleton published in Brassey et al. (2018).

Although peer-reviewed articles including reconstructions of postcranial hominin skeletons are lacking in the scientific literature, there have been a number of reconstructions produced and published in books intended for a general audience. For example, in 2013 the skeleton of the *Paranthropus boisei* specimen OH5 was reconstructed by John Gurche for a display at the Smithsonian Museum of Natural History, and is featured in Gurche's (2013) book *Shaping Humanity*. The height of the skeleton appears to have been informed by a regression model developed in Gidna and Domínguez-Rodrigo (2013) and used by

Domínguez-Rodrigo et al. (2013) to produce minimum stature of 156 cm for this individual. However, the prediction model was developed using anatomically modern human anatomy, which Domínguez-Rodrigo et al. (2013) concede may not be appropriate in the case of the *Paranthropus* genus. We would like to highlight that even if the predicted minimum stature was correct, it does not provide the actual height for this individual nor the measurements of specific lengths of long bones. As of today, the only postcranial fossil that has been assigned to this species is the proximal end of an adult left femur. No other postcranial fossils have been confidently assigned to this species. Gurche provides a brief description for how he extrapolated the body from other australopithecine specimens (Gurche, 2013), but the results are highly speculative and virtually impossible to verify without the discovery of postcranial fossils belonging to *Paranthropus boisei*. The fact is that this reconstruction of *Paranthropus boisei* really only acts as an ill-informed hypothesis that is largely untestable. This is a notion that not only pertains to skeletal reconstructions of this species but to the practice of hominin reconstruction as a whole. What this rather obviously shows is that we are in desperate need of more fossil evidence, especially since bones serve as the starting point in all reconstructions of ancient primates.

Reconstructing Soft Tissues

Fossilized specimens of soft tissue are exceptionally rare. To the knowledge of the authors only one has ever been found for a primate (Franzen et al., 2009; Lingham-Soliar and Plodowski, 2010). The discovery was described as *Darwinius masillae*, an Eocene primate that lived 47 million years ago. What is most exceptional about this specimen is the almost complete skeleton, which is surrounded by a dark shadow representing the outline of the body and clearly showing gross anatomical details, such as the size of muscles surrounding the long bones, as well as minute details, such as the size of the external ears. Fossilized soft tissues have been found for other species, such as a specimen of the Cretaceous dinosaur, *Psittacosaurus* (Lingham-Soliar and Plodowski, 2010), and the Pliocene vulture, *Gyps fulvus* (Iurino et al., 2014). However, no such material has ever been found for any Plio-Pleistocene hominin species and, given the absence of soft tissue in the fossil record, there is no direct evidence for practitioners to extrapolate the soft tissues from or to compare their results with. Practitioners of facial reconstruction must therefore employ methods developed in studies of anatomically modern humans, which have mainly focused on the face. The foundations for these methods were laid in the nineteenth century by anatomists Hermann Welcker and Wilhelm His (Welcker, 1883; His, 1895). Welcker and His carried out the first documented research on the relationship between skull morphology and the soft tissues of the face by collecting soft tissue depths measurements at nine facial points from European cadavers, of which 37 were male and four female. A facial reconstruction was subsequently performed on a plaster cast of the skull of German composer and musician Johann Sebastian Bach using the measured thicknesses to construct the tissues of the face. This work has been often cited as one of the first facial reconstructions (Prag and Neave, 1997). Another well-known early facial reconstruction was performed by Kollman and Büchly (1898). Kollman and Büchly reconstructed the face of a Neolithic woman from Auvernier in Switzerland. The reconstruction was a joint effort, where Kollman collected soft tissue measurements from hundreds of female cadavers and produced a plan for the procedure and Büchly modeled the tissues onto the skull to produce the face. These early attempts of reconstructing faces to approximate the appearance of the deceased are cited in almost all of the literature on forensic facial reconstruction (Prag and Neave, 1997; Wilkinson, 2004).

Today, methods detailing the reconstruction process of the face are ubiquitous in the facial approximation literature (Stephan, 2003a,b,c; Stephan et al., 2003, 2013; Wilkinson, 2004; Hanebrink, 2006; Stephan and Simpson, 2008; Guyomarc'h et al., 2012; Richmond, 2015). Part of the challenge for any practitioner of hominin facial reconstruction is deciding which methods to use since a single anatomical feature may be reconstructed using a number of separate methods. In reconstructing the soft tissues of hominins faces, measurements at various cephalometric landmarks on the face must be determined. There are currently only three methods available to practitioners for reconstructing hominin soft tissues: (1) the thicknesses can be derived from mean values taken from measurements of modern humans—the best resource for deriving mean values comes from a recent meta-analysis of all the data drawn from across all of the literature (Stephan, 2017)—(2) the thicknesses can be derived from regression models developed from measurements of modern human skeletons and corresponding soft tissues, or (3) the thicknesses can be derived from mean values taken from measurements of great apes (chimpanzees, gorillas, and orangutans).

There are a few recognized reasons why mean values derived from either modern humans or apes, especially chimpanzees, may not be appropriate for reconstructing the face of Plio-Pleistocene hominins. First, means only express averages and thus do not represent the reality of individual variation within populations and, in fact, they completely ignore it. Furthermore, extrapolation of modern human depth data to archaic hominin skulls like those belonging to robust *Australopithecus*, such as the OH5 specimen, is predicated on the assumption that soft tissues depths between separate hominin species are identical, which is false based on what soft tissue measurements have been taken from chimpanzees (Hanebrink, 2006), and while extrapolation of mean chimpanzee values may produce less error than those for modern humans, very few measurements have ever been obtained for chimpanzees and therefore much of the face is still subject to artistic interpretation. For the above reasons, we rejected the use of averages in our own reconstructions. Conversely, the use of equations for predicting facial tissue thicknesses from craniometric measurements is gaining traction (Sutton, 1969; Simpson and Henneberg, 2002; Dinh et al., 2011; Stephan and Sievwright, 2018). Multiple significant correlations have been identified in samples of modern humans and regression models have been produced. As such, craniometric measurements of the skull can be used to produce facial tissue depths from regression models alone. Given that the soft tissues are tailored to each skull and are based on

the verified relationships between soft tissue and craniometric dimensions, this method ought to be explored further, especially in great ape material, for the possibility of producing a set of regression models that have inter-species compatibility could reduce most of the variability between facial reconstructions of the same individual.

In our own experiments, results varied depending on whether intuition or equations were used. Given that practitioners of hominin reconstruction have chosen not to publish their methods it is not possible to link methods to any given reconstruction for the sake of comparison, so here we can only analyze our own facial reconstructions as a means of exploring the strengths and weaknesses of each method. To do so, we point to our reconstructions of the Taung child. The first reconstruction was produced using GV's sculptural and anatomical intuition alone, while the second was produced a year later using the same method except under the supervision of MH. As can be seen in **Figure 3**, there are obvious differences in their appearance. If intuited reconstructions that are produced by the same practitioner can vary, in particular with input from outside sources, then one can see clearly why reconstructions of the same individual produced by separate practitioners could vary wildly from museum to museum.

There are also other aspects beyond soft tissue thicknesses at specific points on hominin skulls that affect the variability exhibited between reconstructions of the same individual. The placement of the eyeballs within the orbits, eyebrow position, mouth width, and ear size arguably have more of an impact on the appearance than soft tissues alone. Much like soft tissue thickness, these features have been either reconstructed intuitively or using methods derived from studies of anatomically modern humans and great apes. In Gurche's reconstruction of the *Australopithecus africanus* specimen Sts-5, Gurche reconstructed the mouth width based on measurements of *Pan troglodytes* (Gurche, 2013), and eyeball position based on an unspecified ratio described in the appendix of his publication. In our reconstruction of the Taung child, we found that if official methods were not followed the reconstruction could be made to appear in a number of different ways. The mouth of the reconstruction in **Figure 3A** appears more prognathic than the reconstruction shown in **Figure 3B**. The ears are also larger and the flexure wrinkles more pronounced, which is more akin to young bonobos than to modern humans. In hindsight, it appears a concerted effort may have been at play to depict the subject as more ape-man (A) in one case and more man-ape (B) in the other.

In an effort to move away from intuition, our second facial reconstruction of Lucy (**Figure 4**) used equations derived from regression analyses of anatomically modern humans (Simpson and Henneberg, 2002). As one can see, it differs in appearance from the earlier reconstruction of Lucy in **Figure 2**, which was done intuitively without empirical data. This reconstruction may be perceived as an improvement over the previous Lucy since an empirical method was used, however, we believe that this is not at all the case. We must be fully transparent in stating that a number of the predicted values produced by the regression model yielded negative results, i.e., tissue thicknesses below 0.0 mm. Since it is not possible for soft tissue to be negative or equal to zero, these landmarks were excluded from the reconstruction and instead were extrapolated from the nearest relative predicted value. This error is likely a result of extreme values of the

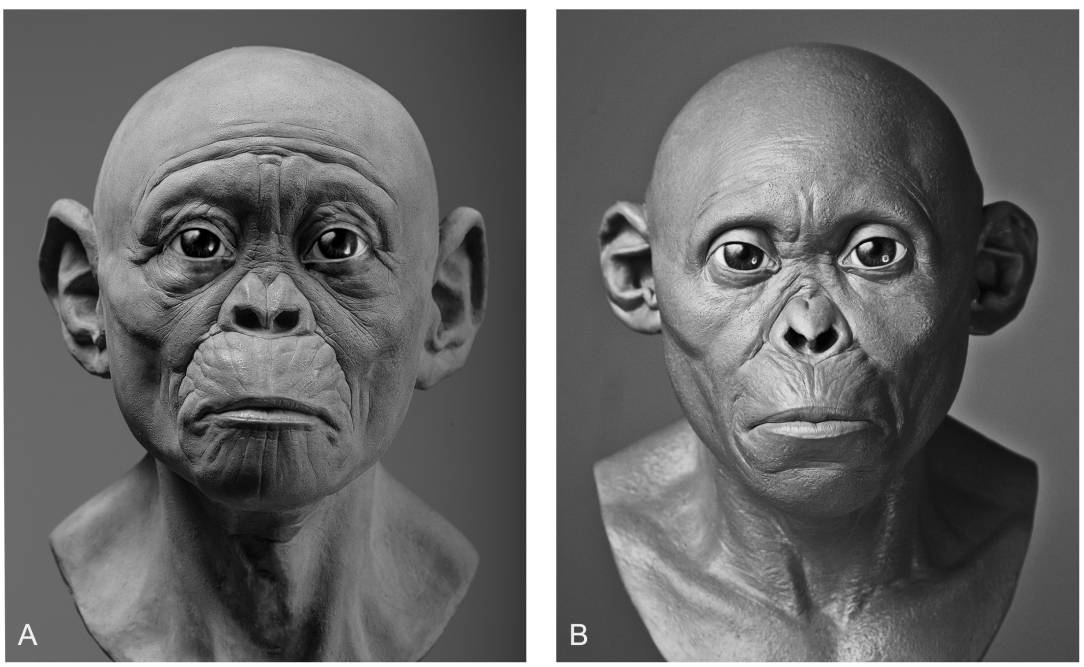

FIGURE 3 | Two facial reconstructions of the Taung child (without hair and pigment) that were produced one year apart. Please note how variability between these reconstructions is exemplified by the subjective decision to depict the subject as more apelike **(A)** or more humanlike **(B)**.

FIGURE 4 | A facial reconstruction of Lucy (without hair and pigment) produced in 2019 that employed facial soft tissue regression models developed in Simpson and Henneberg (2002) from modern human material.

independent variable. While some points did seem to conform to biological reality, based on mean comparisons, the fact that some points were entirely outside of possibility should cast doubt on the entire efficacy of human-derived regression models for reconstructing facial soft tissue in australopithecines. Thus, these equations are perhaps only appropriate for reconstructing hominins with craniometrics that are inside the normal range of variation observed in samples of anatomically modern humans.

Our reconstruction of the Neandertal specimen Amud 1 (**Figure 5**), for example, exhibits less of the aforementioned issues. The more proximal relationship of Neandertals to modern humans makes the use of the equations more viable. A number of other empirical methods derived from modern humans were also used, including positioning the eyeballs according to Guyomarc'h et al. (2012), the profile of the nose according to Prokopec and Ubelaker (2002), and the width of the mouth according to Stephan and Henneberg (2003). The final facial reconstruction of Amud 1 shown in **Figure 6** is similar to other reconstructions of Neandertals, especially in the size of the nose, suggesting that there is less variability in individuals that are compatible with existing methods of facial reconstruction derived from modern humans, although an explanation for this compatibility remains unclear. It is important to note here that while no values were reported as negative, unlike in our facial reconstruction of Lucy, we think the lack of lateral points on the skull offered by the equations resulted in too much intuition at these areas. This is because facial reconstruction methods have focused only on points of the face for the purposes of identification, whereas differences in the appearance between species can extend beyond the face to the whole head, like the temporalis muscles of OH5 for example. Thus, a more comprehensive study involving more measurements and points around the entire skull warrants further investigation.

Regarding soft tissue reconstructions of hominin bodies, the only published method we could find is described by Gurche (2013). This method, which has no empirical basis, was used to reconstruct the body of a number of Plio-Pleistocene hominins. We used the same method in our reconstruction of the body of Lucy in **Figure 2**. Like Gurche, we inferred the muscle proportions from comparative studies of fossil hominins and great apes. One of these studies reported that the ulnae of A.L. 288-1 have short, proximally oriented olecranons, whereas all great apes have long distally oriented olecranons (Drapeau, 2003). This difference in olecranon morphology is reported to be the result of different functional requirements. The long olecranons of the ape ulnae reflect powerful triceps brachii muscles adapted for arboreal use, whereas the short olecranons of A.L. 288-1 reflect triceps brachii muscles adapted for manipulative activities, such as tool making (Drapeau, 2003). Thus, in our reconstruction of Lucy's body, we reconstructed the upper limbs to reflect the functional predictions we could extrapolate from the ulnae. Unfortunately, comparative studies such as those described are lacking for the trunk and lower limbs, so these are highly speculative and subject to change. As a whole, we found that the intuitive method for reconstructing the soft tissues of hominin bodies far too imprecise.

Another point of contention is skin color, which is the single most under-researched feature in relation to hominin reconstruction and there is no known method for reliably reconstructing skin color in hominins. In modern humans, mass migration has made it impossible to predict skin color with any precision. This is mainly due to interbreeding and mismatches between the ancestral environments that shaped our appearance and the environments we inhabit now (Jablonski, 2013). This is perhaps the reason why no effort has been made to develop a method for reconstructing skin color in ancient hominins. The consequence of not having a method for determining the appearance of hominin skin is illustrated in the varying reconstructions produced by Gurche, Daynès, Sawyer, Deak, and the Kennis brothers, as well as in our own reconstructions. As can be seen in the completed facial reconstructions of Lucy (A) and the Taung child (B) presented in **Figure 7**, their skin tones differ significantly. We have interpreted this difference as a result of not having an empirical method for reliably reconstructing

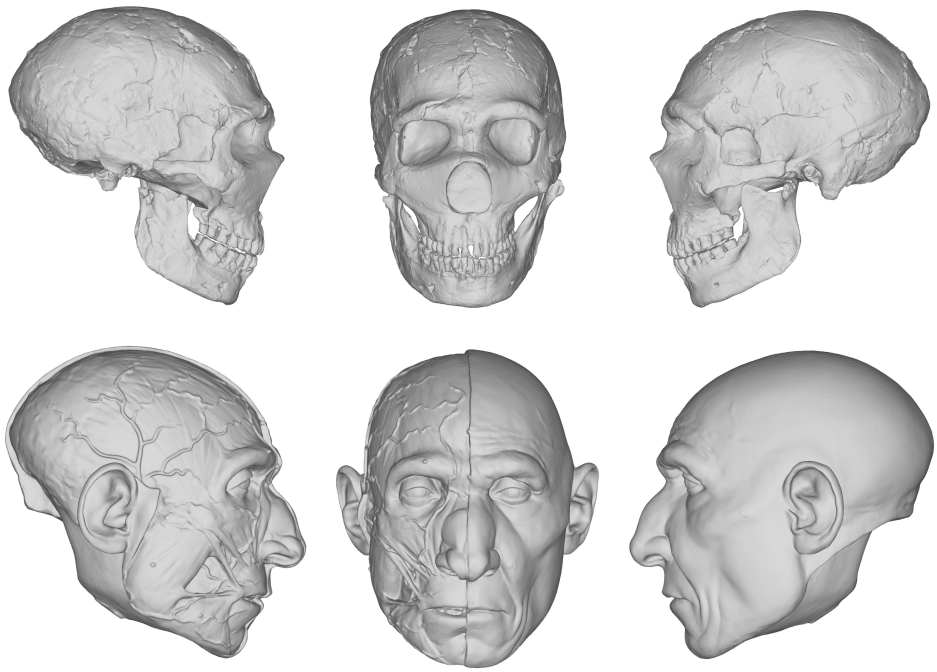

FIGURE 5 | Digital models showing the progression of the facial reconstruction procedure. Subject is based on a reconstruction of the Neanderthal Amud 1 cranium and associated mandible originally reconstructed by Suzuki and Takai (1970). Facial soft tissues were reconstructed using regression models developed in Simpson and Henneberg (2002) from modern human material.

epidermal melanin concentrations in australopithecines. The color of the Taung child's skin was reconstructed to appear similar to modern *Homo sapiens* native to Southern Africa. The decision to reconstruct the skin in this way is based on what is known about the function of epidermal melanin. Melanin evolved as a physical and chemical barrier to filter ultraviolet radiation. In humans there is a strong relationship between latitude and skin color and variation in skin color is the result of differences in concentrations of melanin (Blum, 1969; Relethford, 1998; Barsh, 2003; Chaplin, 2004; Jablonski, 2013). High concentrations of melanin are evolutionary advantages for populations in close proximity to the equator because it is the optimal arrangement for ultraviolet filtration in that environment. We assumed that for the Taung child to survive in Southern Africa there would have been no advantage in having low concentrations of melanin. Indeed, since it would have been a disadvantage and since ultraviolet radiation is the only known selective pressure for evolutionary change in melanin concentrations, we inferred that the skin of the Taung child would have been dark in appearance. However, even if this assumption is true, Lucy was reconstructed using exactly the same logic, although the results are very different. The appearance of the skin may be altered based on one's own subjective interpretation of the taxonomic position of these specimens. Both the African great apes, such as gorillas and chimpanzees, and modern humans have dark skin but "dark" is not nearly as descriptive as one may initially think. Regression models for reconstructing skin tone have been developed in Jablonski and Chaplin (2000), however, they measured melanin concentrations by skin reflectance, which does not provide the practitioner with a visual representation of the skin color of the subject. Research in this area offers the opportunity to present hominin populations with melanin concentrations that actually match their ancestral environments.

The color of primate pelage and differences between species further complicate the process of reconstructing surface appearance in hominins. For our reconstruction of Lucy and the Taung child presented in **Figure 7**, each hair was individually implanted into silicone casts of the reconstructions using a crown punching needle following the direction of hair in *Homo sapiens* and great apes described in Kidd (1903). We found that pelage was the most challenging feature to reconstruct because the pattern and distribution of hair cannot currently be extrapolated from bone alone. We tried to follow current hypotheses regarding thermoregulation via exploitation of exocrine sweating, which is often cited as a potential influence on the evolution of hairlessness in *Homo sapiens* (Wheeler, 1991, 1992), however, these hypotheses do not provide a current phenotype for specific species. Even considering further hypotheses about how hairlessness evolved from spending more time in aquatic environments (Hardy, 1960; Morgan, 1997), and in order to free our ancestors from external parasites (Pagel and Bodmer, 2003), neither of these explanations provided us with the specific instructions required to determine hair color and density. For all of these reasons, pelage poses a problem for museum displays. It has been said that baldness is preferable in an evidence-based reconstruction (Hayes et al., 2013). We do not necessarily agree with this as any reconstruction without hair may be perceived as incomplete or suggest that hominins did not have hair. This does

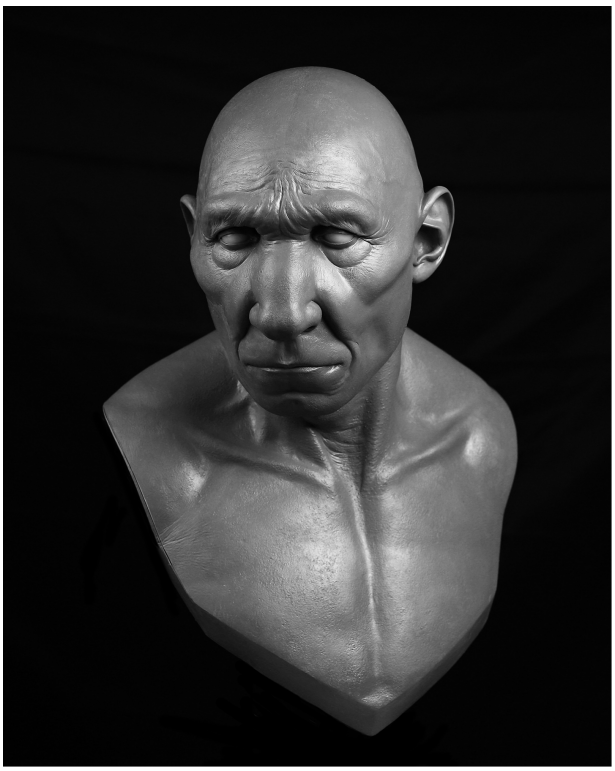

FIGURE 6 | Facial reconstruction of Amud 1 (without hair and pigment) produced in 2019 that employed facial soft tissue regression models developed in Simpson and Henneberg (2002) from modern human material.

not mean that we advocate for imaginary speculation in this area merely for the purpose of completing the reconstruction, rather, we would strongly encourage further research in this area.

FUTURE RESEARCH

The detection and analysis of DNA in extinct hominin finds is an emerging field and offers the exciting possibility of greatly enhancing reconstruction methods. Today, genetic research relevant to the practice includes the following: comparison between the genomes of *Pan troglodytes*, *Pan paniscus*, and *Homo sapiens* has revealed similarities between species and has enabled scientists to reconstruct the ancestry between them (Prüfer et al., 2012); the DNA of the Neandertals has been sequenced from a 38,000 year-old-fossil that was free from contamination with modern human DNA (Green et al., 2006), which has made it possible to compare the Neandertal genome to that of modern humans; and lastly, efforts to reconstruct the skeletal anatomy of the Denisovan's using DNA analysis generated body plans for these archaic hominins (Gokhman et al., 2019), as noted in the introduction, although the results are far from certain. Due to the chemical structure of DNA molecules, it is unlikely that they will preserve for more than several scores of thousands of years, thus there is little hope to obtain DNA of Pliocene/Early Pleistocene hominins. Proteomics seems to be able to study aminoacid sequences in ancient bones of greater antiquity since molecular structure of polypeptides preserves better than structure of DNA.

However, genetics does not currently provide the precise measurements needed for the reconstruction of both hominin soft tissues and underlying bone structures. The morphology of the bones in the illustration showing the Denisovans body plan is highly subjective (Gokhman et al., 2019). There is currently no known method for deriving anthropometric measurements from genomes, highlighting a major problem with the proposed body plan. The main purpose of the illustration appears to be providing an example rather than a precise depiction of anatomical forms from the past. Therefore, it seems that anatomical data are best provided by direct observations of anatomical structures. There is the possibility that genetic research will provide information about hominin appearances that cannot be determined from bone alone. Eye, hair, and skin color are just some aspects of hominin appearances that may be determined from the sequencing of ancient hominin genomes. Unfortunately, this information will be restricted to specimens from the late hominin record (Neandertals, Denisovans, and LB1) because, as stated, DNA extraction is not possible from fragments that are older than a few hundred thousand years. Worse still, DNA extraction from fossils is impossible. Fossils are bones that have all organic compounds replaced by minerals from soil and do not contain DNA. Alas, the only hominin remains that will be available for genetic research will be those that are not fossilized.

THE ETHICS OF RECONSTRUCTION AND SOCIETAL IMPLICATIONS

Given what Anderson (2011) has shown regarding the variability present in reconstructions of the same individual across separate museum displays, it is clear that very little effort has been made to produce reconstructions that are substantiated by strong empirical science. This is surprising given how museums boast about decades of success presenting scientific knowledge and education to the public. While in large part this is true and they provide an invaluable service to society, with respect to hominin reconstructions, they appear to exaggerate the methods used or this information is left out of their displays entirely. The reasons for this are not certain so we can only hypothesize as to the reasons why. It can most likely be attributed to factors outside the control of science, namely economic and social concerns. The immense pressure for museums to produce exhibits that are exciting may get in the way of any efforts to present reconstructions that are based on actual scientific knowledge, which requires time and effort. Exciting exhibits that feature large and very complete objects may attract non-traditional audiences, whereas small exhibits that grow over time presenting what is actually known about the appearance of Plio-Pleistocene hominins may only be of interest to a narrow audience.

Museums are often hubs for scientists and educators to share ideas with each other and find practices to excite the public with their enthusiasm. Truly, despite our criticisms, we acknowledge that generations of learners of all ages, educators, artists, and all forms of curious people have benefited greatly

FIGURE 7 | Pigmented silicone casts of facial reconstructions of Lucy **(A)** and the Taung child **(B)** showing different skin tones. Lucy's tone has been reconstructed to appear more similar to that of bonobos, whereas the Taung child's tone is more similar to that of anatomically modern humans native to South Africa.

from the existence of museums. However, presenting information that is not known diminishes the value of that which *is* known and may lead to confusion and discourage further interest in human evolutionary theory. There are potential educational harms in presenting unscientific reconstructions of hominins under the shroud of presumed validity. Therefore, with the cultural role of a museum and any educational institution, or any educational tool at all, comes an added responsibility to take pains to avoid accidentally, or worse, willfully misinforming the public.

While institutions showcasing and not challenging these empirical errors is troubling, other errors less concerned with what hominins looked like can be potentially far more damaging to social perceptions of evolution and its implications. To explore this point, it is important to introduce a couple of terms and a sentiment from an artistic perspective. For the academic art community, understanding iconography and iconology when creating representational works is crucial. In the visual arts, iconography is the study of subject matter itself and iconology is an attempt to analyze the significance of that subject matter in relation to the culture and individuals that produced it. This distinction is important because depictions of hominins do not exist in a vacuum, rather they are seated in the historical contexts of not just science but also those of the arts and cultures. This issue has been discussed in many books, including Moser's (1996) *Ancestral images: the iconography of human origins*, which analyzes how biases, prejudices, and stereotypes had been crucial in such reconstructions and further reinforced by them. Therefore, like an institution can be held accountable for what it promotes and showcases to the public, artists too can be held accountable for how they represent their subjects in their artworks.

In Van Laar and Diepeveen (1998) the roles artists function under within society are explored. One of these roles is that of the artist as an intellectual. This role is exemplified as the artist who deals with areas of human knowledge and contributes to them; the paradigmatic career of Leonardo Da Vinci comes to mind as the example that fits this mold. The tradition of artists working within the disciplines of science has undoubtedly contributed to scientific knowledge. As such, it can easily be argued that artists working in the field of hominin reconstruction operate under a similar role. However, as Laar and Diepeveen point out, with the obvious benefits to this role comes the danger of elitism being exercised by the artist. Artists tend to get self-absorbed in their claims about art and culture, making artwork that is seldom understood by the public and often disagreed with by art professionals. In other words, what begins with a sincere interest to contribute to human knowledge can become an ideological arms race in a competitive art field regarding the insights of individual artists who constantly jostle for artistic relevance. While this point is being made within the context of the art world, this same danger is present in the field of hominin reconstruction. Artists who are commissioned to sculpt models for museums tend to be highly skilled in the sculptural arts and their interest to contribute to science is at times overshadowed by what they can do artistically. Like the ideological arms races of heady conceptual artists, the museum display circuits can also be subjected to a similar form of competition. They can be so much more concerned with making science exciting that they can forget the underlying mission of their role in this context, which

is to disseminate and contribute to actual scientific knowledge. Artists who purport to facilitate the dissemination of scientific material, whose works are also hosted by renowned institutions of learning, are understandably perceived by the public as experts in their field. However, when artists operating as disseminators of science fail to make sure their models showcase the best available evidence, they fall short in their role of not just educators but artists as well. When work is being consumed by the public for scientific understanding, that status comes with immense responsibility and accountability. Throughout history, people of all ages have looked to artists for inspiration, contemplation, and in many cases like the ones in question, information. Artists who do not take into account or even exploit their contextual roles are at risk of doing society a disservice.

For example, consider the most iconic image of human evolution: Rudolf Zallinger's The March of Progress, also known as The Road to *Homo sapiens*. Gould (1989) was the first to point out the flaws in this reconstruction, which perpetuates a number of misleading, and potentially harmful, ideas about human evolution. First, it presents the erroneous view that evolution entails a linear progression from animal to ape, to ape-man to the so-called "Negroid race" and then to the "Caucasoid race." This Euro-centric bias not only makes biological errors but also projects ethical insensitivities. Note that the Zallinger's image was printed in a series of Science books for public consumption in America in 1965 at the height of the civil rights movement in a country wherein people were afforded different sets of rights and often denied basic freedoms, all based upon variations in skin color. Based on the pernicious bias out of which this image was made, it is hardly appropriate to use it for disseminating scientific information about human evolution. However, imagery of this kind is still being used today. In a promotional video advertising Gurche's reconstructions present at the Smithsonian Museum of Natural History[1], the same errors are present. It shows a linear progression through evolutionary time, transitioning from one genus to the next from *Sahelanthropus tchadensis* to *Australopithecus* to *Homo erectus*, to *Homo heidelbergensis* to a Neandertal and then finally to *Homo sapiens* represented by a photo of Gurche himself, who is of European ancestry. Visual material of linear simplified progressions of this sort, even if accidental, can act as a tone-deaf reminder of the history of Europeans holding a place in academia dictating to minorities where they come from and often where they stand in this unscientific hierarchy. This is perhaps most easily seen in the history of art museums and natural history museums housing art in a segregated manner. As expressed in Stanish (2008), art museums have historically showcased the art of the European masters, whereas natural history museums housed the art of indigenous peoples. This Eurocentric myopia has the effect of alienating minorities by putting their artwork in the context of natural history; the domain where we observe the natural world as a separate entity from it. Conversely, the art museum is the domain of artistic achievement. The act of segregating minority culture's artworks to the building where we study animals is akin to only representing African bodies as a steppingstone on the progression of evolution behind the European body. It may not sound like a point of scientific relevance, but in the field of visual arts one's audience, content, and context are inextricably linked. Artists who show imagery that has relevance to the very identity of our species should be well versed in the troubling iconology surrounding these types of imagery. If education and dissemination are the aims of museums and textbooks, then an extra level of care should be employed in not just what we depict, but how they are depicted and an intimate understanding of who the audience is. Consider how young, would-be academics of minority groups feel as they are readily encountered by not just scientifically unsubstantiated material, but material that echoes a history of racist attitudes toward groups that look like them. One could understand how visual material of this sort can discourage interest in science.

It is important to note here that it is not the intention of the authors to discourage artistic expressions of scientific ideas. If anything, we whole-heartedly support such explorations. As previously noted, artists have held various roles in society and often operate as an inspirational force that can inspire new perspectives outside of the purview of more methodological domains like science. To expand on this point, an artwork by one of us (GV) is presented in **Figure 8**. Shown is a work inspired by the artist's involvement within the sciences while employing formal and conceptual cues from art history to explore ideas of identity, origin stories, and even use the formal elements of the veiled cloth as a metaphor for how much is yet to be unveiled about the appearances of our ancestors and evolutionary history as a whole. This work, and other artwork involving the depictions of scientific ideas and/or specimens, serve to invoke thoughts, emotions, and concepts that are of a socio-political and philosophical nature. Thus, works like this have domains in which they are more or less appropriate. Within the domain of the contemporary art gallery or art museum, the scientific inaccuracies or artistic choices are of little consequence since the context puts more weight on the work's philosophical implications. Conversely, picture for a moment this statue, labeled as an artistic rendition of Lucy, in a natural history museum. Unless there are clear plaques and context-giving aids revealing that the body and its proportions are speculative, and that the use of cloth is a conceptual artistic freedom, this statue would surely mislead adult and, especially, younger museum goers due to the museum-imposed context of education and trust. As the opportunity for confusion outweighs the possibility of education, the prospect of such a work in a natural history museum is perhaps an inappropriate context barring exceptional caveats. Yet, there may not be a need to draw such a dichotomous view; if the statue served as an entrance piece that primes the viewers to think about how much we do not yet know, and how heavily veiled the truths about our past are, it can begin a healthy dialogue about what the rest of this imagined exhibit may present to its visitors in the way of fossils and other remains. This is but one example of a way of an artistic object exercising artistic license can operate in an educational context. Yet, this kind of conceptual artistic license is not the one usually taken in museums of natural

[1]https://www.youtube.com/watch?v=ru8ifph_q9o

FIGURE 8 | A marble sculpture titled "Santa Lucia" carved in 2019 following the body-composition of the intuitive reconstruction of Lucy previously shown in **Figure 2**.

history, instead practitioners of reconstructions take *scientific license* and create works much less founded on science than the museums prop them up to be. This is a case of a dim use of the word "art" and "license" operating as handwaving to simply allow artists to fill in the massive gaps in the available evidence with their "vision" without being honest with the public that they are engaged in highly speculative representation. The issue then becomes one of transparency, wherein exhibits could (and perhaps should) take care to show viewers the very exciting and wonderful facts we have uncovered and how much more we do not yet know. This would make what is shown in exhibits scientifically relevant and not inadvertently (or worse purposefully) making claims through their exhibits that are unfounded scientifically as previously discussed. Not taking full account of the context and role both the artist and museum serve together in the aims of scientific dissemination in society can have an adverse effect on the ability of these institutions to fulfill their self-stated aims of societal outreach and education.

Therefore, models, illustrations, and videos published by reputable institutions and trusted names like the Smithsonian Museum of Natural History should be held to a similar level of scrutiny as papers published in peer-reviewed journals. This is justified given the quantity of daily visits to museums around the world and the amount of visual consumption of content from museum displays, their websites, and printed material, which is far more accessible to the general public than any scientific article. For these reasons, scientists, artists, and museum curators involved in reconstructing our evolutionary antecedents must be very conscious of their role in society as arbiters of scientific facts and the consequences of not conforming tightly to this responsibility. These institutions are ones with a long history of community outreach which have no doubt touched many lives for the better, the authors included. These places have long served as a space where people come to learn and be exposed to not just science, but also to its questions and complexities. Where facts about hominin appearances are unknown, institutions can look to highlight the process of scientific discovery and be transparent instead of relying on artistic liberties and interpretations. Where interpretations or artistic speculation is undertaken, appropriate caveats and information should be readily offered until further research improves on these assumptions. While reconstructions currently displayed in museums globally are impressive for their technical achievement, their lack of scientific foundation paired with an overstatement of their scientific validity may undercut the trust of the public and betrays the very responsibility of dissemination that is expected from such spaces of potential learning.

CONCLUSION

The choice of hominins as a case study for this introductory paper of this special issue on muscle reconstructions is due to its value for broader discussions on such reconstructions and on both their ethics and societal implications. Muscle reconstructions are not only of interest to, and used by, scientists, rather they are used in art, textbooks, the press, social media, museums, schools, universities, and many other institutions. That said, the practice of hominin reconstruction has been mostly disregarded as a scientific activity and consequently has not been held to the same standard of scrutiny as peer-reviewed research, despite how the practice is currently perceived. The practice has essentially fallen into the hands of artists who, with no scientific framework of methods yet established for the reconstruction of Plio-Pleistocene hominins, performed the procedure however they wished. Some artists have relied mostly on their intuition regarding the soft tissues, while others have employed the use of forensic facial approximation methods generated from studies of modern human material. However, highlighting such complexities and difficulties also allows us to be aware of the fascinating opportunities that we face: it is a real opportunity for science to offer an alternative and to develop the practice of hominin reconstruction from one that is mostly an artistic activity to one that is a strong empirical science.

The question of whether the aforementioned is worth exploring in science seems to be mostly a matter of subjective opinion. Here, the authors would like to propose that no argument can be made against its exploration. Surely, if there

is even the slightest evidence to suggest that the practice may improve, then exploration and growth in this area should be encouraged rather than dismissed. Hominin reconstructions are predominately used for the dissemination of scientific information to the public in museum displays and students in university courses, which will influence the way we perceive our common origins, our fellow human beings, and the way we perceive and define humanity more generally. Thus, biologically accurate reconstructions built upon strong scientific foundations will be a non-trivial improvement that will enhance their efficacy and have a positive impact on the public understanding of evolutionary science; a branch of science concerned with our own ancestors and history. This underscores our responsibility regarding their depiction and dissemination because regardless of whether it concerns apes, monkeys, earlier tetrapods, or earlier fish, they are all our evolutionary relatives in the ever-branching biological tree of life.

AUTHOR CONTRIBUTIONS

RC initiated the investigation into scientifically accurate hominin reconstructions, analyzed the literature, wrote the majority of the manuscript, and edited the whole version of the manuscript. GV wrote the section under the heading "The Ethics of Reconstruction and Societal Implications," carved the sculpture featured in **Figure 8**, modeled all reconstructions featured in **Figures 1–7** in partnership with RC, and edited the whole version of the manuscript. MH advised the reconstructions featured in **Figures 2–7**, was involved in the 6 year partnership reconstructing hominins with RC and GV, and edited the whole version of the manuscript. RD had the idea of doing this manuscript for this special issue, wrote the section under the heading "Introduction: Why Study and Reconstruct Muscles?", and edited the whole version of the manuscript. All authors contributed to the article and approved the submitted version.

REFERENCES

Aiello, L., and Dean, D. (1990). *An Introduction to Human Evolutionary Anatomy*. London: Academic Press.

Amano, H., Kikuchi, T., Morita, Y., Kondo, O., Suzuki, H., Ponce, et al. (2015). Virtual reconstruction of the Neanderthal Amud 1 cranium. *Am. J. Phys. Anthropol.* 158, 185–197. doi: 10.1002/ajpa.22777

Anderson, K. (2011). *Hominin Representations in Museum Displays: Their Role in Forming Public Understanding Through The Non-Verbal Communication of Science*. Ph.D. Dissertation. Adelaide: The University of Adelaide.

Balter, M. (2009). Bringing hominins back to life. *Science* 325, 136–139. doi: 10.1126/science.325_136

Barsh, G. S. (2003). What controls variation in human skin color? *PLoS Biol.* 1:e27. doi: 10.1371/journal.pbio.0000027

Bastir, M., García-Martínez, D., Williams, S. A., Recheis, W., Torres-Sánchez, I., García Río, F., et al. (2017). 3D geometric morphometrics of thorax variation and allometry in Hominoidea. *J. Hum. Evol.* 113, 10–23. doi: 10.1016/j.jhevol.2017.08.002

Benazzi, S., Bookstein, F. L., Strait, D. S., and Weber, G. W. (2011). A new OH5 reconstruction with an assessment of its uncertainty. *J. Hum. Evol.* 61, 75–88. doi: 10.1016/j.jhevol.2011.02.005

Berger, L. R., de Ruiter, D. J., Churchill, S. E., Schmid, P., Carlson, K. J., Dirks, P. H. G. M., et al. (2010). Australopithecus sediba: a new species of homo-like Australopith from South Africa. *Science* 328:195. doi: 10.1126/science.1184944

Blum, H. F. (1969). Is sunlight a factor in the geographical distribution of human skin color? *Geogr. Rev.* 59, 557–581. doi: 10.2307/213862

Brassey, C. A., O'Mahoney, T. G., Chamberlain, A. T., and Sellers, W. I. (2018). A volumetric technique for fossil body mass estimation applied to Australopithecus afarensis. *J. Hum. Evol.* 115, 47–64. doi: 10.1016/j.jhevol.2017.07.014

Broom, R. (1947). Discovery of a new skull of the South African ape-man, *Plesianthropus*. *Nature* 159, 672–672. doi: 10.1038/159672a0

Brown, F., Harris, J., Leakey, R., and Walker, A. (1985). Early *Homo erectus* skeleton from west Lake Turkana, Kenya. *Nature* 316, 788–792. doi: 10.1038/316788a0

Brown, P., Sutikna, T., Morwood, M. J., Soejono, R. P., Jatmiko, Wayhu Saptomo, E., et al. (2004). A new small-bodied hominin from the Late Pleistocene of Flores, Indonesia. *Nature* 431, 1055–1061. doi: 10.1038/nature02999

Chaplin, G. (2004). Geographic distribution of environmental factors influencing human skin coloration. *Am. J. Phys. Anthropol.* 125, 292–302. doi: 10.1002/ajpa.10263

Dilkes, D. (2000). Appendicular myology of the hadrosaurian dinosaur Maiasaura peeblesorum from the Late Cretaceous (Campanian) of Montana. *Earth Environ. Sci. Trans. R. Soc. Edinb.* 90, 87–125. doi: 10.1017/s0263593300007185

Dinh, Q. H., Ma, T. C., Bui, T. D., Nguyen, T. T., and Nguyen, D. T. (2011). "Facial soft tissue thicknesses prediction using anthropometric distance," in *New Challenges for Intelligent Information and Database Systems*, eds N. T. Nguyen, B. Trawiński, and J. J. Jung (Berlin: Springer-Verlag), 117–126. doi: 10.1007/978-3-642-19953-0_12

Diogo, R. (2018). First detailed anatomical study of bonobos reveals intra-specific variations and exposes just-so stories of human evolution, bipedalism, and tool use. *Front. Ecol. Evol.* 6:53. doi: 10.3389/fevo.2018.00053

Diogo, R., and Wood, B. (2013). The broader evolutionary lessons to be learned from a comparative and phylogenetic analysis of primate muscle morphology. *Biol. Rev.* 88, 988–1001. doi: 10.1111/brv.12039

Domínguez-Rodrigo, M., Pickering, T. R., Baquedano, E., Mabulla, A., Mark, D. F., Musiba, C., et al. (2013). First partial skeleton of a 1.34-million-year-old *Paranthropus boisei* from Bed II, Olduvai Gorge, Tanzania. *PLoS One* 8:e80347. doi: 10.1371/journal.pone.0080347

Drapeau, M. S. M. (2003). Functional anatomy of the olecranon process in hominoids and plio-pleistocene hominins. *Am. J. Phys. Anthropol.* 124, 297–314. doi: 10.1002/ajpa.10359

Franzen, J. L., Gingerich, P. D., Habersetzer, J., Hurum, J. H., von Koenigswald, W., and Smith, B. H. (2009). Complete primate skeleton from the Middle Eocene of Messel in Germany: morphology and paleobiology. *PLoS One* 4:e5723. doi: 10.1371/journal.pone.0005723

Gerasimov, M. (1971). *The Face Finder*. London: Hutchinson & Co.

Gidna, A. O., and Domínguez-Rodrigo, M. (2013). A method for reconstructing human femoral length from fragmented shaft specimens. *Homo* 64, 29–41. doi: 10.1016/j.jchb.2012.09.006

Gokhman, D., Mishol, N., de Manuel, M., de Juan, D., Shuqrun, J., Meshorer, E., et al. (2019). Reconstructing denisovan anatomy using DNA methylation maps. *Cell* 179, 180.e10–192.e10. doi: 10.1016/j.cell.2019.08.035

Gould, S. J. (1989). *Wonderful Life: The Burgess Shale and the Nature of History*. New York, NY: Norton WW.

Green, R. E., Krause, J., Ptak, S. E., Briggs, A. W., Ronan, M. T., Simons, J. F., et al. (2006). Analysis of one million base pairs of Neanderthal DNA. *Nature* 444, 330–336. doi: 10.1038/nature05336

Gunz, P., and Mitteroecker, P. (2013). Semilandmarks: a method for quantifying curves and surfaces. *HYSTRIX* 24, 103–109. doi: 10.4404/hystrix-24.1-6292

Gunz, P., Mitteroecker, P., Neubauer, S., Weber, G. W., and Bookstein, F. L. (2009). Principles for the virtual reconstruction of hominin crania. *J. Hum. Evol.* 57, 48–62. doi: 10.1016/j.jhevol.2009.04.004

Gurche, J. (2013). *Shaping Humanity: How Science, Art and Imagination Help Us Understand Our Origins*. New Haven: Yale University Press.

Guyomarc'h, P., Dutailly, B., Couture, C., and Coqueugniot, H. (2012). Anatomical placement of the human eyeball in the orbit—validation using CT scans of living adults and prediction for facial approximation. *J. For. Sci.* 57, 1271–1275. doi: 10.1111/j.1556-4029.2012.02075.x

Hanebrink, J. R. (2006). *Datum is Only Skin Deep: In Vivo Measurements of Facial Tissue Thickness in Chimpanzees*. Ph.D. Dissertation. Baton Rouge, LA: Louisiana State University.

Hardy, A. (1960). Was man more aquatic in the past? *New Sci.* 7, 642–645.

Hayes, S., Sutikna, T., and Morwood, M. (2013). Faces of *Homo floresiensis* (LB1). *J. Archaeol. Sci.* 40, 4400–4410. doi: 10.1016/j.jas.2013.06.028

His, W. (1895). Anatomische Forschungen über Johann Sebastian Bach Gabeine und Antlitz nebst Bemerkungen über dessen Bilder. *Abhandlungen der mathermatisch-physikalischen Klasse der Königlichen Sachsischen Gesellschaft der Wissenschaften* 22, 379–420.

Iurino, D. A., Bellucci, L., Schreve, D., and Sardella, R. (2014). Exceptional soft tissue fossilization of a Pleistocene vulture (*Gyps fulvus*): new evidence for emplacement temperatures of pyroclastic flow deposits. *Quatern. Sci. Rev.* 96, 180–187. doi: 10.1016/j.quascirev.2014.04.024

Jablonski, N. G. (2013). *Skin: A Natural History*. Berkeley, CA: University of California Press.

Jablonski, N. G., and Chaplin, G. (2000). The evolution of human skin coloration. *J. Hum. Evol.* 39, 57–106. doi: 10.1006/jhev.2000.0403

Jelínek, J. (1975). *The Pictorial Encyclopedia of The Evolution of Man*. London: Hamlyn

Johanson, D. C. (1981). *Lucy, The Beginnings of Humankind*. New York, NY: Simon and Schuster.

Johanson, D. C., Lovejoy, C. O., Kimbel, W. H., White, T. D., Ward, S. C., Bush, M. E., et al. (1982). Morphology of the Pliocene partial hominid skeleton (A.L. 288-1) from the Hadar formation, Ethiopia. *Am. J. Phys. Anthropol.* 57, 403–451. doi: 10.1002/ajpa.1330570403

Kidd, W. (1903). *The Direction of Hair in Animals and Man*. London: Ballantyne, Hanson & Co.

Kikuchi, T., and Ogihara, N. (2013). Computerized assembly of neurocranial fragments based on surface extrapolation. *Anthropol. Sci.* 121, 115–122. doi: 10.1537/ase.130618

Kimbel, W. H., and Rak, Y. (2010). The cranial base of *Australopithecus afarensis*: new insights from the female skull. *Philos. Trans. R. Soc. Lond. Biol. Sci.* 365, 3365–3376. doi: 10.1098/rstb.2010.0070

Kimbel, W. H., and White, T. D. (1988). A revised reconstruction of the adult skull of *Australopithecus afarensis*. *J. Hum. Evol.* 17, 545–550. doi: 10.1016/0047-2484(88)90042-5

Kimbel, W. H., White, T. D., and Johanson, D. C. (1984). Cranial morphology of *Australopithecus afarensis*: a comparative study based on a composite reconstruction of the adult skull. *Am. J. Phys. Anthropol.* 64, 337–388. doi: 10.1002/ajpa.1330640403

Kollman, J., and Büchly, W. (1898). Die Persistenz der Rassen und die reconstruction der Physiognomie prähistorischer Schädel. *Archiv. r Anthropol.* 25, 329–359.

Laird, M. F., Schroeder, L., Garvin, H. M., Scott, J. E., Dembo, M., Radovèiæ, D., et al. (2017). The skull of Homo naledi. *J. Hum. Evol.* 104, 100–123. doi: 10.1016/j.jhevol.2016.09.009

Leakey, M. D. (1981). Tracks and tools. *Philos. Trans. R. Soc. Lond. Ser. B Biol. Sci.* 292, 95–102.

Leakey, M. D., and Hay, R. L. (1979). Pliocene footprints in the Laetolil Beds at Laetoli, northern Tanzania. *Nature* 278:317. doi: 10.1038/278317a0

Lingham-Soliar, T., and Plodowski, G. (2010). The integument of Psittacosaurus from Liaoning Province, China: taphonomy, epidermal patterns and color of a ceratopsian dinosaur. *Die Naturwissenschaften* 97, 479–486. doi: 10.1007/s00114-010-0661-3

Morgan, E. (1997). *The Aquatic Ape Hypothesis*. London: Souvenir Press.

Moser, S. (1996). *Ancestral Images: The Iconography of Human Origins.* New York, NY: Cornell University Press.

Mounier, A., and Mirazón Lahr, M. (2016). Virtual ancestor reconstruction: revealing the ancestor of modern humans and Neandertals. *J. Hum. Evol.* 91, 57–72. doi: 10.1016/j.jhevol.2015.11.002

Pagel, M., and Bodmer, W. (2003). A Naked Ape would have fewer parasites. *Proc. Biol. Sci.* 270, S117–S119.

Prag, J., and Neave, R. (1997). *Making Faces: Using Forensic and Archaeological Evidence*. London: British Museum Press.

Prokopec, M., and Ubelaker, D. H. (2002). Reconstructing the shape of the nose according to the skull. *For. Sci. Commun.* 4, 1–4.

Prüfer, K., Munch, K., Hellmann, I., Akagi, K., Miller, J. R., Walenz, B., et al. (2012). The bonobo genome compared with the chimpanzee and human genomes. *Nature* 486, 527–531. doi: 10.1038/nature11128

Relethford, J. H. (1998). Hemispheric difference in human skin color. *Am. J. Phys. Anthropol.* 104, 449–457. doi: 10.1002/(SICI)1096-8644(199712)104:4<449::AID-AJPA2<3.0.CO;2-N

Richmond, M. (2015). *Evaluation of Craniofacial Superimposition as a Technique for Measuring Mountain Gorilla Facial Soft Tissue Depth and Implications for Hominid Facial Approximation*. Greenville, NC: East Carolina University.

Roberts, A. (2018). *Evolution: The Human Story*. London: Dorling Kindersley.

Sartono, S. (1972). Discovery of another hominid skull at Sangiran. Central Java. *Curr. Anthropol.* 13, 124–126. doi: 10.1086/201255

Senck, S., Bookstein, F., Benazzi, S., Kastner, J., and Weber, G. (2015). Virtual reconstruction of modern and fossil hominoid crania: consequences of reference sample choice. *Anat. Rec.* 298, 827–841. doi: 10.1002/ar.23104

Simpson, E., and Henneberg, M. (2002). Variation in soft-tissue thicknesses on the human face and their relation to craniometric dimensions. *Am. J. Phys. Anthropol.* 118, 121–133. doi: 10.1002/ajpa.10073

Stanish, C. S. (2008). On museums in a postmodern world. *Daedalus* 137, 147–149. doi: 10.1162/daed.2008.137.3.147

Stephan, C., and Henneberg, M. (2003). Predicting mouth width from inter-canine width - a 75% rule. *J. For. Sci.* 48, 725–727. doi: 10.1520/JFS2002418

Stephan, C. N. (2003a). Anthropological facial 'reconstruction' – recognizing the fallacies, 'unembracing' the errors, and realizing method limits. *Sci. Just.* 43, 193–200. doi: 10.1016/S1355-0306(03)71776-6

Stephan, C. N. (2003b). Facial approximation: an evaluation of mouth-width determination. *Am. J. Phys. Anthropol.* 121, 48–57. doi: 10.1002/ajpa.10166

Stephan, C. N. (2003c). Predicting mouth width from inter-canine width—a 75% rule. *J. For. Sci.* 48, 725–727.

Stephan, C. N. (2017). 2018 tallied facial soft tissue thicknesses for adults and sub-adults. *For. Sci. Int.* 280, 113–123. doi: 10.1016/j.forsciint.2017.09.016

Stephan, C. N., Henneberg, M., and Sampson, W. (2003). Predicting nose projection and pronasale position in facial approximation: a test of published methods and proposal of new guidelines. *Am. J. Phys. Anthropol.* 122, 240–250. doi: 10.1002/ajpa.10300

Stephan, C. N., and Sievwright, E. (2018). Facial soft tissue thickness (FSTT) estimation models—and the strength of correlations between craniometric dimensions and FSTTs. *For. Sci. Int.* 286, 128–140. doi: 10.1016/j.forsciint.2018.03.011

Stephan, C. N., and Simpson, E. K. (2008). Facial soft tissue depths in craniofacial identification (part I): an analytical review of the published adult data. *J. For. Sci.* 53, 1257–1272. doi: 10.1111/j.1556-4029.2008.00852.x

Stephan, C. N., Simpson, E. K., and Byrd, J. E. (2013). Facial soft tissue depth statistics and enhanced point estimators for craniofacial identification: the debut of the shorth and the 75-Shormax. *J. For. Sci.* 58, 1439–1457. doi: 10.1111/1556-4029.12252

Sutton, P. R. N. (1969). Bizygomatic diameter: the thickness of the soft tissues over the zygions. *Am. J. Phys. Anthropol.* 30, 303–310. doi: 10.1002/ajpa.1330300215

Suwa, G., Asfaw, B., Kono, R. T., Kubo, D., Lovejoy, C. O., and White, T. D. (2009). The *Ardipithecus ramidus* skull and its implications for hominid origins. *Science* 326:68. doi: 10.1126/science.1175825

Suzuki, H., and Takai, F. (1970). *The Amud Man and His Cave Site*. Tokyo: Keigaku Publishing.

Tattersall, I., and Sawyer, G. J. (1996). The skull of "Sinanthropus" from Zhoukoudian, China: a new reconstruction. *J. Hum. Evol.* 31, 311–314. doi: 10.1006/jhev.1996.0063

Ullrich, H., and Stephan, C. N. (2016). Mikhail Mikhaylovich Gerasimov's authentic approach to plastic facial reconstruction. *Anthropologie* 52, 97–107.

Van Laar, T., and Diepeveen, L. (1998). *Active Sights: Art As Social Interaction*. Menlo Park, CA: Mayfield.

Welcker, H. (1883). *Schiller's Schädel und Todenmaske nebst Mittheilungen über Schädel und Todenmaske Kants*. Braunschweig: Vieweg und Sohn.

Wheeler, P. E. (1991). The thermoregulatory advantages of hominid bipedalism in open equatorial environments: the contribution of increased convective heat

loss and cutaneous evaporative cooling. *J. Hum. Evol.* 21, 107–115. doi: 10.1016/0047-2484(91)90002-D

Wheeler, P. E. (1992). The thermoregulatory advantages of large body size for hominids foraging in savannah environments. *J. Hum. Evol.* 23, 351–362. doi: 10.1016/0047-2484(92)90071-G

Wilkinson, C. (2004). *Forensic Facial Reconstruction*. Cambridge: Cambridge University Press.

Zollikofer, C. P. E., Ponce, de León, M. S., Lieberman, D. E., Guy, F., Pilbeam, D., et al. (2005). Virtual cranial reconstruction of *Sahelanthropus tchadensis*. *Nature* 434, 755–759. doi: 10.1038/nature03397

Conflict of Interest: The authors declare that the research was conducted in the absence of any commercial or financial relationships that could be construed as a potential conflict of interest.

frontiers in Ecology and Evolution

CORRECTION
published: 08 July 2021
doi: 10.3389/fevo.2021.719193

Corrigendum: Visual Depictions of Our Evolutionary Past: A Broad Case Study Concerning the Need for Quantitative Methods of Soft Tissue Reconstruction and Art-Science Collaborations

Ryan M. Campbell[1*†], *Gabriel Vinas*[2†], *Maciej Henneberg*[1,3†] *and Rui Diogo*[4†]

[1] *Department of Anatomy & Pathology, University of Adelaide, Adelaide, SA, Australia,* [2] *Department of Sculpture, Arizona State University, Tempe, AZ, United States,* [3] *Institute of Evolutionary Medicine, University of Zurich, Zurich, Switzerland,* [4] *Department of Anatomy, Howard University, Washington, DC, United States*

Keywords: artistic license, facial approximation, hominid, hominin, hard tissue, soft tissue

Edited and reviewed by:
Stefano Dominici,
University of Florence, Italy

***Correspondence:**
Ryan M. Campbell
ryan.campbell@adelaide.edu.au

***ORCID:**
Ryan M. Campbell
orcid.org/0000-0003-2630-1701
Gabriel Vinas
orcid.org/0000-0003-3374-3460
Maciej Henneberg
orcid.org/0000-0003-1941-2286
Rui Diogo
orcid.org/0000-0002-9008-1910

Specialty section:
This article was submitted to Paleontology, a section of the journal Frontiers in Ecology and Evolution

Received: *02 June 2021*
Accepted: *16 June 2021*
Published: *08 July 2021*

Citation:
Campbell RM, Vinas G, Henneberg M and Diogo R (2021) Corrigendum: Visual Depictions of Our Evolutionary Past: A Broad Case Study Concerning the Need for Quantitative Methods of Soft Tissue Reconstruction and Art-Science Collaborations. Front. Ecol. Evol. 9:719193. doi: 10.3389/fevo.2021.719193

A Corrigendum on

Visual Depictions of Our Evolutionary Past: A Broad Case Study Concerning the Need for Quantitative Methods of Soft Tissue Reconstruction and Art-Science Collaborations
by Campbell, R. M., Vinas, G., Henneberg, M., and Diogo, R. (2021). Front. Ecol. Evol. 9:639048. doi: 10.3389/fevo.2021.639048

In the original article, there were the following errors:

There was an error in the word "genetic tool," which should have been written as "genetic tools."

A correction has been made to the first sentence in the section titled **INTRODUCTION: WHY STUDY AND RECONSTRUCT MUSCLES on Line 30 of the corrected manuscript:**

At a time in which we are increasingly exposed to acclaims about new powerful genetic tools in the media and academia, one may wonder as to why we would focus on muscle reconstructions at all in this introductory paper of this special issue.

There was an error in the naming of a Figure. We wrote Figure 3 when we meant to say Figure 2.

A correction has been made to the first sentence in the section titled **Methods and Techniques Used for Reconstructing Hominids**, **Reconstructing Soft Tissues**, **paragraph 6 on Line 490 of the corrected manuscript:**

In an effort to move away from intuition, our second facial reconstruction of Lucy (Figure 4) used equations derived from regression analyses of anatomically modern humans (Simpson and Henneberg, 2002). As one can see, it differs in appearance from the earlier reconstruction of Lucy in Figure 2, which was done intuitively without empirical data.

There was an error in the figure caption for Figure 3. We wrote "1 year" when we should have written one year.

A correction has been made to figure caption 3 in the section titled **Figure captions on Line 1110 of the corrected manuscript:**

Figure 3. Two facial reconstructions of the Taung child (without hair and pigment) that were produced one year apart. Please note how variability between these reconstructions is exemplified by the subjective decision to depict the subject as more apelike **(A)** or more humanlike **(B)**.

There was an error repeating the same word twice. For ease of reading, this word should be removed.

A correction has been made to the last sentence in the first paragraph in the section titled **A Brief History of Hominin Facial Reconstruction on Line 140 of the corrected manuscript**:

We would like to be transparent with the reader and admit that this section is by no means a complete list of all the reconstructions that have ever been produced, however, it does include the most well-recognized practitioners and reconstructions that were featured in scholarly publications, scientific textbooks, and on display at institutions of international repute.

An in-text citation for Weidernreich and Swan was incorrectly formatted throughout a paragraph in the manuscript.

A correction has been made to in-text citation in the section titled **Methods and Techniques Used for Reconstructing Hominids**, **Reconstructing Hard Tissues**, **paragraph 2 of the corrected manuscript**:

Methods for the reconstruction of hominin crania have been, and are still being, developed (Kimbel et al., 1984; Kimbel and White, 1988; Zollikofer et al., 2005; Gunz et al., 2009; Suwa et al., 2009; Kimbel and Rak, 2010; Benazzi et al., 2011; Amano et al., 2015; Brassey et al., 2018). In 1984, Kimbel, White, and Johanson reconstructed a male *Australopithecus afarensis* skull. The skull was a composite reconstruction that incorporated the skeletal elements from 12 different supposedly male fossil specimens found from sediments at A.L. 200-1a and one specimen found at A.L. 333/333w. This skull was later revised after the discovery of further fossil evidence (Kimbel and White, 1988). Similarly, in 1996, Tattersal and Sawyer revised Weidernreich and Swan's 1937 reconstruction of the skull of *Homo erectus* from a collection of casts from Zhoukoudian, China (Tattersall and Sawyer, 1996). This reconstruction was different from the Weidenreich and Swann skull, which was reconstructed as a female, whereas Tattersal and Sawyer reconstructed the skull as a male (Tattersall and Sawyer, 1996). To the knowledge of the authors, these are two of the only physical reconstructions of hominin skulls that have had their initial reconstruction and subsequent revision formally published. What this means for all other reconstructions of hominin skulls is unclear.

There was an error in the description of Figure 7 in the main text. We wrote "the Taung child (A) and Lucy (B)," but we meant to say "Lucy (A) and the Taung child (B)."

A correction has been made to the sentence in the section titled **Methods and Techniques Used for Reconstructing Hominids**, **Reconstructing Soft Tissues**, **paragraph 9 on Line 547 of the corrected manuscript**:

As can be seen in the completed facial reconstructions of Lucy (A) and the Taung child (B) presented in Figure 7, their skin tones differ significantly.

The order of names in a figure were written back to front. It was written as "the Taung child and Lucy," but it should have been written as "Lucy and the Taung child."

A correction has been made to the sentence in the section titled **Methods and Techniques Used for Reconstructing Hominids**, **Reconstructing Soft Tissues**, **paragraph 10 on Line 574 of the corrected manuscript**:

For our reconstruction of Lucy and the Taung child presented in Figure 7, each hair was individually implanted into silicone casts of the reconstructions using a crown punching needle following the direction of hair in *Homo sapiens* and great apes described in Kidd (1903).

There is a spelling error in the keywords of the original article. A word is written in Australian English as "License" but should have been written as "license" in American English.

A correction has been made to the **Keywords on Line 27 of the corrected manuscript:**

keywords: artistic license, facial approximation, hominid, hominin, hard tissue, soft tissue

There is an error in the order of words that impedes legibility in the middle of a sentence. The sentence initially read as "but also to learn," but should be "but to also learn."

A correction has been made to the sentence in the section titled **Introduction: Why Study and Reconstruct Muscles? Third paragraph, line 77 of the corrected manuscript:**

This therefore illustrates how crucial it is to undertake accurate muscle reconstructions of fossils, to not only understand their functional morphology, and biology as a whole—bones do *not* move without muscles—but to also learn more about their evolutionary relationships, history, and adaptations.

A word was missing. The word missing was "of," which should have come before the words "years ago." It should be "of years ago."

A correction has been made to the sentence in the section titled **Introduction: Why Study and Reconstruct Muscles? Fourth paragraph, line 94 of the corrected manuscript:**

Over the last century, there has been a huge interest in reconstructing the face of members of our human lineage that lived many thousands, or even some millions, of years ago.

There was an error of unnecessary words that calls for their removal. "the entire" should be removed so the sentence just reads "…underlying evolutionary science."

A correction has been made to the sentence in the section titled **Introduction: Why Study and Reconstruct Muscles? Fourth paragraph, line 106 of the corrected manuscript:**

It is based on Charles Lyell's uniformitarian principle underlying evolutionary science.

There is an error in the use of past tense. We used "were" when it should have been "are."

A correction has been made to the sentence in the section titled **A Brief History of Hominin Facial Reconstruction**: First **paragraph, line 142 of the corrected manuscript:**

We would like to be transparent with the reader and admit that this section is by no means a complete list of all the reconstructions that have ever been produced, however, it does include the most well-recognized practitioners and reconstructions that are featured in scholarly publications, scientific textbooks, and on display at institutions of international repute.

There was an error with the use of a comma, where a transition would have sufficed.

A correction has been made to the sentence in the section titled **A Brief History of Hominin Facial Reconstruction**: **third paragraph, line 162 of the corrected manuscript:**

Is it important to note here that not all reconstructions of hominins have been produced in 3D since 2D reconstructions are arguably more numerous and thus any review would be incomplete without acknowledging them.

There was an error in the use of the singular "tissue." It should be a plural and written as "tissues."

A correction has been made to the sentence in the section titled **Reconstructing Hard Tissues**: First **paragraph, line 251 of the corrected manuscript:**

Therefore, before the soft tissues for any hominin can be considered, the osteological material must first be reconstructed.

There is an unnecessary use of descriptive words "better preserved." For ease of reading these words "better preserved" should be removed.

A correction has been made to the sentence in the section titled **Reconstructing Hard Tissues**: Fifth **paragraph, line 315 of the corrected manuscript:**

Since Lucy was discovered, other skulls have been found.

There is a missing plural "s" after the word "reconstruction." It should read "reconstructions"

A correction has been made to the sentence in the section titled **Reconstructing Soft Tissues**: Fourth **paragraph, line 459 of the corrected manuscript:**

Given that the soft tissues are tailored to each skull and are based on the verified relationships between soft tissue and craniometric dimensions, this method ought to be explored further, especially in great ape material, for the possibility of producing a set of regression models that have inter-species compatibility could reduce most of the variability between facial reconstructions of the same individual.

There is an unnecessary "the" in a sentence and it should be removed.

A correction has been made to the sentence in the section titled **Reconstructing Soft Tissues**: Fifth **paragraph, line 477 of the corrected manuscript of the corrected manuscript:**

Much like soft tissue thickness, these features have been either reconstructed intuitively or using methods derived from studies of anatomically modern humans and great apes.

There is a missing comma after the word "evidence."

A correction has been made to the sentence in the section titled **The Ethics of Reconstruction and Societal Implications Fourth paragraph, line 694 of the corrected manuscript:**

However, when artists operating as disseminators of science fail to make sure their models showcase the best available evidence, they fall short in their role of not just educators but artists as well.

There is a grammar issue with the word "ones." It should have been written as "one's."

A correction has been made to the sentence in the section titled **The Ethics of Reconstruction and Societal Implications Fifth paragraph, line 730 of the corrected manuscript:**

It may not sound like a point of scientific relevance, but in the field of visual arts one's audience, content, and context are inextricably linked.

There is a misuse of the prefix "un." It needs to be moved from "scientifically" to the word "substantiated" to read "scientifically unsubstantiated."

A correction has been made to the sentence in the section titled **The Ethics of Reconstruction and Societal Implications, Fifth paragraph, line 736 of the corrected manuscript:**

Consider how young, would-be academics of minority groups feel as they are readily encountered by not just scientifically unsubstantiated material, but material that echoes a history of racist attitudes toward groups that look like them.

There is a missing comma after "Yet" at the start of a sentence.

A correction has been made to the sentence in the section titled **The Ethics of Reconstruction and Societal Implications, Fifth paragraph, line 760:**

Yet, there may not be a need to draw such a dichotomous view; if the statue served as an entrance piece that primes the viewers to think about how much we do not yet know, and how heavily veiled the truths about our past are, it can begin a healthy dialogue about what the rest of this imagined exhibit may present to its visitors in the way of fossils and other remains.

There is a spelling error of the word "analyzed." It Is currently in Australian English as "analysed" but should be changed to US spelling.

A correction has been made to the sentence in the section titled **Author Contributions, line 853:**

RC initiated the investigation into scientifically accurate hominin reconstructions, analyzed the literature, wrote the majority of the manuscript, and edited the whole version of the manuscript.

The authors apologize for these errors above and state that they do not change the scientific conclusions of the article in any way. The original article has been updated.

REFERENCES

Amano, H., Kikuchi, T., Morita, Y., Kondo, O., Suzuki, H., Ponce, et al. (2015). Virtual reconstruction of the Neanderthal Amud 1 cranium. *Am. J. Phys. Anthropol.* 158, 185–197. doi: 10.1002/ajpa.22777

Benazzi, S., Bookstein, F. L., Strait, D. S., and Weber, G. W. (2011). A new OH5 reconstruction with an assessment of its uncertainty. *J. Hum. Evol.* 61, 75–88. doi: 10.1016/j.jhevol.2011.02.005

Brassey, C. A., O'Mahoney, T. G., Chamberlain, A. T., and Sellers, W. I. (2018). A volumetric technique for fossil body mass estimation applied to Australopithecus afarensis. *J. Hum. Evol.* 115, 47–64. doi: 10.1016/j.jhevol.2017.07.014

Gunz, P., Mitteroecker, P., Neubauer, S., Weber, G. W., and Bookstein, F. L. (2009). Principles for the virtual reconstruction of hominin crania. *J. Hum. Evol.* 57, 48–62. doi: 10.1016/j.jhevol.2009.04.004

Kidd, W. (1903). *The Direction of Hair in Animals and Man.* London: Ballantyne, Hanson & Co.

Kimbel, W. H., and Rak, Y. (2010). The cranial base of *Australopithecus afarensis*: new insights from the female skull. *Philos. Trans. R. Soc. Lond. Biol. Sci.* 365, 3365–3376. doi: 10.1098/rstb.2010.0070

Kimbel, W. H., and White, T. D. (1988). A revised reconstruction of the adult skull of *Australopithecus afarensis*. *J. Hum. Evol.* 17, 545–550. doi: 10.1016/0047-2484(88)90042-5

Kimbel, W. H., White, T. D., and Johanson, D. C. (1984). Cranial morphology of *Australopithecus afarensis*: a comparative study based on a composite reconstruction of the adult skull. *Am. J. Phys. Anthropol.* 64, 337–388. doi: 10.1002/ajpa.1330640403

Simpson, E., and Henneberg, M. (2002). Variation in soft-tissue thicknesses on the human face and their relation to craniometric dimensions. *Am. J. Phys. Anthropol.* 118, 121–133. doi: 10.1002/ajpa.10073

Suwa, G., Asfaw, B., Kono, R. T., Kubo, D., Lovejoy, C. O., and White, T. D. (2009). The *Ardipithecus ramidus* skull and its implications for hominid origins. *Science* 326:68. doi: 10.1126/science.1175825

Tattersall, I., and Sawyer, G. J. (1996). The skull of "Sinanthropus" from Zhoukoudian, China: a new reconstruction. *J. Hum. Evol.* 31, 311–314. doi: 10.1006/jhev.1996.0063

Zollikofer, C. P. E., Ponce, de León, M. S., Lieberman, D. E., Guy, F., Pilbeam, D., et al. (2005). Virtual cranial reconstruction of *Sahelanthropus tchadensis*. *Nature* 434, 755–759. doi: 10.1038/nature03397

frontiers in Ecology and Evolution

ORIGINAL RESEARCH
published: 19 March 2021
doi: 10.3389/fevo.2021.640345

Brain Reconstruction Across the Fish-Tetrapod Transition; Insights From Modern Amphibians

Alice M. Clement[1], Corinne L. Mensforth[1], T. J. Challands[2], Shaun P. Collin[3] and John A. Long[1]*

[1] College of Science and Engineering, Flinders University, Adelaide, SA, Australia, [2] School of Geosciences, Grant Institute, University of Edinburgh, Edinburgh, United Kingdom, [3] School of Life Sciences, La Trobe University, Bundoora, VIC, Australia

The fish-tetrapod transition (which incorporates the related fin-limb and water-land transitions) is celebrated as one of the most important junctions in vertebrate evolution. Sarcopterygian fishes (the "lobe-fins") are today represented by lungfishes and coelacanths, but during the Paleozoic they were much more diverse. It was some of these sarcopterygians, a lineage of the tetrapodomorph fishes, that gave rise to tetrapods (terrestrial vertebrates with limbs bearing digits). This spectacular leap took place during the Devonian Period. Due to the nature of preservation, it is the hard parts of an animal's body that are most likely to fossilize, while soft tissues such as muscular and brain tissues, typically fail to do so. Thus, our understanding of the adaptations of the hard skeletal structures of vertebrates is considerably greater than that of the soft tissue systems. Fortunately, the braincases of early vertebrates are often ossified and thereby have the potential to provide detailed morphological information. However, the correspondence between brain and endocast (an internal mold of the cavity) has historically been considered poor in most "lower" vertebrates and consequently neglected in such studies of brain evolution. Despite this, recent work documenting the spatial relationship in extant basal sarcopterygians (coelacanth, lungfish, axolotl, and salamander) has highlighted that this is not uniformly the case. Herein, we quantify and illustrate the brain-endocast relationship in four additional extant basal tetrapod exemplars: neobatrachian anurans (frogs) *Breviceps poweri* and *Ceratophrys ornata*; and gymnophionans (caecilians) *Gegeneophis ramaswamii* and *Rhinatrema bivittatum*. We show that anurans and caecilians appear to have brains that fill their endocasts to a similar degree to that of lungfishes and salamanders, but not coelacanth. *Ceratophrys* has considerably lower correspondence between the brain and endocast in the olfactory tract and mesencephalic regions, while *Breviceps* has low correspondence along its ventral endocranial margin. The brains of caecilians reflect their endocasts most closely (vol. ∼70%). The telencephalon is tightly fitted within the endocast in all four taxa. Our findings highlight the need to adequately assess the brain-endocast relationship in a broad range of vertebrates, in order to inform neural reconstructions of fossil taxa using the Extant Phylogenetic Bracket approach and future studies of brain evolution.

Keywords: Sarcopterygii, Anura, Gymnophiona, neurobiology, brain, endocast, diceCT

OPEN ACCESS

Edited by:
Ingmar Werneburg,
University of Tübingen, Germany

Reviewed by:
Min Zhu,
Institute of Vertebrate Paleontology and Paleoanthropology, Chinese Academy of Sciences, China
Jing Lu,
Institute of Vertebrate Paleontology and Paleoanthropology, Chinese Academy of Sciences, China

****Correspondence:***
Alice M. Clement
alice.clement@flinders.edu.au

Specialty section:
This article was submitted to Paleontology, a section of the journal Frontiers in Ecology and Evolution

Received: *11 December 2020*
Accepted: *25 February 2021*
Published: *19 March 2021*

Citation:
Clement AM, Mensforth CL, Challands TJ, Collin SP and Long JA (2021) Brain Reconstruction Across the Fish-Tetrapod Transition; Insights From Modern Amphibians. Front. Ecol. Evol. 9:640345. doi: 10.3389/fevo.2021.640345

INTRODUCTION

Plants and invertebrates had already ventured onto land in the Silurian Period (419–443 million years ago), well before the transition onto land by the first vertebrates (back-boned animals) during the Devonian Period (359–419 million years ago). Nevertheless, the move from water to land by these animals, known as the "fish-tetrapod transition," is widely celebrated as a highly significant evolutionary leap which eventually gave rise to roughly half of all today's vertebrate diversity (including humans).

Due to the nature of fossilization, changes over time in the skeleton are much better documented and understood (e.g., Cloutier et al., 2020) than the related soft tissues such as muscle and brain. In particular, preserved brains are exceedingly rare in the fossil record (although see Pradel et al., 2009), and where they are preserved they unlikely reflect brain morphology during life due to desiccation. As such, the internal part of the skull that houses the brain, or "endocast" has instead been used as a proxy for visualizing the brain, the shape of its component parts and quantitatively assessing their size, in a field of study known as palaeoneurology (Edinger, 1921).

By analyzing cranial endocasts (the internal space within the cranial cavity) of fossil taxa, certain inferences about behavior can be drawn, guided by the principle of proper mass, whereby "the mass of neural tissue controlling a particular function is appropriate (proportionate) to the amount of information processing involved in performing the function" (Jerison, 1973, pg. 8). That is to say, the more important or acute a sense or behavior is to an animal, the more likely that brain region will be relatively larger than would otherwise be expected, and consequently be reflected in the shape of the braincase internally. Applying this principal to endocasts of fossils can be problematic in those taxa which brains incompletely fill their endocasts, and the internal spatial relationship between brain and endocast is not known.

Despite the significance afforded to the fish-tetrapod transition, there remain relatively few known cranial endocasts of tetrapodomorph fishes (stem-tetrapods). The best-known example is that of *Eusthenopteron foordi*, a tristichopterid fish from the Late Devonian (mid-Frasnian) Escuminac Formation in Canada (Whiteaves, 1883). Using Sollas' grinding method common in embryology, palaeoichthyologists from the "Stockholm School" and elsewhere, serially ground several Paleozoic 3D-preserved early vertebrates to reconstruct their endocasts, including that of *Eusthenopteron foordi* (Jarvik, 1980). Romer (1937) followed the same method to reconstruct the endocast of the Permian megalichthyid *Ectosteorhachis* from the United States.

More recently, advances in computed tomography (CT) scanning technology have enabled several more endocasts to be investigated non-destructively. *Gogonasus*, from the Late Devonian (Frasnian) Gogo Formation in Australia is known from complete, exceptionally-preserved 3D material (Holland, 2014), while *Tungsenia* from the Early Devonian (Pragian) of China, and *Spodichthys* from the Late Devonian (Frasnian) of East Greenland, have had only their ethmosphenoid regions modeled (Snitting, 2008; Lu et al., 2012). Work currently underway (Clement, pers. comm.) will soon add a complete endocast of *Cladarosymblema*, a megalichthyinid from the Carboniferous of Australia, to the list of those stem-tetrapods where the morphology of the endocast has been examined.

The record of endocasts for basal tetrapods is similarly depauperate, and includes the following: a partial endocast from the well-known Devonian tetrapod *Ichthyostega* (Clack et al., 2003); a cranial endocast from the early Carboniferous tetrapod *Lethiscus* (Pardo et al., 2017b); an otic capsule endocast from the Carboniferous temnospondyl, *Dendrerpeton* (Robinson et al., 2005); two Permian temnospondyls, *Eryops* and *Edops*, had their endocasts described in good detail but were made using destructive techniques (Dempster, 1935; Romer and Edinger, 1942); the Permian recumbirostran *Brachydectes* examined using non-destructive tomographic methods (Pardo and Anderson, 2016); and the Triassic stegocephalians *Deinosuchus*, *Lyrocephalus*, and *Aphaneramma* (Stensiö, 1963). This is, in part, due to many basal crown tetrapods possessing neurocrania that are poorly ossified compared to many tetrapodomorph fishes.

However, despite this pioneering work on these early vertebrates, most comparative neurological or palaeoneurological studies continue to focus on birds and mammals, due to their brains largely filling the cranial vault with a tight correspondence with their braincases (Jerison, 1973). The brains of "lower" (anamniote) vertebrates generally incompletely fills the internal braincase space, and therefore have been considered of limited use for interpreting brain morphology. Jerison (1973, pg. 121) claims that the brain of lungfishes is only 10% as big as the endocast, and that it would thus be "difficult, although not impossible, to understand the brain's anatomy from an endocranial cast." Although a large disparity was recorded between the lungfish brain and endocast, the disparity is even greater still in the coelacanth (*Latimeria*) with a brain just 1% of its endocranial volume (Millot and Anthony, 1965).

Recent work based on CT and magnetic resonance imaging (MRI) scans has interrogated these assertions. Clement et al. (2015) revealed that the brain of a sub-adult Australian lungfish (*Neoceratodus*) fills the majority of its endocast (∼80%), while the adult coelacanth (*Latimeria*) was confirmed to indeed have a brain one hundredth of the volume of its capacious cavity (Dutel et al., 2019). While it is well understood that ontogeny can have an effect on relative brain size, adult specimens from both extant lungfish families (Neoceratodontidae, Lepidosirenidae) were later found to have a brain filling upward of 40% of their endocasts, even without correction for ostensible shrinkage (Challands et al., 2020), a proportion that is significantly higher than the reported 10% from Jerison (1973). In fact, more recent data (Yopak et al., 2010; Iwaniuk, 2017; Striedter and Northcutt, 2020) continues to show a more nuanced picture with greater degree of overlap in brain volume to body mass between the "lower" and "higher" vertebrates, and thus we consider that it can be reasonably

expected that the relationship between brain and endocast is similarly complicated.

The "heat-map" surface-surface distance measurement method of quantifying the brain-endocast spatial relationship in the Australian lungfish developed by Clement et al. (2015), was recently applied to six basal sarcopterygian taxa as a proxy to elucidate the changes that occurred over the fish-tetrapod transition (Challands et al., 2020). Taxa investigated included the coelacanth (*Latimeria chalumnae*), Australian lungfish (*Neoceratodus forsteri*), African lungfish (*Protopterus aethiopicus, P. dolloi*), the axolotl (*Ambystoma mexicanum*) and fire newt [*Triturus (Cynops) pyrrhogaster*].

Challands et al. (2020) confirmed earlier work that showed the coelacanth to be an outlier, with a miniscule brain lying within a cavernous endocast (Dutel et al., 2019), which is in stark contrast to the brain of lungfishes and salamanders that occupy ∼40–50% of the endocast. Those authors found that the Australian and African lungfishes have quite a good fit between brain and endocast internally, although the olfactory tract morphology in *Protopterus* spp. is not faithfully reflected in its endocast. In the salamanders, *Triturus (Cynops)* and *Ambystoma*, there is also quite a tight fit except for the region where the trigeminal nerve complex exits the braincase. Overall, these findings suggest that certain inferences can be made about the size of the brain from its endocast in basal sarcopterygians, in particular with respect to some brain regions, such as the telencephalon (forebrain).

Challands et al. (2020) suggested that the closeness of fit of different regions of the brain to the brain cavity may be influenced by the mandibular musculature and so, to a certain extent, could be predicted from the skull morphology where musculature can be reconstructed. Regions of lowest brain-endocast disparity occurred where bony reinforcement of the neurocranium lies adjacent to mandibular musculature, whereas regions of highest disparity were found in regions with lower reinforcement (e.g., where mandibular masticatory musculature mass was lower or absent). Such regions included where the trigeminal nerve complex exits the braincase and where endolymphatic sacs are present within the braincase.

There are three living genera of lungfishes and one genus of coelacanth, which united represent the only extant piscine sarcopterygians, and are therefore of particular relevance to the fish-tetrapod transition. Conversely, on the other side of the extant phylogenetic bracket are lissamphibians, such as frogs, salamanders and caecilians, which can also likely provide equally valuable insights into brain evolution of the first tetrapods. For the purposes outlined in this paper, we have adopted the phylogeny of extant amphibians from Pyron and Wiens (2011) and do not herein attempt to comment of the controversy surrounding the origins of Lissamphibia (Marjanovic and Laurin, 2007; Ruta and Coates, 2007). We accept that the first tetrapods appeared during the Devonian, the tetrapod crown node arose during the Carboniferous, and the extant amphibian orders most likely have their origins dating back throughout the Permo-Triassic (Anderson et al., 2008; Clack, 2012; Pardo et al., 2017a).

Since we cannot assume *a priori* that salamanders are necessarily the best representatives to interpret the condition of the first tetrapods, we hereby aim to quantify the brain-endocast spatial relationship in four more extant lissamphibian basal tetrapod exemplars: neobatrachian anurans *Breviceps poweri*, and *Ceratophrys ornata*; and gymnophionans *Gegeneophis ramaswamii* and *Rhinatrema bivittatum*. We hypothesize that these taxa will have brains that fill their endocasts to a similar degree as that of lungfishes and salamanders, and the region of closest fit will be around the forebrain. As more 3D morphological data such as these are created, brain reconstruction models, such as that of Clement et al. (2016), can be further refined by incorporating data from the full extant phylogenetic bracket for any given fossil taxon.

MATERIALS AND METHODS

Tomographic Data

Diffusible iodine-based contrast-enhanced computed tomography (diceCT) scan data of *B. poweri* (Power's Rain Frog), Media number: M13270-22958, was obtained under CC BY-NC-SA copyright from MorphoSource[1]. The pixel size was 21 microns (μm).

The *C. ornata* (Argentine Horned Frog) diceCT scan data was originally generated by Kleinteich and Gorb (2015), but later downloaded for this study from Dryad Digital Repository[2] under a CC0 1.0 Universal Public Domain Dedication license. The pixel size was 27 μm.

The *G. ramaswamii* (tenmalai blind caecilian) and *R. bivittatum* (two-lined caecilian) diceCT scan data were downloaded from Duke University (see text footnote 1), with Media numbers: M71659-133946 and M33276-61864, and obtained under -CC BY-NC-SA- attribution. Florida Museum of Natural History, University of Florida provided access to these data, the collection of which was funded by oVert TCN; NSF DBI-1701714. The *Gegeneophis* dataset was subsequently subsampled so the resultant pixel size was 25 μm, whereas the *Rhinatrema* data were subsampled to 32 μm.

All data were segmented and rendered, and stereolithographs (STL's) produced, in MIMICS v.18–19 (Materialise, 1992–2020).

Surface Distance Analysis and Visualization

The "closeness of fit" between 3D surface mesh STL's of the brain and the braincase's internal "endocast" were analyzed using the "Surface-to-Surface Distance Measurement Script" of Clement et al. (2015) using Python, with script updates from Challands et al. (2020). This custom script is publicly available from[3]. The resulting images visualize the surface-to-surface distance between STL's using a "heat map" whereby cooler colors (blue) indicate smaller distances (a closer fit), and warmer colors (red) indicate greater distance.

[1] www.morphosource.org

[2] https://doi.org/10.5061/dryad.066mr

[3] https://www.researchgate.net/publication/345917984_Surface-to-surface_distance_measurement_script

Comparison of volumes were calculated from 3D model volume values obtained from MIMICS. Figures were prepared and assembled in Adobe Photoshop and Illustrator, GIMP and Inkscape.

RESULTS

The segmented brains (gray) and the brain-endocast overlays (gray and red), and surface-surface distance "heat maps" are shown in **Figures 1**, **2**. Brain volume as a percentage of endocast volume in mm^3 is given in **Table 1**.

Breviceps poweri

The brain of *B. poweri* measures 3.0 mm long from the anterior edge of the olfactory bulbs to the spinal cord, 1.3 mm across the widest point of the brain, and 1.4 mm at the highest point of the brain (**Figure 1A**). The forebrain (consisting of the telencephalon and diencephalon) comprises 48% of the total brain length, the midbrain (mesencephalon) 21%, and the hindbrain (metencephalon and myelencephalon) 31%. The cranial endocast of *B. poweri* measures 3.4 mm in length, 1.8 mm at its widest point, and 1.6 mm dorsoventrally.

The forebrain of *B. poweri* is dominated by the large, bulbous, oval-shaped telencephalic (tel) hemispheres which are slightly wider than they are long (**Figure 1A**). The boundary between the olfactory bulbs and the telencephalon is difficult to discern. There is 0.1 mm of olfactory nerve visible between the olfactory epithelium and the olfactory bulbs. The area around the diencephalon constricts in all axes, and then expands dorsoventrally to accommodate the optic tectum [mes (ot)] in the midbrain. The spinal cord is angled upward dorsally at about 45° from the rest of the brain. The trigeminal (n.V) and auditory (n.VIII) nerves are visible emerging from the hindbrain from the scan data.

The cranial endocast of *B. poweri,* when viewed laterally, steadily increases in both dorsoventral and lateral diameter from the olfactory bulbs through to the hindbrain and then rapidly constricts near the spinal cord (**Figures 1B,C**). When viewing the cranial endocast dorsally, the shape of forebrain is almost circular, with an abrupt widening from the olfactory bulbs and then constricting behind the optic tecta. The endocast is close to the surface of the brain (<0.1 mm) on the ventral side of the olfactory tracts, the dorsal side of the olfactory bulbs, and the dorsal and lateral sides of the optic tecta in the midbrain. The greatest distance between the brain and cranial endocast is on the ventral side of the brain, where distances are >0.17 mm over the majority of the area (**Figure 1C**).

Ceratophrys ornata

The brain of *C. ornata* (**Figure 1D**) measures 4.2 mm from the anterior edge of the olfactory bulbs to the spinal cord and is 1.1 mm at its widest point and 1.2 mm at the highest point of the brain. The forebrain comprises 43% of the total brain length, the midbrain 31%, and the hindbrain 26%. The cranial endocast of *C. ornata* measures 5.2 mm long, 2.1 mm at the widest point, and 1.7 mm in height.

The olfactory tracts (olf) extend a relatively long way into the cranial endocast (1.2 mm, 23% of the length of the endocast). The olfactory tracts run parallel to each other and lie 0.3 mm apart. The olfactory bulbs (ob) are recognizable as a separate bulge distinct from the telencephalon (tel) anteriorly, which extends anteroventrally from the olfactory tracts as triangular-shaped structures. The telencephalic hemispheres are small, paired, oval prominences. The brain narrows considerably in the diencephalic region and the mid- and hindbrain angles ventrally downward some 45° from the preceding forebrain. The hypophyseal region (hyp) is short and angled posteroventrally. The brain expands only slightly in the midbrain (mes) to accommodate the optic tecta. The brain then narrows toward the hindbrain (med) and the anterior edge of the spinal cord. The trigeminal (n.V), facial (n.VII), auditory (n.VIII), glossopharyngeal (n.IX) and vagus nerves (n.X) are visible from the scan data in the hindbrain region (**Figure 1D**).

In contrast to the bulbous brain, the cranial endocast of *C. ornata* is smooth and lacking obvious protuberances (**Figure 1E**). It slowly widens from the olfactory epithelia to the midbrain. Following the course of the brain, the mid- and hindbrain endocast regions also angles down ventrally to the anterior end of the spinal cord. Dorsally, the widest region accommodates the midbrain and the nerves emerging from the hindbrain (n.V-X), and then tapers toward the hindbrain ventral edge. The surface-surface distances between the cranial endocast and brain of *C. ornata* are <0.1 mm on the ventral surfaces of the diencephalon and hindbrain, and on the dorsal surfaces of the telencephalon and optic tecta. There are larger distances of >0.2 mm between the brain and the endocast on the dorsal surface, where the olfactory nerves extend into the endocast, and on the lateral surfaces near the trigeminal nerve's entry to the brain (**Figure 1F**).

Gegeneophis ramaswamii

The brain of *G. ramaswamii* measures 6.0 mm from the anterior edge of the olfactory bulbs to the spinal cord, is 3.4 mm wide across the broadest point of the brain, and is 1.2 mm in height (**Figure 2A**). The forebrain contributes 61% of the total brain length, while the midbrain and hindbrain contribute 17 and 22%, respectively. The cranial endocast measures 6.2 mm in length, 3.7 mm in width, and 1.2 mm in height.

The scans of the brain and cranial endocast of *G. ramaswamii* have resulted in some compression on the right lateral edge of the specimen. However, this is the only distortion visible on the scans and anatomical features are still recognizable and measurements have been approximated along the compressed edge.

The forebrain of *G. ramaswamii* consists of large telencephalic hemispheres (tel) that are much longer than they are wide (**Figure 2A**). When viewed laterally, the height of the brain slowly increases from the anterior edge of the olfactory bulbs (ob) to the midpoint of the telencephalon, and then slightly decreases in height toward the posterior edge of the hindbrain. The brain narrows behind the midbrain (mesencephalon) before it expands as a conical structure in the hindbrain toward the spinal cord.

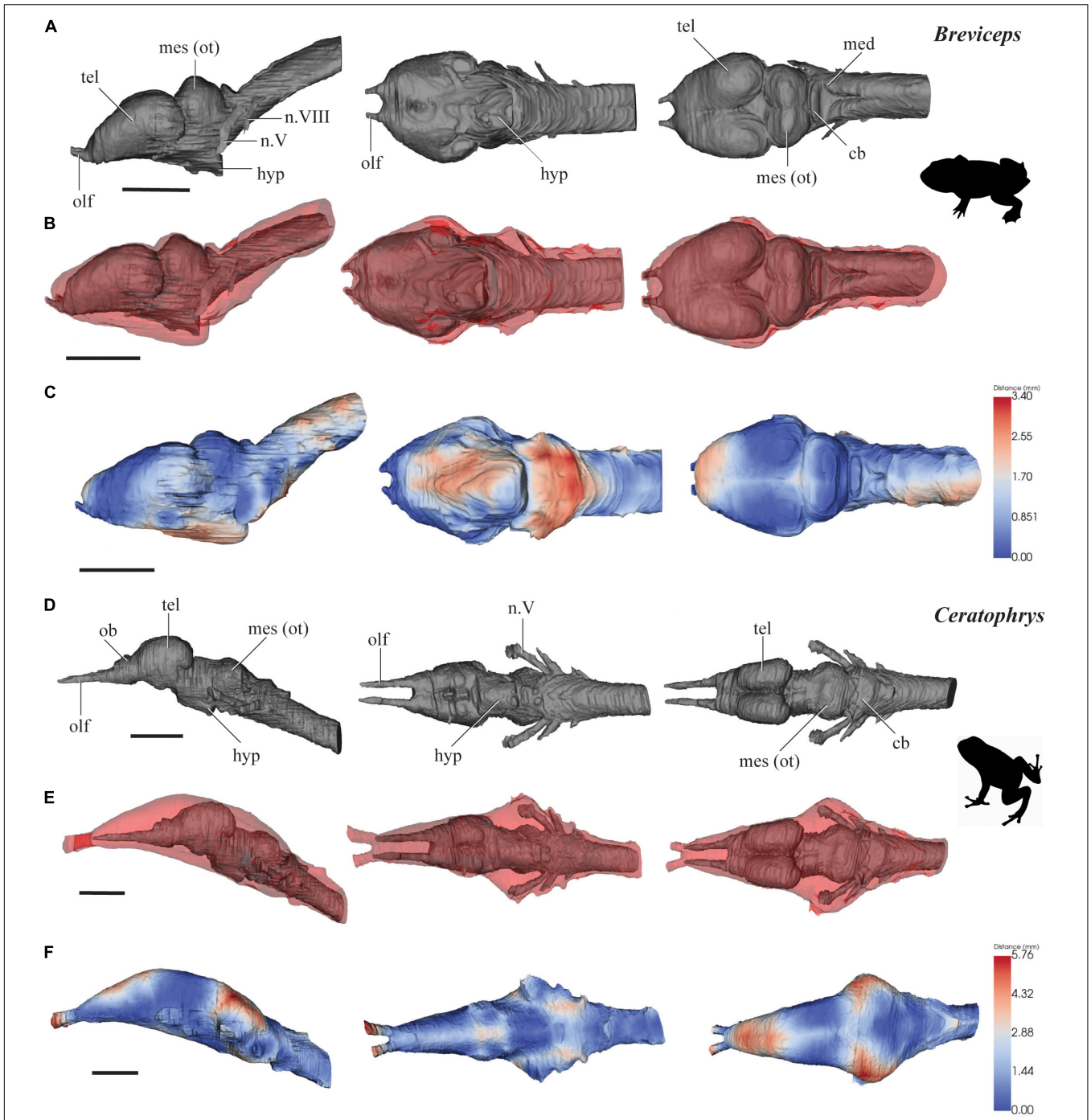

FIGURE 1 | 3D models of brains (gray), endocasts (red), and surface-surface distance heatmaps of two anurans in left lateral, ventral and dorsal views. **(A–C)** *Breviceps*; **(D–F)** *Ceratophrys*. Anterior to the left. cb, cerebellum; hyp, hypophysis; med, medulla oblongata; mes (ot), mesencephalon/optic tectum; tel, telencephalon; ob, olfactory bulb; olf, olfactory tract; n.V, trigeminal nerve complex; n.VIII, auditory nerve. Scale 10 mm.

The optic tectum (mes) appears as a single protuberance rather than a paired structure. From the lateral view, the brain appears approximately linear.

The cranial endocast of *G. ramaswamii* fits very tightly around the forebrain (**Figures 2B,C**), with <0.2 mm gap between the brain and the endocast. The brain and endocast constrict to slightly different degrees in the mid- and hindbrain region, leaving distances of >0.3 mm in these regions.

Rhinatrema bivittatum

The brain of *R. bivittatum* measures 5.5 mm from the anterior edge of the olfactory bulbs to the spinal cord, is 2.1 mm wide

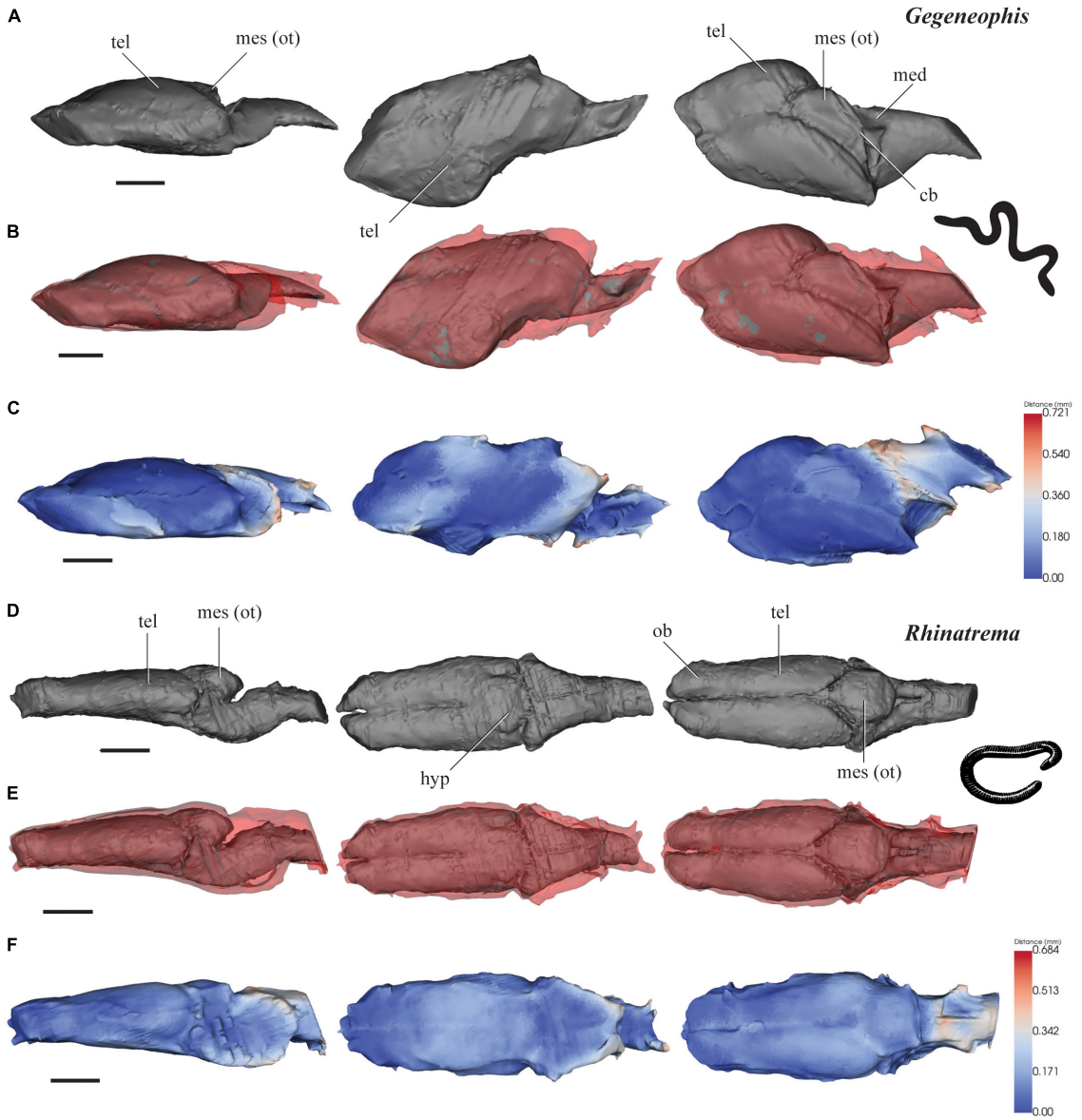

FIGURE 2 | 3D models of brains (gray), endocasts (red), and surface-surface distance heatmaps of two caecilians in left lateral, ventral and dorsal views. **(A–C)** *Gegeneophis*; and **(D–F)** *Rhinatrema*. Anterior to the left. cb, cerebellum; med, medulla oblongata; mes (ot), mesencephalon/optic tectum; tel, telencephalon; ob, olfactory bulb. Scale 1 mm.

across the broadest point at the midbrain, and is 1.7 mm in height at the highest part of the brain (**Figure 2D**). The forebrain contributes 63% of the total brain length, with the midbrain and hindbrain contributing 24 and 13%, respectively. The cranial endocast measures 5.7 mm in length, 2.3 mm in width and 2.0 mm in height.

When observing the brain of *R. bivittatum* dorsally, the forebrain (tel) maintains a similar width along the majority of the telencephalon, which appears as an elongated pair of rectangular structures without any expansion postero-laterally (**Figure 2D**). The olfactory bulbs (ob) are recognizable anteriorly, where the brain narrows slightly and the two hemispheres are separated by a small groove. The midbrain increases in diameter along all axes around the optic tecta, and the hindbrain tapers toward the spinal cord. From the lateral view, the brain appears approximately linear except for some dorsal expansion of the mesencephalic region (mes).

The cranial endocast of *R. bivittatum* closely mirrors the shape of the forebrain, with <0.3 mm of distance between the brain and endocast (**Figures 2E,F**). The endocast widens where the midbrain expands, and maintains the short distance of <0.3 mm between the brain and braincase. The endocast then slightly narrows around the posterior edge of the midbrain and the hindbrain, but not to the same extent that the midbrain contracts,

TABLE 1 | Brain volume as a percentage of endocast volume in mm^3 in extant piscine sarcopterygians and select Lissamphibian taxa.

Taxon	Source	Brain vol. (mm^3)	Endocast vol. (mm^3)	Percentage filled%
Latimeria (adult)	Challands et al., 2020	1,973	201,276	1
Neoceratodus (juv.)	Clement et al., 2015	5.3	6.8	78
Neoceratodus (adult)	Challands et al., 2020	630	1,403	45
Protopterus aethiopicus	Challands et al., 2020	457	1,097	42
Protopterus dolloi	Challands et al., 2020	407	857	47
Rhinatrema	This study	9	14	64
Gegeneophis	This study	14	18	78
Ambystoma	Challands et al., 2020	28	74	38
Triturus (Cynops)	Challands et al., 2020	14	34	41
Breviceps	This study	26	41	63
Ceratophrys	This study	38	77	49

Additional comparative data from Clement et al. (2015) and Challands et al. (2020) also included.

leaving distances >0.3 mm between the majority of these areas (**Figures 2E,F**).

DISCUSSION

The Extant Phylogenetic Bracket method (EPB), whereby two or more extant outgroups are used to provide rigorous limits of biological inference to a fossil taxon in question (Witmer, 1995), is a valued approach to aid in the reconstruction of soft tissues in extinct taxa. Although extant tetrapods are separated by over 360 million years from the first terrestrial vertebrates, the anatomy and morphology of their closest piscine relatives (sarcopterygian fishes) and basal tetrapods (lissamphibians) can provide invaluable insight into the condition of their long extinct kin.

The brain-endocast relationships of piscine sarcopterygians and salamanders have been considered elsewhere (Clement et al., 2015; Dutel et al., 2019; Challands et al., 2020) but are complemented by the additions in this study investigating frogs and caecilians to fulfill the EPB for Palaeozoic stem tetrapods (**Figure 3**). By quantifying the spatial relationship between the brain and internal cavity of the braincase (the endocast) across sarcopterygians ranging from the coelacanth, both lungfish families, and all three orders of extant amphibians, we have provided further information that can be used to identify a range of brain volumes for early stem tetrapods (assuming the EPB method is robust), and thus have established likely minimum volumes for the brains of these animals.

Caecilians are enigmatic and generally poorly understood animals although recent work has elucidated data on their crania relating to its musculature (Kleinteich and Haas, 2007), shape (Müller et al., 2009; Sherratt et al., 2014), and modularity (Marshall et al., 2019). Work on braincase morphology (Maddin et al., 2012a,b) and the labyrinth system (Maddin and Anderson, 2012; Maddin and Sherratt, 2014) has provided a breadth of new information, but to the best of our knowledge, we are herein the first to produce cranial endocasts for the lineage.

As the sister-group to all other caecilians (Pyron and Wiens, 2011), the Rhinatrematidae retain features lacking in other taxa (e.g., still possessing a tail), and as one of the most basal caecilians it may thus reasonably be expected to retain a more plesiomorphic condition of the brain and braincase. Indeed, the telencephalic hemispheres of *Rhinatrema* are elongate, remaining narrow along their whole length without the expansion posterolaterally as in other more derived caecilians such as *Ichthyophis* (Nieuwenhuys et al., 1998) and *Typhlonectes* (Schmidt et al., 1996; Striedter and Northcutt, 2020). In this aspect the telencephalon actually resembles those of several other sarcopterygians more so than other caecilians (Challands et al., 2020) and perhaps reflects the plesiomorphic condition. The braincase of a stem caecilian from the Jurassic Period, *Eocaecilia*, suggests that earliest members of this lineage retained a more robust skull than is found in more recent, derived taxa (Maddin et al., 2012a).

In contrast, as a member of the Caeciliidae, *Gegeneophis* is a more derived caecilian than *Rhinatrema* (Pyron and Wiens, 2011), and its brain shape, with posterolaterally-expanded telencephalic hemispheres, is more typical for the group. Being a blind animal, one might expect the optic tectum to be reduced in *Gegeneophis* but it appears to remain as prominent as in other taxa (**Figure 1**). Nevertheless, the entire morphology of caecilians is strongly modified in association with their ecology, and the close correspondence internally between their brain and braincase likely reflects morphological constraints related to their fossorial lifestyle.

Compared to caecilians, anurans are a much more diverse and well-studied group. The brains of frogs and toads have been considered relatively similar across taxa, although there is evidence of variation in brain morphology correlated with seasonality (Luo et al., 2017), habitat and locomotion (Taylor et al., 1995; Manzano et al., 2017). The brains of both *Breviceps* and *Ceratophrys* are both a similar size in proportion to their overall body size (brain length 20–22% of snout/vent length), but that of *Breviceps* fills its endocast to a greater degree than *Ceratophrys,* by almost 15%. While the olfactory canals are short in *Breviceps*, those in *Ceratophrys* extend far anteriorly before exiting the braincase, similar to the condition in some lungfishes (*Protopterus* spp., see Challands et al., 2020, **Figure 6**). *Breviceps* is a burrowing frog (Hofrichter, 2000), thus its close

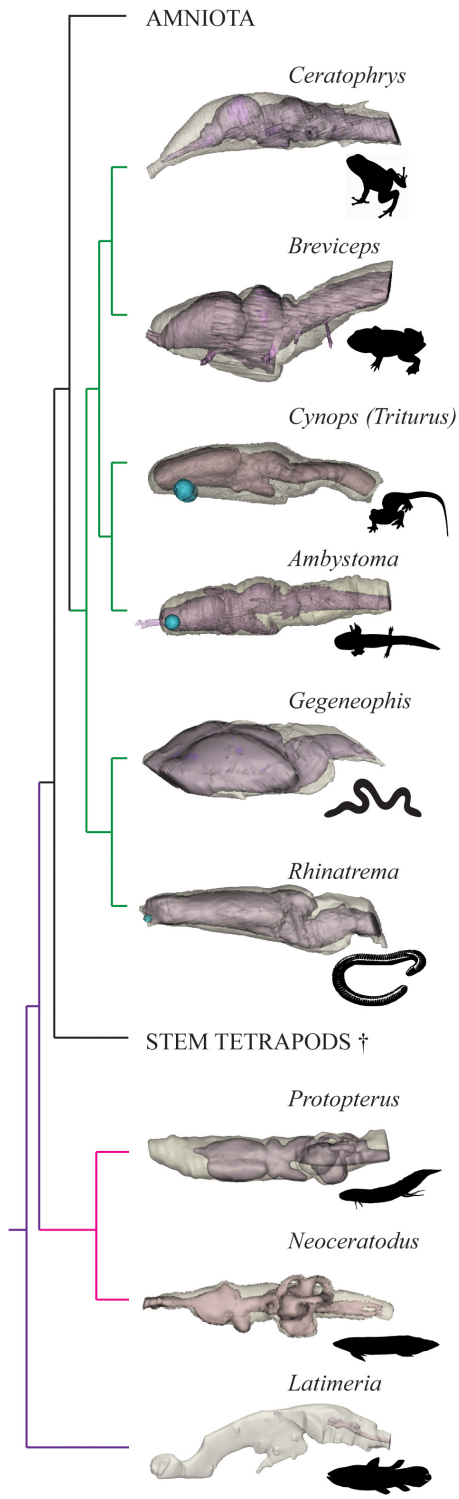

FIGURE 3 | Brain-braincase relationship in extant piscine sarcopterygians and select Lissamphibian taxa. Endocasts (light brown) shown in transparent overlay on brains (pink) in left lateral view. *Latimeria, Neoceratodus, Protopterus, Ambystoma*, and *Cynops* from Challands et al. (2020), phylogeny adapted from Amemiya et al. (2013) and Pyron and Wiens (2011). Images not to scale. *Gegeneophis* silhouette drawn by AMC, all other animal silhouettes from http://phylopic.org, see Acknowledgments for individual image credits.

relationship between the brain and braincase may be related to its highly fossorial lifestyle, as we have hypothesized for caecilians also. However, of the six frog brain morphotypes shown in Manzano et al. (2017), we note that the brain of *Breviceps* is most similar in overall morphology to that of the "hopper-walker" *Rhinella fernandezae*, the Bella Vista Toad. On the other hand, *Ceratophrys* has a brain more similar to the waxy monkey tree frog, *Phyllomedusa sauvagii*, a "climber-walker," or largely arboreal frog (Manzano et al., 2017). It is clear that further work is required to elucidate brain ecomorphology in the hyper diverse and specialized anurans.

While employing the full Extant Phylogenetic Bracket to reconstruct soft tissue in fossils is considered a relatively rigorous approach, the inclusion of particularly specialized or derived groups must only be done so with caution. One may consider that the lower limit of brain volume in the first tetrapods may be similar to the condition found in *Latimeria*, although we do not believe this to be the case. Extant coelacanths live in the deep ocean and retain an intracranial joint, while lungfish and tetrapods lost this feature early in their history. The enlargement of the notochord in *Latimeria* (Dutel et al., 2019) and the persistence of the intracranial joint both plausibly contribute to the large disparity between the brain and endocast in this taxon, where its expansion is most likely limited by both ecological and biomechanical constraints. Furthermore, it is known that fish living in the deep-sea and less complex environments tend to have smaller brains compared to their shallow water counterparts (Kotrschal, 1998).

Moreover, both caecilians and anurans are considered to be highly adapted to their respective modes of life as fossorial animals or specialized jumpers and vocalizers. Consideration of the ecology and habitat of the first tetrapods (Clack, 2012) lends support to the use of lungfishes and salamanders as the best extant representatives for interpreting the brain morphology in the earliest terrestrial vertebrates. The combination of data from the coelacanth, lungfish and now all three orders of extant amphibians herein demonstrates the importance of considering ecology and habit when using the EPB.

If the coelacanth, caecilians and frogs are used to estimate and constrain the brain volume of extinct stem and/or early tetrapods then we might expect a range of brain volumes of between 1–78% of the internal brain cavity/endocast. Such a range is hardly informative and using the EPB may perhaps more useful in constraining character states in extinct taxa. For example, we may infer the presence of elongate parallel telencephalic hemispheres in extinct early tetrapod taxa seeing as this condition is seen in the extant, yet basal, caecilian *Rhinatrema*.

Eliminating those taxa that possess characters not seen in early tetrapods (e.g., *Latimeria* due to the presence of an intracranial joint) and those taxa that are ecologically highly specialized (Gymnophiona and Anura) limits brain volume estimates to be restricted to those seen in extant Dipnoi and Caudata i.e., between 38–47%. That said, many early tetrapods were themselves highly specialized in terms of ecology and habit, for example the limbless *Lethiscus* (Pardo et al., 2017b) and the robust, possibly burrowing recumbirostran *Brachydectes* (Pardo and Anderson, 2016), and so it may be expected that in some taxa,

the brain volume in these extreme cases may be more similar to different extant, but ecologically similar taxa. The emphasis here is on selecting a suitable EPB that reflects both phylogeny and ecology so as to obtain informed estimates of features in extinct taxa rather than using a wholesale approach.

CONCLUSION

In conclusion, we analyzed the correspondence between the brain and endocast in two anurans, *B. poweri* and *C. ornata*, and two caecilians, *R. bivittatum* and *G. ramaswamii*, using diceCT data. We found that these taxa had brains that filled their endocasts to a greater extent than that of extant salamanders and lungfishes, and infer that such disparity may be a product of their highly specialized ecology and habit. The telencephalon (forebrain) was the region of closest fit across all taxa. *Ceratophrys* differed from the other taxa in that it had considerable surface-surface distance surrounding the olfactory tracts and mesencephalon. Our findings help to constrain the minimum and maximum expected brain volumes for extinct tetrapods employing an Extant Phylogenetic Bracket approach. However, we emphasize the need to make an informed choice for the EPB and not to assume inferences can be made from the phylogenetic position of the EPB taxa alone, but also to consider ecology, habit and lifestyle. Lastly, we have created the first virtual cranial endocasts for frogs and caecilians and envisage that these will be useful for future analyses of endocast shape in amphibians.

DATA AVAILABILITY STATEMENT

The original contributions presented in the study are included in the article/**Supplementary Materials**, further inquiries can be directed to the corresponding author/s.

ETHICS STATEMENT

Ethical review and approval was not required for the animal study because data already existed freely available online (we did not deal with the animals scanned ourselves, the data was from previous studies).

AUTHOR CONTRIBUTIONS

AC conceived and designed the study. AC and CM performed the 3D segmentation and wrote the first draft of the manuscript. TC analyzed the data. AC and TC created figures and **Supplementary Data**. SC, TC, and JL inputted to the writing of the manuscript. JL provided materials and software. All authors contributed to the interpretation of results, editing of the manuscript, and have approved this final version for re-submission.

FUNDING

AC, SC, CM, and JL are supported by funding from Australian Research Council grant DP 200103398. TC was supported by Callidus Services Ltd., United Kingdom.

ACKNOWLEDGMENTS

We would like to thank Thomas Kleinteich for use of the *Ceratophrys* dataset and Hugo Dutel for supplying STL's of *Latimeria* for use in **Figure 3**. We would also like to thank Catherine Early and David Blackburn for bringing my attention to caecilian scan data available on MorphoSource (https://www.morphosource.org/). Animal silhouettes displayed in figures are copyright-free images courtesy of PhyloPic (http://www.phylopic.org/): *Latimeria*, *Rhinatrema*, Yan Wong; *Neoceratodus*, Roberto Díaz Sibaja; *Protopterus*, *Ceratophrys*, Steven Traver; *Ambystoma*, Jake Warner; *Cynops*, Neil Kelley; and *Breviceps*, under CC BY 3.0 from Nobu Tamura at http://phylopic.org/image/a3b917bc-142d-4314-aa82-2215f5487daf/. We would also like to thank two reviewers and Guest Associate Editor Ingmar Werneburg for their criticisms that improved an earlier draft of this manuscript.

SUPPLEMENTARY MATERIAL

The Supplementary Material for this article can be found online at: https://www.frontiersin.org/articles/10.3389/fevo.2021.640345/full#supplementary-material

REFERENCES

Amemiya, C. T., Alfoldi, J., Lee, A. P., Fan, S. H., Philippe, H., MacCallum, I., et al. (2013). The African coelacanth genome provides insights into tetrapod evolution. *Nature* 496, 311–316. doi: 10.1038/Nature12027

Anderson, J. S., Reisz, R. R., Scott, D., Frobisch, N. B., and Sumida, S. S. (2008). A stem batrachian from the Early Permian of Texas and the origin of frogs and salamanders. *Nature* 453, 515–518. doi: 10.1038/nature06865

Challands, T. J., Pardo, J. D., and Clement, A. M. (2020). Mandibular musculature constrains brain-endocast disparity between sarcopterygians. *R. Soc. Open Sci.* 7, 1–20.

Clack, J. A. (2012). *Gaining Ground: The Origin and Evolution of Tetrapods*. Bloomington, IN: Indiana University Press.

Clack, J. A., Ahlberg, P. E., Finney, S. M., Dominguez Alonso, P., Robinson, J., and Ketcham, R. A. (2003). A uniquely specialized ear in a very early tetrapod. *Nature* 425, 65–69. doi: 10.1038/nature01904

Clement, A. M., Nysjö, J., Strand, R., and Ahlberg, P. E. (2015). Brain – endocast relationship in the Australian lungfish, *Neoceratodus forsteri*, elucidated from tomographic data (Sarcopterygii: Dipnoi). *PLoS One* 10:e0141277. doi: 10.1371/journal.pone.0141277

Clement, A. M., Strand, R., Nysjö, J., Long, J. A., and Ahlberg, P. E. (2016). A new method for reconstructing brain morphology: applying the brain-neurocranial spatial relationship in an extant lungfish to a fossil endocast. *R. Soc. Open Sci.* 3:160307. doi: 10.1098/rsos.160307

Cloutier, R., Clement, A. M., Lee, M. S. Y., Noël, R., Béchard, I., Roy, V., et al. (2020). Elpistostege and the origin of the vertebrate hand. *Nature* 579, 549–554. doi: 10.1038/s41586-020-2100-8

Dempster, W. T. (1935). The brain case and endocranial cast of Eryops megacephalus (Cope). *J. Comp. Neurol.* 62, 171–196. doi: 10.1002/cne.900620108

Dutel, H., Galland, M., Tafforeau, P., Long, J. A., Fagan, M. J., Janvier, P., et al. (2019). Neurocranial development of the coelacanth and the evolution of the sarcopterygian head. *Nature* doi: 10.1038/s41586-019-1117-3

Edinger, T. (1921). Über nothosaurus, ein steinkern der schädelhöhle. *Senckenbergiana* 3, 121–129.

Hofrichter, R. (2000). Amphibians: the world of frogs, toads, salamanders and newts.

Holland, T. (2014). The endocranial anatomy of Gogonasus andrewsae Long, 1985 revealed through micro CT-scanning. *Earth Environ. Sci. Trans. R. Soc. Edinb.* 105, 9–34. doi: 10.1017/s1755691014000164

Iwaniuk, A. N. (2017). "The evolution of cognitive brains in non-mammals," in *Evolution of the Brain, Cognition, and Emotion in Vertebrates*, eds S. Watanabe, M. A. Hofman, and T. Shimizu (Berlin: Springer), 101–124. doi: 10.1007/978-4-431-56559-8_5

Jarvik, E. (1980). *Basic Structure and Evolution of Vertebrates*. London: Academic Press.

Jerison, H. J. (1973). *Evolution of the Brain and Intelligence*. Cambridge, MA: Academic Press, Inc.

Kleinteich, T., and Gorb, S. N. (2015). Frog tongue acts as muscle-powered adhesive tape. *R. Soc. Open Sci.* 2:150333. doi: 10.1098/rsos.150333

Kleinteich, T., and Haas, A. (2007). Cranial musculature in the larva of the caecilian, *Ichthyophis kohtaoensis* (Lissamphibia: Gymnophiona). *J. Morphol.* 268, 74–88. doi: 10.1002/jmor.10503

Kotrschal, K. (1998). Fish brains: evolution and environmental relationships. *Rev. Fish Biol. Fish.* 8, 373–408.

Lu, J., Zhu, M., Long, J. A., Zhao, W., Senden, T. J., Jia, L. T., et al. (2012). The earliest known stem-tetrapod from the Lower Devonian of China. *Nat. Commun.* 3:1160. doi: 10.1038/ncomms2170

Luo, Y., Zhong, M. J., Huang, Y., Li, F., Liao, W. B., and Kotrschal, A. (2017). Seasonality and brain size are negatively associated in frogs: evidence for the expensive brain framework. *Sci. Rep.* 7:16629.

Maddin, H. C., and Anderson, J. S. (2012). Evolution of the amphibian ear with implications for lissamphibian phylogeny: insight gained from the caecilian inner ear. *Fieldiana Life Earth Sci.* 76, 59–77. doi: 10.3158/2158-5520-5.1.59

Maddin, H. C., Jenkins, F. A. J., and Anderson, J. S. (2012a). The braincase of *Eocaecilia micropodia* (Lissamphibia, Gymnophiona) and the origin of caecilians. *PLoS One* 7:e50743. doi: 10.1371/journal.pone.0050743

Maddin, H. C., Russell, A. P., and Anderson, J. S. (2012b). Phylogenetic implications of the morphology of the braincase of caecilian amphibians (Gymnophiona). *Zool. J. Linn. Soc.* 166, 160–201.

Maddin, H. C., and Sherratt, E. (2014). Influence of fossoriality on inner ear morphology: insights from caecilian amphibians. *J. Anat.* 225, 83–93. doi: 10.1111/joa.12190

Manzano, A. S., Herrel, A., Fabre, A. C., and Abdala, V. (2017). Variation in brain anatomy in frogs and its possible bearing on their locomotor ecology. *J. Anat.* 231, 38–58. doi: 10.1111/joa.12613

Marjanovic, D., and Laurin, M. (2007). Fossils, molecules, divergence times, and the origin of lissamphibians. *Syst. Biol.* 56, 369–388. doi: 10.1080/10635150701397635

Marshall, A. F., Bardua, C., Gower, D. J., Wilkinson, M., Sherratt, E., and Goswami, A. (2019). High-density three-dimensional morphometric analyses support conserved static (intraspecific) modularity in caecilian (Amphibia: Gymnophiona) crania. *Biol. J. Linn. Soc.* 126, 721–742. doi: 10.1093/biolinnean/blz001

Materialise (1992–2020). *Materialise Mimics*. Leuven: Materialise.

Millot, J., and Anthony, J. (1965). *Anatomie de Latimeria Chalumnae: Système Nerveux et Organes des sens. Centre National de la Recherche Scientifique*. Paris: Centre National de la Recherche Scientifique.

Müller, H., Wilkinson, M., Loader, S. P., Wirkner, C. S., and Gower, D. J. (2009). Morphology and function of the head in foetal and juvenile Scolecomorphus kirkii (Amphibia: Gymnophiona: Scolecomorphidae). *Biol. J. Linn. Soc.* 96, 491–504. doi: 10.1111/j.1095-8312.2008.01152.x

Nieuwenhuys, R., Donkelaar, H. J., and Nicholson, C. (1998). *The Central Nervous System of Vertebrates*. Berlin: Springer.

Pardo, J. D., and Anderson, J. S. (2016). Cranial morphology of the Carboniferous-Permian tetrapod *Brachydectes newberryi* (Lepospondyli, Lysorophia): new data from μCT. *PLoS One* 11:1–34.

Pardo, J. D., Small, B. J., and Huttenlocker, A. K. (2017a). Stem caecilian from from the Triassic of Colorado sheds light on the origins of Lissamphibia. *Proc. Natl. Acad. Sci. U. S. A.* 114, E5389–E5395. doi: 10.1073/pnas.1706752114

Pardo, J. D., Szostakiwskyj, M., Ahlberg, P. E., and Anderson, J. S. (2017b). Hidden morphological diversity among early tetrapods. *Nature* 546, 642–645. doi: 10.1038/nature22966

Pradel, A., Langer, M., Maisey, J. G., Geffard-Kuriyama, D., Cloetens, P., Janvier, P., et al. (2009). Skull and brain of a 300-million-year-old chimaeroid fish revealed by synchrotron holotomography. *Proc. Natl. Acad. Sci. U. S. A.* 106, 5224–5228. doi: 10.1073/pnas.0807047106

Pyron, R. A., and Wiens, J. J. (2011). A large-scale phylogeny of Amphibia including over 2800 species, and a revised classification of extant frogs, salamanders, and caecilians. *Mol. Phylogenet. Evol.* 61, 543–583. doi: 10.1016/j.ympev.2011.06.012

Robinson, J., Ahlberg, P. E., and Koentges, G. (2005). The braincase and middle ear region of *Dendrerpeton acadianum* (Tetrapoda: Temnospondyli). *Zool. J. Linn. Soc.* 143, 577–597. doi: 10.1111/j.1096-3642.2005.00156.x

Romer, A. S. (1937). The braincase of the Carboniferous Crossopterygian *Megalichthys* nitidus. *Bull. Mus. Comp. Zool.* 132, 1–73. doi: 10.1007/978-3-319-23534-9_1

Romer, A. S., and Edinger, T. (1942). Endocranial casts and brains of living and fossil amphibia. *J. Comp. Neurol.* 77, 355–389. doi: 10.1002/cne.900770203

Ruta, M., and Coates, M. I. (2007). Dates, nodes and character conflict: addressing the lissamphibian origin problem. *J. Syst. Palaeontol.* 5, 69–122. doi: 10.1017/s1477201906002008

Schmidt, A., Wake, D. B., and Wake, M. H. (1996). Motor nuclei of nerves innervating the tongue and hypoglossal musculature in a caecilian (Amphibia: Gymnophiona), as revealed by HRP transport. *J. Comp. Neurol.* 370, 342–349. doi: 10.1002/(sici)1096-9861(19960701)370:3<342::aid-cne5>3.0.co;2-4

Sherratt, E., Gower, D. J., Klingenberg, C. P., and Wilkinson, M. (2014). Evolution of cranial shape in Caecilians (Amphibia: Gymnophiona). *Evol. Biol.* 41, 528–545. doi: 10.1007/s11692-014-9287-2

Snitting, D. (2008). A redescription of the anatomy of the Late Devonian *Spodichthys buetleri* Jarvik, 1985 (Sarcopterygii, Tetrapodomorpha) from East Greenland. *J. Vertebr. Paleontol.* 28, 637–655. doi: 10.1671/0272-4634(2008)28[637:arotao]2.0.co;2

Stensiö, E. (1963). *The Brain and the Cranial Nerves in Fossil, Lower Craniate Vertebrates*. Oslo: Skrifter utgitt av Det Norske Videnskaps-Akademi, 1–120.

Striedter, G. F., and Northcutt, R. G. (2020). *Brains Through Time: A Natural History of Vertebrates*. New York, NY: Oxford University Press.

Taylor, G. M., Nol, E., and Boire, D. (1995). Brain regions and encephalization in anurans: adaptation or stability? *Brain Behav. Evol.* 45, 96–109. doi: 10.1159/000113543

Whiteaves, J. F. (1883). Recent discoveries of fossil fishes in the Devonian rocks of Canada. *Am. Nat.* 17, 158–164. doi: 10.1086/273271

Witmer, L. M. (1995). "The extant phylogenetic bracket and the importance of reconstructing soft tissues in fossils," in *Functional Morphology in Vertebrate Palaeontology*, ed. J. Thomason (Cambridge: Cambridge University Press), 19–33.

Yopak, K. E., Lisney, T. J., Darlington, R. B., Collin, S. P., Montgomery, J. C., and Finlay, B. L. (2010). A conserved pattern of brain scaling from sharks to primates. *Proc. Natl. Acad. Sci. U. S. A.* 107, 12946–12951. doi: 10.1073/pnas.1002195107

Conflict of Interest: The authors declare that the research was conducted in the absence of any commercial or financial relationships that could be construed as a potential conflict of interest.

frontiers in Ecology and Evolution

ORIGINAL RESEARCH
published: 09 April 2021
doi: 10.3389/fevo.2021.641657

Ontogenetic Changes of the Aquatic Food Uptake Mode in the Danube Crested Newt (*Triturus dobrogicus* Kiritzescu 1903)

Nikolay Natchev[1,2], Kristina Yordanova[1], Sebastian Topliceanu[3,4,5], Teodora Koynova[1], Dimitar Doichev[1] and Dan Cogălniceanu[3,4]*

[1] Department of Biology, Faculty of Natural Sciences, Shumen University, Shumen, Bulgaria, [2] Department of Integrative Zoology, Vienna University, Vienna, Austria, [3] Faculty of Natural and Agricultural Sciences, Ovidius University of Constanţa, Constanţa, Romania, [4] Asociatia Chelonia Romania, Bucharest, Romania, [5] CEDMOG Research Center, Ovidius University of Constanţa, Constanţa, Romania

The study of the feeding mechanisms in vertebrates requires an integrative approach since the feeding event consists of a chain of behaviors. In the present study we investigated the food uptake behavior in different ontogenetic stages in the Danube crested newt (*Triturus dobrogicus*). We focused on the coordination in the kinematics of the elements of the locomotor and the feeding systems at the transition between the approach of the newt to the prey and the food uptake start. In the feeding strategy of the larvae of *T. dobrogicus*, the phase of food search is replaced by an initial "food detection phase." In both larvae and adult specimens, the animals approached the food to a close distance by a precise positioning of the snout besides the food item. The larvae were able to reach food items offered at over 80° relative to the longitudinal midline of the head. When the food was offered at a large distance or laterally, the food uptake was either not successful or the coordination chain at the transition between food approach and food uptake was interrupted. In young larvae we detected an abrupt change in the activity of the locomotor system and the feeding system. The larvae approached the food by tail undulation and after reaching the final position of attack, no further activity of the locomotor apparatus was detectable. The larvae used a pure form of inertial suction to ingest food. In pre-metamorphic larvae and adults we registered an integrated activation of the locomotor apparatus (both limbs and tail) and the feeding apparatus during prey capture in the form of compensatory suction. The drastic change in the feeding mode of the pre-metamorphotic larvae and the adults compared to the younger larvae in *T. dobrogicus* may indicate the evolutionary development of a defined relation in the activity of the locomotor system and the control of the feeding apparatus. We propose that in newts, the interaction between the control execution in both systems switched from successive (body movement – feeding) into integrated (body movement – body movement and feeding) during the ontogeny. The main trigger for such a switch (at least in *T. dobrogicus*) is the formation of functional limbs during the late larval development.

Keywords: locomotion, feeding, coordination, larvae, water-land transition, urodela

OPEN ACCESS

Edited by:
Julia L. Molnar,
New York Institute of Technology, United States

Reviewed by:
Anthony Herrel,
Muséum National d'Histoire Naturelle, France
Ana Ivanović,
University of Belgrade, Serbia

****Correspondence:***
Nikolay Natchev
natchev@shu.bg

Specialty section:
This article was submitted to Evolutionary Developmental Biology, a section of the journal Frontiers in Ecology and Evolution

Received: *06 January 2021*
Accepted: *15 March 2021*
Published: *09 April 2021*

Citation:
Natchev N, Yordanova K, Topliceanu S, Koynova T, Doichev D and Cogălniceanu D (2021) Ontogenetic Changes of the Aquatic Food Uptake Mode in the Danube Crested Newt (Triturus dobrogicus Kiritzescu 1903). Front. Ecol. Evol. 9:641657. doi: 10.3389/fevo.2021.641657

INTRODUCTION

In vertebrates, the movements of the cranial and post-cranial element during the feeding events can be integrated to different levels (Montuelle and Kane, 2019). In many vertebrate groups, the kinematics of the feeding apparatus during the initial phases of the feeding process (see Schwenk, 2000) is well documented by using high-speed videography and cineradiography (for an overview see Bels and Whishaw, 2019). Schwenk and Rubega (2005) define the feeding stages which follow after the reaching of a distance that allows for successful food uptake, as discrete stages: (i) the capture/subjugation (present in snakes, some birds and mammals), (ii) the food ingestion, (iii) the intraoral food transport, (iv) the food processing (sometimes simultaneously occurring with the transport), and (v) the swallowing. The stages of capture/subjugation (when present) and ingestion are regarded as the initial stages of the feeding process *sensu stricto*. Montuelle and Kane (2019) define two behavioral phases which precede the prey capture – the "searching" and the "approaching." The activity of the sensors and the locomotion system during searching and approaching, allows the predator to recognize and access the prey before the initial stages of the feeding process. The activity of the locomotion system during the searching phase may be absent in some "sit and wait" predators.

Such a theoretical framework allows for an exact description of the food uptake mode and behavior in most ectothermic vertebrates, where often the capture/subjugation stage is integrated within the ingestion phase. However, in some species a discrete capture/subjugation feeding stage can be recognized. Very specific pre-ingestion phase is for example the forming of the so-called "hydrodynamic tongue" in mudskippers (Michel et al., 2015). Some specialized fish species may immobilize their prey by using electric current (Catania, 2014, 2019; Mendes-Júnior et al., 2020), or may use their rostrums to confuse, hurt or kill prey before ingestion (Wisner, 1958; Scott and Tibbo, 1968; Stillwell and Kohler, 1985; Shimose et al., 2006). The "scooping" behavior, typical for some frog species like *Xenopus leviae* (Carreño and Nishikawa, 2010), *Pipa pipa* (O'Reilly et al., 2002; Carreño and Nishikawa, 2010; Cundall et al., 2017), and *Pelophylax ridibundus* (Yordanova et al., 2017) involves the forelimbs in prey capture. In this feeding behavior, the limbs are used as a barrier that prohibits the prey from leaving the oropharynx of the predator (the limbs are not involved directly in prey capture and the capture itself is based on the use of hydrodynamic forces).

The hydrodynamics of the aquatic food ingestion in lower tetrapods are influenced by several factors (see Heiss et al., 2018). Some frogs like *X. laevis* and *P. pipa* (as adults) rely on suction feeding (Carreño and Nishikawa, 2010; Cundall et al., 2017). Due to the lack of gill slits, the frogs which can feed underwater use bidirectional water suction mode (see Lauder and Shaffer, 1986). The adult anurans are restricted in their ability to engulf large volumes of water in a suction cycle and suction feeding demand specialization of the feeding apparatus. A unique specialization was described in *P. pipa*, where the ability to suction feed impacted the whole body plan and even had led to the reorganization of some muscle insertions (Cundall et al., 2017). The metamorphosed urodelans also rely on bidirectional suction feeding (e.g., Lauder and Reilly, 1988; Deban and Wake, 2000; Deban et al., 2001; Deban, 2003). To date, a significant delay in the hyoid retraction start relative to the gape opening start was reported only for cryptobranchids (Reilly and Lauder, 1992; Heiss et al., 2013b). In the Chinese giant salamander (*Andrias davidianus*), the suction forces are generated initially and predominantly by the displacement of the upper and the lower jaw (Heiss et al., 2013b). In contrast – the under-pressure within the buccal cavity in most salamanders is generated by a rapid retraction of the hyo-lingual complex prior to peak gape (Lauder and Shaffer, 1986; Lauder and Reilly, 1994). Several studies were published on the aquatic feeding behavior and kinematic in adult newts (Heiss et al., 2013a, 2015, 2016, 2017, 2018, 2019; Lukanov et al., 2016; Schwarz et al., 2020a,b,c), but data on the food uptake in newt larvae are still scarce especially in the early larval stages. The current knowledge on the prey capture behavior in urodelans is biased toward investigations on late larval stages and adult specimens (see Lauder and Reilly, 1988; Lauder and Shaffer, 1988; Schwarz et al., 2020a,b,c).

The feeding fitness of the larvae is of a crucial importance for the viability of fishes and amphibians. The feeding success rate of the larvae depends on the proper execution both of the approach to the food and the execution of the food uptake (Sanderson and Kupferberg, 1999). In the present study we investigate the food uptake behavior of the Danube crested newt (*Triturus dobrogicus*) during different ontogenetic stages. We focus on the locomotor kinematics of both larvae and adults during the approach phases and the timing of the execution of the final approach and the food uptake. We then describe the integration of the motor control of the locomotor and the feeding apparatuses and their functional implications.

MATERIALS AND METHODS

The Danube Crested Newt has a restricted distribution area, being present in floodplains of large rivers from eastern Austria to Danube Delta (Fahrbach and Gerlach, 2018). The species is characterized by its long body and short limbs. The Danube Crested Newt is the most water related species and has the longest larval stage among *Triturus* species (Furtula et al., 2009).

On 14.02.2020, we captured nine adult males and eight adult females of *T. dobrogicus* from a temporary pond located in southeast Romania, part of Danube Delta Biosphere Reserve (Grindul Lupilor, 44°37′15.83″N, 28°48′24.92″E). Immediately after capture, the adults were transported to the laboratory for "Functional Morphology" at "Konstantin Preslavsky" University of Shumen, Bulgaria.

We randomly assigned three females and three males per aquarium (50 cm × 33 cm × 20 cm), except for one aquarium where only two females were housed with three males. The aquaria were filled with 30 L of aged tap water and provided with plastic strips used for oviposition. We renewed the plastic strips every two days and collected the eggs. All the eggs were considered with the date when they were deposited. Half of the water volume was changed every 3 days.

To avoid overcrowding, we housed the eggs in eight plastic aquaria (25 cm × 16 cm × 15 cm), with no more than 14 eggs in each. The aquaria were filled with 6L aged tap water and half of the volume was refreshed weekly. The measured water physico-chemical parameters were constant during the experiment period (mean values: pH: 7.98; dissolved oxygen: 8.36 mg/l; conductivity: 395 μS). Ambient temperature was maintained constant at 20°C ± 1°C and the animals were kept under natural photoperiod throughout the experiment. We checked for eggs that were not developing and removed them from aquaria to avoid fungal infections. After hatching, we moved the freshly hatched larvae to the experimental boxes. These aquaria were filled with 3 L of aged tap water, 1/3 of the water from the aquaria was refreshed with aged tap water every 4 days. When the active feeding started after the yolk resorption, the larvae were fed *ad libitum* with Cladocera (*Daphnia* sp., *Moina* sp.) and Copepoda (*Cyclops* sp.). At the later larval stages (after 42), we supplemented the food with a mixture of dry low-fat meat (beef liver and beef heart) every day. Metamorphosed animals were housed until the end of the experiment when all the juveniles together with the adults were released at the point of capture.

We started the feeding kinematics investigation at larval stage 42 (according to the developmental stages of Bernabò and Brunelli, 2019). Before the recordings we housed the specimens with no food for 24 h, then we moved the larvae individually in the experimental aquaria where they were filmed. The larvae of *T. dobrogicus*, are strictly carnivorous (Stojanov et al., 2011) and feed only on moving prey. To simulate movements of the prey, we used same sized pellets of beef liver-heart mixture. Since larvae of the Pacific giant salamander (genus *Dicamptodon*) were reported to react to larger prey offered at longer distances (Parker, 1994), to exclude the effect of prey size we used calibrated food pellets.

The particles were allowed to drop from the water surfaces to the bottom of the experimental water basin, aimed to sink directly in front of the larvae snout. During sinking, the food pellets usually deviated from the target, landing at the bottom at different distances from the predator and at different angles relative to the longitudinal axis of the larval head (see **Figure 1**). Each feeding event (successful or not) was recorded in order to assess the effects of the recorded variables on the final feeding success. The performance of the experiments was complicated due to the problems related to the food offering. However, we were able to record a total of 78 films in larval stages 42 to 50 (from stage 42 – 4 films from 2 specimens; stage 43 – 16 films from 5 specimens; stage 44 – 2 films from 1 specimen; stage 46 – 23 films from 5 specimens; stage 47 – 2 films from 2 specimens; stage 48 – 9 films from 2 specimens; stage 49 – 6 films from 3 specimens, stage 50 – 7 films from 2 specimens).

We refer further in the text to the larvae from stages before 50 as "young larvae." We noticed that when the larvae entered the pre-metamorphosis stages (around stage 50), the animals started to swim and maneuver very actively. The food was attacked by the predator almost at the water surface – not allowing the particle to drop. This activity hampered us in gathering information concerning the feeding behavior in a comparable way we collected it for the "young larvae" (we produced only seven films from dorsal view). For kinematical comparison we documented three feeding events in our largest larva from stage 50 – we filmed that animal in lateral view when food (domestic fly) was offered at the water surface. We also documented 19 feeding events in two females and two male adult Danube crested newts. The adults were filmed laterally, which allowed for detailed observations of the kinematics of the elements of the feeding apparatus during prey capture.

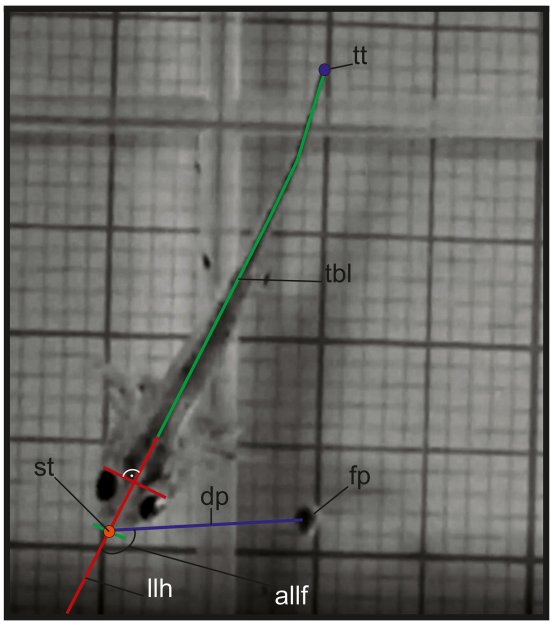

FIGURE 1 | Variables measured in the kinematic analysis in larval feeding**:** allf, angle between the longitudinal axis of the head and the prey; dp, distance between the tip of the snout and the center of mass of the food item; fp, food particle; llh, longitudinal axis of the head; tbl, total body length; st, snout tip; tt, tail tip.

For high-speed video documentation we used a "Sony RX-III" video system (Sony corporation, Minato, Tokyo, Japan). The films were performed with 1,000 fps (set at "quality mode": 1136 × 384 p) and for illumination we used two "Ledlenser T-16" (LEDLENSER GmbH & Co. KG, Solingen, North Rhine-Westphalian, Germany) light sources. The videos were imported in Movavi Video Editor v20.1.0 Plus for video processing and frame extraction. The images were digitized by the use of "SIMI-MatchiX" (SIMI Reality Motion Systems, Unterschleißheim, Germany). For larvae we extracted the following variables: **A**, angle between the food particle center of mass and the longitudinal axis of the larvae head (in degrees); **D**, prey distance (cm); **S**, speed of the larvae to the prey during the approach stage (cm/s); **TL**, Length of the larvae (cm); **TT**, length of the trajectory of the tail tip (cm); **ST**, max. speed of the movement of the tail tip during the approach stage (cm/s); **SDi**, distance traveled by the snout tip during the inertial suction (cm); **SS**, speed of the displacement of the snout tip during

TABLE 1 | Descriptive table of larval feeding behavior.

Parameter	Successful feeding			Parameter	Unsuccessful feeding		
	n	Mean ± SD	Min–Max		*n*	Mean ± SD	Min–Max
A	52	30.73 ± 27.9	0–90	A	17	35.29 ± 31.14	0–120
D	33	0.4 ± 0.35	0.01–1.48	D	16	0.66 ± 0.26	0.26–1.21
S	33	0.31 ± 0.17	0.02–0.7	S	16	0.33 ± 0.17	0.18–0.89
TL	52	2.09 ± 2.9	1.53–2.9	TL	17	2.01 ± 0.27	1.66–2.65
TT	50	1.4 ± 1.87	0.11–12.05	TT	17	2.16 ± 1.03	0.39–3.97
ST	52	0.61 ± 0.52	0.10–2.25	ST	17	1 ± 0.33	0.22–1.53
SDi	48	0.19 ± 0.1	0.05–0.63	Sdi	10	0.24 ± 0.07	0.15–0.39
SS	48	0.23 ± 0.2	0.02–1.25	SS	10	0.17 ± 0.05	0.05–0.22

n, sample size; Mean ± SD, average values ± standard deviation; Min – Max, minimum and maximum; A, prey angle related to longitudinal axis of the larvae head (in degrees); D, prey distance (cm); S, speed of the larvae to the prey (cm/s); TL, Length of the larvae (cm); TT, trajectory of the tail tip (cm); ST, max. speed of the movement of the tail tip (cm/s); SDi, distance of the snout tip displacement traveled during the inertial suction (cm); SS, speed of displacement of the snout tip during the inertial suction (cm/s).

the inertial suction (cm/s) – see **Table 1**. For the adults we collected data concerning: La, start of limbs before gape opening (s); Dag, delay of limb adduction end to start gape opening (s); Dla, duration of limb adduction (s) – see **Table 3** and **Figure 2**.

Each variable was checked for normality using Shapiro-Wilk test. Next we used a Generalized Linear Model (GLM) to check the effect of our variables on the larval success in feeding. For all tests, differences were significant at $p < 0.05$. We performed all of the statistical analyses using RStudio Version 1.3.1093© 2009-2020 RStudio, PBC.

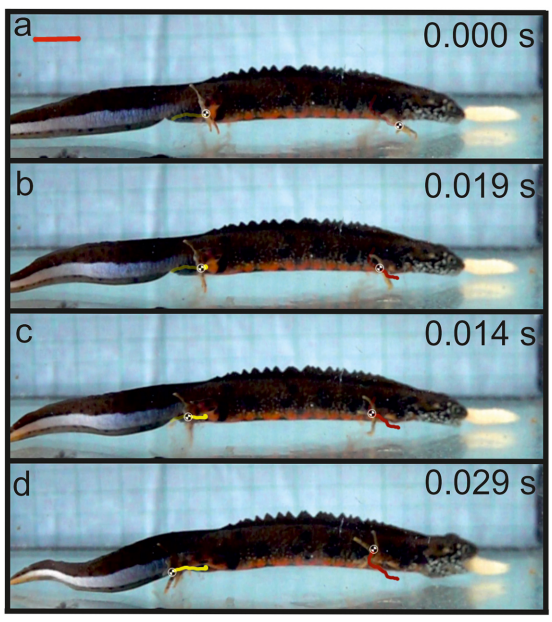

FIGURE 2 | Prey capture event in an adult *T. dobrogicus*. **(a)** Start of the limb adduction; **(b)** start of gape opening; **(c)** start of hyoid depression; **(d)** end of limb adduction; the red line indicates the trajectory of the metapodium of the fore-limb and the yellow line indicates the trajectory of the metapodium of the hind-limb.

RESULTS

The relations between the position of the food and the distance to the snout and the feeding success is presented in **Tables 1**, **2** and **Figure 3**. A binomial logistic regression performed by using Generalized Linear Models (GLMs) assessed the effects of: (a) **A**, angle between the center of mass of the food item to longitudinal axis of the larvae head; (b) **D**, food item distance (cm); (c) **S**, speed of the larvae during approach (cm/s); (d) **TL**, Length of the larvae body (cm); (e) **TT**, trajectory of the tail tip (cm); (f) **ST**, speed of the movement of the tail tip (cm/s); (g) **SDi**, inertial suction distance (cm) and (h) **SS**, speed of the inertial suction displacement of the snout tip (cm/s) (**Table 2** and **Figure 3**). The logistic regression model was statistically significant in case of **D** (Wald = −2.32, $p = 0.02$) and **ST**. The larvae fed successfully with decreasing of the distance to the food item. In case of successful feeding, a higher ST indicates a lower probability of feeding.

Our experiments demonstrated that the initial distance between newt and prey had a significant effect on the feeding behavior in the larvae of *T. dobrogicus*. When the food particle

TABLE 2 | Binomial regression coefficients of the following parameters related to success of feeding.

Variable	Std. Error	*z*-value	*P*-value
Prey angle related to longitudinal axis of the larvae head (A)	0.01	0.459	0.6465
Prey distance (cm) (D)	**1.03**	**−2.322**	**0.0203**
Speed of the larvae to the prey (cm/s) (S)	1.82	−0.322	0.747
Length of the larvae (cm) (TL)	1.002	−1.001	0.317
Trajectory of the tail tip (cm) (TT)	0.172	1.38	0.167
Speed of the movement of the tail tip (cm/s) (ST)	**0.590**	**2.51**	**0.011**
Inertial suction distance (cm) (SDi)	3.144	1.389	0.164
Speed of the inertial suction displacement (cm/s) (SS)	3.8105	−0.806	0.420

Bold values represent significant differences ($p < 0.05$).

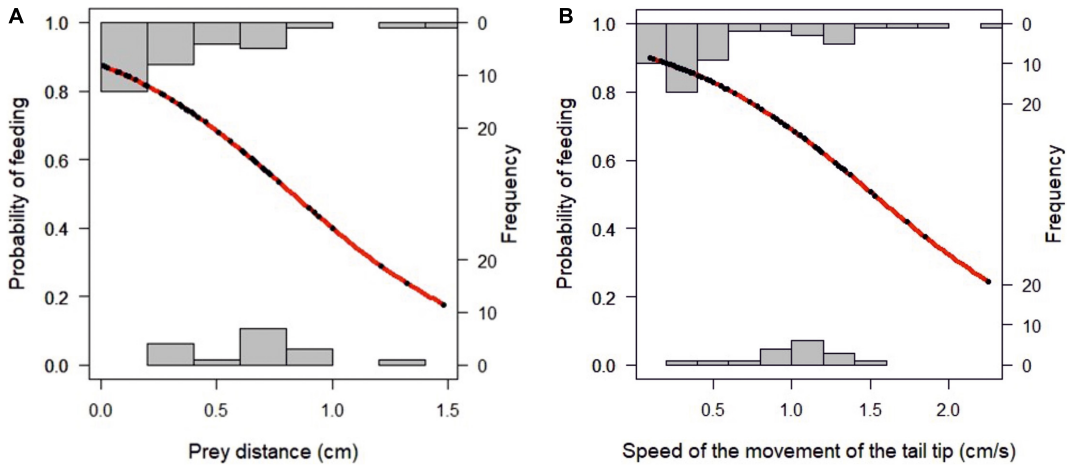

FIGURE 3 | (A) Effects of prey distance on probability of successful feeding; **(B)** effect of speed on probability of successful feeding.

landed on the bottom of the aquarium at relatively long distance (but less than 74% of the total body length), the larvae actively swam toward the item, adjusting the head position and correcting the angle of alignment of the head and the food. In the young larvae, the locomotion was performed only by tail undulation. No involvement of the limbs was detected as the larvae approached the food in a way that the tip of the snout was positioned very close to the food, almost touching it. In the next phase, the food pellet was captured by suction feeding (**Figure 4**). In case the pellet sank at a distance of less than 6% of the larval body length, it was immediately attacked by the larvae without any activity of the locomotor system (**Figure 5**).

When the particles landed at a distance larger than 74% of the body length, the larvae reacted in two different manners. In most cases, the animals did not react to the stimulus at all. In 17 cases however, the larvae swam toward the food item and positioned their snouts like in the strike demonstrated on **Figure 5**, hence no further prey capture occurred.

In the pre-metamorphosis larvae from stage 50, the newts approached the prey to a very close distance and then stopped. The active prey capture started by simultaneously activation of the tail and the limbs, followed by the start of the gape opening (**Figure 6**). In adult Danube crested newts, during the start of the ingestion, we detected a simultaneous activation of the limbs and tail prior jaw opening (**Table 3** and **Figure 2**). The kinematical

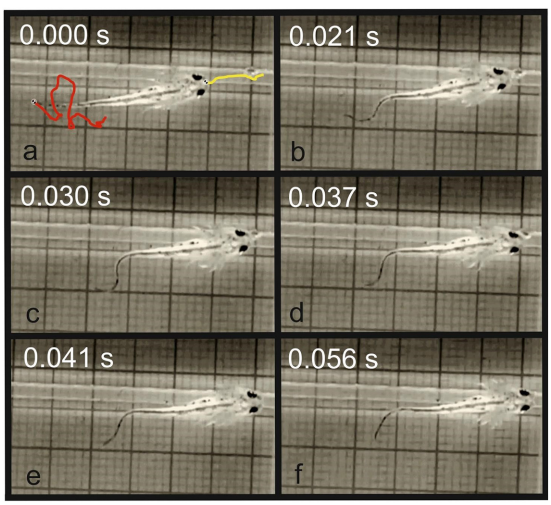

FIGURE 4 | Prey capture in *T. dobrogicus* larvae. **(a)** Start of the approach phase (the yellow line represents the trajectory of the tip of the snout and the red line represents the trajectory of the tail tip); **(b)** end of the approach phase; **(c)** stationary position of the predator; **(d)** start of the suction feeding; **(e)** suction of the food item; **(f)** end of the food uptake cycle.

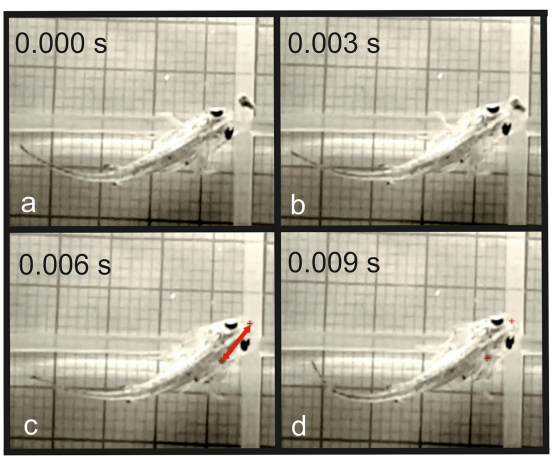

FIGURE 5 | Inertial suction feeding event in *T. dobrogicus* larvae. **(a)** Start of mouth opening; **(b)** start of the movement of the food toward the predator; **(c)** the food item is ingested in the oropharyngeal cavity; **(d)** end of the forward movement of the predator; the red crosses indicate the initial and the final position of the food item; the red arrow indicates the distance traveled by the food item during ingestion.

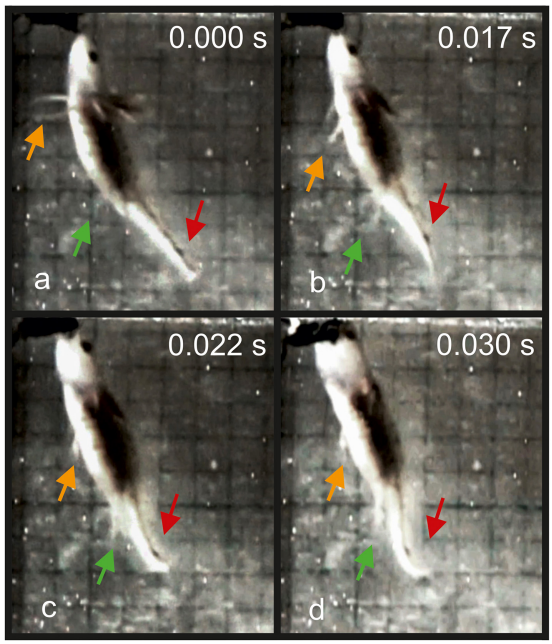

FIGURE 6 | Kinematics of the prey capture in a *T. dobrogicus* larvae stage 50. **(a)** Start of the approach phase; **(b)** start of jaw opening (notice the change in the position of the limbs and the tail); **(c)** end of limb adduction; **(d)** reaching peak gape. The yellow arrow indicates the position of the fore-limb metapodium; the green arrow indicates the position of the hind-limb metapodium; the red arrow indicates the undulation of the tail.

data measured in adults did not differ significantly between the specimens and sexes (**Table 3**).

DISCUSSION

Based on our results, we propose a theoretical framework concerning the evolution of the integration of the motor programs of the locomotor and feeding apparatus in newts. Only shortly before metamorphosis, the limbs became operational and this impacted the feeding strategy of the developing larvae to large scale. The young larvae in *T. dobrogicus* are operating predominantly on the bottom and have more or less a two dimensional hunting field. Only after the development of operational limbs in the late pre-metamorphic phases, the larvae started to exploit the whole 3-D volume of the water basin and were able to attack prey from multiple directions (see **Figure 6**). In the younger stages of the development in *T. dobrogicus*, the feeding strategy is impacted by the poor potential of the larvae to perform any forms of ram feeding (for overview see Heiss et al., 2018; Montuelle and Kane, 2019).

TABLE 3 | Descriptive table of adults feeding behavior.

Variable	Females (n = 10)		Males (n = 9)	
	Mean ± SD	Min–Max	Mean ± SD	Min–Max
La	0.25 ± 0.12	0.11–0.44	0.15 ± 0.05	0.1–0.27
Dag	0.18 ± 0.09	0.07–0.35	0.22 ± 0.04	0.16–0.28
Dla	0.44 ± 0.1	0.28–0.61	0.37 ± 0.08	0.31–0.55

n, sample size; Min, minimum; Max, maximum; Range, max-min; Mean, average values; SD, standard deviation. La, start of limbs before gape opening (s); Dag, delay of limb adduction end to start gape opening (s); Dla, duration of limb adduction (s).

In newts with seasonal shifts of terrestrial and aquatic life stages, the specialization of the feeding apparatus for underwater prey capture may be constrained. The seasonal change of feeding media (water vs air) is not related only to shifts in the motocontrol programs of the feeding apparatus (suction vs. lingual or jaw prehension), but may lead even to reorganization of the oropharyngeal morphology (Heiss et al., 2013a, 2015, 2016, 2017, 2018; Van Wassenbergh and Heiss, 2016). These authors provide a detailed analysis of the feeding ecology and the functional morphology of the feeding apparatus in the adults of the Alpine newt (*Ichthiosaura alpestris*) and the Smooth newt (*Lissotriton vulgaris*). Heiss and De Vylder (2016) report on aquatic suction feeding in the predominantly terrestrial living Himalayan newt (*Tylototriton verrucosus*). It seems that the Smooth newt (at least in aquatic phase) and the Himalayan newt use predominantly inertial suction for prey capture. The data provided for the aquatic feeding kinematics in the Balkan-Anatolian crested newt (*Triturus ivanbureschi*) also indicate on the predominant use of inertial suction in this species (Lukanov et al., 2016). The alpine newt, when fed underwater during the terrestrial life stage, is moving forward during suction and the angles of the joints in the forelimb are changing during ingestion (see Heiss et al., 2013a). The involvement of the limb movement in ingestion indicates a similar feeding behavior as described here for the adults in the Danube crested newt. In adult *T. dobrogicus*, the ingestion stage starts with the simultaneous movement of the fore- and the hind-limbs, in combination with tail undulation (**Figure 2**). The locomotor apparatus is active until the start of the fast closing gape phase (see Bramble and Wake, 1985), indicating that the adult Danube crested newt use a form of compensatory suction (sensu Aerts et al., 2001) during food ingestion.

Even small differences in the shape and the volume of the oropharynx may largely impact the efficiency of the suction performance (see Lauder, 1979). A larger oropharyngeal space contributes to the execution of powerful suction (see Lemell et al., 2002; Heiss et al., 2013b). The relatively small skull and the bidirectional water suction mode which is used by the adult Danube newts do not allow them to engulf a large amount of water - the bow wave has to be compensated by a lounge of the predator toward the prey. Thus, it is possible that the suction mechanism in *T. dobrogicus* does not allow the adults to rely on inertial suction and the activity of the locomotor system has to be integrated in the ingestion phase to support successful prey capture. The timing coordination in the activation of the locomotor system and the feeding apparatus is rather uniform and does not indicate significant differences concerning the sexes in the adults in *T. dobrogicus*.

Our results demonstrate a major difference in the feeding modes used by the young larvae and the adults in the Danube crested newt. In larvae we observed two scenarios of

successful feeding depending on food position – a pure inertial suction, when the food was offered close to the snout, and the swimming/stop/suction behavior when the food was offered further from the predator. In the second case, the larvae swam by tail undulations toward the offered food until the snout was positioned at a very close distance to the particle. Then the locomotion apparatus was deactivated and the feeding apparatus was activated during the ingestion stage. The larvae, however, were not motionless during the ingestion stage and moved forward, despite the fact that the locomotor apparatus was not functioning. Such forward movement of the larvae during the ingestion phase was described by Deban and Olson (2002). These authors studied the ingestion mechanism of a tiny pipid frog larvae and found that in *Hymenochirus boettgeri,* the prey is captured by the extension of a tubular formed mouth that approaches the food. This way the predatory larvae reduces the bow wave - a remarkable convergence to feeding apparati in some teleost species (Osse, 1985). The larvae of *H. boettgeri* moved only slightly forward during ingestion. For larvae that rely on inertial suction (*sensu* Aerts et al., 2001), but lack protrudable snouts, they have to engulf more water and the generated momentum is greater – contributing to the forward movement of the whole predator (see Muller and Osse, 1984). In other words, the larvae "suck themselves forward" (Deban and Olson, 2002).

The body form impacts the efficiency of the swimming and steering in the amphibian larvae. In the evolution of the amphibians, the larvae have lost the sturdy plates in form of skeletal fin elements characteristic for the bony fishes and their body execute significant lateral undulation in low *Re* numbers swimming (Wassersug and Hoff, 1985). The tadpoles show a high yaw rotation during swimming (Wassersug and Hoff, 1985). The bauplan of the salamander larvae is not principally different concerning the hydrodynamics and the streamlining is additionally impacted by the external bushy gills (Sanderson and Kupferberg, 1999). According to Blight (1976), the main difference of the swimming mode in salamander larvae compared to fish, is the high amplitude to which the larvae rotate laterally their heads in swimming (larvae wobble). The yaw of the head during swimming is not significant for the feeding efficiency in most anuran larvae, because they are mostly greasers or rely on filtration (Wassersug and Hoff, 1985). In predators the estimation of distance is crucial for successful prey capture. The highly specialized carnivorous larvae of *H. boettgeri* possess large eyes which are directed forwards (Deban and Olson, 2002). To reduce yaw in prey capture, these larvae use only the most posterior part of their tail to propel themselves. This results in lack of lateral oscillation of the head (Wassersug and Hoff, 1985). The swimming mode in the young larvae of *T. dobrogicus* is not contributing to the stabilization of the head. Unlike in *H. boettgeri*, the tail undulation is initiated in the midsection of the body and the whole tail is involved in swimming (**Figures 7a,b**). The high lateral displacement of the head prevents from exact aiming of the mouth toward the prey during active swimming. During the food approach phase, the snout tip is constantly redirected left and right off-target due to the wobbling (**Figures 7b,c**). Directly before the ingestion, the locomotor activity stops and the snout is correctly aimed (**Figure 7d**).

The young larvae of *T. dobrogicus* have to approach the food item to a very close distance for a successful grasp - this occurs as the locomotion system transports the predator near the prey. These larvae do not use the tail (or the legs) during the food ingestion. That indicates a strict succession in the execution of the motor control programs of the locomotor and the feeding apparati. Both systems were switched in succession – the locomotor system was active during the prey approach phase and the feeding apparatus was activated in the following ingestion phase. A very interesting point is, that when the larvae had to travel a distance of over 74% body length toward the prey, they successfully took the position of final head fixation (see Lemell and Weisgram, 1997), but the activity of the feeding apparatus was not triggered to start the ingestion stage. This may indicate that the motor programs of the locomotor system and the feeding system are time correlated. The execution of the ingestion may start only within a defined period of time after the activation of the locomotor system, as a reaction to the prey detection in a particular strike. Such a coordination may prevent the energy loss from feeding attempt which could be potentially unsuccessful. We were not able to test that hypothesis, since due to technical limitations, we were forced to use food pellets and not living prey in our experiments with the "young larvae". In case of active movements of the prey after the predator approached it, a new feeding situation could occur and the larvae may lounge a new attack in reaction to the new stimulus. As *Triturus* adults are known to feed on immobile prey (see Careddu et al., 2020), a topic for further research is the detection of the ontogenetic stage at which the animals switch their mode of reaction concerning the mobility of the prey.

The larvae changed their feeding strategy at the developmental stage 50. The kinematics in this pre-metamorphosis stage (see Bernabò and Brunelli, 2019) resembles that of the adult specimens. The limbs and the tail were involved in the prey ingestion mode and the prey capture starts with the activation of the locomotor apparatus - the gape opened with a delay relative to the limb and tail activation. The involvement of the functional limbs and the tail in the food ingestion process allowed for a principal change in the execution of the prey capture. The larvae switched from inertial suction to a form of compensatory suction (Heiss et al., 2018) with a component of lounge of the whole body toward the prey. This shift may allow the larvae for hunting of larger and more agile prey, which in turn increase feeding efficiency and may result in improvement of the general fitness of the specimens.

From a biomechanical perspective (see Neenan et al., 2014), one of the crucial factors for the shift in the feeding mode during the ontogeny in *T. dobrogicus* is the development of movable limbs. In the post 50-stage the limbs can be stretched before the strike in a manner to stabilize the position of the head toward the prey for attack from many possible directions. Possibly, the limbs are also contributing to development of thrust, however at the late larval stages the main momentum was presumably gained by the tail. We suggest that during the prey capture, the forward thrust is delivered predominantly by the tail and the correct

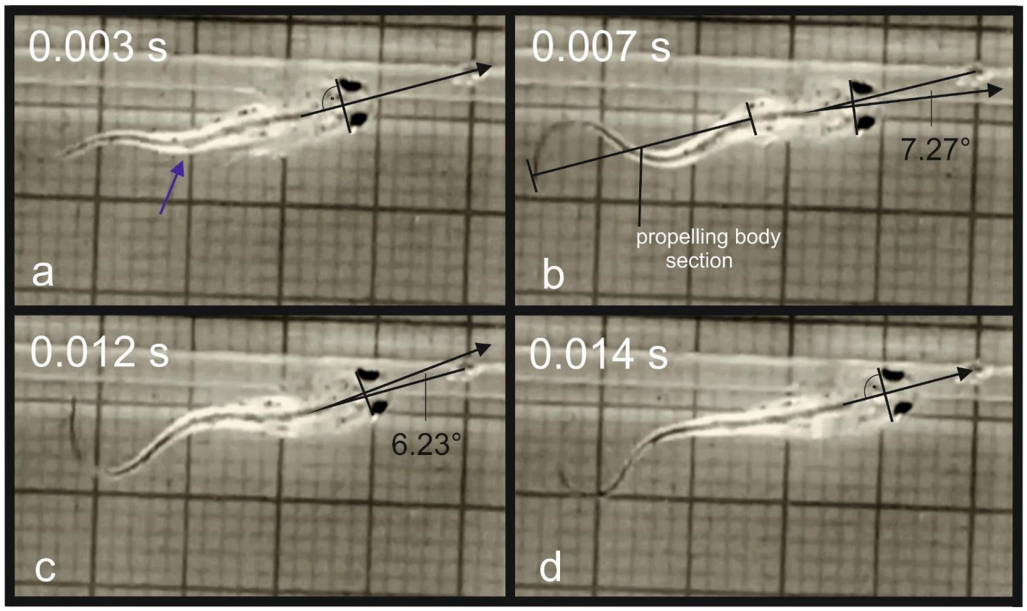

FIGURE 7 | Movement of the tip of the snout during a food uptake event in *T. dobrogicus* larvae: **(a)** start of the approach phase (the blue arrow indicates the point where undulation was initially generated); **(b)** displacement of the snout tip to the right from the correct direction due to head yaw; **(c)** displacement of the snout tip to the left from the correct direction due to head yaw; **(d)** stop of the tale undulation.

lounge direction was maintained with the support of the lateral appendages. During the ingestion, the function of the limbs may be crucial for preventing head yaw and in securing precise aiming of the gaping mouth toward the prey. This function of the lateral appendages may converge to the function of the paired fins in teleost food uptake (Wainwright, 1983; Westneat et al., 2004; Higham, 2007).

The ontogenetic shift may impact the feeding behavior to a large degree in newts (see Schwarz et al., 2020c). Even specimens from closely following ontogenetic phases, like late larval phases and early metamorphosed newts may differ in the execution of some feeding stages. In the case of *I. alpestris*, the development of the tongue during the metamorphosis has a deep impact on the food processing mode of the newt (Schwarz et al., 2020c). The drastic change in the feeding mode of the pre-metamorphic larvae and adults compared to the younger larvae in *T. dobrogicus* indicates the evolutionary development of a defined relation in the activity of the locomotor system and the control of the feeding apparatus. We propose that in newts, the interaction between the control execution in both systems switches from successive (body movement – feeding) into integrated (body movement – body movement and feeding) during ontogeny. Our results indicate that this shift in feeding behavior occurrs prior to metamorphosis, and can be crucial for maintaining continuous feeding through metamorphosis. In the genus *Triturus*, during the postembryonic phase (i.e., the brief period between hatching and feeding) the larvae rely on the rest of the yolk sac. The further development is convoyed by crucial changes in the skeletal morphology (Fahrbach and Gerlach, 2018) and presumably in the skull kinetics, which allows the larvae to include larger and more mobile prey in their diet. Further studies are needed to unravel the levels of integration in the movements of the locomotor system and the hyoid apparatus (as the main generator of suction forces) in *Triturus* larvae. An important aspect for the in-depth understanding of the ontogenetic shift in the feeding motorics would be the direct comparison of the 3D movements of components of the feeding apparatus in larvae and adults.

DATA AVAILABILITY STATEMENT

The original contributions presented in the study are included in the article/supplementary material, further inquiries can be directed to the corresponding author/s.

ETHICS STATEMENT

The animal study was reviewed and approved by the ethical committee of Ovidius University of Constanţa, Danube Delta Biosphere Reserve Administration.

AUTHOR CONTRIBUTIONS

NN prepared the concept for the manuscript, performed the experiments, digitized the films, calculated variables, provided tables and figures, and wrote the manuscript. KY digitized the films, provided tables and figures, and wrote the manuscript. ST prepared the concept for the manuscript, performed the experiments, calculated variables, provided tables and figures, and wrote the manuscript. TK performed the experiments, calculated variables, provided tables and figures, and wrote

the manuscript. DD calculated variables, provided tables and figures, and wrote the manuscript. DC prepared the concept for the manuscript, provided tables and figures, and wrote the manuscript. All authors contributed to the article and approved the submitted version.

FUNDING

This work was supported by the project ANTREPRENORDOC, in the frame work of Human Resources Development Operational Program 2014–2020, financed from the European Social Fund under the contract number 36355/23.05.2019 HRD OP/380/6/13 – SMIS Code: 123847, the fund for support of publication at "Konstantin Preslavsky" University of Shumen, the Research Fund of the "Konstantin Preslavsky" University of Shumen (Grant Nos. RD-08-104/30.01.2020 and RD-08-67/25.01.2021).

ACKNOWLEDGMENTS

The comments of two reviewers contributed significantly to the improvement of the manuscript.

REFERENCES

Aerts, P., van Damme, J., and Herrel, A. (2001). Intrinsic mechanics and control of fast cranio-cervical movements in aquatic feeding turtles. *Amer. Zool.* 41, 1299–1310. doi: 10.1093/icb/41.6.1299

Bels, V., and Whishaw, I. Q. (2019). *Feeding in Vertebrates: Evolution, Morphology, Behavior, Biomechanics*. Switzerland: Springer, doi: 10.1007/978-3-030-13739-7

Bernabò, I., and Brunelli, E. (2019). Comparative morphological analysis during larval development of three syntopic newt species (*Urodela*: *Salamandridae*). *Eur. Zool. J.* 86, 38–53. doi: 10.1080/24750263.2019.1568599

Blight, A. R. (1976). Undulatory swimming with and without waves of contraction. *Nature* 264, 352–354. doi: 10.1038/264352a0

Bramble, D. M., and Wake, D. B. (1985). "Feeding mechanisms of lower tetrapods," in *Functional Vertebrate Morphology*, Vol. 13, eds M. Hildebrand, D. M. Bramble, K. F. Liem, and D. B. Wake (Cambridge, MA: Harvard University Press), 230–261.

Careddu, G., Carlini, N., Romano, A., Rossi, L., Calizza, E., Caputi, S., et al. (2020). Diet composition of the Italian crested newt (*Triturus carnifex*) in structurally different artificial ponds based on stomach contents and stable isotope analyses. *Aquat. Conserv.: Mar. Freshw. Ecosyst.* 30, 1505–1520. doi: 10.1002/aqc.3383

Carreño, C. A., and Nishikawa, K. C. (2010). Aquatic feeding in pipid frogs: the use of suction for prey capture. *J. Exp. Biol.* 213, 2001–2008. doi: 10.1242/jeb.043380

Catania, K. (2014). The shocking predatory strike of the electric eel. *Science* 346, 1231–1234. doi: 10.1126/science.1260807

Catania, K. (2019). The astonishing behavior of electric eels. *Front. Integr. Neurosc.* 13:23. doi: 10.3389/fnint.2019.00023

Cundall, D., Fernandez, E., and Irish, F. (2017). The suction mechanism of the pipid frog, *Pipa pipa* (Linnaeus, 1758). *J. Morphol.* 278, 1229–1240. doi: 10.1002/jmor.20707

Deban, S. M. (2003). "Constraint and convergence in the evolution of salamander feeding," in *Vertebrate Biomechanics and Evolution*, eds J. Gasc, A. Casinos, and V. Bels (Oxford: BIOS Scientific Publishers), 163–180.

Deban, S. M., and Olson, W. M. (2002). Suction feeding by a tiny predatory tadpole. *Nature* 420, 41–42. doi: 10.1038/420041a

Deban, S. M., O'Reilly, J. C., and Nishikawa, K. C. (2001). The evolution of the motor control of feeding in Amphibians. *Amer. Zool.* 41, 1280–1298. doi: 10.1093/icb/41.6.1280

Deban, S. M., and Wake, D. B. (2000). "Aquatic feeding in salamanders," in *Feeding: Form, Function, and Evolution in Tetrapod Vertebrates*, ed. K. Schwenk (San Diego, CA: Academic Press), 65–94.

Fahrbach, M., and Gerlach, U. (2018). *The genus Triturus*. Frankfurt: Chimaira.

Furtula, M., Todorović, B., Simić, V., and Ivanović, A. (2009). Interspecific differences in early life-history traits in crested newts (*Triturus cristatus* superspecies, Caudata, Salamandridae) from the Balkan Peninsula. *J. Nat. Hist.* 43, 469–477. doi: 10.1080/00222930802585794

Heiss, E., Aerts, P., and Van Wassenbergh, S. (2015). Flexibility is everything: prey capture throughout the seasonal habitat switches in the smooth newt *Lissotriton* vulgaris. *Org. Divers. Evol.* 15, 127–142. doi: 10.1007/s13127-014-0187-1

Heiss, E., Aerts, P., and Van Wassenbergh, S. (2018). Aquatic-terrestrial transitions of feeding systems in vertebrates: a mechanical perspective. *J. Exp. Biol.* 221:jeb154427. doi: 10.1242/jeb.154427

Heiss, E., and De Vylder, M. (2016). Dining dichotomy: aquatic and terrestrial prey capture behavior in the Himalayan newt *Tylototriton verrucosus*. *Biol. Open* 5, 1500–1507. doi: 10.1242/bio.020925

Heiss, E., Handschuh, S., Aerts, P., and Van Wassenbergh, S. (2016). Musculoskeletal architecture of the prey capture apparatus in salamandrid newts with multiphasic lifestyle: does anatomy change during the seasonal habitat switches? *J. Anat.* 228, 757–770. doi: 10.1111/joa.12445

Heiss, E., Handschuh, S., Aerts, P., and Van Wassenbergh, S. (2017). A tongue for all seasons: extreme phenotypic flexibility in salamandrid newts. *Sci. Rep.* 7:1006. doi: 10.1038/s41598-017-00674-y

Heiss, E., Aerts, P., and Van Wassenbergh, S. (2013a). Masters of change: seasonal plasticity in the prey-capture behavior of the Alpine newt *Ichthyosaura alpestris* (Salamandridae). *J. Exp. Biol.* 216, 4426–4434. doi: 10.1242/jeb.091991

Heiss, E., Natchev, N., Gumpenberger, M., Weissenbacher, A., and Van Wassenbergh, S. (2013b). Biomechanics and hydrodynamics of prey capture in the Chinese giant salamander reveal a high-performance jaw-powered suction feeding mechanism. *J. R. Soc. Interface* 10:20121028. doi: 10.1098/rsif.2012.1028

Heiss, E., Schwarz, D., and Konow, N. (2019). Chewing or not? Intraoral food processing in a salamandrid newt. *J. Exp. Biol.* 222:jeb189886. doi: 10.1242/jeb.189886

Higham, T. E. (2007). Feeding, fins and braking maneuvers: locomotion during prey capture in centrarchid fishes. *J. Exp. Biol.* 210, 107–117. doi: 10.1242/jeb.02634

Lauder, G. V. (1979). Feeding mechanisms in primitive teleosts and in the halecomorph fish *Amia calva*. *J. Zool.* 187, 543–578. doi: 10.1111/j.1469-7998.1979.tb03386.x

Lauder, G. V., and Reilly, S. M. (1988). Functional design of the feeding mechanism in salamanders: causal bases of ontogenetic changes in function. *J. Exp. Biol.* 134, 219–233.

Lauder, G. V., and Reilly, S. M. (1994). "Amphibian feeding behavior: comparative biomechanics and evolution," in *Biomechanics of Feeding in Vertebrates*, eds V. Bels, M. Chardon, and P. Vandwalle (Berlin: Springer), 163–195. doi: 10.1007/978-3-642-57906-6_7

Lauder, G. V., and Shaffer, H. B. (1986). Functional design of the feeding mechanism in lower vertebrates: unidirectional and bidirectional flow systems in the tiger salamander. *Zoo. J. Linn. Soc.* 88, 277–290. doi: 10.1111/j.1096-3642.1986.tb01191.x

Lauder, G. V., and Shaffer, H. B. (1988). Ontogeny of functional design in tiger salamanders (*Ambystoma tigrinum*): are motor patterns conserved during major morphological transformations? *J. Morphol.* 197, 249–268. doi: 10.1002/jmor.1051970302

Lemell, P., Lemell, C., Snelderwaard, P., Gumpenberger, M., Wochesländer, R., and Weisgram, J. (2002). Feeding patterns of *Chelus fimbriatus* (*Pleurodira*: *Chelidae*). *J. Exp. Biol.* 205, 1495–1506.

Lemell, P., and Weisgram, J. (1997). Feeding patterns of *Pelusios castaneus*. *Neth. J. Zool.* 47, 429–441.

Lukanov, S., Tzankov, N., Handshuh, S., Heiss, E., Naumov, B., and Natchev, N. (2016). On the amphibious food uptake and prey manipulation behavior in the Balkan-Anatolian crested newt (*Triturus ivanbureschi*, Arntzen and Wielstra, 2013). *Zoology* 119, 224–231. doi: 10.1016/j.zool.2016.02.002

Mendes-Júnior, R. N. G., Sá-Oliveira, J. C., Vasconcelos, H. C. G., Costa-Campos, C. E., and Araújo, A. S. (2020). Feeding ecology of electric eel *Electrophorus varii* (Gymnotiformes: Gymnotidae) in the Curiaú River Basin, Eastern Amazon. *Neotrop. Ichthyol.* 18:e190132. doi: 10.1590/1982-0224-2019-0132

Michel, K. B., Heiss, E., Aerts, P., and Van Wassenbergh, S. (2015). A fish that uses its hydrodynamic tongue to feed on land. *Proc. R. Soc. B.* 282:20150057. doi: 10.1098/rspb.2015.0057

Montuelle, S. J., and Kane, E. A. (2019). "Food capture in vertebrates: a complex integrative performance of the cranial and postcranial systems," in *Feeding in Vertebrates, Fascinating Life Sciences*, eds V. Bels and I. Q. Whishaw (Cham: Springer), 71–137. doi: 10.1007/978-3-030-13739-7_4

Muller, M., and Osse, J. W. M. (1984). Hydrodynamics of suction feeding in fish. *Trans. Zool. Soc. Lond.* 37, 51–135.

Neenan, J. M., Ruta, M., Clack, J. A., and Rayfield, E. J. (2014). Feeding biomechanics in *Acanthostega* and across the fish–tetrapod transition. *Proc. R. Soc. B.* 281:20132689. doi: 10.1098/rspb.2013.2689

O'Reilly, J. C., Deban, S. M., and Nishikawa, K. C. (2002). "Derived life history characteristics constrain the evolution of aquatic feeding behavior in adult amphibians," in *Topics in Functional and Ecological Vertebrate Morphology*, eds P. Aerts, K. D'Aout, A. Herrel, and R. Van Damme (Maastricht: Shaker Publishing), 153–190.

Osse, J. W. M. (1985). "Jaw protrusion, an optimization of the feeding apparatus of teleosts?," in *Architecture in Living Structure*, eds G. A. Zweers and P. Dullemeijer (Dordrecht: Springer), doi: 10.1007/978-94-009-5169-3_10

Parker, M. S. (1994). Feeding ecology of stream-dwelling pacific giant salamander larvae (*Dicamptodon tenebrosus*). *Copeia* 3, 705–718. doi: 10.2307/1447187

Reilly, S. M., and Lauder, G. V. (1992). Morphology, behavior, and evolution: comparative kinematics of aquatic feeding in salamanders. *Brain Behav. Evol.* 40, 182–196. doi: 10.1159/000113911

Sanderson, S. L., and Kupferberg, S. J. (1999). "Development and evolution of aquatic larval feeding mechanisms," in *The Origin and Evolution of Larval Forms*, eds B. K. Hall and M. H. Wake (San Diego, CA: Acad. Press), 301–377. doi: 10.1016/B978-012730935-4/50011-0

Schwarz, D., Gorb, S. N., Kovalev, A., Konow, N., and Heiss, E. (2020a). Flexibility of intraoral food processing in the salamandrid newt *Triturus carnifex*: effects of environment and prey type. *J. Exp. Biol.* 223:jeb232868. doi: 10.1242/jeb.232868

Schwarz, D., Konow, N., Roba, Y. T., and Heiss, E. (2020b). A salamander that chews using complex, three-dimensional mandible movements. *J. Exp. Biol.* 223:jeb.220749. doi: 10.1242/jeb.220749

Schwarz, D., Konow, N., Porro, L. B., and Heiss, E. (2020c). Ontogenetic plasticity in cranial morphology is associated with a change in the food processing behavior in Alpine newts. *Front. Zool.* 17:34. doi: 10.1186/s12983-020-00373-x

Schwenk, K. (2000). "Tetrapod feeding in the context of vertebrate morphology," in *Feeding: Form, Function, and Evolution in Tetrapod Vertebrates*, ed. K. Schwenk (San Diego, CA: Academic Press), 3–20.

Schwenk, K., and Rubega, M. (2005). "Diversity of vertebrate feeding systems," in *Physiological and Ecological Adaptations to Feeding in Vertebrates*, eds J. M. Starck and T. Wang (New Hampshire: Science Publishers), 1–41.

Scott, W. B., and Tibbo, S. N. (1968). Food and feeding habits of Swordfish, *Xiphias gladius*, in the Western North Atlantic. *J. Fish. Res. Bd. Canada* 25, 903–919. doi: 10.1139/f68-084

Shimose, T., Shono, H., Yokawa, K., Saito, H., and Tachihara, K. (2006). Food and feeding habits of blue marlin, *Makaira nigricans*, around Yonaguni Island, southwestern Japan. *Bull. Mar. Sci.* 79, 761–775.

Stillwell, C. E., and Kohler, N. E. (1985). Food and feeding ecology of the swordfish *Xiphias gladius* in the western North Atlantic Ocean with estimates of daily ration. *Mar. Ecol. Prog. Ser.* 22, 239–247.

Stojanov, A., Tzankov, N., and Naumov, B. (2011). *Die Amphiben und Reptilien Bulgariens*. Frankfurt: Chimaira.

Van Wassenbergh, S., and Heiss, E. (2016). Phenotypic flexibility of gape anatomy fine-tunes the aquatic prey-capture system of newts. *Sci. Rep.* 6:29277. doi: 10.1038/srep29277

Wainwright, S. A. (1983). "To bend a fish," in *Fish Biomechanics*, eds P. W. Webb and D. Weihs (New York, NY: Praeger), 68–91.

Wassersug, R. J., and Hoff, K. (1985). The kinematics of swimming in anuran larvae. *J. Exp. Biol.* 119, 1–30.

Westneat, M. W., Thorsen, D. H., Walker, J. A., and Hale, M. E. (2004). Structure, function, and neural control of pectoral fins in fishes. *IEEE J. Ocean. Eng.* 29, 674–683. doi: 10.1109/JOE.2004.833207

Wisner, R. L. (1958). Is the spear of istiophorid fishes used in feeding? *Pac. Sci.* 12, 60–70.

Yordanova, K., Lukanov, S., and Natchev, N. (2017). "Preliminary data indicate hard-wired coordination between locomotor and feeding systems in the Marsh frog (*Pelophylax ridibundus* Pallas, 1771) when catching prey on the water surface," in *Proceedings of the 5th Student Scientific Conference "Ecology and Environment"*, (Shumen: Konstantin Preslavsky University Press), 30–31.

Conflict of Interest: The authors declare that the research was conducted in the absence of any commercial or financial relationships that could be construed as a potential conflict of interest.

frontiers in Ecology and Evolution

METHODS
published: 14 April 2021
doi: 10.3389/fevo.2021.642255

Geographical Information System Applied to a Biological System: Pelvic Girdle Ontogeny as a Morphoscape

Virginia Abdala[1,2], Luciana Cristobal[1], Mónica C. Solíz[3] and Daniel A. Dos Santos[1,4]*

[1] Instituto de Biodiversidad Neotropical, UNT-CONICET, San Miguel de Tucumán, Argentina, [2] Cátedra de Biología General, Facultad de Ciencias Naturales e IML, Universidad Nacional de Tucumán, San Miguel de Tucumán, Argentina, [3] Cátedra de Vertebrados, Facultad de Ciencias Naturales, Universidad Nacional de Salta (UNSa), Salta, Argentina, [4] Cátedra de Biología Animal, Facultad de Ciencias Naturales e IML, Universidad Nacional de Tucumán, San Miguel de Tucumán, Argentina

OPEN ACCESS

Edited by:
Catherine Anne Boisvert, Curtin University, Australia

Reviewed by:
Rohan Mansuit, UMR 7207 Centre de Recherche sur la Paléobiodiversité et les Paléoenvironnements (CR2P), France
Terry A. Gates, North Carolina State University, United States

***Correspondence:**
Virginia Abdala
virginia@webmail.unt.edu.ar
orcid.org/0000-0002-4615-5011

Specialty section:
This article was submitted to Paleontology, a section of the journal Frontiers in Ecology and Evolution

Received: *15 December 2020*
Accepted: *22 March 2021*
Published: *14 April 2021*

Citation:
Abdala V, Cristobal L, Solíz MC and Dos Santos DA (2021) Geographical Information System Applied to a Biological System: Pelvic Girdle Ontogeny as a Morphoscape. Front. Ecol. Evol. 9:642255. doi: 10.3389/fevo.2021.642255

Geographic Information System (GIS) is a system that captures, stores, manipulates, analyzes, manages, and presents spatial or geographical data. As this technological environment has been created to deal with space problems, it is perfectly adaptable to solve these type of issues in the context of vertebrate comparative morphology. The pectoral and pelvic girdles are key structures that relate the axial skeleton with the limbs in tetrapods. Owed to their importance in locomotion, the morphology, development, and morphogenesis of these structures have been widely studied. The complexity of the structures and tissues implied in the development of the girdles make quantitative approaches extremely difficult. The use of GIS technology provides a visual interpretation of the histological data, a general quantitative assessment of the processes taking place during the ontogeny of any structure, and would allow collecting information about the changes in the surface occupied by the different tissues across the ontogenetic processes of any vertebrate taxa. GIS technology applied to map morphological structures would be a main contribution to the construction of the vertebrate ontologies, as it would facilitate the identification and location of the structures. GIS technology would allow also us to construct a shared database of histological quantitative changes across the ontogeny in any vertebrate. The main objective of this study is to use GIS technology for spatial analysis of histological samples such as these of the pelvic girdle using histological cuts of anurans and chicken, allowing thus to construct a morphoscape, analogous to a landscape. This is the first attempt to apply GIS tools to ontogenetic series to infer biological properties of the spatial analysis in the context of comparative biology. More frequent use of this technology would contribute to obtaining more profitable and biologically informative results.

Keywords: methodological options in anatomy, histology, biological information systems, morphoscape, GIS

INTRODUCTION

Geographic Information System (GIS) is a system that captures, stores, manipulates, analyzes, manages, and presents spatial or geographical data (Madurika and Hemakumara, 2017). This technology is used to compare layers of different types of data connected by locations in geographic space (Ungar and Williamson, 2000). Many tools of GIS are designed to model the physical surface of the earth (Zuccotti et al., 1998). As this technological environment has been created to deal with space problems, it is perfectly adaptable to solve these type of issues in the context of vertebrate comparative morphology. GIS software has been explored in the context of analyzing topography of the dentition (Zuccotti et al., 1998; Jernvall and Selänne, 1999; Ungar and Williamson, 2000; M'Kirera and Ungar, 2003; Ungar, 2004, 2007; Evans et al., 2007; Plyusnin et al., 2008; Eronen et al., 2009; Wilson et al., 2012; Salazar-Ciudad and Marin-Riera, 2013), spatial analysis of histological traits in human bone (Rose et al., 2012), conodont morphologies (Manship, 2004; Manship et al., 2006; Yacobucci and Manship, 2011; Knauss, 2012, 2013), skeletal structures of echinoderms (Sheffield et al., 2012; Zachos, 2012, 2015), and for morphometric analysis of the ammonoid shells (Knauss and Yacobacci, 2014). Additionally, GIS software is used to contribute to interoperability and data reuse (Fonseca and Egenhofer, 1999; Fonseca and Sheth, 2002), biological data mining (Plyusnin et al., 2008), and additionally could be used in developing terminological standardizations for the anatomy of vertebrates, such as the anatomical ontologies proposed for anurans (Maglia et al., 2007) or any other vertebrate. Techniques of GIS could be also used to find a tissue, helping to find out what exists at a particular location. This location can be described in many ways, using, for example, name or color of a tissue, or even topographic references relative to the area surveyed.

The pectoral and pelvic girdles are key structures that relate the axial skeleton with the limbs in tetrapods. Owed to their importance in locomotion, the anatomy, development and morphogenesis of these structures have been widely studied (Borkhvardt, 1991; Kaplan, 2000; Baleeva, 2001, 2009; Malashichev, 2001; Borkhvardt and Baleeva, 2002; Malashichev et al., 2005, 2008; Ročková and Roček, 2005; Shearman, 2005, 2008; Manzano and Barg, 2005; Pomikal and Streicher, 2010; Robovská-Havelková, 2010; Pomikal et al., 2011; Valasek et al., 2011; Don et al., 2013; Manzano et al., 2013; Nowlan and Sharpe, 2014; Nagashima et al., 2016; Soliz et al., 2018 among many others) mainly from a qualitative perspective. The complexity of the structures and tissues implied in the development of the girdles made quantitatives approximations very limited (but see Roddy et al., 2009; Pomikal and Streicher, 2010; Pomikal et al., 2011).

The main objective of this study is to use GIS technology for spatial analysis of histological samples, taking as examples the pelvic girdle of anurans and chicken, allowing to construct a morphoscape analogous to a landscape. Analyzing and representing pelvic girdle ontogeny with GIS tools provides a frame of reference for normal development and can be used for a visual interpretation of the data, and in a quantification of the growth of any structures or tissues of the vertebrate body. We used these unrelated taxa as examples of the possibilities of this approach, and are sure that more frequent use of this technology would contribute to obtaining more profitable and biologically informative results.

MATERIALS AND METHODS

Histology

Four specimens of *Lysapsus limellum* FML 28180 (Fundación Miguel Lillo, Tucumán, Argentina. Stages 37, 40, 44, 46 of Gosner, 1960) and three specimens of *Boana riojana* FML (Stages 37, 44, 46 of Gosner, 1960) were used in this study. These species were selected because previous work on the girdles by our team (Soliz et al., 2018) provided the necessary histological samples in the required sections. We also use images of four histological cuts of a developing chicken pelvic girdle, Stages 30–35 of Hamburger and Hamilton (1951) from Nowlan and Sharpe (2014). Images of the chicken histological cuts were nicely made available by Dr. Niamh Nowlan (Imperial College, London). We refer to our two species as Anuran Model because differences between them are minor in comparison with those of the Anuran and Chicken Models.

Specimens were dehydrated through a graded ethanol series, cleared in xylene and embedded in Paraplast. Embedded specimens were sectioned in serial and semi-serial sections of 5–10 μm. Sections were then deparaffinized, hydrated, and stained with Hematoxylin–Eosin (H-E). All sections were once again dehydrated, bathed in xylene, and sealed with Canada Balsam under a cover slip. Terminology of girdles tissue and structures follows Baleeva (2001); Shearman (2008), Diogo and Abdala (2010); Manzano et al. (2013), Diogo and Molnar (2014); Soliz et al. (2018).

GIS Application

As a way to facilitate the application of this technology, we include a tutorial (**Supplementary Material**). From more than 100 cuts, a colored section of the same structures from each of the two anuran species, in all four different developmental stages were selected, photographed and digitized, at the same magnification. The original cross-sectional cuts composite image and the SMA.jpg image were imported into a single map in QGIS. To calibrate the measures and enable the accurate use of measuring tools, we built our own reference system. We assign milimeters as the unit of measure. The cuts were scaled 200 μm. In all images the scale was respected. The 200 μm segment of the original cut was rescaled into 0.2 mm. QGIS was used to refer all images to a single reference system. To this end, we used the transverse Mercator reference system. After that, we identified the plane of bilateral symmetry or the sagittal plane, and defined a work area of 1.60 × 0.8 mm, which represents 100% of our area of analysis (**Figure 1**). After several trials, we found that this size of area allowed us to comfortably follow the anatomical structures through the different ontogenetic stages. New map layers were created in QGIS to represent four cartilaginous structures for the anuran species: pelvic hemigirdle, femur epiphysis and diaphysis, and

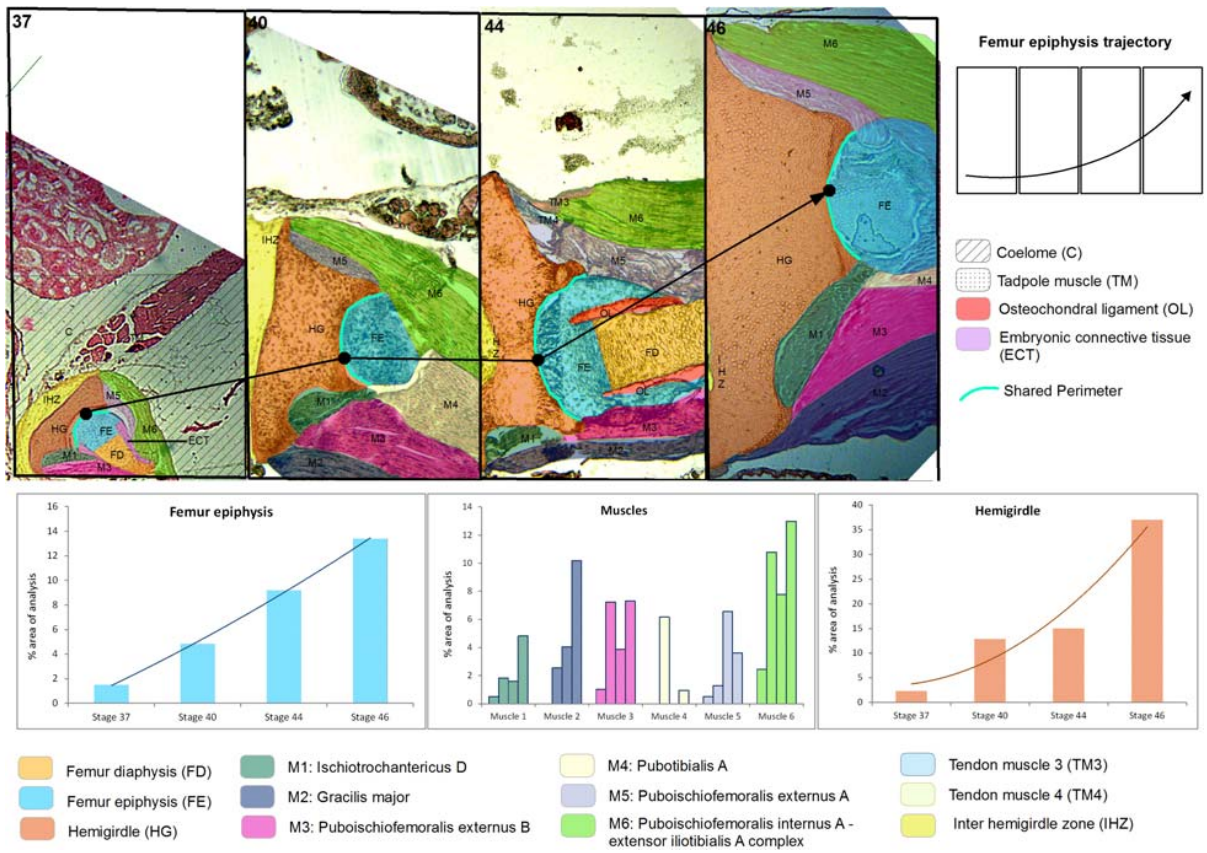

FIGURE 1 | *Lisapsus limellum*. Selected area and the ontogenetic Stages 37–46 showing the increase in size and change of location of pelvic girdle tissues and structures. In the frequency histograms the growth of the structures is depicted.

the lateral articular cartilage; six muscles: ischiotrochantericus D, gracilis major, puboschiofemoralis externus B, pubotibialis A, puboischiofemoralis externus A, puboischiofemoralis internus A-extensor iliotibialis A complex, and two tendons: tendon of the puboschiofemoralis externus B and pubotibialis A. We also identify the connective tissue area that separates both hemigirdles. In regard to the chicken, we identify four cartilaginous structures: ischium, ilium, femur epiphysis and diaphysis; a cavity filled with mesenchimatic tissue (**Figure 3**). We also identify cell nuclei, the matrix of cartilaginous tissue, dense and lax mesenchimatic tissue and empty areas, which in the Stages 34 and 35 included the acetabular joint cavity. Unsupervised digital classifications of 10× images of the chicken cuts (Nowlan and Sharpe, 2014), another commonly used GIS technique to mark areas, were used to identify the tissues, a procedure commonly used with satellite images. A digital classification of the jpg images of the histological cuts of *Gallus gallus* was made. Image classification refers to the task of extracting information classes from a multiband raster image, in this case three bands (RGB). The raster resulting from the image classification can be used to create thematic maps. In this case, an almost non-supervised classification (iso clusters) was made. Unsupervised classification searches for spectral classes (or clusters) in a multiband image without the analyst's intervention. Ten initial classes were defined and from them were recovered those that responded similarly in their RGB combinations (which in GIS would correspond to spectral similarity). Finally, five different types of structures were identified: core, cartilaginous matrix, dense mesenchyme, lax mensenchyme and cavity.

These structures and tissues were manually identified and annotated (**Figures 1**–**3**), and their scores were recorded in the attribute table for each layer (**Figures 1**, **3**). The attribute table relates any type of data, such as tissue types, and different structures that have been spatially located in the GIS. QGIS was used to create a separate layer containing the images of the histological sections for separate viewing. This was accomplished with the geographical data-base by creating an edited histodatabase. A histodatabase is a data model constructed in standard database formats, allowing for storage of a variety of different layer types within GIS environment. A data repository with all original jpg images, images with reference system, results of digital classifications in raster format and shapefiles used for this work (in a QGIS Project) will be available in a web repository[1]. After preparation of the appropriate layers, several tools within QGIS were used to identify distributional patterns of histological features. Thus, we obtained, the growth

[1]https://ibn.conicet.gov.ar/recursos/

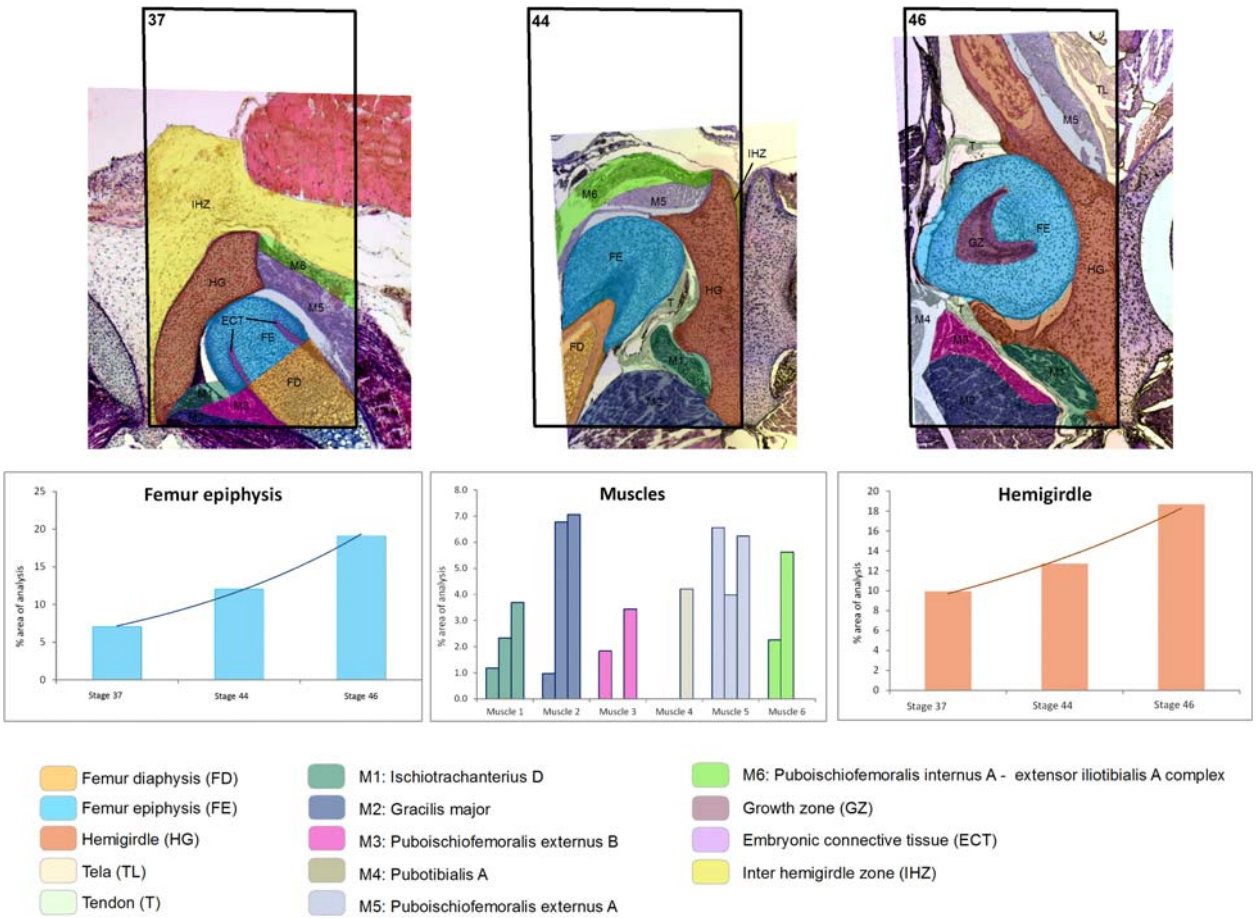

FIGURE 2 | *Boana riojana*. Selected area and the ontogenetic Stages 37–44–46 showing the increase in size and change of location of the pelvic girdle tissues and structures. Note the embryonic connective tissue restricted to the future osteochondral ligament. In the frequency histograms the growth of the structures is depicted.

percentages of selected structures and tissues through the ontogenetic stages. We also identify the middle point of the femur epiphysis and follow it in the cuts of all stages of anuran and chicken development, which allowed us to build a trajectory for easy visual recognition of this bone movement thoroughly during development (**Figures 1**, **3**). Additionally, we calculated the shared perimeter between the anatomical structures (**Supplementary Material**).

RESULTS

Anuran Model

Sequence of the Ontogenetic Stages of the Anuran Pelvic Girdles Structures and Tissues

Lisapsus limellum and *Boana riojana*

At Stage 37, both species *Lisapsus limellum*, **Figure 1** and **Table 1**; *Boana riojana*, **Figure 2** and **Table 2**) present the hemigirdle as a single pre-cartilaginous piece, almost rectangular and at an angle of around 50° with respect to the sagittal plane. This structure occupies 2.4% of the analyzed structures, which are 11.5% of the delimited area in *Lisapsus limellum*. In *Boana riojana* the hemigirdle occupies 9.9% of the analyzed structures, which are 61.1% of the delimited area. The space between the sagittal plane is occupied by a loose connective tissue, with abundant ground substance and relatively few fibers and cells, filling the inter hemigirdle zone, 2% of the analyzed area in *L. limellum*. In *B. riojana* the central loose connective tissues occupies 23.8% and the typical connective tissue occupies 0.5%, and a part of the tadpole coelome. The acetabular fossa is already observable, housing the pre-cartilaginous femoral head, which occupies the 1.2% of the analyzed area in *L. limellum* and 7.1% in *B. riojana*. The femur diaphysis is also observable occupying 1.2% of the analyzed area in *L. limellum* and 6.9% in *B. riojana*. Four premyogenic masses corresponding to the ischiotrochantericus D, puboschiofemoralis externus B, puboischiofemoralis externus A, and puboischiofemoralis internus A are visible. All these premuscle or muscle masses occupied the 4.5% of the analyzed area in *L. limellum* and 12.9% in *B. riojana*. Considering tissues instead of structures, it could be seen that the cartilaginous tissue occupies 4.7% of the analyzed area, almost the same percentage as the premyogenic masses in *L. limellum* (4.5%),

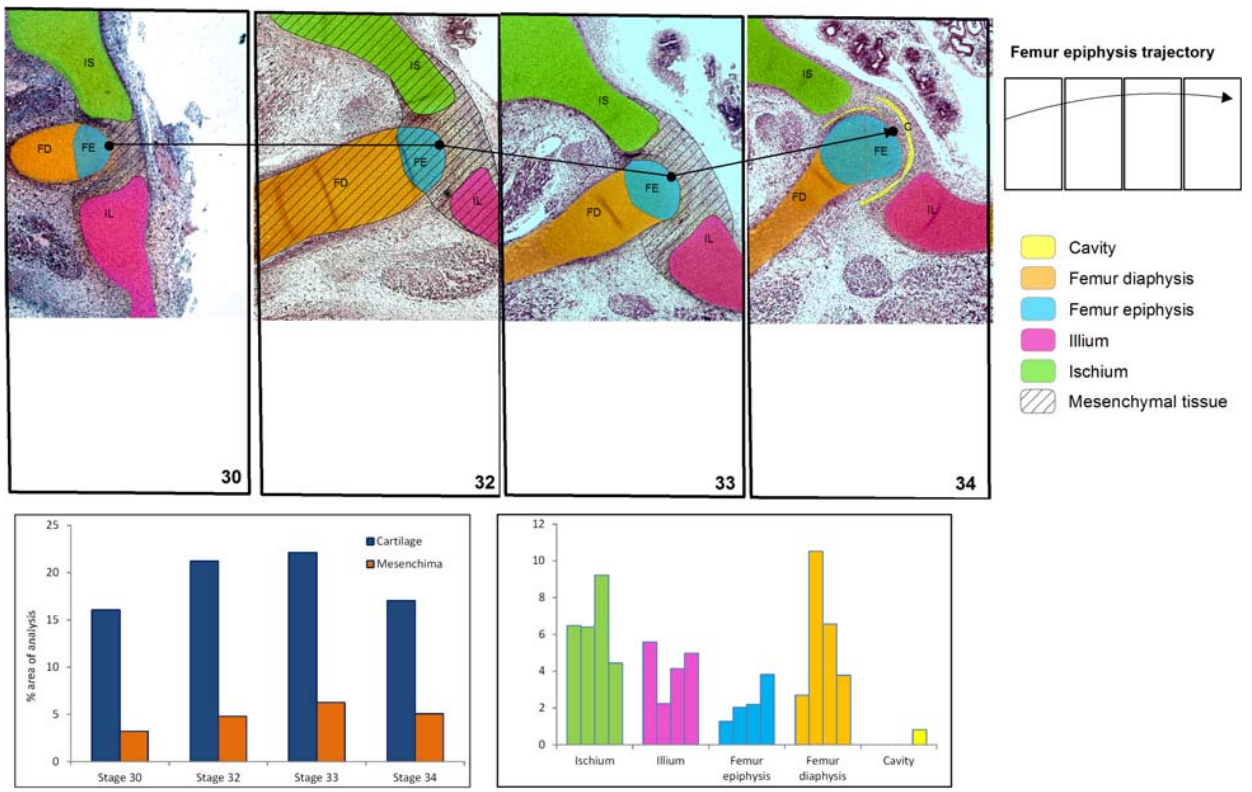

FIGURE 3 | Chicken histological cuts between Stages 30 and 34 HH (Nowlan and Sharpe, 2014) showing the increase in size and change of location of the pelvic girdle tissues and structures. In the frequency histograms the growth of the structures is depicted.

whereas in *B. riojana*, cartilage corresponds to 23.9% of the analyzed area and the premyogenic masses to 12.9%. The central loose connective tissue occupies 2% of the analyzed area, whereas the typical connective tissue of the femur epiphysis 0.3% in *L. limellum*.

In *Lisapsus limellum* at stage 40 the pre-cartilaginous structures have increased their size. The entire hemigirdle-femur framework is closer to the sagittal plane at an angle of around 30°. The hemigirdle occupies 12.9% of the analyzed area and the femur epiphysis 4.8%. The femur diaphysis is indistinguishable. The space between the hemigirdle and the sagittal plane is entirely occupied by a loose connective tissue (3.8% of the analyzed area). The premyogenic masses also increased their size to occupy 29.8% of the analyzed area. The displacement of the hemigirdle-femur framework allows distinguishing the future gracilis major along with the other five premuscle masses.

Results on the shared perimeters between the structures analyzed in this paper are included in the **Supplementary Table 1**. The shared perimeter between the femur epiphysis and the hemigirdle is shown in **Figure 1**.

Lisapsus limellum and *Boana riojana Comparison*

At Stage 44 the hemigirdle is parallel to the sagittal plane and attached to the other hemigirdle along almost all the medial surface. In *Lisapsus limellum* the hemigirdle occupies 15.1% of the analyzed area, and in *Boana riojana* 12.7%. In the center of the attachment region between both hemigirdles is an oval open region filled with the loose connective tissue that is reduced to 1.5% of the analyzed area in *Lisapsus limellum*. In *Boana riojana* this connective tissue occupies a long area between the hemigirdles that corresponds to 0.5% of the analyzed area. In the femur epiphysis (9.2%) the lateral articular cartilages are clearly visible, along with the osteochondral ligament (2.2%) in *L. limellum*. In *B. riojana*, the femur epiphysis occupies 12.1% of the analyzed area. The osteochondral ligament is not visible in this histological cut. The femur diaphysis is clearly recognizable (6.6%) in *L. limellum*. In *B. riojana* it is ossified and occupies 2.3% of the analyzed area. In *L. limellum*, at Stage 44, the muscles have lengthened compared to the Stage 40, but their covered a smaller area (23.8% vs. 29.8 in Stage 40). In *B. riojana*, at Stage 44, the muscles have also lengthened but with a greater area than in the Stage 37 (18.7%). In *B. riojana* tendons are visible at Stage 44, occupying 2.9% of the analyzed area. At Stage 46 both hemigirdles (37%) are completely attached, leaving just vestiges of the loose connective tissue (0.3%) in *Lisapsus limellum*. In *Boana riojana*, the hemigirdle is composed by a cartilaginous part (18.7%) and an ossified part (6.1%), so the total hemigirdle occupies 24.8%.The femur epiphysis (13.4% in *L. limellum*; 19.1% in *B. riojana*) is totally adjusted to the acetabulum. The femur diaphysis is indistinguishable in *L. limellum*, and *Boana riojana*. All muscular masses are composed of mature tissue and occupy 39.9% of the analyzed area in *L. limellum* and 24.6% in *B. riojana*.

TABLE 1 | Tissues (light brown) and structures (light blue) percentages (%) in relation to the analyzed area (*Lisapsus limellum*).

Tissue	Structure	Stage 37		Stage 40		Stage 44		Stage 46	
Cartilage	Femur diaphysis	4.7	1.2	17.7		30.9	6.6	50.4	
	Femur epiphysis		1.2		4.8		9.2		13.4
	Hemigirdle		2.4		12.9		15.1		37.0
Connective	Femur epiphysis	2.3	0.3	3.9		3.7		0.3	
	Interzone				0.1				
	Inter hemigirdle zone		2.0		3.8		1.5		0.3
	Osteochondral ligament						2.2		
Premuscle	Muscle 1	4.5	0.5	29.8	1.8	23.8	1.6	39.9	4.8
	Muscle 2				2.5		4.1		10.2
	Muscle 3		1.0		7.2		3.9		7.3
	Muscle 4				6.2				1.0
	Muscle 5		0.5		1.3		6.6		3.6
	Muscle 6		2.4		10.8		7.8		13.0
Tendon	Tendon muscle 3					1.4	0.6		
	Tendon muscle 4						0.8		
Total		**11.5**		**51.4**		**59.7**		**90.6**	
Liquid	Coelome	23.7	23.7						
Muscle	Tadpole muscle	7.1	7.1						

TABLE 2 | Tissues (light brown) and structures (light blue) percentages (%) in relation to the analyzed area (*Boana riojana*).

Tissue	Structure	Stage 37		Stage 44		Stage 46	
Cartilage	Femur diaphysis	23.9	6.9	24.8		41.2	
	Femur epiphysis		7.1		12.1		19.1
	Hemigirdle		9.9		12.7		18.7
	Growth zone						3.4
Connective	Embryonic connective tissue	24.3	0.5	0.5		5.3	
	Inter hemigirdle zone		23.8		0.5		
	Tela						5.3
Muscle	Muscle 1	12.9	1.2	18.7	2.3	24.6	3.7
	Muscle 2		1.0		6.8		7.1
	Muscle 3		1.8				3.4
	Muscle 4						4.2
	Muscle 5		6.6		4.0		6.2
	Muscle 6		2.3		5.6		
Tendinous	Tendon				2.9		2.3
Pre bone	Femur diaphysis			2.1	2.1		
Bone	Femur diaphysis			2.3	2.3	6.1	
	Hemigirdle						6.1
Total		**61.1**		**51.3**		**78.6**	

The cartilaginous tissue occupies 50.4% of the analyzed area in *L. limellum* and 41.2% in *B. riojana*. In *B. riojana* the tendons occupy 2.3% of the analyzed area.

Both hemigirdles are moving to the sagittal plane of the body. Growth of cartilaginous structures tend to be proportional through all stages, with the hemigirdle and femur epiphysis being the largest at Stage 46. This pattern of proportional growth is not so obvious in relation to the muscles in *L. limellum*, which exhibit more variability; in *B. riojana* the growth of the muscles is as proportional as the cartilaginous structures. In both cases a higher overall growth between the Stages 44 and 46 is noticeable. Tendinous tissue appears late in the ontogeny and remains comparatively small.

TABLE 3 | Tissues (light brown) and structures (light blue) percentages (%) in relation to the analyzed area (*Gallus gallus*).

Tissue	Structure	Stage 30		Stage 32		Stage 33		Stage 34	
Cartilage	Femur diaphysis	16.0	2.7	21.2	10.5	22.1	6.6	17.0	3.8
	Femur epiphysis		1.3		2.0		2.2		3.8
	Illium		5.6		2.2		4.1		5.0
	Ischium		6.5		6.4		9.2		4.4
Mesenchima	Cavity	3.2		4.8		6.3		5.1	0.8
Total		**19.2**		**26**		**28.4**		**22.1**	

Chicken Model

Sequence of the Ontogenetic Stages of the Chicken Pelvic Girdles Tissues and Structures

In the chicken model (**Figure 3**), at Stage 30, the hemigirdle is composed of two pieces, the ischium and the ilium, separated by mesenchimatic tissue. The hemigirdle is located almost paralell to the sagital plane of the body at Stage 30, and rotates to reach almost 55° at Stage 32. Both hemigirdles are moving away from the sagittal plane of the body. The femur epiphysis and diaphysis are distinguishable. Percentages of the different structures and tissues in relation to the analyzed area are shown in **Table 3**. Growth of the cartilaginous structures tends to increase to the last stages, with some inconsistencies probably owed to the depth of the histological cuts. The mesenchime of the cavity surrounding the femur epiphysis tend to grow up to the Stage 33 (6.3%), and then shows a soft decrease in Stage 34 (5.1%) owed to the increase of the area occupied by the femur epiphysis (from 1.3% in Stage 30–3.8 in Stage 34).

DISCUSSION

Our results show that GIS technology is an effective interface to study spatial problems even to microscopic scales. However, as far as we know, apart from ours there has been only one attempt to apply GIS environment to ontogenetic series to infer biological properties of the spatial analysis in the context of comparative biology (see Zachos, 2015). The application of this technology exhibits some shortcomings more related to the difficulties of obtaining appropriate histological cuts than to the technology itself. Thus, we think that the small area of the tendinous tissue in our results and the decrease of the area occupied by some muscles in later stages compared to earlier ones, can be artifacts owed to the lack of cuts at the same deep. The comparison of samples coming from different species or stages of different sizes would be also a problem. However, in view of analytical benefits the effort to achieve standard samples is worth to carry out. Whenever the focus is put on the analysis of shapes, structures of different sizes can be accommodated within a window of standard size

(for instance, the square unit). In spite of these limitations, GIS tools are a powerful technology that could allow discovery of interesting trends in the growth of tissues and structures along all the ontogenetic periods of any living organism.

The use of GIS imaging has facilitated the quantification of several features of pelvic girdle development that could not be possible using whole-mount data and be very difficult with histological data. The major advantage in using GIS is the fast visual perspective of the tissues and structures, as well as the option of a quick collection and catalog of histological and structural data. The possibility to set the same reference area for all specimens allowed us to highlight differences in the trajectories of the hemigirdles between the studied species. Our data clearly demonstrate that in frogs, rotation of the pelvis with respect to the sagittal body plane makes both closer to each other (see also Pomikal et al., 2011), whereas the opposite happens in the chicken (see also Nowlan and Sharpe, 2014). Data on the rotation angles of the hemigirdles in the chicken show that they move away from the sagittal plane of the body. At earlier stages, the angle between the hemigirdle and the sagittal plane of the body is very small, and grows to about 55° in only one stage. In the chicken all the structures occupy only half of the area compared to frogs, and changes in the location of the femur epiphyses are more gradual. The location of the femur epiphyses change more acutely in frogs, from the lower quadrant to the superior one. The more radical growth of the girdle structures and the change in the locations of the femur epiphyses in frogs could be easily related to the dramatic change from an aquatic to a terrestrial habitat, which requires fully functional limbs (Muntz, 1975; Pomikal et al., 2011). It could be also inferred that the opposite direction of the rotation of the femur and girdles in the chicken can be owed to the bipedal position of the hindlimb in birds that requires a more vertical location of this bone. We are aware that these data are visible with histological cuts, however, the use of GIS mapping highlight trends that remain hidden in the complex landscape of serial histological sampling.

Analyses of the anuran pelvic girdle growth during development using GIS tools reveal interesting patterns worth considering. At Stage 37 around 60% of the analyzed area of *Lisapsus limellum* and 40% of *B. riojana* are occupied by tissues and structures of the tadpole. The connective tissue that fills the inter hemigirdles zones is more extensive in *Boana riojana* at Stage 37, 23.9% of the studied area, which corresponds to 61.1% of the total area. At the same stage, in *Lisapsus limellum* it occupies 2.3%, which corresponds to a 11.5% of the studied area. Remarkably, at Stage 37, in both species the connective tissue of the inter hemigirdle zone is almost the same percentage of the connective tissue in general, 2 of 2.3% in *L. limellum* (0.3%) and 23.8 of 24.3% in *B. riojana* (0.5%). Pomikal et al. (2011) reported a highly detailed description of the ilio-sacral connector, a strand of connective tissue linking the ilium and the sacrum in several anuran species. It could be inferred that the big area of connective tissue between the hemigirdles at the earlier stages (IHZ in our **Figures 1**, **2**), which persists as a small region at Stage 46 in *Lisapsus limellum* and has practically disappeared at Stage 44 in *Boana riojana*, could also be a hemigirdle connector. As can be observed in the figures, the hemigirdle-connector tissue appears highly different to the surrounding tissues, and-as was demonstrated in *Rana temporaria* by Pomikal et al. (2011)—growth of the cartilaginous structures is performed at the expense of the connective strand. It would be very interesting to analyze its composition and compare it with the ilio-sacral connector and to the mesenchymal bridge described by Malashichev (2001) that connects the lizard ribs.

The fastest growing of all cartilaginous structures in the anuran model occurs between Stages 44 and 46. It is remarkable and similar to what occurs with muscles. This outcome is surprising considering the sequence proposed by Muntz (1975) in which tadpoles of Stage 42 should have fully functional limbs with their tissues fully differentiated, suggesting that the faster growth should occur to reach that stage. The growth between Stages 44 and 46 of most structures is faster indeed, passing in, e.g., the femur epiphysis of *L. limellum* from 9.2 to 13.4% and in *B. riojana* from 12.1 to 19.1% of the total area considered. This fast growth suggests that although functional, tissues and structures in Stage 42 have to reach their most adjusted phenotype to perform the physical activities of the organism.

The images of the chicken development show the gradual change in the femur orientation, which acquires a more vertical position. It is interesting that a previous study of Carrano and Biewener (1999) has showed that an experimental change in

TABLE 4 | List of GIS functionalities that can enhance the work of morphoanatomists.

GIS analysis functions	Short description	Applicability
Retrieval	Selective search manipulation	Information from database tables can be accessed directly through the mapped anatomic structure
Classification	Procedure of identifying groups and defining patterns	Using spectral decomposition of images, clusters of cells can be isolated
Overlay	Layers with a shared spatial extent are joined. Composite maps by combining diverse data sets are created	Two different anatomical layers (e.g., muscles and nerves) can be crossed
Neighborhood	Analyzing the relationship between an object and similar surrounding objects	It is of interest to assess the character of a certain outlined area. Analysis of a kind of structure is next to what kinds of structure can be done
Topographic	Dealing with surface characteristics with continuously changing value over an area	Representation of data such as concentration of nuclei in a sample as a digital elevation model. It aids to visualize better patterns of change
Interpolation	Predicting unknown values using the known values at neighboring locations	Anatomical samples could be either corrupted or incomplete. The void in data can be filled by using interpolation
Connectivity	Analyzing different features associated with network of elements (structures connected through links)	Anatomical networks are increasingly studied. Muscular-skeletal networks can be identified here

the location of the center of mass of a chicken by adding postacetabular weigths, provoked a more horizontal femur orientation. The change in the orientation of the femur through chicken development suggests that the center of mass of the embryo is shifting to a more anterior position. On the contrary, the orientation of the femur in *Lisapsus limellum* is in the opposite sense, probably indicating a shift of the center of mass to a posterior location. These changes are more clearly perceived and showed because of the GIS technology used here.

The shared perimeter between the hemigirdle and the femur epiphysis of *Lisapsus limellum* increases progressively until Stage 44, being shorter at Stage 46. As **Figure 1** shows, this shortening could be an artifact, as in the image, muscles cover the terminal prominences of the hemigirdle. The **Supplementary Table 1** shows that the longest perimeter of the embryonic tissue present at Stage 37 is shared by the diaphysis of the femur. It could be predicted that this embryonic tissue will differentiate into diaphysis tissue. This type of data will help to uncover other growth patterns of the tissued through the ontogeny.

In this paper we showed that GIS software can be used to document, describe, and compare a variety of different structures and tissues through histological mapping. We thus make a histomorphoscape, in this case applied to girdles development. This method allows the consideration of a new scale at which to evaluate the variability of the histomorphology of a structure (Rose et al., 2012). GIS technology would allow also to construct a shared database of histological quantitative changes across the ontogeny in any vertebrate. These data would be more efficiently recovered and useful for comparisons at a higher scale than with the tools available until now. In this way, any researcher from the field of comparative morphology could achieve a snapshot of possible analyzes involving shapes, measurement of features, and topographic relationships among structures. GIS provides tools that allow a fresh and dynamic new way (**Table 4**). For example, the function of interpolation could assist in dealing with non-complete samples. It sheds light on the underlying nature of structures otherwise absent, which is intrinsic to many GIS software, but not easily available in other resources from digital image analysis. Sweat streams drained by a rough skin could be analyzed with the same rationale as in a continental watershed, presenting an unprecedented way to study a natural phenomenon.

DATA AVAILABILITY STATEMENT

Publicly available datasets were analyzed in this study. This data can be found here: https://ibn.conicet.gov.ar/recursos/.

ETHICS STATEMENT

Ethical review and approval was not required for the animal study because we worked with histological cuts from a collection.

AUTHOR CONTRIBUTIONS

VA conceived this study and realized drafting of the manuscript. LC applied GIS technology. MS provided the anuran cuts. VA, LC, and DD interpreted the data. All authors critically revised the manuscript.

FUNDING

PIP CONICET 0389 to VA; PICT 2016-2772 – PICT 2018-00832 to VA.

ACKNOWLEDGMENTS

We are very grateful to Niamh Nowlan (Department of Bioengineering, Imperial College London) for making the chicken pictures available.

SUPPLEMENTARY MATERIAL

The Supplementary Material for this article can be found online at: https://www.frontiersin.org/articles/10.3389/fevo.2021.642255/full#supplementary-material

REFERENCES

Baleeva, N. (2001). Formation of the scapular part of the pectoral girdle in anuran larvae. *Russian J. Herpetol.* 8, 195–204.

Baleeva, N. (2009). Formation of the coracoid region of the anuran pectoral girdle. *Russ. J. Herpetol.* 16, 41–50.

Borkhvardt, V., and Baleeva, N. (2002). Development of the pectoral girdle in larvae of Siberian salamander *Salamandrella keyserlingii* (Amphibia. Hynobiidae). *Russ. J. Herpetol.* 9, 177–184.

Borkhvardt, V. G. (1991). Regularities of the development of the cartilaginous elements in vertebrate ontogenesis. *Zh. Obshch. Biol.* 52, 627–640.

Carrano, M. T., and Biewener, A. A. (1999). Experimental alteration of limb posture in the chicken (Gallus gallus) and its bearing on the use of birds as analogs for dinosaur locomotion. *J. Morphol.* 240, 237–249. doi: 10.1002/(sici)1097-4687(199906)240:3<237::aid-jmor3>3.0.co;2-n

Diogo, R., and Abdala, V. (2010). *Muscles of Vertebrates*. Hauppauge, NY: Science Publishers.

Diogo, R., and Molnar, J. (2014). Comparative anatomy, evolution, and homologies of tetrapod hindlimb muscles, comparison with forelimb muscles, and deconstruction of the forelimb-hindlimb serial homology hypothesis. *Anat. Rec.* 297, 1047–1075. doi: 10.1002/ar.22919

Don, E. K., Currie, P. D., and Cole, N. J. (2013). The evolutionary history of the development of the pelvic fin/hindlimb. *J. Anat.* 222, 114–133. doi: 10.1111/j.1469-7580.2012.01557.x

Eronen, J. T., Evans, A. R., Fortelius, M., and Jernvall, J. (2009). The impact of regional climate on the evolution of mammals: a case study using fossil horses. *Evolution* 64, 398–408. doi: 10.1111/j.1558-5646.2009.00830.x

Evans, A. R., Wilson, G. P., Fortelius, M., and Jernvall, J. (2007). High-level similarity of dentitions in carnivorans and rodents. *Nature* 445, 78–81. doi: 10.1038/nature05433

Fonseca, F., and Egenhofer, M. (1999). "Ontology-driven geographic information systems," in *GIS '99: Proceedings of the 7th ACM International Symposium on Geographic Information Systems*, ed. C. B. Medeiros (New York, NY: Association for Computing Machinery), 14–19.

Fonseca, F., and Sheth, A. (2002). *The Geospatial Semantic Web*. Available online at: https://corescholar.libraries.wright.edu/knoesis/679

Gosner, K. L. (1960). A simplified table for staging anuran embryos and larvae with notes on identification. *Herpetologica* 16, 183–190.

Hamburger, V., and Hamilton, H. L. (1951). A series of normal stages in the development of the chick embryo. *J. Morphol.* 88, 49–92. doi: 10.1002/jmor.1050880104

Jernvall, J., and Selänne, L. (1999). Laser confocal microscopy and geographic information systems in the study of dental morphology. *Paleontol. Electronica* 2:18.

Kaplan, M. (2000). The pectoral girdles of *Rana rugulosa* (Ranidae) and *Nesomantis thomasseti* (Sooglossidae). *Herpetologica* 56, 188–195.

Knauss, M. J. (2012). Quantifying morphological variability in ammonoids using GIS spatial analyses. *Geol. Soc. Am.* 44:442.

Knauss, M. J. (2013). Quantifying ornamental variabilityin an ammonoid clade using GIS spatial analyses. *Geol. Soc. Am.* 45:475.

Knauss, M. J., and Yacobacci, M. M. (2014). Geographic information systems technology as a morphometric tool for quantifying morphological variation in an ammonoid clade. *Palaeontol. Electron.* 17:19A.

Madurika, H. K. G. M., and Hemakumara, G. P. T. S. (2017). Gis based analysis for suitability location finding in the residential development areas of Greater Matara Region. *Int. J. Sci. Technol. Res.* 4, 96–105.

Maglia, A. M., Leopold, J. L., Pugener, A., and Gauch, S. (2007). An anatomical ontology for amphibians. *Pac. Symp. Biocomput.* 12, 367–378.

Malashichev, Y. (2001). Sacrum and pelvic girdle development in lacertidae. *Russ. J. Herpetol.* 8, 1–16.

Malashichev, Y., Borkhvardt, V., Christ, B., and Scaal, M. (2005). Differential regulation of avian pelvic girdle development by the limb field ectoderm. *Anat .Embryol.* 210, 187–197. doi: 10.1007/s00429-005-0014-8

Malashichev, Y., Christ, B., and Pröl, F. (2008). Avian pelvis originates from lateral plate mesoderm and its development requires signals from both ectoderm and paraxial mesoderm. *Cell. Tissue Res.* 331, 595–604. doi: 10.1007/s00441-007-0556-6

Manship, L., Strauss, R. E., and Barrick, J. (2006). "Discrimination of frasnian (Late Devonian) Palmatolepis species using multivariate analysis of platform elements," in *Proceedings of the Programme & Abstracts, First International Conodont Symposium 2006 (ICOS 2006)*, Leicester, 55.

Manship, L. L. (2004). *Pattern Matching: Classification of Ammonitic Sutures Using GIS*. Lubbock, TX: Department of Geosciences.

Manzano, A., Abdala, V., Ponssa, M. L., and Soliz, M. C. (2013). Ontogeny and tissue differentiation of the pelvic girdle and hind limbs of anurans. *Acta Zool.* 94, 420–436.

Manzano, A., and Barg, M. (2005). The iliosacral articulation in Pseudinae (Anura. Hylidae). *Herpetologica* 61, 259–267. doi: 10.1655/04-28.1

M'Kirera, F., and Ungar, P. S. (2003). Occlusal relief changes with molar wear in Pan troglodytes troglogytes and Gorilla gorilla gorilla. *Amer. J. Primatol.* 60, 31–41. doi: 10.1002/ajp.10077

Muntz, L. (1975). Myogenesis in the trunk and leg during development of the tadpole of *Xenopus laevis* (Daudin 1802). *J. Embryol. Exp. Morph.* 33, 757–774.

Nagashima, H., Sugahara, F., Watanabe, K., Shibata, M., Chiba, A., and Sato, N. (2016). Developmental origin of the clavicle, and its implications for the evolution of the neck and the paired appendages in vertebrates. *J. Anat.* 229, 536–548. doi: 10.1111/joa.12502

Nowlan, N. C., and Sharpe, J. (2014). Joint shape morphogenesis precedes cavitation of the developing hip joint. *J. Anat.* 224, 482–489. doi: 10.1111/joa.12143

Plyusnin, I., Evans, A. R., Karme, A., Gionis, A., and Jernvall, J. (2008). Automated 3D phenotype analysis using data mining. *PLoS One* 3:e1742. doi: 10.1371/journal.pone.0001742

Pomikal, C., Blumer, R., and Streicher, J. (2011). Four–dimensional analysis of early pelvic girdle development in Rana temporaria. *J. Morphol.* 272, 287–301. doi: 10.1002/jmor.10913

Pomikal, C., and Streicher, J. (2010). 4D–analysis of early pelvic girdle development in the mouse (Mus musculus). *J. Morphol.* 271, 116–126. doi: 10.1002/jmor.10785

Robovská-Havelková, P. (2010). How can ontogeny help us to understand the morphology of anuran pectoral girdle? *Zoomorphology* 129, 121–132. doi: 10.1007/s00435-010-0105-9

Ročková, H., and Roček, Z. (2005). Development of the pelvis and posterior part of the vertebral column in the Anura. *J. Anat.* 206, 17–35. doi: 10.1111/j.0021-8782.2005.00366.x

Roddy, K. A., Nowlan, N. C., Prendergast, P. J., and Murphy, P. (2009). 3D representation of the developing chick knee joint: a novel approach integrating multiple components. *J. Anat.* 214, 374–387. doi: 10.1111/j.1469-7580.2008.01040.x

Rose, D. C., Agnew, A., Gocha, T. P., Stout, S. D., and Field, J. S. (2012). Technical note: the use of geographical information systems software for the spatial analysis of bone microstructure. *Amer. J. Phys. Anthropol.* 148, 648–654. doi: 10.1002/ajpa.22099

Salazar-Ciudad, I., and Marin-Riera, M. (2013). Adaptive dynamics under development-based genotype-phenotype maps. *Nature* 497, 361–365. doi: 10.1038/nature12142

Shearman, R. (2005). Growth of the pectoral girdle of the leopard frog. Rana pipiens (Anura, Ranidae). *J. Morphol.* 264, 94–104. doi: 10.1002/jmor.10322

Shearman, R. (2008). Chondrogenesis and ossification of the Lissamphibian pectoral girdle. *J. Morphol.* 269, 479–495. doi: 10.1002/jmor.10597

Sheffield, S. L., Zachos, L. G., and Lewis, R. D. (2012). A morphometric study of Erisocrinus (Crinoidea) using ArcGIS. *Geol. Soc. Am.* 44:232.

Soliz, M. C., Ponssa, M. L., and Abdala, V. (2018). Comparative anatomy and development of pectoral and pelvic girdles in hylid anurans. *J. Morphol.* 279, 904–924. doi: 10.1002/jmor.20820

Ungar, P. (2004). Dental topography and diets of *Australopithecus afarensis* and early Homo. *J. Human Evol.* 46, 605–622. doi: 10.1016/j.jhevol.2004.03.004

Ungar, P. (2007). "Dental topograpy and human evolution," in *Dental Perspectives on Human Evolution: State of the Art Research in Dental Paleoanthropology*, eds S. E. Bailey and J. J. Hubling (Berlin: Springer Science & Business Media), 411.

Ungar, P., and Williamson, M. (2000). Exploring the effects of tooth wear on functional morphology: a preliminary study using dental topograpic analysis. *Palaeontol. Electron.* 31:18.

Valasek, P., Theis, S., De Laurier, A., Hinitsf, Y., Lukea, G. L., Ottoa, J., et al. (2011). Cellular and molecular investigations into the development of the pectoral girdle. *Devel. Biol.* 357, 108–116. doi: 10.1016/j.ydbio.2011.06.031

Wilson, G. P., Evans, A. R., Corfe, I. J., Smits, P. D., Fortelius, M., and Jernvall, J. (2012). Adaptive radiation of multituberculate mammals before the extinction of dinosaurs. *Nature* 483, 457–460. doi: 10.1038/nature10880

Yacobucci, M. M., and Manship, L. L. (2011). Ammonoid septal formation and suture asymmetry explored with a geographic information systems approach. *Palaeontol. Electron.* 14:3A.

Zachos, L. G. (2012). Morphometric analysis of fossils using heads-up digitizing and geographic information system (GIS) software. *Geol. Soc. Am.* 44:18.

Zachos, L. G. (2015). Holistic morphometric analysis of growth of the sand dollar *Echinarachnius parma* (Echinodermata:Echinoidea:Clypeasteroida). *Zootaxa* 4052, 151–179. doi: 10.11646/zootaxa.4052.2.1

Zuccotti, L. F., Williamsom, M. D., Limp, W. F., and Ungar, P. S. (1998). Technical note: modeling primate occlusal topography using geographic information systems technology. *Amer. J. Phys. Anthropol.* 107, 137–142. doi: 10.1002/(sici)1096-8644(199809)107:1<137::aid-ajpa11>3.0.co;2-1

Conflict of Interest: The authors declare that the research was conducted in the absence of any commercial or financial relationships that could be construed as a potential conflict of interest.

frontiers in Ecology and Evolution

ORIGINAL RESEARCH
published: 11 May 2021
doi: 10.3389/fevo.2021.671006

Variation in Articular Cartilage Thickness Among Extant Salamanders and Implications for Limb Function in Stem Tetrapods

*Julia L. Molnar**

Department of Anatomy, New York Institute of Technology, College of Osteopathic Medicine, Old Westbury, NY, United States

The size and shape of articular cartilage in the limbs of extant vertebrates are highly variable, yet they are critical for understanding joint and limb function in an evolutionary context. For example, inferences about unpreserved articular cartilage in early tetrapods have implications for how limb length, joint range of motion, and muscle leverage changed over the tetrapod water-land transition. Extant salamanders, which are often used as functional models for early limbed vertebrates, have much thicker articular cartilage than most vertebrate groups, but the exact proportion of cartilage and how it varies across salamander species is unknown. I aimed to quantify this variation in a sample of 13 salamanders representing a broad range of sizes, modes of life, and genera. Using contrast-enhanced micro-CT, cartilage dimensions and bone length were measured non-destructively in the humerus, radius, ulna, femur, tibia, and fibula of each specimen. Cartilage correction factors were calculated as the combined thickness of the proximal and distal cartilages divided by the length of the bony shaft. Articular cartilage added about 30% to the length of the long bones on average. Cartilage was significantly thicker in aquatic salamanders (42 ± 14% in the humerus and 35 ± 8 in the femur) than in terrestrial salamanders (21 ± 7% in both humerus and femur). There was no consistent relationship between relative cartilage thickness and body size or phylogenetic relatedness. In addition to contributing to limb length, cartilage caps increased the width and breadth of the epiphyses by amounts that varied widely across taxa. To predict the effect of salamander-like cartilage correction factors on muscle leverage, a simplified model of the hindlimb of the Devonian stem tetrapod *Acanthostega* was built. In this model, the lever arms of muscles that cross the hip at an oblique angle to the femur was increased by up to six centimeters. Future reconstructions of osteological range of motion and muscle leverage in stem tetrapods and stem amphibians can be made more rigorous by explicitly considering the possible effects of unpreserved cartilage and justifying assumptions based on available data from extant taxa, including aquatic and terrestrial salamanders.

Keywords: early tetrapods, salamanders, cartilage, soft tissue, joint, muscle leverage, Acanthostega, water–land transition

OPEN ACCESS

Edited by:
Zerina Johanson, Natural History Museum (United Kingdom), United Kingdom

Reviewed by:
Pavel Skutschas, Saint Petersburg State University, Russia
Jürgen Kriwet, University of Vienna, Austria

***Correspondence:**
Julia L. Molnar
Julia.molnar@nyit.edu

Specialty section:
This article was submitted to Paleontology, a section of the journal Frontiers in Ecology and Evolution

Received: *22 February 2021*
Accepted: *19 April 2021*
Published: *11 May 2021*

Citation:
Molnar JL (2021) Variation in Articular Cartilage Thickness Among Extant Salamanders and Implications for Limb Function in Stem Tetrapods. Front. Ecol. Evol. 9:671006. doi: 10.3389/fevo.2021.671006

INTRODUCTION

Articular cartilage morphology in extant taxa has been used as a basis to infer the extent of unpreserved cartilage in fossils animals for the purpose of reconstructing joint and limb function (e.g., Hutchinson et al., 2005; Jannel et al., 2019; Tsai et al., 2020; Molnar et al., 2021). Articular cartilage seldom fossilizes, so its morphology in extant taxa may provide the best guide for reconstructing this tissue in extinct animals. Failure to account for unpreserved articular cartilage may result in underestimation of limb lengths and thus stride length and speed, as well as affecting joint congruence and thus posture and range of motion (Holliday et al., 2010). Furthermore, the amount of articular cartilage affects the relative position of muscle attachments, so assumptions about cartilage thickness will affect reconstructions of muscle leverage (Dao et al., 2020).

In the case of stem tetrapods, salamanders may provide the most informative extant model for articular cartilage. Salamanders are often used as models for limb-based locomotion in stem tetrapods because of their similar body proportions and amphibious lifestyle (Ashley-Ross, 2004; Kawano and Blob, 2013; Pierce et al., 2013). On a histological level, however, the analogy becomes more complicated, and some background in tetrapod bone development is necessary to understand the similarities and differences between and among the two groups. As in other vertebrates, ossification in the long bones of extant salamanders begins with a cartilaginous template, and bone is deposited around the periphery of the shaft (perichondral ossification), increasing the bone's diameter (Francillon-Vieillot et al., 1990). Simultaneously, the length of the bone is increased by periosteal bone deposited toward the epiphyses (Sanchez et al., 2010b). This epiphyseal cartilage hypertrophies and becomes calcified, and much of it is later resorbed to form the marrow cavity, which expands from the mid-shaft toward the epiphyses as the bone grows longer. Between the hypertrophic cartilage and the undifferentiated cartilage that will become the articular surface is a region of "seriated" or "stratified" cartilage in which the chondrocytes are organized in columns (Francillon-Vieillot et al., 1990). The erosion of the cartilage by the marrow forms a series of longitudinal projections called "marrow processes" within the hyptertrophic cartilage (Haines, 1942). Medullary trabecula following the same longitudinal pattern as the chondrocytes are formed by endochondral ossification (Haines, 1942).

Although the basic processes of endochondral ossification are similar among tetrapods, there are several differences in the epiphyses of salamanders, some of which are shared with early vertebrates. First, secondary ossification centers do not develop in salamanders or in vertebrates close to the tetrapod water–land transition, such as the tetrapodomorph fish *Eusthenopteron* (Sanchez et al., 2014) and the limbed tetrapodomorph *Acanthostega* (Sanchez et al., 2016), or even in many stem amniotes (Sanchez et al., 2008). This similarity between salamanders and stem tetrapods is important for soft tissue reconstruction because articular cartilages in adult long bones are much thicker in animals that develop secondary centers of ossification (mammals and lepidosaurs) than in turtles, crocodylians, and salamanders, which do not (Haines, 1942; Xie et al., 2020). Second, the columnar organization of the stratified cartilage is more pronounced in mammals and birds and less so in salamanders and turtles (Haines, 1942; Francillon-Vieillot et al., 1990), and in amphibians ossification does not occur in the stratified region (Estefa et al., 2021). Furthermore, in neotenic salamanders such as *Cryptobranchus* and *Proteus* the chondrocytes and the trabecula that replace them tend to be irregularly disposed without much organization at all (Haines, 1938, 1942). A similar condition was described in the facultatively neotenic, semi-aquatic newt *Pleurodeles waltl* (Quilhac et al., 2014). In contrast, a longitudinal arrangement of medullary trabecula has been described in stem tetrapods both with and without limbs (Sanchez et al., 2014, 2016; Kamska et al., 2018), suggesting that, like extant amniotes, their most likely mechanism of bone elongation is endochondral ossification of longitudinal columns of hypertrophic cartilage (Estefa et al., 2021). Third, in some neotenic salamanders such as *Proteus* endochondral ossification is minimal; the cartilage within the shaft persists, calcified cartilage is retained in the adult, and no primary medullary cavity is formed (Haines, 1938; Francillon-Vieillot et al., 1990). In this respect neotenic salamanders resemble stem tetrapods, which also lacked a central marrow cavity (Estefa et al., 2021).

Although bone structure in salamanders is well described, quantitative studies of articular cartilage in salamanders are rare. Descriptive studies of various species (von Eggeling, 1869; Klintz, 1912; Francis, 1934; Haines, 1938) illustrate ossified/calcified and cartilaginous epiphyses with a wide range of sizes, shapes and structures. Using contrast-enhanced micro-CT (DiceCT) to non-destructively visualize bone and cartilage morphology, I aimed to estimate variation among and identify correlates of articular cartilage thickness within extant salamanders. These results, in combination with fossil morphology, provide a basis for estimating how unpreserved articular cartilage affects reconstructions of joint range of motion and, particularly, muscle leverage in early limbed vertebrates.

MATERIALS AND METHODS

Specimens and Measurements

Salamander species were chosen to represent a wide range of genera (10), size (4.0–20.5 cm snout-vent length [SVL]), and mode of life (five aquatic, two semi-aquatic, and six terrestrial) (**Table 1**). All of the aquatic taxa were neotenic, having visible external gills and tailfins (Lynn, 1961; Wakahara, 1996), and all of the semi-aquatic and terrestrial taxa were fully metamorphosed. Seven specimens were scanned for this project, and an additional six DiceCT scans were downloaded from MorphoSource[1]. DiceCT was chosen because it provides much better contrast and resolution (very important for small specimens) than traditional methods for measuring cartilage thickness such as CT, ultrasound, and MRI, and it is less destructive than anatomical sectioning. Nevertheless, only museum specimens available for destructive testing were

[1] www.morphosource.org

TABLE 1 | Specimens and scanning.

Taxon			Specimen				Scanning		
Scientific name	**Adult habitat**	**Adult size/sexual maturity (cm)**	**Source**	**Number**	**SVL (cm)**	**Mass (g)**	**Source**	**Media ID**	**Resolution**
*Pleurodeles waltl**	Semi-aquatic (10)	11–30 total length (10)	AMNH	A-168418	3.7	2.21	NYIT		8.9
Bolitoglossa porrasorum	Terrestrial (3)	5.8–6.2 SVL (3)	UF	156522	4.4	-	MorphoSource	doi: 10.17602/M2/M43742	25.1
Hynobius nebulosus	Terrestrial (6)	4–7 SVL (6)	UF	24315	5.9	-	MorphoSource	ark:/87602/m4/M133947	22.1
Pseudotriton ruber	Aquatic and terrestrial (4)	5.5 SVL (4)	NYIT	MG-1257	6.1	6.56	NYIT		12.9
Plethodon cinereus	Terrestrial (4)	3.2–4.1 SVL (4)	AMNH	A-159522	4.0	1.02	NYIT		7.1-5.7
*Ambystoma tigrinum**	Terrestrial (not neotenic) (4)	7.6–16.5 SVL (2)	AMNH	FS-26619	6.6	11.81	NYIT		19.9
Ambystoma maculatum	Terrestrial (4)	5.6–7.8 SVL (4)	UF	26607	7.6	-	Morpho-source	ark:/87602/m4/M141549	35.3
Salamandra salamandra	Terrestrial (8)	9.4–10.6 total length (7)	AMNH	FS-26618	7.7	15.3	NYIT		27.9
Ambystoma mexicanum	Aquatic (3)	15–45 total length (9)	AMNH	A-144861	10.1	69.91	NYIT		27.1
Siren intermedia	Primarily aquatic (4)	15–18 SVL (4)	UF	123993	13.2	-	MorphoSource	ark:/87602/m4/M141555	46.8
Siren lacertina	Aquatic (4)	50–98 total length (5)	AMNH	A-171810	15.4	79.08	NYIT		25
Cryptobranchus alleganiensis	Aquatic (4)	30–40 total length (4)	UF	10881	16.0	-	MorphoSource	ark:/87602/m4/M67234	67.6
Necturus maculatus	Aquatic (4)	17.5–20 total length (4)	AMNH	FS-26617	20.5	123.62	NYIT		32.5-33.9

*References: 1 (Natis, 2018), 2 (Raffaëlli, 2014), 3 (Lannoo, 2005), 4 (Petranka, 1998), 5 (Goris and Maeda, 2005), 6 (Najbar et al., 2020), 7 (AmphibiaWeb, 2020), 8 (Helmenstine, 2020), and 9 (Joven et al., 2015). *indicates specimens with unilateral broken or missing limb(s). SVL, snout-vent length; AMNH, American Museum of Natural History; NYIT, New York Institute of Technology; UF, University of Florida. MorphoSource: University of Florida provided access to these data, the collection of which was funded by oVert TCN; NSF DBI-1701714. The files were downloaded from www.MorphoSource.org, Duke University.*

used because of concerns about damage resulting from the contrast staining procedure. All specimens had been preserved in ethanol. Specimens were stained by immersion in 9% potassium iodide solution for approximately 2 weeks (Metscher, 2009). After staining, they were imaged using a Skyscan 1173 high-energy desktop micro-CT scanner (www.skyscan.be) at 8–35 μm resolution. Scans were reconstructed in NRecon software[2].

Reconstructed scans were imported into Amira2020.2 software[3]. The contrast medium made it possible to visually distinguish between mineralized tissue, cartilage, and other soft tissues in the scans (**Figures 1A–D**). Proximal cartilage cap, bony shaft, and distal cartilage cap of each humerus, femur, radius, and ulna were semi-automatically segmented (in the two *Siren* species, only the forelimb elements were present) (**Figures 1E–H**). Length of each element was measured using the 3D measure tool in Amira (**Figure 1I**, **Table 2**). Some specimens had concave mineralized epiphyses with tapering cartilage cones that extended toward the marrow cavity (arrows in **Figures 1A,B**). In these specimens, measurements of cartilage thickness did not include the portion sheathed in bone because this portion would not affect the length of the limb element or the shape of its articular surface. However, cartilage within the shaft would affect the material properties of the limb. Measurements were taken bilaterally from the humerus and femur in specimens with four intact limbs (see **Table 1**). In addition, length of the long and short axes of the mineralized and cartilaginous epiphyses of the humerus and femur was measured unilaterally (**Figures 1J,K**).

Statistical Analysis

Statistical analyses were performed in SPSS version 27. Cartilage thickness as a percentage of bone length ("cartilage correction factor" or CCF, sensu Holliday et al., 2010) was calculated as the sum of the thickness of the proximal and distal cartilages divided by the length of the bony shaft (because it is a ratio, CCF is independent of body size). Taxa were coded as terrestrial, semi-terrestrial, or aquatic based on descriptions from the literature (**Table 1**).

Three hypotheses were tested: 1) mean cartilage correction factors for the humerus and femur are significantly different between aquatic and terrestrial taxa, 2) the humerus and femur contain a similar proportion of cartilage, and 3) mean cartilage correction factor is not correlated with body size. To test hypothesis 1, independent-samples *T*-tests were conducted with CCF as the test variable and habit (terrestrial or aquatic) as the grouping variable. To meet the assumption of independent samples, left and right limbs were averaged and the humerus and femur were analyzed separately. Semi-aquatic salamanders were excluded from this analysis because there were only two taxa; i.e., not enough for a robust test. To test hypothesis 2, an additional independent-samples *T*-test was conducted with CCF as the test variable and bone (humerus or femur) as the grouping variable. Parametric tests were used because samples

[2]www.microphotonics.com

[3]www.thermofisherscientific.com

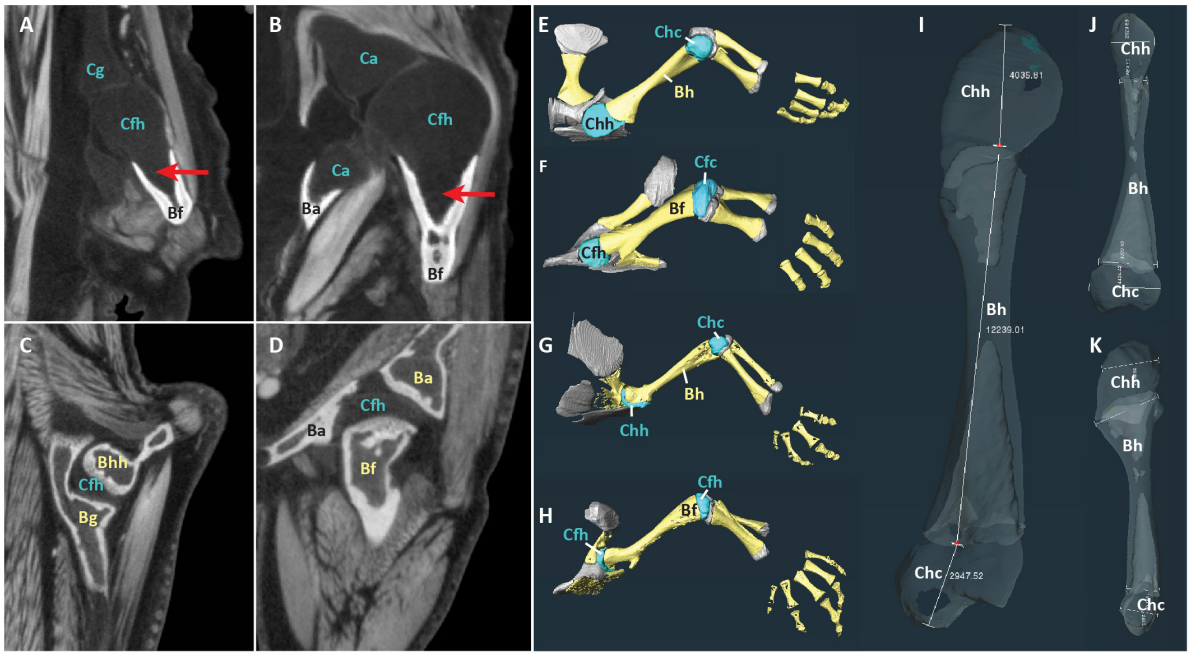

FIGURE 1 | Scans of representative aquatic and terrestrial salamanders showing morphological differences and measurement methods. **(A–D)** DiceCT slices through shoulder **(A)** and hip **(B)** joints of the aquatic salamander *Necturus maculatus* and the shoulder **(C)** and hip **(D)** joints of the terrestrial salamander *Pseudotriton ruber*. Red arrows show cartilage cones within bony shaft. **(E–H)** 3-D surfaces of bones (yellow) and cartilages (blue and gray) in the forelimb of *N. maculatus* **(E)**, the hindlimb of *N. maculatus* **(F)**, the forelimb of *P. ruber* **(G)**, and the hindlimb of *P. ruber* **(H)** (carpals not shown). **(I–K)** Humerus of *N. maculatus* showing linear measurements in μm of cartilage thickness and bony shaft **(I)** and the long and short axes of the mineralized and cartilaginous epiphyses **(J,K)**. Abbreviations: bony acetabulum (Ba), bony femoral shaft (Bf), bony glenoid (Bg), bony humeral shaft (Bh), cartilaginous acetabulum (Ca), cartilaginous femoral condyles (Cfc), cartilaginous femoral head (Cfh), cartilaginous glenoid (Cg), cartilaginous humeral condyles (Chc), cartilaginous humeral head (Chh).

within each group did not violate the assumptions of normality (assessed using Shapiro–Wilk test). Significance levels were adjusted appropriately if data violated the assumption of equal variance under Levene's Test. To test hypothesis 3, a Pearson product-moment correlations coefficient was computed to assess the relationship between CCF in the humerus and femur and snout-vent length.

Testing for Phylogenetic Signal

Ancestor reconstruction was performed in Mesquite 3.6[4] using the maximum parsimony method and a time-calibrated phylogeny from TimeTree (timetree.org; Hedges et al., 2006). Seven characters were traced: average CCF for humerus and femur and individual CCFs for humerus, femur, radius, ulna, tibia, and fibula. The "phylosig" function in R (Revell, 2012) was used to test for phylogenetic signal in average CCF for the humerus and femur. A second test was conducted using alternative divergence times (Marjanoviæ and Laurin, 2014).

Moment Arm Analysis

To predict the effect of unpreserved articular cartilage on reconstructions of muscle leverage, two-dimensional muscle moment arms were calculated using a custom script in MATLAB[5] (**Supplementary Table 1**). The inputs were CCF and XY coordinates of the origin and insertion of each muscle relative to the joint center of rotation. For simplicity, the limb was assumed to be in a horizontal position. Outlines of the pelvis and femur of the stem tetrapod *Acanthostega* (Coates, 1996) were added for visualization purposes. *Acanthostega* was chosen because it is, along with *Ichthyostega*, the earliest limbed vertebrate represented by extensive post-cranial material (Clack, 2012), and because limb range of motion and muscle leverage have been reconstructed in this animal (Dao et al., 2020; Molnar et al., 2021). Basic graphing functions were used to calculate the moment arm: first, the equation of a line representing the muscle's line of action relative to the joint center (set at the origin of the plot) was calculated, then a line was plotted perpendicular to the line of action and passing through the origin, and finally the distance between the origin and the intercept of the two lines (the moment arm). The insertion point was adjusted by the CCF, and the moment arm calculation was repeated. The muscles used in this example are abstractions used to demonstrate the range of effect sizes. However, the same code could be used to predict the effects of a particular CCF on a biologically realistic muscle using origin and insertion coordinates from an anatomically accurate illustration or model.

[4] mesquiteproject.org

[5] mathworks.com

TABLE 2 | Measurements of cartilage thickness and bony shaft length taken from humerus and femur (μm) and calculated percentage of humerus or femur length composed of cartilage.

Species	Humerus				Femur			
	Proximal cartilage	Distal cartilage	Bony shaft	CCF	Proximal cartilage	Distal cartilage	Bony shaft	CCF
Ambystoma maculatum	370	720	8,930	12.2%	720	280	8,990	11.1%
	350	600	9,030	10.5%	710	340	8,930	11.8%
Ambystoma mexicanum	1774.37	1438.27	13204.18	24.3%	2248.86	1307.71	13992.4	25.4%
	1795.32	1310.64	13037.12	23.8%	2311.5	1277.75	13935.68	25.8%
Ambystoma tigrinum	1365.61	1066.72	10110.05	24.1%	1275.82	836.35	8513.98	24.8%
	-	-	-		-	-	-	
Bolitoglossa porrasorum	420	1,020	4,550	31.6%	580	950	4,620	33.1%
	390	940	4,570	29.1%	570	860	4,680	30.6%
Cryptobranchus alleganiensis	3,150	3,150	12,730	49.5%	2,980	1,970	14,020	35.3%
	2,990	3,290	12,900	48.7%	2,520	2,460	13,160	37.8%
Hynobius nebulosus	560	530	6,640	16.4%	480	350	6,190	13.4%
	480	650	6,600	17.1%	600	340	6,250	15.0%
Necturus maculatus	4035.81	2947.52	12239.01	57.1%	3683.7	1838.98	13288.84	41.6%
	3846.77	2862.33	12091.66	55.5%	3583.38	1972.53	13457.88	41.3%
Plethodon cinereus	71.23	441.74	2954.41	17.4%	308.45	327.45	3077.7	20.7%
	72.89	456.34	2930.93	18.1%	311.57	306.11	3090.32	20.0%
Pleurodeles waltl	931.88	1542.45	4732.74	52.3%	719.47	1289.93	4599.83	43.7%
	-	-	-		-	-	-	
Pseudotriton ruber	332.7	889.09	5567.48	21.9%	451.74	605.3	6312.44	16.7%
	283.4	914.86	5566.26	21.5%	461.65	605.57	6220.99	17.2%
Salamandra salamandra	815.45	1877.5	10911.9	24.7%	1358.82	948.22	11017.1	20.9%
	870.27	1756.52	11000.66	23.9%	1485.07	1000.03	10766.16	23.1%
Siren intermedia	1,200	1,210	4,720	51.1%	-	-	-	-
	1,240	1,120	4,720	50.0%	-	-	-	-
Siren lacertina	1520.28	1335.4	8701.9	32.8%	-	-	-	-
	1309.08	1258.89	8861.18	29.0%	-	-	-	-

RESULTS

Among the taxa measured, articular cartilage added approximately 25–30% to the length of the humerus and femur on average (**Figure 2**). Cartilage made up a similar proportion of the distal limb bones (radius, ulna, tibia, and fibula). Relatively thicker cartilage caps were found in larger, more aquatic taxa, whereas phylogenetic relatedness did not predict relative cartilage thickness. The unexpected finding of thicker cartilage in larger taxa likely is related to the correlation of large body size with aquatic mode of life. Differences between forelimb and hindlimb and between proximal and distal cartilages were relatively small (about 5% on average), and the magnitude and direction of these differences were inconsistent across taxa (**Table 2**). In addition to contributing to the length of the humerus and femur, cartilages increased the dimensions of the articular surfaces in most salamanders.

Qualitative Results

Articular cartilage was visible in both ends of each long bone and, in some specimens, at the tip of the greater trochanter of the femur (**Figure 2**). Two different epiphyseal structures were identifiable: one with concave mineralized epiphyses in which the cartilage cap continued toward the midpoint of the shaft, and one with flat or convex epiphyses in which the cartilage cap was clearly separated from the marrow cavity (compare **Figures 1A–D**). The first type was mainly found in aquatic taxa with relatively thick cartilage (*N. maculatus*, *C. alleganiensis*, *P. waltl, S. lacertina*, and *S. intermedia*).

Differences Within Individuals

The humerus contained slightly more cartilage than the femur on average, but the difference was not statistically significant (**Figure 3**, **Table 2**). The 13 humeri (M = 31.4%, SD = 15.3%) compared to the 11 femora (M = 26.3%, SD = 10.8%) had non-significantly thicker articular cartilage, $t(22) = 0.94$, $p = 0.184$. In six taxa the cartilages in the humerus were noticeably thicker (particularly *Cryptobranchus*, which had unusually thick cartilages on the distal end of the humerus), and in five taxa the cartilages in the femur were slightly thicker (**Figure 2**, **Table 2**). Thickness of proximal and distal cartilage caps (humeral condyles) was similar on average, except that the distal caps on the humerus were slightly thicker than in the other three locations ($17.5 \pm 7.5\%$ versus $12.3 \pm 14.0\%$; **Table 2**). Individual taxa showed much greater differences; for example, in the femur of *Necturus maculatus* the proximal cartilage caps were twice as

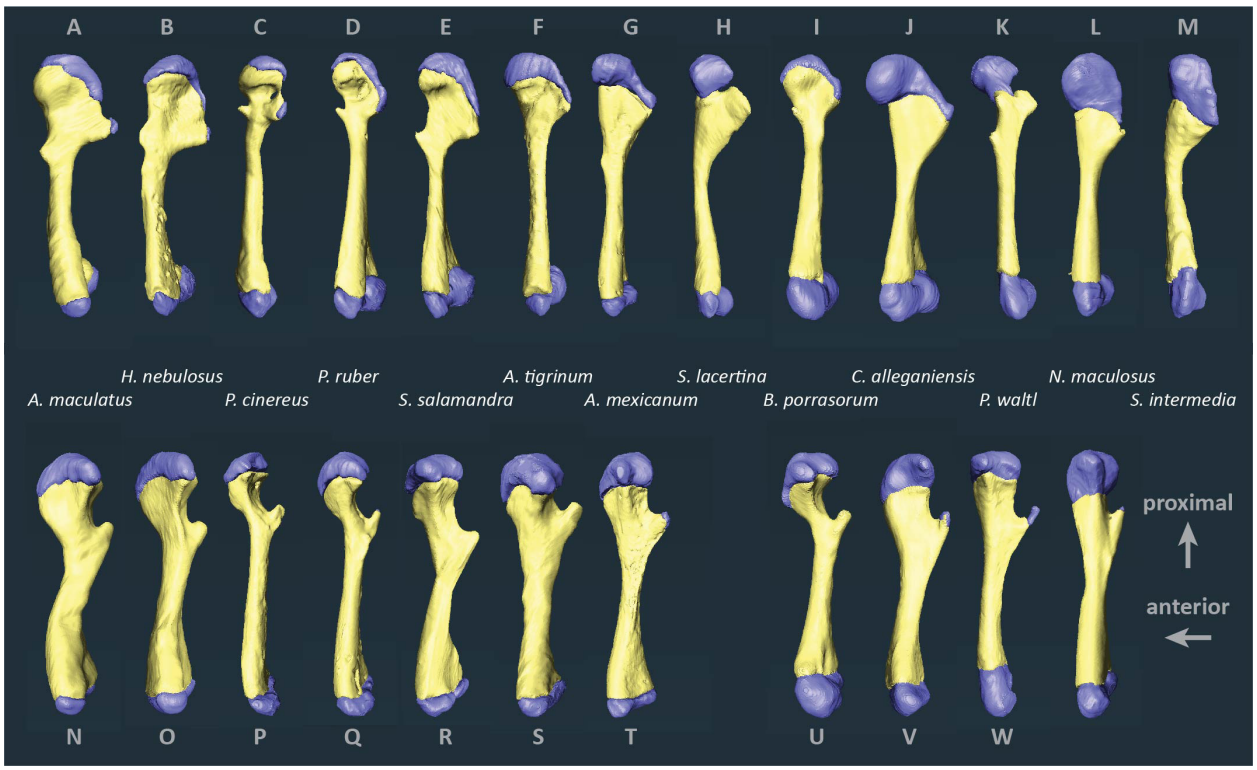

FIGURE 2 | Segmented humeri and femora of scanned salamanders showing mineralized and cartilaginous elements. Surface renderings of left humeri **(A–M)** and left femora **(N–X)** in dorsal view showing bone (yellow) and cartilage (blue). Taxa are ordered by average cartilage correction factor in the humerus and femur (total cartilage thickness divided by length of the bony shaft), with the smallest factor on the left (*A. maculatum,* 11.4%) and the largest on the right (*S. intermedia*, 50.5%).

thick as the distal caps, whereas in the humerus of *Plethodon cinereus* the distal cartilages were six times as thick as the proximal ones (**Figure 2**, **Table 2**). Some left-right asymmetry was observed: 5–8% in the thickness of cartilage caps, but only 1–2% in the bony shafts (**Table 2**). This discrepancy may indicate a biological difference or it may reflect measurement error, segmentation error, and/or cartilage deformation in preserved specimens. However, because CCF is expressed as a percentage of the length of the shaft, even a 10% difference in cartilage thickness would change CCF by only about 3–5%.

The distal elements contained a similar proportion of cartilage to the humerus and femur. Among the limb bones, the thickest articular cartilage was found in the proximal end of the ulna where it made up most of the olecranon process (27.9% bone length on average; **Table 3**). The thinnest cartilages on average were found in the proximal ends of the radius and tibia (8.7–10.1%). Because of the large olecranon cartilage, the cartilage correction factor was greatest in the ulna (44.1% bone length on average versus 25–29% in the radius, tibia, and fibula).

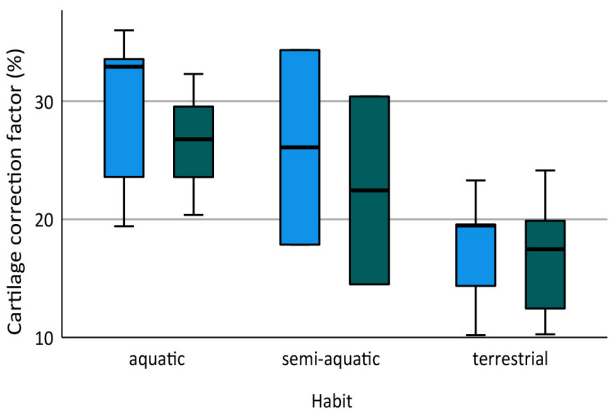

FIGURE 3 | Box plot showing cartilage correction factors (CCF) for the humerus and femur in aquatic, semi-aquatic, and terrestrial salamanders. CCF was calculated as the sum of the proximal and distal cartilage thickness divided by the length of the bony shaft.

Body Size and Terrestriality

Aquatic salamanders had significantly thicker articular cartilage in the humerus and femur than terrestrial salamanders (**Figure 3**). In the humerus, the five aquatic salamanders (M = 42.2%, SD = 13.9%) compared to the six terrestrial salamanders (M = 20.7%, SD = 6.8%) had significantly thicker articular cartilage, $t(6) = 3.2$, $p = 0.022$ (equal variances not assumed). In the femur, the three aquatic salamanders with hindlimbs (M = 34.5%, SD = 8.1%) compared to the six terrestrial salamanders (M = 20.8%, SD = 7.4%) had significantly

TABLE 3 | Measurements of cartilage thickness and bony shaft length taken from radius, ulna, tibia, and fibula (μm) and calculated cartilage correction factors for each bone (CCF).

Species	Radius			Ulna			Tibia			Fibula		
	Proximal cartilage	Bony shaft	Distal cartilage	Proximal cartilage	Bony shaft	Distal cartilage	Proximal cartilage	Bony shaft	Distal cartilage	Proximal cartilage	Bony shaft	Distal cartilage
Ambystoma maculatum	0	4,250	360	410	5,710	420	220	5,310	380	200	5,170	420
Ambystoma mexicanum	801.83	7478.12	518.44	799.16	7068.53	314.2	519.25	8939.05	956.5	913.17	7829.97	791.32
Ambystoma tigrinum	406.57	5326.73	632.55	1022.28	6118.79	502.04	487.32	5071.31	1130.92	763.84	4905.63	488.81
Bolitoglossa porrasorum	240	2,870	500	600	2,810	510	350	2,880	530	480	2,820	460
Cryptobranchus alleganiensis	780	6,250	1,560	3,260	6,060	1,170	1,260	7,100	1,790	1,060	6670	1860
Hynobius nebulosus	140	3,340	430	740	3,680	380	210	3,710	240	370	3,360	410
Necturus maculatus	612.49	5963.49	896.71	2763.62	6303.57	928.72	962.09	5649.33	894.47	878.86	5383.92	791.13
Plethodon cinereus	50.93	1683.86	264.23	168.35	1749.13	182.26	103.39	1811.57	249.46	96.41	1790.98	208.91
Pleurodeles waltl	223.35	2311.99	726.27	1027.87	2304.02	592.77	457.53	2174.14	494.18	618.47	2201.51	663.23
Pseudotriton ruber	158.08	3146.07	662.53	472.88	2967.95	468.44	229.48	3533.1	498.76	431.24	3388.58	367.4
Salamandra salamandra	339.2	6205.67	880.66	1489.92	5910.92	943.32	429.45	5690.47	633.11	714.73	5432.4	819.66
Siren intermedia	540	2,010	770	1,260	2,310	540						
Siren lacertina	456.64	4216.73	942.49	1805.89	4249.25	981.96						
Average	365.31	4234.82	703.38	1216.92	4403.24	610.29	475.32	4715.36	708.85	593.34	4450.27	661.86

thicker articular cartilage, $t(7) = 2.6$, $p = 0.037$. The thickest cartilages (>45% bone length) were found in large aquatic salamanders: the mudpuppy *N. maculatus* (41.3–57.1%), the limb-reduced *S. intermedia* (50.0–51.1% in the forelimb), the giant salamander *C. alleganiensis* (35.3–49.5%), and the semi-aquatic newt *P. waltl* (43.7–52.3%) (**Table 2**). Qualitatively, the salamanders with the thickest cartilage (*N. maculatus*, *C. alleganiensis*, *P. waltl*, and both *Siren* species) lacked ossified or calcified epiphyses, and cones of cartilage extended deep to the cortical bone within the diaphysis (see **Figures 1A,B**). The thinnest cartilages (<22%) were found in the small to medium-sized terrestrial salamanders *A. maculatum* (10.5–12.2%), *H. nebulosus* (13.4–17.1%), *P. cinereus* (16.5–20.7%), and *P. ruber* (16.7–21.9%). Intermediate amounts of cartilage (23–35%) were found both in aquatic salamanders (*A. mexicanum* [23.8–25.8%] and *S. lacertina* [29.0–32.8%]) and terrestrial salamanders (*S. salamandra* [20.9–25.1%], *A. tigrinum* [24.1–24.8%], and *B. porrasorum* [29.1–33.1%]).

A similar relationship between cartilage thickness and terrestriality was found in the radius, ulna, tibia, and fibula. The thickest cartilages were found in *S. intermedia* (71.5% bone length), *P. waltl* (53.4%), *S. lacertina* (49.4%), *C. alleganiensis* (49.3%), and *N. maculatus* (36.9%) and the thinnest in *A. maculatum* (11.6%), *A. mexicanum* (17.9%), *P. cinereus* (18.8%), and *H. nebulosus* (20.7%). The most notable difference was *S. lacertina*, which had an intermediate proportion of cartilage in the humeri (similar to *B. porrasorum*) but a large proportion in the radius and ulna (similar to *C. alleganiensis*).

Because aquatic salamanders tend to be larger, it is difficult to examine the effects of body size separately from mode of life. Cartilages were thicker in larger salamanders in this study (a positive correlation between CCF and SVL), and the correlation was statistically significant in the humerus ($r = 0.577$, $n = 13$, $p = 0.036$) though not in the femur ($r = 0.499$, $n = 11$, $p = 0.118$). However, the effect disappeared when salamanders were separated by mode of life: among aquatic salamanders there was a positive correlation between SVL and relative cartilage thickness, but among terrestrial and semi-aquatic salamanders the correlation was negative (**Figure 4**). Within the sample there was no overlap in size between aquatic salamanders (>10 cm SVL) and terrestrial salamanders (<8 cm SVL). Because mode of life was a far better predictor of cartilage thickness than body size was, and because there is no reason to expect that larger animals would have thicker cartilages, the most likely explanation is that the positive relationship between body size and CCF is an artifact of the relationship between body size and mode of life. A larger, more extensive sample would be required to verify or exclude a relationship between relative cartilage thickness and body size.

Phylogenetic Relatedness

No phylogenetic signal was detected in the average CCFs for the humerus and femur (Blomberg's $K = 0.271$, $p = 0.355$), and no phylogenetic pattern was apparent in the ancestor reconstruction (**Figure 5**). Large variations were present within genera: among the three *Ambystoma* species, cartilage correction factors in the humerus and femur ranged from very small in *A. maculatum* (11.4%) to medium in *A. mexicanum* and

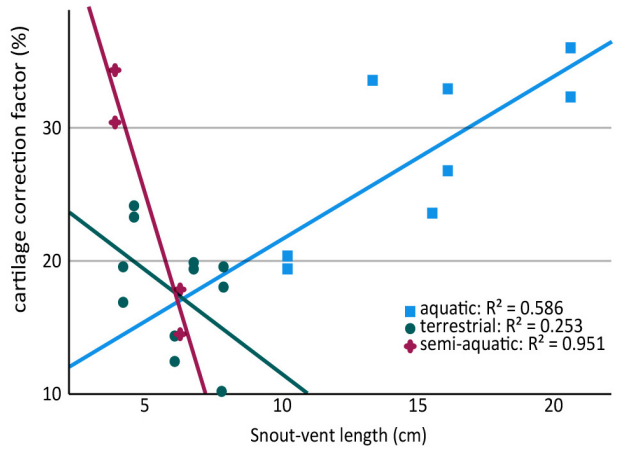

FIGURE 4 | Scatter plot showing relationship between snout-vent length (SVL) and cartilage thickness in the humerus and femur of aquatic, semi-aquatic, and terrestrial salamanders. There is a positive relationship between cartilage thickness and SVL in aquatic salamanders and a negative relationship in semi-aquatic and terrestrial salamanders. Note that there are two data points per specimen (humerus and femur).

A. tigrinum (24.4–24.8%), and between the two *Siren* species from medium in *S. lacertina* (30.9%) to large in *S. intermedia* (50.1%). Ancestor reconstruction showed intermediate values at the nodes leading to the three major clades: Cryptobranchoidea (30.7%), Salamandroidea (31.8%), and Sirenidae (40.6%) (**Figure 5**). Separate ancestor reconstructions on each individual bone yielded similar results (**Supplementary Data Sheet 1**). A second analysis using divergence times from a more recent timetree (Marjanoviæ and Laurin, 2014) also failed to detect a phylogenetic signal (Blomberg's $K = 0.259$, $p = 0.309$).

Dimensions of Articular Surfaces

The dimensions of the cartilaginous epiphyses were greater than their mineralized (ossified or calcified) equivalents in most cases, and in many their proportions were substantially different. Like the thickness of articular cartilages, the magnitude of the differences between dimensions of cartilaginous and mineralized epiphyses appear to be related to mode of life. The smallest cartilage correction factors on average (<15%) were found in semi-aquatic and terrestrial salamanders (*A. maculatum*, *H. nebulosus*, *P. ruber*, and *P. cinereus*) and the largest (>30%) were found in aquatic and semi-aquatic ones (*P. waltl and N. maculatus*). There were also noticeable differences between the humerus and femur, and between the proximal and distal cartilages. In the humerus, the cartilaginous epiphyses were more spherical than their mineralized counterparts: cartilage added 24.8–27.8% on average to the short axes of the humeral head and condyles but only 11.1–17.4% to their long axes (**Table 4**). In the femur the average increase was similar in both dimensions, resulting most commonly in an increase in size without a change in shape. However, in the femur there was a big difference in CCF between the femoral head and the condyles (+29.8% versus +13.9% on average). There was a lot of variation within each group and quite a bit of overlap between aquatic and terrestrial taxa, so it would be difficult to predict the shape of articular cartilage based on mineralized epiphyses in salamanders.

DISCUSSION

Salamanders often are used as extant models for early limbed vertebrates, so the range, variability, and correlates of articular cartilage thickness in salamanders will affect inferences about limb function over the tetrapod water–land transition. Because ossification of the tetrapod postcranial skeleton is thought to be functionally related to gravitational forces encountered during terrestrial locomotion (e.g., Carter et al., 1998), and because the effect of gravity scales proportionally with body mass, I predicted that the percentage of cartilage would be greater in smaller and more aquatic salamanders. This prediction was partially borne out by the data: no consistent relationship was observed between cartilage thickness and size (quantified by snout-vent length), but the proportion of cartilage was significantly greater in aquatic salamanders than terrestrial ones. No obvious phylogenetic pattern was observed. The results were applied to a mathematical model of the hip joint of a limbed Devonian tetrapodomorph, demonstrating that salamander-like articular cartilage would have substantially increased the leverage of muscles that cross the hip at an oblique angle to the femur. These results emphasize the importance of articular cartilage for reconstruction of limb length, range of motion, and muscle leverage in extinct tetrapods such as early salamanders and stem tetrapods and provide an empirical starting point to account for these effects.

Limitations

Much of the observed variation in articular cartilage thickness could not be explained by terrestriality alone. For example, the Spotted Salamander *A. maculatum* had much less cartilage in the humerus and femur than the other terrestrial taxa (only about 10% of each element). To my knowledge, there is nothing about the species or specimen to suggest that it should have an unusually small amount of cartilage. Another member of the genus, the Axolotl *A. mexicanum*, also had much less cartilage in the humerus and femur than would be predicted by mode of life (19–21%, compared with an average of 35–42% among all aquatic salamanders). It is possible that these results reflect a small phylogenetic effect that is masked by mode of life, and that *Ambystoma* species tend to have relatively less cartilage than other genera. Alternatively, the relatively thin cartilage in *A. mexicanum* may be attributed to metamorphic plasticity in this species: unlike the other "aquatic" taxa in this sample, metamorphosis can be hormonally induced in *A. mexicanum* (Wakahara, 1996). In addition, relative cartilage thickness was very different between the two semi-aquatic species: with a CCF of 44–52% in the humerus and femur, the Iberian Ribbed Newt *P. waltl* falls in the middle of the range of aquatic salamanders, whereas the Red Salamander *P. ruber*, at 17–22%, falls in the middle of the range of terrestrial salamanders. However, the unexpectedly large CCF in *P. waltl* might be explained by sexual maturity (see below). Finally, although the two species

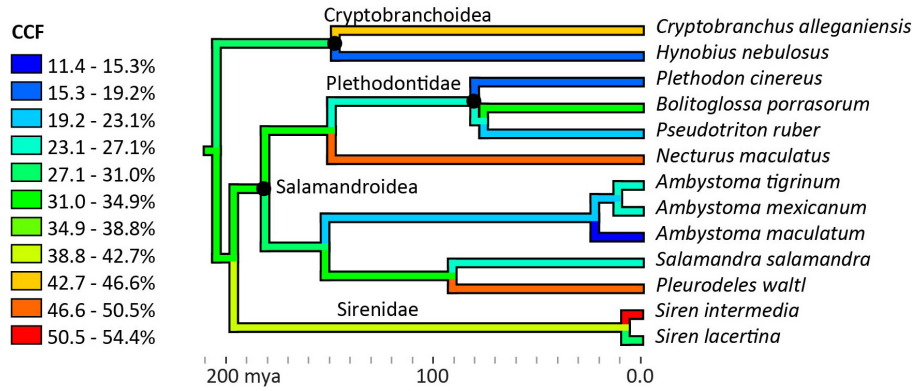

FIGURE 5 | Ancestor reconstruction of cartilage correction factors using maximum parsimony. Time calibrated phylogeny from Timetree.org (Hedges et al., 2006). A test for phylogenetic signal in the data was non-significant (Blomberg's $K = 0.271$, $p = 0.355$). See SI for individual ancestor reconstructions on cartilage correction factors in the humerus, femur, radius, ulna, tibia, and fibula.

TABLE 4 | Dimensions of cartilaginous epiphyses compared to mineralized epiphyses. Values represent the percentage increase in long and short axes of the cartilaginous epiphyses over the mineralized epiphyses.

Species	Humeral head		Humeral condyles		Femoral head		Femoral condyles	
	Long axis	Short axis	Long axis	Short axis	Long axis	Short axis	Long axis	Short axis
Ambystoma maculatum	0.0%	0.0%	0.3%	7.6%	11.5%	11.5%	1.0%	0.0%
Ambystoma mexicanum	23.0%	46.4%	−1.0%	36.5%	40.1%	51.8%	6.7%	−8.8%
Ambystoma tigrinum	16.1%	19.9%	1.8%	31.1%	31.2%	37.7%	13.5%	5.2%
Bolitoglossa porrasorum	15.1%	0.0%	17.5%	19.5%	36.2%	26.0%	14.8%	53.8%
Cryptobranchus alleganiensis	28.5%	60.5%	1.2%	29.3%	51.0%	10.9%	17.6%	0.8%
Hynobius nebulosus	9.4%	21.2%	−2.1%	14.6%	14.5%	17.6%	3.7%	3.2%
Necturus maculatus	29.7%	55.1%	18.9%	24.7%	55.7%	63.5%	14.2%	−0.7%
Plethodon cinereus	0.0%	0.0%	3.1%	20.5%	4.9%	20.8%	18.1%	32.7%
Pleurodeles waltl	40.0%	65.2%	84.3%	61.7%	7.2%	34.0%	61.3%	18.2%
Pseudotriton ruber	17.3%	3.2%	−0.7%	4.8%	14.2%	17.1%	8.5%	26.7%
Salamandra salamandra	−0.1%	9.5%	4.6%	47.1%	42.0%	56.2%	10.5%	4.4%
Siren intermedia	26.6%	31.1%	16.9%	−2.3%	-	-	-	-
Siren lacertina	21.0%	49.0%	0.1%	26.7%	-	-	-	-
Average	17.4%	27.8%	11.1%	24.8%	28.0%	31.6%	15.5%	12.3%

are closely related and very similar in morphology and ecology, relative cartilage thickness was much greater in the lesser siren *S. intermedia* than in the greater siren *S. lacertina* (51% versus 31% in the humerus). The large variation present within extant salamanders increases the uncertainty of cartilage reconstruction in their extinct relatives.

The study was not designed to examine the effects of sexual maturity on cartilage thickness, but, because the process of cartilage erosion and bone deposition continues until adulthood (Sanchez et al., 2010b), it is likely that immature specimens have a greater percentage of cartilage. Similarly, negative allometry of cartilage thickness across ontogeny has been demonstrated in the long bones of *Alligator* (Holliday et al., 2010) and frogs (e.g., Erismis and Chinsamy, 2010). Two specimens, the terrestrial Pijol Salamander *Bolitoglossa porrasorum* and the semi-aquatic Iberian News *Pleurodeles waltl*, were substantially smaller than average length at sexual maturity (**Table 1**), and both had unusually large cartilage correction factors in the humerus and femur for their mode of life (30.4–31.8% and 44–52%, respectively). However, excluding *B. porrasorum* from the analysis did not change the result that mean CCF is significantly larger in aquatic salamanders: the differences between aquatic and terrestrial salamanders were still significant, with marginally larger effect sizes (t = 3.4–3.5 versus 2.6–3.2) and smaller p-values (p = 0.015–0.016 versus 0.022–0.037) (*P. waltl* was not included in either analysis because it is classed as semi-aquatic). An additional specimen, the California Giant Salamander *Dicamptodon ensatus*, fell within the range of adult lengths but was excluded from the analysis because it retained a remnant of external gills and thus, as a facultative neotenic species (Wakahara, 1996), it could not be classified confidently as aquatic or terrestrial. This specimen had extraordinarily thick cartilage caps (97% in the humerus and 121% in the femur)

(Dao et al., 2020). An examination of larvae, juveniles, and adults of known age and reproductive status would be necessary to test the relationship between sexual maturity and cartilage thickness in salamanders.

Another limitation of the dataset is the relatively sparse sampling at the upper end of the body size range. The sample was restricted to specimens that were available for destructive testing from local museums or from colleagues, plus DiceCT scans available on Morphosource.com. The largest salamander in the sample is *C. alleganiensis* (16 cm SVL), but this species can reach 40 cm SVL (Petranka, 1998; Raffaëlli, 2014). The largest extant salamanders are the Chinese and Japanese Giant Salamanders (*Andrias davidianus* and *A. japonicus*, respectively), and males of these species can reach 102 cm total length (comparable to the Devonian stem tetrapod *Acanthostega*), though the average size of adults is much smaller (Kawamichi and Ueda, 1998). Unfortunately, large *Andrias* specimens are rare and none were available for DiceCT. However, a micro-CT scan without contrast reveals that, like those of *Cryptobranchus* and other aquatic neotenic salamanders, the mineralized portions of the humerus and femur in *Andrias japonicus* are concave at either end, presumably accommodating large cartilage cones (specimen from Florida Museum of Natural History, Amphibians and Reptiles: 31536; ark:/87602/m4/M77893; www.MorphoSource.org, Duke University). Therefore, a 30–50% CCF would be expected in *Andrias*, similar to the other aquatic salamanders. In addition to extra-large aquatic salamanders, the dataset lacks very large terrestrial salamanders. The largest terrestrial salamander in the sample is *S. Salamandra* at 7.7 cm SVL, although this species can reach 20–30 cm total length (Raffaëlli, 2014). A specimen was acquired of the largest terrestrial salamander, the California Giant Salamander *Dicamptodon ensatus*, but, as explained above, it was excluded because it was incompletely metamorphosed. As DiceCT becomes more broadly available, future studies with greater sampling of large body sizes will be able to test whether or not the correlation between relative cartilage thickness and SVL is an artifact of the tendency toward larger body sizes in aquatic salamanders.

The girdles of salamanders contain varying amounts of cartilage, which was not measured for this study. Some, such as the Common Mudpuppy *N. maculatus*, have completely cartilaginous glenoids and acetabula, while others, such as the Red Salamander *P. ruber*, have bony glenoids and acetabula covered by a very thin layer of articular cartilage (**Figures 1A–D**). The cartilaginous component of the girdles would have little effect on limb length but a large effect on range of motion because in salamanders like *N. maculatus* cartilage makes up the entire glenoid and acetabulum. In addition, cartilaginous parts of the girdles provide the origins of muscles that attach to the limbs in all taxa (e.g., the cartilaginous suprascapula forms the origin of m. dorsalis scapulae [deltoideus]; Francis, 1934).

Comparison to Other Tetrapods

The epiphyseal structure of salamanders is unique among extant tetrapods, and articular cartilage makes up a larger proportion of the length of long bones in salamanders than in any other tetrapod reported thus far. Mammals and lepidosaurs develop secondary centers of ossification and have very thin articular cartilage (Haines, 1942). Archosaurs and turtles do not have secondary ossification centers, but their epiphyses contain bony protrusions which play a similar mechanical role (Xie et al., 2020). Some frogs have epiphyses formed from calcified cartilage (Haines, 1942; Carter et al., 1998). Differences in the structure and composition of epiphyses are thought to relate to the presence or absence of mechanical stresses imposed by rapid growth in a terrestrial environment (Xie et al., 2020).

The humeri of salamanders have a cartilage correction factor almost four times as large as that of American Alligators, which have the greatest proportion of cartilage reported among archosaurs (31 $\pm$ 15% versus 8 $\pm$ 3%) (Holliday et al., 2010). In the femur, CCF was 26 $\pm$ 10% in salamanders compared to 6 $\pm$ 2% in alligators. The disparity was even more pronounced in the distal limb bones: average CCF in the radius, ulna, tibia, and fibula among the salamanders in this study ranged from 26 to 44%, while in alligators it ranged from 5 to 9%. Unlike in salamanders, the ulna in alligators did not have a particularly large CCF compared to the other long bones. Effect on width and breadth of epiphyses were comparable between the two groups. For example, articular cartilage added 13–27% to the craniocaudal and mediolateral dimensions of the humeral head in alligators (Holliday et al., 2010) and 17–28% to the corresponding dimensions (long and short axes, respectively) in salamanders. For comparison, in adult ostriches the CCF was only 2% in length of the humerus and 9–11% in the humeral head (Holliday et al., 2010).

Implications for Fossil Reconstruction

In addition to physical constraints, data from extant animals are one of the most valuable resources for placing bounds on uncertainty about unpreserved attributes (Witmer, 1995; Hutchinson, 2011). For example, the range of cartilage thickness in extant salamanders provides a reasonable starting point for estimating cartilage thickness in early limbed tetrapodomorphs because the two groups are similar in body proportions, mode of life, and, to some extent, the structure of the mineralized portions of their epiphyses. Even more valuable are data from extant animals within a phylogenetic context combined with osteological correlates in fossils ("extant phylogenetic bracket"; Witmer, 1995). Though beyond the bounds of the current study, identifying and tracing osteological correlates of various cartilage thicknesses in stem amphibians and stem amniotes would strengthen inferences about articular cartilage in stem tetrapods. Potential correlates of thick articular cartilage have been identified in extinct archosaurs, including rough, weakly convex articular surfaces that are not congruent with each other (Holliday et al., 2010; Tsai et al., 2020).

Relative cartilage thickness was very different between aquatic and terrestrial salamanders in this study, raising the question, which group is a better model for the first vertebrates with limbs? In many ways the aquatic group seems most appropriate because Devonian tetrapodomorphs with limbs such as *Acanthostega* and *Ichthyostega* probably were fully aquatic and shared features with neotenic salamanders such as functional gills and a large tail fin

(Coates and Clack, 1991; Clack and Coates, 1995; Clack et al., 2003). Like aquatic salamanders, stem tetrapods lacked a central marrow cavity (Estefa et al., 2021), possibly reflecting their habits; aquatic animals may benefit from having a larger amount of cartilage because cartilage is less brittle than bone and thus less likely to fracture, or because it is metabolically less costly to maintain (Haines, 1942), whereas a complete medullary cavity is thought to help accommodate the torsional loads incurred during terrestrial locomotion (Sanchez et al., 2010a). However, the unusual histological organization of the long bones of neotenic salamanders (described in the introduction) is thought to be a derived feature within urodeles (Haines, 1938, 1942). In contrast, the epiphyses of *Dicynodon* (a therapsid from the Upper Permian (Kammerer et al., 2011) contain a regular, radiate arrangement of bony trabecula similar to that found in turtles, crocodiles, and (to a lesser extent) in terrestrial salamanders, which Haines (1938, 1942) identified as the ancestral tetrapod condition. Recent work on *Acanthostega* and the closely related fishes *Eusthenopteron* and *Hyneria* describes a similar structure, with tubular marrow processes at the base of their epiphyses (Sanchez et al., 2014, 2016; Kamska et al., 2018). Therefore, even aquatic tetrapodomorphs may have had epiphyseal morphology and relative cartilage dimensions more like those of extant terrestrial salamanders, or even amniotes such as turtles and crocodiles (Haines, 1938; Estefa et al., 2021).

These results inform predictions about articular cartilage thickness in extinct animals in several ways. First, they help to predict differences among taxa by identifying traits that are correlated with thicker cartilage in salamanders and likely in their extinct relatives (more aquatic habits, flat or convex mineralized epiphyses, and, possibly, sexual immaturity) and ones that are not (absolute body size and phylogenetic relatedness). Second, these results provide a starting point for determining cartilage correction factors in extinct taxa, which can then be used in a sensitivity analysis. Returning to stem tetrapods, a cartilage correction factor of 21 ± 7% in the femur could be used, corresponding to the mean and standard deviation in terrestrial salamanders in this study. These results can reasonably be applied to most stem tetrapods, with some caveats. Although often presented as a prototypical Devonian stem tetrapod, *Acanthostega* is not necessarily a good representative of the ancestral condition in terms of long bone histology and life history. Most notably, the degree of ossification in the humerus is seemingly unrelated to body size, and ossification did not begin until the animals reached nearly full size (Sanchez et al., 2016). This long delay in ossification might affect the ultimate size and shape of the cartilaginous epiphyses. In contrast, other Devonian and Early Carboniferous limbed vertebrates such as *Ichthyostega*, *Whatcheeria*, and *Pederpes* had more heavily ossified limb bones but appear to lack ossified or calcified epiphyses (Jarvik, 1996; Clack and Finney, 2005; Otoo et al., 2021), similar to extant salamanders. However, in *Pederpes* the ossified epiphyses are distinctly concave, suggesting very thick articular cartilage and an aquatic and/or juvenile condition (Clack and Finney, 2005). In contrast, terrestrial salamanders probably are not the best model for the epiphyses of many crown tetrapods. While prolonged juvenile stage is thought to be ancestral for limbed vertebrates (Sanchez et al., 2014, 2016; Kamska et al., 2018), some

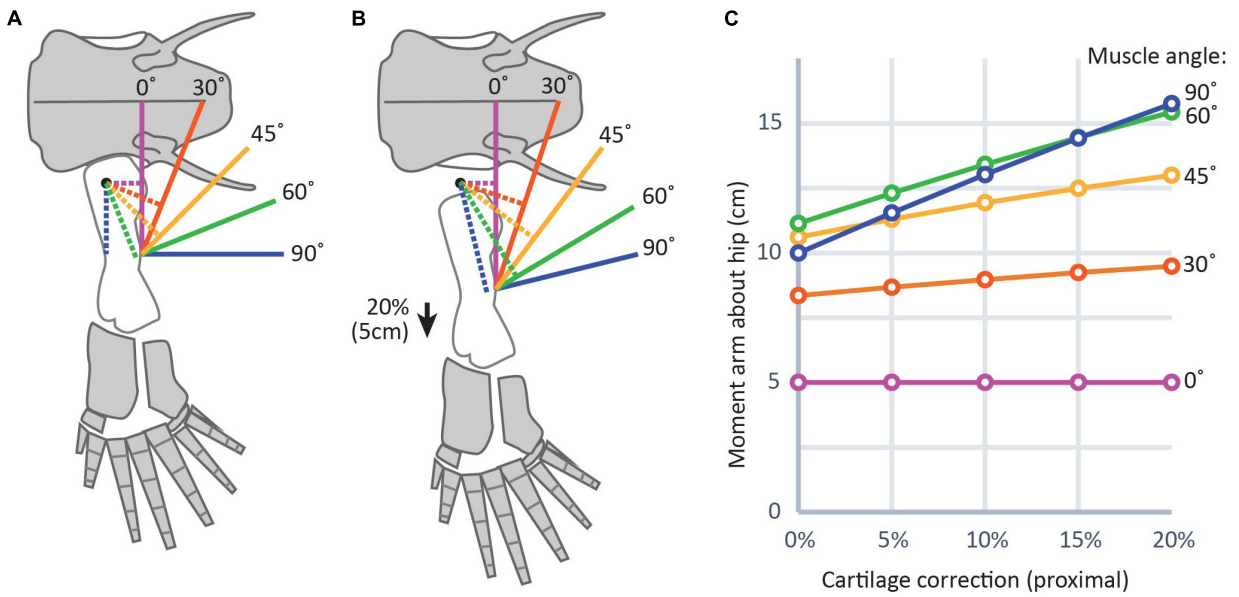

FIGURE 6 | Graphical representation of the effect of cartilage corrections on two-dimensional moment arms about the hip joint. **(A)** and **(B)** show a diagram of the hindlimb in *Acanthostega* (bone outlines modified from Coates, 1996) (25 cm femur length used for simplicity) without cartilage correction **(A)** and with cartilage correction of 20% femur length **(B)**, roughly equivalent to the thickness of proximal cartilage caps in the femur of *Necturus*. Solid lines indicate muscles and dotted lines indicate moment arms. **(C)** Shows a plot of change in moment arms of the modeled muscles with different cartilage correction factors. Muscles with lines of action nearly parallel to the long axis of the femur (purple, red) show smaller effect sizes; i.e., flatter slopes in part **(C)**, while those with lines of action more nearly perpendicular to the femur (green, blue) show greater effect sizes; i.e., steeper slopes in part **(C)**.

stem amniotes such as *Seymouria* exhibited much faster bone growth than extant salamanders (Estefa et al., 2020), and the epiphyses of extant lepidosaurs might be a better analog. On the other extreme, some stem salamanders such as *Apateon* show pedomorphic growth patterns (Estefa et al., 2021) and might be more analogous to aquatic or semi-aquatic salamanders. One cautionary note: although no correlation between absolute size and cartilage thickness was observed in this study, many stem tetrapods [including *Acanthostega*, at approximately 60 cm total length (Coates, 1996), and *Ichthyostega*, which is slightly larger (Ahlberg et al., 2005)] fall outside the size range of the sampled taxa, producing some additional uncertainty.

The effect of unpreserved articular cartilage on range of motion in fossils is difficult to predict, and such a prediction was not attempted in this study. A preliminary study of the hindlimb of *Acanthostega* showed that a similar correction factor (cartilage cap 13% bone length on the proximal end; similar to the Fire Salamander *S. Salamandra*) would increase osteological range of motion of the hip by a modest 15–30° (Dao et al., 2020). However, this model assumes that cartilage is infinitely deformable and does not in itself restrict range of motion. Based on salamanders in the current study, the CCF for the length and width of the femoral head would be approximately 30% (**Table 4**), likely producing a more congruent hip joint and restricting range of motion. The results from these salamanders suggest that the dimensions of the femoral head are affected by articular cartilage to a greater degree than the humeral head, humeral condyles, or femoral condyles (although this varies among taxa).

Because adding a cartilage correction moves muscle insertion points distally further from their insertions, reconstructed muscle leverage would also be affected (Dao et al., 2020). Changes in muscle leverage will be greatest in muscles whose axes of movement are nearly perpendicular to the femur. In a model of a hindlimb with a 25 cm femur and a 20% CCF on the proximal end, slightly above the average for aquatic salamanders in this study (**Figure 6**), changes in moment arms of 4–6 cm were found for muscles that run nearly perpendicular to the femur, as opposed to those muscles whose axes were nearly parallel (0–2 cm). This result is logical: moving the insertion more distally (i.e., along the long axis of the bone) has the effect of lengthening a muscle whose line of action is parallel to the long axis of the femur but does not change its orientation (**Figure 6**, purple lines). However, for a muscle whose line of action is oblique to the femur, moving the insertion distally will both lengthen the line of action and change its orientation by decreasing the angle between the muscle and the femur (**Figure 6**, blue lines). Because a muscle's lever arm by definition is perpendicular to the line of action (e.g., Sherman et al., 2013), changing the orientation of the latter directly affects the former. Therefore, even without explicitly modeling moment arms it is possible to predict the effects of different assumptions about unpreserved articular cartilage on limb function. For example, our previous work on *Acanthostega* used a 7.5% CCF in the humeral head (Molnar et al., 2021). Had we used a CCF drawn from the average for terrestrial salamanders in this study (approximately 10%), the moment arms of shoulder retractors like latissimus dorsi and pectoralis posterior probably would have been several centimeters larger, while those of elbow extensors such as triceps brachii would have been minimally affected.

DATA AVAILABILITY STATEMENT

The original contributions presented in the study are included in the article/**Supplementary Material**, further inquiries can be directed to the corresponding author/s.

ETHICS STATEMENT

Ethical review and approval was not required for the animal study because this research used only preserved specimens from existing collections.

AUTHOR CONTRIBUTIONS

JM conceived the study, collected and analyzed data, and wrote and edited the manuscript.

FUNDING

This project was supported by startup grant from NYIT to JM.

ACKNOWLEDGMENTS

I am grateful to Dan Gibbons for writing the MATLAB script, to Meredith Taylor for de-staining specimens, and to Kelsi Hurdle for assisting with micro-CT scanning. Access to the micro-CT scanner was provided with funding from NSF MRI 1828305. David Kizirian at the American Museum of Natural History and Michael Granatosky at NYIT provided specimens for scanning. Aki Watanabe performed a phylogenetic signal test in R and shared his contrast staining protocol, and the biomechanics research group at NYIT contributed ideas and feedback. Special thanks to Brandon Dao and Christine Chevalier-Horgan for the preliminary work that sparked this manuscript, and thanks to the two reviewers whose suggestions greatly improved it.

SUPPLEMENTARY MATERIAL

The Supplementary Material for this article can be found online at: https://www.frontiersin.org/articles/10.3389/fevo.2021.671006/full#supplementary-material

Supplementary Table 1 | Ancestor reconstruction of cartilage correction factors for humerus, femur, radius, ulna, tibia, and fibula using maximum parsimony

Supplementary Data Sheet 1 | MATLAB script for calculating two-dimensional moment arms with a cartilage correction factor.

Supplementary datasets | (available on MorphoSource.com upon publication): 15 DiceCT datasets representing the fore- and hindlimbs of various salamanders.

1. Right forelimb of *Pleurodeles waltl* (AMNH A168418)

2. Right hindlimb of *Pleurodeles waltl* (AMNH A168418)
3. Forelimbs of *Pseudotriton ruber* (NYIT MG1257)
4. Hindlimbs of *Pseudotriton ruber* (NYIT MG1257)
5. Forelimb of *Plethodon cinereus* (AMNH A159522)
6. Hindlimb of *Plethodon cinereus* (AMNH A159522)
7. Forelimbs of *Ambystoma tigrinum* (AMNH 26619)
8. Hindlimbs of *Ambystoma tigrinum* (AMNH 26619)
9. Forelimb of *Salamandra salamandra* (AMNH 26618)
10. Hindlimb of *Salamandra salamandra* (AMNH 26618)
11. Forelimbs of *Ambystoma mexicanum* (AMNH A144861)
12. Hindlimbs of *Ambystoma mexicanum* (AMNH A144861)
13. Forelimbs of *Siren lacertina* (AMNH A171810)
14. Forelimbs of *Necturus maculatus* (AMNH 26617)
15. Hindlimbs of *Necturus maculatus* (AMNH 26617)

REFERENCES

Ahlberg, P. E., Clack, J. A., and Blom, H. (2005). The axial skeleton of the Devonian tetrapod Ichthyostega. *Nature* 437, 137–140. doi: 10.1038/nature03893

AmphibiaWeb (2020). *Salamandra salamandra: Fire Salamander*. Available online at: http://amphibiaweb.org/species/4284 (accessed Jan 26, 2021)

Ashley-Ross, M. A. (2004). Kinematics of the transition between aquatic and terrestrial locomotion in the newt *Taricha torosa*. *J. Exp. Biol.* 207, 461–474. doi: 10.1242/jeb.00769

Carter, D., Mikiæ, B., and Padian, K. (1998). Epigenetic mechanical factors in the evolution of long bone epiphyses. *Zool. J. Linn. Soc.* 123, 163–178.

Clack, J., and Coates, M. I. (1995). *Acanthostega gunnari*, a primitive, aquatic tetrapod? *Bull. Muséum. Natl. Hist. Nat. Sect. C Sci. Terre. Paléontol. Géologie Minéralogie* 17, 359–372.

Clack, J. A. (2012). *Gaining Ground: The Origin and Evolution of Tetrapods, Second*. Bloomington, IN: Indiana University Press.

Clack, J. A., Ahlberg, P. E., Finney, S. M., Dominguez Alonso, P., Robinson, J., and Ketcham, R. A. (2003). A uniquely specialized ear in a very early tetrapod. *Nature* 425, 65–69. doi: 10.1038/nature01904

Clack, J. A., and Finney, S. M. (2005). *Pederpes finneyae*, an articulated tetrapod from the Tournaisian of Western Scotland. *J. Syst. Palaeontol.* 2, 311–346. doi: 10.1017/S1477201904001506

Coates, M. I. (1996). The Devonian tetrapod *Acanthostega gunnari* Jarvik: postcranial anatomy, basal tetrapod interrelationships and patterns of skeletal evolution. *Trans. R Soc. Edinb.* 87, 363–421.

Coates, M. I., and Clack, J. A. (1991). Fish-like gills and breathing in the earliest known tetrapod. *Nature* 352, 234–236.

Dao, B., Chevalier-Horgan, C. L., Pierce, S. E., and Molnar, J. L. (2020). The effect of cartilage thickness on reconstructions of range of motion and muscle leverage in extinct tetrapods. *FASEB J.* 34, 1–1.

Erismis, U. C., and Chinsamy, A. (2010). Ontogenetic changes in the epiphyseal cartilage of *rana (Pelophylax) caralitana* (Anura: Ranidae). *Anat. Rec.* 293, 1825–1837. doi: 10.1002/ar.21241

Estefa, J., Klembara, J., Tafforeau, P., and Sanchez, S. (2020). Limb-bone development of seymouriamorphs: implications for the evolution of growth strategy in stem amniotes. *Front. Earth Sci.* 8:97. doi: 10.3389/feart.2020.00097

Estefa, J., Tafforeau, P., Clement, A. M., Klembara, J., Niedźwiedzki, G., Berruyer, C., et al. (2021). New light shed on the early evolution of limb-bone growth plate and bone marrow. *Elife* 10:e51581.

Francillon-Vieillot, H., de Buffrénil, V., Castanet, J., Géraudie, J., Meunier, F. J., Sire, J. Y., et al. (1990). Microstructure and mineralization of vertebrate skeletal tissues. *Skelet. Biominer. Patterns Process. Evol. Trends* 1, 471–530.

Francis, E. (1934). *The Anatomy of the Salamander*. Oxford: Clarendon Press.

Goris, R. C., and Maeda, N. (2005). *Guide to the Amphibians and Reptiles of Japan*. Malabar, FL: Krieger Publishing Company.

Haines, R. W. (1938). The primitive form of epiphysis in the long bones of tetrapods. *J. Anat.* 72, 323–343.

Haines, R. W. (1942). The evolution of epiphyses and of endochondral bone. *Biol. Rev.* 17, 267–292.

Hedges, S. B., Dudley, J., and Kumar, S. (2006). TimeTree: a public knowledge-base of divergence times among organisms. *Bioinformatics* 22, 2971–2972.

Helmenstine, A. M. (2020). *All About the Axolotl (Ambystoma mexicanum)*. New York, NY: ThoughtCo.

Holliday, C. M., Ridgely, R. C., Sedlmayr, J. C., and Witmer, L. M. (2010). Cartilaginous epiphyses in extant archosaurs and their implications for reconstructing limb function in dinosaurs. *PLoS One* 5:e13120. doi: 10.1371/journal.pone.0013120

Hutchinson, J. R. (2011). On the inference of function from structure using biomechanical modelling and simulation of extinct organisms. *Biol. Lett.* 8, 115–118. doi: 10.1098/rsbl.2011.0399

Hutchinson, J. R., Anderson, F. C., Blemker, S. S., and Delp, S. L. (2005). Analysis of hindlimb muscle moment arms in *Tyrannosaurus rex* using a three-dimensional musculoskeletal computer model: implications for stance, gait, and speed. *Paleobiology* 31, 676–701.

Jannel, A., Nair, J. P., Panagiotopoulou, O., Romilio, A., and Salisbury, S. W. (2019). "Keep your feet on the ground": simulated range of motion and hind foot posture of the middle jurassic sauropod *Rhoetosaurus brownei* and its implications for sauropod biology. *J. Morphol.* 280, 849–878. doi: 10.1002/jmor.20989

Jarvik, E. (1996). The Devonian tetrapod Ichthyostega. *Foss. Strata.* 40, 1–207.

Joven, A., Kirkham, M., and Simon, A. (2015). "Husbandry of Spanish ribbed newts (*Pleurodeles waltl*)," in *Salamanders in Regeneration Research*, eds A. Kumar and A. Simon (New York, NY: Springer), 47–70.

Kammerer, C. F., Angielczyk, K. D., and Fröbisch, J. (2011). A comprehensive taxonomic revision of Dicynodon (Therapsida, Anomodontia) and its implications for dicynodont phylogeny, biogeography, and biostratigraphy. *J. Vertebr. Paleontol.* 31, 1–158. doi: 10.1080/02724634.2011.627074

Kamska, V., Daeschler, E., Downs, J., Ahlberg, P. E., Tafforeau, P., and Sanchez, S. (2018). Long-bone development and life-history traits of the Devonian tristichopterid *Hyneria lindae*. *Earth Environ. Sci. Trans. R Soc. Edinb.* 109, 1–12. doi: 10.1017/S175569101800083X

Kawamichi, T., and Ueda, H. (1998). Spawning at nests of extra-large males in the giant salamander *Andrias japonicus*. *J. Herpetol.* 32, 133–136.

Kawano, S. M., and Blob, R. W. (2013). Propulsive forces of mudskipper fins and salamander limbs during terrestrial locomotion: implications for the invasion of land. *Integr. Comp. Biol.* 53, 1–12. doi: 10.1093/icb/ict051

Klintz, J. H. (1912). Die enchondrale Ossifikation bei den Amphibien (*Salamandra maculosa* Laur.). *Arb. Ueber. Zool. Inst. Wien.* 19, 165–194.

Lannoo, M. J. (2005). *Amphibian Declines: The Conservation Status of United States Species*. Berkeley, CA: University of California Press.

Lynn, W. G. (1961). Types of amphibian metamorphosis. *Am. Zool.* 1, 151–161.

Marjanoviæ, D., and Laurin, M. (2014). An updated paleontological timetree of lissamphibians, with comments on the anatomy of Jurassic crown-group salamanders (Urodela). *Hist. Biol.* 26, 535–550.

Metscher, B. D. (2009). MicroCT for comparative morphology: simple staining methods allow high-contrast 3D imaging of diverse non-mineralized animal tissues. *BMC Physiol.* 9:11. doi: 10.1186/1472-6793-9-11

Molnar, J. L., Hutchinson, J. R., Diogo, R., Clack, J. A., and Pierce, S. E. (2021). Evolution of forelimb musculoskeletal function across the fish-to-tetrapod transition. *Sci. Adv.* 7:eabd7457.

Nafis, G (2018). *A Guide to the Amphibians and Reptiles of California*. Corvallis, OR: California Herps.

Najbar, A., Konowalik, A., Halupka, K., Najbar, B., and Ogielska, M. (2020). Body size and life history traits of the fire salamander *Salamandra salamandra* from Poland. *Amphib. Reptil.* 41, 63–74. doi: 10.1163/15685381-20191135

Otoo, B. K. A., Bolt, J. R., Lombard, R. E., Angielczyk, K. D., and Coates, M. I. (2021). The postcranial anatomy of *Whatcheeria deltae* and its implications for the family Whatcheeriidae. *Zool. J. Linn. Soc.* zlaa182. doi: 10.1093/zoolinnean/zlaa182

Petranka, J. W. (1998). *Salamanders of the United States and Canada*. Washington, DC: Smithsonian Institution Press.

Pierce, S. E., Hutchinson, J. R., and Clack, J. A. (2013). Historical perspectives on the evolution of tetrapodomorph movement. *Integr. Comp. Biol.* 53, 209–223.

Quilhac, A., de Ricqlès, A., Lamrous, H., and Zylberberg, L. (2014). Globuli ossei in the long limb bones of *Pleurodeles waltl* (Amphibia, Urodela, Salamandridae). *J. Morphol.* 275, 1226–1237. doi: 10.1002/jmor.20296

Raffaëlli, J. (2014). *Les Urodèles du Monde*, 2nd Edn. McLean, VA: Penden.

Revell, L. J. (2012). phytools: an R package for phylogenetic comparative biology (and other things). *Methods Ecol. Evol.* 3, 217–223.

Sanchez, S., Germain, D., De RicqlèS, A., Abourachid, A., Goussard, F., and Tafforeau, P. (2010a). Limb-bone histology of temnospondyls: implications for understanding the diversification of palaeoecologies and patterns of locomotion of Permo-Triassic tetrapods. *J. Evol. Biol.* 23, 2076–2090. doi: 10.1111/j.1420-9101.2010.02081.x

Sanchez, S., Klembara, J., Castanet, J., and Steyer, J. S. (2008). Salamander-like development in a seymouriamorph revealed by palaeohistology. *Biol. Lett.* 4, 411–414. doi: 10.1098/rsbl.2008.0159

Sanchez, S., Ricqlès, A. D., Schoch, R., and Steyer, J. S. (2010b). Developmental plasticity of limb bone microstructural organization in Apateon: histological evidence of paedomorphic conditions in branchiosaurs. *Evol. Dev.* 12, 315–328. doi: 10.1111/j.1525-142X.2010.00417.x

Sanchez, S., Tafforeau, P., and Ahlberg, P. E. (2014). The humerus of Eusthenopteron: a puzzling organization presaging the establishment of tetrapod limb bone marrow. *Proc. R. Soc. B Biol. Sci.* 281:20140299. doi: 10.1098/rspb.2014.0299

Sanchez, S., Tafforeau, P., Clack, J. A., and Ahlberg, P. E. (2016). Life history of the stem tetrapod Acanthostega revealed by synchrotron microtomography. *Nature* 537:408.

Sherman, M. A., Seth, A., and Delp, S. L. (2013). "What is a moment arm? Calculating muscle effectiveness in biomechanical models using generalized coordinates," in *Proceedings of the ASME Engineering Technical Conferences V07BT10A052* (New York, NY: American Society of Mechanical Engineers).

Tsai, H. P., Middleton, K. M., Hutchinson, J. R., and Holliday, C. M. (2020). More than one way to be a giant: convergence and disparity in the hip joints of saurischian dinosaurs. *Evolution* 74, 1654–1681.

von Eggeling, H. (1869). *Der Aufbau der Skeletteile in den Freien Gliedmassen der Wirbeltiere; Untersuchungen an Urodelen Amphibien*. Jena: Fischer.

Wakahara, M. (1996). Heterochrony and neotenic salamanders: possible clues for understanding the animal development and evolution. *Zoolog. Sci.* 13, 765–776. doi: 10.2108/zsj.13.765

Witmer, L. M. (1995). "The extant phylogenetic bracket and the importance of reconstructing soft tissues in fossils," in *Functional Morphology in Vertebrate Paleontology*, ed. J. J. Thomason (Cambridge, MA: Cambridge University Press), 19–33.

Xie, M., Gol'din, P., Herdina, A. N., Estefa, J., Medvedeva, E. V., and Li, L. (2020). Secondary ossification center induces and protects growth plate structure. *eLife* 9:e55212. doi: 10.7554/eLife.55212

Conflict of Interest: The author declares that the research was conducted in the absence of any commercial or financial relationships that could be construed as a potential conflict of interest.

frontiers in Ecology and Evolution

ORIGINAL RESEARCH
published: 22 July 2021
doi: 10.3389/fevo.2021.679633

Development of the Pectoral Lobed Fin in the Australian Lungfish *Neoceratodus forsteri*

Tatsuya Hirasawa[1], Camila Cupello[2], Paulo M. Brito[2], Yoshitaka Yabumoto[3], Sumio Isogai[4], Masato Hoshino[5] and Kentaro Uesugi[5]*

[1] Department of Earth and Planetary Science, Graduate School of Science, The University of Tokyo, Tokyo, Japan, [2] Departamento de Zoologia, Instituto de Biologia/IBRAG, Universidade do Estado do Rio de Janeiro, Rio de Janeiro, Brazil, [3] Kitakyushu Museum of Natural History and Human History, Kitakyushu, Japan, [4] Department of Anatomy, Iwate Medical University School of Medicine, Morioka, Japan, [5] Japan Synchrotron Radiation Research Institute, Sayo, Japan

The evolutionary transition from paired fins to limbs involved the establishment of a set of limb muscles as an evolutionary novelty. In parallel, there was a change in the topography of the spinal nerves innervating appendicular muscles, so that distinct plexuses were formed at the bases of limbs. However, the key developmental changes that brought about this evolutionary novelty have remained elusive due to a lack of data on the development of lobed fins in sarcopterygian fishes. Here, we observed the development of the pectoral fin in the Australian lungfish *Neoceratodus forsteri* (Sarcopterygii) through synchrotron radiation X-ray microtomography. *Neoceratodus forsteri* is a key taxon for understanding the fin-to-limb transition due to its close phylogenetic relationships to tetrapods and well-developed lobed fins. At the onset of the fin bud in *N. forsteri*, there is no mesenchyme at the junction between the axial body wall and the fin bud, which corresponds to the embryonic position of the brachial plexus formed in the mesenchyme in tetrapods. Later, concurrent with the cartilage formation in the fin skeleton, the fin adductor and abductor muscles become differentiated within the surface ectoderm of the fin bud. Subsequently, the girdle muscle, which is homologous to the tetrapod serratus muscle, newly develops at the junction between the axial body wall and the fin. Our study suggests that the acquisition of embryonic mesenchyme at the junction between the axial body wall and the appendicular bud opened the door to the formation of the brachial plexus and the specialization of individual muscles in the lineage that gave rise to tetrapods.

Keywords: Sarcopterygii, Dipnomorpha, Tetrapodomorpha, fish-tetrapod transition, migratory muscle precursor cell, limb muscle, brachial plexus

OPEN ACCESS

Edited by:
Catherine Anne Boisvert, Curtin University, Australia

Reviewed by:
Koh Onimaru, RIKEN Center for Life Science Technologies, Japan
Zerina Johanson, Natural History Museum, United Kingdom

****Correspondence:***
Tatsuya Hirasawa
hirasawa@eps.s.u-tokyo.ac.jp

Specialty section:
This article was submitted to Evolutionary Developmental Biology, a section of the journal Frontiers in Ecology and Evolution

Received: *12 March 2021*
Accepted: *01 July 2021*
Published: *22 July 2021*

Citation:
Hirasawa T, Cupello C, Brito PM, Yabumoto Y, Isogai S, Hoshino M and Uesugi K (2021) Development of the Pectoral Lobed Fin in the Australian Lungfish Neoceratodus forsteri. Front. Ecol. Evol. 9:679633. doi: 10.3389/fevo.2021.679633

INTRODUCTION

One of the pivotal challenges of the animals' water-to-land transition is the difficulty in weight support and locomotion on land under gravity constraints. The tetrapod limbs had evolved from paired fins during the Devonian (Ahlberg, 2019), and were decisive for the success of this transition. Although fossil transitional forms from the fin to the limb potentially bridge the gap, tetrapod limbs differ from paired fins in mode of evolutionary change, or variational

modality, thereby representing an evolutionary novelty (Wagner, 2014). The origin of this novelty involved the functional integration of the musculoskeletal and nervous systems necessary for terrestrial and aerial movement, and represents one of the most drastic morphological changes in vertebrate evolution.

Attempts to understand the evolution of the limb and the developmental basis of the morphological transition have involved comparative anatomy, paleontology, and evolutionary developmental biology. Since soft-tissues are poorly preserved in the fossil record, much emphasis is currently placed on the skeletal systems. In particular, the evolutionary origin of the digit and wrist (i.e., the autopod) has been gradually unraveled through paleontological studies of Devonian fossils (Shubin et al., 2006; Cloutier et al., 2020) and through evolutionary developmental studies focused mainly on the *5'Hox* genes expressed in fin and limb buds (Shubin and Alberch, 1986; Davis et al., 2007; Johanson et al., 2007; Nakamura et al., 2016; Tanaka, 2016; Woltering et al., 2020). These studies have dispelled any uncertainty about the homologies of proximal (i.e., the stylopod and zeugopod) skeletal elements in fins and limbs, and the morphological transitions from one to the other have been traced in relation to the evolution of tetrapod limb movement (Shubin et al., 2004, 2006; Pierce et al., 2012; Miyake et al., 2016; Molnar et al., 2017; Ahlberg, 2019; Wynd et al., 2019).

Despite this progress, however, the process of the soft-tissue evolution remains elusive. So far, morphologies of the muscles (Braus, 1901; Shann, 1920, 1924; Diogo et al., 2016; Miyake et al., 2016; Molnar et al., 2017, 2018), spinal nerves (Fürbringer, 1888; Braus, 1901; Hirasawa and Kuratani, 2018), and vascular system (Ura, 1956; Saito, 1988a,b) have been compared between fins and limbs, but their homologies are still, at least partly, uncertain. In fossil taxa, data about muscle attachments can provide clues for muscle morphologies (Sanchez et al., 2013; Molnar et al., 2017), but it is quite difficult to capture the complete picture of the musculoskeletal system of non-tetrapodomorph and tetrapodomorph fishes, as well as early tetrapods. The extant tetrapods possess a common set of limb muscles and corresponding spinal nerves, and the topographies of both systems have remained largely consistent during the evolution of tetrapod crown groups. Recent studies on the evolution of limb muscles (Molnar et al., 2017, 2018) suggest that the full set of limb muscles was acquired in a stepwise manner in the early evolution of limbed tetrapods. Also, the plexus of spinal nerves formed at the base of the limb is likely an evolutionary novelty in the tetrapod lineage (Hirasawa and Kuratani, 2018). Formation of the limb-innervating plexus potentially facilitated the complex control of movement by the columnar organization of neurons in the spinal cord (i.e., the lateral motor column) (Murakami and Tanaka, 2011; Jung et al., 2018), by enabling axons from neurons at different cranio-caudal levels to innervate a single muscle together.

From the developmental point of view, modes of migration of somite-derived muscle progenitor cells have been compared between tetrapods and fishes, in particular elasmobranchs, whose fin muscles are arranged in parallel to the somites (Okamoto et al., 2017; Turner et al., 2019). Although data on the mode of limb muscle development in lissamphibians remains insufficient, at least for amniotes there is ample evidence that the limb muscle progenitor cells dissolve their somitic segmentation patterns upon entrance to the limb bud (Dietrich et al., 1998; Gross et al., 2000; Hirasawa and Kuratani, 2018). Almost simultaneously with the migration of muscle progenitor cells into the limb bud, the developing spinal nerves form the brachial plexus within the mesenchyme at the junction between the axial body wall and the limb bud (i.e., the plexus mesenchyme), which is required for normal development of nerves innervating limb muscles (Wright and Snider, 1996; Haase et al., 2002; Kramer et al., 2006). This dissolution of the segmentation pattern of the musculature and spinal nerves at the junction between the axial body wall and limb bud may represent a developmental process required for the establishment of limb muscles in extant tetrapods. On the other hand, based on the descriptions of pectoral fin development in the sturgeon (Mollier, 1897) and zebrafish (Grandel and Schulte-Merker, 1998), no distinct mesenchyme develops at the junction between the axial body wall and fin bud in these actinopterygian fishes.

Because the tetrapod limb evolved from the lobed fin of ancestral sarcopterygian fishes, the development of lobed fins in extant non-tetrapod sarcopterygians including coelacanths and lungfishes potentially provides clues to understanding key evolutionary changes in muscle and nerve development. Among the extant non-tetrapod sarcopterygians, in which lungfishes are closer to tetrapods than coelacanths (Amemiya et al., 2013; Betancur-R et al., 2017), the Australian lungfish *Neoceratodus forsteri* provides the best model for developmental studies of lobe-finned fishes; other species present problems either because of the inaccessibility of large embryonic samples (e.g., coelacanths) or secondary modifications in fin morphology (e.g., African and South American lungfishes, having undeveloped filamentous paired fins). Indeed, recent studies on the development of the lobed fin in *N. forsteri* have revealed the developmental mechanism of skeletal patterning (Johanson et al., 2004, 2007; Woltering et al., 2020). However, our current understanding of muscle and nerve development in lobed fins largely relies on descriptions and illustrations from classical literature (e.g., Semon, 1898; Salensky, 1899; Greil, 1913), which are insufficient for comparison with recent developmental studies. In this study, we seek to provide a basis for future developmental studies by describing the development of muscles in the pectoral lobed fin of *N. forsteri* based on three-dimensional observations at a cellular level.

MATERIALS AND METHODS

Fertilized *Neoceratodus forsteri* eggs were legally collected from the Department of Biological Sciences, Macquarie University, Sydney, Australia, and transported with the permission of CITES (Certificate No. 2009-AU-564836) in 2009. The embryos and larvae were fixed with 10% neutral buffered formalin after Berlin blue dye injection to blood vessels by using a previously described method (Kamei et al., 2010), and stored in 10% neutral buffered formalin. All specimens are registered to the Iwate Medical University Ura Ryozi Collection (IMU-UR; **Table 1**).

TABLE 1 | List of specimens examined in this study.

Specimen No.	Stage	Total length (mm)
IMU-RU-SI-0010	41	8.5
IMU-RU-SI-0013 (**Figure 1**)	46	13.5
IMU-RU-SI-0017 (**Figure 2**)	47 (early phase)	16.0
IMU-RU-SI-0019	47 (late phase)	17.0
IMU-RU-SI-0022	47 (late phase)	17.0
IMU-RU-SI-0037 (**Figure 3**)	47 (late phase)	17.5
IMU-RU-SI-0038	48 (early phase)	19.0
IMU-RU-SI-0039 (**Figure 4**)	48 (mid-phase)	20.5
IMU-RU-SI-0040	48 (late phase)	24.0

In this study, embryos were staged according to the Kemp (1982) stage table.

High-resolution X-ray tomography of the embryonic samples was performed at the synchrotron radiation facility SPring-8 in Sayo-cho, Hyogo Prefecture, Japan. The entire body of each embryo was placed in a polypropylene tube filled with normal saline in the experimental hutch of the beamline BL20B2 and scanned by means of propagation-based X-ray phase-contrast tomography (Paganin et al., 2002) with a voxel size of 2.70 μm at an energy of 15 keV. A visible-light conversion type X-ray image detector was used to detect X-ray transmission images. Incident X-ray image onto the detector was converted into visible light image by a Gadox scintillator with a thickness of 15 μm. Combinations of two camera lenses, 1st lens: a camera lens with a focal length of 35 mm (AI AF Nikkor 35 mm f/2D; Nikon, Tokyo, Japan); 2nd lens: a camera lens with a focal length of 85 mm (AI AF Nikkor 85 mm f/1.4D IF; Nikon, Tokyo, Japan), were used to form the image on a sCMOS image sensor (ORCA Flash C11440-22C; Hamamatsu Photonics, Hamamatsu, Japan). The distance from the sample to the X-ray image detector was 600 mm. A total of 1,800 projections covering 180° were taken with an exposure time of 200 ms per projection. Slices were reconstituted by using a filtered back-projection algorithm implemented on homemade software (Uesugi et al., 2010).

The stacks of images were examined by using the image-processing software package Fiji (Schindelin et al., 2012) in orthogonal views. The images were reconstructed three-dimensionally, using the Avizo software (Thermo Fisher Scientific, Waltham, MA, United States). Each embryonic component was manually labeled on the sections and subsequently combined to generate a three-dimensional model.

RESULTS

Onset of the Pectoral Fin Bud

The earliest developmental stage we observed was stage 41 (**Table 1**). By this stage, the dorsal axial muscles have become differentiated, and the pronephros has developed at the caudal end of the pharynx. The prospective field of the pectoral fin bud, which is observable lateral to the pronephros, consists of the epidermis and mesenchyme, which together are as large as the pronephric duct as previously observed by Hodgkinson et al. (2009). At this stage, the mesenchyme, which later develops into ventral axial muscles and fin buds, does not extend ventrally to the pronephros.

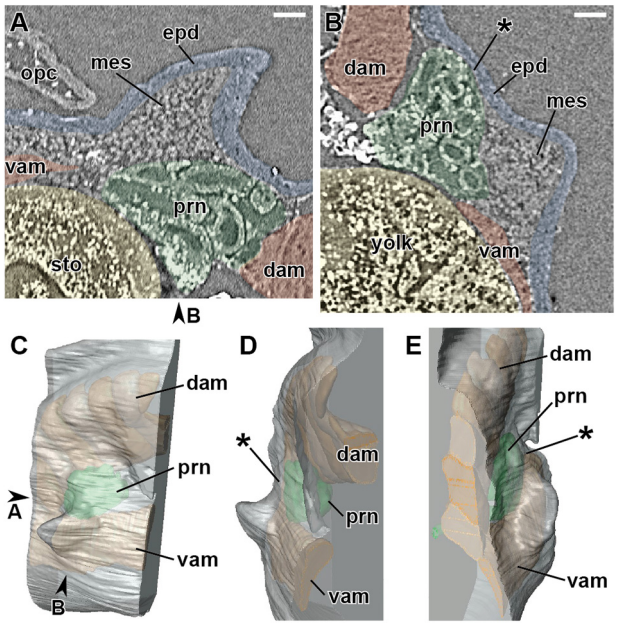

FIGURE 1 | Developing right pectoral fin of *Neoceratodus forsteri* at stage 46 (total length = 13.5 mm). **(A)** Coronal section. **(B)** Transverse section. **(C)** Lateral view. **(D)** Cranial view. **(E)** Caudal view. dam, dorsal axial muscle; epd, epidermis; mes, mesenchyme; opc, operculum; prn, pronephros; sto, stomach; vam, ventral axial muscle. Arrowheads indicate the respective sectioned levels. The asterisk marks the junction between the axial body wall and fin bud, where no mesenchymal tissue is observable at this developmental stage. Scale bar = 100 μm.

At stage 46 (**Figure 1** and **Table 1**), the pectoral fin bud protrudes laterally at the junction of the lateroventral aspect of the pronephros and the laterodorsal aspect of the ventral axial muscles. At this stage, the fin bud consists of the epidermis and mesenchyme, and the latter is homogeneous and structureless. Dorsal to the fin bud, there is little space between the epidermis and pronephros, and no mesenchymal tissue is observable. Positional relationships among the pectoral fin, pronephros, and ventral axial muscles are maintained throughout the observed developmental stages (stages 46–48).

Differentiation of the Pectoral Fin Muscles

Differentiation of the pectoral fin muscles occurs during stage 47. Here, we divide stage 47 into two phases (**Table 1**) based on when myotubes of the pectoral fin muscles become identifiable.

In the early phase of stage 47 (**Figure 2**), a mass of cartilage develops at the base of the pectoral fin. A dense mesenchymal cell mass (premuscle mass) surrounds the cartilage in the proximal part of the fin bud (**Figures 2B–D**). In the cranial part of the fin bud, a small number of mesenchymal cells (just five or six cells across at the thickest) occupy the space between the laterodorsal aspect of the pronephros and epidermis (**Figure 2C**).

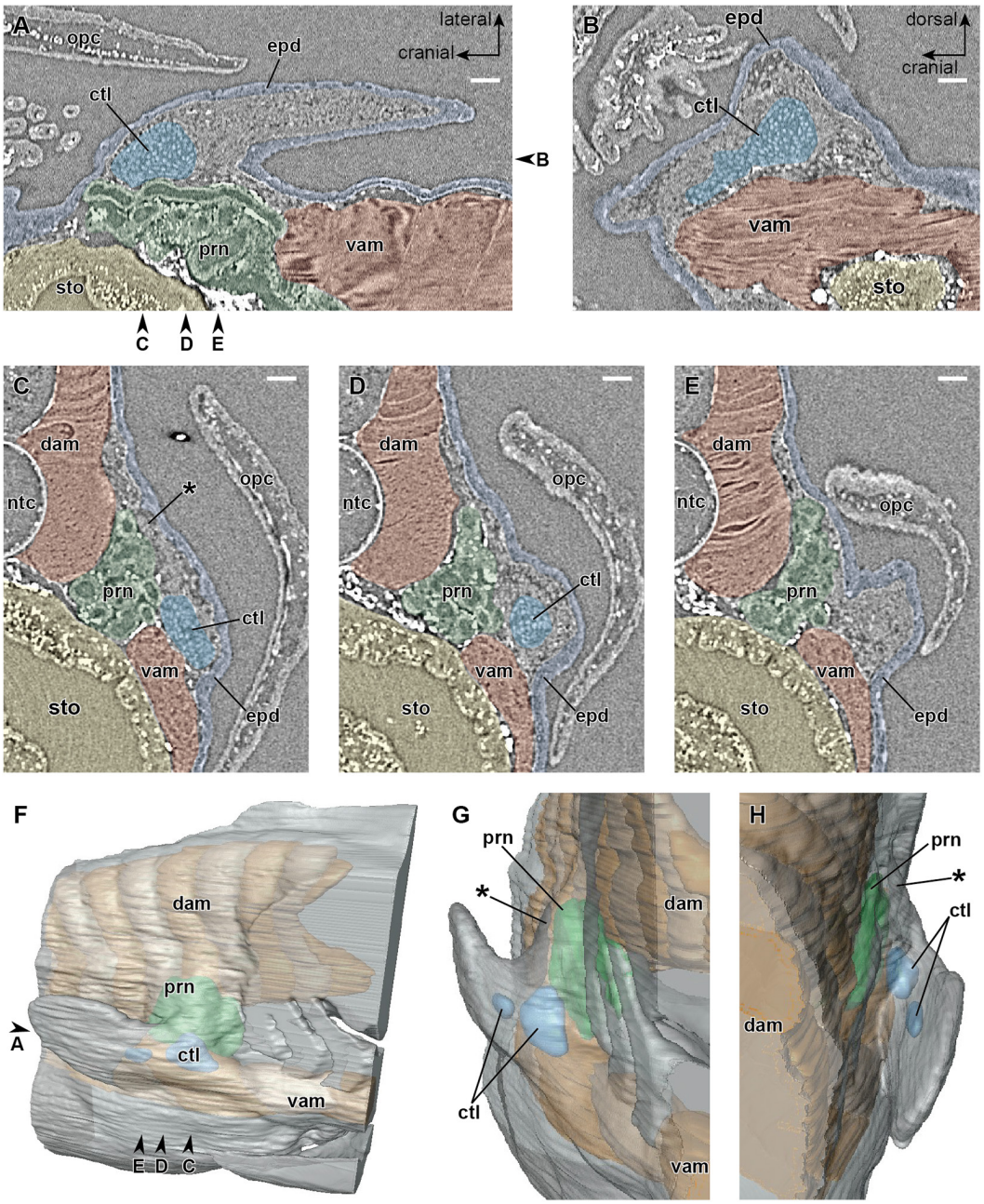

FIGURE 2 | Developing right pectoral fin of *Neoceratodus forsteri* during the early phase of stage 47 (total length = 16.0 mm). **(A)** Coronal section. **(B)** Sagittal section. **(C–E)** Transverse section. **(F)** Lateral view. **(G)** Cranial view. **(H)** Caudal view. ctl, cartilage; dam, dorsal axial muscle; epd, epidermis; ntc, notochord; opc, operculum; prn, pronephros; sto, stomach; vam, ventral axial muscle. Arrowheads indicate the respective sectioned levels. The asterisk marks the cranial part of the junction between the axial body wall and fin bud, filled by a small number of mesenchymal cells at this developmental stage, which later form the cleithrum. Scale bar = 100 μm.

This mesenchyme becomes thinner caudally (**Figure 2D**), and in the caudal part, there is little space between them (**Figure 2E**).

In the late phase of stage 47 (**Figure 3**), the primary myotubes of the pectoral fin adductor (**Figures 3A,B**) and abductor (**Figures 3B,C**) muscles become differentiated. The cartilage of the scapulocoracoid, humerus, and ulna are now recognizable separately (**Figure 3B**). It is identifiable that the adductor and abductor muscles are connected proximally to the scapulocoracoid and distally to the humerus and ulna, while separation of superficial and deep layers (superficiales and profunduses) of these muscles is not observable. At the cranial part of the junction between the pectoral fin and trunk, which corresponds approximately to the thickest part of the mesenchyme intervening between the pronephros and epidermis

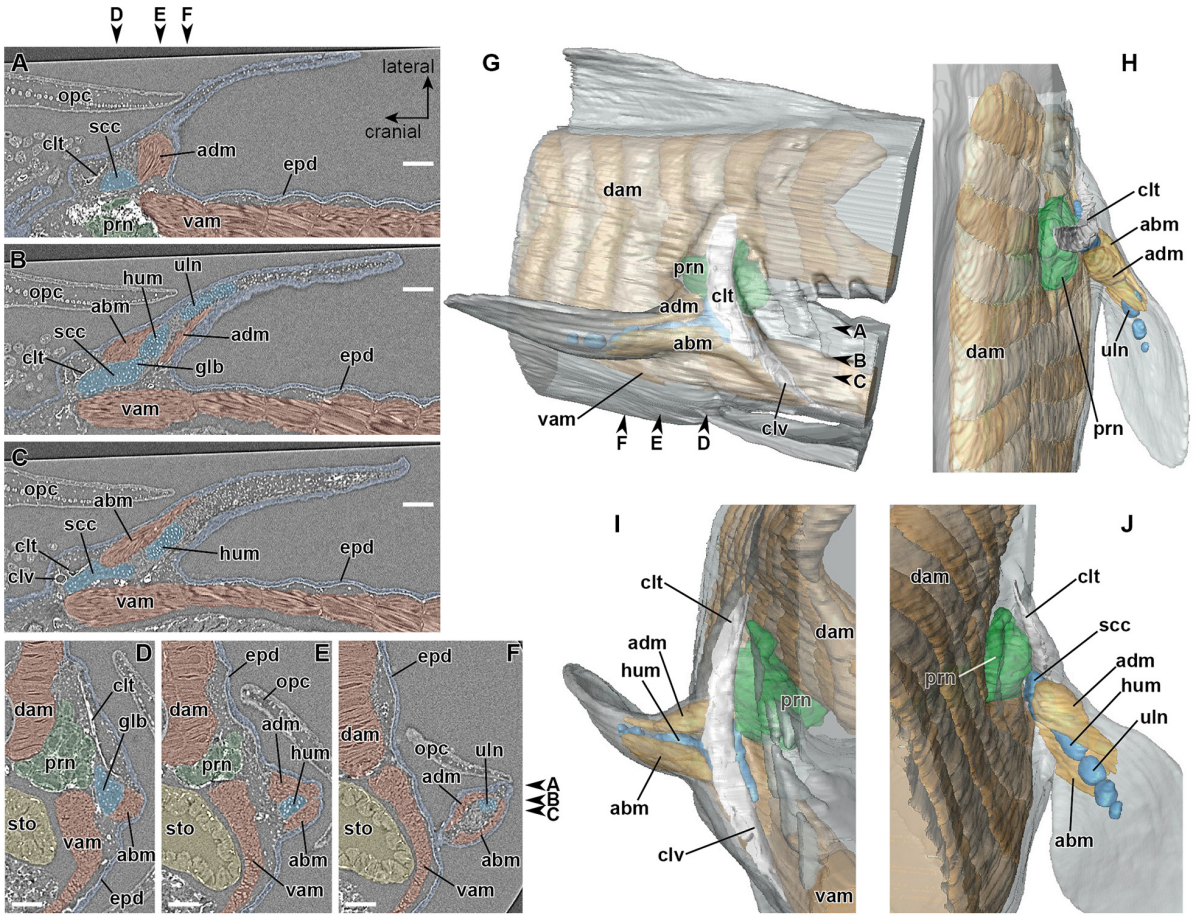

FIGURE 3 | Developing right pectoral fin of *Neoceratodus forsteri* during the late phase of stage 47 (total length = 17.5 mm). **(A–C)** Coronal section. **(D–F)** Transverse section. **(G)** Lateral view. **(H)** Dorsal view. **(I)** Cranial view. **(J)** Caudal view. abm, abductor muscle; adm, adductor muscle; clt, cleithrum; clv, clavicle; dam, dorsal axial muscle; epd, epidermis; glb, glenoid buttress of the scapulocoracoid; hum, humerus; opc, operculum; prn, pronephros; scc, scapulocoracoid; sto, stomach; uln, ulna; vam, ventral axial muscle. Arrowheads indicate the respective sectioned levels. Scale bar = 200 μm.

during the early phase of stage 47 (**Figure 2C**), the cleithrum develops as a dermal bone (**Figures 3A–D**) filling the space between the pronephros and epidermis (**Figure 3D**).

Development of the Girdle Muscle

The axial skeleton develops from stage 47 onward. During the late phase of stage 47, the vertebral elements, namely the neural arch and basiventral arcualium, develop around the notochordal sheath. Subsequently, at the beginning of stage 48 (**Table 1**), the cranial rib extends toward the junction between the dorsal and ventral axial muscles at a level caudal to the pronephros. At this phase, no muscle tissue connected to the cleithrum is recognizable.

Later, in the mid-phase of stage 48 (**Table 1**), the girdle muscle, which corresponds to the retractor lateralis ventralis pectoralis (e.g., Diogo et al., 2016) and to the retractor cleithri muscle (Greil, 1913), becomes differentiated (**Figure 4**). This girdle muscle is connected proximally to the distal end of the cranial rib (**Figures 4C,I**), and distally to the medial surface of the cleithrum (**Figures 4D,E,I**). No connection of the girdle muscle to connective tissue associated with the axial muscles is observable.

Subsequently, in the late phase of stage 48 (**Table 1**), the pectoral fin adductor and abductor muscles subdivide into superficial and deep layers (superficiales and profunduses), and the superficial layers of both muscles expand their proximal connections to the medial surface of the cleithrum.

DISCUSSION

Developmental Environment for the Pectoral Fin Muscles and Their Innervating Nerves

In this study, we used synchrotron phase-contrast microtomography to perform histological observations of pectoral fin development in *N. forsteri*, in light of recent knowledge of vertebrate development. As the examined embryos and larvae possessed large yolk sacs and some mesenchymal tissues characterized by low cell densities, they were not suited for

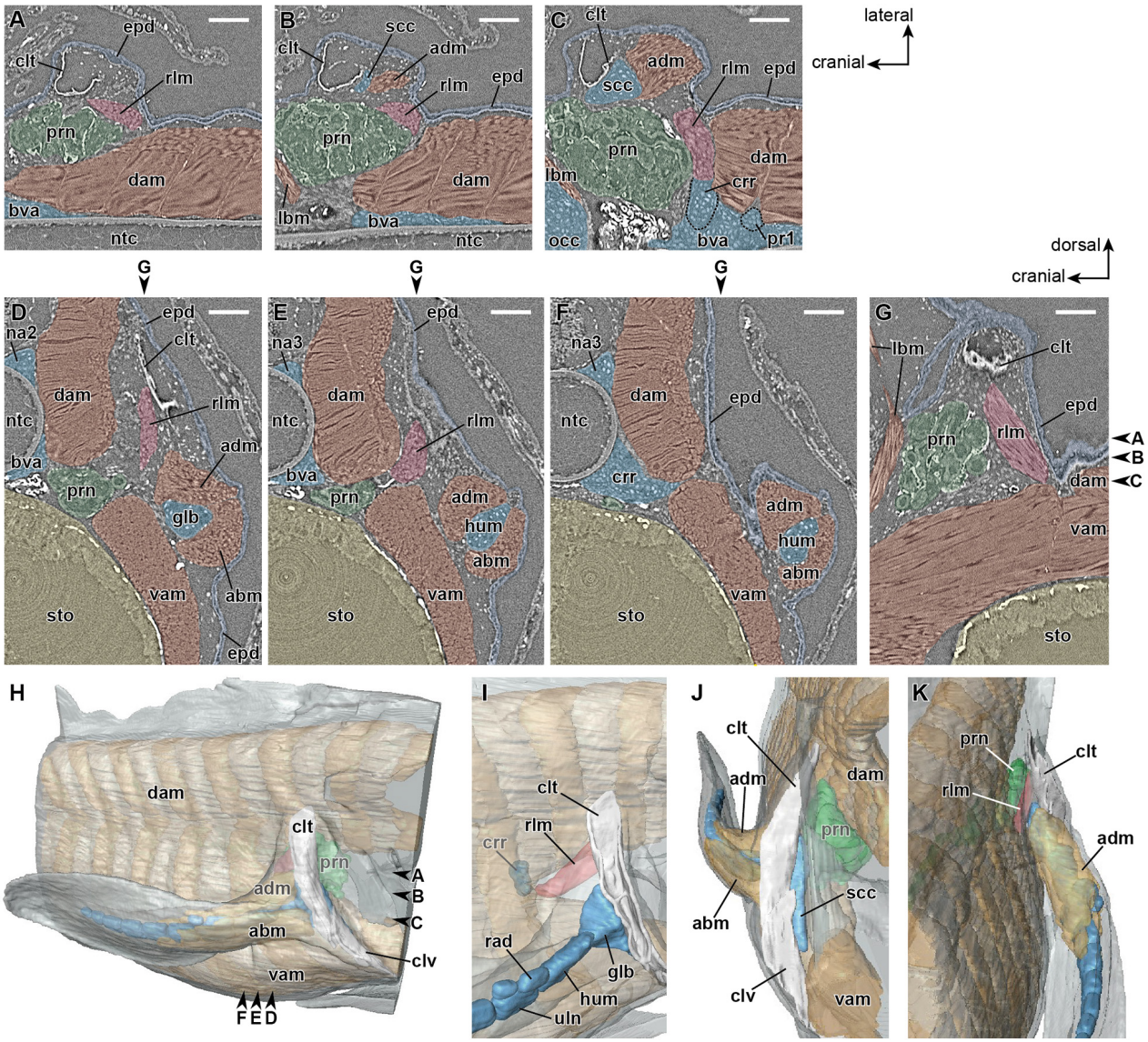

FIGURE 4 | Developing right pectoral fin of *Neoceratodus forsteri* at stage 48 (total length = 20.5 mm). **(A–C)** Coronal section. **(D–F)** Transverse section. **(G)** Sagittal section. **(H)** Lateral view. **(I)** Enlarged image of the retractor laterralis ventralis pectoralis muscle in caudolateral view. **(J)** Cranial view. **(K)** Caudal view. abm, abductor muscle; adm, adductor muscle; bva, basiventral arcualium; clt, cleithrum; clv, clavicle; dam, dorsal axial muscle; crr, cranial rib; epd, epidermis; glb, glenoid buttress of the scapulocoracoid; lbm, levator arcuum branchialium five muscle (i.e., the dorsopharyngeus muscle in Greil, 1913); hum, humerus; na2, neural arch 2; na3, neural arch 3; ntc, notochord; opc, operculum; prn, pronephros; pr1, pleural rib 1; scc, scapulocoracoid; rad, radius; rlm, retractor lateralis ventralis pectoralis muscle (i.e., the retractor cleithri muscle in Greil, 1913); sto, stomach; uln, ulna; vam, ventral axial muscle. Arrowheads indicate the respective sectioned levels. Scale bar = 200 μm.

physical sectioning, which requires retention of heterogeneous tissues on slide glass. On the other hand, virtual sectioning by X-ray microtomography, as a non-destructive technique, can keep the morphologies of all tissues intact, and enables three-dimensional observation at a high resolution. Although resolutions are generally higher in physically prepared sections with staining, or the conventional histological technique, technological advances in X-ray microtomography will continue to provide indispensable contribution to comparative morphology. Future morphological and histological studies may request three-dimensional observations based on X-ray microtomography data. In addition, since the technique used in this study does not require any specific fixation nor chemical treatment, it will be useful to obtain three-dimensional data prior to other experiments, such as analyses on gene expressions.

Our results demonstrate that the pectoral fin of *N. forsteri* develops adjacent to the pronephros, and that there is only a small space available to accommodate the mesenchyme between the axial body wall and fin bud (**Figures 1B**, **2C–E**). The minor mesenchyme intervening between the epidermis

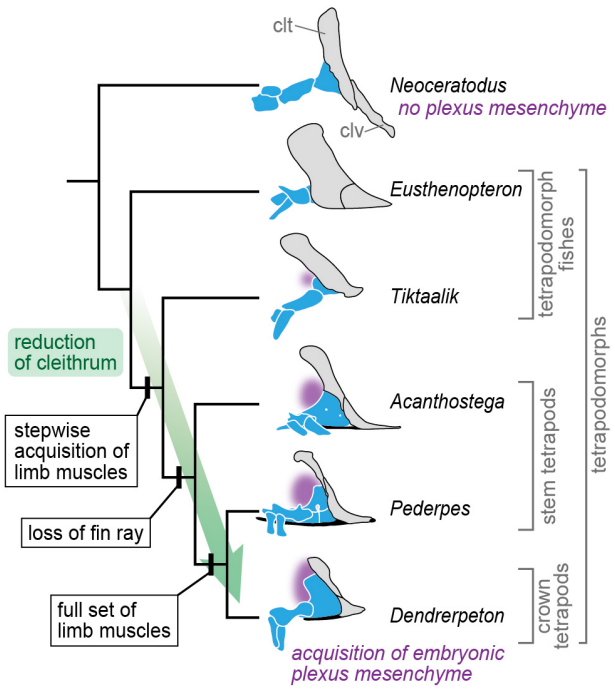

FIGURE 5 | A scenario for evolution of the plexus mesenchyme. In the evolution leading to the crown tetrapods, the cleithrum gradually became reduced, and concurrently, the full set of limb muscles was acquired in a stepwise manner (Molnar et al., 2017). At this transitional phase, the brachial plexus might become evolutionarily fixed, being accompanied with an acquisition of the embryonic plexus mesenchyme, which replaced the cleithrum-forming embryonic domain. The cleithrum and clavicle are gray, endoskeletal shoulder girdle and limb skeleton blue, interclavicle black, and position of the plexus mesenchyme (in embryonic development) purple. Abbreviations: clt, cleithrum; clv, clavicle. The tetrapodomorph skeletons are redrawn from Andrews and Westoll (1970), Coates (1996), Clack and Finney (2005), Shubin et al. (2006), and Clack (2012).

and pronephros at the cranial part of the fin bud base (asterisk in **Figure 2C**) later produces the dermal bone of the cleithrum (**Figures 3D,H–J**), thereby substantially narrowing the migratory routes of the somite-derived muscle progenitor cells and spinal nerve axons. Based on these observations, it is likely that the "plexus mesenchyme" (Wright and Snider, 1996) does not develop in *N. forsteri*. Among extant tetrapods, the mesenchyme occupying the space between the axial body wall and limb bud is similarly small during forelimb development in lissamphibians (Byrnes, 1898; Chen, 1935). In contrast to *N. forsteri*, however, the lack of a cleithrum in lissamphibians allows the mesenchymal environment to remain relatively large. Although further comparative analyses between *N. forsteri* and lissamphibians are needed, it is possible that the evolutionary reduction of the cleithrum in the basal tetrapodomorph lineage (Romer, 1924; Shubin et al., 2006; Molnar et al., 2017; **Figure 5**) allowed the establishment of a novel developmental environment, i.e., the "plexus mesenchyme."

Muscles Connected to the Cleithrum

Our observations roughly show the developmental processes of muscles connected to the cleithrum, including the girdle muscle (retractor lateralis ventralis pectoralis or retractor cleithri) and the superficial adductor and abductor muscles of the pectoral fin.

As the girdle muscle is connected proximally to the distal end of the rib and distally to the medial surface of the cleithrum, it is likely homologous with the tetrapod serratus muscle, which develops as an axial muscle (Valasek et al., 2010, 2011). We demonstrate that the girdle muscle in *N. forsteri* develops distinctly later than the dorsal and ventral axial muscles do (**Figure 4**), but could not identify its primordial cells probably due to rapid differentiation of the girdle muscle; similarly, the detailed developmental process of the tetrapod serratus muscle has also remained elusive (Pu et al., 2016). Nevertheless, in *N. forsteri*, the girdle muscle develops through either dorsocranial extension of the developing muscle from the junction between the dorsal and ventral axial muscles at the level of the cranial rib or differentiation of the mesenchyme occupying the space medial to the cleithrum, because the cleithrum and the axial muscles are separated at the corresponding developmental stage (**Figures 3**, **4**).

In *N. forsteri*, the superficial layers of pectoral fin adductor and abductor muscles, which are homologous with the latissimus dorsi and pectoralis muscles, respectively, become differentiated substantially later than do the deep layers (**Figure 3**). In limb muscle development, these superficial muscles (latissimus dorsi and pectoralis) develop through an "in-out" process, in which the muscle progenitor cells, upon entering the limb bud, extend out from the limb bud onto the axial body wall (Valasek et al., 2011). Based on our observations, in *N. forsteri*, it is probable that the superficial adductor and abductor muscles develop not through the "in-out" process, as the fin bud is occupied by myotubes of the deep adductor and abductor muscles and includes very few undifferentiated muscle progenitor cells (**Figure 3**). This suggests that the "in-out" developmental process of superficial limb muscles first evolved in the tetrapodomorph lineage.

PERSPECTIVES AND CONCLUSION

The tetrapod limb is an evolutionary novelty: new muscles were acquired in the early evolution of limbed tetrapods (Molnar et al., 2017, 2018), and a new variational modality of neuromuscular morphology was established during the fin-to-limb transition (Hirasawa and Kuratani, 2018). Soft-tissue anatomy of fossil vertebrates can often be reconstructed by using phylogenetic bracketing approach (Witmer, 1995), but such approach is ineffective for inferring a transitional state prior to an origin of an evolutionary novelty. Therefore, the process of the soft-tissue evolution during the fin-to-limb transition cannot be deciphered solely through comparative morphological analyses between extant and fossil taxa, although these analyses, together with biomechanics, potentially contribute to an understanding of functional transitions independent of the origin of the evolutionary novelty. Instead, like the vertebrate jaw, another example of evolutionary novelty (Shigetani et al., 2002), the origin of the novel limb soft-tissue patterns will be elucidated by analyzes of developmental genetic bases.

In this study, we conducted three-dimensional observations of the pectoral lobed fin of *N. forsteri* in light of recent knowledge of vertebrate development, by using synchrotron radiation X-ray microtomography. We found that the mesenchyme occupying the junction between the axial body wall and fin bud is quite small in *N. forsteri*, implying the absence of the "plexus mesenchyme" seen in tetrapods. In addition, our observations highlighted the late differentiation timings of the girdle muscle and superficial adductor and abductor fin muscles separate from those of the other axial muscles and deep adductor and abductor fin muscles, respectively. These characteristics of pectoral lobed fin development in *N. forsteri* will lead to a better understanding of the fin-to-limb transition from the viewpoint of evolutionary developmental biology.

DATA AVAILABILITY STATEMENT

The raw data supporting the conclusions of this article will be made available by the authors, without undue reservation.

ETHICS STATEMENT

Ethical review and approval was not required for the animal study because fish species are beyond the scope of ethical review in Japan. However, we conducted the research under self-assessment of ethics.

AUTHOR CONTRIBUTIONS

TH conceived the project. SI collected and prepared the embryonic samples. TH and CC wrote the draft. All authors read and approved the final version of the manuscript and together conducted the synchrotron radiation X-ray tomography of the embryonic samples.

FUNDING

This work was supported by JSPS KAKENHI grant nos. 17H06385 and 19K04061 (to TH), Coordenação de Aperfeiçoamento de Pessoal de Nível Superior, Brasil (CAPES) Finance Code 001-Programa Nacional de Pós Doutorado and UERJ Programa de Apoio à Docência (PAPD) process number E-26/007/10661/2019 (to CC), and CNPq #310101/2017-4 and FAPERJ #E-26/202.890/2018 grants (to PMB).

ACKNOWLEDGMENTS

We thank Jean Joss (Macquarie University) for providing *Neoceratodus* embryos, and Iwate Medical University for their management of the collection of all specimens used in this study. We also appreciate two referees for providing useful comments, which definitely improved our manuscript.

REFERENCES

Ahlberg, P. E. (2019). Follow the footprints and mind the gaps: a new look at the origin of tetrapods. *Earth Environ. Sci. Trans. R. Soc. Edinb.* 109, 115–137. doi: 10.1017/s1755691018000695

Amemiya, C. T., Alfoldi, J., Lee, A. P., Fan, S. H., Philippe, H., MacCallum, I., et al. (2013). The African coelacanth genome provides insights into tetrapod evolution. *Nature* 496, 311–316.

Andrews, S. M., and Westoll, T. S. (1970). The postcranial skeleton of *Eusthenopteron foodi* whiteaves. *Trans. R. Soc. Edinb.* 68, 207–329. doi: 10.1017/s008045680001471x

Betancur-R, R., Wiley, E. O., Arratia, G., Acero, A., Bailly, N., Miya, M., et al. (2017). Phylogenetic classification of bony fishes. *BMC Evol. Biol.* 17:162. doi: 10.1186/s12862-017-0958-3

Braus, H. (1901). Die muskeln und nerven der ceratodusflosse. Ein beitrag zur vergleichenden morphologie der freien gliedmaasse bei niederen fischen und zur archipterygiumtheorie. *Denkschr. Med. Naturwiss. Ges. Jena* 4, 137–300.

Byrnes, E. F. (1898). Experimental studies on the development of limb muscles in amphibia. *J. Morphol.* 14, 105–140. doi: 10.1002/jmor.1050140202

Chen, H. K. (1935). Development of the pectoral limb of *Necturus maculosus*. *Illinois Biol. Monogr.* 14, 1–71. doi: 10.2307/1437018

Clack, J. A. (2012). *Gaining Ground: The Origin and Evolution of Tetrapods*, 2nd Edn. Bloomington: Indiana University Press.

Clack, J. A., and Finney, S. M. (2005). Pederpes finneyae, an articulated tetrapod from the Tournaisian of Western Scotland. *J. Syst. Palaeontol.* 2, 311–346. doi: 10.1017/s1477201904001506

Cloutier, R., Clement, A. M., Lee, M. S. Y., Noel, R., Bechard, I., Roy, V., et al. (2020). *Elpistostege* and the origin of the vertebrate hand. *Nature* 579, 549–554. doi: 10.1038/s41586-020-2100-8

Coates, M. I. (1996). The devonian tetrapod *Acanthostega gunnari* jarvik: postcranial anatomy, basal tetrapod interrelationships and patterns of skeletal evolution. *Trans. R. Soc. Edinb. Earth Sci.* 87, 363–421. doi: 10.1017/s0263593300006787

Davis, M. C., Dahn, R. D., and Shubin, N. H. (2007). An autopodial-like pattern of Hox expression in the fins of a basal actinopterygian fish. *Nature* 447, 473–476. doi: 10.1038/nature05838

Dietrich, S., Schubert, F. R., Healy, C., Sharpe, P. T., and Lumsden, A. (1998). Specification of the hypaxial musculature. *Development* 125, 2235–2249. doi: 10.1242/dev.125.12.2235

Diogo, R., Johnston, P., Molnar, J. L., and Esteve-Altava, B. (2016). Characteristic tetrapod musculoskeletal limb phenotype emerged more than 400 MYA in basal lobe-finned fishes. *Sci. Rep.* 6:37592.

Fürbringer, M. (1888). *Untersuchungen zur Morphologie und Systematik der Vögel: zugleich ein Beitrag zur Anatomie der Stütz- und Bewegungsorgane*. Amsterdam: Van Holkema, 1751.

Grandel, H., and Schulte-Merker, S. (1998). The development of the paired fins in the zebrafish (*Danio rerio*). *Mech. Dev.* 79, 99–120. doi: 10.1016/s0925-4773(98)00176-2

Greil, A. (1913). Entwickelungsgeschichte des Kopfes und des Blutgefäßsystems von *Ceratodus forsteri*. II. Die epigenetischen Erwerbungen während der Stadien 39-48. *Denkschr. Med. Naturwiss. Ges. Jena* 4, 935–1492.

Gross, M. K., Moran-Rivard, L., Velasquez, T., Nakatsu, M. N., Jagla, K., and Goulding, M. (2000). *Lbx1* is required for muscle precursor migration along a lateral pathway into the limb. *Development* 127, 413–424. doi: 10.1242/dev.127.2.413

Haase, G., Dessaud, E., Garcès, A., de Bovis, B., Birling, M. C., Filippi, P., et al. (2002). GDNF acts through PEA3 to regulate cell body positioning and muscle innervation of specific motor neuron pools. *Neuron* 35, 893–905. doi: 10.1016/s0896-6273(02)00864-4

Hirasawa, T., and Kuratani, S. (2018). Evolution of the muscular system in tetrapod limbs. *Zoolog. Lett.* 4:27.

Hodgkinson, V. S., Ericsson, R., Johanson, Z., and Joss, J. M. P. (2009). The apical ectodermal ridge in the pectoral fin of the Australian lungfish (*Neoceratodus forsteri*): keeping the fin to limb transition in the fold. *Acta Zool.* 90, 253–263. doi: 10.1111/j.1463-6395.2008.00349.x

Johanson, Z., Joss, J., Boisvert, C. A., Ericsson, R., Sutija, M., and Ahlberg, P. E. (2007). Fish fingers: digit homologues in sarcopterygian fish fins. *J. Exp. Zool. B Mol. Dev. Evol.* 308, 757–768. doi: 10.1002/jez.b.21197

Johanson, Z., Joss, J. M. P., and Wood, D. (2004). The scapulocoracoid of the queensland lungfish *Neoceratodus forsteri* (Dipnoi : Sarcopterygii): morphology, development and evolutionary implications for bony fishes (Osteichthyes). *Zoology* 107, 93–109. doi: 10.1016/j.zool.2004.01.001

Jung, H., Baek, M., D'Elia, K. P., Boisvert, C., Currie, P. D., Tay, B. H., et al. (2018). The ancient origins of neural substrates for land walking. *Cell* 172, 667–682. doi: 10.1016/j.cell.2018.01.013

Kamei, M., Isogai, S., Pan, W., and Weinstein, B. M. (2010). Imaging blood vessels in the zebrafish. *Methods Cell Biol.* 100, 27–54. doi: 10.1016/b978-0-12-384892-5.00002-5

Kemp, A. (1982). The embryological development of the queensland lungfish, *Neoceratodus forsteri* (Krefft). *Mem. Queensl. Mus.* 20, 553–597.

Kramer, E. R., Knott, L., Su, F. Y., Dessaud, E., Krull, C. E., Helmbacher, F., et al. (2006). Cooperation between GDNF/Ret and ephrinA/EphA4 signals for motor-axon pathway selection in the limb. *Neuron* 50, 35–47. doi: 10.1016/j.neuron.2006.02.020

Miyake, T., Kumamoto, M., Iwata, M., Sato, R., Okabe, M., Koie, H., et al. (2016). The pectoral fin muscles of the coelacanth *Latimeria chalumnae*: functional and evolutionary implications for the fin-to-limb transition and subsequent evolution of tetrapods. *Anat. Rec.* 299, 1203–1223. doi: 10.1002/ar.23392

Mollier, S. (1897). Die paarigen extremitäten der wirbeltiere. III. Die entwickelung der paarigen flossen des stöhrs. *Anat. Hefte* 8, 1–74. doi: 10.1007/bf02316963

Molnar, J. L., Diogo, R., Hutchinson, J. R., and Pierce, S. E. (2017). Reconstructing pectoral appendicular muscle anatomy in fossil fish and tetrapods over the fins-to-limbs transition. *Biol. Rev.* 93, 1077–1107. doi: 10.1111/brv.12386

Molnar, J. L., Diogo, R., Hutchinson, J. R., and Pierce, S. E. (2018). Evolution of hindlimb muscle anatomy across the tetrapod water-to-land transition, including comparisons with forelimb anatomy. *Anat. Rec.* 303, 218–234. doi: 10.1002/ar.23997

Murakami, Y., and Tanaka, M. (2011). Evolution of motor innervation to vertebrate fins and limbs. *Dev. Biol.* 355, 164–172. doi: 10.1016/j.ydbio.2011.04.009

Nakamura, T., Gehrke, A. R., Lemberg, J., Szymaszek, J., and Shubin, N. H. (2016). Digits and fin rays share common developmental histories. *Nature* 536, 225–228. doi: 10.1038/nature19322

Okamoto, E., Kusakabe, R., Kuraku, S., Hyodo, S., Robert-Moreno, A., Onimaru, K., et al. (2017). Migratory appendicular muscles precursor cells in the common ancestor to all vertebrates. *Nat. Ecol. Evol.* 1, 1731–1736. doi: 10.1038/s41559-017-0330-4

Paganin, D., Mayo, S. C., Gureyev, T. E., Miller, P. R., and Wilkins, S. W. (2002). Simultaneous phase and amplitude extraction from a single defocused image of a homogeneous object. *J. Microsc.* 206, 33–40. doi: 10.1046/j.1365-2818.2002.01010.x

Pierce, S. E., Clack, J. A., and Hutchinson, J. R. (2012). Three-dimensional limb joint mobility in the early tetrapod *Ichthyostega*. *Nature* 486, 523–526. doi: 10.1038/nature11124

Pu, Q., Huang, R., and Brand-Saberi, B. (2016). Development of the shoulder girdle musculature. *Dev. Dyn.* 245, 342–350. doi: 10.1002/dvdy.24378

Romer, A. S. (1924). Pectoral limb musculature and shoulder-girdle structure in fish and tetrapods. *Anat. Rec.* 27, 119–143. doi: 10.1002/ar.1090270210

Saito, H. (1988a). Development of the vasculature of the pectoral fin in the Australian lungfish, *Neoceratodus forsteri*. *Am. J. Anat.* 182, 183–196. doi: 10.1002/aja.1001820208

Saito, H. (1988b). The development of the vasculature of the pelvic fin in the Australian lungfish, *Neoceratodus forsteri*. *Tohoku J. Exp. Med.* 156, 359–373. doi: 10.1620/tjem.156.359

Salensky, W. (1899). "Entwicklungsgeschichte des ichthyopterygiums," in *Proceedings of the 4th International Congress of Zoology*, Cambridge, 177–183.

Sanchez, S., Dupret, V., Tafforeau, P., Trinajstic, K. M., Ryll, B., Gouttenoire, P. J., et al. (2013). 3D microstructural architecture of muscle attachments in extant and fossil vertebrates revealed by synchrotron microtomography. *PLoS One* 8:e56992. doi: 10.1371/journal.pone.0056992

Schindelin, J., Arganda-Carreras, I., Frise, E., Kaynig, V., Longair, M., Pietzsch, T., et al. (2012). Fiji: an open-source platform for biological-image analysis. *Nat. Methods* 9, 676–682. doi: 10.1038/nmeth.2019

Semon, R. (1898). Die entwickelung der paarigen flossen des *Ceratodus forsteri*. *Denkschr. Med. Naturwiss. Ges. Jena* 4, 59–111.

Shann, E. W. (1920). The comparative myology of the shoulder girdle and pectoral fin of fishes. *Trans. R. Soc. Edinb.* 52, 531–570. doi: 10.1017/s0080456800004452

Shann, E. W. (1924). Further observations on the myology of the pectoral region in fishes. *Proc. Zool. Soc. Lond.* 94, 195–215. doi: 10.1111/j.1096-3642.1924.tb01497.x

Shigetani, Y., Sugahara, F., Kawakami, Y., Murakami, Y., Hirano, S., and Kuratani, S. (2002). Heterotopic shift of epithelial-mesenchymal interactions in vertebrate jaw evolution. *Science* 296, 1316–1319. doi: 10.1126/science.1068310

Shubin, N. H., and Alberch, P. (1986). A morphogenetic approach to the origin and basic organization of the tetrapod limb. *Evol. Biol.* 20, 319–387. doi: 10.1007/978-1-4615-6983-1_6

Shubin, N. H., Daeschler, E. B., and Coates, M. I. (2004). The early evolution of the tetrapod humerus. *Science* 304, 90–93. doi: 10.1126/science.1094295

Shubin, N. H., Daeschler, E. B., and Jenkins, F. A. (2006). The pectoral fin of *Tiktaalik roseae* and the origin of the tetrapod limb. *Nature* 440, 764–771. doi: 10.1038/nature04637

Tanaka, M. (2016). Fins into limbs: autopod acquisition and anterior elements reduction by modifying gene networks involving 5'Hox, Gli3, and Shh. *Dev. Biol.* 413, 1–7. doi: 10.1016/j.ydbio.2016.03.007

Turner, N., Mikalauskaite, D., Barone, K., Flaherty, K., Senevirathne, G., Adachi, N., et al. (2019). The evolutionary origins and diversity of the neuromuscular system of paired appendages in batoids. *Proc. R. Soc. B Biol. Sci.* 286:20191571. doi: 10.1098/rspb.2019.1571

Uesugi, K., Hoshino, M., Takeuchi, A., Suzuki, Y., Yagi, N., and Nakano, T. (2010). Development of fast (sub-minute) micro-tomography. *AIP Conf. Proc.* 1266, 47–50.

Ura, R. (1956). Kontribuo al ontogenio de vazsistemo de antauaj membroj, precipe ce *Hymobius naevius*: unu provo solvi membroproblemon. *Okajimas Folia Anat. Jpn.* 28, 256–285.

Valasek, P., Theis, S., DeLaurier, A., Hinits, Y., Luke, G. N., Otto, A. M., et al. (2011). Cellular and molecular investigations into the development of the pectoral girdle. *Dev. Biol.* 357, 108–116. doi: 10.1016/j.ydbio.2011.06.031

Valasek, P., Theis, S., Krejci, E., Grim, M., Maina, F., Shwartz, Y., et al. (2010). Somitic origin of the medial border of the mammalian scapula and its homology to the avian scapula blade. *J. Anat.* 216, 482–488. doi: 10.1111/j.1469-7580.2009.01200.x

Wagner, G. P. (2014). *Homology, Genes, and Evolutionary Innovation*. Princeton, NY: Princeton University Press, 496.

Witmer, L. M. (1995). "The extant phylogenetic bracket and the importance of reconstructing soft tissue in fossils," in *Functional Morphology in Vertebrate Paleontology*, ed. J. J. Thomason (Cambridge: Cambridge University Press), 19–33.

Woltering, J. M., Irisarri, I., Ericsson, R., Joss, J. M. P., Sordino, P., and Meyer, A. (2020). Sarcopterygian fin ontogeny elucidates the origin of hands wiith digits. *Sci. Adv.* 6:eabc3510. doi: 10.1126/sciadv.abc3510

Wright, D. E., and Snider, W. D. (1996). Focal expression of glial cell line-derived neurotrophic factor in developing mouse limb bud. *Cell Tissue Res.* 286, 209–217. doi: 10.1007/s004410050689

Wynd, B. M., Daeschler, E. B., and Stocker, M. R. (2019). Evolutionary homology in the fin-to-limb transition: evaluating the morphology of foramina in a late devonian humerus from the catskill formation, Clinton County, Pennsylvania. *J. Vertebr. Paleontol.* 39:e1718682. doi: 10.1080/02724634.2019.1718682

Conflict of Interest: The authors declare that the research was conducted in the absence of any commercial or financial relationships that could be construed as a potential conflict of interest.

frontiers in Ecology and Evolution

PERSPECTIVE
published: 03 August 2021
doi: 10.3389/fevo.2021.702576

The Evolution of Appendicular Muscles During the Fin-to-Limb Transition: Possible Insights Through Studies of Soft Tissues, a Perspective

Rohan Mansuit[1,2]* *and Anthony Herrel*[2]

[1] UMR 7207, CNRS, Département Origines and Evolution, Centre de Recherche en Paléontologie, Muséum National d'Histoire Naturelle, Sorbonne Université, Paris, France, [2] UMR 7179, CNRS, MECADEV, Département Adaptations du Vivant, Muséum National d'Histoire Naturelle, Sorbonne Université, Paris, France

The evolution of the appendages during the fin-to-limb transition has been extensively studied, yet the majority of studies focused on the skeleton and the fossil record. Whereas the evolution of the anatomy of the appendicular musculature has been studied, the changes in the muscular architecture during the fin-to-limb transition remain largely unstudied, yet may provide important new insights. The fin-to-limb transition is associated with the appearance of a new mode of locomotion and the associated shift from pectoral to pelvic dominance. Here, we propose ways to investigate this question and review data on muscle mass and muscle architecture of the pectoral and pelvic muscles in extant vertebrates. We explore whether changes in appendage type are associated with changes in the muscular architecture and the relative investment in different muscle groups. These preliminary data show a general increase in the muscle mass of the appendages relative to the body mass during the fin-to-limb transition. The locomotor shift suggested to occur during the fin-to-limb transition appears supported by our preliminary data since in "fish" the pectoral fins are heavier than the pelvic fins, whereas in tetrapods, the forelimb muscles are less developed than the hind limb muscles. Finally, a shift in the investment in different muscle groups with an increase of the contribution of the superficial groups in tetrapods compared to "fish" appears to take place. Our study highlights the potential of investigating quantitative features of the locomotor muscles, yet also demonstrates the lack of quantitative data allowing to test these ideas.

Keywords: appendages, muscle architecture, locomotor shift, homology, functional morphology

OPEN ACCESS

Edited by:
Ingmar Werneburg,
University of Tübingen, Germany

Reviewed by:
Virginia Abdala,
IBN, CONICET-UNT, Argentina
David Marjanović,
Museum of Natural History Berlin (MfN), Germany

***Correspondence:**
Rohan Mansuit
rohan.mansuit@mnhn.fr

Specialty section:
This article was submitted to Paleontology, a section of the journal Frontiers in Ecology and Evolution

Received: *29 April 2021*
Accepted: *13 July 2021*
Published: *03 August 2021*

Citation:
Mansuit R and Herrel A (2021) The Evolution of Appendicular Muscles During the Fin-to-Limb Transition: Possible Insights Through Studies of Soft Tissues, a Perspective. Front. Ecol. Evol. 9:702576. doi: 10.3389/fevo.2021.702576

INTRODUCTION

The water-to-land transition of vertebrates is associated with a number of morphological transformations of the body (Brazeau and Ahlberg, 2006; Daeschler et al., 2006), including the transformation from fins into limbs (Coates et al., 2002; Ahlberg et al., 2005; Cole et al., 2011; Pierce et al., 2012). The evolution of the appendages in sarcopterygians has been extensively studied, but the majority of the studies to date have focused on the skeleton as it is well documented in the

fossil record (Andrews and Westoll, 1970; Coates et al., 2002; Boisvert, 2005; Daeschler et al., 2006; Shubin et al., 2006; Boisvert et al., 2008; Pierce et al., 2012). Previous studies on the development (Shubin and Alberch, 1986; Joss and Longhurst, 2001; Cole et al., 2011; Boisvert et al., 2013), the genetics (Coates, 1995; Johanson et al., 2007; Zhang et al., 2010; Nakamura et al., 2016), and the musculature (Boisvert et al., 2013; Diogo et al., 2016; Molnar et al., 2018, 2020) of fins and limbs have shed light on the evolution of the tetrapod limb. However, the changes in the investment in different muscle groups as well as the architecture (i.e., muscle mass, fiber length, pennation angle, and cross-section area) of the appendicular muscles during the fin-to-limb transition remain virtually unstudied. However, as the fin-to-limb transition is marked by the appearance of a new mode of locomotion (Ahlberg et al., 2005; Cole et al., 2011; Pierce et al., 2012), changes in muscle architecture as well as the differential investment in different functional groups can be expected. Soft-tissue preservation is typically very incomplete in fossils and consequently it is not possible to directly study the evolution of the appendicular muscles during the fin-to-limb transition. Although some exceptionally preserved stem-tetrapods like *Ossinodus pueri* have allowed a reconstruction of the forelimb muscles (Bishop, 2014), quantitative data like muscle masses cannot be extrapolated from the fossils.

Osteichthyans are divided in actinopterygians and sarcopterygians, two clades partly defined on the anatomy of the pectoral and pelvic appendages (Janvier, 1996). Actinopterygians have poly-basal articulated paired fins, with dermal fin rays that insert at the level of the pectoral and pelvic girdles by means of several radial elements connected to three basal cartilages and covered by small muscles located within the body wall. Sarcopterygians have mono-basal articulated paired appendages with an endoskeletal metapterygial axis formed by the alignment of several endoskeletal elements between the pectoral and pelvic girdles and the fin rays/digits. This metapterygial axis is covered by large muscles located at least partly outside of the body wall. The metapterygial axis is connected to the girdles by a single proximal element (Rosen et al., 1981; Janvier, 1996), but see Mansuit et al. (2021) for the coelacanth *Latimeria* where two proximal elements are connected to the pelvic girdle. Living sarcopterygians include the coelacanth, lungfish and tetrapods. In actinopterygians locomotion is mainly driven by body undulation generated by the axial musculature and the use of the pectoral fins. In contrast, in tetrapods, there is a dominance of the pelvic appendages in generating propulsion (Coates et al., 2002; Boisvert, 2005; Cole et al., 2011; Boisvert et al., 2013). The evolution from "front-to-rear-wheel drive" has been studied in early tetrapodomorph fossils (Carroll et al., 2005; Clack, 2012), yet has rarely been explored using living analogs. Quantitative information such as the muscle mass, fiber length, or muscle cross-section area is, however, crucial to be able interpret the ecological and locomotor changes that may have occurred during the fin-to-limb transition.

Although the relative mass of the limb muscles in tetrapods seems at first sight greater than that of the paired fins in "fishes", this has never been investigated quantitatively. Here, we survey the literature to extract quantitative data on the muscle architecture of pectoral and pelvic appendages in extant vertebrates to investigate the hypothesis that a switch to a hindlimb-driven locomotion, as suggested by the skeletal anatomy of the appendages of tetrapodomorphs, is associated with changes in the limb muscles. We further explored whether changes in appendage type (fins or limbs) are associated with changes in muscle architecture and the investment in different muscle groups of the fore- and hind limbs. As quantitative data are scant, our preliminary analyses should be seen as a proof of concept and will hopefully stimulate researchers to investigate limb muscles more systematically and in a quantitative manner.

MATERIALS AND METHODS

For this study we used data on muscle mass or architecture (e.g., cross-sectional area of a muscle) from published studies on the appendages of actinopterygians and sarcopterygians. The functional role of muscles can only be assessed by quantifying their size as well as their architecture. Architectural variables encompass muscle fiber length, fiber orientation and pennation, and the derived muscle cross-sectional areas which are a good proxy of the force-generating capacity of a muscle. Data for actinopterygians were taken from Thorsen and Westneat (2005), Dickson and Pierce (2019), and Crawford et al. (2020). Unfortunately, there was no study that compared the muscle architecture of the pectoral and pelvic fins in the same species; therefore, data were compiled across different studies. The data on the muscle architecture of the pectoral and pelvic fins of the extant coelacanth *Latimeria chalumnae*, as a model of a sarcopterygian fish, were taken from Huby et al. (2021). We used here data on *Latimeria* because it is the only sarcopterygian fish with data on the muscular architecture of its appendages, even if it is not the closest living relative to Tetrapoda. Concerning tetrapods, we excluded all birds from our dataset since they have highly derived forelimbs specialized for flight, but we covered a diversity of tetrapods that use quadrupedal locomotion. We included the data on the alligator *Alligator mississippiensis* (Allen et al., 2010), varanid lizards (Dick and Clemente, 2016; Cieri et al., 2020), and several mammals (Payne et al., 2005a; Ercoli et al., 2013, 2015; Moore et al., 2013; Rupert et al., 2015; Warburton et al., 2015; Olson et al., 2016; Martin et al., 2019). The publications on the coelacanth (Huby et al., 2021), the alligator (Allen et al., 2010), the varanids (Dick and Clemente, 2016; Cieri et al., 2020), the short-nosed bandicoot *Isoodon* (Warburton et al., 2015; Martin et al., 2019) and the grison *Galictis* (Ercoli et al., 2013, 2015) include both the pectoral and pelvic appendages. The data for the American badger, *Taxidea taxus* (Moore et al., 2013), the nine-banded armadillo, *Dasypus novemcinctus* (Olson et al., 2016), and the marmot *Marmota monax* (Rupert et al., 2015) pertain only to the forelimb, whereas the data for the horse *Equus caballus* (Payne et al., 2005a) pertain only to the hind limb.

The muscles were classified in homologous groups, using the homologies between fin and limb muscles proposed by Diogo et al. (2016) and Molnar et al. (2018, 2020). Four intrinsic muscle groups are considered here: the *abductor superficialis, abductor profundus, adductor superficialis* and *adductor profundus* groups

(**Figure 1**). Concerning the pelvic limb of tetrapods, the *caudofemoralis* muscle is not considered in this study, despite being an important muscle for the retraction of the limb. As it originates from the axial musculature of the body it was considered not to be a limb muscle *sensu stricto*. Homologies between the muscles of the pectoral and pelvic appendages in each species included in this study are shown in **Supplementary Tables 1, 2**.

We first investigated the evolution of the muscle architecture of the pectoral and pelvic appendages, using the measurements obtained from the literature provided in **Table 1**. Only the data that allow the comparison between the pectoral and pelvic appendages are used here, i.e., for the coelacanth, the alligator, the varanid lizard and the short-nosed bandicoot. Although the data on the grison, *Galictis*, correspond to fore- and hind limbs, it is not possible to compare the two appendages since the muscle mass in the publications are given only in a relative proportion to the total muscle mass of the corresponding limb, and not to the total body mass (Ercoli et al., 2013, 2015).

We also explored the evolution of the distribution of the muscle groups in the appendages, using the measurements provided in **Table 1**. Since we focus on the distribution of the muscle groups inside an appendage, we can here also use the data from species for which only one appendage is available. We used data presented relative to body mass or relative to the overall appendicular muscle mass (*Galictis,* Ercoli et al., 2013, 2015) as well as the data on the physiological cross-sectional area (PCSA) of the fin muscles in fish (*Cryptopsaras, Antennarius,* and *Carrasius*; Dickson and Pierce, 2019; Crawford et al., 2020). The data are, however, not complete enough to statistically test the observed trends. Unfortunately, quantitative data on complete limbs are rare and data for both front and hind limbs of the same species are even rarer. Yet, such data are needed to statistically test hypotheses pertaining to the fin-to-limb transition.

RESULTS

Evolution of the Muscle Architecture of the Pectoral and Pelvic Appendages

In the sarcopterygian fish *Latimeria*, the muscle mass of the pectoral limb is greater than that of the pelvic limb (0.43 vs. 0.30% of total body mass). In tetrapods, the muscle mass of the pectoral limb is smaller than that of the pelvic limb (**Table 1**). Moreover, it appears that in tetrapods, the muscle mass of the limbs is proportionally greater than in fish-like animals. Indeed, in actinopterygians and *Latimeria*, each appendage has a mass relative to the body mass inferior to 1% (**Table 1**), whereas in tetrapods, the mass, relative to body mass, is greater (>1.7%; up to 8.5% in the short-nosed bandicoot).

Evolution of the Architecture of the Muscle Groups

In actinopterygians, both for the pectoral and pelvic fins, the muscle groups that contribute the most to the overall fin muscle mass are the deep groups (*abductor/adductor profundus*) (**Table 1**). Similarly, in the sarcopterygian fish *Latimeria*, the muscle groups that contribute the most to the total muscle mass are the deep muscles (*abductor/adductor profundus* groups) (**Table 1**), irrespective of the limb. However, in tetrapods, the muscle groups that contribute most to the mass of the appendages are the superficial groups (*abductor/adductor superficialis*), both for the fore- and hind limbs. In this data set only the horse *Equus caballus* stands out since the *adductor profundus* group is heavier than the *adductor superficialis* group.

DISCUSSION

Shift From Pectoral to Pelvic Appendage Dominance

The fin-to-limb transition has been proposed to be characterized by a shift from the pectoral to pelvic dominance causing changes in its size and proportions (Coates et al., 2002; Boisvert, 2005; Don et al., 2013). Indeed, in actinopterygians and sarcopterygian fishes the pectoral fin is greater than the pelvic fin and the pelvic girdle is small and "free" from the axial skeleton. The muscular data from the different studies included in our meta-analysis tend to confirm this hypothesis. Indeed, for the sarcopterygian fish *Latimeria*, the pectoral fin has a greater muscle mass than the pelvic fin, whereas in tetrapods, the hind limb has a greater mass than the forelimb. The fins are also proportionally smaller than the limbs of tetrapods since the summed muscle mass of each fin represents less than 1% of the total body mass of the organism (**Table 1**). In tetrapods, the relative size of each limb is greater, reaching up to nearly 6% of the total body mass. According to Andrews and Westoll (1970), the size difference between fins and limbs is probably due to their different function. Indeed, in fish locomotion and propulsion is mainly produced by lateral undulation of the body and the use of the caudal fin (Bainbridge, 1963; Lighthill, 1971; Webb, 1982; Lauder, 2000; George and Westneat, 2019). The paired fins are mainly used for different types of maneuvers (Webb, 1982; Wilga and Lauder, 1999; Lauder, 2000; Drucker and Lauder, 2003; Standen, 2008). During terrestrial locomotion in tetrapods the limbs need to support the body against gravity in addition to providing propulsion. In support of this idea, it has been demonstrated that in a more terrestrial living environment the endoskeleton of the pectoral fin of *Polypterus* becomes longer and more robust due to the increased use of the fins for locomotion and in the lifting the anterior part of the body above the substrate (Standen et al., 2014; Du and Standen, 2020). The terrestrial environment and a walking-type locomotion thus appear to require greater forces to move the appendages, compared to swimming (Du and Standen, 2017). Interestingly, in benthic anglerfish that walk on the substrate the pectoral fins are also stronger and more robust (Dickson and Pierce, 2019). Moreover, the muscles of the pectoral fin are heavier and stronger compared to body size, compared to the pelagic anglerfishes that swim. Dickson and Pierce (2019) showed, for example, that the benthic anglerfish *Antennarius* has four times stronger fin muscles than the pelagic anglerfish *Carrassius*. This stronger fin is associated with a larger muscle volume and mass. The larger and stronger fins or limbs

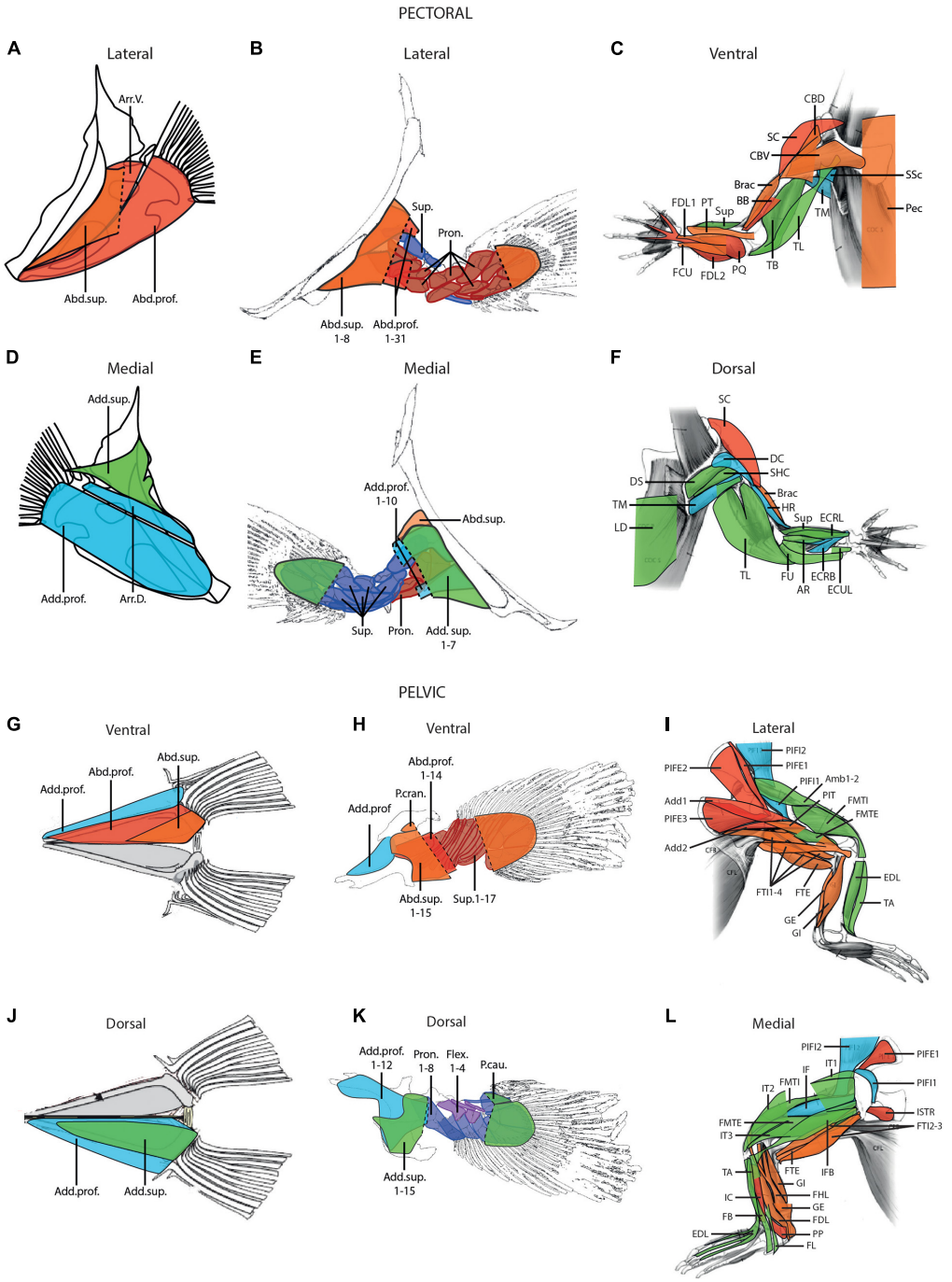

FIGURE 1 | Hypotheses of homology of the muscles of the pectoral **(A–F)** and pelvic **(G–L)** appendages in fish **(A,D,G,J)**, the coelacanth, *Latimeria* **(B,E,H,K)**, and the alligator **(C,F,I,L)**; modified from Thorsen and Westneat (2005), Allen et al. (2010), and Huby et al. (2021). Blue, *adductor profundus* group; green, a*dductor superficialis* group; orange, *abductor superficialis* group; red, *abductor profundus* group. Note that for the coelacanth *Latimeria* **(B,E,H,K)** the profundus groups are separated in two different layers. Abd.prof., *abductor profundus*; Abd.sup., *abductor superficialis*; Add.prof., *adductor profundus*; Add.sup., *adductor superficialis*; Add, *adductor*; Amb, *ambiens*; Arr.D., *arrector dorsalis*; Arr.V., *arrector ventralis*; AR, *abductor radialis*; BB, *biceps brachii*; Brac, *brachialis*; CBD, *coracobrachialis dorsalis*; CBV, *coracobrachialis ventralis*; DC, *deltoideus clavicularis*; DS, *deltoideus scapularis*; ECRB, *extensor carpi radialis brevis*; ECRL, *extensor carpi radialis longus*; ECUL, *extensor carpi ulnaris longus*; EDL, *extensor digitorum longus*; FB, *fibularis brevis*; FCU, *flexor carpi ulnaris*; FDL, *flexor digitorum longus*; FHL, *flexor hallucis longus*; FL, *fibularis longus*; FMTE, *femorotibialis externus*; FMTI, *femorotibialis internus*; FTE, *flexor tibialis externus*; FTI, *flexor tibialis internus*; FU, *flexor ulnaris*; GE, *gastrocnemius externus*; GI, *gastrocnemius internus*; HR, *humeroradialis*; IC, *interosseus cruris*; IF, *iliofemoralis*; IFB, *iliofibularis*; ISTR, *ischiotrochantericus*; IT, *iliotibialis*; LD, *latissimus dorsi*; Pec, *pectoralis*; PIFE, *puboischiofemoralis externus*; PIFI, *puboischiofemoralis internus*; PIT, *puboischiotibialis*; PP, *pronator profundus*; PQ, *pronator quadratus*; Pron., *pronator*; PT, *pronator teres*; SC, *supracoracoideus*; SHC, *scapulohumeralis caudalis*; SSc, *subscapularis*; Sup, *supinator*; TA, *tibialis anterior*; TB, *triceps brevis*; TL, *triceps longus*; TM, *teres major*.

TABLE 1 | Distribution of the muscle groups of the pectoral and pelvic appendages.

	Pectoral					Pelvic				
	Abductor superficialis	***Abductor profundus***	***Adductor superficialis***	***Adductor profundus***	**Total**	***Abductor superficialis***	***Abductor profundus***	***Adductor superficialis***	***Adductor profundus***	**Total**
Abudefduf saxatilis [M_{muscle}/M_{body} (%)]	0.13	0.23	0.15	0.18	**0.69**	–	–	–	–	–
Cryptopsaras [normalized PCSA (mm^2)]	0.19	0.22	0.02	0.26	**0.69**	–	–	–	–	–
Antennarius [normalized PCSA (mm^2)]	0.53	1.13	0.12	1.31	**3.08**	–	–	–	–	–
Carassius auratus [normalized PCSA (mm^2)]	–	–	–	–	–	7.46E-04	2.06E-03	8.45E-04	3.32E-03	**6.97E-03**
Latimeria chalumnae [M_{muscle}/M_{body} (%)]	0.08	0.16	0.09	0.10	**0.43**	0.07	0.10	0.04	0.10	**0.30**
Alligator mississippiensis [M_{muscle}/M_{body} (%)]	0.86	0.20	0.45	0.24	**1.76**	1.15	0.55	0.85	0.72	**3.27**
Varanidae [M_{muscle}/M_{body} (%)]	1.48	0.24	1.23	0.12	**3.07**	1.68	0.27	1.44	0.59	**3.98**
Isoodon sp. [M_{muscle}/M_{body} (%)]	1.41	0.41	1.15	0.30	**3.26**	4.25	0.40	2.90	0.97	**8.52**
Galictis cuja [M_{muscle}/M_{limb} (%)]	54.17	20.54	71.20	15.84	**101.08**	47.23	7.42	30.39	11.66	**96.70**
Taxidea taxus [M_{muscle}/M_{body} (%)]	0.76	0.42	1.34	0.31	**2.83**	–	–	–	–	–
Dasypus novemcinctus [M_{muscle}/M_{body} (%)]	0.74	0.28	1.38	0.26	**2.66**	–	–	–	–	–
Marmota monax [M_{muscle}/M_{body} (%)]	0.85	0.31	1.30	0.41	**2.86**	–	–	–	–	–
Equus caballus [M_{muscle}/M_{limb} (%)]	–	–	–	–	–	42.33	8.95	17.17	28.20	**96.65**

The gray rows correspond to values that are not expressed relative to body mass. The bold values are correspond to the sum of the different muscle groups of the appendage.

are considered as essential to support the larger pushing forces against the substrate, necessary for locomotion (Du and Standen, 2017). Thus, larger muscles allow to produce the greater forces needed to support the body and to move on the substrate by walking both in benthic and terrestrial environments. It is, however, necessary to be cautious with these generalizations. Indeed, most of the data sets are incomplete and only focus on one appendage, thus complicating the interpretations of the results. Furthermore, even if there are numerous studies that focus on the muscle architecture of the limbs in mammals, data for other tetrapods are scarce, especially for lissamphibians. Data on the pelvic fins of fishes are also particularly scant. A larger sample of fish and tetrapods is clearly needed to be able to generalize these results, and may allow to test many of the trends observed here.

Distribution of the Muscle Groups

The distribution of the muscle groups along the appendages, based on the homologous relations described by Diogo et al. (2016) (**Supplementary Tables 1, 2**), is different between "fishes" and tetrapods. The *abductor* and *adductor superficialis* muscle groups are heavier than the deep muscle groups in tetrapods, both for the pectoral and pelvic appendages. In fish, the distribution of the muscle groups is different since the deep muscle groups are more developed. Thus, during the fin-to-limb transition there was a shift in the distribution of the muscle groups with a reduction of the deep muscles in tetrapods and the development of the superficial muscle groups in term of mass and strength. The heavier *adductor profundus* compared to *adductor superficialis* in the hind limb of *Equus caballus* represents an unusual condition among tetrapods. It is possible that this distribution of the muscle groups in the hind limb of the horse is linked with the adaptation for cursoriality and the skeletal anatomy of the limb. However, it would be necessary to look at the distribution of the muscle groups inside the forelimb of the horse to validate this hypothesis, yet the data in the literature are incomplete concerning this limb. The extrinsic muscle anatomy of this limb and the distal muscle anatomy were studied in two different studies (Brown et al., 2003; Payne et al., 2005b), and the compilation of the data does not allow to obtain a full overview of the fore limb muscle anatomy. Except for the horse which presents functional features of the fore- and hind limbs associated with a highly specialized cursorial locomotion, it appears that the increase in size and development of the muscles of the superficial groups may be linked to the adaptations of the limbs to terrestrial locomotion. However, the change in muscles distribution might not only be linked to this "new" mode of locomotion. Indeed, in walking anglerfishes, the distribution of the muscle groups is similar to that of swimming fishes with deep muscles that are stronger than the superficial muscles. It is thus likely that other constraints are involved in the changes in relative muscle development observed in tetrapods. Specifically, terrestrial tetrapods need to support their body mass whereas in anglerfish buoyancy helps to support body mass. It is consequently essential to complete the dataset with fish that "walk" in a terrestrial environment to test the idea that buoyancy has an impact on the distribution of the muscles in "walking" fishes.

Whereas in terrestrial tetrapods the change in muscle distribution seems directly linked to walking and the support of the body against gravity, specialized locomotor modes (e.g., digging, running, flying, or swimming) may cause animals to deviate from this general pattern. Adding species with specialized locomotor behaviors could help reconstruct the muscles in early tetrapods with different life styles.

CONCLUSION

This preliminary study presents promising results on the evolution of the muscular anatomy of the appendages during the fin-to-limb transition and shows that these types of data may help to better understand this major evolutionary transition. The general increase in the muscle mass of the appendages relative to body size in tetrapods is in line with observations on the skeletal

elements in the fossil record. More strongly developed muscles are often associated with an increase in the force developed by the muscles directly linked to the function of the appendages. Indeed, in fishes, propulsion is mainly produced by the axial muscles involved in the lateral undulation of the body and the caudal fin, whereas in terrestrial tetrapods the limbs support the body and produce most of the thrust for the propulsion. The proposed shift from "front-" to "rear-wheel drive," suggested by the changes in skeletal anatomy during the evolutionary history of tetrapodomorphs, is also corroborated by the muscle distribution data available in the literature. Indeed, in fish the pectoral fins are heavier than the pelvic fins, whereas in terrestrial tetrapods the forelimbs are smaller and lighter than the hind limbs relative to body size. Finally, this study highlights a shift in the distribution of the muscle groups during the fin-to-limb transition with an increase of the contribution of the superficial muscle groups in tetrapods compared to "fish." However, as quantitative data in the literature are often fragmentary and incomplete, it is crucial to add quantitative data from dissections to be able to formally test these hypotheses.

DATA AVAILABILITY STATEMENT

The original contributions presented in the study are included in the article/ **Supplementary Material**, further inquiries can be directed to the corresponding author.

AUTHOR CONTRIBUTIONS

RM and AH designed the study and interpreted the results. RM wrote the manuscript. AH revised the manuscript. Both authors contributed to the article and approved the submitted version.

FUNDING

This work was supported by a grant from Agence Nationale de la Recherche in the LabEx ANR-10-LABX-0003-BCDiv, program "Investissements d'avenir" no. ANR-11-IDEX-0004-02.

ACKNOWLEDGMENTS

We thank Gaël Clément and Marc Herbin from the MNHN for their advice that improved our work. We are grateful to Catherine Boisvert and Julia Molnar for their invitation to contribute to this research collection. We also thank reviewers for constructive comments that improved this manuscript.

SUPPLEMENTARY MATERIAL

The Supplementary Material for this article can be found online at: https://www.frontiersin.org/articles/10.3389/fevo.2021.702576/full#supplementary-material

Supplementary Table 1 | Hypotheses of homology between pectoral appendicular muscles of fishes and tetrapods used in this manuscript, based on Diogo et al. (2016).

Supplementary Table 2 | Hypotheses of homology between pelvic appendicular muscles of fishes and tetrapods used in this manuscript, based on Diogo et al. (2016).

REFERENCES

Ahlberg, P. E., Clack, J. A., and Blom, H. (2005). The axial skeleton of the Devonian tetrapod *Ichthyostega*. *Nature* 437, 137–140. doi: 10.1038/nature03893

Allen, V. R., Elsey, R. M., Jones, N., Wright, J., and Hutchinson, J. R. (2010). Functional specialization and ontogenetic scaling of limb anatomy in *Alligator mississippiensis*. *J. Anat.* 216, 423–445. doi: 10.1111/j.1469-7580.2009.01202.x

Andrews, S. M., and Westoll, T. S. (1970). The postcranial skeleton of *Eusthenopteron foordi* Whiteaves. *Earth Environ. Sci. Trans. R. Soc. Edinburgh* 68, 207–329.

Bainbridge, R. (1963). Caudal fin and body movement in the Propulsion of some Fish. *J. Exp. Biol.* 40, 23–56.

Bishop, P. J. (2014). The humerus of *Ossinodus pueri*, a stem tetrapod from the Carboniferous of Gondwana, and the early evolution of the tetrapod forelimb. *Alcheringa* 38, 209–238. doi: 10.1080/03115518.2014.861320

Boisvert, C. A. (2005). The pelvic fin and girdle of Panderichthys and the origin of tetrapod locomotion. *Nature* 438, 1145–1147. doi: 10.1038/nature04119

Boisvert, C. A., Joss, J. M., and Ahlberg, P. E. (2013). Comparative pelvic development of the axolotl (Ambystoma mexicanum) and the Australian lungfish (Neoceratodus forsteri): conservation and innovation across the fish-tetrapod transition. *EvoDevo* 4, 1–19. doi: 10.1186/2041-9139-4-3

Boisvert, C. A., Mark-Kurik, E., and Ahlberg, P. E. (2008). The pectoral fin of *Panderichthys* and the origin of digits. *Nature* 456, 636–638. doi: 10.1038/nature07339

Brazeau, M. D., and Ahlberg, P. E. (2006). Tetrapod-like middle ear architecture in a Devonian fish. *Nature* 439, 318–321. doi: 10.1038/nature04196

Brown, N. A. T., Kawcak, C. E., McIlwraith, C. W., and Pandy, M. G. (2003). Architectural properties of distal forelimb muscles in horses, *Equus caballus*. *J. Morphol.* 258, 106–114. doi: 10.1002/jmor.10113

Carroll, R. L., Irwin, J., and Green, D. M. (2005). Thermal physiology and the origin of terrestriality in vertebrates. *Zool. J. Linn. Soc.* 143, 345–358. doi: 10.1111/j.1096-3642.2005.00151.x

Cieri, R. L., Dick, T. J. M., and Clemente, C. J. (2020). Monitoring muscle over three orders of magnitude: widespread positive allometry among locomotor and body support musculature in the pectoral girdle of varanid lizards (Varanidae). *J. Anat.* 237, 1114–1135. doi: 10.1111/joa.13273

Clack, J. A. (2012). *Gaining Ground: The Origin and Evolution of Tetrapods. Second Edition*. Bloomington: Indiana University Press.

Coates, M. I. (1995). Fish fins or tetrapod limbs - a simple twist of fate? *Curr. Biol.* 5, 844–848.

Coates, M. I., Jeffery, J. E., and Ruta, M. (2002). Fins to limbs: what the fossils say. *Evol. Dev.* 4, 390–401.

Cole, N. J., Hall, T. E., Don, E. K., Berger, S., Boisvert, C. A., Neyt, C., et al. (2011). Development and evolution of the muscles of the pelvic fin. *PLoS Biol.* 9:e1001168. doi: 10.1371/journal.pbio.1001168

Crawford, C. H., Randall, Z. S., Hart, P. B., Page, L. M., Chakrabarty, P., Suvarnaraksha, A., et al. (2020). Skeletal and muscular pelvic morphology of hillstream loaches (Cypriniformes: Balitoridae). *J. Morphol.* 281, 1280–1295. doi: 10.1002/jmor.21247

Daeschler, E. B., Shubin, N. H., and Jenkins, F. A. (2006). A Devonian tetrapod-like fish and the evolution of the tetrapod body plan. *Nature* 440, 757–763. doi: 10.1038/nature04639

Dick, T. J. M., and Clemente, C. J. (2016). How to build your dragon: scaling of muscle architecture from the world's smallest to the world's largest monitor lizard. *Front. Zool.* 13:5. doi: 10.1186/s12983-016-0141-5

Dickson, B. V., and Pierce, S. E. (2019). How (and why) fins turn into limbs: insights from anglerfish. *Earth Environ. Sci. Trans. R. Soc. Edinburgh* 109, 87–103. doi: 10.1017/S1755691018000415

Diogo, R., Johnston, P., Molnar, J. L., and Esteve-Altava, B. (2016). Characteristic tetrapod musculoskeletal limb phenotype emerged more than 400 MYA in basal lobe-finned fishes. *Sci. Rep.* 6, 1–9. doi: 10.1038/srep37592

Don, E. K., Currie, P. D., and Cole, N. J. (2013). The evolutionary history of the development of the pelvic fin/hindlimb. *J. Anat.* 222, 114–133. doi: 10.1111/j.1469-7580.2012.01557.x

Drucker, E. G., and Lauder, G. V. (2003). Function of pectoral fins in rainbow trout: behavioral repertoire and hydrodynamic forces. *J. Exp. Biol.* 206, 813–826. doi: 10.1242/jeb.00139

Du, T. Y., and Standen, E. M. (2017). Phenotypic plasticity of muscle fiber type in the pectoral fins of Polypterus senegalus reared in a terrestrial environment. *J. Exp. Biol.* 220, 3406–3410. doi: 10.1242/jeb.162909

Du, T. Y., and Standen, E. M. (2020). Terrestrial acclimation and exercise lead to bone functional response in Polypterus pectoral fins. *J. Exp. Biol.* 223(Pt 11):jeb217554. doi: 10.1242/jeb.217554

Ercoli, M. D., Álvarez, A., Stefanini, M. I., Busker, F., and Morales, M. M. (2015). Muscular anatomy of the forelimbs of the lesser grison (*Galictis cuja*), and a functional and phylogenetic overview of mustelidae and other Caniformia. *J. Mamm. Evol.* 22, 57–91. doi: 10.1007/s10914-014-9257-6

Ercoli, M. D., Echarri, S., Busker, F., Álvarez, A., Morales, M. M., and Turazzini, G. F. (2013). The functional and phylogenetic implications of the myology of the lumbar region, tail, and hind limbs of the lesser grison (*Galictis cuja*). *J. Mamm. Evol.* 20, 309–336. doi: 10.1007/s10914-012-9219-9

George, A. B., and Westneat, M. W. (2019). Functional morphology of endurance swimming performance and gait transition strategies in balistoid fishes. *J. Exp. Biol.* 222:jeb194704.

Huby, A., Mansuit, R., Herbin, M., and Herrel, A. (2021). Revision of the muscular anatomy of the paired fins of the living coelacanth *Latimeria chalumnae* (Actinistia, Sarcopterygii). *Biol. J. Linn. Soc.* 2020:blab047. doi: 10.1093/biolinnean/blab047

Janvier, P. (1996). *Early Vertebrates*. Oxford: Oxford University Press.

Johanson, Z., Joss, J., Boisvert, C. A., Ericsson, R., Sutija, M., and Ahlberg, P. E. (2007). Fish fingers: digit homologues in sarcopterygian fish fins. *J. Exp. Zool. Part B Mol. Dev. Evol.* 308, 757–768. doi: 10.1002/jez.b.21197

Joss, J., and Longhurst, T. (2001). "Lungfish paired fins," in *Major Events in Early Vertebrate Evolution*, ed. P. E. Ahlberg (London: Taylor and Francis), 370–376.

Lauder, G. V. (2000). Function of the caudal fin during locomotion in fishes: kinematics, flow visualization, and evolutionary patterns. *Am. Zool.* 40, 101–122.

Lighthill, M. J. (1971). Large-amplitude elongated-body theory of fish locomotion. *Proc. R. Soc. London. Ser. B. Biol. Sci.* 179, 125–138.

Mansuit, R., Clément, G., Herrel, A., Dutel, H., Tafforeau, P., Santin, M. D., et al. (2021). Development and growth of the pelvic fin in the extant coelacanth *Latimeria chalumnae*. *Anat. Rec.* 304, 541–558. doi: 10.1002/ar.24452

Martin, M. L., Warburton, N. M., Travouillon, K. J., and Fleming, P. A. (2019). Mechanical similarity across ontogeny of digging muscles in an Australian marsupial (*Isoodon fusciventer*). *J. Morphol.* 280, 423–435. doi: 10.1002/jmor.20954

Molnar, J. L., Diogo, R., Hutchinson, J. R., and Pierce, S. E. (2018). Reconstructing pectoral appendicular muscle anatomy in fossil fish and tetrapods over the fins-to-limbs transition. *Biol. Rev.* 93, 1077–1107. doi: 10.1111/brv.12386

Molnar, J. L., Diogo, R., Hutchinson, J. R., and Pierce, S. E. (2020). Evolution of hindlimb muscle anatomy across the tetrapod water-to-land transition, including comparisons with forelimb anatomy. *Anat. Rec.* 303, 218–234. doi: 10.1002/ar.23997

Moore, A. L., Budny, J. E., Russell, A. P., and Butcher, M. T. (2013). Architectural specialization of the intrinsic thoracic limb musculature of the American badger (*Taxidea taxus*). *J. Morphol.* 274, 35–48. doi: 10.1002/jmor.20074

Nakamura, T., Gehrke, A. R., Lemberg, J., Szymaszek, J., and Shubin, N. H. (2016). Digits and fin rays share common developmental histories. *Nature* 537, 225–228. doi: 10.1038/nature19322

Olson, R. A., Womble, M. D., Thomas, D. R., Glenn, Z. D., and Butcher, M. T. (2016). Functional morphology of the forelimb of the nine-banded armadillo (*Dasypus novemcinctus*): comparative perspectives on the myology of dasypodidae. *J. Mamm. Evol.* 23, 49–69. doi: 10.1007/s10914-015-9299-4

Payne, R. C., Hutchinson, J. R., Robilliard, J. J., Smith, N. C., and Wilson, A. M. (2005a). Functional specialisation of pelvic limb anatomy in horses (*Equus caballus*). *J. Anat.* 206, 557–574.

Payne, R. C., Veenman, P., and Wilson, A. M. (2005b). Erratum: the role of the extrinsic thoracic limb muscles in equine locomotion (Journal of Anatomy (2004)). *J. Anat.* 206, 193–204.

Pierce, S. E., Clack, J. A., and Hutchinson, J. R. (2012). Three-dimensional limb joint mobility in the early tetrapod *Ichthyostega*. *Nature* 486, 523–526. doi: 10.1038/nature11124

Rosen, D. E., Forey, P. L., Gardiner, B. G., and Patterson, C. (1981). Lungfishes, tetrapods, paleontology, and plesiomorphy. *Bull. Am. Museum Nat. Hist.* 167, 159–276.

Rupert, J. E., Rose, J. A., Organ, J. M., and Butcher, M. T. (2015). Forelimb muscle architecture and myosin isoform composition in the groundhog (*Marmota monax*). *J. Exp. Biol.* 218, 194–205. doi: 10.1242/jeb.107128

Shubin, N. H., and Alberch, P. (1986). A morphogenetic approach to the origin and basic organization of the tetrapod limb. *Evol. Biol.* 20, 319–387.

Shubin, N. H., Daeschler, E. B., and Jenkins, F. A. (2006). The pectoral fin of Tiktaalik roseae and the origin of the tetrapod limb. *Nature* 440, 764–771. doi: 10.1038/nature04637

Standen, E. M. (2008). Pelvic fin locomotor function in fishes: three-dimensional kinematics in rainbow trout (*Oncorhynchus mykiss*). *J. Exp. Biol.* 211, 2931–2942. doi: 10.1242/jeb.018572

Standen, E. M., Du, T. Y., and Larsson, H. C. E. (2014). Developmental plasticity and the origin of tetrapods. *Nature* 513, 54–58. doi: 10.1038/nature13708

Thorsen, D. H., and Westneat, M. W. (2005). Diversity of pectoral fin structure and function in fishes with labriform propulsion. *J. Morphol.* 263, 133–150. doi: 10.1002/jmor.10173

Warburton, N. M., Malric, A., Yakovleff, M., Leonard, V., and Cailleau, C. (2015). Hind limb myology of the southern brown bandicoot (*Isoodon obesulus*) and greater bilby (*Macrotis lagotis*) (Marsupialia: Peramelemorphia). *Aust. J. Zool.* 63, 147–162. doi: 10.1071/ZO14087

Webb, P. W. (1982). Locomotor patterns in the evolution of actinopterygian fishes. *Am. Zool.* 22, 329–342.

Wilga, C. D., and Lauder, G. V. (1999). Locomotion in sturgeon: function of the pectoral fins. *J. Exp. Biol.* 202, 2413–2432.

Zhang, J., Wagh, P., Guay, D., Sanchez-Pulido, L., Padhi, B. K., Korzh, V., et al. (2010). Loss of fish actinotrichia proteins and the fin-to-limb transition. *Nature* 466, 234–237. doi: 10.1038/nature09137

Conflict of Interest: The authors declare that the research was conducted in the absence of any commercial or financial relationships that could be construed as a potential conflict of interest.

frontiers in Ecology and Evolution

ORIGINAL RESEARCH
published: 05 August 2021
doi: 10.3389/fevo.2021.659039

Modeling Sprawling Locomotion of the Stem Amniote *Orobates*: An Examination of Hindlimb Muscle Strains and Validation Using Extant *Caiman*

*Michelle Zwafing[1], Stephan Lautenschlager[2], Oliver E. Demuth[3,4] and John A. Nyakatura[1]**

[1] Lehrstuhl für Vergleichende Zoologie, Institut für Biologie, Humboldt Universität zu Berlin, Berlin, Germany, [2] School of Geography, Earth and Environmental Sciences, University of Birmingham, Birmingham, United Kingdom, [3] Department of Earth Science, University of Cambridge, Cambridge, United Kingdom, [4] Structure and Motion Laboratory, Department of Comparative Biomedical Sciences, Royal Veterinary College, London, United Kingdom

OPEN ACCESS

Edited by:
Julia L. Molnar, New York Institute of Technology, United States

Reviewed by:
Stephanie E. Pierce, Harvard University, United States
Emanuel Andrada, Friedrich Schiller University Jena, Germany

***Correspondence:**
John A. Nyakatura
john.nyakatura@hu-berlin.de

Specialty section:
This article was submitted to Paleontology, a section of the journal Frontiers in Ecology and Evolution

Received: *26 January 2021*
Accepted: *15 July 2021*
Published: *05 August 2021*

Citation:
Zwafing M, Lautenschlager S, Demuth OE and Nyakatura JA (2021) Modeling Sprawling Locomotion of the Stem Amniote Orobates: An Examination of Hindlimb Muscle Strains and Validation Using Extant Caiman. Front. Ecol. Evol. 9:659039. doi: 10.3389/fevo.2021.659039

The stem amniote *Orobates pabsti* has been reconstructed to be capable of relatively erect, balanced, and mechanically power-saving terrestrial locomotion. This suggested that the evolution of such advanced locomotor capabilities preceded the origin of crown-group amniotes. We here further investigate plausible body postures and locomotion of *Orobates* by taking soft tissues into account. Freely available animation software BLENDER is used to first reconstruct the lines of action of hindlimb adductors and retractors for *Orobates* and then estimate the muscle strain of these muscles. We experimentally varied different body heights in modeled hindlimb stride cycles of *Orobates* to find the posture that maximizes optimal strains over the course of a stride cycle. To validate our method, we used *Caiman crocodilus*. We replicated the identical workflow used for the analysis of *Orobates* and compared the locomotor posture predicted for *Caiman* based on muscle strain analysis with this species' actual postural data known from a previously published X-ray motion analysis. Since this validation experiment demonstrated a close match between the modeled posture that maximizes optimal adductor and retractor muscle strain and the *in vivo* posture employed by *Caiman*, using the same method for *Orobates* was justified. Generally, the use of muscle strain analysis for the reconstruction of posture in quadrupedal vertebrate fossils thus appears a promising approach. Nevertheless, results for *Orobates* remained inconclusive as several postures resulted in similar muscle strains and none of the postures could be entirely excluded. These results are not in conflict with the previously inferred moderately erect locomotor posture of *Orobates* and suggest considerable variability of posture during locomotion.

Keywords: locomotion, posture, gait, extrinsic muscles, fossil, animation, muscle strain, virtual experiment

INTRODUCTION

The reconstruction of the biomechanics of fossils is a valuable approach to understand and investigate extinct life. While largely determining musculo-skeletal function, soft tissues like muscles are rarely preserved in fossils (Lautenschlager, 2016). However, with the development of new computational modeling techniques alternative possibilities to reconstruct and investigate the soft tissues of extinct species have emerged (Cunningham et al., 2014). In particular, the development and increasing availability of computed tomography (CT) had a fundamental impact on paleobiological research (e.g., Cunningham et al., 2014). Traditional reconstructions of soft tissues such as muscles were restricted to a theoretical, usually two-dimensional framework with drawings. The advent of CT not only allows the visualization of bone internal structures (Sutton, 2008; Cunningham et al., 2014), but also more sophisticated musculo-skeletal models (e.g., Bates and Falkingham, 2012; Hutchinson, 2012; Lautenschlager, 2015; Bishop et al., 2021). This potential to create three-dimensional models has led to a diversification of techniques to investigate fossils regarding functional morphology and biomechanical behavior including the role of soft tissues (Anderson et al., 2012; Cunningham et al., 2014; Manafzadeh and Padian, 2018; Demuth et al., 2020; Lautenschlager, 2020).

Modern Amniota represent a highly successful and diverse clade, comprising roughly 75% of extant tetrapods including lizards, snakes, turtles, crocodiles, birds, and mammals as well as a suite of large, but extinct radiations such as pterosaurs, sauropterygians, and non-avian dinosaurs (Reisz, 1997; Clack and Bénéteau, 2012). Fossil evidence suggests an origin of amniotes in the Carboniferous period (e.g., Laurin and Reisz, 1997; Clack, 2006; Coates and Ruta, 2007). Some authors argue that only with the evolution of the first amniotes, the transition of vertebrates to living on land was completed, because the reproduction was not directly dependent on open water anymore (Martin and Sumida, 1997; Nyakatura et al., 2014). This transition also necessitated the evolution of increasingly effective locomotion in terrestrial habitats.

To gain further insight into the locomotor characteristics of early amniotes, the focus of this study is on the extrinsic hindlimb muscles of the putative stem amniote *Orobates pabsti*. *Orobates* is a basal diadectid from the early to mid-Permian Tambach formation of central Germany (Berman et al., 2004). Diadectidae is most often hypothesized to represent the fossil sister group of Amniota (Laurin and Reisz, 1995, 1997; Lee and Spencer, 1997; Coates and Ruta, 2007), but *Orobates* also has been reconstructed within the crown group (Marjanović and Laurin, 2019). In addition to body fossils, fossil trackways were recovered from the same site, some of which could be assigned to *Orobates* as the trackmaker (Voigt et al., 2007). This combination of track and trackmaker offers a unique possibility to reconstruct the locomotion of this fossil species (Berman et al., 2004; Voigt et al., 2007; Nyakatura et al., 2015, 2019). A previous study integrated kinematic and dynamic modeling and employed a bioinspired robot to understand the locomotion of *Orobates* (Nyakatura et al., 2019). We here built on this previous study and utilized the modeling of soft tissues, specifically the muscle strain in the extrinsic hindlimb muscles, to further our understanding of the posture and locomotion in this key taxon. With this analysis of muscle strains we tested previous locomotor reconstructions in an independent way using a variant of multibody dynamics analysis (MDA). MDA is a computational analysis method including solid components connected by joints which restrict the movements by internal and external forces (Lautenschlager, 2020). It is a non-invasive method to simulate and test different scenarios and complex designs (Lautenschlager, 2015, 2020). The method was often used in comparative biomechanics research, e.g., to investigate human jaw movement (Koolstra and van Eijden, 1995), bite forces of theropod dinosaurs (Bates and Falkingham, 2012), or neck function in extinct vertebrates (Snively et al., 2013).

Here we simulated *Orobates* locomotion and used an MDA-like method linking rigid skeletal elements and simulating movements, but not accounting for forces. We modeled abstracted hindlimb adductor and retractors (reduced to a straight line of action) and quantified the occurring muscle strains of these muscles in diverse postures ranging from a "very low" (essentially belly-dragging) posture to a "very high" posture with maximally extended limbs at touch down. We aimed to identify the body posture which maximizes the occurrence of optimal muscle strains (and to identify anatomically implausible excessive compression/tension). Extrinsic hindlimb muscles are connecting the torso with the limb and are particularly important for posture and the generation of forward propulsion (Ashley-Ross, 1994; Fischer et al., 2002; Schilling et al., 2009). We, therefore, focused on extrinsic hindlimb muscles in this study. In terms of the posture of a sprawling tetrapod, the extrinsic hindlimb adductors depress the femur to pull the knee toward the sagittal plane and thus lift the trunk off the ground (Russell and Bels, 2001). In terms of the generation of propulsion, extrinsic hindlimb retractors pull the femur posteriorly and, when the foot is in contact with the ground, thereby propel the body forward.

The rationale of the modeling approach of this paper is based on the assumption that tetrapods engage postures and gaits during locomotion, which maximize the occurrence of optimal muscle strains. Importantly, we first tested this assumption in *Caiman crocodilus*, of which detailed 3D kinematics are known from a previous kinematic study using X-ray motion analysis (Nyakatura et al., 2019). It was tested whether a posture, as predicted by extrinsic hindlimb muscle strain analysis, matches the actual posture found in the kinematic analysis. Successful validation justified transferring our modeling approach to the extrinsic hindlimb muscles in *Orobates*. More generally, for the first time muscle strain analysis is used to constrain the reconstruction of the posture of a fossil tetrapod.

MATERIALS AND METHODS

Digital Model and Gait Simulation of *Caiman* Crocodilus

To first test the assumption of postures that minimize problematic muscle strains are being preferred, we validated the method using a modern amniote, *Caiman crocodilus*. An

available digital skeletal model of extant *Caiman crocodilus* from a previous study (Nyakatura et al., 2019) was used, an idealized gait was animated and different locomotor postures were simulated (Nyakatura and Demuth, 2019). *Caiman* kinematics are also known from a previous X-ray motion analysis (Nyakatura et al., 2019). If our assumption holds true, the methodology outlined above should be able to predict the naturally chosen posture of *Caiman*. Thus, we used the identical workflow that is used for the investigation of *Orobates* (detailed below) and compared the posture predicted for *Caiman* based on muscle strain analysis with this species' actual postural data known from X-ray motion analysis.

All procedures involving live animals were strictly following pertinent animal welfare regulations and were authorized by the Thüringer Landesamt für Verbraucher- und Umweltschutz (registration number: 02-008/11) in the state of Thuringia, Germany. Two *Caiman* individuals were originally borrowed from a zoo (La Ferme aux crocodiles, Pierrelatte, France) and analyzed (Nyakatura et al., 2019). After the investigation, the two borrowed *Caiman* were returned to the zoo unharmed. For this study, only videos of the female were selected for the idealized animation of the complete skeletal movement during locomotion, to directly match its skeleton to its movement.

We created an idealized animation based on a collage of X-ray videos to capture the movement of the whole skeleton (**Supplementary Video 1**). When passing by the 38 cm image intensifiers of the system, only a part of the individual was within the field of view. A set of a synchronized dorsal and a lateral video of the *Caiman* walking through this narrow field of view was imported into ADOBE AFTER EFFECTS (Adobe Inc., San José, California, United States). The videos were duplicated several times and they were arranged and timed in such a way that the impression of an X-ray video with a much-extended field of view showing almost the entire specimen emerged (see **Supplementary Video 1**). This visualization was first conceived and prepared by Jonas Lauströer (as part of our previous study Nyakatura et al., 2019), but was later on improved by one of us (OED). This allowed us to montage an X-Ray video of the entire skeleton for a complete, idealized walk cycle of *C. crocodilus*.

The 3D bone models were obtained from medical CT data collected at the Friedrich Schiller University Hospital and segmented in the software package AMIRA (Thermo Fisher Scientific, Zuse Institut Berlin, Germany) (Nyakatura et al., 2019). Using these 3D bone models, a digital marionette of the female *C. crocodilus* (specimen no.: PMJ Rept 665, Phyletisches Museum Jena, Germany) was created, scaled to match the video, and superimposed onto the idealized X-ray collage (**Figure 1**). A hierarchical joint marionette (Gatesy et al., 2010; Arnold et al., 2014), i.e., an inverse kinematic (IK) rig (Watt and Watt, 1992), was used to match the bones with their x-ray shadows in the software package AUTODESK MAYA (Version 2015; Autodesk Inc., San Rafael, California, United States) (see Wiseman et al., 2021). For further analysis, the model was transferred from AUTODESK MAYA into BLENDER.

Actual kinematic data of *Caiman crocodilus* was measured *in vivo* using XROMM (X-ray reconstruction of moving morphology; Brainerd et al., 2010) in a previous study (Nyakatura et al., 2019 cf. SM14 of the cited reference). These published data were then used to evaluate the model predicted posture, which maximizes optimal muscle strains, against *in vivo* kinematic data.

Digital Model and Gait Simulation of *Orobates pabsti*

The digital version of the holotype specimen of *Orobates pabsti* (specimen number MNG 10,181) was available for this study (Nyakatura et al., 2015, 2019). Moreover, we used the animated digital skeleton from a previous study (Nyakatura et al., 2019). Please refer to our previous publications for specifics of how the digital specimen was generated and the rationale for animation properties (Nyakatura et al., 2015, 2019; Nyakatura, 2017, 2019). In brief, the holotype specimen was microCT-scanned and individual bone fragments were segmented and thus freed from the surrounding rock matrix. Bone fragments of a single skeletal

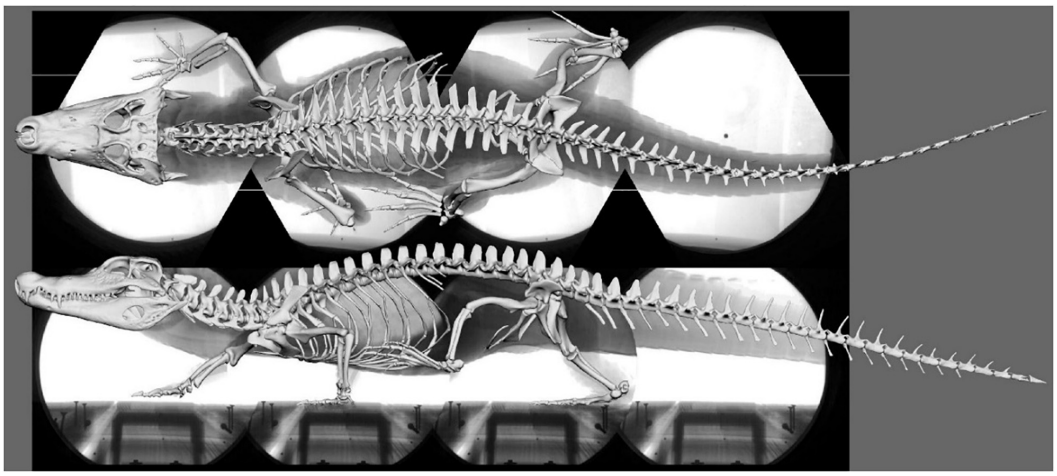

FIGURE 1 | Superimposed skeleton on the X-ray video collage in dorsal (top) and lateral (bottom) view (**Supplementary Video 1**).

element were fused and all skeletal elements were undistorted (Nyakatura et al., 2015). For the animated step cycle, fossil trackways assigned to *Orobates* (cf. Voigt et al., 2007) were analyzed and used as a hard constraint, i.e., each manus and pes was forced to match the trackways (Nyakatura, 2019; Nyakatura et al., 2019). Limb and spine kinematics were animated in accordance with general biomechanical principles of sprawling tetrapod locomotion identified in a previous study and were anatomically plausible in terms of joint mobility (Nyakatura et al., 2019). Specifically, this refers to the relationship of stylopodial long-axis rotation to stylopodial protraction/retraction.

Importantly, the Maya rig controlling *Orobates*' simulated locomotion as well as the rig controlling *Caiman* allowed to set and adjust body height (i.e., lifting of the trunk off the ground; cf. Nyakatura et al., 2019). Despite using the same set of hip kinematics for all of our modeled body heights, this affected not only femoral adduction/abduction, but also resulted in changes of protraction/retraction and long-axis rotation due to the interdependency of rotations when describing 3D joint movements with Euler angles (Sullivan, 2007). Like the model of *Caiman,* the model of *Orobates* was transferred into BLENDER as .fbx files which retained the movement and animation paths of the rigs. To simplify the model only the movement sequence of the hindlimb was used. The rest of the skeletal elements were combined in a single component as the movement of these was not necessary for the study.

Abstracted Muscle Models and Analysis of Muscle Strains

Muscles fibers are made up of myofibrils which consist of contractile units, the sarcomeres. Within the sarcomeres, crossbridges between overlapping Myosin and Actin filaments are built. Contraction is realized through a conformation change of Myosin heads and resulting relative movement between the linked filaments (i.e., the power stroke). Due to this internal structure, muscles have a tension/compression range in which a maximum tetanic contraction can be achieved (Sherwood et al., 2013). The optimal range for the generation of force is between 70 and 130% of resting length, while maximum compression and tension of a muscle is approximately reached at 30 and 170% of resting length, respectively (Sherwood et al., 2013; Lautenschlager, 2015). Thus, simulated step cycles that invoke muscle compression below 30% and tension beyond 170% resting length can be regarded as problematic and are considered here as unlikely to occur in cyclic, steady-state walking. More generally, we expect animals to choose gaits and postures that maximize optimal muscle strains (and minimize problematic muscle compression and extension).

For the modeling of abstracted muscles and for the analysis of muscle strains of *Caiman* and *Orobates* the freely available three-dimensional (3D) visualization software BLENDER[1] was used, which allows the animation and manipulation of models (Garwood and Dunlop, 2014). This software also provides the possibility for analytical approaches and automatization using the in-built python interpreter (Lautenschlager, 2015). For measuring the muscle strain over the course of a step cycle, a python script was created which measures the strain of each muscle and calculates the muscle strain ratios between a defined reference length (see below) and stretched/compressed muscle conditions. Data of all recorded parameters were automatically exported to a text file for post-processing.

In the digital models of *Caiman* and *Orobates*, the hindlimb could be moved relative to the pelvis. First, the muscles of the adductors and retractors were reconstructed in each model. The following primary hindlimb adductors critical for the animals' hip height were considered in this study: *M. adductor femoris* (ADD), *M. puboischiofemorales externus* (PIFE), *M. puboischiotibialis* (PIT). In addition to the adductors, we also modeled the primary retractors of the femur and thus hindlimb of sprawling tetrapods: *M. caudofemoralis longis* (CFL) and *M. caudofemoralis brevis* (CFB).

For *Caiman* the muscle origins and insertions were modeled in accordance with a detailed anatomical description of *Caiman latirostris* (**Figure 2**; Otero et al., 2010). Muscle reconstruction in fossils is challenging, as they are often not preserved. Yet, reconstruction of *Orobates*' muscles was critical for the purpose of this study. One widely used approach to infer the presence of soft-tissues in fossil vertebrates is the examination of the extant phylogenetic bracket (Witmer, 1995). This involves comparing the osteological attachments sites in fossil species with extant taxa (Molnar et al., 2020; Bishop et al., 2021). The muscle attachment sites in *Orobates* were determined by comparing the presence of muscles in modern amphibians and modern selected sprawling amniotes using published anatomical descriptions (we did not consider highly derived amniote postcrania represented in e.g., mammals, turtles, snakes, or birds). For this purpose, various previous studies that reported muscle attachment sites (Ashley-Ross, 1992; Otero et al., 2010; Diogo et al., 2016; Molnar et al., 2020) were examined for differences and similarities in extrinsic hindlimb muscles between amphibians and sprawling amniotes. Based on this, we inferred the presence or absence of these muscles as well as their attachment sites for *Orobates* (see "Results"). Importantly, the 3D reconstructed bone models of *Orobates* (from Nyakatura et al., 2015) lack obvious morphological indicators of muscle attachments and the reconstruction of simplified muscle lines of action, therefore, remains uncertain.

In BLENDER the muscles were abstracted as simple cylinders between the origin and the insertion, thus along a straight line of action (Lautenschlager, 2015). The ends of each cylinder representing a muscle were fixed to the reconstructed muscle attachment sites on the bone models. Although these muscle models can potentially penetrate bones and one another, it was not observed in any of our modeled trials. Thus, when joint movement was animated and the skeletal elements were moved relative to one another, the cylinders were compressed or stretched. We defined the reference length (i.e., 100% muscle length in our models) to occur at 50% of the contact phase, i.e., at mid-stance. Here the assumption is made that at mid-stance limb

[1] www.blender.org; version 2.81

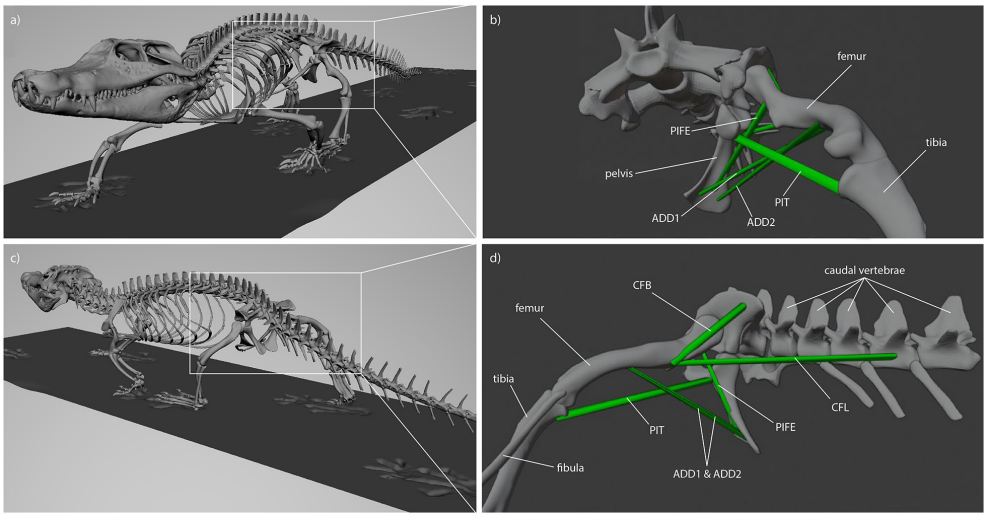

FIGURE 2 | Muscle attachments and lines of action in *Caiman* (see Otero et al., 2010). **(a)** Latero-frontal view of *Caiman*, **(b)** latero-frontal view of relevant skeletal elements to show adductor muscles (ADD1, ADD2, PIFE 3rd head, PIT) at reference length (mid-stance), **(c)** latero-caudal view of *Caiman*, **(d)** latero-caudal view of relevant skeletal elements to show retractor muscles (CFB, CFL) at reference length (mid-stance).

posture resembles posture of still-standing animals and presents a replicable posture. For each modeled body height (see below) all muscle strain measures were taken relative to the mid-stance reference pose.

Modeling Postures

To be able to identify postures in which problematic muscle strains were minimized, we modeled multiple different postures in our simulated stride cycles in a "virtual experiment" (Nyakatura and Demuth, 2019). Particularly, we analyzed muscle strains in five simulated postures characterized by different degrees of sprawling (**Figure 3**): "very low," "low," "intermediate," "high," and "very high." We consider the "very low" and the "very high" postures to encompass anatomical plausibility. In the "very low" posture the limb posture at various instances during the stride cycle was "hypersprawled," i.e., the knee is positioned more dorsal than the hip and the belly is in contact with the ground (Nyakatura et al., 2014). In the "very high" posture the hindlimb was extended as much as possible at touch down and any further extension would have resulted in disarticulated joints (see Nyakatura et al., 2019). "Low," "intermediate," and "high" postures were modeled at evenly spaced increments between these extremes. Additionally, the modeled postures were also quantified using hip height expressed as percentage of inter girdle distance (IGD) at mid-stance in order to provide a way to replicate the modeled postures. Note that the different modeled postures did not occur at identical relative hip heights. In *Caiman* these vary from IGD 0.28 ("very low" posture) to 0.69 ("very high" posture) (**Figure 4**). In *Orobates*, these vary from the IGD 0.37 ("very low" posture) to 0.52 ("very high" posture) (**Figure 5**).

In order to identify the posture for *Orobates* which minimizes excessive strains, we used the identical workflow that was used for *Caiman*. Therefore, for each modeled muscle of both models (*Caiman*, *Orobates*) and for all five simulated postures, the muscle strain was measured over the course of the simulated stride cycle. The estimated muscle strains were plotted against the percentage of the stride cycle. To visualize whether muscle strains during a stride cycle at a specific simulated posture are involving problematic values, we highlighted the respective areas in the graphs. In these graphs, the green area represents optimal compression/tension muscle strains (i.e., within 70 and 130% of reference length), the orange area represents non-optimal, but feasible strains, and the red area indicates that compression/tension are no longer considered possible (i.e., below 30% and above 170%). For each modeled hip height, we then determined the percentage of the stride in which optimal strains were maintained and used this percentage as a metric for comparison between simulated postures following the principle "the-higher-the-value-the-better," but body heights that induced muscle strains <30 and $>170\%$ were ruled out.

RESULTS

Validation: *Caiman* Crocodilus

Taking all simulated postures together, in *Caiman* muscle strain values for ADD1 ranged from 93 to 203% and for ADD2 from 94 to 190% over the course of a stride cycle (**Figures 6A,B**). These two muscles showed the greatest range of values. For the muscles PIFE3 and PIT, we measured values of 99–115% and 95–127%, respectively (**Figures 6C,D**). The femoral retractors CFB and CFL exhibited values from 44 to 114% and 76 to 111%, respectively, over the course of a step cycle (**Figures 6E,F**).

In the "very high" posture (IGD = 0.69) the highest strains for the adductor's ADD1 and ADD2 occurred. These were $>170\%$

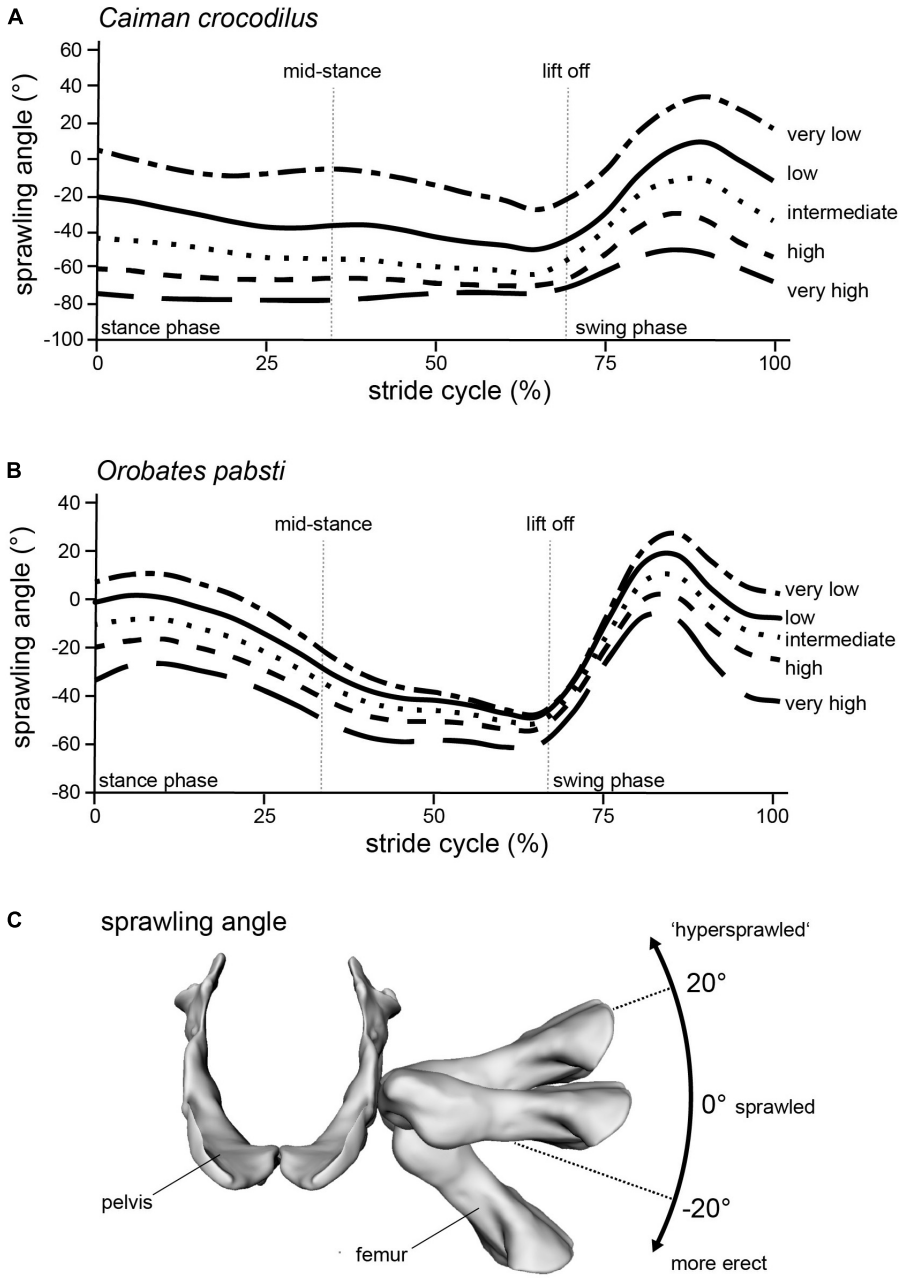

FIGURE 3 | Modeling different postures from "very low" to "very high" in **(A)** *Caiman* and **(B)** *Orobates* is reflected in the **(C)** sprawling angle (frontal view of the pelvis and femur of *Orobates* with differently ad/abducted femur). Raw data provided as **Supplementary Material**.

of reference length (**Figures 6A,B**). Also, the CFB showed strains out of the optimal tension area (**Figure 6E**).

Skeletal muscle here is only considered to function properly at a strain value of > 30 and < 170% of the reference length. Only the "very high" posture involved implausible strains and was excluded as a possibility for *Caiman*. In turn, all other simulated body heights were considered plausible reflecting the diverse locomotor postures observed in modern crocodilians from "low walks" to "high walks." However, at the "low" and "intermediate" postures (IGD of 0.39 and 0.49) not only entirely avoided implausible muscle strains, but also strains remained within the optimal length (i.e., > 70 and < 130% of reference length; the green areas in **Figures 4**, **6**) for an average of above 95% for all six modeled muscles over the course of the stride cycle (**Table 1**). Our modeling approach thus predicts that *Caiman* adopts a "low" to "intermediate" hip height in accordance with the assumption that optimal muscle strains are maximized and critical muscle strains are avoided in living animals. Indeed, the value for the "intermediate" posture model almost exactly matched *in vivo Caiman* data which documented hip height of

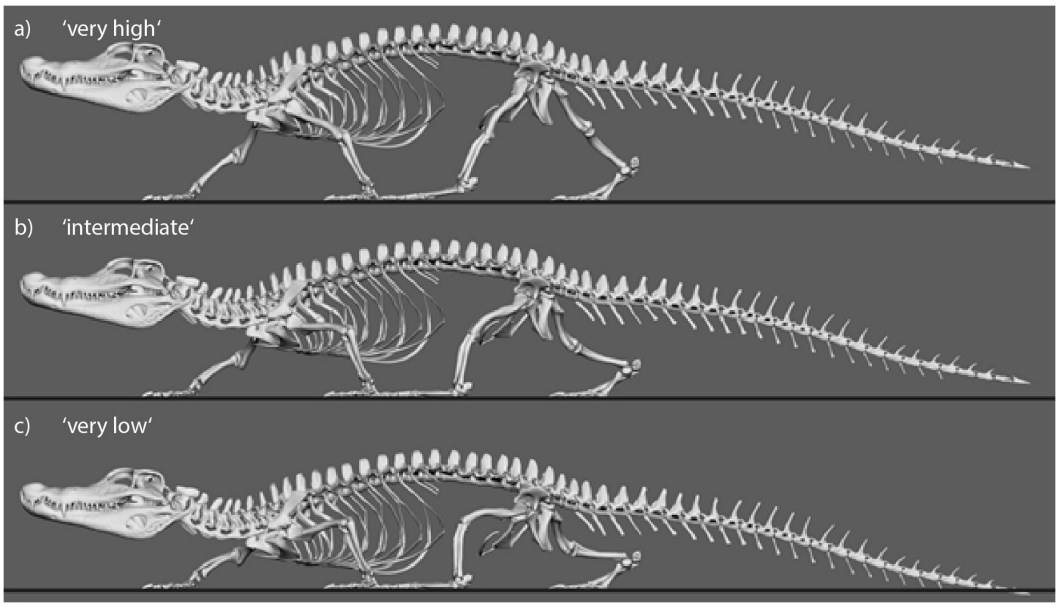

FIGURE 4 | Still images from animated *Caiman* locomotor cycle to illustrate the experimental variation of body height. Three of five variations are shown. **(a)** "Very high" with IGD = 0.69. **(b)** "Intermediate" with IGD = 0.49. **(c)** "Very low" with IGD = 0.29.

IGD = 0.502 (± 0.021) (Nyakatura et al., 2019; the specimens of *Caiman* never chose low walks in this previous study). We used this close match as a justification to employ our muscle strain modeling approach to the simulated gaits of *Orobates pabsti*.

Muscle Attachments in *Orobates* Hindlimb and Proposed Function

Reconstruction of muscle line of actions is a necessary prerequisite for the modeling of muscle strains in *Orobates*. Several adductors contribute to hip height and thus posture. During the contact phase, ADD1 prevents the limb from collapsing by resisting femoral abduction. The muscles ADD2, *M. puboischiotibialis* (PIT) and PIFE assist in this function (Gatesy, 1997; Hutchinson and Gatesy, 2000). In *Caiman* the *M. adductor femoris* (ADD) is comprised of two heads, the *M. adductor femoris 1* (ADD1) and *M. adductor femoris 2* (ADD2), with longitudinal fibers and triangular shape (Otero et al., 2010; **Figure 2**). ADD1 originates over the anterolateral surface of the ischium, close to the obturator process and inserts along the posterior surface of the femoral shaft. ADD2 has its origin on the postero-lateral portion of the ischium and also inserts along the posterior surface of the femoral shaft *in Caiman*. The muscles ADD1 and ADD2 are separated through *M. puboischiofemoralis externus* (PIFE) (Otero et al., 2010). In salamanders, the *adductor femoris* muscle is also present but has only one head that features the same origin and insertion sites of ADD1 in *Caiman* (Diogo et al., 2016; Molnar et al., 2020). In diadectids (which include *Orobates*) the muscle attachment sites are wider (Romer, 1922) suggesting a similar triangular shape as in *Caiman*. Therefore in *Orobates* two muscle portions were modeled and examined for the adductors (ADD1, ADD2; **Figure 7**). The PIT is a small muscle that arises in *Caiman* from the anterolateral surface of the ischium and inserts on the proximomedial aspect of the tibia (Otero et al., 2010). In salamanders this muscle originates from the puboischiac plate and inserts on the proximal two-thirds of the anteromedial face of the tibia (Ashley-Ross, 1992). Because of the similarities in origin and insertion of the PIT in both the amniote *Caiman* and anamniote salamanders, we reconstruct similar muscle attachment points in *Orobates*. The PIFE is undivided in non-archosaurian taxa (Hutchinson, 2001). This muscle also assists in the adduction of the femur and therefore prevents the body from collapsing to the ground. In *Caiman* the PIFE has three heads, in our study we investigate the third head of PIFE (i.e., PIFE3) which originates on the lateral aspect of the ischium between ADD1 and ADD2 and inserts on the major trochanter of the femur (Gatesy, 1997; Hutchinson and Gatesy, 2000; Otero et al., 2010). In amphibians like salamanders an undivided PIFE arises from the lateral aspect of the ischium and inserts onto the femoral trochanter (Ashley-Ross, 1992). In *Orobates* we modeled an undivided muscle. However, the muscle attachment sites in Archosauria for PIFE3 and PIFE in amphibians are similar, thus we assumed the same muscle attachment (**Figure 7**).

M. caudofemoralis longis (CFL) and *M. caudofemoralis brevis* (CFB) are the main retractors of the femur. In archosaurs like *Caiman* the CFL has its origin from the lateral sides of haemal arches and the base of proximal caudal vertebral centra. This muscle joins the CFB to insert via a tendon on the fourth trochanter of the femur (Otero et al., 2010). The smaller muscle CFB lays anterior to the CFL and has two sites of origin in *Caiman*. The first arises from the postero-ventral part of the illium and the second site arises from the centrum and the base of the transverse processes of the anterior caudal vertebrae.

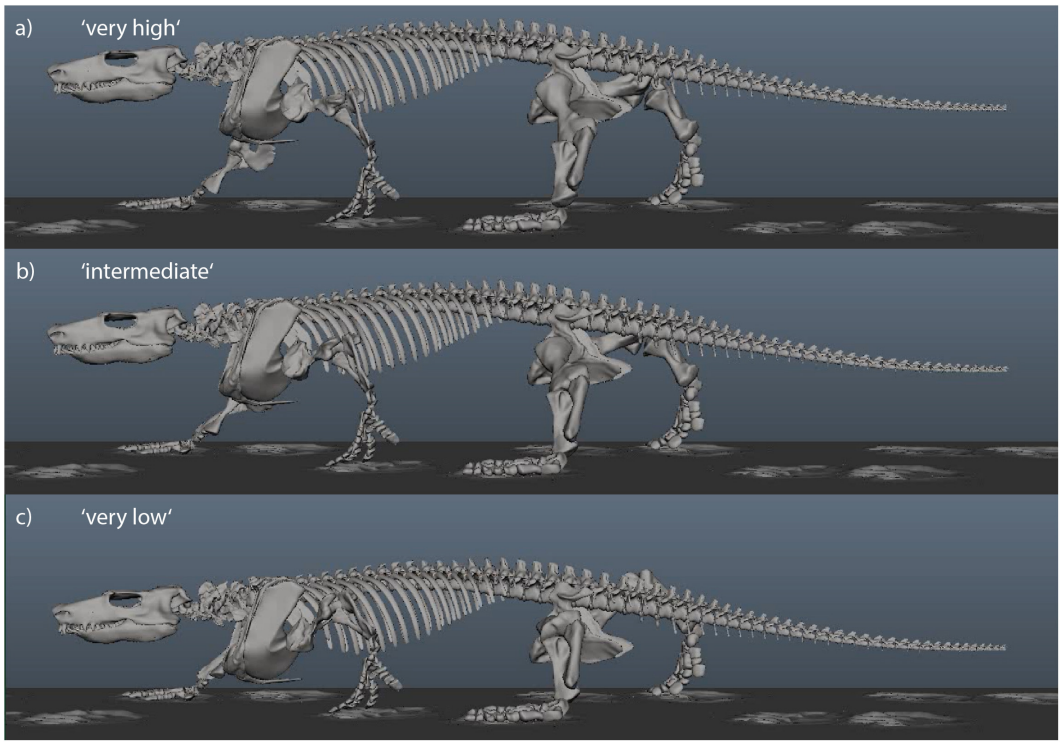

FIGURE 5 | Still images from animated *Orobates* locomotor cycle to illustrate the experimental variation of body height. Three of five variations are shown. Animation from Nyakatura et al. (2019). **(a)** "Very high" with IGD = 0.52. **(b)** "Intermediate" with IGD = 0.45. **(c)** "Very low" with IGD = 0.38.

The muscle inserts on the femur close to the fourth trochanter (Gatesy, 1997; Otero et al., 2010). In salamanders just one portion of the *M. caudofemoralis* is usually distinguished and shares the same muscle attachment sites like the CFL in archosaurs (Ashley-Ross, 1992; Molnar et al., 2020). As with the ADD, the muscle attachment site of the *M. caudofemoralis* is wider in Diadectidae (Romer, 1922). Therefore, we again used two muscle portions to examine the muscle strain of the *caudofemoralis* in *Orobates* (we distinguished between CFL and CFB in *Orobates*; **Figure 7**).

Obvious sites of attachment for any of these muscles were not visible on the 3D reconstructed bone models of *Orobates pabsti* (from Nyakatura et al., 2015) and reconstructed muscle attachment sites should therefore be treated with caution.

Muscle Strain Analysis for *Orobates* Pabsti

Taking all simulated postures together in *Orobates* muscle strain values for ADD1 ranged from 82 to 108% and for ADD2 from 68 to 123% over the course of a stride cycle (**Figures 8A,B**). For the muscles PIFE and PIT we measured values of 44–156% and 93–133%, respectively (**Figures 8C,D**). The femoral retractors CFB and CFL displayed values ranging from 39 to 150% and from 61 to 123% over the course of a stride cycle (**Figures 8E,F**). None of the simulated postures involved strain values of < 30 or $> 170\%$ of reference length. Thus, all simulated postures (from "very low" to "very high") can be considered plausible and no posture can be discarded outright. The absolutely highest strain values were found at the "very high" posture with peak PIFE muscle strain of 156.33% of reference length. The absolutely lowest muscle strain value occurred in the CFB at the "high" posture (with a minimum value of 39.65% of reference length). The least critical body posture for *Orobates* was found to be "intermediate" (89.24% optimal strain values across all muscles over the entire stride cycle), but the "very low" (88.59%) and the "high" (88.98%) postures similarly maximized the occurrence of optimal muscle strains between 70 and 130% of the reference length (**Table 2**).

DISCUSSION

The aim of this study was to predict plausible body height (posture) and therefore further constrain the locomotion of the stem amniote *Orobates pabsti* by taking soft tissues, specifically the extrinsic hindlimb muscles, into account. In our modeling approach, we estimated the muscle strains of six muscles in five simulated body postures from "very low" to "very high." We identified postures for *Orobates* that maximize optimal strains over the course of a stride cycle. The identical workflow was first used for *Caiman crocodilus* to validate our modeling approach since for *Caiman* the model-predicted values could be compared to *in vivo* postural data from a previous study (Nyakatura et al., 2019). Although only the "very high" posture could be eliminated outright due to the occurrence of implausible strains, we found a

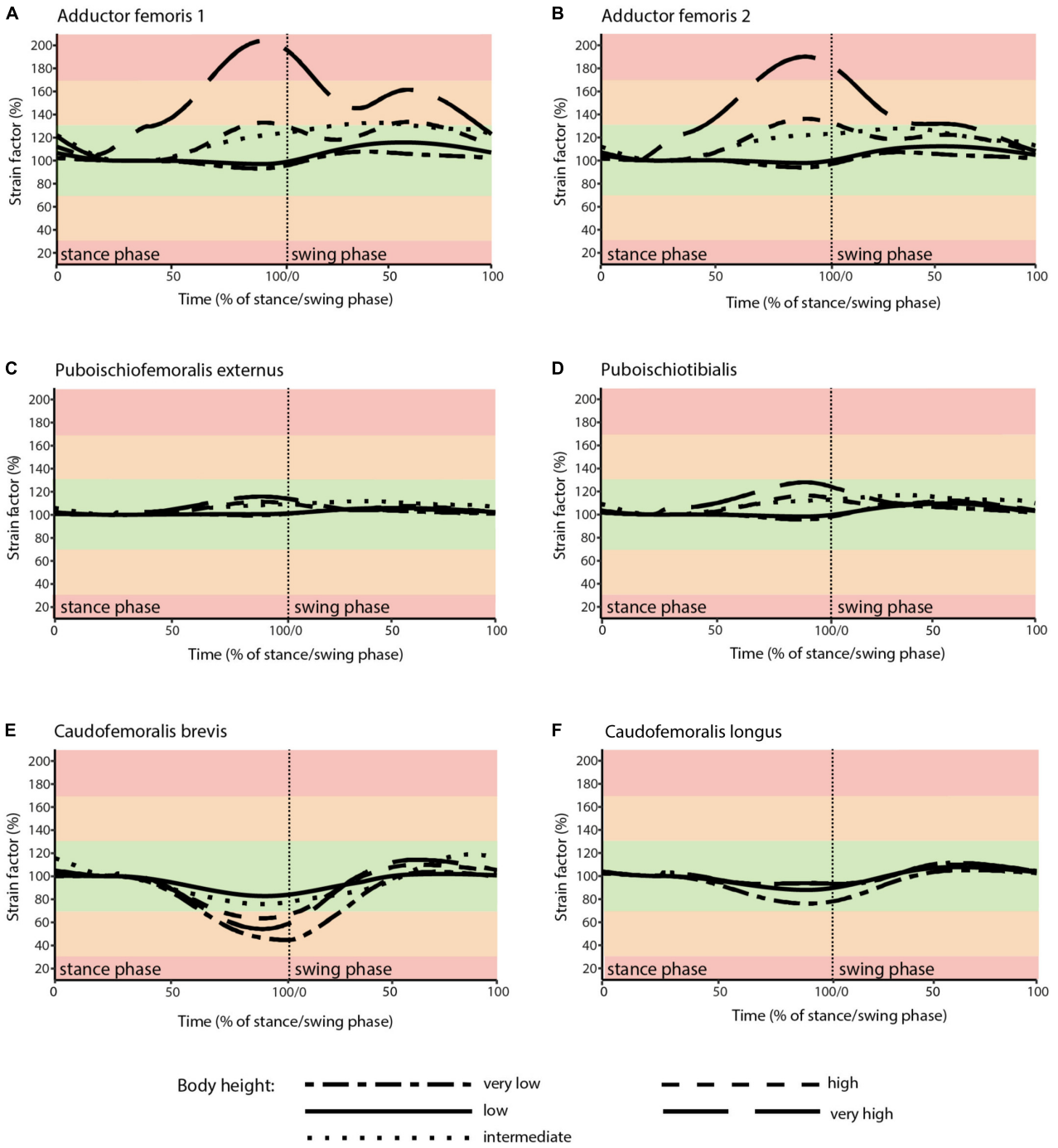

FIGURE 6 | Muscle strains plotted against percentage of stance and swing phase in *Caiman* for each of the five analyzed body heights. **(A)** ADD1; **(B)** ADD2; **(C)** PIFE; **(D)** PIT; **(E)** CFB; **(F)** CFL. Red areas of the plots involve muscle tension beyond 170% or compression below 30% of reference length and were considered implausible in this study. Green areas of the plots represented optimal muscle length for the generation of force (between 70 and 130% of reference length). Orange areas represent feasible muscle strains with limited potential for force generation.

close match between the predicted posture (maximizing optimal strains) and the *in vivo* posture of *Caiman* and used this to justify employing our modeling approach to *Orobates*.

Previous work into the reconstruction of *Orobates*' locomotor capabilities relied on information provided by fossil trackways (Voigt et al., 2007) and integrated kinematic and dynamic simulations as well as biorobotics (Nyakatura et al., 2019). This previous work proposed a relatively erect (intermediate to high body height with no belly dragging) posture, which was further interpreted to indicate a balanced and mechanical energy-saving

TABLE 1 | Percentage of the stride cycle that each modeled muscle maintained optimal muscle strain (i.e., within 70 and 130% of reference length) in *Caiman*.

	Hip height	PIT	PIFE3	ADD1	ADD2	CFB	CFL	Total
Stance phase	"Very low"	100%	100%	100%	100%	62.5%	100%	
	"Low"	100%	100%	100%	100%	100%	100%	
	"Intermediate"	100%	100%	100%	100%	100%	100%	
	"High"	100%	100%	82.5%	73.75%	70%	100%	
	"Very high"	100%	100%	41.25%	43.75%	65%	100%	
Swing phase	"Very low"	100%	100%	100%	100%	75.71%	100%	
	"Low"	100%	100%	100%	100%	100%	100%	
	"Intermediate"	100%	100%	58.75%	100%	100%	100%	
	"High"	100%	100%	74.29%	95.71%	95.71%	100%	
	"Very high"	100%	100%	5.71%	35.71%	90%	100%	
Complete stride cycle	"Very low"	100%	100%	100%	100%	69.11%	100%	94.85%
	"Low"	100%	100%	100%	100%	100%	100%	100%
	"Intermediate"	100%	100%	79.38%	100%	100%	100%	96.56%
	"High"	100%	100%	78.4%	84.73%	82.86%	100%	90.99%
	"Very high"	100%	100%	23.48	39.73%	77.5%	100%	73.45%

*ADD, M. adductor femoris; PIFE, M. puboischiofemorales externus; PIT, M. puboischiotibialis; CFL, M. caudofemoralis longis; CFB, M. caudofemoralis brevis. See **Figure 6** for graphical illustration of muscle strains.*

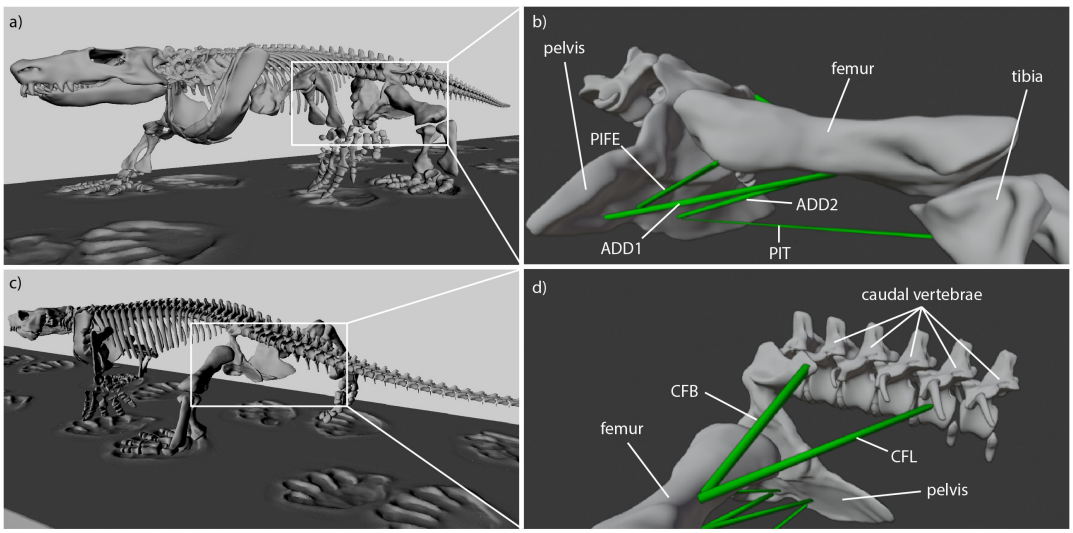

FIGURE 7 | Reconstructed muscle attachments and lines of action in *Orobates*. **(a)** Latero-frontal view of *Orobates*, **(b)** latero-frontal view of relevant skeletal elements to show adductor muscles (ADD1, ADD2, PIFE, PIT) at reference length (mid-stance), **(c)** latero-caudal view of *Orobates*, **(d)** latero-caudal view of relevant skeletal elements to show retractor muscles (CFB, CFL) at resting length (mid-stance).

gait (Nyakatura et al., 2019). Especially the latter previous quantitative study lends support to earlier qualitative assessments of *Orobates*' locomotion which hypothesized this species to have been capable of "increased speed, greater maneuverability, and more efficient support" than earlier tetrapods (Berman and Henrici, 2003). While uncertainty was acknowledged and even a website was published alongside the paper to allow readers to explore the gaits of *Orobates* and the consequences of changes made to any of the tested kinematic variables[2], several of the most plausible gait solutions identified for *Orobates* –including the solution featured in the main text of the paper– clustered around a body height of 44% IGD. Our results based on the assessment of muscle strains in various simulated gaits with differing body heights found the strongest support for an "intermediate" body height (45% IGD; but note that other modeled body heights yielded almost equal results within a single percentage point). Thus, the results of the current study based on an independent line of evidence do not directly contradict and one of the favored models is in agreement with a moderately erect posture and gait of *Orobates* (but see discussion of limitations to the here used approach below).

The presence of such more erect limb posture when compared to earlier tetrapods (Kawano and Blob, 2013; Nyakatura et al., 2014) suggests the capability to facilitate improved acceleration

[2]https://go.epfl.ch/Orobates

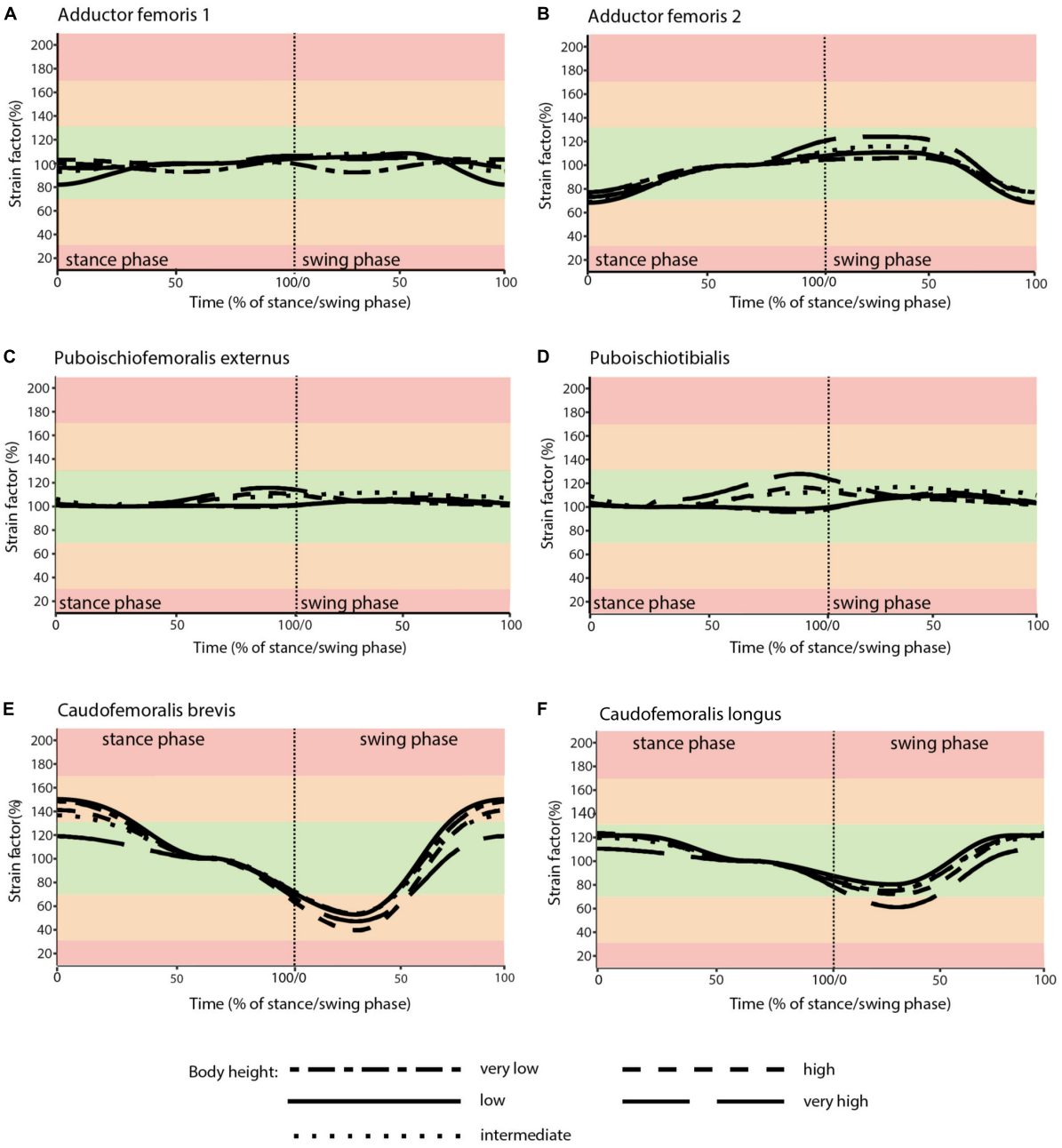

FIGURE 8 | Muscle strains plotted against percentage of stance and swing phase in *Orobates* for each of the five analyzed body heights. **(A)** ADD1; **(B)** ADD2; **(C)** PIFE; **(D)** PIT; **(E)** CFB; **(F)** CFL. Red areas of the plots involve muscle tension beyond 170% or compression below 30% of resting length and is considered implausible in this study. Green areas of the plots represented optimal muscle length for the generation of force (between 70 and 130% of reference length). Orange areas represent feasible muscle strains with limited potential for force generation.

of the body into the direction of travel (Riskin et al., 2016), greater overall capacity for speed (Reilly et al., 2005; Fuller et al., 2011), and reduced torsional stresses at limb long bone midshafts (Blob, 2001). Our results thus lend further tentative support to the possibility of such advanced locomotion (as outlined in the previous sentence) already present in the last common ancestor of diadectids and crown amniotes. Given the most common recovered phylogenetic position of diadectids as stem amniotes (e.g., Laurin and Reisz, 1995, 1997; Lee and Spencer, 1997; Coates and Ruta, 2007), this would imply that advanced terrestrial locomotion beneficial to navigating fully terrestrial habitats preceded the origin of crown amniotes in contrast to previous suggestions (Sumida and Modesto, 2001).

While the earlier study of Nyakatura et al. (2019) used complex permutations of several interdependent variables of sprawling tetrapod locomotion, the current study focuses solely

TABLE 2 | Percentage of the stride cycle that a modeled muscle maintained optimal muscle strain (i.e., within 70 and 130% of reference length) in *Orobates*.

	Hip height	PIT	PIFE	ADD1	ADD2	CFB	CFL	Total
Stance phase	"Very low"	100%	78.75%	100%	100%	70.00%	100%	
	"Low"	100%	71.25%	100%	91.25%	67.50%	100%	
	"Intermediate"	100%	81.25%	100%	93.75%	78.75%	100%	
	"High"	87.50%	100%	100%	100%	68.75%	100%	
	"Very high"	100%	91.25%	100%	100%	97.50%	100%	
Swing phase	"Very low"	100%	84.29%	100%	100%	30.00%	100%	
	"Low"	74.29%	74.29%	100%	92.86%	27.14%	100%	
	"Intermediate"	100%	85.71%	100%	94.28%	37.14%	100%	
	"High"	92.86%	91.43%	100%	100%	27.14%	100%	
	"Very high"	100%	34.29%	100%	100%	45.71%	61.43%	
Complete stride cycle	"Very low"	100%	81.52%	100%	100%	50%	100%	88.59%
	"Low"	87.15%	72.77%	100%	92.06%	47.32%	100%	83.22%
	"Intermediate"	100%	83.48%	100%	94.02%	57.95%	100%	89.24%
	"High"	90.18%	95.72%	100%	100%	47.95%	100%	88.98%
	"Very high"	100%	62.77%	100%	100%	71.61%	80.72%	85.85%

*ADD, M. adductor femoris; PIFE, M. puboischiofemorales externus; PIT, M. puboischiotibialis; CFL, M. caudofemoralis longis; CFB, M. caudofemoralis brevis. See **Figure 8** for graphical illustration of muscle strains.*

on one kinematic variable, which is body height (as reflected by the sprawling angle or expressed as percentage of IGD). The influence of body height was tested, but other hip kinematic properties (pro-/retraction, long-axis rotation) were unavoidably affected by the IK rig due to the interdependency of rotations when using Euler angles to describe 3D joint movements (Sullivan, 2007). In addition to this, it remains unexplored what consequences systematic changes to other kinematic variables of sprawling locomotion such as long-axis rotation, pre-/retraction, and spine bending (Barclay, 1946; Ashley-Ross, 1994; Karakasiliotis et al., 2016) have on the muscle strains of the extrinsic hindlimb muscles in *Orobates*. Moreover, we cannot fully exclude any of the tested body heights for *Orobates*, because none of them reached implausible values of muscle tension (>170% of resting length) or muscle compression (<30% of resting length) (Sherwood et al., 2013; Lautenschlager, 2015). Hence, even though the "intermediate" posture reached the overall maximized optimal muscle strains, data for muscle strain assessed here remains inconclusive, but does not contradict previous reconstructions of posture and gait for *Orobates*. Animals generally engage in diverse behaviors that often involve larger joint excursions and thus also muscle strains than cyclic steady-state walking. *Orobates* was potentially capable of locomotion at different body heights (cf. the "low walks" and "high walks" of crocodiles, e.g., Gatesy, 1991; Reilly et al., 2005). Regardless, the results derived from our modeling approach should be considered tentative steps into the incorporation of soft tissue anatomy into the reconstruction of locomotor properties.

We acknowledge that the muscle models used here are highly abstracted and simplified. It is, however, very encouraging that this simple approach was capable of closely predicting the *in vivo* posture exhibited in our validation experiments using the *Caiman*. Again, "low" and "intermediate" (hip height of 0.49 IGD) postures maximized optimal muscle strains over the course of an entire stride, almost matching the *in vivo* hip height of 0.5 IGD *in vivo*. The degree of muscle tension and compression is most relevant during activity of a muscle (although even during inactivity the risk of muscle injury remains). Available electromyographic (EMG) data for *Caiman* is scarce, but Gatesy (1989) mentioned that the observed preliminary data of the extrinsic hindlimb muscles of *Caiman crocodilus* (referred to by its synonym *Caiman sclerops* in Gatesy, 1989) appear to be similar to more robust data from *Alligator mississippiensis*. While in our analysis the most critical muscle strains occur in the ADD1 and ADD2 as well as in the CFB muscles during late stance and swing phase, available EMG data points to reduced activity of postural and propulsive muscles of crocodilians during that time of the stride cycle. Importantly, however, to our knowledge no data has been published for the ADD2 and CFB muscles in either *Alligator* or in *Caiman* highlighting the need for such *in vivo* muscle activation pattern data. Still, our validation was able to predict the posture of *Caiman*, albeit that other postures scored similarly high. This validation lends support, not only for the transfer of our method to the modeling of *Orobates*' locomotion, but also to the more general assumption we made here. Specifically, we hypothesized that tetrapods will choose postures and gaits that will maximize the occurrence of optimal muscle strains. While this clearly needs further empiric evidence from other species, when further corroborated this relationship could be utilized for the inference of posture and gaits in other fossil taxa, too.

Further simplifications in the model setup were made, such as modeling muscles as simple point-to-point connections. In reality, however, muscles are not straight lines like we reconstruct them in our models of *Caiman* and *Orobates,* and they would curve around other muscles and bones or could attach to connective tissue. This would increase or decrease the muscle length and can affect the measured muscle strains. Even the individual muscle microstructure such as differences in the pennation angle likely affects the muscle strain assessment (Lautenschlager, 2015). Nevertheless, a similar modeling approach as has been used here has been employed

to study cranial musculature and showed that this approach can lead to meaningful results, i.e., that predictions even from such simplified muscle models match empirical data well (Lautenschlager, 2015). Undoubtedly, the approach needs further testing in the context of locomotion. Again, if established, it would present a very useful technique to gain insight into the posture and gait of extinct tetrapod species.

Nevertheless, the modeling approach utilized here failed to single out one specific predicted posture or even to rule out a suite of modeled postures for *Orobates*. Indeed, none of the modeled postures did involve problematic excessive strains. This result could simply demonstrate a postural variability of *Orobates* which even exceeded that of modern *Caiman* (see above). Alternatively, this could point to limited prediction strength of the method. Potentially, prediction strength could be improved by including additional (intrinsic) limb muscles such as knee and ankle extensors, more elaborate optimization criteria, and more detailed muscle anatomy (e.g., pennation angles, variable lengths of muscles and tendons, etc.). Instantaneous muscle lever arms could further help to constrain postures as was recently attempted in a study on Nile crocodiles (Wiseman et al., 2021). In sophisticated musculo-skeletal models of vertebrate postcranial function most of these issues are taken into account and even muscle activation patterns may be predicted (e.g., recent papers by Bishop et al., 2021; Stark et al., 2021), but necessitate considerable modeling effort. A simpler approach such as the muscle strain analysis used in the current study therefore offers an alternative, for example for a first reduction of the solution space of potential postures especially in broader scaled comparative studies.

CONCLUSION

The current study builds on previous work on the locomotion of *Orobates pabsti*, a putative stem amniote from the Permian period, by taking soft tissues into account. The proposed modeling approach of highly abstracted muscles responsible for lifting the trunk off the ground and for the generation of propulsion during walking locomotion at different simulated body heights was able to approximately predict the posture of extant *Caiman crocodilus*. This finding derived from "virtual experiments" that systematically varied body height, justified the transfer of the methodology to *Orobates* in order to gain further insight into the locomotor capabilities of this key early tetrapod. Muscle models were added to an already existing skeletal reconstruction of the holotype specimen of *Orobates*. Further, the animated locomotion stemming from a previous study was used. As in the validation experiment of *Caiman*, body height was systematically varied. While none of the simulated step cycles at different body heights resulted in the occurrence of implausible muscle strains and thus no posture could be dismissed outright, an "intermediate" posture minimized deviations from optimal muscle strains between 70 and 130% of the resting length (however, only due to a slightly better result than almost equally good results for other body heights). Body height at this "intermediate" posture is consistent with independent results from kinematic and dynamic simulations of the previous study (Nyakatura et al., 2019). Thus, our current study, albeit not narrowing posture down even more, does not contradict the hypothesized advanced locomotor capabilities of *Orobates* and strengthens previous evidence for the locomotor reconstruction of the last common ancestor of diadectids and crown amniotes. More generally and even though overall prediction strength may be weaker than comparable more sophisticated musculo-skeletal modeling approaches, the here employed methodology of simplified muscle modeling, which is relatively easy to implement, could be useful especially in comparative studies into the reconstruction of posture of extinct tetrapods.

DATA AVAILABILITY STATEMENT

The original contributions presented in the study are included in the article/**Supplementary Material**, further inquiries can be directed to the corresponding author/s.

ETHICS STATEMENT

The animal study was reviewed and approved by the Thüringer Landesamt für Verbraucher- und Umweltschutz (registration number: 02-008/11).

AUTHOR CONTRIBUTIONS

JN and SL conceived of the study. OD prepared interactive animation of *Caiman crocodilus*. SL transferred models from Maya into Blender. MZ and JN reconstructed muscles, conducted the muscle strain modeling, analyzed the data, drafted figures, and prepared the manuscript draft. All authors interpreted data, and revised, read, and approved the manuscript.

FUNDING

This study received funding from a Volkswagen Foundation grant (AZ 90222 to JN) and a Daimler and Benz Foundation grant (32-08/12 to JN). JN was also supported by the German Research Council (DFG EXC 1027, DFG EXC 2025).

ACKNOWLEDGMENTS

We thank La Ferme aux Crocodiles (Pierrelatte, France) for making two *Caiman crocodilus* available for this study. We further thank R. Petersohn, I. Weiß, S. Clemens, and V. Allen for their contribution to the X-ray motion analysis of live *Caiman* specimens. We are indebted to J. Lauströer and A. Andikfar for their initial concept of a X-ray video collage of *Caiman*. We thank the two reviewers for their critical comments on a previous version, which greatly helped to improve the manuscript.

SUPPLEMENTARY MATERIAL

The Supplementary Material for this article can be found online at: https://www.frontiersin.org/articles/10.3389/fevo.2021.659039/full#supplementary-material

REFERENCES

Anderson, P. S. L., Bright, J. A., Gill, P. G., Palmer, C., and Rayfield, E. J. (2012). Models in palaeontological functional analysis. *Biol. Lett.* 8, 119–122. doi: 10.1098/rsbl.2011.0674

Arnold, P., Fischer, M. S., and Nyakatura, J. A. (2014). Soft tissue influence on ex vivo mobility in the hip of Iguana: comparison with in vivo movement and its bearing on joint motion of fossil sprawling tetrapods. *J. Anat.* 225, 31–41. doi: 10.1111/joa.12187

Ashley-Ross, M. (1994). Hindlimb kinematicas during terrestrial locomotion in a salamander (*Dicamptodon Tenebrosus*). *J. Exp. Biol.* 193, 255–283.

Ashley-Ross, M. A. (1992). The comparative myology of the thigh and crus in the salamanders *Ambystoma tigrinum* and *Dicamptodon tenebrosus*. *J. Morphol.* 211, 147–163. doi: 10.1002/jmor.1052110204

Barclay, O. (1946). The mechanics of amphibian locomotion. *J. Exp. Biol.* 23:177. doi: 10.1242/jeb.23.2.177

Bates, K. T., and Falkingham, P. L. (2012). Estimating maximum bite performance in *Tyrannosaurus* rex using multi-body dynamics. *Biol. Lett.* 8, 660–664. doi: 10.1098/rsbl.2012.0056

Berman, D. S., and Henrici, A. C. (2003). Homology of the astragalus and structure and function of the tarsus of Diadectidae. *J. Paleontol.* 77, 172–188. doi: 10.1017/S002233600004350X

Berman, D. S., Henrici, C. M. Y., Richard, A., Sumida, S. S., and Martens, T. (2004). A new Diadectid (Diadectomorpha), Orobates Pabsti, from the early Permian of central Germany. *Bull. Carnegie Mus. Nat. Hist.* 35, 1–36. doi: 10.2992/0145-9058(2004)35[1:anddop]2.0.co;2

Bishop, P. J., Cuff, A. R., and Hutchinson, J. R. (2021). How to build a dinosaur: musculoskeletal modeling and simulation of locomotor biomechanics in extinct animals. *Paleobiology* 58, 1–38. doi: 10.1017/pab.2020.46

Blob, R. W. (2001). Evolution of hindlimb posture in nonmammalian therapsids: biomechanical tests of paleontological hypotheses. *Paleobiology* 27, 14–38. doi: 10.1666/0094-8373(2001)027<0014:eohpin>2.0.co;2

Brainerd, E. L., Baier, D. B., Gatesy, S. M., Hedrick, T. L., Metzger, K. A., Gilbert, S. L., et al. (2010). X-ray reconstruction of moving morphology (XROMM): precision, accuracy and applications in comparative biomechanics research. *J. Exp. Zool. Part A Ecol. Genet. Physiol.* 313, 262–279.

Clack, J. A. (2006). The emergence of early tetrapods. *Palaeogeogr. Palaeoclimatol. Palaeoecol.* 232, 167–189. doi: 10.1016/j.palaeo.2005.07.019

Clack, J. A., and Bénéteau, A. (2012). *Gaining Ground: The Origin and Evolution of Tetrapods*, Second Edn. Bloomington: Indiana University Press

Coates, M. I., and Ruta, M. (2007). *Skeletal Changes in the Transition from Fins to Limbs*. Chicago, IL: Univ. of Chicago Press.

Cunningham, J. A., Rahman, I. A., Lautenschlager, S., Rayfield, E. J., and Donoghue, P. C. J. (2014). A virtual world of paleontology. *Trends Ecol. Evol.* 29, 347–357. doi: 10.1016/j.tree.2014.04.004

Demuth, O. E., Rayfield, E. J., and Hutchinson, J. R. (2020). 3D hindlimb joint mobility of the stem-archosaur *Euparkeria capensis* with implications for postural evolution within Archosauria. *Sci. Rep.* 10:15357. doi: 10.1038/s41598-020-70175-y

Diogo, R., Johnston, P., Molnar, J. L., and Esteve-Altava, B. (2016). Characteristic tetrapod musculoskeletal limb phenotype emerged more than 400 MYA in basal lobe-finned fishes. *Sci. Rep.* 6:37592. doi: 10.1038/srep37592

Fischer, M. S., Schilling, N., Schmidt, M., Haarhaus, D., and Witte, H. (2002). Basic limb kinematics of small therian mammals. *J. Exp. Biol.* 205, 1315–1338. doi: 10.1242/jeb.205.9.1315

Fuller, P. O., Higham, T. E., and Clark, A. J. (2011). Posture, speed, and habitat structure: three-dimensional hindlimb kinematics of two species of Padless geckos. *Zoology* 114, 104–112. doi: 10.1016/j.zool.2010.11.003

Garwood, R., and Dunlop, J. (2014). The walking dead: blender as a tool for paleontologists with a case study on extinct arachnids. *J. Paleontol.* 88, 735–746. doi: 10.1666/13-088

Gatesy, S. M. (1989). *Archosaur Neuromuscular and Locomotor Evolution*. Ph.D. thesis. Cambridge, MA: Harvard University.

Gatesy, S. M. (1991). Hind limb movements of the American alligator (*Alligator mississippiensis*) and postural grades. *J. Zool.* 224, 577–588. doi: 10.1111/j.1469-7998.1991.tb03786.x

Gatesy, S. M. (1997). An electromyographic analysis of hindlimb function in *Alligator* during terrestrial locomotion. *J. Morphol.* 234, 197–212. doi: 10.1002/(sici)1097-4687(199711)234:2<197::aid-jmor6>3.0.co;2-9

Gatesy, S. M., Baier, D. B., Jenkins, F. A., and Dial, K. P. (2010). Scientific rotoscoping: a morphology-based method of 3-D motion analysis and visualization. *J. Exp. Zool. A Ecol. Genet. Physiol.* 313, 244–261. doi: 10.1002/jez.588

Hutchinson, J. R. (2001). The evolution of pelvic osteology and soft tissues on the line to extant birds (Neornithes). *Zool. J. Linn. Soc.* 131, 123–168. doi: 10.1006/zjls.2000.0254

Hutchinson, J. R. (2012). On the inference of function from structure using biomechanical modelling and simulation of extinct organisms. *Biol. Lett.* 8, 115–118. doi: 10.1098/rsbl.2011.0399

Hutchinson, J. R., and Gatesy, S. M. (2000). Adductors, abductors, and the evolution of archosaur locomotion. *Paleobiology* 26, 734–751. doi: 10.1666/0094-8373(2000)026<0734:aaateo>2.0.co;2

Karakasiliotis, K., Thandiackal, R., Melo, K., Horvat, T., Mahabadi, N. K., Tsitkov, S., et al. (2016). From cineradiography to biorobots: an approach for designing robots to emulate and study animal locomotion. *J. R. Soc. Interface* 13:20151089. doi: 10.1098/rsif.2015.1089

Kawano, S. M., and Blob, R. W. (2013). Propulsive forces of mudskipper fins and salamander limbs during terrestrial locomotion: implications for the invasion of land. *Integr. Comp. Biol.* 53, 283–294. doi: 10.1093/icb/ict051

Koolstra, J. H., and van Eijden, T. M. (1995). Biomechanical analysis of jaw-closing movements. *J. Dent. Res.* 74, 1564–1570. doi: 10.1177/00220345950740091001

Laurin, M., and Reisz, R. R. (1995). A reevaluation of early amniote phylogeny. *Zool. J. Linn. Soc.* 113, 165–223. doi: 10.1111/j.1096-3642.1995.tb00932.x

Laurin, M., and Reisz, R. R. (1997). "A new perspective on tetrapod phylogeny," in *Amniote Origins: Completing the Transition to Land*, eds S. Sumida and K. Martin (San Diego, CA: Academic Press), 9–59. doi: 10.1016/b978-012676460-4/50003-2

Lautenschlager, S. (2015). Estimating cranial musculoskeletal constraints in theropod dinosaurs. *R. Soc. Open Sci.* 2:150495. doi: 10.1098/rsos.150495

Lautenschlager, S. (2016). Digital reconstruction of soft-tissue structures in fossils. *Paleontol. Soc. Pap.* 22, 101–117. doi: 10.1017/scs.2017.10

Lautenschlager, S. (2020). Multibody dynamics analysis (MDA) as a numerical modelling tool to reconstruct the function and palaeobiology of extinct organisms. *Palaeontology* 63, 703–715. doi: 10.1111/pala.12501

Lee, M. S. Y., and Spencer, P. S. (1997). "Crown-Clades, key characters and taxonomic stability: when is an amniote not an amniote?," in *Amiote Origins - Completing the Transition to Land*, eds S. S. Sumida and K. L. Martin (San Diego, CA: Academic Press)

Manafzadeh, A. R., and Padian, K. (2018). ROM mapping of ligamentous constraints on avian hip mobility: implications for extinct ornithodirans. *Proc. R. Soc. B Biol. Sci.* 285:20180727. doi: 10.1098/rspb.2018.0727

Marjanović, D., and Laurin, M. (2019). Phylogeny of Paleozoic limbed vertebrates reassessed through revision and expansion of the largest published relevant data matrix. *PeerJ* 6:e5565. doi: 10.7717/peerj.5565

Martin, K., and Sumida, S. S. (1997). *Amniote Origins: Completing the Transition to Land*. San Diego, CA: Academic Press

Molnar, J. L., Diogo, R., Hutchinson, J. R., and Pierce, S. E. (2020). Evolution of hindlimb muscle anatomy across the tetrapod water-to-land transition, including comparisons with forelimb anatomy. *Anat. Rec. (Hoboken)* 303, 218–234. doi: 10.1002/ar.23997

Nyakatura, J. A. (2017). "Description, experiment, and model. reading traces in paleobiological research exemplified by a morpho-functional analysis," in *Traces*, ed. B. Bock von Wülfingen (Berlin: De Gruyter), 15–28.

Nyakatura, J. A. (2019). Making use of a track-trackmaker association: locomotor inference of an early amniote with help of "fossilized behavior". *Hallesches Jahrbuch Geowissenschaften Beiheft* 46, 67–75.

Nyakatura, J. A., Allen, V. R., Lauströer, J., Andikfar, A., Danczak, M., Ullrich, H.-J., et al. (2015). A three-dimensional skeletal reconstruction of the stem amniote *Orobates pabsti* (Diadectidae): analyses of body mass, centre of mass position, and joint mobility. *PLoS One* 10:e0137284. doi: 10.1371/journal.pone.0137284

Nyakatura, J. A., and Demuth, O. E. (2019). "Modellieren. Virtuelle Experimente zur funktionellen Morphologie," in *Experimentieren: Einblicke in Praktiken und Versuchsaufbauten zwischen Wissenschaft und Gestaltung*, eds S. Marguin, H. Rabe, W. Schäffner, and F. Schmidgall (Bielefeld: Transcript Verlag)

Nyakatura, J. A., Andrada, E., Curth, S., and Fischer, M. S. (2014). Bridging "Romer's Gap": limb mechanics of an extant belly-dragging lizard inform debate on tetrapod locomotion during the early carboniferous. *Evol. Biol.* 41, 175–190. doi: 10.1007/s11692-013-9266-z

Nyakatura, J. A., Melo, K., Horvat, T., Karakasiliotis, K., Allen, V. R., Andikfar, A., et al. (2019). Reverse-engineering the locomotion of a stem amniote. *Nature* 565, 351–355. doi: 10.1038/s41586-018-0851-2

Otero, A., Gallina, P. A., and Herrera, Y. (2010). Pelvic musculature and function of *Caiman latirostris*. *Herpetol. J.* 20, 173–184.

Reilly, S. M., Willey, J. S., Biknevicius, A. R., and Blob, R. W. (2005). Hindlimb function in the alligator: integrating movements, motor patterns, ground reaction forces and bone strain of terrestrial locomotion. *J. Exp. Biol.* 208, 993–1009. doi: 10.1242/jeb.01473

Reisz, R. R. (1997). The origin and early evolutionary history of amniotes. *Trends Ecol. Evol.* 12, 218–222. doi: 10.1016/S0169-5347(97)01060-4

Riskin, D. K., Kendall, C. J., and Hermanson, J. W. (2016). The crouching of the shrew: mechanical consequences of limb posture in small mammals. *PeerJ* 4:e2131. doi: 10.7717/peerj.2131

Romer, A. S. (1922). The locomotor apparatus of certain primitive and mammal-like reptiles. *Bull. AMNH* 46, article 10, 517–606.

Russell, A. P., and Bels, V. (2001). Biomechanics and kinematics of limb-based locomotion in lizards: review, synthesis and prospectus. *Comp. Biochem. Physiol. Part A Mol. Integr. Physiol.* 131, 89–112. doi: 10.1016/s1095-6433(01)00469-x

Schilling, N., Fischbein, T., Yang, E. P., and Carrier, D. R. (2009). Function of the extrinsic hindlimb muscles in trotting dogs. *J. Exp. Biol.* 212, 1036–1052. doi: 10.1242/jeb.020255

Sherwood, L., Klandorf, H., and Yancey, P. H. (2013). *Animal Physiology: From Genes to Organisms*. Pacific Grove, CA: Calif. Brooks/Cole.

Snively, E., Cotton, J. R., Ridgely, R., and Witmer, L. M. (2013). Multibody dynamics model of head and neck function in *Allosaurus* (Dinosauria, Theropoda). *Palaeontol. Electron.* 16:11A.

Stark, H., Fischer, M. S., Hunt, A., Young, F., Quinn, R., and Andrada, E. (2021). A three-dimensional musculoskeletal model of the dog. *Sci. Rep.* 11:11335.

Sullivan, C. S. (2007). *Function and Evolution of the Hind Limb in Triassic Archosaurian Reptiles.* Ph.D. thesis. Cambridge, MA: Harvard University.

Sumida, S. S., and Modesto, S. (2001). A phylogenetic perspective on locomotory strategies in early amniotes. *Integr. Comp. Biol.* 41, 586–597. doi: 10.1093/icb/41.3.586

Sutton, M. D. (2008). Tomographic techniques for the study of exceptionally preserved fossils. *Proc. Biol. Sci.* 275, 1587–1593. doi: 10.1098/rspb.2008.0263

Voigt, S., Berman, D. S., and Henrici, A. C. (2007). First well-established track-trackmaker association of paleozoic tetrapods based on *Ichniotherium* trackways and diadectid skeletons from the Lower Permian of Germany. *J. Vertebr. Paleontol.* 27, 553–570.

Watt, A., and Watt, M. (1992). *Advanced Animation and Rendering Techniques: Theory and Practice*. New York, NY: ACM Press

Wiseman, A. L. A., Bishop, P. J., Demuth, O. E., Cuff, A. R., Michel, K. B., and Hutchinson, J. R. (2021). Musculoskeletal modelling of the Nile crocodile (*Crocodylus niloticus*) hindlimb: effects of limb posture on leverage during terrestrial locomotion. *J. Anat. JOA* 239, 424–444. doi: 10.1111/joa.13431

Witmer, L. M. (1995). "The extant phylogenetic bracket and the importance of reconstruction soft tissues in fossils," in *Functional Morphology in Vertebrate Paleontology*, ed. J. J. Thomason (Cambridge: Cambridge University Press) 19–33.

Conflict of Interest: The authors declare that the research was conducted in the absence of any commercial or financial relationships that could be construed as a potential conflict of interest.

Publisher's Note: All claims expressed in this article are solely those of the authors and do not necessarily represent those of their affiliated organizations, or those of the publisher, the editors and the reviewers. Any product that may be evaluated in this article, or claim that may be made by its manufacturer, is not guaranteed or endorsed by the publisher.

frontiers in Ecology and Evolution

ORIGINAL RESEARCH
published: 09 February 2022
doi: 10.3389/fevo.2021.812561

Imaging With the Past: Revealing the Complexity of Chimaeroid Pelvic Musculature Anatomy and Development

*Jacob B. Pears[1,2], Carley Tillett[3], Rui Tahara[4], Hans C. E. Larsson[4] and Catherine A. Boisvert[1,2]**

[1] School of Molecular and Life Sciences, Curtin University, Perth, WA, Australia, [2] Curtin Health Innovation Research Institute, Curtin University, Perth, WA, Australia, [3] Hub for Immersive Visualization and eResearch, Curtin University, Perth WA, Australia, [4] Redpath Museum, McGill University, Montreal, QC, Canada

Chondrichthyans are now widely adopted as models for examining the development and evolution of the stem gnathostome body plan. The fins of some cartilaginous fish are recognized for their plesiomorphic form and mode of muscular development, i.e., epithelial extension. Despite detailed molecular and descriptive examinations of these developmental mechanisms, there has been little contemporary examination of the ontogeny and morphology of the musculature in chondrichthyans including that of the paired fins. This gap represents a need for further examination of the developmental morphology of these appendicular musculatures to gain insight into their evolution in gnathostomes. The elephant shark is a Holocephalan, the sister group of all other chondrichthyans (Holocephali: *Callorhinchus milii*). Here, we use nano-CT imaging and 3D reconstructions to describe the development of the pelvic musculature of a growth series of elephant shark embryos. We also use historical descriptions from the nineteenth century and traditional dissection methods to describe the adult anatomy. This combined approach, using traditional methods and historical knowledge with modern imaging techniques, has enabled a more thorough examination of the anatomy and development of the pelvic musculature revealing that chimaeroid musculatures are more complex than previously thought. These data, when compared to extant and extinct sister taxa, are essential for interpreting and reconstructing fossil musculatures as well as understanding the evolution of paired fins.

Keywords: chimaeroid, muscle development, nano-CT, elephant shark, appendicular muscles, pelvic anatomy, clasper

OPEN ACCESS

Edited by:
David Ellard Keith Ferrier, University of St Andrews, United Kingdom

Reviewed by:
Katharine Criswell, University of Cambridge, United Kingdom
Richard Dearden, Muséum National d'Histoire Naturelle, France

***Correspondence:**
Catherine A. Boisvert
Catherine.Boisvert@curtin.edu.au

Specialty section:
This article was submitted to Evolutionary Developmental Biology, a section of the journal Frontiers in Ecology and Evolution

Received: *10 November 2021*
Accepted: *17 December 2021*
Published: *09 February 2022*

Citation:
Pears JB, Tillett C, Tahara R, Larsson HCE and Boisvert CA (2022) Imaging With the Past: Revealing the Complexity of Chimaeroid Pelvic Musculature Anatomy and Development. Front. Ecol. Evol. 9:812561. doi: 10.3389/fevo.2021.812561

INTRODUCTION

Comparative anatomy has been essential in the study of the evolution of paired fins. By comparing the anatomy and development of sister taxa at phylogenetically significant intervals, researchers have been able to distinguish plesiomorphic and derived traits to better understand how fins have evolved in the gnathostome clade (Neyt et al., 2000; Tanaka et al., 2002; Cole and Currie, 2007; Cole et al., 2011; Wilhelm et al., 2015; Ziermann et al., 2017). In these analyses, cartilaginous fish (Chondrichthyes) are often assumed to represent the pleisomorphic condition relative to osteichthyans. This dates back to the comparative anatomists of the late nineteenth century (Balfour, 1878, 1881), who used chondrichthyans as the best extant models for the "primitive"

condition of the jawed vertebrate body plan (Cole and Currie, 2007; Coolen et al., 2008; Brazeau and Friedman, 2015; Larouche et al., 2017). Although chondrichtyans do retain pleisomorphic characteristics, some, like the presence of mineralized cartilage, are autapomorphies. On their own, they do not represent the "primitive bauplan" of jawed vertebrates but present phylogenetically important anatomies. In order to understand the origin and evolution of paired fins, their anatomy must be compared to that of other extant and extinct sister taxa.

In recent years, comparative anatomy, specifically examinations of the musculature, has been used, by a vocal minority, to challenge the long held view that pectoral and pelvic fins are serial homologs (Diogo and Molnar, 2014; Diogo and Ziermann, 2015; Ziermann et al., 2017; Diogo, 2020; Siomava et al., 2020). Among these studies, only a single paper (Ziermann et al., 2017) has looked at fin muscle development despite its essential role in addressing questions such as the validity of serial homology (Ziermann et al., 2017). Current studies of chondrichthyan muscle development are sparse, with the majority of the research having been conducted in the late nineteenth (Balfour, 1878, 1881; Dohrn, 1884; Mollier, 1892; Braus, 1899) and early twentieth centuries (Goodrich, 1906; Edgeworth, 1911, 1935). Contemporary research has focused on the developmental mechanisms of fins (Neyt et al., 2000; Tanaka et al., 2002; Cole and Currie, 2007; Cole et al., 2011; Freitas et al., 2014) with the exception of Ziermann et al. (2017), which does describe the development of specific muscles across ontogeny as opposed to solely examining the mechanisms of appendicular muscle development. The historical literature has also examined an array of different elasmobranch taxa, including members of the Squaliformes (Braus, 1898, 1899), Carcharhiniformes (Balfour, 1878; Dohrn, 1884; Mollier, 1892; Goodrich, 1906), and Torpediniformes (Dohrn, 1884; Mollier, 1892; Braus, 1899). While this body of work is vast, detailed and almost exclusively in German, it is also generally limited to observations of the mesodermal cells that form the fin muscles and their early development, with no description of the development of specific muscles. This scarcity of developmental data indicate a need for more detailed morphological descriptions of the ontogeny of the musculature in cartilaginous fish to better address currently debated homology questions.

Holocephalans are the sister group of all other chondricthyans (Sharks, skates, and rays) (Ehrlich, 2010; Inoue et al., 2010; Maisey, 2012; Venkatesh et al., 2014) and have been used as models for examining gnathostome vertebrate morphology and development (Trinajstic et al., 2013, 2018), including the development of the musculature of paired fins (Cole et al., 2011). In contrast with elasmobranchs, selachians in particular, the appendicular muscles of holocephalans have not been described in an array of different species. As far as we are aware, there is only one contemporary description of chimaeroid pelvic fin muscle anatomy, that of the ratfish (*Hydrolagus colliei*) (Diogo and Ziermann, 2015), and one in the historical literature of the rabbit fish (*Chimaera monstrosa*) (Davidoff, 1879). Further, only two descriptions of the pelvic clasper musculature of *C. monstrosa* and *Callorhynchus antarcticus* (sic) are present in the historical literature (Davidoff, 1879; Jungersen, 1899). To date there has been no study describing the morphology of these muscles across ontogeny.

Callorhinchid chimaeras such as the elephant shark (*Callorhinchus milii*) are the sister group to all living holocephalans (Inoue et al., 2010; Cole et al., 2011; Venkatesh et al., 2014) and therefore represent a unique model to examine gnathostome development. Here, we have examined the development and morphology of the pelvic musculature of *C. milii* via nano Computed Tomography (CT) imaging and anatomical dissection. In contrast with traditional methods, this nano-CT imaging allows for the non-destructive visualization of the anatomy in fine detail *in situ*, which can be reproduced in 3D models of the pelvic skeleton and musculature. Further, we compare our description of adult morphology with those of other chimaeroids in the historical and contemporary literature to determine any muscle homologies. Through these analyses, we aim to address the lack of developmental and anatomical data and better inform current understandings and hypotheses on the evolution and nature of the vertebrate fin skeleton.

MATERIALS AND METHODS

Adult and Embryonic Materials

To source the embryonic growth series, multiple adult female *Callorhinchus milii* were caught by rod and reel from Western Port bay, Victoria, Australia (License Numbers: DPR RP1000, RP1003, and RP1112). These individuals were transported, housed and kept according to established practice (Boisvert et al., 2015) until eggs were laid, after which they were released in the wild. Eggs were raised in a closed system aquarium (Boisvert et al., 2015) and euthanized at different stages of development using Tricaine. Specimens were staged according to their length and external morphology as per Didier et al. (1998). Where it could be determined by external morphology, male embryonic specimens were selected to enable the description of the developing claspers. Specimens were then fixed in 4% paraformaldehyde (PFA) in phosphate buffer solution (PBS) and dehydrated in ethanol or methanol. All procedures were conducted following the directions and authorization of the Monash University Animal Ethics Committee (Permit: MAS/ARMI/2010/01).

Adult specimens were also caught by rod and reel from Western Port bay, Victoria, Australia (License Numbers: DPR RP RP1000, RP1003, and RP1112). Individuals were transported and housed by the same practices, but died in captivity and were used for dissections. All procedures were conducted following the directions and authorization of the Monash University Animal Ethics Committee (Permit: MAS/ARMI/2010/01).

Nano Computed Tomography Imaging

To examine muscular development across ontogeny in a non-destructive manner, a growth series (stages 30, 32, and 34; Didier et al., 1998) of elephant shark (*Callorhinchus milii*) embryos were stained using 1% phosphotungstic acid (PTA) (1% PTA dissolved in 70% EtOH). Embryos were quickly washed with 70% EtOH to remove excessive stain on the surface, and then nano-CT scanned in 0.5% agarose on a Zeiss Xradia 520 Versa (Carl Zeiss Canada

Ltd., ON, Canada) at McGill University. The staining duration and imaging parameters for each stage are given in **Table 1**.

3D Modeling

Nano-CT data was reconstructed using Reconstructor (Carl Zeiss Canada Ltd., ON, Canada) and 3D models of the pelvic muscles were visualized using *Dragonfly* version 2020.1 (Object Research Systems)[1].

Dissection and Gross Anatomy

Adult male and female *C. milii* were dissected with scalpel and forceps to examine the gross anatomy of the pelvic musculature. They were photographed with a Canon digital camera.

Nomenclature

There are currently two known descriptions of holocephalan pelvic musculatures: rabbit fish (*Chimaera monstrosa*) (Davidoff, 1879) and the spotted ratfish (*Hydrolagus colliei*) (Diogo and Ziermann, 2015). Our description of the pelvic musculature of *C. milii* is more similar to that of *C. monstrosa* than *H. colliei*. We have therefore translated the terminology of *C. monstrosa* from German into English, to use for the present study, but, in cases where this terminology did not include structures found in *C. milii*, that of *H. colliei* was used (**Tables 2–4**).

There are three descriptions of pelvic clasper musculature in chimaeroids, those of *C. monstrosa* and *Callorhynchus antarcticus* (Jungersen, 1899) and another of *C. monstrosa* (Davidoff, 1879). In our description of the muscles of the pelvic claspers of *C. milii*, we have adapted the terminology of Davidoff (1879) as applied by Jungersen (1899) to describe *C. antarcticus* as this is from the same genus and is very similar in morphology to *C. milii* (**Table 5**). Another muscle associated with the pre-pelvic tenaculum was observed in *C. monstrosa* (Davidoff, 1879) and *C. antarcticus* (Parker, 1886), however, remained unnamed (**Table 6**). We propose a new name for this muscle (see below).

[1]https://www.theobjects.com/dragonfly/new.html

RESULTS

Adult Pelvic Musculature

Dorsal Musculature

The dorsal musculature consists of the portio prima, portio tertia, portio secunda, and deep dorsal layer. The dorsal half of the iliac ramus of the pelvic girdle is situated atop the hypaxial musculature, ranging from the midline to the middle of the hypaxial musculature at a 45° angle. The pelvic girdle is covered

TABLE 1 | Staining duration and imaging parameters of embryonic specimens.

Stage	Staining (days)	Voltage (kV)	Power (W)	Exp. time (sec)	Scan time (h)	Voxel size (μm)
30	27	60	5	3.0	5.0	3.0
32	67	60	5	4.5	6.5	4.0
34	69	60	5	5.0	7.0	5.5

TABLE 2 | Chimaeroid dorsal pelvic musculature and their points of origin (O) and insertion (I).

Muscle	*Chimaera monstrosa* (Davidoff, 1879)	*Callorhinchus milii* (This study)	Muscle	*Hydrolagus colliei* (Diogo and Ziermann, 2015)
Portio prima	O: External aponeurosis I: Front fin secondary skeleton (Ceratotrichia)	O: Body muscle fascia and Iliac ramus I: Ceratotrichia and Deep dorsal layer	Adductor superficialis	O: Body muscle fascia I: Dorsal radial cartilage
Portio tertia	O: Ilium I: Deep dorsal layer	O: Iliac ramus I: Deep dorsal layer	Not described	
Portio secunda	O: External aponeurosis and Ilium I: Second fin metapterygium (♀)/Basal appendage (♂)	O: Fascia of the body muscle, pelvic girdle and cloaca I: Second fin metapterygium (♀)/Anterior clasper cartilage (♂)	Levator 5	O: Body muscle fascia I: Basipterygium and Medial radial cartilages
Deep dorsal layer (tiefe dorsale Schicht)	O: Dorsal surface of basipterygium I: Radial muscles	O: Dorsal surface of basipterygium I: Dorsal radial cartilage	Adductor (Deep bundle)	O:Basipterygium I: Dorsal Radial Cartilage

TABLE 3 | Chimaeroid lateral pelvic musculature and their points of origin (O) and insertion (I).

Muscle	*Chimaera monstrosa* (Davidoff, 1879)	*Callorhinchus milii* (This study)	Muscle	*Hydrolagus colliei* (Diogo and Ziermann, 2015)
Protractor	Not described (But see *Lateral musculature*)	O: Body muscle fascia and Pelvic girdle I: Basipterygial process	Protractor	O: Pelvic girdle I: Propterygium
Abdominal adductor	Not described	O: Body muscle fascia I: Pelvic girdle	Not described	

TABLE 4 | Chimaeroid ventral pelvic musculature and their points of origin (O) and insertion (I).

Muscle	*Chimaera monstrosa* (Davidoff, 1879)	*Callorhinchus milii* (This study)	Muscle	*Hydrolagus colliei* (Diogo and Ziermann, 2015)
Basio-radial layer (Basio-radiale Schicht)	O: Ventral surface of basipterygium I: Ventral radial cartilage	O: Ventral surface of basipterygium I: Ventral radial cartilages	Abductor distalis	O: Basipterygium I: Ventral radial cartilage
Superficial ventral layer (oberflächliche ventrale Schicht)	O: Aponeurotic band and Ventral surface of ventral pelvic segment I: Anterior portion of basio-radial layer	O: Ventral surface of pelvic girdle I:Ceratotrichia and Anterior portion of basio-radial layer	Abductor proximalis	O: Puboischiac bar I: Basipterygium
Proximal radial layer	Not described	O: Proximal edge of the basipterygium and second fin metapterygium (♀)/Anterior clasper cartilage(♂) I: Proximal fin radials	Not described	

TABLE 5 | Chimaeroid clasper musculature and their points of origin (O) and insertion (I).

Muscle	*Chimaera monstrosa* (Jungersen, 1899)	*Chimaera monstrosa* (Davidoff, 1879)		*Callorhynchus antarcticus* (Jungersen, 1899)		*Callorhinchus milii* (This study)	
Adductor	O: Ventral surface of pelvic girdle and inter-pelvic band I: b1 cartilage	Adductor	O: Medial surface 1st and 2nd cartilages I: Medial surface ventral process	Dilatator (sic) dorsal portion	O: b1 cartilage (anterior clasper cartilage I: Appendix-stem (Posterior clasper cartilage)	Adductor	O: Dorsal surface of the pelvic girdle cartilage I: Posterior clasper cartilage
Dilatator (sic)	O: Hinder end of basale and b1 cartilage I: Anterior part of b1 cartilage	Flexor	O: Basal metapterygii I: Ventral process of clasper cartilage	Dilatator (sic) ventral portion	O: Basale I: Appendix-stem (Posterior clasper cartilage)	Flexor	O: Base of basipterygium I: Posterior clasper cartilage
Compressor	O: Lateral edge of β cartilage I: Lateral surface b1 cartilage and appendix-stem	Abductor	O: Lateral edge of 3rd cartilage I: Ventral process	Compressor	O: Lateral edge of b1 cartilage I: Appendix-stem (Posterior clasper cartilage)	Abductor	O: Anterior clasper cartilage I: Posterior clasper cartilage
Pelvico-basal layer (pelvico-basale Schicht)	O: Dorsal surface of the pelvis and Tendinous pelvic band I: Medial edge of basal, b1 and process (♂)	O: Dorsal surface of ventral pelvic segment I: Basipterygium (♀)/Basal appendage process (♂)		Not described		O: Dorsal surface of ventral pelvic segment I: Second fin metapterygium (♀)/Anterior clasper cartilage(♂)	

TABLE 6 | Points of origin (O) and insertion (I) of the muscle associated with the pre-pelvic tenaculum.

Chimaera monstrosa (Davidoff, 1879)		*Callorhynchus antarcticus* (Parker, 1886)		*Callorhinchus milii* (This study)	
Saw plate (Sägeblatt) muscle	O: Dorsal surface of pelvic girdle I: Saw plate (Tenaculum)	Strong muscle	O: Inner surface of pelvic cartilage I: Anterior clasper (Tenaculum)	Tenaculum muscle	O: Dorsal surface of pelvic girdle I: Tenaculum

dorsally by the portio prima and laterally by the protractor and hypaxial muscles (**Figures 1A,B**, **2** and **Supplementary Figures 1, 2**). The portio prima takes the form of a rounded chevron originating in a jagged manner from the fascia of the middle third of the iliac ramus and adjacent hypaxial musculature, following the anterior leading edge of the pelvic girdle (**Figures 1A,B**). This muscle is aligned with the pelvic fin, covering its dorsal surface and inserting into the ceratotrichia and deep dorsal layer. The portio tertia is situated beneath the portio prima and is separated from this muscle by a tendon running along the pelvic girdle ramus (**Figure 1B**). The portio tertia originates from the ventral surface of the iliac ramus of the pelvic girdle extending ventrally to insert into the deep dorsal layer (**Figure 1B**). The deep dorsal layer is also located beneath the portio prima, originating from the dorsal surface of the basipterygium, near the acetabulum of the pelvic girdle, extending distally over the fin skeleton and inserts into the dorsal fin radials (**Figure 1B**). The portio secunda is situated immediately behind and largely covered by the portio prima laterally and posteriorly borders the portio tertia, from which it is separated by a tendon running from the ventral surface of the iliac ramus to the basipterygium (**Figures 1A,B**). This muscle originates from the fascia of the hypaxial musculature, pelvic girdle, and the cloaca (**Figure 1B**). The points of insertion for this

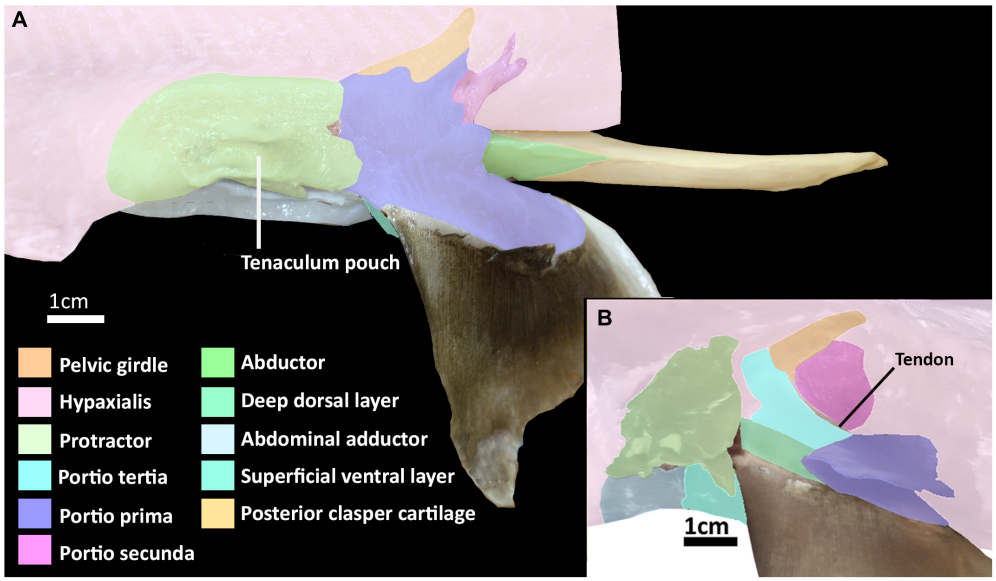

FIGURE 1 | Dissection of the pelvic musculature of the elephant shark (*Callorhinchus milii*). **(A)** Lateral view of the superficial dorsal musculature of an adult male, **(B)** lateral view of the deep dorsal musculature of an adult female with superficial muscles partly removed.

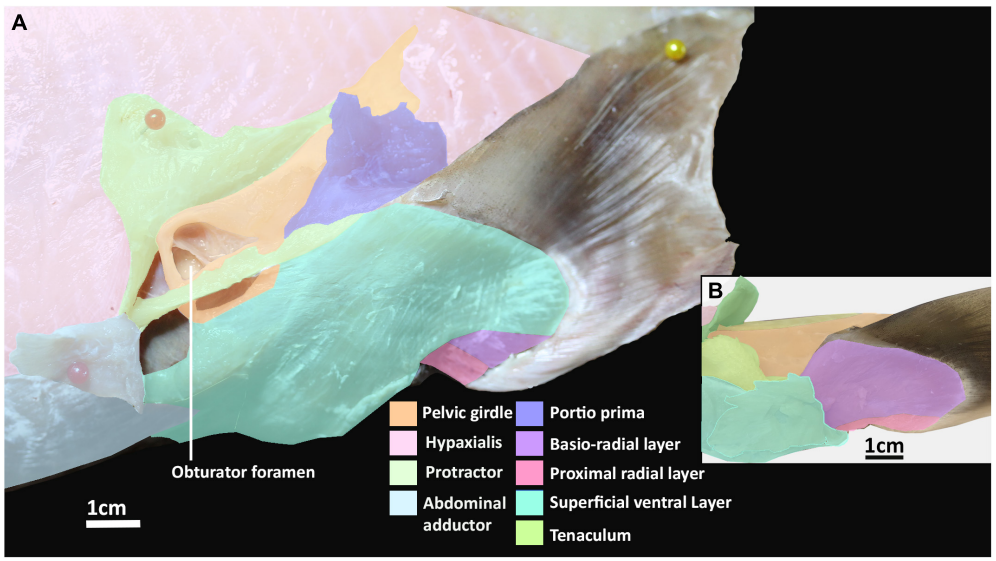

FIGURE 2 | Dissection of the pelvic musculature of an adult elephant shark (*Callorhinchus milii*). **(A)** Lateral view of the ventral musculature of a female elephant shark, which has been partially dissected, **(B)** ventral view of the pelvic fin of an adult male elephant shark.

muscle are sexually dimorphic. In females this muscle inserts into distal surface of the second fin metapterygium (**Supplementary Figure 1**; *sensu* Riley et al., 2017) and in males it inserts into the distal surface of the anterior clasper cartilage (**Figure 3A**).

Lateral Musculature

The abdominal adductor and protractor form the lateral musculature. The protractor superficially overlies the lower third of the hypaxial musculature, extending along the abdomen with fibers perpendicular to those of the hypaxial musculature and caudally abutting with the portio prima (**Figures 1A**, **2A**). This muscle originates from the fascia of the hypaxial musculature and extends posteriorly forming two points of attachment immediately anterior of the portio prima, giving it the appearance of a stout letter Y rotated 90° posteriorly (**Figure 1**). This muscle is sexually dimorphic. In males the protractor has a hole in its lower half from which the pre-pelvic tenaculum protrudes (**Figure 2B**). In females the pocket is not as prominent. More deeply, this muscle overlays the fascia of the entire anterior third of the pelvic girdle to which it inserts. It also has a

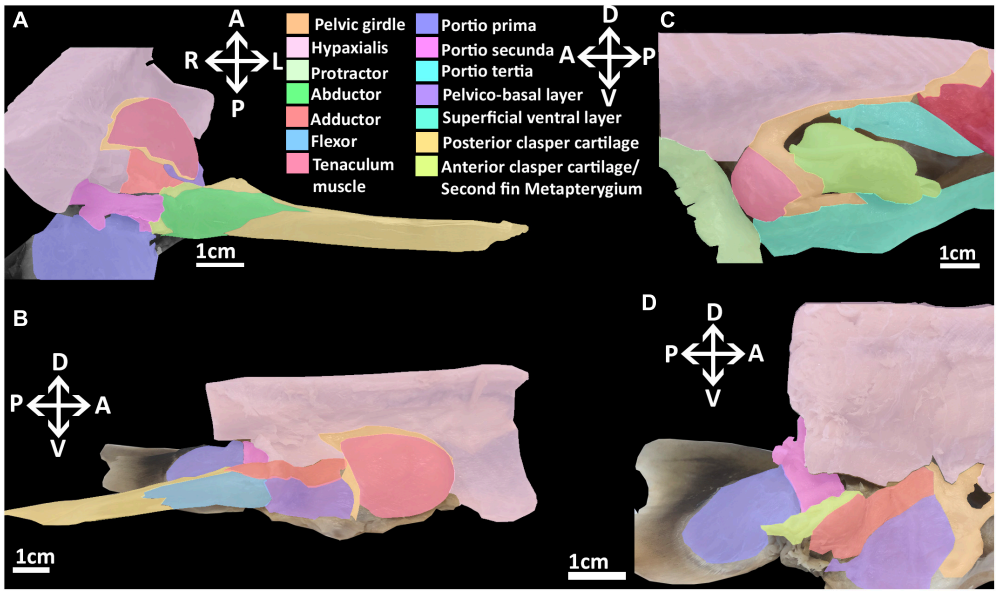

FIGURE 3 | Dissection of the musculature of the pelvic fin and clasper cartilages of the elephant shark (*Callorhinchus milii*). **(A)** Posterior view of a dissected male elephant shark, with the pelvic clasper drawn out proximally, **(B)** medial view of a bisected male elephant shark, showing the internal reproductive musculature, **(C)** lateral view of a male elephant shark with the protractor and abdominal adductor muscles removed, **(D)** medial view of a dissected female elephant shark showing the musculature associated with the second fin metapterygium. Anatomical planes and position indicated by lettering: A, Anterior; P, Posterior; D, Dorsal; V, Ventral; R, Right, L, Left.

deeper attachment extending from the ventral surface of the obturator foramen to the basipterygial process (*sensu* Riley et al., 2017; **Figure 2**, **Supplementary Figure 3**). Below the protractor is the abdominal adductor, which takes the form of a very narrow but long isosceles triangle situated along the base of the abdomen over the hypaxial muscles (**Figures 1A,B**, **2A**). The shortest side of this triangle borders with the dorsal end of the superficial ventral layer next to the protractor, while the longer two sides extend anteriorly with protractor extending nearly to the pectoral fin (**Figures 1A,B**, **2A**). This muscle is very superficial, originating from the fascia of the body wall and inserting into the ventral surface of the pelvic girdle near the midline (**Figure 2A**).

Ventral Musculature

The ventral musculature is composed of one superficial and two deep components. The superficial ventral layer originates from the ventral surface of the ventral segment of the pelvic girdle where it is most prominent and extends distally to partly cover the ventral surface of the pelvic fin and inserts over most of the basio-radial layer and ceratotrichia anteriorly (**Figures 2A,B** and **Supplementary Figure 3**). The basio-radial layer originates from the ventral surface of the basipterygium, near the acetabulum. This muscle extends over most of the surface of the pelvic fin under the superficial ventral layer and inserts into all but the two most proximal fin radials. The proximal radial layer is much smaller relative to these other muscles, originating from the proximal edge of the ventral surface of the basipterygium and anterior clasper cartilage in males and second fin metapterygium in females (**Supplementary Figure 1**), near their point of articulation, close to the clasper flexor, extending over the proximal side of the ventral surface of the fin skeleton to insert into the two most proximal fin radials (**Figures 2A,B**).

Reproductive Musculature

The reproductive musculature of males includes the clasper abductor, adductor and flexor, pelvico-basal layer. In males, the pelvic clasper consists of two cartilaginous components: the anterior clasper cartilage, articulating to the proximal side of the basipterygium, and the posterior clasper cartilage. The latter is a sheet of folded cartilage forming a rod attached to the distal portion of the anterior clasper cartilage (Didier, 1995). In addition to the portio secunda and proximal radial layer, there are four other muscles that attach to the pelvic claspers: an adductor, an abductor, a flexor, and the pelvico basal layer (**Figures 3A,B** and **Supplementary Figure 4**). The adductor originates from the dorsal surface of the ventral segment of the pelvic girdle, abutting with the hypaxial musculature and pelvico-basal layer. The adductor extends posteriorly partially covering the pelvico-basal layer and forming a thick bundle on the dorsal surface, proximal to the central groove, of the anterior clasper cartilage, and spans diagonally to wrap around the central groove of the clasper, inserting into the posterior cartilage (**Figures 3A,B**). The flexor is situated along the proximal side of the pelvic clasper next to the adductor. It originates from the base of the basipterygium near its articulation with the anterior clasper cartilage and extends posteriorly over a third of the clasper inserting into the posterior cartilage (**Figure 3B**). The abductor originates from the base of the distal side of

the anterior clasper cartilage and extends posteriorly over this anterior element to insert laterally into the distal side of the posterior clasper cartilage, wrapping around and covering about a quarter of the clasper's length (**Figure 3A**). The pelvico-basal layer originates from the dorsal surface of the ventral pelvic segment, below the adductor. This muscle is partially covered by the adductor and extends posteriorly over the girdle to insert into the anterior clasper cartilage below the adductor and in front of the flexor (**Figure 3B**). The tenaculum muscle, a new term we introduce in this study (see section "Tenaculum Muscle"), originates proximo-laterally from the dorsal surface of the pelvic girdle, specifically the dorsal cartilage of the obturator foramen. This muscle is very broad and covers the proximal side of the obturator foramen. It follows the anterior portion of the pelvic girdle, curving around its most distal point to insert into the base of the pre-pelvic tenaculum. This muscle has no contact with the tenaculum through the obturator foramen, being separated by a fine membrane covering this foramen (**Figure 3C**).

Females lack pelvic claspers and instead possess a second fin metapterygium. In females, the clasper abductor and flexor muscles are absent. The clasper adductor and pelvico-basal layer are present, but smaller relative to that of males (**Figure 3D**). These muscles originate from the dorsal surface of the pelvic girdle as they do in males whereas both extend posteriorly to insert into the second fin metapterygium in females. The abductor inserts broadly over the proximal side of the second fin metapterygium covering the attachment of the pelvico-basal layer.

Development of Pelvic Musculature

Stage 30

Endoskeleton

At stage 30, very few elements of the pelvic musculature and skeleton are present or easily discerned (**Figure 4**). The basipterygium and radials can be identified but they are all peripherally diffuse. The basipterygium is the most clearly discerned skeletal element, having extended distally to form most of the length of the main bar of this structure, but not its width. In contrast to the basipterygium, the fin radials are more diffuse. Only the most proximal radials appear clearly while the more distal elements are more diffuse or absent. None of the radials have any connections with the musculature yet. Rudiments of the pelvic girdle have formed, but these are very diffuse and have not formed across their full span anteriorly or posteriorly.

Dorsal Musculature

At this stage, a dorsal agglomeration of muscle that bears a resemblance to both the portio prima and deep dorsal layer in its attachments to the skeleton has formed, ranging from the dorsal rudiments of the pelvic girdle to the basipterygium and fin radials (**Figure 4**). This muscle mass originates from the hypaxial muscle and dorsal rudiments of pelvic girdle and inserts into dorsal surface of the proximal edge of the basipterygium. These are similar to the points of origin of the portio prima and deep dorsal layer, respectively, in the adult. While this muscle has extended over the fin skeleton that has formed so far, it has no contact with the fin radials and instead inserts into the dorsal surface basipterygium, near the proximal fin radials. The portio secunda and portio tertia are absent.

Lateral Musculature

The protractor and abdominal adductor are both present (**Figure 4A**), but are very small and thin at this stage. Neither are in contact nor in close proximity with the fin musculature or skeleton. The protractor originates laterally from the hypaxial musculature and at this stage also inserts into the hypaxial musculatures having not yet made contact with the fin skeleton or the rudiments of the pelvic girdle. The abdominal adductor abuts the protractor ventrally, and at this stage also originates from and inserts into the protractor and hypaxial muscles.

Ventral Musculature

A ventral agglomeration of muscles has formed (**Figures 4A,C,D**), extending from where the pelvic girdle would be located anteriorly and rudiments of the inter-pelvic band and extends distally near the ventral surface of the basipterygium and fin radials. The location of this agglomeration is reminiscent of both the superficial ventral layer and basio-radial layer, but these cannot be distinguished from within this mass at this stage. This mass originates from the inter-pelvic band and inserts along the ventral surface of the basipterygium. The proximal radial layer is absent.

Reproductive Skeleton and Musculature

The male reproductive and accessory organs and their muscles are absent in this stage.

Stage 32

Endoskeleton

At this stage, the pelvic endoskeleton and associated musculature are more distinct (**Figure 5**). The pelvic girdle is well developed, filling most of the area found in the adult, except for its most ventral and most dorsal points and the incomplete obturator foramen, which are diffuse. The fin skeleton has also expanded to a state more similar to that of the adult, with all of its elements being clearly identifiable and only the most distal radials being somewhat diffuse.

Dorsal Musculature

At this stage, all of the dorsal muscles can be identified. The portio prima is larger than the dorsal agglomeration in stage 30, extending dorsally to cover approximately two thirds of the iliac process length and posteriorly over the deep dorsal layer. This muscle originates from the middle of the iliac ramus only just inserting into the ceratotrichia in a manner similar to the adult, but less broadly and directly (**Figure 5A**). Whilst the portio prima extends laterally over part of the hypaxial musculature and pelvic girdle, it does not have the same breadth as that of adults and has not formed its final point of origin over the hypaxial musculature nor the dorsal portion of the iliac ramus. The deep dorsal layer distally covers the fin radials into which it inserts. The portio secunda spans a length similar to that of the adult, but is much thinner overall at this stage. It originates from tissue near the skin, the iliac ramus and cloaca, but is separated from the hypaxial muscle. It becomes thicker ventrally, particularly

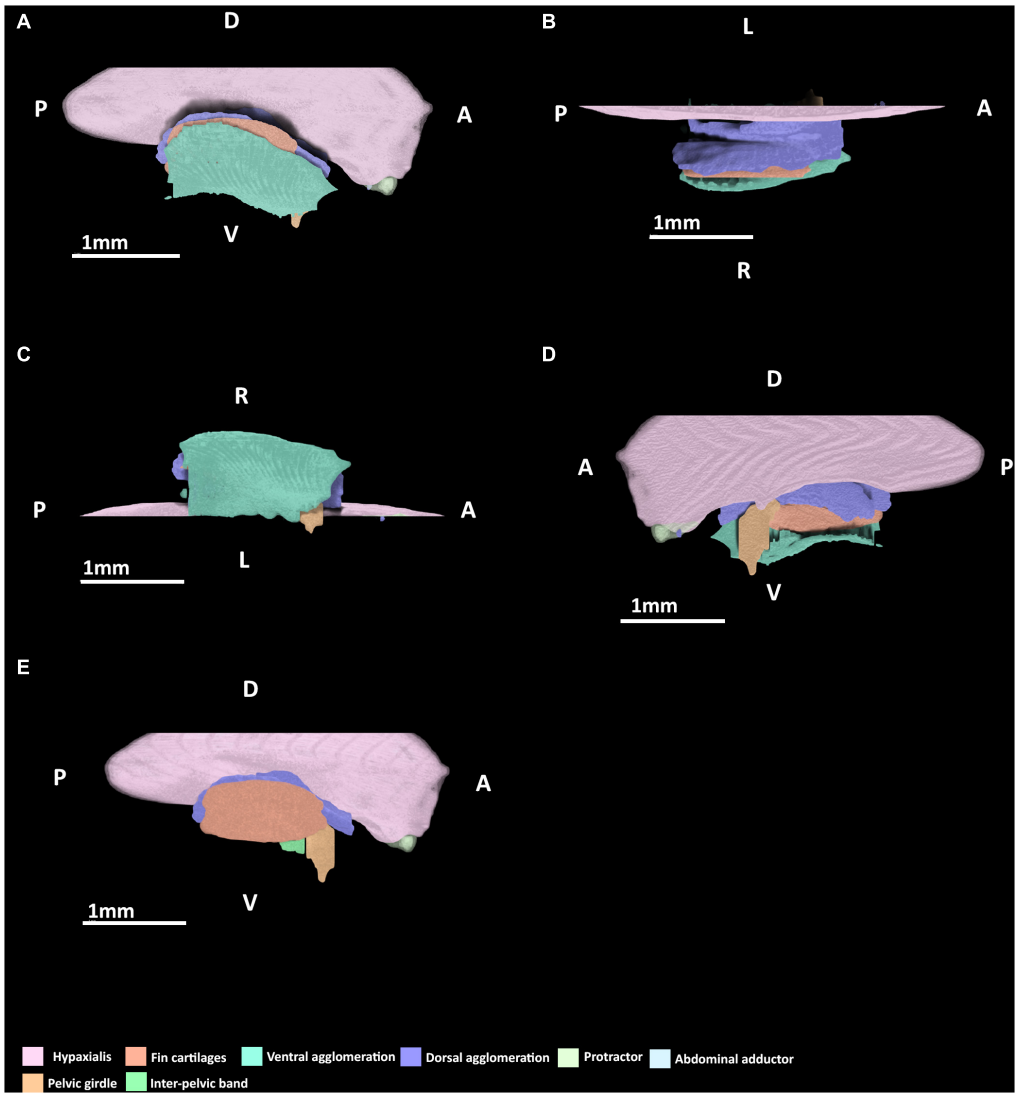

FIGURE 4 | 3D model of the right pelvic musculature of a stage 30 male elephant shark (*Callorhinchus milii*) embryo. **(A)** Lateral view of musculature, **(B)** dorsal view of the dorsal musculature, **(C)** ventral view of musculature, **(D)** medial view of musculature, **(E)** lateral view with the ventral agglomeration removed. Anatomical planes and position indicated by lettering: A, Anterior; P, Posterior; D, Dorsal; R, Right; L, Left.

near its point of insertion, but its insertion with the anterior clasper cartilage with very few fibers connecting to this cartilage at this point remains narrow. The portio tertia has the same points of origin and insertion as the adult, originating from the ventral surface of the lower quarter of the iliac ramus of the pelvic girdle and inserting into the proximal end of the deep dorsal layer, immediately posterior of the portio tertia's most ventral point (**Figure 5B**). However, this muscle is much thinner than that of the adult and does not broadly cover the portions of the girdle it attaches to.

Lateral Musculature

The protractor extends further posteriorly relative to stage 30, but still has not made contact with the fin skeleton nor the pelvic girdle and so still originates from and inserts into the hypaxial musculature. The abdominal adductor has also extended posteriorly and is in close proximity with the pelvic girdle, specifically into the diffuse ventral arc partially forming the obturator foramen, but has still not yet inserted into this part of the skeleton (**Figures 5A,C**).

Ventral Musculature

At this stage, the superficial ventral and basio-radial layers still form a ventral agglomeration and cannot be completely distinguished from one another (**Figures 5C,D**). This mass originates from the inter-pelvic band, the ventral surface of the anterior segment of the pelvic girdle and the ventral surface of the basipterygium near the acetabulum, which are also the points of origin of the superficial ventral layer and basio-radial layer, respectively, in the adult. This ventral agglomeration spans

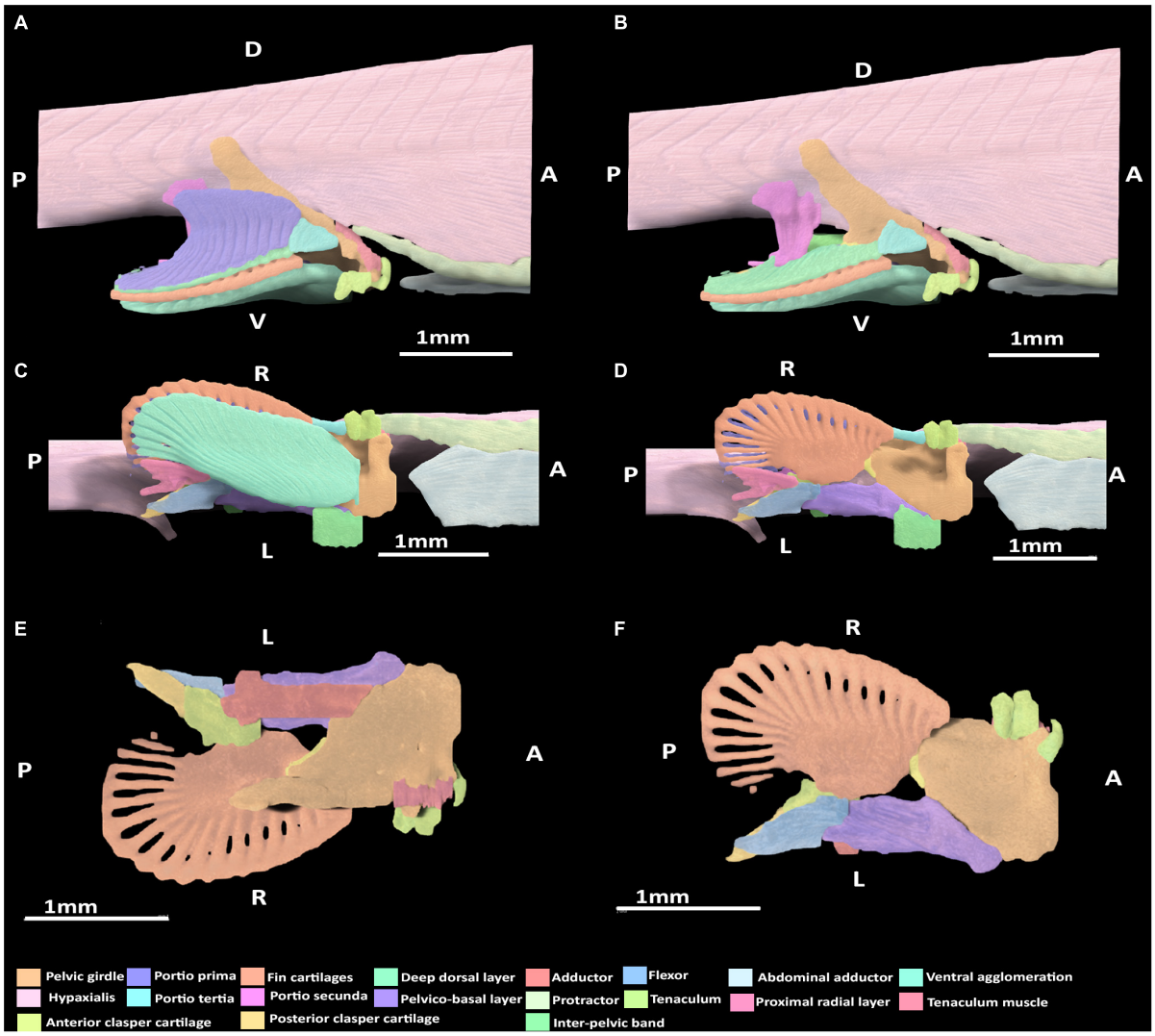

FIGURE 5 | 3D model of the right pelvic musculature of a stage 32 male elephant shark (*Callorhinchus milii*) embryo. **(A)** Lateral view of musculature, **(B)** lateral view with the portio prima removed, **(C)** ventral view of musculature, **(D)** ventral view with the superficial ventral layer removed, **(E)** dorsal view of the reproductive musculature, **(F)** ventral view of the reproductive musculature. Anatomical planes and position indicated by lettering: A, Anterior; P, Posterior; D, Dorsal; R, Right; L, Left.

most of the ventral surface of the fin skeleton, inserting into the distal portion of the basipterygium and covering, but not connecting with, all but the most proximal fin radials. This muscle is similar in shape to the ventral pelvic musculature, the superficial ventral layer and basio-radial layer, of the adult but does not insert as distally into the fin radials. The proximal radial layer can be identified at this stage and is distinct from the ventral agglomeration. This muscle originates from proximal edge of the basipterygium and anterior clasper cartilage, but whilst it is close proximity with the most proximal fin radials, it has not yet inserted into these cartilages.

Reproductive Skeleton and Musculature

At this stage, the rudiments of the pelvic clasper cartilages and pre-pelvic tenaculum have begun to form. Despite these structures being diffuse, particularly the posterior clasper cartilage and tenaculum, their associations with the musculature that has formed at this stage can be discerned (**Figures 5B,D,E**). The tenaculum muscle originates from the dorsal surface of the anterior pelvic girdle, near the developing obturator foramen. This muscle inserts into the base of the tenaculum. The clasper abductor is not present at this stage. The clasper flexor, situated on the proximal side of the pelvic clasper, can be seen to originate ventro-laterally from the basipterygium near its articulation with anterior clasper cartilage, abutting the point of insertion of the pelvico-basal layer. The clasper flexor extends posteriorly to insert proximo-ventrally into the developing posterior clasper cartilage, which it surpasses in length. The clasper adductor has begun to form, being situated on the dorsal surface of the pelvic girdle above the pelvico basal layer. This muscle has not

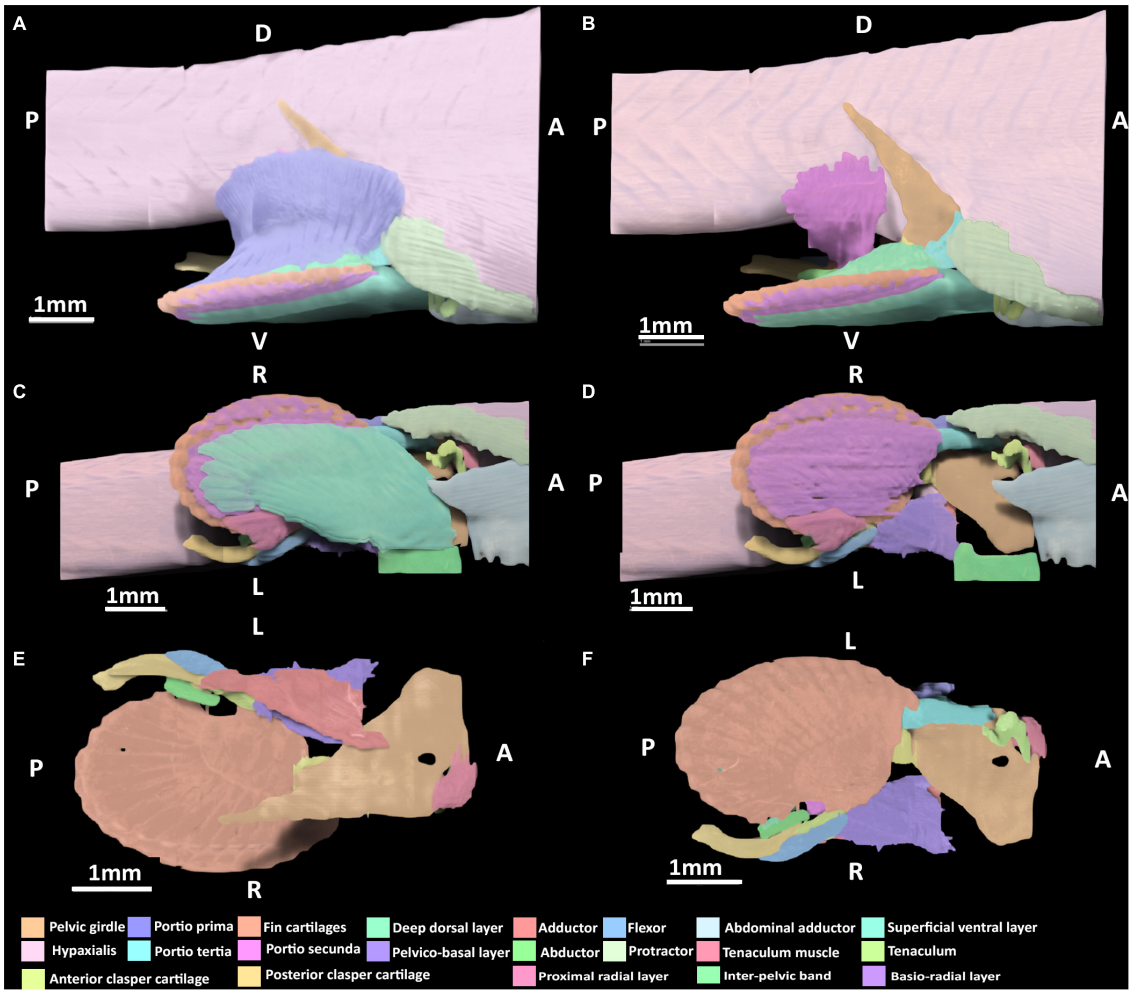

FIGURE 6 | 3D model of the right pelvic musculature of a stage 34 male elephant shark (*Callorhinchus milii*) embryo. **(A)** Lateral view of musculature, **(B)** same view but with the portio prima removed, **(C)** ventral view of musculature, **(D)** ventral view with the superficial ventral layer removed, **(E)** dorsal view of the reproductive musculature, **(F)** ventral view of the reproductive musculature. Anatomical planes and position indicated by lettering: A, Anterior; P, Posterior; D, Dorsal; R, Right; L, Left.

made contact with the posterior clasper cartilage and instead inserts into the dorsal surface of the anterior clasper cartilage. The pelvico-basal layer originates broadly dorso-laterally from the surface of the ventral segment of the pelvic girdle and the inter-pelvic band, and extends posteriorly to insert laterally and ventrally, into the anterior clasper cartilage, bearing a close resemblance with the adult morphology (**Figures 5D,E**).

Stage 34

Endoskeleton

The endoskeleton has become more defined and expanded relative to stage 32 (**Figure 6**). The fin skeleton in particular is now more complete. Beyond this broadening and expansion there are no other significant change to the endoskeleton.

Dorsal Musculature

The portio prima has expanded dorsally and laterally, forming its point of origin with the hypaxial musculature and the ramus of the pelvic girdle, very similar to the morphology of an adult (**Figure 6A**). Compared to stage 32, it has also broadened posteriorly to insert more securely into the deep dorsal layer and more directly into the ceratotrichia as in the adult. The deep dorsal layer, and portio tertia are very similar in terms of their points of origin and insertion to those of stage 32 (**Figures 5A,B,D**), but are substantially broader and thicker both in terms of size and their respective attachments, bearing a much closer resemblance to the morphology of adults (**Figures 6A,B**). The portio secunda spans over the hypaxial musculature from which it now originates broadly, in a similar manner to the adult (**Figure 6B**). This muscle has also become thicker along its length and has broader insertion dorsally into the proximal side of the anterior clasper cartilage.

Lateral Musculature

The protractor extends further posteriorly compared to stage 32, but has no contact with the fin skeleton and its points of origin

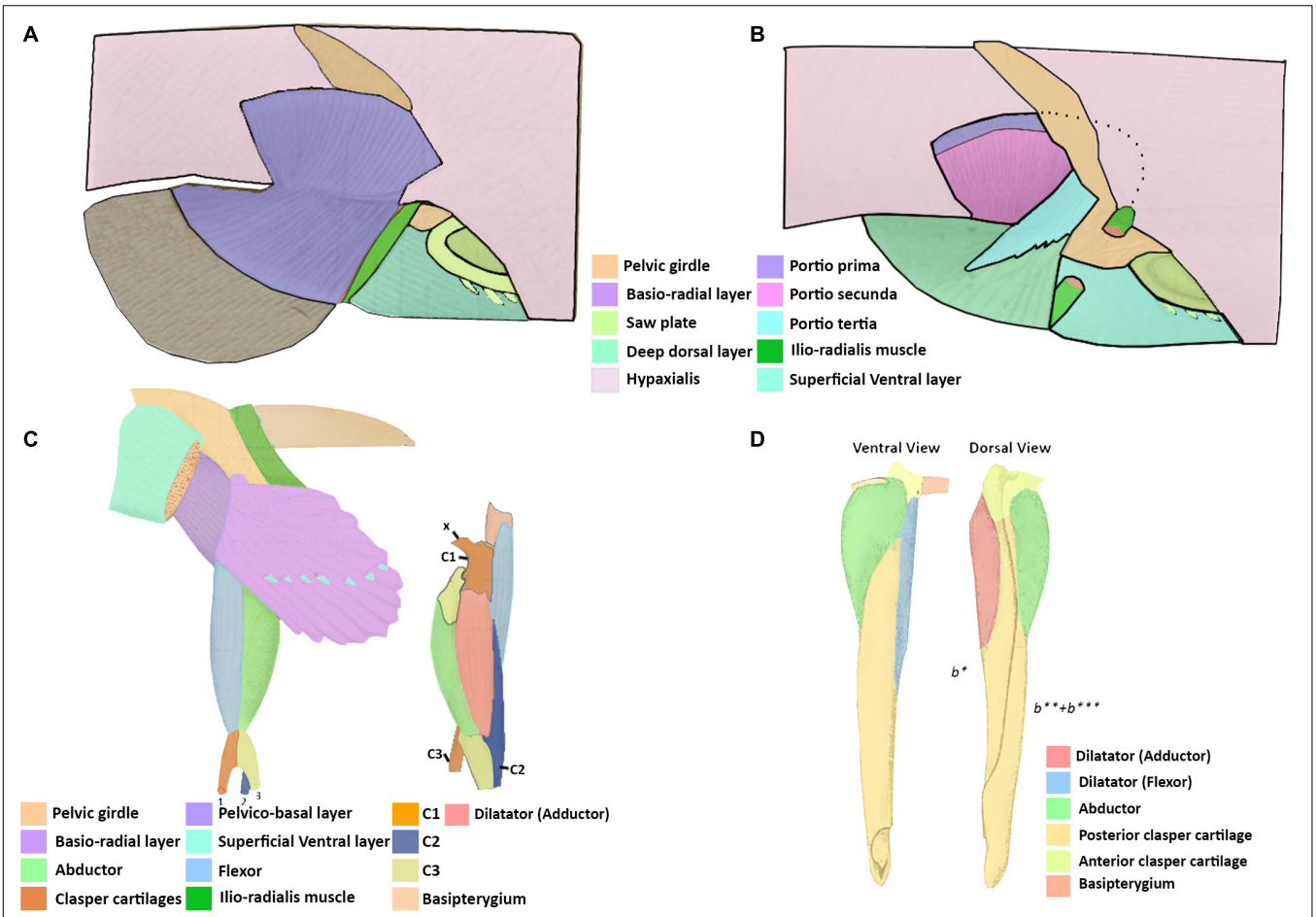

FIGURE 7 | Illustrations adapted from Davidoff (1879) of the pelvic and clasper musculature of *Chimaera monstrosa* and from Jungersen (1899) of the clasper musculature of *Callorhynchus antarcticus*. **(A)** Right lateral view of the superficial dorsal pelvic musculature of *C. monstrosa*, **(B)** same view of the deep dorsal pelvic musculature of *C. monstrosa*, **(C)** ventral view of left pelvic musculature and lateral left view of clasper musculature of *C. monstrosa*, **(D)** ventral and dorsal views of the right pelvic clasper of *C. antarcticus*. x, ventral process; C1, first cartilage; C2, second cartilage; C3, third cartilage; b*, first cartilage; b**, second cartilage; b***, third cartilage.

and insertion remain the same as in stage 32 (**Figures 6A,C**). The abdominal adductor is similar in terms of its points of origin and insertion to those of stage 32 (**Figure 5A**), but is broader in its span and attachment with the pelvic girdle.

Ventral Musculature

The superficial ventral layer, basio-radial layer and proximal radial layer are now clearly distinct from each other and their arrangement and span more closely resemble those of the adult (**Figures 6C,D**). The superficial ventral layer originates from the ventral surface of the anterior pelvic segment and inter-pelvic band, extending posteriorly over the basio-radial layer, into which it inserts distally. The basio-radial layer originates from the ventral surface of the basipterygium near its contact with the pelvic girdle and extends posteriorly over the fin skeleton to insert into the fin radial cartilages. The proximal radial layer has broadened greatly relative to stage 32 and inserts into the most proximal fin radials, and now covers these radials.

Reproductive Skeleton and Musculature

The skeleton of the pelvic claspers and tenaculum are more developed and distinct relative to stage 32, however, the posterior regions of the posterior clasper cartilage and tenaculum cartilages are still diffuse. At this stage, all of the reproductive muscles are now present (**Figures 6B,D,E**). The abductor can be identified, originating from the distal side of the anterior clasper cartilage wrapping around the clasper and extending posteriorly to insert into the posterior clasper cartilage. The clasper adductor now inserts dorso-laterally into the posterior clasper cartilage but does not extend along this cartilage as far as it does in the adult. The clasper flexor is longer posteriorly, extending over almost a third of the posterior clasper cartilage into which it inserts ventro-laterally. Its span across these cartilages is now similar to that of the adult, though it is still shorter posteriorly. The tenaculum muscle has expanded ventrally to more directly attach to the tenaculum cartilages, bearing a closer resemblance to the arrangement of this muscle in the adult, but still much smaller in size. The pelvico-basal layer has thickened relative

to stage 32 and attaches more broadly to the same points of origin and insertion.

DISCUSSION

Chimaeroid Pelvic Musculature

Currently, there are only two published descriptions of the pelvic musculature of extant chimaeroids: both are of members from the family *Chimaeridae,* the spotted ratfish (*Hydrolagus colliei*) (Diogo and Ziermann, 2015) and rabbit fish (*Chimaera monstrosa*) (Davidoff, 1879). These descriptions, separated by 136 years, differ significantly in their descriptions and terminology (**Table 2**). Below, we compare and contrast these descriptions to propose homologies and establish a better understanding of the pelvic anatomy of extant chimaeroids.

Dorsal Musculature

The dorsal pelvic musculature of *H. colliei, C. monstrosa*, and *C. milii* are all composed of superficial and deep portions. However, the points of origin and divisions of these muscles differ (**Table 2**). The dorsal musculature of *C. milii* corresponds very closely with that of *C. monstrosa*, in that both are divided into four portions and that these have similar points of origin and insertion. In *C. monstrosa*, the portio prima is described as originating from the "external aponeurosis" extending over the pelvic girdle and adjacent hypaxial muscle, inserting into the ceratotrichia ("secondary fin skeleton") (Davidoff, 1879, p. 477; **Figures 7A,B**) in the same manner as the portio prima in *C. milii,* though we also describe the portio prima as inserting into the deep dorsal layer (**Figures 1A,B**). In both *C. milii* and *C. monstrosa,* the portio tertia is located underneath the portio prima, originating from the ventral surface of the iliac ramus of the pelvic girdle and inserting into the deep dorsal layer (tiefe dorsale Schicht). The deep dorsal layer originates laterally from the dorsal surface of the basipterygium and divides posteriorly into bundles that insert into the fin radials (Davidoff, 1879; **Figures 1B, 7B**). The deep dorsal layer in *C. milii* also originates from the dorsal surface of the basipterygium near the acetabular articulation to the pelvic girdle. This specific location of the point of origin is not explicitly given in the text of the description of *C. monstrosa* but is shown in the figures cited (Davidoff, 1879; **Figure 7A**).

The arrangement of the dorsal pelvic musculature in *H. colliei* differs slightly from that of *C. monstrosa* and *C. milii* in that it is less complex. In *H. colliei*, the dorsal musculature is divided into three groups: two portions of an adductor and a single levator. The adductor superficialis (superficial bundle) originates from the fascia of the body muscle and extends over the pelvic girdle ramus, and the deep bundle of the adductor originates from the basipterygium extending over the fin skeleton to insert into the fin radials, but the exact point is not described (Diogo and Ziermann, 2015). The points of origin and insertion of the superficial and deep portions of the adductor suggest that they correspond with the portio prima and deep dorsal layer, respectively. However, no muscle resembling the portio tertia is described in *H. colliei*. As this muscle is situated closely with the portio prima (adductor superficialis) and inserts into the deep dorsal layer (adductor deep bundle) it is possible that the portio tertia has inadvertently been included as a part of one of the other muscles. Alternatively, the portio tertia may not be present in *H. colliei*. Re-examination is warranted to resolve this issue.

There is more agreement on the muscle known as the portio secunda in *C. monstrosa* and *C. milii* and levator 5 in *H. colliei.* In all of these taxa, this muscle is situated medially behind the more superficial portio prima (adductor superficialis) and posteriorly adjacent to the pelvic girdle (**Figures 1A**, **7B**; Davidoff, 1879; Diogo and Ziermann, 2015). The portio secunda in *C. milii* (**Figures 1**, **2**) originates from the fascia of the hypaxial musculature, pelvic girdle and cloaca and inserts into the second fin metapterygium in females and the clasper cartilages in males (**Figures 1**, **3**). Likewise, in *C. monstrosa*, the portio secunda originates from the "external aponeurosis" of the hypaxial musculature and pelvic girdle, and inserts into the most anterior cartilage of the "basal appendage (clasper)" in males and the "basal (second fin metapterygium)" in females (**Figures 7A,B**; Davidoff, 1879, p. 474). In *H. colliei*, this muscle is referred to as levator 5 and is described as originating from the fascia of the body muscle and connecting to the basipterygium and medial fin radials. This difference over the points of insertion may arise from a lack of specificity regarding the anatomy of the fin skeleton and the fact that the description of *H. colliei* was based only on female specimens (Diogo and Ziermann, 2015).

Lateral Musculature

The lateral musculature consists of the protractor and abdominal adductor (**Table 3**). The protractor described here in *C. milii* (**Figures 1A**, **2**) shares the same points of origin and insertion, the pelvic girdle and basipterygial process (propterygium), respectively, as those described in *H. colliei* (Diogo and Ziermann, 2015), suggesting that these muscles are homologous. This muscle is not explicitly identified in the description of *C. monstrosa*, however, the lateral portions of the hypaxial muscle in the illustrations of the pelvic musculature (Davidoff, 1879, Figure 20, ssv) resemble our description of the protractor and abdominal adductor in *C. milii* (**Figures 1A,B**, **2**), though the arrangement displayed is not entirely congruent as is in alignment with the pelvic girdle and overlying part of it. This may be because this image was drawn after the removal of the integument. The lateral muscles are not named but are described as follows, "The attachment of the lateral muscles to the pelvis includes only the anterior edge of the ventral, the two cranks and the entire inner surface of the dorsal section" (Davidoff, 1879, p. 474). This description resembles our description some of the attachment points of the protractor and abdominal adductor, but it is too vague to distinguish any specific correlation with our own findings. The other point of difference with regards to the lateral musculature may also a result of omission. No muscle in the descriptions of *H. colliei* (Diogo and Ziermann, 2015) or *C. monstrosa* (Davidoff, 1879) appear to correspond with the abdominal adductor in *C. milii* (**Figures 1A,B**, **2**). As this muscle is small and blends in well with the hypaxial musculature and protractor it may be that the muscle was not identified by other investigators.

Ventral Musculature

There are also differences regarding the description of the ventral pelvic musculature among the previous studies and our own findings (**Table 4**). Again, the ventral musculature of *C. milii* and *C. monstrosa* (Davidoff, 1879) are relatively similar, though there is some difference. In *C. monstrosa* the superficial ventral layer (oberflächliche ventrale Schicht) originates from an aponeurotic band connecting the pelvic girdles and the ventral surface of the ventral portion of the pelvic girdle, extending over the "articulation of the basal with the pelvis" to the fin rays where they divide into bundles and insert into muscle bundles below them, covering the ventral surface of the pelvic fin, except for some posterior lobes (**Figures 7C**; Davidoff, 1879). This description largely agrees with that of the superficial ventral layer in *C. milii*, originating from the ventral surface of the pelvic girdle, and an inter-pelvic band in embryos, extending over the acetabulum and basipterygium. We also find that this muscle covers most basio-radial layer in *C. milii*, completely anteriorly where it inserts into the ceratotrichia and tapering off distally toward the end of the fin, exposing the basio-radial layer into which it also inserts (**Figures 2A,B**). The basio-radial layer in both *C. monstrosa* and *C. milii* originates from the basipterygium near the acetabulum and extends posteriorly over the ventral surface of the fin skeleton, however, there is some difference in the span of these muscles over the ventral surface of the fin skeleton. In *C. monstrosa* this muscle is said to cover the entire ventral surface of the pelvic fin, inserting into the radial cartilages (**Figures 2**, **7C**; Davidoff, 1879). In contrast, we find that the basio-radial layer only covers most of the ventral surface of the pelvic fin whereas a distinct proximal radial layer roofs the most proximal regions of the fin skeleton. As the proximal radial layer is subtle in its distinction from the basio-radial layer it may have inadvertently included as a part of the basio-radial layer in the description of *C. monstrosa*, or this may be an interspecific difference. The other main difference with our findings and the description of *C. monstrosa*, is an extra muscular mass situated between the basio-radial layer and superficial ventral layer, which we have not found in *C. milii*. In *C. monstrosa*, this mass is described as "beginning at the medial anterior angle of the fin and running obliquely backwards and laterally," over the fin and connecting with the fascia of the superficial ventral layer and basio-radial layer (Davidoff, 1879, p. 476).

The arrangement of the ventral musculature of the pelvic fin in *H. colliei* is significantly different from that of *C. milii* and *C. monstrosa*. In *H. colliei*, this musculature is divided into proximal and distal portions of an abductor (Diogo and Ziermann, 2015). The proximal portion, abductor proximalis, originates from the puboischiac bar (pelvic girdle) and inserts into the basipterygium whereas the distal bundle originates from the basipterygium and extends distally to insert into the ventral surfaces of the radial cartilages (Diogo and Ziermann, 2015). The abductor distalis appears to correspond with the basio-radial layer in *C. milii* and *C. monstrosa* as they share the same points of origin and insertion. However, as with *C. monstrosa*, the proximal radial layer is not described in *H. colliei* and may be included within the abductor distalis (Davidoff, 1879; Diogo and Ziermann, 2015). The proximal bundle of the abductor in *H. colliei* seems to share a common point of origin with the superficial ventral layer of *C. milii* and *C. monstrosa*, the puboischiac bar (ventral pelvic segment). However, these muscles do not share the same point of insertion, as the proximal bundle is described as "running. . . to the basipterygium" in *H. colliei* (Diogo and Ziermann, 2015, p. 523), whilst the superficial ventral layer in both *C. milii* and *C. monstrosa* extends over the basipterygium and inserts into the basio-radial layer (**Figures 2**, **7C**; Davidoff, 1879).

Reproductive Musculature

The pelvic claspers of chimaeroids have been described in several historical and contemporary studies (Davidoff, 1879; Jungersen, 1899; Leigh-Sharpe, 1922, 1926; Didier, 1995), but with limited description of their associated musculature. As far as we are aware there are three descriptions of the clasper musculature in chimaeroids, two of the rabbit fish (*Chimaera monstrosa*) (Davidoff, 1879; Jungersen, 1899), and one of *Callorhynchus antarcticus* (sic) (Jungersen, 1899). The clasper skeleton among these genera are notably different. The skeleton of the claspers of *C. milii* and *C. antarcticus*, both from the same genus appear to be the same, in that both are composed of two components, a small anterior cartilage attached to the basipterygium and a long folded posterior cartilage connected to the anterior cartilage (Jungersen, 1899; Didier, 1995; Riley et al., 2017). In *C. milii*, these two cartilages are simply called the anterior and posterior clasper cartilages (Didier, 1995; Riley et al., 2017) and as b1 and the appendix stem in *C. antarcticus* (Jungersen, 1899), respectively. In contrast, the skeleton of *C. monstrosa* has a branching clasper skeleton composed of three distinct cartilages (Gegenbaur, 1870; Davidoff, 1879; Jungersen, 1899). The first component known as the first cartilage connects with the basipterygium and the other two, the second and third cartilages, branch off from the first cartilage (Davidoff, 1879; C1, C2, C3 in **Figure 7C**). This suggests that the first cartilage of *C. monstrosa* corresponds with the anterior clasper cartilage as they both join the basipterygium with the posterior clasper cartilage/s (Davidoff, 1879; Didier, 1995). Establishing homologies of the posterior cartilages of *C. monstrosa* with those of the callorhinchids requires further embryonic studies focusing on the cartilages in these taxa.

All three descriptions of the clasper musculature in chimaeroids, the two historical accounts and our own, agree that the claspers possess three distinct muscles and superficially appear to have a similar arrangement (**Figures 3A,B**, **7C,D**). However, due to the different nature of the skeleton of *C. monstrosa*, it is not clear how these muscles can be homologized with those of *C. milii* and *C. antarcticus*. As expected, the description and arrangement of the clasper musculature of *C. antarcticus* are similar to those of *C. milii* though the nomenclature used differs to each other (**Table 5**). There are only two notable differences between the two descriptions of the musculature. Firstly, we describe the flexor and adductor as distinct muscles rather than portions of a single dilatator (sic) (**Table 5** and **Figures 3**, **7D**; Jungersen, 1899). Secondly, the adductor is much longer and originates from the dorsal surface of the pelvic girdle. Beyond these two details, the

points of origin and insertion of the muscles in both taxa are the same, though this is not clear at first, as parts of the description of *C. antarcticus* are not given in a direct manner (Jungersen, 1899). For instance, the compressor (abductor in *C. milii*) is described thusly, "...the large muscle (S) (compressor) of the glandular bag, which in no respects shows other relations than in *Chimaera* (*monstrosa*)," (Jungersen, 1899, p. 75). In turn, the same muscle in *C. monstrosa* is described as "...M. compressor, arises from the lateral edge of the piece β [C3 (**Figure 7C**)] (see Figure 69), and is inserted on the lateral surface of the piece b1, and on the appendix-stem," (Jungersen, 1899, p. 73). The appendix stem in *C. antarcticus* corresponds with the posterior clasper cartilage. Similarly, the points of insertion of the portions of the dilatator (sic) are not explicitly stated and are inferred from the figures (see **Figure 7D**).

The clasper musculature of *C. monstrosa* comprises three distinct muscles, similar to *C. milii* and *C. antarcticus* with their arrangement. The flexor is situated laterally on the proximal side of the clasper, the adductor is located dorsally above, and the abductor is situated laterally on the distal side. Despite these superficial similarities, there are notable differences in the arrangement of these muscles with the callorhinchids. Whilst the flexor in all of these taxa arises from the basipterygium, this muscle, as well as the adductor and abductor in *C. monstrosa* insert into the ventral process (x in **Figure 7C**), a component of the first cartilage (Davidoff, 1879; Jungersen, 1899). In turn, the adductor and abductor originate from the medial surface of first and second cartilages and the lateral edge of the third cartilage, respectively (**Table 5** and **Figure 7C**). The adductor is situated dorsally and is located on the distal side of the clasper rather than proximally, similar to *C. milii* and *C. antarcticus* (**Figures 3**, **7C,D**).

An additional muscle called the pelvico-basal layer is also found in both *C. milii* and *C. monstrosa*. In *C. monstrosa*, this muscle is described as originating from the "entire extent of the posterior margin and from part of the dorsal surface of the ventral pelvic segment" and inserting into the process of the pelvic claspers of males and the "basal" (second fin metapterygium) of females (**Figure 5B**; Davidoff, 1879, p. 475). In the other description of *C. monstrosa* (Jungersen, 1899), this muscle is considered as a portion of the ventral muscles of the pelvic fin, originating from a tendinous pelvic band and the dorsal surface of the pelvis and inserting into the medial edge of the "basale" (clasper) and its process. This description of the point of origin agrees with what we have observed in *C. milii* embryos where this muscle arises from an inter-pelvic band and the dorsal surface of the girdle (**Table 5**). The pelvico-basal layer has not been described in *H. colliei* (Diogo and Ziermann, 2015) nor in *C. antarcticus* (Jungersen, 1899). However, as with *C. monstrosa* it may be that this muscle was inadvertently included in the proximal portion of the abductor, which is also described as originating from the puboischiac bar (Diogo and Ziermann, 2015). This might explain the difference in the point of insertion of this muscle and the superficial ventral layer in *C. milii* and *C. monstrosa*. Alternatively, it may be because the muscle was considered out of scope as these authors did not examine the reproductive musculature (Diogo and Ziermann, 2015). It is also possible that as the pelvic musculature of *H. colliei* has only been described in females, it may be that the insertion of the proximal bundle to the "basipterygium" is actually the insertion of the pelvico-basal layer onto the second fin metapterygium. Re-examination of the pelvic musculature in male and female specimens will help clarify this issue.

Tenaculum Muscle

The muscle associated with the pre-pelvic tenaculum has been described in at least two instances, in *C. monstrosa* (Davidoff, 1879) and *C. antarcticus* (Parker, 1886). Both descriptions agree that it arises from the dorsal surface of the pelvic girdle and extends to the pre-pelvic tenaculum (**Table 6**). This agrees with the arrangement of this muscle that we have found in *C. milii* (**Figure 3**). Surprisingly, this muscle has never been named or illustrated and so deserves some attention. In *C. monstrosa* (Davidoff, 1879), it is described only as the muscle associated with the Saw plate (Sägeblatt) and in *C. antarcticus* (Parker, 1886) it is simply called the "strong muscle." For clarity, we propose that this muscle should be known as the tenaculum muscle due to its association with the pre-pelvic tenaculum.

Summary of Interspecific Differences

In terms of the interspecific differences between the pelvic musculatures of the chimaeroids examined here, *C. milii* and *C. monstrosa* are more similar to one another than either are to *H. colliei*. The dorsal musculature of *C. milii* and *C. monstrosa* is divided in the same groups of muscles, the portio prima, portio tertia, portio secunda, and deep dorsal, and only exhibits minor differences (**Table 2**). In contrast, the dorsal muscles of *H. colliei* are divided into three components, a superficial and deep adductor and a levator. These muscles appear to correspond well with the portio prima, deep dorsal layer and portio secunda, respectively. Though there is potentially some differences between the insertion of the portio secunda and levator and the portio tertia is not identified in *H. colliei* (**Table 2**). There may be some differences in the lateral musculature of these taxa, but this is likely due to inadvertent omission in the description of *C. monstrosa* (Davidoff, 1879) and *H. colliei* (Diogo and Ziermann, 2015). In *C. milii* and *H. colliei* the lateral musculature includes a protractor that attaches to the pelvic girdle and part of the fin skeleton. The unidentified muscles are the abdominal adductor in *H. colliei* and *C. monstrosa*, and protractor in *C. monstrosa* (but see section "Lateral Musculature"). The ventral musculature of *C. milii* and *C. monstrosa* is very similar, being composed of a superficial ventral layer and basio-radial layer, with almost the same attachments on the pelvic girdle and fin skeleton, respectively (**Table 4**). However, *C. milii* also possess an additional deep muscle along the fin skeleton and clasper cartilage, the proximal radial layer. The ventral musculature of *H. colliei* is also composed of two components, a distal and proximal abductor, however, their points of origin and insertion on the pelvic girdle and fin skeleton differ greatly from those of the superficial ventral layer and basio-radial layer (**Table 4**).

The reproductive musculature of *C. milii* and *C. antarcticus* are comparable to each other (**Table 5**) as both possess the same clasper skeletal structure and the arrangement of their

muscles, the clasper adductor, abductor and flexor, are largely the same. The only difference between the two taxa is that the flexor and adductor are considered bundles of a single muscle in *C. anatarcticus*. *C. monstrosa* also has three clasper muscles (**Table 5**), the flexor, adductor, and abductor. However, due to differences in the clasper skeleton, these are difficult to compare to *C. milii* and *C. antarcticus* (but see section "Reproductive Musculature"). *C. monstrosa* and *C. milii* both have a pelvico-basal layer with essentially the same origin on the pelvic girdle and insertion on the clasper cartilages (**Table 5**). All three taxa possess a tenaculum muscle originating from the pelvic girdle and inserting into the base of the tenaculum (**Table 6**).

Comments on Development

We provide the first detailed descriptions of developmental origins of the pelvic fin muscles in the embryonic series of *C. milii*. This reveals certain patterns in the growth and development of the muscles. At stage 30, the muscles immediately associated with the fin skeleton, agglomerations of the dorsal (portio prima and deep dorsal layer) and ventral (superficial ventral layer and basio-radial layer) muscles, as well as the protractor and abdominal adductor are the first muscles to appear. These muscles are more prominent anteriorly, dorsally and proximally (**Figure 4**). By stage 32, these muscles have expanded distally, dorsally and posteriorly and the dorsal agglomeration differentiates into the portio prima and deep dorsal layer. At this stage, deeper muscles such as the portio tertia and secunda as well as the muscles associated with reproductive structures (pelvico-basal layer, adductor, flexor, and tenaculum muscle) have formed and are also more prominent dorsally and anteriorly. By stage 34, all of the pelvic and reproductive muscles can be identified and are more prominent relative to stage 32.

In both *C. milii* and the bamboo shark (*Chiloscyllium punctatum*), the pelvic fin muscles form from epithelial extensions of the myotome, with epithelial buds migrating ventrally to form the body wall musculature and extending further ventrally into the pelvic fin mesenchyme to form the fin muscles (Cole et al., 2011). The patterns of pelvic fin muscle growth and development observed here may be explained by the trajectory of these epithelial extensions. The antero-posterior development of the musculature observed in the embryos examined would appear to correspond with the suggestion that this is the direction by which these extensions enter the pelvic mesenchyme to form the fin muscle. The development of more superficial elements or their agglomeration with deep components may also suggest that these projections of the epithelium first spread over surface of the fin skeleton before forming the deeper muscles rather than forming the deeper portions first. To date, there has been no examination of the developmental origins of the musculature related to the pre-pelvic tenaculum nor the pelvic claspers in extant chondrichthyans. The tenaculum muscle is in close proximity with the protractor and hypaxial musculature and may likely also result from epithelial extensions. Similarly, the clasper musculature is in close proximity with the musculature of the pelvic fin and pelvico-basal layer, and may also be the result of epithelial extensions. To determine whether these muscles are produced by the same developmental mechanisms requires the examination of origin and arrangement of these structures in more chondrichthyan taxa. The muscle anatomy of reproductive structures has been examined in increasing detail in elasmobranchs in recent studies, which has emphasized the importance of these details in understanding their phylogenetic systematics (de Figueiredo Petean and de Carvalho, 2018; Moreira and de Carvalho, 2018, 2019). There is a notable lack of contemporary information on the musculature of chimaeroid claspers, which is entirely restricted to accounts from over a century ago (Davidoff, 1879; Jungersen, 1899). This indicates a clear need to examine the musculatures in a range of chimaeroid species to verify these historical accounts, refine systematics and determine any insights these may shine on the evolution of vertebrate reproduction.

The prominent size of the superficial musculature in *C. milii* may have some evolutionary implications for fin muscles. Comparisons of the appendicular musculature between different species of fishes and tetrapods have revealed that superficial muscles are heavier than deep muscles in both limbs of tetrapods whereas deeper muscles are more developed in the fins of fishes (Mansuit and Herrel, 2021). This difference indicates a shift occurred during the fin to limb transition in which tetrapods have experienced a reduction of their deep appendicular muscles and an increase of superficial musculature. This shift is suggested to be an adaptation to the mechanical demands required of terrestrial locomotion, needing more strength to support the body against gravity, as opposed to buoyancy in aquatic habits (Mansuit and Herrel, 2021). Our examination of the musculature indicates that the superficial appendicular musculature is more prominent than the deep musculature in *C. milii*, at least in terms of surface area. This either suggests that more prominent superficial musculature is plesiomorphic, in which case the tetrapod arrangement is a reversal or that the relative prominence of muscles is driven by biomechanical factors. In order to determine this, differences in the prominence of the superficial and deep appendicular musculature of other extant chondrichthyans, actinopterygian, and sarcopterygian fishes should be investigated and compared to the fossil record.

Currently, the appendicular musculature of fossil vertebrates such as placoderms, chondrichthyans and osteichthyans are not well known. Soft tissues do not normally fossilize, however, in certain specimens, such as those from the Gogo formation, soft tissues, including muscles, or muscle attachment scars, are preserved. These specimens can be used to investigate and partially reconstruct the arrangement of the musculature of fossil taxa (Trinajstic et al., 2007, 2013, 2015). This is best demonstrated by the detailed reconstruction of the head, neck and abdominal muscles in arthrodire placoderms from preserved tissues. Muscle scars are present on the pelvic girdle and fin endoskeleton of placoderms from the Gogo formation (pers obs) but have not been described. Chondrichthyan musculatures were thought to be very simple, which appeared incongruent with the complexity of placoderm musculatures found in the Gogo arthrodires (Trinajstic et al., 2013). Here, we have shown that chondrichthyan musculatures are more complex than currently thought providing important details to guide interpretation of fossil musculatures (Lund and Grogan, 1997).

Fossil specimens with preserved musculature or muscle scars should be examined to better understand the arrangement of the appendicular musculature and determine the evolutionary shifts that have occurred in the early evolution of limbs in gnathostomes. Some fossil specimens also possess preserved reproductive claspers (Trinajstic et al., 2015). Studies on these structures and any possible muscle reconstructions compared with those of extant chondrichthyans will help better understand the development and evolution of vertebrate reproduction.

Comparative Development of Pelvic Musculature

To date, only one ontogenetic study of the pelvic muscles in chondrichthyan has been conducted (Ziermann et al., 2017). Ziermann et al. (2017) describe the morphology and development of the cephalic, pectoral and pelvic muscles in the catshark (*Scyliorhinus canicula*) from stages 26 to 33 using a combination of scanning electron microscopy (SEM), traditional histology and whole mount immunostaining. The staging table for *C. milii* is based on that of *S. canicula*, making their respective stages approximately equivalent (Ballard et al., 1993; Didier et al., 1998), and thereby making the comparison of their development fairly straightforward.

In *S. canicula,* muscle projections are thought to ventrally extend to the base of the pelvic fins between stages 27 and 28 but no specific muscles can be identified at these stages. By stage 30, the ventral muscles are present as an undivided abductor and the dorsal muscles as the adductor superficialis (Ziermann et al., 2017). In *C. milii*, by stage 30, agglomerations of the dorsal (portio prima and deep dorsal layer) and ventral (superficial ventral layer and basio-radial layer) muscles have formed (**Figures 4A,C,D**). In terms of morphology and level of development, the two species are similar at this stage. However, in our nano-CT data, we distinguish two muscles, respectively, within both the ventral and dorsal agglomerations through their attachment points on the rudimentary skeleton. Through this nano-CT imaging method we can identify the deep dorsal layer (adductor profundus) within the dorsal agglomeration which was not identified in *S. canicula*, possibly because of the limitations of the techniques used. Through the use of nano-CT imaging, we are also able to identify the lateral musculature, the protractor and abdominal adductor, in *C. milii* at stage 30 (**Figure 4A**), which could not be identified in *S. canicula* at this stage. By stage 32, most components of the pelvic musculature in *C. milii* can be identified (**Figure 5**). The dorsal muscles can be distinguished from one another, and most of the reproductive musculature can be identified, though, apart from the proximal radial layer, the ventral muscles still consist of an agglomeration. The ventral musculature of *S. canicula* at stage 32 and 33 remains undifferentiated and neither the deep dorsal musculature nor the lateral muscles are identified at these stages, with stage 33 being the last stage examined (Ziermann et al., 2017). It is not clear when the deep portion of the adductor or retractor/levator5 is formed in *S. canicula*. These discrepancies in the formation of the musculature may be derived from interspecific differences in the rate of development. Alternatively, these may arise from differences in methodology. The use of nano-CT imaging has allowed us to identify and visualize early differentiations of muscles in 3D, which are difficult to achieve with traditional histology or whole mount immunostaining where structures may obscure one another and prevent a complete analysis of the anatomy. This highlights that the CT imaging and 3D visualization techniques in tandem with traditional methods will help ensure a comprehensive study of the anatomies.

To date, there are no studies on the development of the musculature of the pelvic claspers or tenaculum in other holocephalans or other cartilaginous fish. The examination of the morphology and development of these structures in other chondrichthyans as well as fossil taxa such as placoderms are required to determine any morphological similarities or homologies between the musculature of claspers among these taxa and to further understand the evolution of vertebrate reproduction.

CONCLUSION

Our findings indicate that the pelvic musculature of extant chimaeroids is more complex than suggested by contemporary and historical descriptions (Davidoff, 1879; Diogo and Ziermann, 2015), but agree more with the complexity described in the historical literature (Davidoff, 1879). The revised adult anatomy is essential for interpreting embryonic development. Our work has been greatly aided through reading the historical literature written by the original comparative anatomists and embryologists, much of which appears to have largely been forgotten or overlooked. Such works are treasure stores of much needed anatomical and embryological data that can inform current comparative analyses of different outgroups to bracket evolutionary transitions (Boisvert et al., 2013; Dearden et al., 2021). This will help form hypotheses on evolutionary processes that have shaped the vertebrate skeleton, which can be tested with fossil data that can possess well preserved soft tissues for analyses of the musculature (Trinajstic et al., 2013, 2018). In particular, the holocephalian pelvic musculature described here compares well to the complexity inferred for some Palaeozoic jawless fishes. These anatomies imply an equally complex origin of the pelvis and its musculature. The other great aid to this work has been the use of CT imaging and 3D visualization, which has enabled us to identify the early development of the pelvic musculature and pick apart some of the subtle complexities of the anatomy that are difficult to identify solely through analog dissection. This synthesis, combining the knowledge from the historic literature and analog dissection with modern CT imaging and digital dissections, can shed light on the complexity of anatomy, morphological transformations and their underlying mechanisms underpinning major evolutionary events.

DATA AVAILABILITY STATEMENT

The original contributions presented in the study are included in the article/**Supplementary Material**, further inquiries can be directed to the corresponding author/s.

ETHICS STATEMENT

The animal study was reviewed and approved by the Monash University Animal Ethics Committee (Permit: MAS/ARMI/2010/01).

AUTHOR CONTRIBUTIONS

CB conceived this project and acquired the specimens used. HL and RT conducted the nano-CT imaging. JP and CT segmented and modeled the nano-CT data. JP and CB performed the dissections and analysis of the gross anatomy and interpreted the data, and wrote the manuscript. All authors reviewed the manuscript.

FUNDING

This work was supported by the Curtin Research fellowship: CB, Australian Government Research Training Program Scholarship (AGRTP): JP, ARC discovery grant 1096002. The nano-CT instrument was funded by Canadian Foundation of Innovation project 33122 to the infrastructure of the Integrated Quantitative Biology Initiative (IQBI).

ACKNOWLEDGMENTS

We would like to thank Assoc. Prof. Andrew Woods and the Curtin Hub for Immersive Visualisation and eResearch (HIVE) for their assistance and patience with the modeling of the nano-CT data. We would also like to thank Peter Currie, Carmen Sontaag, and Wendy Chua for elephant shark support. We thank Katharine Criswell and Richard Dearden for their feedback in improving the manuscript.

SUPPLEMENTARY MATERIAL

The Supplementary Material for this article can be found online at: https://www.frontiersin.org/articles/10.3389/fevo.2021.812561/full#supplementary-material

Supplementary Figure 1 | Illustration of the pelvic skeleton of a female elephant shark (*Callorhinchus milii*).

Supplementary Figure 2 | Photographed images of dissected elephant shark pelvic musculature (*Callorhinchus milii*) from **Figure 1** without color overlays.

Supplementary Figure 3 | Photographed images of dissected elephant shark ventral pelvic musculature (*Callorhinchus milii*) from **Figure 2** without color overlays.

Supplementary Figure 4 | Photographed images of dissected elephant shark reproductive musculature (*Callorhinchus milii*) from **Figure 3** without color overlays.

REFERENCES

Balfour, F. M. (1878). *A Monograph on The Development of Elasmobranch Fishes*. Basingstoke: Macmillan. doi: 10.5962/bhl.title.7847

Balfour, F. M. (1881). "On the development of the skeleton of the paired fins of elasmobranchii, considered in relation to its bearings on the nature of the limbs of the vertebrata," in *Proceedings of the Zoological Society of London* (Hoboken, NJ: Wiley Online Library), 656–670. doi: 10.1111/j.1096-3642.1881.tb01323.x

Ballard, W. W., Mellinger, J., and Lechenault, H. (1993). A series of normal stages for development of *Scyliorhinus canicula*, the lesser spotted dogfish (Chondrichthyes: Scyliorhinidae). *J. Exp. Zool.* 267, 318–336. doi: 10.1002/jez.1402670309

Boisvert, C. A., Joss, J. M., and Ahlberg, P. E. (2013). Comparative pelvic development of the axolotl (A*mbystoma mexicanum*) and the Australian lungfish (*Neoceratodus forsteri*): conservation and innovation across the fish-tetrapod transition. *Evodevo* 4, 1–19. doi: 10.1186/2041-9139-4-3

Boisvert, C. A., Martins, C. L., Edmunds, A. G., Cocks, J., and Currie, P. (2015). Capture, transport, and husbandry of elephant sharks (*Callorhinchus milii*) adults, eggs, and hatchlings for research and display. *Zoo Biol.* 34, 94–98. doi: 10.1002/zoo.21183

Braus, H. (1898). Ueber die innervation der paarigen extremitäten bei selachiern, holocephalen und dipnoern. *Jena. Zeitschr. Naturwiss.* 31, 239–486.

Braus, H. (1899). Beiträge zur entwicklung der muskulatur und des peripheren nervensystems der selachier. *Morphol. Jahrbuch* 27, 501–629.

Brazeau, M. D., and Friedman, M. (2015). The origin and early phylogenetic history of jawed vertebrates. *Nature* 520, 490–497. doi: 10.1038/nature14438

Cole, N. J., and Currie, P. D. (2007). Insights from sharks: evolutionary and developmental models of fin development. *Dev. Dyn.* 236, 2421–2431. doi: 10.1002/dvdy.21268

Cole, N. J., Hall, T. E., Don, E. K., Berger, S., Boisvert, C. A., Neyt, C., et al. (2011). Development and evolution of the muscles of the pelvic fin. *PLoS Biol.* 9:e1001168. doi: 10.1371/journal.pbio.1001168

Coolen, M., Menuet, A., Chassoux, D., Compagnucci, C., Henry, S., Lévèque, L., et al. (2008). The dogfish *Scyliorhinus canicula*: a reference in jawed vertebrates. *Cold Spring Harb. Protoc.* 2008:emo111. doi: 10.1101/pdb.emo111

Davidoff, M. (1879). Beitrage zur vergleichenden anatomie der hinteren gliedmassen der fische. *Morphol. Jahrbuch* 5, 450–520.

de Figueiredo Petean, F., and de Carvalho, M. R. (2018). Comparative morphology and systematics of the cookiecutter sharks, genus Isistius Gill (1864)(Chondrichthyes: Squaliformes: Dalatiidae). *PLoS One* 13:e0201913. doi: 10.1371/journal.pone.0201913

Dearden, R. P., Mansuit, R., Cuckovic, A., Herrel, A., Didier, D., Tafforeau, P., et al. (2021). The morphology and evolution of chondrichthyan cranial muscles: a digital dissection of the elephantfish *Callorhinchus milii* and the catshark *Scyliorhinus canicula*. *J. Anatomy* 238, 1082–1105. doi: 10.1111/joa.13362

Didier, D. A. (1995). *Phylogenetic Systematics of Extant Chimaeroid Fishes (Holocephali, Chimaeroidei): American Museum Novitates (3119)*. New York, NY: American Museum of Natural History, 1–88.

Didier, D. A., LeClair, E. E., and Vanbuskirk, D. R. (1998). Embryonic staging and external features of development of the chimaeroid fish, *Callorhinchus milii* (Holocephali, Callorhinchidae). *J. Morphol.* 236, 25–47. doi: 10.1002/(SICI)1097-4687(199804)236:1<25::AID-JMOR2>3.0.CO;2-N

Diogo, R. (2020). Cranial or postcranial—dual origin of the pectoral appendage of vertebrates combining the fin-fold and gill-arch theories? *Dev. Dyn.* 249, 1182–1200. doi: 10.1002/dvdy.192

Diogo, R., and Molnar, J. (2014). Comparative anatomy, evolution, and homologies of tetrapod hindlimb muscles, comparison with forelimb muscles, and deconstruction of the forelimb-hindlimb serial homology hypothesis. *Anat. Rec.* 297, 1047–1075. doi: 10.1002/ar.22919

Diogo, R., and Ziermann, J. (2015). Muscles of chondrichthyan paired appendages: comparison with Osteichthyans, deconstruction of the fore–hindlimb serial homology dogma, and new insights on the evolution of the vertebrate neck. *Anat. Rec.* 298, 513–530. doi: 10.1002/ar.23047

Dohrn, A. (1884). Die paarigen und unpaaren flossen der selachier. Studien zur urgeschichte des wirbeltierkörpers. VI. mitteilungen der zool. *Station Neapel Bd* 5:1884.

Edgeworth, F. (1911). Memoirs: on the morphology of the cranial muscles in some vertebrates. *J. Cell Sci.* 2, 167–316. doi: 10.1242/jcs.s2-56.222.167

Edgeworth, F. H. (1935). *The Cranial Muscles Of Vertebrates*. Cambridge: Cambridge University Press.

Ehrlich, H. (2010). *Biological Materials of Marine Origin*. Dordrecht: Springer. doi: 10.1007/978-90-481-9130-7

Freitas, R., Gómez-Skarmeta, J. L., and Rodrigues, P. N. (2014). New frontiers in the evolution of fin development. *J. Exp. Zool. Part B* 322, 540–552. doi: 10.1002/jez.b.22563

Gegenbaur, C. (1870). Ueber die modificationen des skeletts der hintergliedmassen bei den mannchen der selachier und chimaren. *Jena. Z. Naturwiss.* 5:448.

Goodrich, E. S. (1906). Memoirs: notes on the development, structure, and origin of the median and paired fins of fish. *J. Cell Sci.* 2, 333–376. doi: 10.1242/jcs.s2-50.198.333

Inoue, J. G., Miya, M., Lam, K., Tay, B.-H., Danks, J. A., Bell, J., et al. (2010). Evolutionary origin and phylogeny of the modern holocephalans (Chondrichthyes: Chimaeriformes): a mitogenomic perspective. *Mol. Biol. Evol.* 27, 2576–2586. doi: 10.1093/molbev/msq147

Jungersen, H. F. E. (1899). *On The Appendices Genitales In The Greenland Shark, Somniosus Microcephalus (Bl. Schn.), And Other Selachians*. Copenhagen: Bianco Luno (F. Dreyer). doi: 10.5962/bhl.title.14334

Larouche, O., Zelditch, M. L., and Cloutier, R. (2017). Fin modules: an evolutionary perspective on appendage disparity in basal vertebrates. *BMC Biol.* 15:32. doi: 10.1186/s12915-017-0370-x

Leigh-Sharpe, W. H. (1922). The comparative morphology of the secondary sexual characters of *Holocephali* and elasmobranch fishes. The claspers, clasper siphons, and clasper glands. *J. Morphol.* 36, 199–220. doi: 10.1002/jmor.1050360204

Leigh-Sharpe, W. H. (1926). The comparative morphology of the secondary sexual characters of elasmobranch fishes. The claspers, clasper siphons, and clasper glands. Memoir X. *J. Morphol.* 42, 335–348. doi: 10.1002/jmor.1050420111

Lund, R., and Grogan, E. D. (1997). Relationships of the chimaeriformes and the basal radiation of the chondrichthyes. *Rev. Fish Biol. Fish.* 7, 65–123. doi: 10.1023/A:1018471324332

Maisey, J. (2012). What is an 'elasmobranch'? The impact of palaeontology in understanding elasmobranch phylogeny and evolution. *J. Fish Biol.* 80, 918–951. doi: 10.1111/j.1095-8649.2012.03245.x

Mansuit, R., and Herrel, A. (2021). The evolution of appendicular muscles during the fin-to-limb transition: possible insights through studies of soft tissues, a perspective. *Front. Ecol. Evol.* 9:508. doi: 10.3389/fevo.2021.702576

Mollier, S. (1892). Zur entwickelung der selachierextremitaeten. *Anat. Anzeiger* 7, 351–365.

Moreira, R. A., and de Carvalho, M. R. (2018). Morphology of the clasper musculature in rays (Chondrichthyes; Elasmobranchii: Batoidea), with comments on their phylogenetic interrelationships. *J. Morphol.* 279, 1827–1839. doi: 10.1002/jmor.20904

Moreira, R. A., and de Carvalho, M. R. (2019). Clasper morphology of the japanese sawshark, *Pristiophorus japonicus* Günther, 1870 (Chondrichthyes: Elasmobranchii). *Anat. Rec.* 302, 1666–1670. doi: 10.1002/ar.24082

Neyt, C., Jagla, K., Thisse, C., Thisse, B., Haines, L., and Currie, P. (2000). Evolutionary origins of vertebrate appendicular muscle. *Nature* 408, 82–86. doi: 10.1038/35040549

Parker, T. (1886). On the claspers of *Callorhynchus*. *Nat. Lond.* 34:635. doi: 10.1038/034635a0

Riley, C., Cloutier, R., and Grogan, E. D. (2017). Similarity of morphological composition and developmental patterning in paired fins of the elephant shark. *Sci. Rep.* 7, 1–10. doi: 10.1038/s41598-017-10538-0

Siomava, N., Fuentes, J. S., and Diogo, R. (2020). Deconstructing the long-standing a priori assumption that serial homology generally involves ancestral similarity followed by anatomical divergence. *J. Morphol.* 281, 1110–1132. doi: 10.1002/jmor.21236

Tanaka, M., Münsterberg, A., Anderson, W. G., Prescott, A. R., Hazon, N., and Tickle, C. (2002). Fin development in a cartilaginous fish and the origin of vertebrate limbs. *Nature* 416, 527–531. doi: 10.1038/416527a

Trinajstic, K., Boisvert, C., Long, J. A., and Johanson, Z. (2018). "Evolution of vertebrate reproduction," in *Evolution and Development of Fishes*, eds C. Underwood, M. Richter, and Z. Johanson (Cambridge: Cambridge University Press), 207–226. doi: 10.1017/9781316832172.013

Trinajstic, K., Boisvert, C., Long, J., Maksimenko, A., and Johanson, Z. (2015). Pelvic and reproductive structures in placoderms (stem gnathostomes). *Biol. Rev.* 90, 467–501. doi: 10.1111/brv.12118

Trinajstic, K., Marshall, C., Long, J., and Bifield, K. (2007). Exceptional preservation of nerve and muscle tissues in Late Devonian placoderm fish and their evolutionary implications. *Biol. Lett.* 3, 197–200. doi: 10.1098/rsbl.2006.0604

Trinajstic, K., Sanchez, S., Dupret, V., Tafforeau, P., Long, J., Young, G., et al. (2013). Fossil musculature of the most primitive jawed vertebrates. *Science* 341, 160–164. doi: 10.1126/science.1237275

Venkatesh, B., Lee, A. P., Ravi, V., Maurya, A. K., Lian, M. M., Swann, J. B., et al. (2014). Elephant shark genome provides unique insights into gnathostome evolution. *Nature* 505:174. doi: 10.1038/nature12826

Wilhelm, B. C., Du, T. Y., Standen, E. M., and Larsson, H. C. (2015). Polypterus and the evolution of fish pectoral musculature. *J. Anat.* 226, 511–522. doi: 10.1111/joa.12302

Ziermann, J. M., Freitas, R., and Diogo, R. (2017). Muscle development in the shark *Scyliorhinus canicula*: implications for the evolution of the gnathostome head and paired appendage musculature. *Front. Zool.* 14:31. doi: 10.1186/s12983-017-0216-y

Conflict of Interest: The authors declare that the research was conducted in the absence of any commercial or financial relationships that could be construed as a potential conflict of interest.

Publisher's Note: All claims expressed in this article are solely those of the authors and do not necessarily represent those of their affiliated organizations, or those of the publisher, the editors and the reviewers. Any product that may be evaluated in this article, or claim that may be made by its manufacturer, is not guaranteed or endorsed by the publisher.

frontiers in Ecology and Evolution

ORIGINAL RESEARCH
published: 10 March 2022
doi: 10.3389/fevo.2021.799637

Modeling Skull Network Integrity at the Dawn of Amniote Diversification With Considerations on Functional Morphology and Fossil Jaw Muscle Reconstructions

Ingmar Werneburg[1,2]* *and Pascal Abel*[1,2]

[1] Senckenberg Centre for Human Evolution and Palaeoenvironment at Eberhard Karls Universität Tübingen, Tübingen, Germany, [2] Fachbereich Geowissenschaften der Eberhard Karls Universität Tübingen, Tübingen, Germany

One of the major questions in evolutionary vertebrate morphology is the origin and meaning of temporal skull openings in land vertebrates. Partly or fully surrounded by bones, one, two, or even three openings may evolve behind the orbit, within the ancestrally fully roofed anapsid (*scutal*) skull. At least ten different morphotypes can be distinguished in tetrapods with many modifications and transitions in more crownward representatives. A number of potential factors driving the emergence and differentiation of temporal openings have been proposed in the literature, but only today are proper analytical tools available to conduct traceable tests for the functional morphology underlying temporal skull constructions. In the present study, we examined the anatomical network in the skull of one representative of early amniotes, †*Captorhinus aguti*, which ancestrally exhibits an anapsid skull. The resulting skull modularity revealed a complex partitioning of the temporal region indicating, in its intersections, the candidate positions for potential infratemporal openings. The framework of †*C. aguti* was then taken as a template to model a series of potential temporal skull morphotypes in order to understand how skull openings might influence the modular composition of the amniote skull in general. We show that the original pattern of skull modularity (†*C. aguti*) experiences comprehensive changes by introducing one or two temporal openings in different combinations and in different places. The resulting modules in each skull model are interpreted in regard to the feeding behavior of amniotes that exhibit(ed) the respective skull morphotypes. An important finding is the alternative incorporation of the jugal and palate to different modules enforcing the importance of an integrated view on skull evolution: the temporal region cannot be understood without considering palatal anatomy. Finally, we discuss how to better reconstruct relative jaw muscle compositions in fossils by considering the modularity of the skull network. These considerations might be relevant for future biomechanical studies on skull evolution.

Keywords: Amniota, Reptilia, biomechanics, cranial osteology, temporal skull openings, fenestration

OPEN ACCESS

Edited by:
Michel Laurin,
UMR 7207 Centre de Recherche sur la Paléobiodiversité et les Paléoenvironnements (CR2P), France

Reviewed by:
Diego Rasskin-Gutman,
University of Valencia, Spain
Eduardo Ascarrunz,
Université de Fribourg, Switzerland

***Correspondence:**
Ingmar Werneburg
ingmar.werneburg@senckenberg.de

Specialty section:
This article was submitted to Paleontology, a section of the journal Frontiers in Ecology and Evolution

Received: *21 October 2021*
Accepted: *22 December 2021*
Published: *10 March 2022*

Citation:
Werneburg I and Abel P (2022) Modeling Skull Network Integrity at the Dawn of Amniote Diversification With Considerations on Functional Morphology and Fossil Jaw Muscle Reconstructions. Front. Ecol. Evol. 9:799637. doi: 10.3389/fevo.2021.799637

INTRODUCTION

The evolutionary transition from a mostly aquatic to a fully terrestrial life in vertebrates is associated with a number of fundamental anatomical and physiological changes (Sumida and Martin, 1997; Laurin, 2010; Clack, 2012). These include the evolution of an encapsuled (i.e., amniotic) egg with extraembryonic membranes and the loss of a larval stage in development (Laurin, 2005). As a consequence, morphological adaptative constraints to larval aquatic feeding were skipped, permitting within a few million years an enormous radiation of new feeding types with associated anatomical structures in the early amniotes (Werneburg, 2019). Concurrently, a transition from a primarily suction feeding behavior (Heiss et al., 2013; Natchev et al., 2015) toward a herbivorous (Weishampel, 1997; Sues and Reisz, 1998) or hunting behavior with a weapon-like jaw apparatus (Hülsmann and Wahlert, 1972) took place.

Feeding musculature mainly attaches to the temporal skull region behind the eye and to the posterior part of the palate (Holliday and Witmer, 2007; Jones et al., 2009; Diogo and Abdala, 2010; Werneburg, 2011; Ziermann et al., 2019). In both skull regions, major changes emerged, easily recognizable in all amniote skulls (Lakjer, 1926, 1927; Hanken and Hall, 1993a,b; Novacek, 1993; Rieppel, 1993; Zusi, 1993). In particular, the temporal skull region received much attention in the scientific literature, historically resulting in taxonomic groups mainly defined by the anatomy of their temporal skull region (e.g., Synapsida, Diapsida, "Anapsida"; Case, 1898; Williston, 1904; Broom, 1922; Zdansky, 1923; Frazzetta, 1968; Kuhn-Schnyder, 1980; Rieppel and Gronowski, 1981; Smith et al., 1983; Rieppel, 1984; Frey et al., 2001; Tarsitano et al., 2001; Müller, 2003; Cisneros et al., 2004; Werneburg, 2012, 2013a, 2015, 2019; Haridy et al., 2016; Elzanowski and Mayr, 2018; Abel and Werneburg, 2021) with only few of them still used today. This is because with the rise of phylogenetic systematics and the inclusion of hundreds of other anatomical characters, along with new fossil finds, a more comprehensive picture on amniote interrelationships has been developed (Abel and Werneburg, 2021). Nowadays, the temporal openings are only conditionally relevant for phylogenetic reconstructions. However, they can still be informative on selected phylogenetic levels and in particular taxonomic groups (Ford, 2018) and are considered as highly relevant to understand morphofunctional relationships within the skull.

Recently, Abel and Werneburg (2021) provided a comprehensive review on the diversity and the scientific history of the temporal skull region in land vertebrates. They defined ten skull morphotypes and discussed a series of potential functional factors that shape their temporal region. Proper tests to validate and quantify biomechanical parameters in temporal skull diversification, however, are still lacking.

In the present contribution, we used Anatomical Network Analysis (AnNA; Rasskin-Gutman and Esteve-Altava, 2014) to provide new insights into the complex construction of land vertebrate skulls (Werneburg et al., 2019). For this, we focused on the early Permian †*Captorhinus aguti* (Amniota, Captorhinidae), an early amniote that is known from a high number of three-dimensionally preserved skulls. Even though all major skull morphotypes evolved pretty early after the amniote origin, the skull of captorhinids remained ancestrally anapsid (*scutal sensu* Abel and Werneburg, 2021) with no temporal openings. After analyzing the skull of †*C. aguti*, we used it as a template by removing selected connections to create different skull models in order to estimate which influence the presence of particular temporal openings has on skull integrity. This, in turn, allowed first attempts to interpret alternative functionally distinct regions in the skulls and helped in understanding why these openings might have evolved. Finally, we used these modularity patterns and associated functional considerations to infer potential muscular associations in fossil skulls for which muscle reconstructions are very difficult to perform.

MATERIALS AND METHODS

Anatomical Framework

Skull anatomy of †*C. aguti* is well-documented in the literature (Case, 1911; Sushkin, 1928; Warren, 1961; Fox and Bowman, 1966; Bolt, 1974; Modesto, 1998; Abel et al., 2022). For coding of bone connections, we mainly rely on the study of Fox and Bowman (1966). Uncertainties related to the connection of the lacrimal to the palatine (Bolt, 1974), which we confirm to be present in a μCT-scan that was available to us (see below).

Anatomical Network Analysis

Using a walktrap algorithm, we performed an anatomical network analysis (AnNA; e.g., Rasskin-Gutman and Esteve-Altava, 2014; Esteve-Altava, 2017b; Werneburg et al., 2019; Sookias et al., 2020) for the skull of †*C. aguti* by applying the *igraph* 1.2.6 package (Csardi and Nepusz, 2006) in R (R Core Team, 2020, see also: Esteve-Altava et al., 2011; Esteve-Altava, 2017b,c). For this, an Excel sheet was created, listing the skull bones in an adjacency matrix (i.e., binary coded N × N format) with a value of 1 indicating a contact between two bones and a value of 0 for the lack of such (**Table 1**). The skull of †*C. aguti* consists of 65 bones (i.e., "nodes" in network terminology) and 322 bone contacts (i.e., "links"). The data sheet was imported into RStudio (RStudio Team, 2019) and transformed into an undirected *igraph* object to enable network depiction and calculation of community structures. We used the *cluster_walktrap* function to find community structures based on random walks with the step number being 3 (**Supplementary Table 1**). In network analyses, the resulting community structures (i.e., modules) describe subsets that share more links with each other than with the other nodes of the network, potentially representing different functional units (see discussion and Werneburg et al., 2019). Additionally, we calculated the modularity-value (Q). Q is positive when the number of contacts within the modules exceeds the expected number if all contacts were assigned randomly. Likewise, Q is negative when the number of observed contacts within a module are below the random arrangement.

TABLE 1 | Anatomical network matrix of the skull of †*Captorhinus aguti*. Connections (i.e., "1") are highlighted in blue. Please note that cells representing contacts between identical nodes (e.g., "Angular_left" vs. "Angular_left") are filled black for reading aid. For the analysis, such cells have to be coded as "0". Alterations of this matrix based on **Figures 1A,C** as well as related CSV-files can be found in the accompanying **Supplementary Material**.

	Angular_left	Angular_right	Articular_left	Articular_right	Basioccipital	Coronoid_left	Coronoid_right	Dentary_left	Dentary_right	Epipterygoid_left	Epipterygoid_right	Exoccipital_left	Exoccipital_right	Frontal_left	Frontal_right	Jugal_left	Jugal_right	Lacrimal_left	Lacrimal_right	Maxilla_left	Maxilla_right	Nasal_left	Nasal_right	Opisthotic_left	Opisthotic_right	Palatine_left	Palatine_right	Parabasisphenoid	Parietal_left	Parietal_right	Postfrontal_left	Postfrontal_right	Postorbital_left	Postorbital_right	Postparietal_left	Postparietal_right	Prearticular_left	Prearticular_right	Prefrontal_left	Prefrontal_right	Premaxilla_left	Premaxilla_right	Prootic_left	Prootic_right	Pterygoid_left	Pterygoid_right	Quadrate_left	Quadrate_right	Quadratojugal_left	Quadratojugal_right	Septomaxilla_left	Septomaxilla_right	Splenial_left	Splenial_right	Squamosal_left	Squamosal_right	Stapes_left	Stapes_right	Supraoccipital	Supratemporal_left	Supratemporal_right	Surangular_left	Surangular_right	Vomer_left	Vomer_right
Angular_left		0	1	0	0	0	0	1	0	0	0	0	0	0	0	0	0	0	0	0	0	0	0	0	0	0	0	0	0	0	0	0	0	0	0	0	0	0	0	0	0	0	0	0	0	0	0	0	0	0	0	0	1	0	0	0	0	0	0	0	0	1	0	0	0
Angular_right	0		0	1	0	0	0	0	1	0	0	0	0	0	0	0	0	0	0	0	0	0	0	0	0	0	0	0	0	0	0	0	0	0	0	0	0	0	0	0	0	0	0	0	0	0	0	0	0	0	0	0	0	1	0	0	0	0	0	0	0	0	1	0	0
Articular_left	1	0		0	0	0	0	0	0	0	0	0	0	0	0	0	0	0	0	0	0	0	0	0	0	0	0	0	0	0	0	0	0	0	0	0	1	0	0	0	0	0	0	0	0	0	1	0	0	0	0	0	0	0	0	0	0	0	0	0	0	1	0	0	0
Articular_right	0	1	0		0	0	0	0	0	0	0	0	0	0	0	0	0	0	0	0	0	0	0	0	0	0	0	0	0	0	0	0	0	0	0	0	0	1	0	0	0	0	0	0	0	0	0	1	0	0	0	0	0	0	0	0	0	0	0	0	0	0	1	0	0
Basioccipital	0	0	0	0		0	0	0	0	0	0	1	1	0	0	0	0	0	0	0	0	0	0	1	1	0	0	1	0	0	0	0	0	0	0	0	0	0	0	0	0	0	0	0	0	0	0	0	0	0	0	0	0	0	0	0	1	1	1	0	0	0	0	0	0
Coronoid_left	0	0	0	0	0		0	1	0	0	0	0	0	0	0	0	0	0	0	0	0	0	0	0	0	0	0	0	0	0	0	0	0	0	0	0	1	0	0	0	0	0	0	0	0	0	0	0	0	0	0	0	1	0	0	0	0	0	0	0	0	1	0	0	0
Coronoid_right	0	0	0	0	0	0		0	1	0	0	0	0	0	0	0	0	0	0	0	0	0	0	0	0	0	0	0	0	0	0	0	0	0	0	0	0	1	0	0	0	0	0	0	0	0	0	0	0	0	0	0	0	1	0	0	0	0	0	0	0	0	1	0	0
Dentary_left	1	0	0	0	0	1	0		1	0	0	0	0	0	0	0	0	0	0	0	0	0	0	0	0	0	0	0	0	0	0	0	0	0	0	0	1	0	0	0	0	0	0	0	0	0	0	0	0	0	0	0	1	0	0	0	0	0	0	0	0	1	0	0	0
Dentary_right	0	1	0	0	0	0	1	1		0	0	0	0	0	0	0	0	0	0	0	0	0	0	0	0	0	0	0	0	0	0	0	0	0	0	0	0	1	0	0	0	0	0	0	0	0	0	0	0	0	0	0	0	1	0	0	0	0	0	0	0	0	1	0	0
Epipterygoid_left	0	0	0	0	0	0	0	0	0		0	0	0	0	0	0	0	0	0	0	0	0	0	0	0	0	0	1	0	0	0	0	0	0	0	0	0	0	0	0	0	0	0	0	1	0	0	0	0	0	0	0	0	0	0	0	0	0	0	0	0	0	0	0	0
Epipterygoid_right	0	0	0	0	0	0	0	0	0	0		0	0	0	0	0	0	0	0	0	0	0	0	0	0	0	0	1	0	0	0	0	0	0	0	0	0	0	0	0	0	0	0	0	0	1	0	0	0	0	0	0	0	0	0	0	0	0	0	0	0	0	0	0	0
Exoccipital_left	0	0	0	0	1	0	0	0	0	0	0		0	0	0	0	0	0	0	0	0	0	0	1	0	0	0	0	0	0	0	0	0	0	0	0	0	0	0	0	0	0	0	0	0	0	0	0	0	0	0	0	0	0	0	0	0	0	1	0	0	0	0	0	0
Exoccipital_right	0	0	0	0	1	0	0	0	0	0	0	0		0	0	0	0	0	0	0	0	0	0	0	1	0	0	0	0	0	0	0	0	0	0	0	0	0	0	0	0	0	0	0	0	0	0	0	0	0	0	0	0	0	0	0	0	0	1	0	0	0	0	0	0
Frontal_left	0	0	0	0	0	0	0	0	0	0	0	0	0		1	0	0	0	0	0	0	1	0	0	0	0	0	0	1	0	1	0	0	0	0	0	0	0	1	0	0	0	0	0	0	0	0	0	0	0	0	0	0	0	0	0	0	0	0	0	0	0	0	0	0
Frontal_right	0	0	0	0	0	0	0	0	0	0	0	0	0	1		0	0	0	0	0	0	0	1	0	0	0	0	0	0	1	0	1	0	0	0	0	0	0	0	1	0	0	0	0	0	0	0	0	0	0	0	0	0	0	0	0	0	0	0	0	0	0	0	0	0
Jugal_left	0	0	0	0	0	0	0	0	0	0	0	0	0	0	0		0	1	0	1	0	0	0	0	0	0	0	0	0	0	0	0	1	0	0	0	0	0	0	0	0	0	0	0	1	0	0	0	1	0	0	0	0	0	1	0	0	0	0	0	0	0	0	0	0
Jugal_right	0	0	0	0	0	0	0	0	0	0	0	0	0	0	0	0		0	1	0	1	0	0	0	0	0	0	0	0	0	0	0	0	0	0	0	0	0	0	0	0	0	0	0	0	1	0	0	0	1	0	0	0	0	0	1	0	0	0	0	0	0	0	0	0
Lacrimal_left	0	0	0	0	0	0	0	0	0	0	0	0	0	0	0	1	0		0	1	0	1	0	0	0	1	0	0	0	0	0	0	0	0	0	0	0	0	1	0	0	0	0	0	0	0	0	0	0	0	1	0	0	0	0	0	0	0	0	0	0	0	0	0	0
Lacrimal_right	0	0	0	0	0	0	0	0	0	0	0	0	0	0	0	0	1	0		0	1	0	1	0	0	0	1	0	0	0	0	0	0	0	0	0	0	0	0	1	0	0	0	0	0	0	0	0	0	0	0	1	0	0	0	0	0	0	0	0	0	0	0	0	0
Maxilla_left	0	0	0	0	0	0	0	0	0	0	0	0	0	0	0	1	0	1	0		0	0	0	0	0	1	0	0	0	0	0	0	0	0	0	0	0	0	0	0	1	0	0	0	0	0	0	0	0	0	1	0	0	0	0	0	0	0	0	0	0	0	0	0	0
Maxilla_right	0	0	0	0	0	0	0	0	0	0	0	0	0	0	0	0	1	0	1	0		0	0	0	0	0	1	0	0	0	0	0	0	0	0	0	0	0	0	0	0	1	0	0	0	0	0	0	0	0	0	1	0	0	0	0	0	0	0	0	0	0	0	0	0
Nasal_left	0	0	0	0	0	0	0	0	0	0	0	0	0	1	0	0	0	1	0	0	0		1	0	0	0	0	0	0	0	0	0	0	0	0	0	0	0	1	0	1	0	0	0	0	0	0	0	0	0	1	0	0	0	0	0	0	0	0	0	0	0	0	0	0
Nasal_right	0	0	0	0	0	0	0	0	0	0	0	0	0	0	1	0	0	0	1	0	0	1		0	0	0	0	0	0	0	0	0	0	0	0	0	0	0	0	1	0	1	0	0	0	0	0	0	0	0	0	1	0	0	0	0	0	0	0	0	0	0	0	0	0
Opisthotic_left	0	0	0	0	1	0	0	0	0	0	0	1	0	0	0	0	0	0	0	0	0	0	0		0	0	0	0	0	0	0	0	0	0	0	0	0	0	0	0	0	0	1	0	0	0	0	0	0	0	0	0	0	0	1	0	1	0	1	0	0	0	0	0	0
Opisthotic_right	0	0	0	0	1	0	0	0	0	0	0	0	1	0	0	0	0	0	0	0	0	0	0	0		0	0	0	0	0	0	0	0	0	0	0	0	0	0	0	0	0	0	1	0	0	0	0	0	0	0	0	0	0	0	1	0	1	1	0	0	0	0	0	0
Palatine_left	0	0	0	0	0	0	0	0	0	0	0	0	0	0	0	0	0	1	0	1	0	0	0	0	0		0	0	0	0	0	0	0	0	0	0	0	0	0	0	0	0	0	0	1	0	0	0	0	0	0	0	0	0	0	0	0	0	0	0	0	0	0	1	0
Palatine_right	0	0	0	0	0	0	0	0	0	0	0	0	0	0	0	0	0	0	1	0	1	0	0	0	0	0		0	0	0	0	0	0	0	0	0	0	0	0	0	0	0	0	0	0	1	0	0	0	0	0	0	0	0	0	0	0	0	0	0	0	0	0	0	1
Parabasisphenoid	0	0	0	0	1	0	0	0	0	1	1	0	0	0	0	0	0	0	0	0	0	0	0	0	0	0	0		0	0	0	0	0	0	0	0	0	0	0	0	0	0	1	1	0	0	0	0	0	0	0	0	0	0	0	0	1	1	0	0	0	0	0	0	0
Parietal_left	0	0	0	0	0	0	0	0	0	0	0	0	0	1	0	0	0	0	0	0	0	0	0	0	0	0	0	0		1	1	0	1	0	1	0	0	0	0	0	0	0	0	0	0	0	0	0	0	0	0	0	0	0	1	0	0	0	1	1	0	0	0	0	0
Parietal_right	0	0	0	0	0	0	0	0	0	0	0	0	0	0	1	0	0	0	0	0	0	0	0	0	0	0	0	0	1		0	1	0	1	0	1	0	0	0	0	0	0	0	0	0	0	0	0	0	0	0	0	0	0	0	1	0	0	1	0	1	0	0	0	0
Postfrontal_left	0	0	0	0	0	0	0	0	0	0	0	0	0	1	0	0	0	0	0	0	0	0	0	0	0	0	0	0	1	0		0	1	0	0	0	0	0	0	0	0	0	0	0	0	0	0	0	0	0	0	0	0	0	0	0	0	0	0	0	0	0	0	0	0
Postfrontal_right	0	0	0	0	0	0	0	0	0	0	0	0	0	0	1	0	0	0	0	0	0	0	0	0	0	0	0	0	0	1	0		0	1	0	0	0	0	0	0	0	0	0	0	0	0	0	0	0	0	0	0	0	0	0	0	0	0	0	0	0	0	0	0	0
Postorbital_left	0	0	0	0	0	0	0	0	0	0	0	0	0	0	0	1	0	0	0	0	0	0	0	0	0	0	0	0	1	0	1	0		0	0	0	0	0	0	0	0	0	0	0	0	0	0	0	0	0	0	0	0	0	1	0	0	0	0	0	0	0	0	0	0
Postorbital_right	0	0	0	0	0	0	0	0	0	0	0	0	0	0	0	0	1	0	0	0	0	0	0	0	0	0	0	0	0	1	0	1	0		0	0	0	0	0	0	0	0	0	0	0	0	0	0	0	0	0	0	0	0	0	1	0	0	0	0	0	0	0	0	0
Postparietal_left	0	0	0	0	0	0	0	0	0	0	0	0	0	0	0	0	0	0	0	0	0	0	0	0	0	0	0	0	1	0	0	0	0	0		1	0	0	0	0	0	0	0	0	0	0	0	0	0	0	0	0	0	0	1	0	0	0	1	1	0	0	0	0	0
Postparietal_right	0	0	0	0	0	0	0	0	0	0	0	0	0	0	0	0	0	0	0	0	0	0	0	0	0	0	0	0	0	1	0	0	0	0	1		0	0	0	0	0	0	0	0	0	0	0	0	0	0	0	0	0	0	0	1	0	0	1	0	1	0	0	0	0
Prearticular_left	0	0	1	0	0	1	0	1	0	0	0	0	0	0	0	0	0	0	0	0	0	0	0	0	0	0	0	0	0	0	0	0	0	0	0	0		0	0	0	0	0	0	0	0	0	0	0	0	0	0	0	1	0	0	0	0	0	0	0	0	1	0	0	0
Prearticular_right	0	0	0	1	0	0	1	0	1	0	0	0	0	0	0	0	0	0	0	0	0	0	0	0	0	0	0	0	0	0	0	0	0	0	0	0	0		0	0	0	0	0	0	0	0	0	0	0	0	0	0	0	1	0	0	0	0	0	0	0	0	1	0	0
Prefrontal_left	0	0	0	0	0	0	0	0	0	0	0	0	0	1	0	0	0	1	0	0	0	1	0	0	0	0	0	0	0	0	0	0	0	0	0	0	0	0		0	0	0	0	0	0	0	0	0	0	0	0	0	0	0	0	0	0	0	0	0	0	0	0	0	0
Prefrontal_right	0	0	0	0	0	0	0	0	0	0	0	0	0	0	1	0	0	0	1	0	0	0	1	0	0	0	0	0	0	0	0	0	0	0	0	0	0	0	0		0	0	0	0	0	0	0	0	0	0	0	0	0	0	0	0	0	0	0	0	0	0	0	0	0
Premaxilla_left	0	0	0	0	0	0	0	0	0	0	0	0	0	0	0	0	0	0	0	1	0	1	0	0	0	0	0	0	0	0	0	0	0	0	0	0	0	0	0	0		1	0	0	0	0	0	0	0	0	0	0	0	0	0	0	0	0	0	0	0	0	0	1	0
Premaxilla_right	0	0	0	0	0	0	0	0	0	0	0	0	0	0	0	0	0	0	0	0	1	0	1	0	0	0	0	0	0	0	0	0	0	0	0	0	0	0	0	0	1		0	0	0	0	0	0	0	0	0	0	0	0	0	0	0	0	0	0	0	0	0	0	1
Prootic_left	0	0	0	0	0	0	0	0	0	0	0	0	0	0	0	0	0	0	0	0	0	0	0	1	0	0	0	1	0	0	0	0	0	0	0	0	0	0	0	0	0	0		0	0	0	0	0	0	0	0	0	0	0	0	0	1	0	1	0	0	0	0	0	0
Prootic_right	0	0	0	0	0	0	0	0	0	0	0	0	0	0	0	0	0	0	0	0	0	0	0	0	1	0	0	1	0	0	0	0	0	0	0	0	0	0	0	0	0	0	0		0	0	0	0	0	0	0	0	0	0	0	0	0	1	1	0	0	0	0	0	0
Pterygoid_left	0	0	0	0	0	0	0	0	0	1	0	0	0	0	0	1	0	0	0	0	0	0	0	0	0	1	0	0	0	0	0	0	0	0	0	0	0	0	0	0	0	0	0	0		1	1	0	0	0	0	0	0	0	0	0	1	0	0	0	0	0	0	1	0
Pterygoid_right	0	0	0	0	0	0	0	0	0	0	1	0	0	0	0	0	1	0	0	0	0	0	0	0	0	0	1	0	0	0	0	0	0	0	0	0	0	0	0	0	0	0	0	0	1		0	1	0	0	0	0	0	0	0	0	0	1	0	0	0	0	0	0	1
Quadrate_left	0	0	1	0	0	0	0	0	0	0	0	0	0	0	0	0	0	0	0	0	0	0	0	0	0	0	0	0	0	0	0	0	0	0	0	0	0	0	0	0	0	0	0	0	1	0		0	1	0	0	0	0	0	1	0	1	0	0	0	0	0	0	0	0
Quadrate_right	0	0	0	1	0	0	0	0	0	0	0	0	0	0	0	0	0	0	0	0	0	0	0	0	0	0	0	0	0	0	0	0	0	0	0	0	0	0	0	0	0	0	0	0	0	1	0		0	1	0	0	0	0	0	1	0	1	0	0	0	0	0	0	0
Quadratojugal_left	0	0	0	0	0	0	0	0	0	0	0	0	0	0	0	1	0	0	0	0	0	0	0	0	0	0	0	0	0	0	0	0	0	0	0	0	0	0	0	0	0	0	0	0	0	0	1	0		0	0	0	0	0	1	0	0	0	0	0	0	0	0	0	0
Quadratojugal_right	0	0	0	0	0	0	0	0	0	0	0	0	0	0	0	0	1	0	0	0	0	0	0	0	0	0	0	0	0	0	0	0	0	0	0	0	0	0	0	0	0	0	0	0	0	0	0	1	0		0	0	0	0	0	1	0	0	0	0	0	0	0	0	0
Septomaxilla_left	0	0	0	0	0	0	0	0	0	0	0	0	0	0	0	0	0	1	0	1	0	1	0	0	0	0	0	0	0	0	0	0	0	0	0	0	0	0	0	0	0	0	0	0	0	0	0	0	0	0		0	0	0	0	0	0	0	0	0	0	0	0	0	0
Septomaxilla_right	0	0	0	0	0	0	0	0	0	0	0	0	0	0	0	0	0	0	1	0	1	0	1	0	0	0	0	0	0	0	0	0	0	0	0	0	0	0	0	0	0	0	0	0	0	0	0	0	0	0	0		0	0	0	0	0	0	0	0	0	0	0	0	0
Splenial_left	1	0	0	0	0	1	0	1	0	0	0	0	0	0	0	0	0	0	0	0	0	0	0	0	0	0	0	0	0	0	0	0	0	0	0	0	1	0	0	0	0	0	0	0	0	0	0	0	0	0	0	0		1	0	0	0	0	0	0	0	0	0	0	0
Splenial_right	0	1	0	0	0	0	1	0	1	0	0	0	0	0	0	0	0	0	0	0	0	0	0	0	0	0	0	0	0	0	0	0	0	0	0	0	0	1	0	0	0	0	0	0	0	0	0	0	0	0	0	0	1		0	0	0	0	0	0	0	0	0	0	0
Squamosal_left	0	0	0	0	0	0	0	0	0	0	0	0	0	0	0	1	0	0	0	0	0	0	0	1	0	0	0	0	1	0	0	0	1	0	1	0	0	0	0	0	0	0	0	0	0	0	1	0	1	0	0	0	0	0		0	0	0	0	1	0	0	0	0	0
Squamosal_right	0	0	0	0	0	0	0	0	0	0	0	0	0	0	0	0	1	0	0	0	0	0	0	0	1	0	0	0	0	1	0	0	0	1	0	1	0	0	0	0	0	0	0	0	0	0	0	1	0	1	0	0	0	0	0		0	0	0	0	1	0	0	0	0
Stapes_left	0	0	0	0	1	0	0	0	0	0	0	0	0	0	0	0	0	0	0	0	0	0	0	1	0	0	0	1	0	0	0	0	0	0	0	0	0	0	0	0	0	0	1	0	1	0	1	0	0	0	0	0	0	0	0	0		0	1	0	0	0	0	0	0
Stapes_right	0	0	0	0	1	0	0	0	0	0	0	0	0	0	0	0	0	0	0	0	0	0	0	0	1	0	0	1	0	0	0	0	0	0	0	0	0	0	0	0	0	0	0	1	0	1	0	1	0	0	0	0	0	0	0	0	0		1	0	0	0	0	0	0
Supraoccipital	0	0	0	0	1	0	0	0	0	0	0	1	1	0	0	0	0	0	0	0	0	0	0	1	1	0	0	0	1	1	0	0	0	0	1	1	0	0	0	0	0	0	1	1	0	0	0	0	0	0	0	0	0	0	0	0	1	1		0	0	0	0	0	0
Supratemporal_left	0	0	0	0	0	0	0	0	0	0	0	0	0	0	0	0	0	0	0	0	0	0	0	0	0	0	0	0	1	0	0	0	0	0	1	0	0	0	0	0	0	0	0	0	0	0	0	0	0	0	0	0	0	0	1	0	0	0	0		0	0	0	0	0
Supratemporal_right	0	0	0	0	0	0	0	0	0	0	0	0	0	0	0	0	0	0	0	0	0	0	0	0	0	0	0	0	0	1	0	0	0	0	0	1	0	0	0	0	0	0	0	0	0	0	0	0	0	0	0	0	0	0	0	1	0	0	0	0		0	0	0	0
Surangular_left	1	0	1	0	0	1	0	1	0	0	0	0	0	0	0	0	0	0	0	0	0	0	0	0	0	0	0	0	0	0	0	0	0	0	0	0	1	0	0	0	0	0	0	0	0	0	0	0	0	0	0	0	0	0	0	0	0	0	0	0	0		0	0	0
Surangular_right	0	1	0	1	0	0	1	0	1	0	0	0	0	0	0	0	0	0	0	0	0	0	0	0	0	0	0	0	0	0	0	0	0	0	0	0	0	1	0	0	0	0	0	0	0	0	0	0	0	0	0	0	0	0	0	0	0	0	0	0	0	0		0	0
Vomer_left	0	0	0	0	0	0	0	0	0	0	0	0	0	0	0	0	0	0	0	0	0	0	0	0	0	1	0	0	0	0	0	0	0	0	0	0	0	0	0	0	1	0	0	0	1	0	0	0	0	0	0	0	0	0	0	0	0	0	0	0	0	0	0		1
Vomer_right	0	0	0	0	0	0	0	0	0	0	0	0	0	0	0	0	0	0	0	0	0	0	0	0	0	0	1	0	0	0	0	0	0	0	0	0	0	0	0	0	0	1	0	0	0	1	0	0	0	0	0	0	0	0	0	0	0	0	0	0	0	0	0	1	

We also calculated the number of Q-modules, which describe the best mathematical threshold (red dashed line in **Figures 2**, **4–8**) to define a module. Depending on the algorithm used, this threshold might slightly shift. The Q-module is just a rough orientation to detect meaningful biological modules (see discussion in Werneburg et al., 2019; Sookias et al., 2020), and as such, the choice of the cluster optimization algorithm does not have any importance for the scope of this study (personal communication with Borja Esteve-Altava in 2021).

μCT-Scan of †*Captorhinus aguti*

For illustration of the modularity pattern (**Figures 2–8**), we used a μCT-scan of a skull of †*C. aguti* from Sam Noble Oklahoma Museum of Natural History, University of Oklahoma, Norman, OK, United States (OMNH 44816). This scan was used in a

parallel study (Abel et al., 2022) in which we describe in detail the sutures between adjacent bones to infer potential intracranial mobilities. In the μCT-scanned specimen, the following dermal bones are missing: left jugal, part of left prefrontal, left nasal, both premaxillae, most of the postparietals, and both supratemporals. The missing bones are indicated by semitransparent outlines in **Figure 2**. In other pictures of this specimen and in the skull models derived from it (**Figures 3–8**), these missing bones were not redrawn.

Skull Models

Skull models correspond to the temporal skull types defined by Abel and Werneburg (2021). For the different models of temporal skull openings, the original matrix (**Table 1**; *scutal*, i.e., anapsid type) was modified by removing particular bone connections (i.e., coding "1" replaced by coding "0"; see **Figures 1A,C,D**, Script in **Supplementary Material**). The *infrafenestral*, *bifenestral*, and *fossafenestral* skull types of Abel and Werneburg (2021) were, in the present study, divided in two sub-types each. The *nudital* and *additofenestral* skull types were not modeled within the framework of this study. For a *nudital* model, a number of bones (not just contacts) would need to be deleted, resulting in a non-comparable network as all other models in this study have a stable bone number (N). *Additofenestral* refers to multiple contacts between two adjacent bones (leaving more than one opening in between) which cannot be coded using AnNA methodology.

In the *infrafenestral-1* skull model (**Figure 3B**), which is represented by many early Synapsida [†Caseidae, †Varanopidae; e.g., Romer and Price (1940)] and some †Parareptilia (e.g., MacDougall and Reisz, 2014), the jugal/squamosal contacts of the original matrix were removed on both skull sides (i.e., "1" replaced by "0"), resulting in 318 remaining links.

In the *infrafenestral-2* skull model (**Figure 3C**), which was represented by some †Edaphosauridae and early therapsids, such as †Dinocephalia (Boonstra, 1952; Modesto, 1995; Kammerer, 2011; Lucas et al., 2018), the jugal/quadratojugal and postorbital/squamosal-contacts were removed resulting in 314 remaining links. This general pattern is also developed in many lepidosauromorphs, although their fenestra has evolved from the upper instead of the lower temporal opening (Abel and Werneburg, 2021).

In the *infrafossal* skull model (**Figure 3D**), jugal/squamosal and jugal/quadratojugal-contacts were removed, resulting in 314 remaining links. Early amniote taxa representing this morphotype are some †millerettids, †*Microleter,* and †*Eunotosaurus* (Gow, 1972; Keyser and Gow, 1981; Tsuji et al., 2010), and some "microsaurs" like †*Llistrofus* and related taxa that might also represent early amniotes (Bolt and Rieppel, 2009; Mann et al., 2019).

In the *suprafenestral* skull model (**Figure 3E**), which was represented by †*Araeoscelis* (Reisz et al., 1984), the postorbital/parietal-contact was removed, resulting in 318 remaining links.

In the *suprafossal* skull model (**Figure 3F**), supratemporal/parietal and squamosal/parietal-contacts were removed, resulting in 314 remaining links. Although not included as such by Abel and Werneburg (2021), this skull type mirrors a skull shape, which evolved in many non-amniote taxa (Holmes, 1984; Klembara et al., 2006; Reisz et al., 2009; Klembara, 2011), with the "fossa" representing the otic notch.

In the *bifenestral-1* skull model (**Figure 3G**), which was represented by the early diapsid †*Petrolacosaurus* (Reisz, 1977), postorbital/parietal and jugal/squamosal-contacts were removed, resulting in 314 remaining links.

In the *bifenestral-2* skull model (**Figure 3H**), which was likely represented by the neodiapsid †*Youngina* (Carroll, 1981), postorbital/parietal, postfrontal/parietal, and jugal/squamosal-contacts were removed, resulting in 310 remaining links.

In the *bifossal* skull model (**Figure 3I**), jugal/squamosal, jugal/quadratojugal, supratemporal/parietal, and squamosal/parietal-contacts were removed, resulting in 306 remaining links. This model represents a combination of infra- and suprafossal skull types. To our knowledge, it is not represented in any early amniote, but is a morphotype, which is well-developed in the turtle crown-group (Gaffney, 1979; Werneburg, 2012) and mammals (Novacek, 1993). As the anatomy of these animals is highly derived compared to the ancestral amniote condition (Starck, 1995; Müller, 2003; Werneburg and Maier, 2019), the model might have only little relevance to interpret the diverse skull construction in these groups (but see the section "Discussion").

In the *fossafenestral-1* skull model (**Figure 3J**) which may be represented by †*Claudiosaurus* (Carroll, 1981), jugal/squamosal, jugal/quadratojugal, and postorbital/parietal-contacts were removed, resulting in 306 remaining links.

In the *fossafenestral-2* skull model (**Figure 3K**), which may be present in the neodiapsid †*Hovasaurus* and †*Claudiosaurus* [see *fossafenestral-1* type as alternative] (Currie, 1981; Bickelmann et al., 2009), jugal/squamosal, jugal/quadratojugal, postorbital/parietal, and postfrontal/parietal-contacts were removed, resulting in 310 remaining links. This skull type is also visible in many squamates (Evans, 2008).

Muscle Reconstruction

We provide an attempt to hypothetically interpret some aspects of the functional morphology of jaw musculature in the respective skull models. Our concept was that if muscles attach to different bones of the same skull module, they are interpreted as acting as one functional entity. It has been shown that muscles are very conservatively associated to particular bones through evolution and only rarely change their general attachment sites (Diogo and Abdala, 2010; Werneburg, 2013a). Skull modules have widely been interpreted in a functional manner (Esteve-Altava et al., 2015a,b,c; Werneburg et al., 2019; Plateau and Foth, 2020). With changed osteological modularity, bone-related musculature might change its internal and external structure and functional anatomy. This could mean that the muscles could be partly or fully fused as one muscle mass and receive a common nervous signal to contract at the same time, or they could form separated muscle heads and portions with individual functional properties.

Using AnNA, Esteve-Altava et al. (2015c) have shown that different modules can be obtained when the skeletal and muscular components are modeled separately or together,

arguing against a straightforward relationship between bone modules and functional muscle groups. Despite the fact that different node numbers in an anatomical network may result in different modular integration (e.g., see our models below), this obstacle is mainly related to the premise that, in AnNA, every anatomical element—bone and muscle alike—is treated equally as just a "node" in the anatomical framework. However, bones are already very diverse in their anatomy and ontogenetic history with either their enchondral or dermal origin, resulting in altering internal structural properties (Hall, 2005). Reducing them to nodes has its limitations, but it has been shown to still be informative in anatomical network studies. Muscles are more difficult in this regard.

The conservative and tendinous attachments of muscles to particular bones are derived from neural crest cells early in development (Hall, 2009), making primary muscle-bone correspondences difficult to change through evolution. In contrast, muscles also possess a very plastic structure that functionally adapts—*via* expanded direct muscle fiber attachments to other bones—for particular biomechanical requirements. Therefore, comparing modularity of bones and modularity of muscles (Esteve-Altava et al., 2015c) should be taken with great care and detailed anatomical knowledge is needed to make sufficient correlations. A study in which muscles and bones are treated as equal structural entities (nodes) may result in an interesting overall network relationship, but with little functional meaning. Relative proportions, muscle vectors, and muscle fiber directions, among many other parameters, however, are imperative to make sufficient biomechanical reconstructions. Hence, muscle anatomy and not muscle network need to be discussed in relation to bone modularity for a sufficient functional interpretation. This exploratory, rough heuristic approach, of course, can only be speculative and needs to be tested with proper biomechanic methodology (e.g., finite element analyses: Lautenschlager et al., 2017; Ferreira et al., 2020). Nevertheless, comparative anatomical data already provide well-founded indications on a functional relationship between bone modules and muscle morphology.

For example, Werneburg et al. (2019) discussed bone modularity of five extant species and cited muscle anatomy in clear correspondence between particular bone modules and muscles. In the alligator, an expanded snout (their "red" labeled module) is related to the expanded pterygoid-musculature (Schumacher, 1973). The threefold differentiation of the external adductor muscles is closely related to the encounter of three skull modules ("green," "orange," and "red") in the temporal skull region of alligator and tuatara (Holliday and Witmer, 2007; Jones et al., 2009). Even the derived muscle anatomy of the leatherback turtle with straight jaw muscle orientation in the adductor chamber (Burne, 1905; Schumacher, 1972) directly associates with the unique skull modularity in this species ("green" and "orange"). As differentiation of the external jaw muscles in the opossum, the mammalian temporalis musculature anatomically relates to the expanded braincase module ("yellow"), whereas the complex masseter muscle used for chewing attaches to the jugal, which belongs to the snout module ("red") in this species. Even the rather simple skull modularity of the chicken corresponds to its jaw muscle anatomy (Van Den Heuvel, 1992), taking lower level network hierarchy into account (Werneburg et al., 2019).

Based on the known extant tetrapod jaw muscle diversity (e.g., Diogo and Abdala, 2010; Ziermann et al., 2019), we hypothesize at least seven distinct major jaw muscle portions to be present in the ancestral amniote condition (**Figure 3**: seven-pointed star next to each skull). These include for the external jaw adductor section: (1) musculus (m.) adductor mandibulae externus Pars profundus (AMEP), originating mainly from the parietal, (2) m. adductor mandibulae externus Pars superficialis (AMES), originating mainly from the squamosal, and (3) m. adductor mandibulae Pars medialis (AMEM), which is mainly associated with the jugal (see homology discussion in Abel et al., 2022). The internal jaw adductor section includes the following: (4) m. adductor mandibulae posterior, originating mainly from the quadrate, (5) m. pterygoideus Pars ventralis (PTV), which is mainly associated with the posterior edge and/or ventral side of the pterygoid, (6) m. pterygoideus Pars dorsalis (PTD), originating dorsally from the palatine (in addition to the pterygoid), and (7) m. constrictor internus dorsalis (CID) mainly originating from the epipterygoid. This series of seven muscular units is obviously a simplification of the actual diversity and differentiation of jaw musculature, but this generalization was necessary to fit the focus of this article and is open to revision. Muscle terminology is based on Jones et al. (2009) and Werneburg (2011).

RESULTS

Network Analysis of †*Captorhinus aguti* (Skull Type A: *Scutal*/Anapsid)

The number of contacts per bone varies from two (epipterygoid) to 13 (supraoccipital). Most bones possess three to five contacts.

TABLE 2 | Network parameters of the analyzed networks based on the definitions theoretical background as mostly summarized by Plateau and Foth (2020).

Model	C	D	K	L	Q	Q_{max}
scutal (†*Captorhinus aguti*)	0.428	0.077	322	3.663	7	0.62
infrafenestral-1	0.409	0.076	318	3.684	7	0.62
infrafenestra-2	0.430	0.075	314	3.685	7	0.62
infrafossal	0.432	0.075	314	3.697	7	0.63
suprafenestral	0.411	0.076	318	3.674	7	0.62
suprafossal	0.414	0.075	314	3.702	7	0.62
bifenestral-1	0.387	0.075	314	3.702	7	0.62
bifenestral-2	0.375	0.076	310	3.725	7	0.62
bifossal	0.416	0.074	306	3.750	7	0.62
fossafenestral-1	0.398	0.074	306	3.738	7	0.62
fossafenestral-2	0.410	0.075	310	3.715	7	0.63

For all models, N is the number of nodes (i.e., bones) and is always 65 in our models. C is the mean clustering coefficient and represents the arithmetic mean of the ratio of a node's neighbors that connect among them in a triangular manner. D is the density of connections calculated as the number of links (K) divided by the maximum number of connections possible. L is the mean shortest path length and measures the average of the shortest path length between all pairs of bones. Q is the number of calculated Q-modules. Q_{max} evaluates whether the number of modules identified are better supported than what is expected at random.

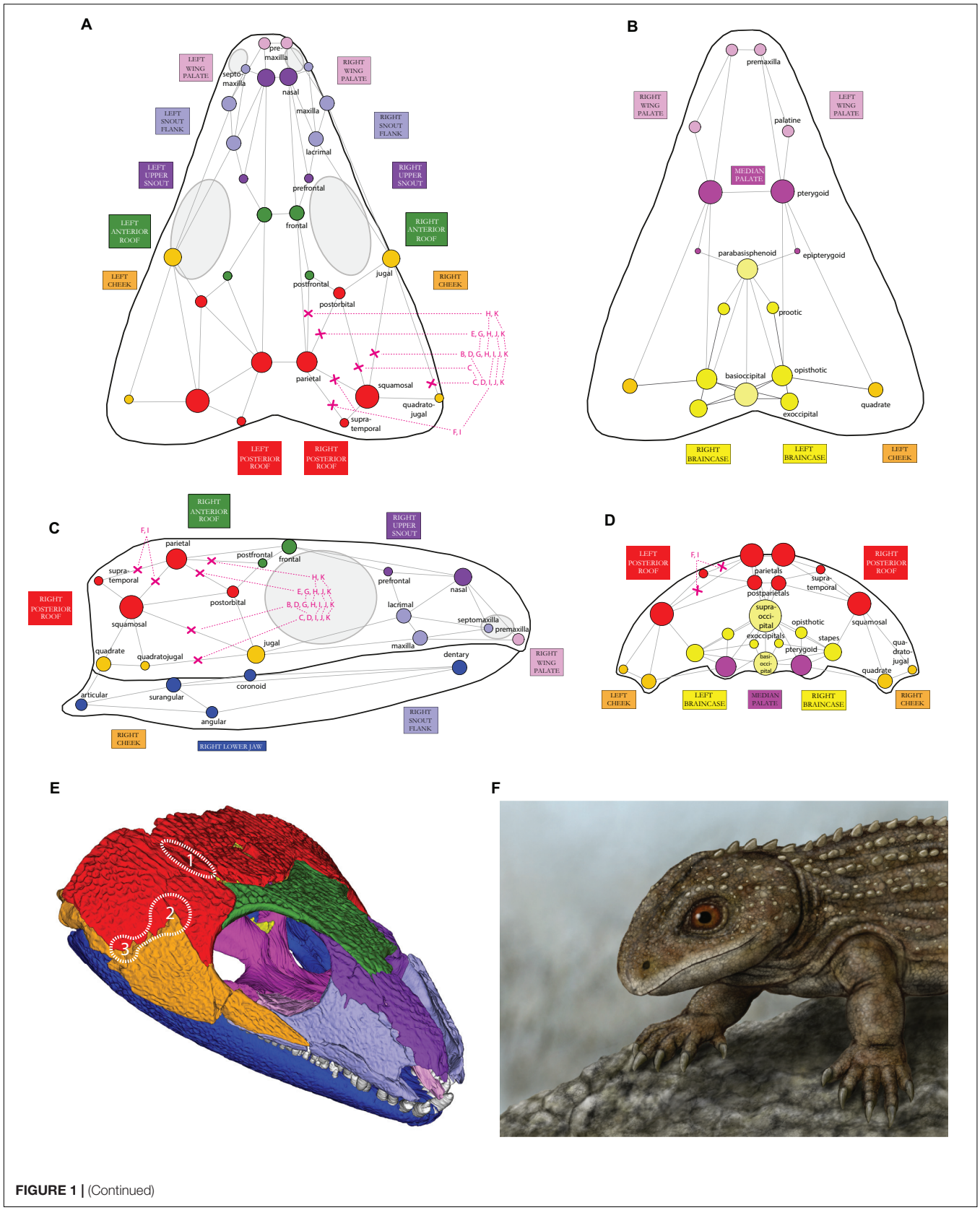

FIGURE 1 | (Continued)

FIGURE 1 | Illustration of the skull network of †*Captorhinus aguti* in **(A)** dorsal, **(B)** ventral, **(C)** lateral, and **(D)** posterior view. Only superficial bones and their connections to other bones ("links" in network terminology) are shown. The relative size of each circle (i.e., node) represents the number of links to the respective bone, incl. also non-illustrated ones (see legend inside Figure). For coding details see **Table 1**. Circles are colored according to the reconstructed cranial network modules (see **Figures 1E**, **2**). In the present study, different network models were created by cutting selected connections between particular bones, herein indicated by red "X"-symbols; letters correspond to respective models and subpanel letters in **Figure 3**). **(E)** oblique view of the 3D-reconstructed skull of †*C. aguti* with colored skull modules (see **Figures 2**, **3A** for labeling). The potential origin sites of temporal openings among early amniotes (1–3) are indicated by dotted lines (compare to **Figure 3A**: right lower corner). **(F)** Digital drawing of †*C. aguti* by paleoartist Markus Bühler (Balingen, Germany); Paläontologische Sammlung der Universität Tübingen, collection number of the drawing: GPIT-PV-112849.

In the temporal region, the squamosal is the most 'integrated' bone (eight contacts). The minimum number can be observed in the postfrontal, supratemporal, and quadratojugal (three contacts). In the conceptual framework of AnNA, integration refers to the number of connections. This is related to the concept of burden (Esteve-Altava et al., 2013a), and it has been adapted for AnNA (see Rasskin-Gutman and Esteve-Altava, 2021).

The analysis with walktrap algorithm, which has been widely used in Anatomical Network literature before, resulted in a modularity index (Q-index) of 0.625. A Q-index > 0 means that the calculated number of contacts inside a module is higher than in a random model (**Figure 2E**). Network parameters and Q-values per model are listed in **Table 2**.

Network Description for †*Captorhinus aguti* (Skull Type A: *Scutal*/Anapsid)

In addition to both left and right-side mandibular rami (dark blue in **Figures 1**–**3A**), a braincase module is present (dark yellow), and it is separated into a left and a right submodule containing prootic/stapes and opisthotic/exoccipital on each side. The unpaired elements of the braincase (light yellow)—parabasisphenoid, basioccipital, and supraoccipital—randomly appear within either one of the contralateral braincase submodules in different runs of the same analysis (see Werneburg et al., 2019 for details on that phenomenon).

The remaining major modules consist of left and right dermal bones of the "cheek," skull roof, snout, and palate regions. Inside these areas, the palate region can be divided into three modules, one left and one right-wing module (light pink), each consisting of premaxilla and palatine/vomer, and one medial palate module (dark pink). The latter plotted closer to the braincase modules (yellow) than to the palatal wing (light pink) inside the dendrogram and consists of the contralateral pterygoids and epipterygoids.

The "cheek" region lateral and posterolateral to the orbit (orange) consists of jugal and the more integrated quadrate/quadratojugal on each side. A certain relationship exists between the "cheek" and the two skull roof modules indicated by neighboring branches in the dendrogram.

The posterior roof module (red) consists of squamosal + parietal/postorbital and postparietal/supratemporal. The anterior roof module (dark green) consists of postfrontal and frontal.

In the snout, two modules can be found on each skull side. The upper snout module (dark purple) consists of prefrontal and nasal. The snout flank module (light purple) consists of maxilla and lacrimal/septomaxilla.

As for the overall network structure, the median palate modules (dark pink), together with the braincase modules (yellow), are placed in between left and right skull side modules on both skull sides functionally separating the skull in a left and right side (**Figure 2E**).

Network Analyses of the Skull Models

All ten skull models (**Figures 3B**–**K**, **4**–**8**) show seven Q-modules each (**Table 2**). We found that compared to the original skull modularity of †*C. aguti* (**Figures 2**, **3A**), the jugal, squamosal, postorbital, and postfrontal usually change their modular association when different temporal openings are modeled. Only in the original skull model, the frontal forms its own module together with postfrontal (green), but it is part of the upper snout module (dark purple) in all ten modeled skulls. Also, different to †*C. aguti*, in all ten modeled skulls, the palatal wing module (light pink) plotted closer to the snout flank module (light purple) than the latter does to the upper snout module (dark purple).

As for the overall network structure, the median palate (dark pink), together with the braincase (yellow) modules, can change their relative position in relation to the palatal wings, snout, cheek, and skull roof modules in each skull model.

In the skull model dendrograms (**Figures 4**–**8**), the original modular association of the respective bone as found in †*C. aguti* is indicated by background coloration of the respective bone name embedded in a different module coloration.

In the *infrafenestral-1* skull model, also different to the original *scutal* skull of †*C. aguti* (see **Figures 1**–**3A** vs. **Figures 3B**, **4A**), the cheek (orange) module plotted closer to the posterior roof module (red) than the latter does to the upper snout module (dark purple), as indicated by parallel white stripes in **Figure 3B**.

In the *infrafenestral-2* skull model (see **Figures 1**–**3A** vs. **Figures 3C**, **4B**), the cheek module split in two separated parts with the jugal integrated within the lateral snout module (light purple). A new module, the postocular module, is formed by postorbital and postfrontal (light green), and the cheek module (orange) is closer associated to the posterior roof module (red). Considering the overall network, the median palate module (dark pink)—together with the braincase module (yellow)—plotted closer to the skull roof (red and blue) and cheek (orange) modules than to the palatal wing (light pink) and the snout modules (light and dark pink) of both skull sides. Hence, the whole skull may be functionally separated into an anterior and a posterior half.

In the *infrafossal* skull model (see **Figures 1**–**3A** vs. **Figures 3D**, **5A**), the cheek module is split with the jugal integrated in the snout flank module (light purple). Postorbital and postfrontal are part of the posterior skull roof module

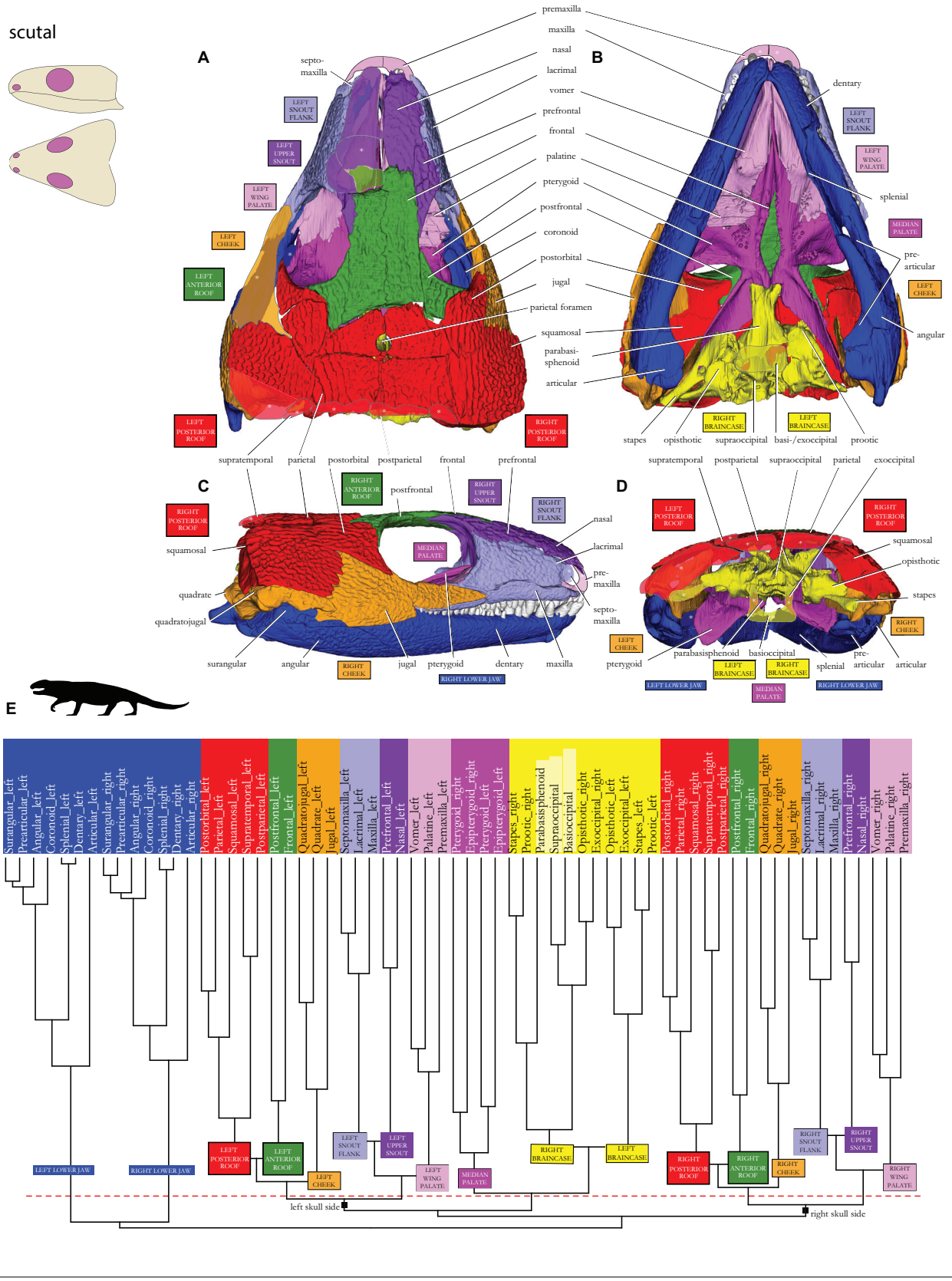

FIGURE 2 | (Continued)

FIGURE 2 | Skull network of †*Captorhinus aguti* in **(A)** dorsal, **(B)** ventral, **(C)** lateral, and **(E)** posterior view. Missing bones of the μCT-scanned skull are redrawn as rough semitransparent outlines. The dendrogram calculated during the network analysis is shown in panel **(E)**: red dashed line indicates the threshold of the Q-modules. Biologically sound morphological modules are indicated by different colors. Unpaired bones of the (yellow) braincase have no robust position in different runs of the same analysis and are shown in light yellow. Major skull network dichotomy in "right" and "left" skull sides is labeled on the basal branches (compare to double-arrows labeled as "right-left" in **Figure 3A**). Sketches of the *scutal* skull type in the upper left corner after Abel and Werneburg (2021). Silhouette in **(E)** drawn after LeBlanc et al. (2018).

(red). Similar to the *infrafenestral-2* model, the median palate module (dark pink), together with the braincase module (yellow), functionally separates the whole skull in an anterior and a posterior half.

In the *suprafenestral* skull model (see **Figures 1**–**3A** vs. **Figures 3E**, **5B**), the squamosal, which originally belonged to the posterior skull roof module (red), is now part of the cheek region (orange). The jugal, which originally belonged to the cheek module, is part of the snout flank module (light purple).

The *suprafossal* skull model (see **Figures 1**–**3A** vs. **Figures 3F**, **6A**) is characterized by an expansion of the posterior skull roof module (red), which now also includes postfrontal and all three (originally orange) cheek bones: quadrate, quadratojugal, and jugal.

The *bifenestral-1* skull model (see **Figures 1**–**3A** vs. **Figures 3G**, **6B**) shows the same patterns as the *infrafenestral-1* model (see **Figures 3B**, **4A**)

In the *bifenestral-2* skull model (see **Figures 1**–**3A** vs. **Figures 3H**, **7A**), postfrontal and postorbital form a new postocular module (light green) that is related to the cheek (orange) and to the posterior skull roof (red) modules.

In the *bifossal skull* model (**Figures 1**–**3A** vs. **Figures 3I**, **7B**), the jugal becomes part of the lateral snout module (light purple). The posterior skull roof module (red) has expanded and integrates the two remaining "cheek elements", quadrate and quadratojugal, along with the postfrontal. Considering the overall network, the median palate module (dark pink)—together with the braincase module (yellow), are closely placed in between the posterior skull roof modules of both skull sides (red), functionally separating the whole skull in an anterior and a posterior half. The anterior half is formed by the palatal wing modules (light pink) and the snout modules (light and dark purple) of both skull sides.

In the *fossafenestral-1* skull model (see **Figures 1**–**3A** vs. **Figures 3J**, **8A**), postfrontal and postorbital form a new, postocular module (light green) that plotted closer to the posterior skull roof (red) module than to the cheek module (orange). The cheek module is split with the jugal, which is now integrated inside the snout flank module (light purple). Median palate modules (dark pink), together with the braincase modules (yellow), are closer related to skull roof (red and light green) and cheek (orange) modules of both skull sides than to the remaining skull modules, again functionally separating the skull in an anterior and a posterior half.

Like in the *fossafenestral-1* skull model (**Figures 3J**, **8A**), the *fossafenestral-2* skull model (see **Figures 1**–**3A** vs. **Figures 3K**, **8B**) shows a postocular module. In this model, however, cheek (orange) and posterior skull roof (red) module plotted closer to each other than both do to the postocular module (light green) (see white parallel stripes in the figure). Like in the *fossafenestral-1* type, the cheek module is also split with the jugal being integrated inside the snout flank module (light purple). Also, as in this skull type, the *fossafenestral-2* skull is functionally separated in an anterior and a posterior half. However, the median palate module (dark pink)—together with the braincase module (yellow)—is even more strongly integrated between roof and cheek modules (red, blue, and orange) of both skull sides.

Muscle Reconstruction

The reconstructed jaw muscle associations directly correspond to the modular pattern of each skull model (i.e., seven-pointed star in **Figure 3**). In the original skull of †*C. aguti* (*scutal*/anapsid type, **Figure 3A**), the following joined muscles are reconstructed and interpreted to act as functional entity: AMEP with AMES (belonging to the red module), CID with PTV (dark purple), and AMP with AMEM (orange). The identity of AMP of either belonging to the internal or external section of the jaw musculature appears to change among taxa based on altering ontogenetic pathways (Rieppel, 1987; summarized by Werneburg, 2011). As such, an association of muscle portions usually assigned to the internal (AMP) or external (AMEM) section of the jaw adductor is not deceptive.

In †*C. aguti*, the pterygoid teeth reach far posteriorly on the ventral surface (**Figure 2B**), preventing broad insertion of PTV. Whether PTV was actually developed as a small muscle portion or whether it was just a small muscle head inserting on the posterior edge of the pterygoid cannot be determined (see discussion by Witzmann and Werneburg, 2017). A PTD could have been partly associated with CID/PTV—as indicated by the half-connected points of the star in **Figure 3A**—as the related bone module (light pink) was not as strongly integrated in the snout modules as both snout modules are into each other (light and dark purple: close association indicated by two parallel white lines in **Figure 3A**).

Muscular associations are different in all of our skull models (**Figures 3B–K**). In the *infrafenestral-1* model (**Figure 3B**), with the anterior expansion of the posterior skull roof module (red), the following muscular associations are hypothesized based on the modular pattern of related bones: AMES with AMEP (red), AMP with AMEM (orange), CID with PTV. AMP and AMES could had been partly connected due to the related modules showing a strong relation to each other.

In the model *infrafenestral-2* (**Figure 3C**), with the formation of a postocular module (light green) and the integration of the jugal into the snout flank (light purple), the following associations are hypothesized: AMES with AMEP (red), CID with PTV. Based on close modular associations, AMP could be partly related to AMES/AMAP, and AMEM to PTD.

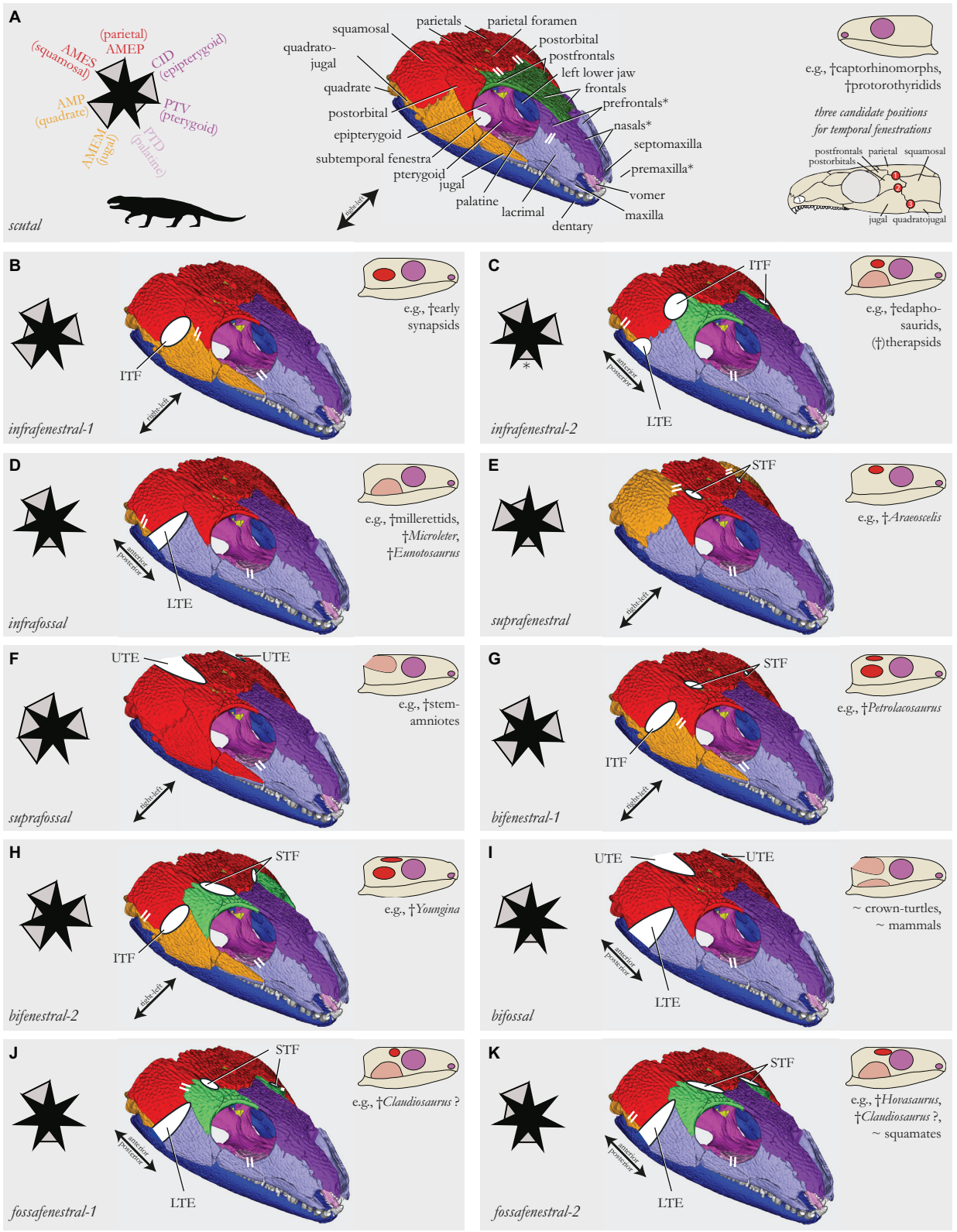

FIGURE 3 | (Continued)

FIGURE 3 | Skull network illustrations of models that simulate different temporal skull morphotypes (see sketches in each subfigure) found in early amniote evolution [based on Abel and Werneburg (2021); *nudital* and *additofenestral* skull types were not possible to model, see text]. The skull of †*Captorhinus aguti* **(A)** was used as model template. Skull models are shown in an anterior dorsolateral view **(B–K)**. Parallel white stripes indicate a closer network relationship of the connected modules when compared to other modules in the anterior (snout) or posterior (temporal) skull half, respectively (compared to dendrograms in **Figures 2E**, **4**–**8**). Modeled temporal fenestrae are shown as white full-ellipses, temporal excavations as white half-ellipses. Star-schemes for each model indicate the differentiation of muscle portions (i.e., the points of the star) inside the jaw adductor chamber [see legend in panel **(A)**; the listed bones serve as major origin sites of these muscle portions; letter coloration based on skull modules]. Muscle portions that putatively act as a joined entity are connected by gray filling between star jags; full filling means that the muscles originate from the same skull module (e.g., red), half filling means that the modules, to which the muscle portions attach, are closely associated to each other in the global anatomical network (compared to dendrograms of **Figures 2E**, **4**–**8**). AMEM, musculus (m.) adductor mandibulae Pars medialis; AMEP, m. adductor mandibulae Pars profundus; AMES, m. adductor mandibulae Pars superficialis; AMP, m. adductor mandibulae posterior; ITF, infratemporal fenestra; LTE, lower temporal excavation; PTD, m. pterygoideus Pars dorsalis; PTV, m. pterygoideus Pars ventralis (perhaps not yet differentiated in †*C. aguti*); STF, supratemporal fenestra; UTE, upper temporal excavation.

In the *infrafossal* model (**Figure 3D**), with the integration of the jugal into the snout flank (light purple), the following association is hypothesized: AMES with AMEP (red). Based on close modular associations, AMP could be partly related to AMES/AMAP, and AMEM to PTD. CID is considered more separate from PTV, because in the skull, which is differentiated in an anterior and a posterior part in overall network composition (**Figure 5A**), the CID-associated epipterygoid might serve a key role in functional anatomy (see section "Discussion").

In the *suprafenestral* model (**Figure 3E**), with the integration of the jugal to the snout flank (light purple) and the integration of the squamosal into the cheek module (orange), following associations are hypothesized: AMES with AMP (orange), CID with PTV (dark purple). AMEP (red) and AMES/AMP (orange) might be partly associated, similar to AMEM (light blue) and PTD (light pink) based on close relationship of the related skull modules.

In the *suprafossal* model (**Figure 3F**), with the expansion of the posterior skull roof module above the whole temporal region (red), the following associations are hypothesized: AMEP with AMES, AMP, and AMEM (red), and CID with PTV (dark pink).

The *bifenestral-1* model (**Figure 3G**) shows the same patterns as the *infrafenestral-1* model (**Figure 1B**).

In the *bifenestral-2* model (**Figure 3H**), with the formation of a postocular module (light green), the following associations are hypothesized: AMEP with AMES (red), AMP with AMEM (orange), and CID with PTV (dark pink). Partial relationship might exist between AMP (orange) and AMES (red).

In the *bifossal* model (**Figure 3I**), with the expansion of the posterior skull roof module to the cheek and postocular region (red) and with integration of the jugal to the snout flank (light purple), the following associations are hypothesized: AMEP with AMES and AMP (red). Partial relationship might exist between AMEM (light purple) and PTD (light pink).

In the *fossafenestral-1* and *-2* models (**Figures 3J–K**), with the formation of a postocular module (light green) and the integration of the jugal into the snout flank (light pink), the following associations are hypothesized: AMEP and AMES (red), and a partial association between AMEM (light purple) and PTD (light pink).

DISCUSSION

Significance of the Anatomical Network Approach

Using the anatomical network approach, we detected seven distinct anatomical modules on each skull side of †*C. aguti* (**Figures 1**–**3A**). These include cheek (orange in Figures), anterior (green) and posterior (red) skull roof, palate wing (light pink), upper snout (purple), snout flank (light blue), and braincase (yellow) modules. In addition, there is a median palate module (dark pink). By modeling changes in skull network composition of †*C. aguti* to mimic skull types of other early amniotes, alterations in the number and fundamental rearrangements in the respective bone composition of skull modules occur, illustrating the sensitivity of the anatomical network approach.

When trying to interpret the functional meaning of module composition, one needs to keep in mind the methodological basis of network analysis which considers as data source just the information on presence and absence of bone connections (1/0 codification) but neglects any detailed morphological characteristic such as suture type, thickness, and gross anatomy of bones. Each level of morphological organization, however, conveys different information, and to understand processes in evolution, each may first be treated separately (Rasskin-Gutman, 2003) before expanding toward a more holistic view on anatomical tissue integration (Maier and Werneburg, 2014). The functional meaning of skull modules, of course, has to be handled with care, and discussion always requires a thorough consideration of other morphological aspects known for the taxon in question and comparable organisms (Werneburg et al., 2019).

Functional considerations of skull anatomy cannot be performed without proper knowledge on muscle anatomy, which is usually barely described in the literature for extant taxa and usually misses relevant information of muscle fiber-compositions and orientations and tendinous components. For extinct taxa, only gross morphology of musculature can be reconstructed on a rough anatomical level, mainly based on phylogenetic bracketing and by considering indications of possible attachment sites on bones (Witzmann and Werneburg, 2017). Nevertheless, anatomical network methodology has been proven to provide basis for reasonable functional conclusions and new hypotheses (Esteve-Altava et al., 2013a,b, 2015a;

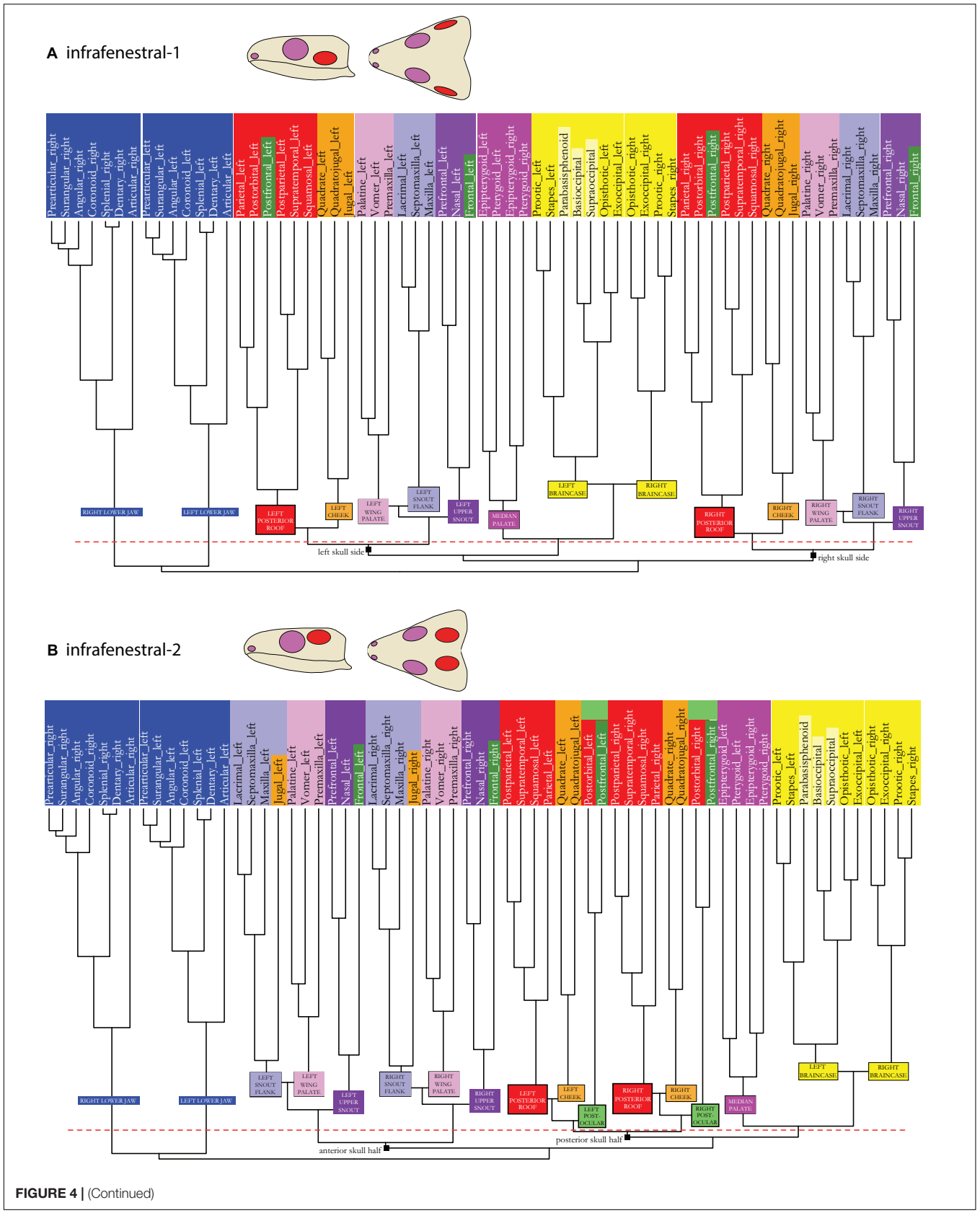

FIGURE 4 | (Continued)

FIGURE 4 | Dendrogram of the skull network of **(A)** the *infrafenestral-1* and **(B)** the *infrafenestral-2* skull types. Compare to caption of **Figure 2E**. The basal dichotomies in left and right skull side **(A)** or in an anterior and a posterior skull part **(B)** are indicated in the dendrogram.

Rasskin-Gutman and Esteve-Altava, 2014; Diogo et al., 2015; Molnar et al., 2017; Lee et al., 2020; Plateau and Foth, 2020; Sookias et al., 2020).

Rasskin-Gutman (2003) provided a first attempt to study skull modularity in relation to temporal openings and found, by comparing nine different tetrapod skulls, that the orbit is surrounded by a rather simple modular arrangement with one element attaching to at least three other adjacent elements. In contrast, the temporal region is rather complex with bones having five or six contacts to other bones which are, eventually, surrounded by bones with triangular connections again. He also found that the snout is less variable in regard to network connections than the postorbital region, which overlaps with the known morphological and trophic diversity of extant taxa (see also Werneburg et al., 2019). As such, the complexity of the anatomy network might provide a reasonable source to understand patterns of functional morphology, in which jaw muscle anatomy it taken into account.

Cranial Kinesis in †*Captorhinus aguti* With Respect to Skull Modularity

Studying the suture anatomy and thickness of dermatocranial bones, Abel et al. (2022) discussed cranial kinesis in †*C. aguti*. The authors discussed metakinesis—a movement of the temporal dermatocranium together with the snout relative to the braincase (Iordansky, 1990)—to be present between parietal/postparietal and supraoccipital and between squamosal and opisthotic. In fact, a metakinetic joint was likely widespread among early amniotes (Carroll, 1969; Gow, 1972; Bramble and Wake, 1985; Iordansky, 1990). This is further supported by the modularity pattern detected in the present study, in which the braincase elements (yellow) are separated from all other skull modules, including the posterior skull roof module with the squamosal (red) and the anterior skull roof module with the frontal (dark green).

Squamosal and parietal are plotted closely within the posterior skull roof module (red). Consequently, a representation of the ancestral "crossopterygian hinge line" (Kemp, 1980) between squamosal and more dorsal bones of the skull roof, which temporarily might have been opened posteriorly as an otic notch in early tetrapods (but see Panchen, 1964), cannot be postulated herein. However, the suture between both elements in †*C. aguti* is not very strong (Abel et al., 2022), which might be mirrored in the even closer modular relationship of the parietal to the postorbital in our reconstruction (**Figure 2E**).

Interdigitation and great thickness of the frontoparietal suture most likely prevented true joint and elasticity-based (sensu Natchev et al., 2016) mesokinetic movement in between the skull roof elements that otherwise could have been moved against each other by the contraction of m. adductor mandibulae externus Pars profundus (AMEP) (Abel et al., 2022). Frontal (dark green) and parietal (red), however, belong to different modules in the skull illustrating that clear modular distinctions between bones must not necessarily indicate a kinetic association of them. Nevertheless, mesokinesis, as widely found in squamates (Iordansky, 2011), might be an evolutionary result from the intersection between the posterior skull roof module (red) and the more anterior dorsal skull bones (dark green and dark purple) already established in an early amniote like †*C. aguti*. In fact, all models with temporal openings (**Figures 3B–K**) show a clear distinction between the posterior skull roof module (red) and the upper snout modules, the latter of which always includes the frontal bone (dark purple), and as such, this condition then might further favor mesokinetic evolution.

A pleurokinetic joint—a mediolateral movement of the quadrate relative to the rest of the skull (Evans, 2008)—was present in †*C. aguti* between quadrate on the one hand and pterygoid, quadratojugal, and squamosal on the other hand, being enabled by the contraction of musculus (m.) adductor mandibulae posterior (AMP) (Abel et al., 2022). In the present modularity study, the quadrate of †*C. aguti* belongs to the cheek module (orange), clearly separated from pterygoid (dark pink) and squamosal (red). Only the quadratojugal (in addition to the jugal) is found to share a modular identity with the quadrate. Apparently, a shared modular identity does not necessarily preclude internal kinetics within a module. The reportedly thin bones of the cheek region (Fox, 1964) likely permitted a certain elasticity of that region, driven by contraction of m. adductor mandibulae Pars medialis (AMEM; sensu Abel et al., 2022) and Pars superficialis (AMES).

Kinesis within the snout (prokinesis and rhynchokinesis) was certainly not possible based on the strong suturing of the snout bones (maxilla, lacrimal, and jugal). Bite forces were likely absorbed by the more elastic sutures in the more dorsal snout bones, namely, between nasal and prefrontal (Abel et al., 2022). Herein, an absorption of biting forces in the upper snout is further supported by the presence of an upper snout module (dark purple) ventrally separated from the snout flank (light purple). The frontal and prefrontal contact is characterized by a simpler (although still thick) suture, that could indicate that this region is less effected by compressional forces (sensu Abel et al., 2022).

A mobility of the palate, a feature that first evolved toward Amniota (Carroll, 1969), was likely possible in †*C. aguti* given the small relative thickness and simple suture types between vomer, palatine, and pterygoid. Also, a potential kinetic articulation between palatine and maxilla was present (Fox and Bowman, 1966; Abel et al., 2022). The latter pattern is mirrored in the modularity of the palate with the elastic vomer and palatine forming a module together with the premaxilla, which functionally belongs to the palatal wing (light pink).

Pro- and retraction of the palate in relation to the rest of the skull might have been enabled by the pterygoid-associated epipterygoid as a basicranial articulation of the

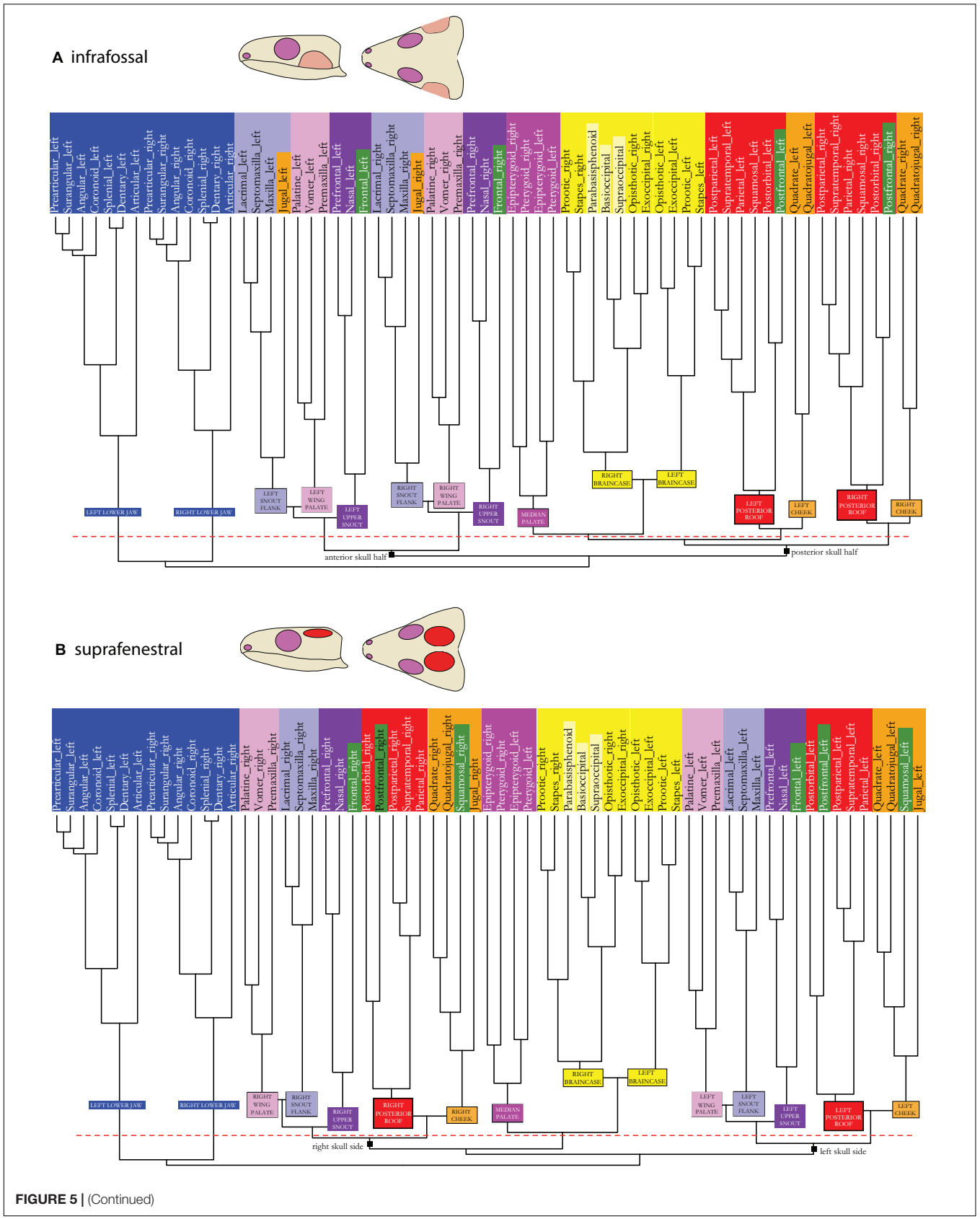

FIGURE 5 | (Continued)

FIGURE 5 | Dendrogram of the skull network of **(A)** the *infrafossal* and **(B)** the *suprafenestral* skull types. Compare to caption of **Figure 2E**. The basal dichotomies in left and right skull sides **(A)** or in an anterior and a posterior skull part **(B)** are indicated in the dendrogram.

epipterygoid to the braincase and a kinetic articulation between palatine and maxilla were present (Abel et al., 2022). Pterygoid and epipterygoid together form a distinct module by their own reflecting their positional intersection between many skull modules and their various moveable and non-moveable articulations with other elements.

In sum, the observations in †*C. aguti* illustrate a relatively good association of cranial kinesis and skull modularity, although both relative thickness and suture type between adjacent bones require a balanced consideration of functional skull morphology (Esteve-Altava, 2017a).

†*Captorhinus aguti* and the Origin of Temporal Skull Openings in Amniotes

It has been repeatedly discussed that particularly thin skull areas are prone to reduction as little forces are acting on these regions (e.g., Jaeckel, 1902; Case, 1924; Romer and Price, 1940; Fox, 1964). Temporal skull openings appear to develop particularly at the intersection between three adjacent bones (Frazzetta, 1968; Kuhn-Schnyder, 1980). Taking †*Captorhinus aguti* as a model, Abel et al. (2022) highlighted the intersections of (1) postorbital, squamosal, and parietal, of (2) jugal, squamosal, and postorbital, and of (3) jugal, squamosal, and quadratojugal as candidate areas for temporal openings in early amniote evolution (see also image with numbers in **Figures 1E, 3A**). In the following, we use the modularity pattern in †*C. aguti* to infer potential areas for temporal openings.

(1) As mentioned above, the ancestral "crossopterygian hinge line" between squamosal and more dorsal skull roof bones could not be recovered in †*C. aguti* herein, because both elements belong to one single module (red). This could indicate that the structural lability of the "crossopterygian hinge line" was stabilized in early amniotes by a close integration of both elements. Nevertheless, †*C. aguti* is still characterized by weak suturing between squamosal and parietal (Abel et al., 2022). As such, this suture could have served as potential origin area of the supratemporal opening later on in evolution ("1" in **Figures 1E, 3A**), as visible in diapsid species, or even - as discussed by Kemp (1980) - as an area that opened to allow dorsal expansion of the infratemporal region in therapsid synapsids.

(2) The modular distinction between jugal (orange) and postorbital/squamosal (red), together with the edge-like geometry of this intersection, makes this area a preferred candidate for the widely occurring infratemporal opening ("2" in **Figures 1E**, **3A**). Force vectors of AMEM (orange) and AMEP (red) musculature, pointing in different directions, will have further triggered the emergence of that opening.

(3) Similar to (2), the relatively rarely occurring opening between quadratojugal, jugal, and squamosal ("3" in **Figures 1E**, **3A**) might mainly result from the intersection of two modules (red and orange), specific arrangements of surrounding musculature (i.e., AMEM, AMES), plus the structural dissolution of the edge-like geometry of this intersection. This edge, however, is less pointy than in (2), which might explain the rare occurrence of this opening. Whether the infratemporal openings (2) and (3) actually have separated phylogenetic origins and whether they emerge from one unique opening or unite to one opening in the respective taxa cannot be evaluated herein. We rather expect the whole sutural area between squamosal and jugal to serve as potential *region* for any infratemporal opening (**Figure 1E**: indicated by white dashed line around "2" and "3"), depending on species-specific configurations and compositions of the surrounding temporal bones. In species with reduced quadratojugal, for example, a more dorsal position of the opening is common (Kemp, 1982).

Rasskin-Gutman (2003) distinguished between "active and passive fenestrae" in the vertebrate skull. Whereas "active" ones between three adjacent bones (i.e., foramina) cannot close because they surround other ("active") tissue like nerves or vessels, the "passive" ones in between four or more bones remain stable ("passive") along a phylogenetic lineage as long as no heterochronic event (relative growth in ontogeny) closes that opening. As such, to better understand transformations in temporal architecture, a greater focus on ontogenetic studies (Rieppel, 1984; Haridy et al., 2016; Werneburg, 2019; Lee et al., 2020) are urgently needed in the future.

As extensively discussed by Abel et al. (2022), taking †*C. aguti* as a model for early temporal skull evolution in amniotes has its limitations given the already derived skull anatomy of this species compared to the assumed ancestral amniote. Nevertheless, indications from their study on suture anatomy plus the present support of modularity patterns provide a reasonable chain of argumentations to understand the origin of temporal openings in early amniotes. To further explore such evolutionary modifications, the modeling of different skull types, as performed in this study, provides a valuable framework to examine the complexity of cranial changes associated with temporal fenestrations.

Modeling Temporal Openings

Modeling temporal openings into the skull network of †*C. aguti* of course comes with limitations. Obviously, there are no taxa in the fossil record that correspond to a fenestrated variant of †*C. aguti*. Skull proportions along with bone number, suture lengths, and suture anatomy can drastically differ in early amniote species with temporal openings when compared to †*C. aguti*. At this point, the above-mentioned simplification of the anatomical network methodology might actually be of a certain advantage as skull proportions and suture morphology are not considered in that approach.

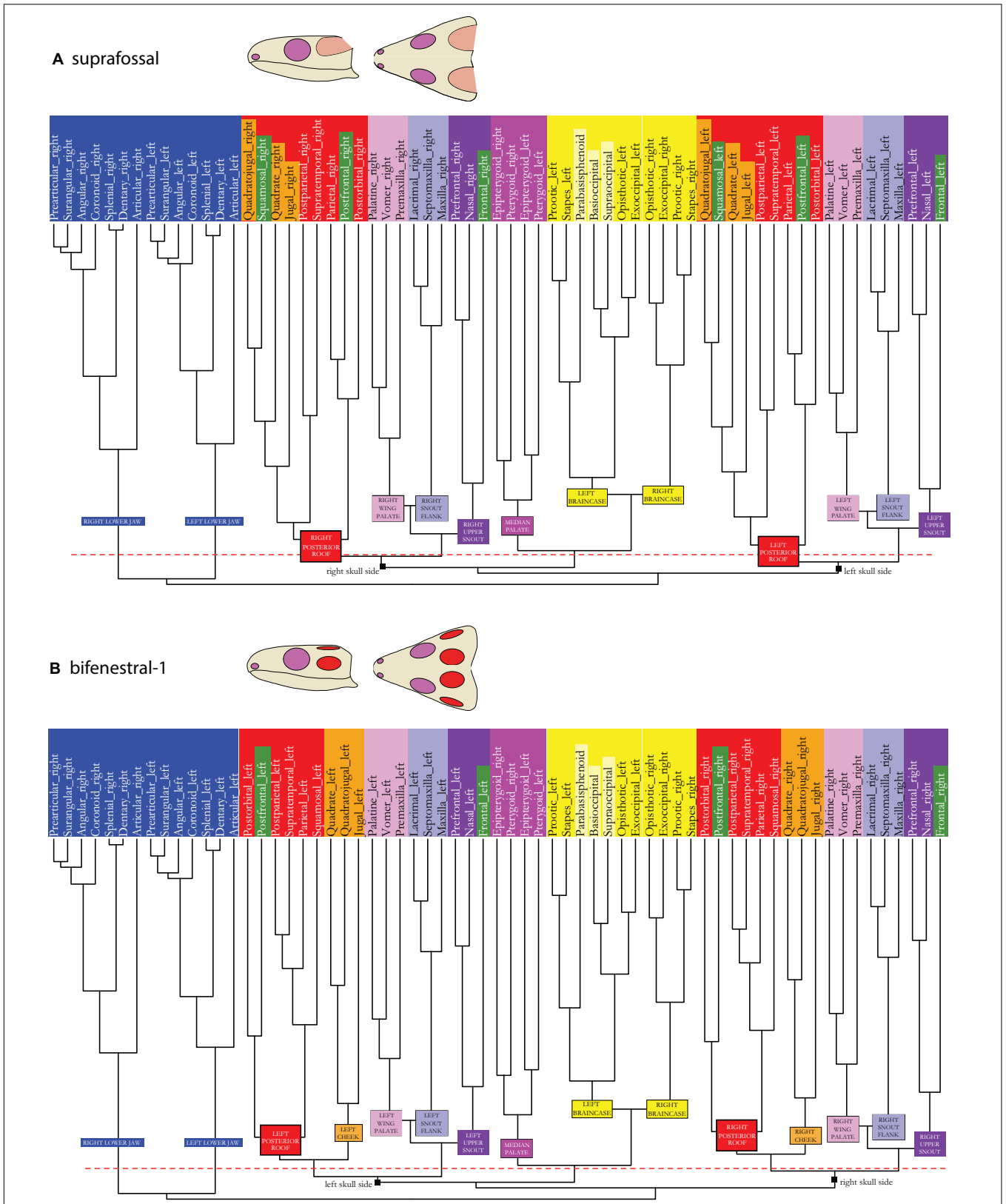

FIGURE 6 | (Continued)

FIGURE 6 | Dendrogram of the skull network of **(A)** the *suprafossal* and **(B)** the *bifenestral-1* skull types. Compare to caption of **Figure 2E**. The basal dichotomies in left and right skull sides are indicated in the dendrogram.

In our models, we kept the number of skull bones and their general connectivity stable to enable direct comparisons between the †*C. aguti* network and the skull models derived from them. However, some bones, postparietal, supratemporal, and septomaxilla in particular (Gaffney, 1990; Koyabu et al., 2014; Higashiyama et al., 2021), are known to get reduced through amniote evolution (Esteve-Altava et al., 2013b). Nevertheless, most early amniotes, which are the focus of our study, still have these bones preserved. Moreover, bones usually do not get lost as such. Particularly, during ontogeny, their ossification centers generally fuse to 'larger' bones (Klembara et al., 2002; Polachowski and Werneburg, 2013; Koyabu et al., 2014; Werneburg et al., 2015; Smith-Paredes et al., 2018), and coding their presence and ancestral connection to "larger" bones, argumentally, can be judged as a reasonable methodological approach to retain comparability in this study.

In our opinion, the only major limitation of our model-comparison is the fact that some early amniotes still have a tabular bone and an ectopterygoid. Most captorhinids, including †*C. aguti*, lack them (e.g., Clack and Carroll, 1973; Berman and Reisz, 1986; Dodick and Modesto, 1995; Müller and Reisz, 2005) and they were, hence, not modeled herein. In this regard, we again highlight the hypothetical character of any model in this study to understand the basic structural relationships inside the amniote skull.

Anatomical network analysis with actual species instead of models should be performed in the future to test and specify our initial attempts. These species would need a comparable observation of suture anatomy (Jones et al., 2011) and muscle reconstruction before, as has been done for †*C. aguti* (Abel et al., 2022). Fossil preservation of early amniotes, however, is poor in many cases and bone connections can be hard to reconstruct.

Evolutionary Changes in Functional Skull Morphology Induced by Temporal Openings

The Palate Is Functionally Associated With Changes in the Temporal Skull Region

The modeling of temporal openings into the anapsid skull (**Figure 3A**; *scutal* skull after Abel and Werneburg, 2021) results in a number of changes in the composition of skull modules. The most frequent skull opening in early amniotes was an infratemporal fenestra (ITF in **Figure 3**), modeled as disconnection between jugal and squamosal herein (**Figures 1A,C**: B-cut; *intrafenestral-1* type). Whereas the modularity of the manipulated temporal skull coverage stays mainly unaltered, the snout flank (light purple) becomes more integrated with the palate wing (light pink) (**Figures 3B**, **4A**). This might be interpreted by a more posterior and, through a shorter lever arm, by a more powerful processing of food items in the center of the mouth. In fact, early synapsids are usually considered to have fed on hard food items associated with carnivore or herbivore feeding (Kemp, 1982; Werneburg, 2019). To process those, they might have been selected for a more powerful jaw adductor musculature. As illustrated herein (seven-pointed star in **Figure 3B**), this might have been permitted by up to four muscle portions acting in union, i.e., AMP, AMEM, AMES, and AMEP.

A close integration of the snout flank (light purple) and the palate wing (light pink) is actually found in all modeled skulls, indicating a general adaptation to different food processing in amniotes when compared to their ancestors with further specifications by positional alteration or addition of opening(s) in the respective taxa. In therapsid synapsids, for example, a strong integration of snout and palate is related to the formation of a secondary palate introduced by neonatal lactation (Maier, 1999) along with a more effective carnivore and herbivore feeding behavior, which required a strengthened palatal region. This change in therapsids was associated with a dorsal shift and expansion of the infratemporal fenestra (ITF) and a lower temporal excavation (LTE) (Abel and Werneburg, 2021). Change in jaw muscle integration might be correlated with the observed bone modularity. With the development of a masseter muscle (i.e., AMEM-related following the argumentation of Abel et al., 2022) and an associated loss of the quadrate from the temporal region (i.e., it moves as incus to the middle ear; Werneburg, 2013b), chewing behavior emerged in cynodont therapsids (Abdala and Damiani, 2004). The adjusted side and inward movements during chewing could actually be mirrored in the postulated functional union of AMEM (masseter) and PTD musculature (asterisk in **Figure 3C**). The greater stability of the skull by formation of a secondary palate to withstand higher suckling and biting forces is also associated with the successive integration of the epipterygoid (as alisphenoid) to the secondary braincase wall toward Mammalia (Maier, 1989, 1999). The certain independency of the median palate module (dark pink) to which the epipterygoid belongs in the anatomical network might have been, in this case, a precondition to uncouple this element from the palate.

The anatomical network modularity of an extant omnivorous mammal (*Didelphis virginiana*: Werneburg et al., 2019), which resembles the *infratemporal-2* skull type, shows a certain similarity to our *infratemporal-2* model in the way that the jugal and palatal region belong to the same module. Noteworthy, the fusion of the orbit with the infratemporal opening in that species has major impact on the modularity of the anterior and posterior dermal skull region. The latter is forming one consistent module with the braincase. This becomes obvious when comparing the results for *D. virginiana* to the pattern observed in primates, in which the postorbital bar is present and the frontal changes its modular association (Esteve-Altava et al., 2015a,c). Changing just one connection in the skull has major impact on general modular compositions.

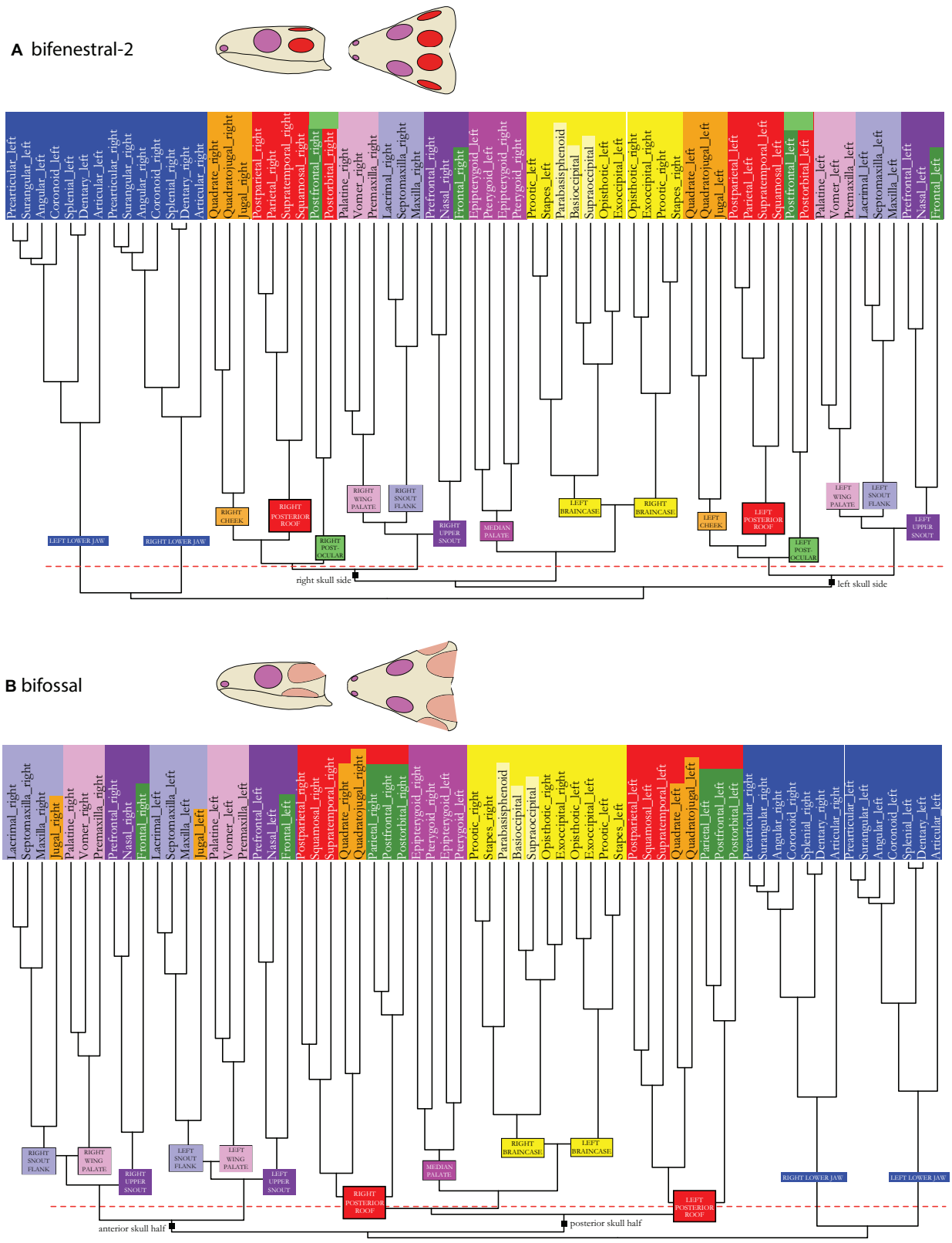

FIGURE 7 | (Continued)

FIGURE 7 | Dendrogram of the skull network of **(A)** the *bifenestral-2* and **(B)** the *bifossal* skull types. Compare to caption of **Figure 2E**. The basal dichotomies in left and right skull sides (A) or in an anterior and a posterior skull part (B) are indicated in the dendrogram.

Convergent Evolution of Stronger Bite in Terrestrial Habitats

The modeling of a lower temporal excavation (LTE) in the skull (**Figure 3D**; *infrafossal* type) results in the integration of the jugal into the snout flank module (light purple), suggesting a more powerful initial capture of hard food items anteriorly in a robust snout, possibly imaginable for †*Eunotosaurus africanus* (Watson, 1914; Keyser and Gow, 1981) and other extinct taxa with similar temporal skull arrangement (e.g., †*Llistrofus*, †*Microleter*, †*Millerosaurus*, †*Milleropsis*). Further food manipulation more posterior in the mouth, for instance by positioning of the food item before swallowing using pterygoid teeth (Gow, 1997), might have been more complex. With the formation of a lower temporal excavation, the overall network integrity falls into an anterior and a posterior skull part (double-headed arrows in **Figures 3C,D**), which could hint to a more important role of the epipterygoid bone (dark pink) as pivot point between them, as indicated by a more independent related CID-musculature in our muscle reconstruction.

The presence of only a supratemporal fenestra (STF), like in the early diapsid †*Araeoscelis,* resulted in a dorsal expansion of the cheek module toward squamosal (orange) (**Figure 3E**; *suprafenestral* type). †*Araeoscelis* "exhibits a suite of unusual cranial features resulting in a massive, sturdily constructed skull, which is interpreted as an adaptation to a specialized diet that probably included invertebrates protected by heavy exoskeletons" (Reisz et al., 1984, p. 57). To enable this strong bite, according to the detected modularity pattern, AMES, AMP, and AMEP on the one hand, and AMEM and PTD on the other hand might have separately worked as unions. The comparison with heavy-snouted *infrafossal* taxa from the Permian (Abel and Werneburg, 2021) shows that different "experimentations" of temporal region anatomy were performed in early amniote evolution to exploit similar food resources that now became available in fully terrestrial habitats.

The presence of an upper temporal excavation (UTE) (**Figure 3F**, *suprafossal* type) results in the greatest expansion of the posterior roof module (red), suggesting high biting forces by joined action of AMEP, AMES, AMP, and AMEM. The otic notch in some potential stem-amniotes like Seymoriamorpha mirrors the modeled upper temporal excavation (Klembara, 1997, 2011). It is likely that these animals were already adapted to a more or less full terrestrial life style with a focus on hard terrestrial food items. Also, strong biting turtles such as Chelydridae, Pelomedusidae, and Platysternidae (Herrel et al., 2002; Ferreira et al., 2020) develop deep upper temporal excavations (posterodorsal emarginations in turtle anatomical terminology *sensu* Werneburg, 2012).

From Robust to Agile—and Back to Robust Prey: Diapsid Evolution

The presence of two temporal openings (*bifenestral-1* and *-2*) as seen in some early diapsids (**Figure 3G**: †*Petrolacosaurus*, **Figure 3H**: †*Youngina*) shows a cheek integration (orange) comparable to that of early synapsids (**Figure 3B**) with AMEP, AMES, AMP, and AMEM acting in union. This could highlight the generally stronger bite and, hence, better adaptation to terrestrial food in both diapsids and synapsids when compared to non-fenestrated early amniotes like †*C. aguti*.

Early diapsids are thought to have been adapted to feeding on agile prey (Evans, 2008), for which an increased intracranial mobility was necessary (see discussion further below). More crownward diapsids (Lee et al., 2020; Plateau and Foth, 2020) differ from the modeled early diapsids. Differences are likely associated with a change to a more carnivorous feeding behavior as exemplified in archosauriform evolution with †*Euparkeria capensis* representing a transitional form (Sookias et al., 2020) or †*Tyrannosaurus rex* showing specific snout adaptations (Werneburg et al., 2019). The relatively larger snouts, together with the orbits, increasingly restricted the space for the temporal region through archosaur evolution. Related to strong bites and long snouts, the pterygoid musculature in crocodiles dominates above the external jaw adductors with influence on bone arrangements and modularity in the respective regions as illustrated by *Alligator mississippiensis* (Werneburg et al., 2019).

The textbook example of an extant diapsid, the tuatara *Sphenodon punctatus* (Lepidosauria), is also highly derived in its skull network modularity (Werneburg et al., 2019) when compared to the herein modeled early diapsid forms. Tuatara secondarily re-evolved the lower temporal arcade (Müller, 2003) and has a number of other derived characters. The degree of its intracranial mobility is debated and seems to depend on ontogenetic changes with, likely, less mobile skulls and stronger bites in adults (Jones et al., 2011; Werneburg and Yaryhin, 2019).

The Never-Ending Turtle Story

The *bifossal* model (**Figure 3I**) resembles a morphotype that is basically established in the turtle crown-group (Werneburg, 2012), a group that reportedly shows several derived characters compared to the ancestral amniote and even to the ancestral turtle condition (Müller, 2003; Joyce, 2007). Hence, the limitation mentioned above for interpreting a network model also applies, particularly, when discussing the turtle skull morphotype. Nevertheless, the simplification in the network methodology permits a comparison to other models.

Compared to †*C. aguti*, the jugal in the *bifossal* model becomes part of the snout flank module (light purple), mirrored by the general robusticity of the snout in turtles, which is ancestrally covered by an edentulous beak (Li et al., 2018). The remainder of the temporal region forms one consistent module (red) likely related to a union of AMEP, AMES, and AMP (**Figure 3I**). In fact, jaw musculature in turtles is (superficially) less diverse than that of all other extant reptilian groups (Schumacher, 1956; Werneburg, 2011, 2013a,b).

With the formation of a deep ventral excavation, the skull network, again, separates into an anterior and a posterior skull part. Whereas this feature resulted in a supposedly

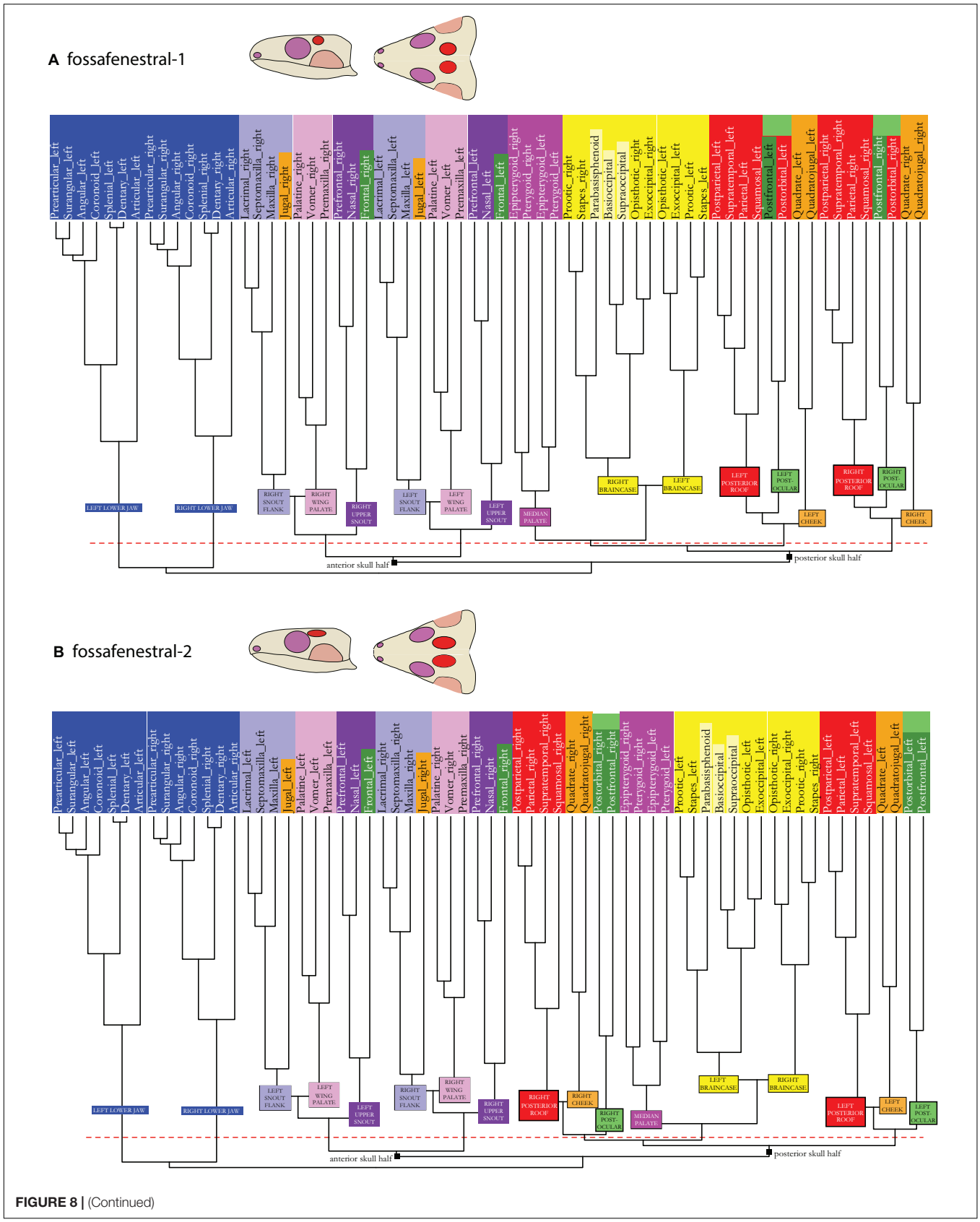

FIGURE 8 | (Continued)

FIGURE 8 | Dendrogram of the skull network of **(A)** the *fossafenestral-1* and **(B)** the *fossafenestral-2* skull types. Compare to caption of **Figure 2E**. The basal dichotomies in an anterior and a posterior skull part are indicated in the dendrogram.

higher independency and mobility of the epipterygoid (dark pink) in taxa like millerettids, †*Microleter*, and †*Eunotosaurus* (**Figure 3D**), the epipterygoid is either lost (Pleurodira) or integrated (Cryptodira) into the secondary braincase wall in crown-turtles (Werneburg and Maier, 2019), decoupling this element from other skull modules (which is associated with the loss of CID musculature in turtles; see Werneburg, 2011) and resulting in an akinetic skull (Werneburg and Maier, 2019). As has been shown by Ferreira et al. (2020), the jaw muscle arrangement and the skull shape of modern turtles is associated with fundamental cranial changes related to the evolutionary increase of neck mobility. Jaw muscle functionality can be seen as a tradeoff between restrictions in space for jaw musculature in the jaw adductor chamber and the retention (but not increase) of the ancestral jaw muscle power. While the jaw musculature of turtles is rather simple in superficial view, it internally shows great tendinous differentiation, which might reflect the concealed anatomical response to that restriction (Schumacher, 1956; Werneburg, 2011, 2013b).

The expansion of the posterior skull roof module (red) in the *bifossal* turtle skull can be associated with a higher integration related to neck mobility. Tensional force of the retracting neck is related to enlarged temporal emarginations (Werneburg, 2012, 2015) and might be buffered by a broadly integrated temporal region (Werneburg et al., 2021).

The leatherback turtle, *Dermochelys coriacea* (Werneburg et al., 2019), largely reduced its ability to retract the neck and, hence, no posterodorsal emarginations are developed in the skull (*sensu* Werneburg, 2015). Notably, in the anatomical network reconstructed for this species, only an integration of frontal and parietal, but not of the cheek region, is present. The close association of frontal and parietal can be interpreted by a still certain degree of embryonic neck muscle tension acting on the roof of its developing skull (Werneburg and Maier, 2019; Werneburg et al., 2021). Different to our model (**Figure 3I**), an ancestral integration of the jugal into the cheek module (orange) is present in the leatherback. This can be interpreted by the specific arrangement of bones, related to unique characters such as a truncated snout and a domed skull in this marine turtle species (Nick, 1912; Schumacher, 1972; Werneburg et al., 2019).

Notably, the *bifossal* skull type (**Figure 3I**) is also present in the akinetic mammals, although the upper temporal excavation derives from an expanded upper temporal fenestra and not by marginal bone reductions (Werneburg, 2019). The convergent separation in an anterior and a posterior skull part and a related simplification of skull network composition (Werneburg et al., 2019) is stunning.

Toward Highly Kinetic Skulls

Whether a *fossafenestral-1* type (**Figure 3J**) was actually developed in †*Claudiosaurus* is debatable based on whether and how much the postfrontal actually contributed to the upper temporal opening (Carroll, 1981). Nevertheless, when compared to the *fossafenestral-2* type (**Figure 3K**), in which the upper temporal opening expands more anteriorly, the general size-influence of an opening becomes obvious, as in this example the posterior skull roof module (red) changes its global modular association (see dendrogram in **Figure 8B** and white parallel stripes in **Figure 3K**).

Among early amniotes, the *fossafenestral-2* type is likely present in †tangasaurids (Bickelmann et al., 2009) and basically represents the skull type found among the neodiapsid squamates. Whenever an upper temporal fenestra is formed together with a lower temporal excavation (**Figures 3C,J–K**), a postocular module (light green) emerges. The same is true for the *bifenestral* skull, in which the supratemporal fenestra is anteriorly expanded (*bifenestral-2* type; **Figure 3H**) as is known for †*Youngina* among early amniotes. Different muscle portions that mainly attach to other bones (star in **Figure 3A**) can partly originate or insert also to the postorbital in extant reptiles (Holliday and Witmer, 2007; Werneburg, 2013a). Having a postocular skull module (light green), which includes postorbital and postfrontal, could indicate to more independent differentiation of those muscle fibers attaching there. Consequently, number and effective direction of muscle vectors will change. As virtually all external adductor muscles insert to the lower jaw, a more complex positioning of agile prey in the mouth can be assumed, as reflected by the insectivorous diet of many taxa with *fossafenestral-2* skull anatomy (i.e., squamates), but also in taxa with *infrafenestral-2* skulls, such as therapsids, which are "on their way" to develop chewing behavior with increased jaw mobility.

The infratemporal openings of *fossafenestral* forms, again, split the skull in an anterior and a posterior part. The epipterygoid (dark pink), with its reconstructed independent CID musculature, could, again, serve as pivot point, in these taxa and enable amphikinetic skull movements (Iordansky, 1990, 2011). In all models described, and in †*C. aguti*, the epipterygoids and pterygoids with their associated musculature form a single module (dark pink), suggesting that they might act together. Whereas the epipterygoid is originally used as lever arm to move the palate in anteroposterior direction—which might still be the case in most taxa—it appears to further act in positioning the pterygoid when handling diverse food items in *bifenestral-2* and *fossafenestral* skulls. In this regard, the former, represented by †*Youngina*, represents a transitional state toward the highly kinetic skull of squamate reptiles.

CONCLUSIONS

Our study tackles one of the big questions in vertebrate evolutionary morphology, namely, the evolution and functional meaning of temporal skull openings in amniotes. Although the used anatomical network theory has a number of limitations due to its simplifying methodology, it allows strategical comparisons among different anatomical models. A careful evaluation of the

observed outcome is necessary and requires a comprehensive morphological discussion.

Here, we modeled the presence or absence of temporal openings into a given skull network to observe the effect on module composition. We demonstrated that changes in the number, position, and expansion of temporal openings have fundamental impact on skull modularity. This is interpreted mainly in regard to feeding behavior in amniotes, where the assumed hardness and agility of prey items are considered. Changes in temporal openings and the resulting skull modules also have impact on cranial kinesis.

The present discussion is highly speculative and remains at a modeling level. It should be understood as a first attempt to interpret complex skull modularity in early amniotes. Obviously, actual skulls need to be studied and coded to get a clearer picture of network modularity in early amniote skulls. By presenting the skull network modularity of the well-known †*C. aguti*, we provide a first attempt in this direction.

A comparison with crown-group amniote skulls, finally, supports the basic functional assumptions that we have derived from our modeling approach. Influenced by changed feeding adaptations and associated changes in skull architecture, however, secondary alterations from the ancestral amniote skull network conditions evolved in crownward taxa. Detecting and describing general patterns of changes across amniote evolution is a desirable outlook on future broad scale taxonomic analysis using the anatomical network methodology.

DATA AVAILABILITY STATEMENT

The original contributions presented in the study are included in the article/**Supplementary Material**, further inquiries can be directed to the corresponding author.

AUTHOR CONTRIBUTIONS

IW: conceptualization, data interpretation, figure preparation, and writing. PA: data acquisition, analysis, and careful annotations on the manuscript. Both authors contributed to the article and approved the submitted version.

ACKNOWLEDGMENTS

We wish to thank Borja Esteve-Altava (Heidelberg), Gerardo Antonio Cordero (Lisbon), and Oleksandr Yaryhin (Plön) for discussion on AnNA-methodology. Diego Rasskin-Gutman and Eduardo Ascarrunz are thanked for critical reading and suggestions to improve the article. This study was supported by DFG-fund WE 5440/6-1 granted to IW.

SUPPLEMENTARY MATERIAL

The Supplementary Material for this article can be found online at: https://www.frontiersin.org/articles/10.3389/fevo.2021.799637/full#supplementary-material

REFERENCES

Abdala, F., and Damiani, R. (2004). Early development of the mammalian superficial masseter muscle in cynodonts. *Palaeontol. Afr.* 40, 23–29.

Abel, P., Pommery, Y., Ford, D. P., Koyabu, D., and Werneburg, I. (2022). "Skull sutures and cranial mechanics in the Permian reptile *Captorhinus aguti* and the evolution of the temporal region in early amniotes," In *The Temporal Region of the Tetrapod Skull Research History, Evolution, and Functional Backgrounds. Dissertation* (Tübingen: University of Tübingen).

Abel, P., and Werneburg, I. (2021). Morphology of the temporal skull region in tetrapods: research history, functional explanations, and a new comprehensive classification scheme. *Biol. Rev.* 96, 2229–2257. doi: 10.1111/brv.12751

Berman, D. S., and Reisz, R. R. (1986). Captorhinid reptiles from the Early Permian of New Mexico, with description of a new genus and species. *Carnegie Mus. Nat. Hist.* 55, 1–28.

Bickelmann, C., Müller, J., and Reisz, R. R. (2009). The enigmatic diapsid *Acerosodontosaurus piveteaui* (Reptilia: Neodiapsida) from the Upper Permian of Madagascar and the paraphyly of "younginiform" reptiles. *Can. J. Earth Sci.* 46, 651–661. doi: 10.1139/E09-038

Bolt, J. R. (1974). Evolution and functional interpretation of some suture patterns in Paleozoic labyrinthodont amphibians and other lower tetrapods. *J. Paleontol.* 48, 434–458.

Bolt, J. R., and Rieppel, O. (2009). The holotype skull of *Llistrofus pricei* Carroll and Gaskill, 1978 (Microsauria: Hapsidopareiontidae). *J. Paleontol.* 83, 471–483. doi: 10.1666/08-076.1

Boonstra, L. D. (1952). N nuwe soort van tapinocephalide deinocephaliër *Struthiocephalus akraalensis* sp. nov. *South Afr. J. Sci.* 48, 247–248.

Bramble, D., and Wake, D. (1985). *Feeding Mechanisms of Lower Tetrapods. In: Functional Vertebrate Morphology*. Cambridge: Harvard University Press, 230–261. doi: 10.4159/harvard.9780674184404.c13

Broom, R. (1922). On the Temporal Arches of the Reptilia. *Proc. Zool. Soc. Lond.* 92, 17–26. doi: 10.1111/j.1096-3642.1922.tb03297.x

Burne, R. H. (1905). Notes on the muscular and visceral anatomy of leathery turtle (*Dermochelys coriacea*). *Proc. Zool. Soc. Lond.* 75, 291–324. doi: 10.1111/j.1469-7998.1905.tb00001.x

Carroll, R. L. (1969). Problems of the origins of reptiles. *Biol. Rev.* 44, 393–432. doi: 10.1111/j.1469-185X.1969.tb01218.x

Carroll, R. L. (1981). Plesiosaur ancestors from the Upper Permian of Madagascar. *Philos. Trans. R. Soc. Lond. Ser. B Biol. Sci.* 293, 315–383. doi: 10.1098/rstb.1981.0079

Case, E. C. (1898). The significance of certain changes in the temporal region of the primitive Reptilia. *Am. Nat.* 32, 69–74. doi: 10.1086/276778

Case, E. C. (1911). *A Revision of the Cotylosauria of North America*. Washington: Carnegie Institution of Washington. doi: 10.5962/bhl.title.45604

Case, E. C. (1924). A possible explanation of fenestration in the primitive reptilian skull, with notes on temporal region of the genus *Dimetrodon*. *Contrib. Mus. Geol. Univ. Mich.* 2, 1–12.

Cisneros, J. C., Damiani, R., Schultz, C., da Rosa, Á, Schwanke, C., Neto, L. W., et al. (2004). A procolophonoid reptile with temporal fenestration from the Middle Triassic of Brazil. *Proc. R. Soc. Lond. B* 271, 1541–1546. doi: 10.1098/rspb.2004.2748

Clack, J., and Carroll, R. L. (1973). Romeriid reptiles from the Lower Permian. *Bull. Mus. Comp. Zool.* 144, 353–407.

Clack, J. A. (2012). *Gaining Ground. The Origin and Evolution of Tetrapods. Second Edition*. Bloomington: Indiana University Press.

Csardi, G., and Nepusz, T. (2006). The igraph software package for complex network research. *Int. J. Complex Syst.* 1659, 1–9.

Currie, P. J. (1981). *Hovasaurus boulei*, an aquatic eosuchian from the Upper Permian of Madagascar. *Palaeontol. Afr.* 24, 99–168.

Diogo, R., and Abdala, V. (2010). *Muscles of Vertebrates*. Enfield: Science Publishers. doi: 10.1201/9781439845622

Diogo, R., Esteve-Altava, B., Smith, C., Boughner, J. C., and Rasskin-Gutman, D. (2015). Anatomical network comparison of human upper and lower, newborn and adult, and normal and abnormal limbs, with notes on development, pathology and limb serial homology vs. homoplasy. *PLoS One* 10:e0140030. doi: 10.1371/journal.pone.0140030

Dodick, J. T., and Modesto, S. P. (1995). The cranial anatomy of the captorhinid reptile *Labidosaurikos meachami* from the Lower Permian of Oklahoma. *Palaeontology* 38, 687–711.

Elzanowski, A., and Mayr, G. (2018). Multiple origins of secondary temporal fenestrae and orbitozygomatic junctions in birds. *J. Zool. Syst. Evol. Res.* 56, 248–269. doi: 10.1111/jzs.12196

Esteve-Altava, B. (2017a). Challenges in identifying and interpreting organizational modules in morphology. *J. Morphol.* 278, 960–974. doi: 10.1002/jmor.20690

Esteve-Altava, B. (2017b). In search of morphological modules: a systematic review. *Biol. Rev.* 92, 1332–1347. doi: 10.1111/brv.12284

Esteve-Altava, B. (2017c). Network Models: connecting Anatomy to Systems Biology. *FASEB J.* 386.2.

Esteve-Altava, B., Boughner, J., Diogo, R., and Rasskin-Gutman, D. (2015a). Anatomical network analysis of primate skull morphology. *FASEB J.* 29:867.3. doi: 10.1096/fasebj.29.1_supplement.867.3

Esteve-Altava, B., Boughner, J. C., Diogo, R., Villmoare, B. A., and Rasskin-Gutman, D. (2015b). Anatomical network analysis shows decoupling of Modular lability and complexity in the evolution of the primate skull. *PLoS One* 10:e0127653. doi: 10.1371/journal.pone.0127653

Esteve-Altava, B., Diogo, R., Smith, C., Diego, J. C. B., and Rasskin-Gutman, D. (2015c). Anatomical networks reveal the musculoskeletal modularity of the human head. *Sci. Rep.* 5:8298. doi: 10.1038/srep08298

Esteve-Altava, B., Marugan-Lobon, J., Botella, H., Bastir, M., and Rasskin-Gutman, D. (2013a). Grist for Riedl's Mill: a network model perspective on the integration and modularity of the human skull. *J. Exp. Zool. B Mol. Dev. Evol.* 320, 489–500. doi: 10.1002/jez.b.22524

Esteve-Altava, B., Marugan-Lobon, J., Botella, H., and Rasskin-Gutman, D. (2013b). Structural constraints in the evolution of the tetrapod skull complexity: Williston's Law revisited using network models. *Evol. Biol.* 40, 209–219. doi: 10.1007/s11692-012-9200-9

Esteve-Altava, B., Marugan-Lobon, J., Botella, H., and Rasskin-Gutman, D. (2011). Network Models in Anatomical Systems. *J. Anthropol. Sci.* 89, 175–184.

Evans, S. E. (2008). "The Skull of Lizards and Tuatara," in *Morphology H: The Skull of the Lepidosauria*, eds C. Gans, A. S. Gaunt, and K. Adler (Salt Lake City: Society for the Study of Amphibians and Reptiles), 1–347.

Ferreira, G. S., Lautenschlager, S., Evers, S. W., Pfaff, C., Kriwet, J., Raselli, I., et al. (2020). Feeding biomechanics suggests progressive correlation of skull architecture and neck evolution in turtles. *Sci. Rep.* 10:5505. doi: 10.1038/s41598-020-62179-5

Ford, D. P. (2018). *The Evolution and Phylogeny of Early Amniotes*. Ph.D. thesis. Oxford: University of Oxford.

Fox, R. C. (1964). The adductor muscles of the jaw in some primitive reptiles. *Univ.Kans. Publ. Mus. Nat. His.* 12, 657–680.

Fox, R. C., and Bowman, M. C. (1966). Osteology and relationships of *Captorhinus aguti* (Cope) (Reptilia: Captorhinomorpha). *Univ. Kans. Paleontol. Contrib.* 11, 1–79.

Frazzetta, T. (1968). Adaptive problems and possibilities in the temporal fenestration of tetrapod skulls. *J. Morphol.* 125, 145–157. doi: 10.1002/jmor.1051250203

Frey, E., Tarsitano, S., Oelofsen, B., and Riess, J. (2001). The origin of temporal fenestrae. *South Afr. J. Sci.* 97, 334–336.

Gaffney, E. S. (1979). Comparative cranial morphology of recent and fossil turtles. *Bull. Am. Mus. Nat. Hist.* 164, 67–376.

Gaffney, E. S. (1990). The comparative osteology of the Triassic turtle *Proganochelys*. *Bull. Am. Mus. Nat. Hist.* 194:263.

Gow, C. (1972). The osteology and relationships of the Millerettidae (Reptilia: Cotylosauria). *J. Zool.* 167, 219–264. doi: 10.1111/j.1469-7998.1972.tb01731.x

Gow, C. E. (1997). A reassessment of *Eunotosaurus africanus* Seeley (Amniota: Parareptilia). *Palaeontol. Afr.* 34, 33–42.

Hall, B. K. (2005). *Bones and Cartilage: Developmental and Evolutionary Skeletal Biology*. Cambridge: Elsevier Academic Press. doi: 10.1016/B978-0-12-319060-4.50065-8

Hall, B. K. (2009). *The Neural Crest and Neural Crest Cells in Vertebrate Development and Evolution*. New York: Springer. doi: 10.1007/978-0-387-09846-3

Hanken, J., and Hall, B. (eds) (1993a). *The Skull. Vol 2, Patterns of Structural and Systematic Diversity*. Chicago: The University of Chicago Press.

Hanken, J., and Hall, B. (eds) (1993b). *The Skull. Vol 3, Functional and Evolutionary Mechanisms*. Chicago: The University of Chicago Press.

Haridy, Y., Macdougall, M. J., Scott, D., and Reisz, R. R. (2016). Ontogenetic change in the temporal region of the early Permian parareptile *Delorhynchus cifellii* and the implications for closure of the temporal fenestra in amniotes. *PLoS One* 11:e0166819. doi: 10.1371/journal.pone.0166819

Heiss, E., Natchev, N., Gumpenberger, M., Weissenbacher, A., and Van Wassenbergh, S. (2013). Biomechanics and hydrodynamics of prey capture in the Chinese giant salamander reveal a high-performance jaw-powered suction feeding mechanism. *J. R. Soc. Interface* 10:20121028. doi: 10.1098/rsif.2012.1028

Herrel, A., O'Reilly, J. C., and Richmond, A. M. (2002). Evolution of bite performance in turtles. *J. Evolu. Biol.* 15, 1083–1094. doi: 10.1046/j.1420-9101.2002.00459.x

Higashiyama, H., Koyabu, D., Hirasawa, T., Werneburg, I., Kuratani, S., and Kurihara, H. (2021). Mammalian face as an evolutionary novelty. *Proc. Nat. Acad. Sci. U. S, A.* 118:e2111876118. doi: 10.1073/pnas.2111876118

Holliday, C. M., and Witmer, L. M. (2007). Archosaur adductor chamber evolution: Integration of musculoskeletal and topological criteria in jaw muscle homology. *J. Morphol.* 268, 457–484. doi: 10.1002/jmor.10524

Holmes, R. (1984). The Carboniferous amphibian *Proterogyrinus scheelei* Romer, and the early evolution of tetrapods. *Philos. Trans. R. Soc. Lond. B Biol. Sci.* 306, 431–524. doi: 10.1098/rstb.1984.0103

Hülsmann, E., and Wahlert, G. V. (1972). *Das Schädelkabinett - Eine erklärende Naturgeschichte der Wirbeltiere*. Basel: Basilius Presse.

Iordansky, N. (1990). Evolution of cranial kinesis in lower tetrapods. *Neth. J. Zool.* 40, 32–54. doi: 10.1163/156854289X00174

Iordansky, N. N. (2011). Cranial kinesis in lizards (*Lacertilia*): origin, biomechanics, and evolution. *Biol. Bull.* 38, 852–861. doi: 10.1134/S1062359011090032

Jaeckel, O. (1902). Ueber *Gephyrostegus bohemicus*. *Zeitschrift der Deutschen Geologischen Gesellschaft* 54, 127–133.

Jones, M. E. H., Curtis, N., Fagan, M. J., O'Higgins, P., and Evans, S. E. (2011). Hard tissue anatomy of the cranial joints in *Sphenodon* (Rhynchocephalia): sutures, kinesis, and skull mechanics. *Palaeontol. Electron.* 14:33604.

Jones, M. E. H., Curtis, N., O'Higgins, P., Fagan, M., and Evans, S. E. (2009). The head and neck muscles accociated with feeding on *Sphenodon* (Reptilia: Lepidosauria: Rynchocephalia). *Palaeontol. Electron.* 12:56.

Joyce, W. G. (2007). Phylogenetic relationships of Mesozoic turtles. *Bull. Peabody Mus. Nat. Hist.* 48, 3–102. doi: 10.3374/0079-032X(2007)48[3:PROMT]2.0.CO;2

Kammerer, C. F. (2011). Systematics of the Anteosauria (Therapsida: Dinocephalia). *J. Syst. Palaeontol.* 9, 261–304. doi: 10.1080/14772019.2010.492645

Kemp, T. S. (1980). Origin of the mammal-like reptiles. *Nature* 283, 378–380. doi: 10.1038/283378a0

Kemp, T. S. (1982). *Mammal-Like Reptiles and the Origin of Mammals*. Cambridge: Academic Press.

Keyser, A. W., and Gow, C. E. (1981). First complete skull of the Permian reptile *Eunotosaurus africanus* Seeley. *South Afr. J. Sci.* 77, 417–421.

Klembara, J. (1997). The cranial anatomy of *Discosauriscus* Kuhn, a seymouriamorph tetrapod from the Lower Permian of the Boskovice Furrow (Czech Republic). *Philos. Trans. R. Soc. Lond. B.* 352, 257–302. doi: 10.1098/rstb.1997.0021

Klembara, J. (2011). The cranial anatomy, ontogeny, and relationships of *Karpinskiosaurus secundus* (Amalitzky) (Seymouriamorpha, Karpinskiosauridae) from the Upper Permian of European Russia. *Zool. J. Linn. Soc.* 161, 184–212. doi: 10.1111/j.1096-3642.2009.00629.x

Klembara, J., Berman, D. S., Henrici, A. C., Cernansky, A., and Werneburg, R. (2006). Comparison of cranial anatomy and proportions of similarly sized *Seymouria sanjuanensis* and *Discosauriscus austriacus*. *Ann. Carnegie Mus.* 30, 37–49. doi: 10.2992/0097-4463(2006)75[37:COCAAP]2.0.CO;2

Klembara, J., Tomasik, A., and Kathe, W. (2002). Subdivisions, fusions and extended sutural areas of dermal skull bones in *Discosauriscus* KUHN (Seymouriamorpha). *Neues Jahrbuch für Geologie und Paläontologie Abhandlungen* 223, 317–349. doi: 10.1127/njgpa/223/2002/317

Koyabu, D., Werneburg, I., Morimoto, N., Zollikofer, C. P. E., Forasiepi, A. M., Endo, H., et al. (2014). Mammalian skull heterochrony reveals modular evolution and a link between cranial development and brain size. *Nat. Commun.* 5:3625. doi: 10.1038/ncomms4625

Kuhn-Schnyder, E. (1980). "Observations on Temporal Openings of Reptilian Skulls and the Classification of Reptiles," in *Aspects of Vertebrate History, Essays in Honor of Edwin Harris Colbert*, ed. L. L. Jacobs (Flagstaff: Museum of Northern Arizona), 153–175.

Lakjer, T. (1926). *Studien über die Trigeminus-versorgte Kaumuskulatur der Sauropsiden*. Copenhagen: Reitsel Buchhandlung.

Lakjer, T. (1927). Studien über die Gaumenregion bei Sauriern im Vergleich mit Anamniern und primitiven Sauropsiden. *Zool. Jahrb.* 49, 57–356.

Laurin, M. (2005). Embryo retention, character optimization, and the origin of the extra-embryonic membranes of the amniotic egg. *J. Nat. Hist.* 39, 3151–3161. doi: 10.1080/00222930500300884

Laurin, M. (2010). *How Vertebrates Left the Water*. Los Angeles: University of California Press. doi: 10.1525/9780520947986

Lautenschlager, S., Gill, P., Luo, Z.-X., Fagan, M. J., and Rayfield, E. J. (2017). Morphological evolution of the mammalian jaw adductor complex: mammalian jaw muscle evolution. *Biol. Rev.* 92, 1910–1940. doi: 10.1111/brv.12314

LeBlanc, A. R. H., MacDougall, M. J., Haridy, Y., Scott, D., and Reisz, R. R. (2018). Caudal autotomy as anti-predatory behaviour in Palaeozoic reptiles. *Sci. Rep.* 8:3328. doi: 10.1038/s41598-018-21526-3

Lee, H. W., Esteve-Altava, B., and Abzhanov, A. (2020). Evolutionary and ontogenetic changes of the anatomical organization and modularity in the skull of archosaurs. *Sci. Re.* 10:16138. doi: 10.1038/s41598-020-73083-3

Li, C., Fraser, N. C., Rieppel, O., and Wu, X. C. (2018). A Triassic stem turtle with an edentulous beak. *Nature* 560, 476–479. doi: 10.1038/s41586-018-0419-1

Lucas, S. G., Rinehart, L. F., and Celeskey, M. D. (2018). The oldest specialized tetrapod herbivore: a new eupelycosaur from the Permian of New Mexico, USA. *Palaeontol. Electron.* 21, 1–42. doi: 10.26879/899

MacDougall, M. J., and Reisz, R. R. (2014). The first record of a nyctiphruretid parareptile from the early Permian of North America, with a discussion of parareptilian temporal fenestration. *Zool. J. Linn. Soc.* 172, 616–630. doi: 10.1111/zoj.12180

Maier, W. (1989). "Ala Temporalis and Alisphenoid in Therian Mammals," in *Trends in Vertebrate Morphology*, eds H. Splechtna and H. Hilgers (Stuttgart: Fischer Verlag), 396–400.

Maier, W. (1999). On the evolutionary biology of early mammals - with methodological remarks on the interaction between ontogenetic adaptation and phylogenetic transformation. *Zool. Anz.* 238, 55–74.

Maier, W., and Werneburg, I. (2014). *Einführung: Zur Methodik der organismischen Evolutionsbiologie. In: Maier W, Werneburg I. Schlüsselereignisse der organismischen Makroevolution*. Zürich: Scidinge Hall Verlag, 11–17.

Mann, A., Pardo, J. D., and Maddin, H. C. (2019). *Infernovenator steenae*, a new serpentine recumbirostran from the 'Mazon Creek' Lagerstätte further clarifies lysorophian origins. *Zool. J. Linn. Soc.* 187, 506–517. doi: 10.1093/zoolinnean/zlz026

Modesto, S. P. (1995). The skull of the herbivorous synapsid *Edaphosaurus boanerges* from the Lower Permian of Texas. *Palaeontology* 38, 213–239.

Modesto, S. P. (1998). New information on the skull of the Early Permian reptile *Captorhinus aguti*. *Paleobios* 18, 21–35.

Molnar, J., Esteve-Altava, B., Rolian, C., and Diogo, R. (2017). Comparison of musculoskeletal networks of the primate forelimb. *Sci. Rep.* 7:10520. doi: 10.1038/s41598-017-09566-7

Müller, J. (2003). Early loss and multiple return of the lower temporal arcade in diapsid reptiles. *Naturwissenschaften* 90, 473–476. doi: 10.1007/s00114-003-0461-0

Müller, J., and Reisz, R. R. (2005). An early captorhinid reptile (Amniota, Eureptilia) from the Upper Carboniferous of Hamilton, Kansas. *J. Vertebr. Paleontol.* 25, 561–568. doi: 10.1671/0272-4634(2005)025[0561:AECRAE]2.0.CO;2

Natchev, N., Handschuh, S., Lukanov, S., Tzankov, N., Naumov, B., and Werneburg, I. (2016). Contributions to the functional morphology of caudate skulls: kinetic and akinetic forms. *PeerJ* 4:e2392. doi: 10.7717/peerj.2392

Natchev, N., Tzankov, N., Werneburg, I., and Heiss, E. (2015). Feeding behaviour in a 'basal' tortoise provides insights on the transitional feeding mode at the dawn of modern land turtle evolution. *PeerJ* 3:e1172. doi: 10.7717/peerj.1172

Nick, L. (1912). Das Kopfskelett von *Dermochelys coriacea* L. *Zoologische Jahrbücher, Abteilung für Anatomie und Ontogenie der Tiere* 33, 1–238.

Novacek, M. J. (1993). "Patterns of Diversity in the Mammalian Skull," in *The Skull, Volume 2: Patterns of Structural and Systematic Diversity*, eds J. Hanken and B. Hall (Chicago: University of Chicago Press), 438–545.

Panchen, A. L. (1964). The cranial anatomy of two coal measure anthracosaurs. *Philos. Trans. R. Soc.* 247, 593–637. doi: 10.1098/rstb.1964.0006

Plateau, O., and Foth, C. (2020). Birds have peramorphic skulls, too: anatomical network analyses reveal oppositional heterochronies in avian skull evolution. *Commun. Biol.* 3:195. doi: 10.1038/s42003-020-0914-4

Polachowski, K. M., and Werneburg, I. (2013). Late embryos and bony skull development in *Bothropoides jararaca* (Serpentes, Viperidae). *Zoology* 116, 36–63. doi: 10.1016/j.zool.2012.07.003

R Core Team (2020). *R: A language and environment for statistical computing*. Vienna: R Foundation for Statistical Computing. URL. https://www.R-project.org/

Rasskin-Gutman, D. (2003). "Boundary Constraints for the Emergence of Form," in *Origination of Organismal Form. Beyond the Gene in Developmental and EvolutionaryBiology*, eds G. B. Müller and S. A. Newman (Cambridge: MIT Press), 305–322.

Rasskin-Gutman, D., and Esteve-Altava, B. (2014). Connecting the dots: anatomical network analysis in morphological EvoDevo. *Biol. Theory* 9, 178–193. doi: 10.1007/s13752-014-0175-x

Rasskin-Gutman, D., and Esteve-Altava, B. (2021). "Concept of Burden in Evo-Devo," in *Evolutionary Developmental Biology. A Reference Guide*, eds L. Nuño de la Rosa and G. B. Müller (Berlin: Springer), 39–49. doi: 10.1007/978-3-319-32979-6_48

Reisz, R. R. (1977). *Petrolacosaurus*, the oldest known diapsid reptile. *Science* 196, 1091–1093. doi: 10.1126/science.196.4294.1091

Reisz, R. R., Berman, D. S., and Scott, D. (1984). The anatomy and relationships of the Lower Permian reptile *Araeoscelis*. *J. Vertebr. Paleontol.* 4, 57–67. doi: 10.1080/02724634.1984.10011986

Reisz, R. R., Schoch, R. R., and Anderson, J. S. (2009). The armoured dissorophid *Cacops* from the Early Permian of Oklahoma and the exploitation of the terrestrial realm by amphibians. *Naturwissenschaften* 96, 789–796. doi: 10.1007/s00114-009-0533-x

Rieppel, O. (1984). The upper temporal arcade of lizards: an ontogenetic problem. *Revue suisse Zool.* 91, 475–482. doi: 10.5962/bhl.part.81891

Rieppel, O. (1987). The development of the trigeminal jaw adductor musculature and associated skull elements in the lizard *Podarcis sicula*. *J. Zool.* 212, 131–150. doi: 10.1111/j.1469-7998.1987.tb05120.x

Rieppel, O. (1993). "Patterns of Diversity in the Reptilian Skull," in *The Skull, Volume 2: Patterns of Structural and Systematic Diversity*, eds J. Hanken and B. Hall (Chicago: University of Chicago Press), 344–389.

Rieppel, O., and Gronowski, R. W. (1981). The loss of the lower temporal arcade in diapsid reptiles. *Zool. J. Linn. Soc.* 72, 203–217. doi: 10.1111/j.1096-3642.1981.tb01570.x

Romer, A. S., and Price, L. W. (1940). *Review of the Pelycosauria*. New York: Geological Society of America. doi: 10.1130/SPE28-p1

RStudio Team (2019). *RStudio: Integrated Development for R*. Boston, MA: RStudio, PBC.

Schumacher, G. H. (1956). Über die Fascien des Kopfes der Schildkröten nebst einigen Bemerkungen zu der Arbeit von Lakjer, 1926. *Zool. Anz.* 156, 35–54.

Schumacher, G. H. (1972). *Die Kopf- und Halsregion der Lederschildkröte* Dermochelys coriacea *(LINNAEUS 1766) - Anatomische Untersuchungen im Vergleich zu anderen rezenten Schildkröten - Mit 7 Figuren im Text und 31 Tafeln*. Berlin: Akademie-Verlag.

Schumacher, G. H. (1973). "The Head Muscles and Hyolaryngeal Skeleton of Turtles and Crocodilians," in *Biology of the Reptilia*, eds G. Gans and T. S. Parsons (New York: Academic Press).

Smith, H. M., Chiszar, D., and Frey, M. J. (1983). The terminology of amniote temporal vacuities. *Trans. Kans. Acad. Sci.* 86, 48–54. doi: 10.2307/3628423

Smith-Paredes, D., Núñez-León, D., Soto-Acuna, S., O'Connor, J., Botelho, J. F., and Vargas, A. O. (2018). Dinosaur ossification centres in embryonic birds uncover developmental evolution of the skull. *Nat. Ecol. Evol.* 2, 1966–1973. doi: 10.1038/s41559-018-0713-1

Sookias, R. B., Dilkes, D., Sobral, G., Smith, R. M. H., Wolvaardt, F. P., Arcucci, A. B., et al. (2020). The craniomandibular anatomy of the early archosauriform *Euparkeria capensis* and the dawn of the archosaur skull. *R. Soc. Open Sci.* 7:200116. doi: 10.1098/rsos.200116

Starck, D. (1995). *5. Teil: Säugetiere. 5/1: Allgemeines, Ordo 1-9*. Gustav: Fischer Verlag Jena.

Sues, H.-D., and Reisz, R. R. (1998). Origins and early evolution of herbivory in tetrapods. *Tree* 13, 141–145. doi: 10.1016/S0169-5347(97)01257-3

Sumida, S. S., and Martin, K. L. M. (eds) (1997). *Amniote Origins: Completing the Transition to Land*. San Diego: Academic Press.

Sushkin, P. P. (1928). Contributions to the cranial morphology of *Captorhinus* Cope (Reptilia, Cotylosauria, Captorhinidae). *Palaeobiologica* 1, 263–280.

Tarsitano, S. F., Oelofsen, B., Frey, E., and Riess, J. (2001). The origin of temporal fenestra. *South Afr. J. Sci.* 97, 334–336.

Tsuji, L. A., Müller, J., and Reisz, R. R. (2010). *Microleter mckinzieorum* gen. et sp. nov. from the Lower Permian of Oklahoma: the basalmost parareptile from Laurasia. *J. Syst. Palaeontol.* 8, 245–255. doi: 10.1080/14772010903461099

Van Den Heuvel, W. F. (1992). Kinetics of the skull in the chicken (*Gallus gallus domesticus*). *Neth. J. Zool.* 42, 461–582. doi: 10.1163/156854292X00071

Warren, J. W. (1961). The basicranial articulation of the early Permian cotylosaur, *Captorhinus*. *J. Paleontol.* 35, 561–563.

Watson, D. M. S. (1914). *Eunotosaurus africanus* Seeley, and the ancestry of the Chelonia. *Proc. Zool. Soc. Lond.* 11, 1011–1020.

Weishampel, D. B. (1997). Herbivory and reptiles. *Lethaia Rev.* 29:224. doi: 10.1111/j.1502-3931.1996.tb01654.x

Werneburg, I. (2011). The cranial musculature in turtles. *Palaeontol. Electron.* 14:99.

Werneburg, I. (2012). Temporal bone arrangements in turtles: an overview. *J. Exp. Zool. B Mol. Dev. Evol.* 318, 235–249. doi: 10.1002/jez.b.22450

Werneburg, I. (2013a). Jaw musculature during the dawn of turtle evolution. *Org. Divers. Evol.* 13, 225–254. doi: 10.1007/s13127-012-0103-5

Werneburg, I. (2013b). The tendinous framework in the temporal skull region of turtles and considerations about its morphological implications in amniotes: a review. *Zool. Sci.* 31, 141–153. doi: 10.2108/zsj.30.141

Werneburg, I. (2015). Neck motion in turtles and its relation to the shape of the temporal skull region. *C. R. Palevol* 14, 527–548. doi: 10.1016/j.crpv.2015.01.007

Werneburg, I. (2019). Morphofunctional categories and ontogenetic origin of temporal skull openings in amniotes. *Front. Earth Sci.* 7:13. doi: 10.3389/feart.2019.00013

Werneburg, I., Esteve-Altava, B., Bruno, J., Torres Ladeira, M., and Diogo, R. (2019). Unique skull network complexity of *Tyrannosaurus rex* among land vertebrates. *Sci. Rep.* 9:1520. doi: 10.1038/s41598-018-37976-8

Werneburg, I., Evers, S. E., and Ferreira, G. (2021). On the "cartilaginous rider" in the endocasts of turtle brain cavities. *Vertebr. Zool.* 71, 403–418.

Werneburg, I., and Maier, W. (2019). Diverging development of akinetic skulls in cryptodire and pleurodire turtles: an ontogenetic and phylogenetic study. *Vertebr. Zool.* 69, 113–143.

Werneburg, I., Polachowski, K., and Hutchinson, M. (2015). Bony skull development in the Argus monitor (Squamata, Varanidae, *Varanus panoptes*) with comments on developmental timing and adult anatomy. *Zoology* 118, 225–280. doi: 10.1016/j.zool.2015.02.004

Werneburg, I., and Yaryhin, A. (2019). Character definition and tempus optimum in comparative chondrocranial research. *Acta Zool.* 100, 376–388. doi: 10.1111/azo.12260

Williston, S. (1904). The temporal arches of the Reptilia. *Biol. Bull.* 7, 175–192. doi: 10.2307/1535794

Witzmann, F., and Werneburg, I. (2017). The palatal interpterygoid vacuities of temnospondyls and the implications for the associated eye- and jaw musculature. *Anat. Rec.* 300, 1240–1269. doi: 10.1002/ar.23582

Zdansky, O. (1923). Über die Temporalregion des Schildkrötenschädels. *Bull. Geol. Inst. Univ. Upsala* 19, 89–114.

Ziermann, J. M., Diaz, R. E., and Diogo, R. (2019). *Heads, Jaws, and Muscles: Anatomical, Functional, and Developmental Diversity in Chordate Evolution*. Cham: Springer. doi: 10.1007/978-3-319-93560-7

Zusi, R. L. (1993). "Patterns of Diversity in the Avian Skull," in *The Skull, Volume 2: Patterns of Structural and Systematic Diversity*, eds J. Hanken and B. Hall (Chicago: University of Chicago Press), 391–437.

Conflict of Interest: The authors declare that the research was conducted in the absence of any commercial or financial relationships that could be construed as a potential conflict of interest.

frontiers | Frontiers in Ecology and Evolution

ORIGINAL RESEARCH
published: 18 May 2022
doi: 10.3389/fevo.2022.841784

Skull Sutures and Cranial Mechanics in the Permian Reptile *Captorhinus aguti* and the Evolution of the Temporal Region in Early Amniotes

*Pascal Abel[1,2], Yannick Pommery[1,3], David Paul Ford[4], Daisuke Koyabu[5] and Ingmar Werneburg[1,2]**

[1] Senckenberg Centre for Human Evolution and Palaeoenvironment (SHEP), Tübingen, Germany, [2] Fachbereich Geowissenschaften, Eberhard-Karls-Universität, Tübingen, Germany, [3] Biogéosciences, Université Bourgogne Franche-Comté, Dijon, France, [4] Evolutionary Studies Institute, University of Witwatersrand, Johannesburg, South Africa, [5] Research and Development Center for Precision Medicine, University of Tsukuba, Tsukuba, Japan

OPEN ACCESS

Edited by:
Haijun Song,
China University of Geosciences Wuhan, China

Reviewed by:
David Marjanović,
Museum of Natural History Berlin (MfN), Germany
Josep Fortuny,
Institut Català de Paleontologia Miquel Crusafont, Spain

***Correspondence:**
Ingmar Werneburg
ingmar.werneburg@senckenberg.de

Specialty section:
This article was submitted to Paleontology, a section of the journal Frontiers in Ecology and Evolution

Received: *22 December 2021*
Accepted: *13 April 2022*
Published: *18 May 2022*

Citation:
Abel P, Pommery Y, Ford DP, Koyabu D and Werneburg I (2022) Skull Sutures and Cranial Mechanics in the Permian Reptile Captorhinus aguti and the Evolution of the Temporal Region in Early Amniotes. Front. Ecol. Evol. 10:841784. doi: 10.3389/fevo.2022.841784

While most early limbed vertebrates possessed a fully-roofed dermatocranium in their temporal skull region, temporal fenestrae and excavations evolved independently at least twice in the earliest amniotes, with several different variations in shape and position of the openings. Yet, the specific drivers behind this evolution have been only barely understood. It has been mostly explained by adaptations of the feeding apparatus as a response to new functional demands in the terrestrial realm, including a rearrangement of the jaw musculature as well as changes in strain distribution. Temporal fenestrae have been retained in most extant amniotes but have also been lost again, notably in turtles. However, even turtles do not represent an optimal analog for the condition in the ancestral amniote, highlighting the necessity to examine Paleozoic fossil material. Here, we describe in detail the sutures in the dermatocranium of the Permian reptile *Captorhinus aguti* (Amniota, Captorhinidae) to illustrate bone integrity in an early non-fenestrated amniote skull. We reconstruct the jaw adductor musculature and discuss its relation to intracranial articulations and bone flexibility within the temporal region. Lastly, we examine whether the reconstructed cranial mechanics in *C. aguti* could be treated as a model for the ancestor of fenestrated amniotes. We show that *C. aguti* likely exhibited a reduced loading in the areas at the intersection of jugal, squamosal, and postorbital, as well as at the contact between parietal and postorbital. We argue that these "weak" areas are prone for the development of temporal openings and may be treated as the possible precursors for infratemporal and supratemporal fenestrae in early amniotes. These findings provide a good basis for future studies on other non-fenestrated taxa close to the amniote base, for example diadectomorphs or other non-diapsid reptiles.

Keywords: Amniota, Captorhinidae, biomechanics, functional morphology, cranial osteology, temporal openings

INTRODUCTION

Amniota, the clade comprising mammals, turtles, lepidosaurs, crocodylians, birds, and their extinct relatives, emerged no later than the early Pennsylvanian (ca. 319 Ma ago; Ford and Benson, 2020). In contrast to the majority of coeval limbed vertebrates, the earliest amniotes and their closest extinct relatives adopted a predominantly or even exclusively terrestrial lifestyle (Sumida, 1997; Nyakatura et al., 2019; Buchwitz et al., 2021). This ecological shift had been accomplished by innovations in their developmental strategies (e.g., Packard and Seymour, 1997; Werneburg, 2019; Blackburn and Stewart, 2021) and was accompanied by further changes in their general anatomy, involving the appendicular skeleton and vertebral column (Sumida, 1997), as well as the skull (Bramble and Wake, 1985; Iordansky, 1990). Especially, the adaptations in the skull are an essential aspect of amniote terrestrialization, as life outside of the aquatic realm makes specific demands on sensorial abilities, respiration, and feeding (Olson, 1961; Lauder and Gillis, 1997; Laurin, 2010).

One of the most recurrent differences in the skull morphology between early amniotes and most other Paleozoic limbed vertebrates are the reductions of the dermatocranium in the temporal region, leading to the formation of temporal fenestrae or marginal excavations (Werneburg, 2012, 2019; Abel and Werneburg, 2021). Such temporal openings evolved at least twice independently in early amniotes (Ford and Benson, 2020), corroborating the notion that they were a response to new functional demands (e.g., Case, 1924; Fox, 1964; Frazzetta, 1968; for a review see Abel and Werneburg, 2021), likely caused by a greater role of the external jaw adductor musculature and corresponding changes in force distribution (e.g., Versluys, 1919; Case, 1924; Lakjer, 1926; Frazzetta, 1968). Initially, this might have been also bound to amniote terrestrialization and accompanied adaptations like weight reduction, higher mobility of the atlanto-occipital joint, and change from a kinetic-inertial to a static-pressure biting system (Gaupp, 1895; Versluys, 1919; Olson, 1961; Fox, 1964; Kuhn-Schnyder, 1980). Overall, temporal openings have been hypothesized to form especially within "weak" regions of the dermatocranium that could easily have been reduced. Those include generally thin areas (e.g., Case, 1924; Romer and Price, 1940; Fox, 1964), intersections of more than two bones (Frazzetta, 1968; Kuhn-Schnyder, 1980), and bone articulations (Kemp, 1980).

Yet, the ancestral configuration without temporal openings (*scutal sensu* Abel and Werneburg, 2021) was retained in many Paleozoic amniotes ("Anapsida"; e.g., Carroll and Baird, 1972; Clark and Carroll, 1973), and also secondarily reevolved in groups like the Permian pareiasauromorphs (MacDougall and Reisz, 2014) and turtles (Gaffney, 1990; Jones et al., 2012). However, no ancestrally scutal amniote is known from post-Paleozoic strata and even extant turtles may not be a good analog due to their unique cranial adaptations (e.g., Kilias, 1957; Werneburg, 2011, 2012, 2013a, 2015; Ferreira and Werneburg, 2019; Werneburg and Maier, 2019). Consequently, any hypothesis regarding the functional morphology in the ancestral scutal skull and its role in the evolution of temporal openings is dependent upon the assessment of fossil material.

Here, we use the skull of the Permian reptile (*sensu* Modesto and Anderson, 2004) *Captorhinus aguti* Cope, 1882 (Amniota, Captorhinidae) as a model for the cranial functional morphology in an early "anapsid." We chose *Captorhinus*, because species of this genus represent some of the best documented early scutal reptiles with easily accessible articulated skull material and a wealth of literature on their cranial anatomy (e.g., Branson, 1911; Case, 1911; Sushkin, 1928; Price, 1935; Romer, 1956; Fox and Bowman, 1966; Heaton, 1979; Modesto, 1998; Kissel et al., 2002; Egberts, 2008), including discussions on their jaw musculature, cranial kinesis, and its relevance in understanding the origin of temporal fenestration (Warren, 1961; Fox, 1964; Fox and Bowman, 1966; Bolt, 1974; Heaton, 1979; Jones and Zikmund, 2012; Werneburg and Abel, 2022).

It is worth mentioning that *C. aguti* postdated the oldest known amniotes by ca. 30 Ma (Woodhead et al., 2010; Ford and Benson, 2020) and already exhibited some adaptations that might be considered derived relative to earlier scutal reptiles, especially in its dentition, feeding mechanics, and skull proportions (Heaton, 1979; Dodick and Modesto, 1995; Hotton et al., 1997; Modesto et al., 2007). Nevertheless, *C. aguti* appears to be still rather generalized in its overall cranial morphology in relation to some other contemporary taxa with a scutal temporal region (e.g., *Labidosaurus* Cope, 1895, moradisaurine captorhinids, and probably *Mesosaurus* Gervais, 1865; Dodick and Modesto, 1995; Modesto, 2006; Modesto et al., 2007) and its temporal morphology is overall similar to other early scutal reptiles (Carroll and Baird, 1972; Clark and Carroll, 1973; Heaton, 1979), among them the oldest known unambiguous amniotes (e.g., *Hylonomus lyelli* Dawson, 1860; *Paleothyris acadiana* Carroll, 1969b). Notable differences in its temporal region, especially to non-captorhinid taxa, are the distinctly reduced supratemporals and absent tabulars (Fox and Bowman, 1966; Heaton, 1979; compare to Koyabu et al., 2012).

We provide a detailed description of the suture morphology within the dermatocranium of *C. aguti* and its adjacent contacts with the viscero- and neurocranium to better understand the general stability and integrity of the hypothetical ancestral amniote skull. We identified possible "weak" regions in the dermatocranium and discuss their implications for strain distribution. Using a conservative reconstruction of the jaw adductor musculature, we further discuss the possibilities of cranial kinesis and elastic bone movements in the temporal region of *C. aguti*, and how our interpretation compares to previous studies involving this taxon. Lastly, we outline how the cranial mechanics in the ancestral amniote probably differed from other Paleozoic limbed vertebrates and how they might have provided preconditions for the evolution of temporal openings.

MATERIALS AND METHODS

For this study, we used an almost complete, three-dimensionally preserved skull of *Captorhinus aguti*, housed at the Sam Noble Oklahoma Museum of Natural History [OMNH 44816; **Figure 1**;

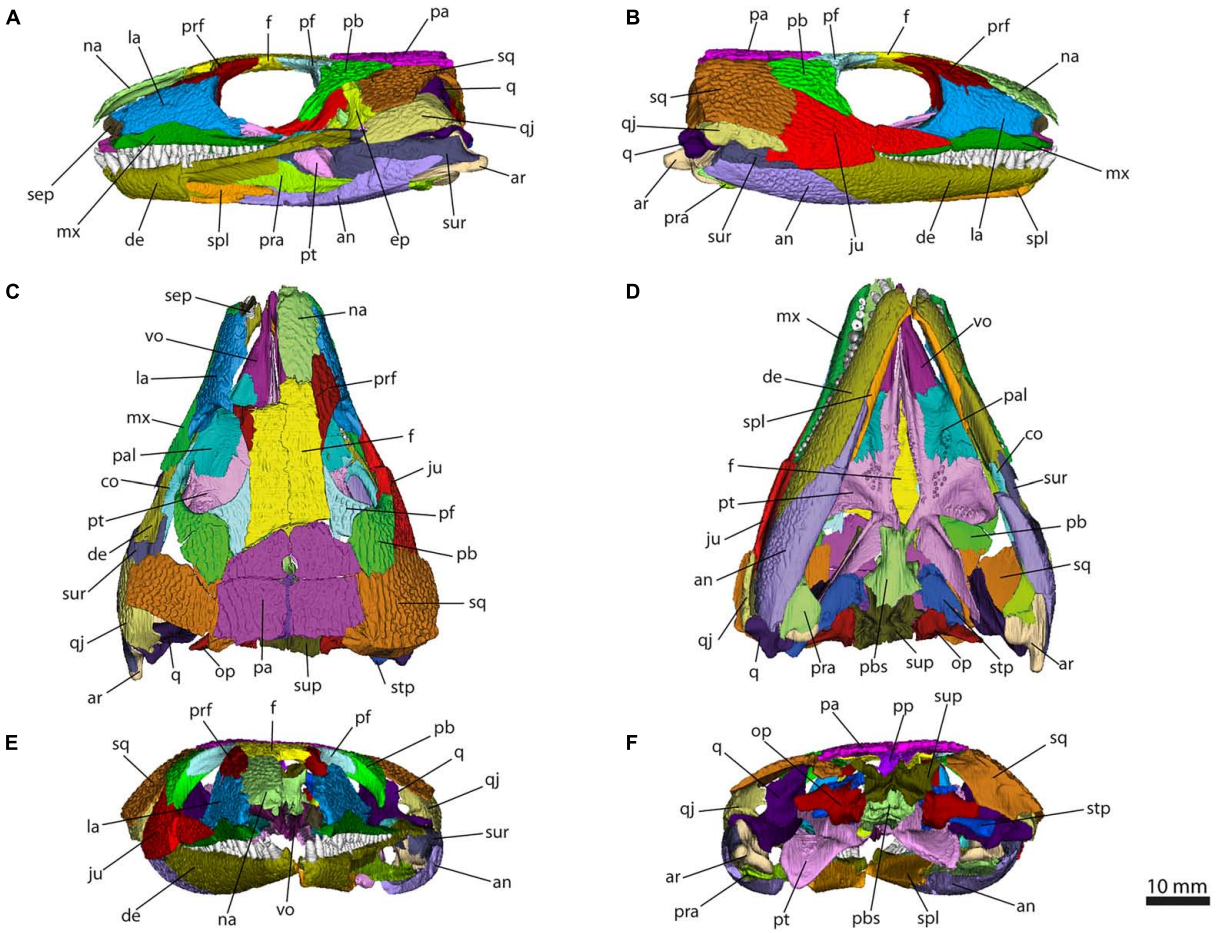

FIGURE 1 | 3D model generated from the scan of OMNH 44816 in left lateral **(A)**, right lateral **(B)**, dorsal **(C)**, ventral **(D)**, anterior **(E)**, and posterior view **(F)**. Abbreviations: an, angular; ar, articular; co, coronoid; de, dentary; ep, epipterygoid; f, frontal; ju, jugal; la, lacrimal; mx, maxilla; na, nasal; op, opisthotic; pa, parietal; pal, palatine; pb, postorbital; pf, postfrontal; pp, postparietal; pra, prearticular; prf, prefrontal; pbs, parabasisphenoid; pt, pterygoid; q, quadrate; qj, quadratojugal; sep, septomaxilla; spl, splenial; sq, squamosal; stp, stapes; sup, supraoccipital; sur, surangular; vo, vomer.

see also Werneburg and Abel (2022)]. As documented by the OMNH, the specimen derives from an unspecified Cisuralian fissure filling in Comanche County, Oklahoma. It is likely that this refers to the well-documented Richards Spur speleothem, which is Artinskian in age (ca. 289 Ma; Woodhead et al., 2010). OMNH 44816 is missing bones especially in the left half of the skull, namely the left nasal and jugal. The left prefrontal and squamosal, the parabasisphenoid and supraoccipital, as well as the left dentary, angular, and surangular are incomplete. The right septomaxilla is probably present but metallic inclusions precluded a proper segmentation. Completely missing in the skull are the premaxillae, prootics, basioccipital, and exoccipitals. Some bones are broken, but nevertheless completely preserved, these are most notably the right palatine, left postorbital, right maxilla and jugal, and both parietals.

OMNH 44816 was scanned by Matthew Colbert with an NSI scanner at the University of Texas High-Resolution X-ray Computed Tomography Facility (UTCT), Austin, United States, in February 2017. The scanner is powered by a Fein Focus High Power source with 180 kV and 0.15 mA. It uses an aluminum filter and a Perkin Elmer detector. The scan has a voxel size of 33.5 μm and consists of 1897 single slices. Further corrections were performed by Jessica Maisano. MicroCT images are deposited in MorphoSource (morphosource.org/concern/media/000439915).

Each bone was virtually extracted using manual segmentation in Avizo 8.13D renderings of the external surface of the bones and the teeth were generated and converted into meshes. Meshes were saved as PLY-files and were projected as 3D models in MorphoDig 1.5 (Lebrun, 2018; **Figures 1–9**). Renderings are available in Abel et al. (in press).

The thickness of the sutures of the dermatocranium was measured using the 2D Length Tool in Avizo 8.1. The measurements were taken in the orientation in which the suture was most complete and visible. Not being homogeneous over the entire suture length, the suture thickness was measured in five different spots. These spots are quite regularly distributed along the whole suture to obtain an accurate and well-representative

mean. All measurements and means of the suture thickness are listed in **Supplementary Table 2**.

For this paper, the term "suture" is generally applied for the contact of two bones, including their non-preserved soft-tissue components. The bone areas that articulate with each other are referred to as "articulation facets," the externally visible area incorporating the suture is the "external surface" (**Figure 2**).

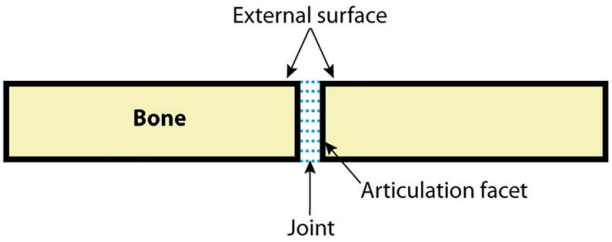

FIGURE 2 | Simplified cross section of a skull suture, illustrating the terminology used in this manuscript.

RESULTS

We identified and defined eight different suture types in the dermatocranium of *Captorhinus aguti* (**Figure 10**). Most used suture type terminology follows Jones et al. (2011). The type "stepped interdigitation" (8 in **Figure 10**) is a combination of "stepped joint" (7 in **Figure 10**) and "Type-B interdigitation" (5 in **Figure 10**) *sensu* Jones et al. (2011). Sutures can vary in the presence and type of interdigitations as well as in the presence of a bony lamina that extends from one of the suturing bones medially to its respective contralateral neighbor, forming an additional medial contact. Like observed for other taxa (e.g., Clack, 2002; Rayfield, 2005), sutures also can vary in suture type and thickness along the contact of two bones. In some cases, the type of suturing could not be directly observed, because the relevant bones were missing in OMNH 44816 or had been disarticulated. Articulations between dermal bones and those of the neuro- and viscerocranium are briefly described but not categorized after the scheme in **Figure 10**, because they fall out of our research question and have a very different, enchondral type of ossification (Koyabu et al., 2014) and related suture formation. Likewise, contacts between such non-dermal bones were also not described.

Preorbital Region

The preorbital region of *C. aguti* consists of the premaxilla, septomaxilla, maxilla, nasal, lacrimal, prefrontal, as well as of the anterior portions of the frontal and jugal. Only some preorbital sutures exhibit a simple structure. Interdigitating contacts appear especially close to the orbits.

The maxilla (**Figure 4**) forms laterally a facial lamina that fits into a ventral notch of the lacrimal ("tongue-and-groove joint"; 2 in **Figure 10**). The posterior half of the maxilla is overlapped by the jugal by a "stepped joint" (7 in **Figure 10**). The palatine contacts the maxilla laterally by what may be referred to as a low "slot joint" (3 in **Figure 10**). Anteriorly, the maxilla would have overlapped the non-preserved premaxilla (Fox and Bowman, 1966; Heaton, 1979).

The ventral margin of the lacrimal (**Figure 5**) is concave to house the facial lamina of the maxilla. Overall, the ventral margin forms a medially expanded rim that forms the external surface with the maxilla. On its dorsal margin, it underlies the nasal, the bones interdigitate externally ("stepped interdigitation"; 8 in **Figure 10**). Posteriorly to the lacrimal-nasal contact, the lacrimal exhibits a similar contact with the prefrontal, the latter underlies the lacrimal. Posteroventrally, it sutures with the jugal by a stepped joint. At its anterior end, the lacrimal is slightly overlapping the septomaxilla laterally. The lacrimal section of the orbital rim medially overlaps a dorsal ridge of the palatine, forming a slot joint.

Excluding its lateral contact with the prefrontal, the nasal (**Figure 5**) interdigitates with all its preserved neighboring bones. Its anterior tip would have underlain the premaxilla. Posterior to the nasal-lacrimal contact, the nasal forms a "butt joint" with the prefrontal (1 in **Figure 10**). The remainder of the nasal-prefrontal contact can be described as a stepped interdigitation. A stepped interdigitation can be also observed at the posterior end of the nasal for its contact with the frontal, where the frontal underlies the nasal.

Apart from its already described sutures with the lacrimal and nasal, the prefrontal (**Figure 6**) medially contacts the frontal by a stepped joint posterior to the prefrontal-nasal contact.

The posterior suture of the frontal (**Figure 6**) with the parietal is overall similar to the frontal-nasal contact. Posterolaterally, the frontal forms a "Type-A interdigitation" (4 in **Figure 10**) with the postfrontal. Additionally, a complex inter-frontal suture is present ("Type-C interdigitation"; 6 in **Figure 10**). Only the posterior end of the frontal that contacts the postfrontal and parietal contributes to the temporal region.

Temporal Region

The temporal part of the dermatocranium in *C. aguti* consists of the posterior portion of the jugal and frontal, as well as the postfrontal, postorbital, squamosal, quadratojugal, parietal, postparietal, and supratemporal. Interdigitating contacts are especially formed on the external surfaces in the "cheeks" (i.e., jugal, squamosal, postorbital, and quadratojugal).

The posterior jugal (**Figure 7**) dorsally underlies the postorbital, forming a stepped joint (7 in **Figure 10**). At its posterior end, the jugal also underlies the squamosal; both bones form a stepped interdigitation (8 in **Figure 10**). The jugal is similarly contacted by the quadratojugal at its posteroventral edge, although the interdigitation sequence is short. A medial contact with the pterygoid has been reported for *Captorhinus* and other captorhinids (Fox and Bowman, 1966; Heaton, 1979; Dodick and Modesto, 1995; Modesto et al., 2007). However, such a contact is not preserved in OMNH 44816. This is likely due to the loss of the anteromedial process that would have connected the jugal to the pterygoid and a slight displacement of the palate.

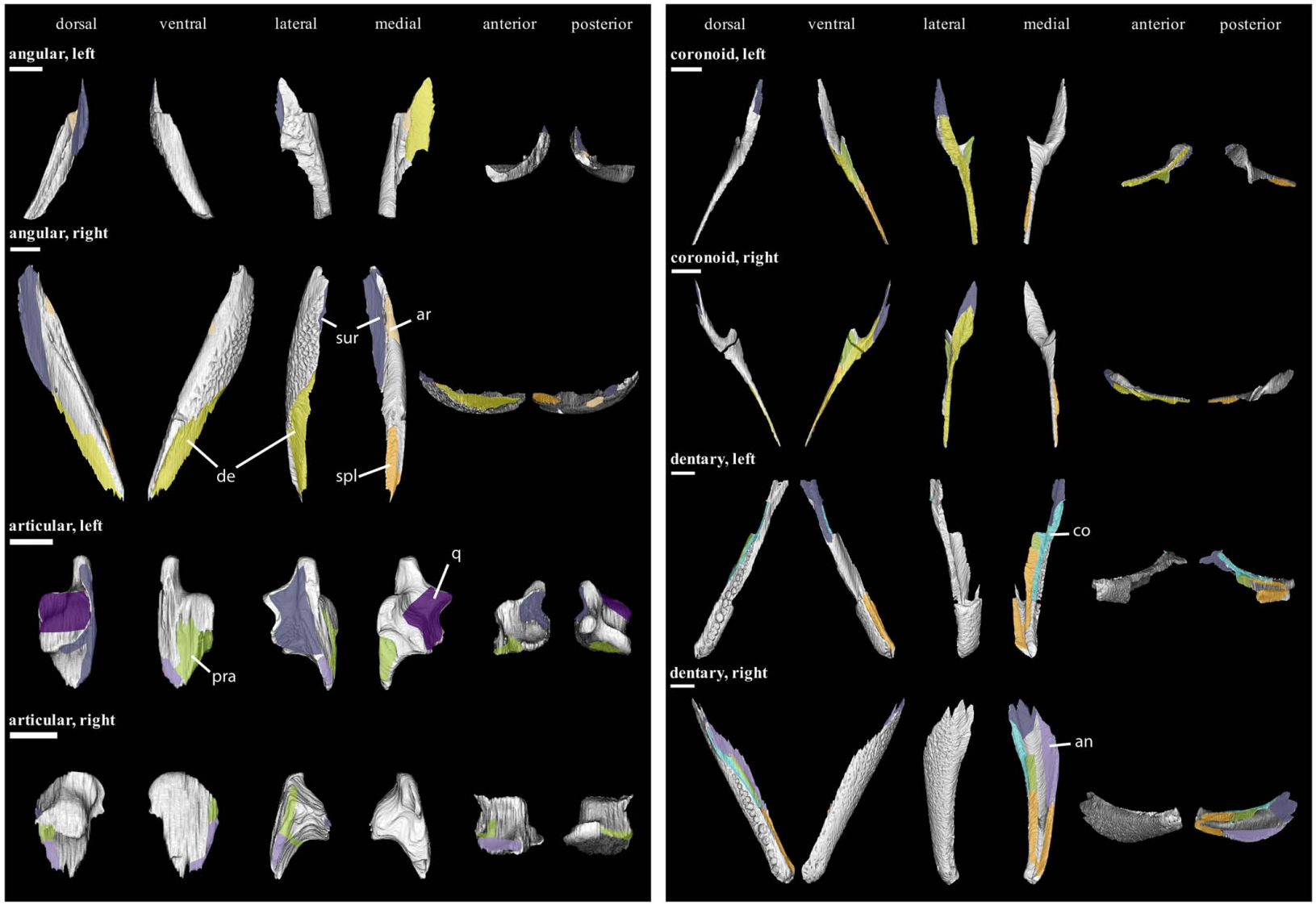

FIGURE 3 | Isolated bones in dorsal, ventral, lateral, medial, anterior and posterior views. Articulation areas with other bones are colored. Left and right angular, left and right articular, left and right coronoid, and left and right dentary are shown. Scale bar = 10 mm. For abbreviations see caption to **Figure 1**.

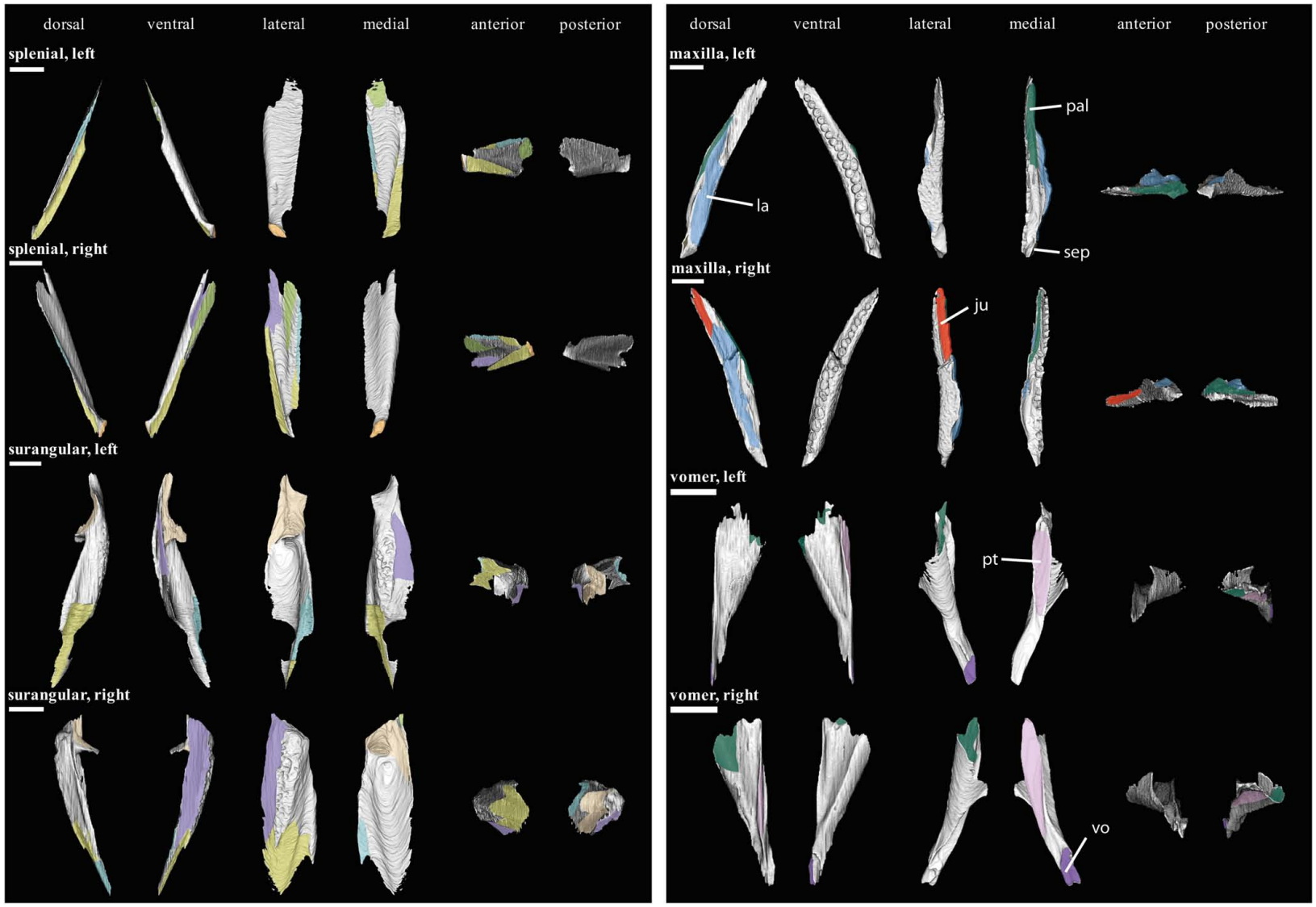

FIGURE 4 | Isolated bones in dorsal, ventral, lateral, medial, anterior and posterior views. Articulation areas with other bones are colored. Left and right splenial, left and right surangular, left and right maxilla, and left and right vomer are shown. Scale bar = 10 mm. For abbreviations see caption to **Figure 1**.

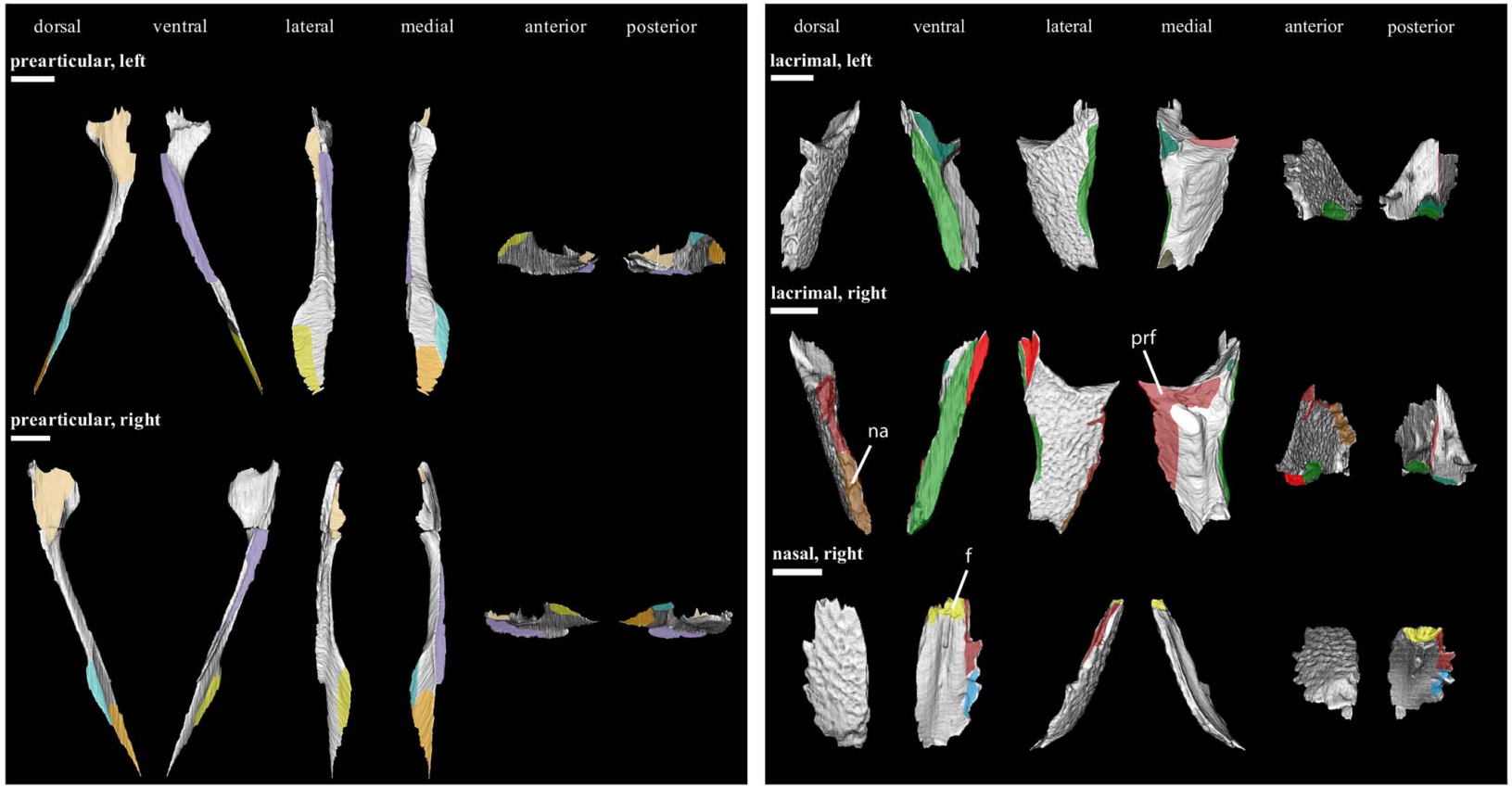

FIGURE 5 | Isolated bones in dorsal, ventral, lateral, medial, anterior and posterior views. Articulation areas with other bones are colored. Left and right prearticular, left and right lacrimal, and right nasal are shown. Scale bar = 10 mm. For abbreviations see caption to **Figure 1**.

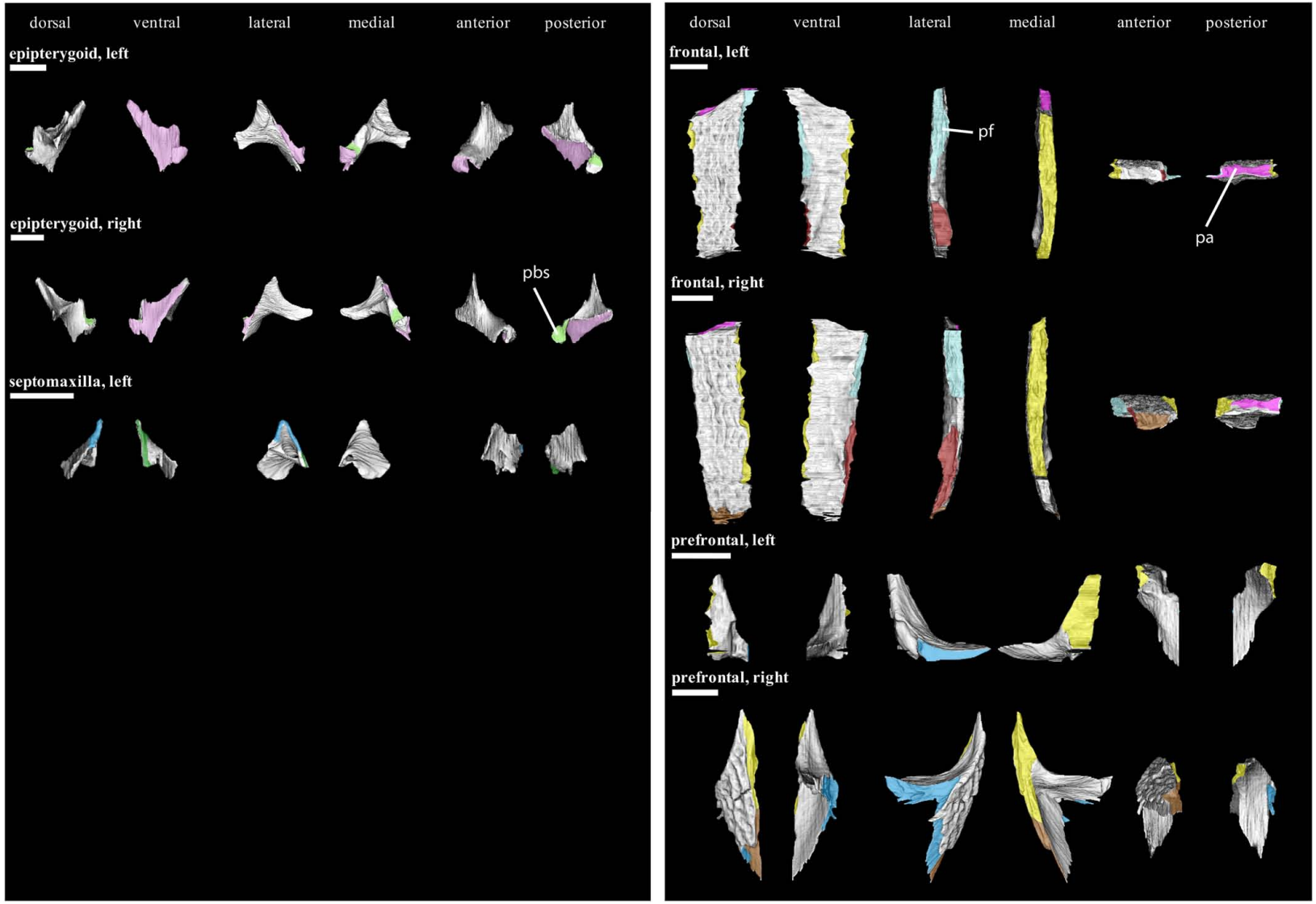

FIGURE 6 | Isolated bones in dorsal, ventral, lateral, medial, anterior and posterior views. Articulation areas with other bones are colored. Left and right epipterygoid, left septomaxilla, left and right frontal, and left and right prefrontal are shown. Scale bar = 10 mm. For abbreviations see caption to **Figure 1**.

FIGURE 7 | Isolated bones in dorsal, ventral, lateral, medial, anterior and posterior views. Articulation areas with other bones are colored. Left and right pterygoid, left and right palatine, right jugal, and left and right quadratojugal are shown. Scale bar = 10 mm. For abbreviations see caption to **Figure 1**.

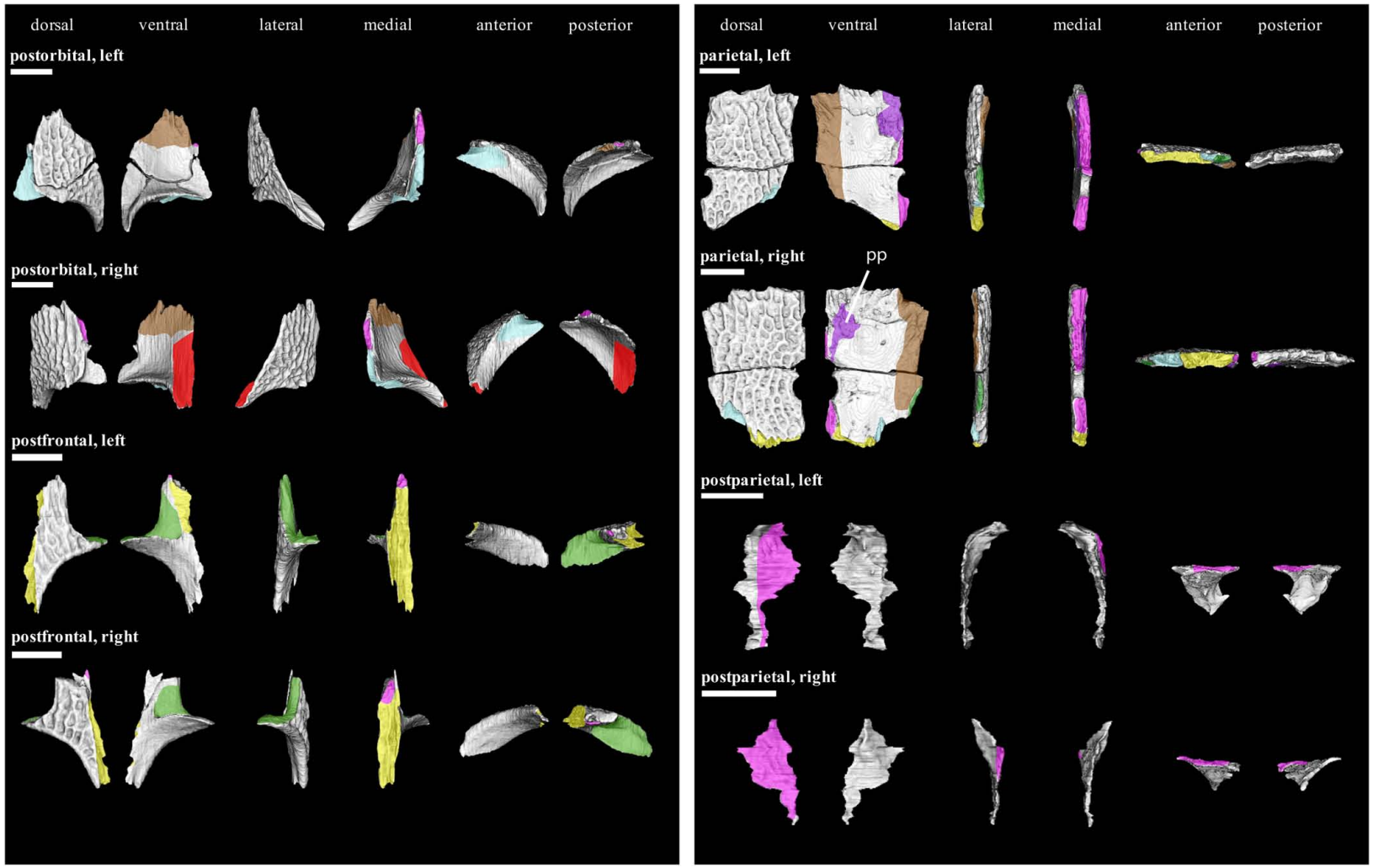

FIGURE 8 | Isolated bones in dorsal, ventral, lateral, medial, anterior and posterior views. Articulation areas with other bones are colored. Left and right postorbital, left and right postfrontal, left and right parietal, and left and right postparietal are shown. Scale bar = 10 mm. For abbreviations see caption to **Figure 1**.

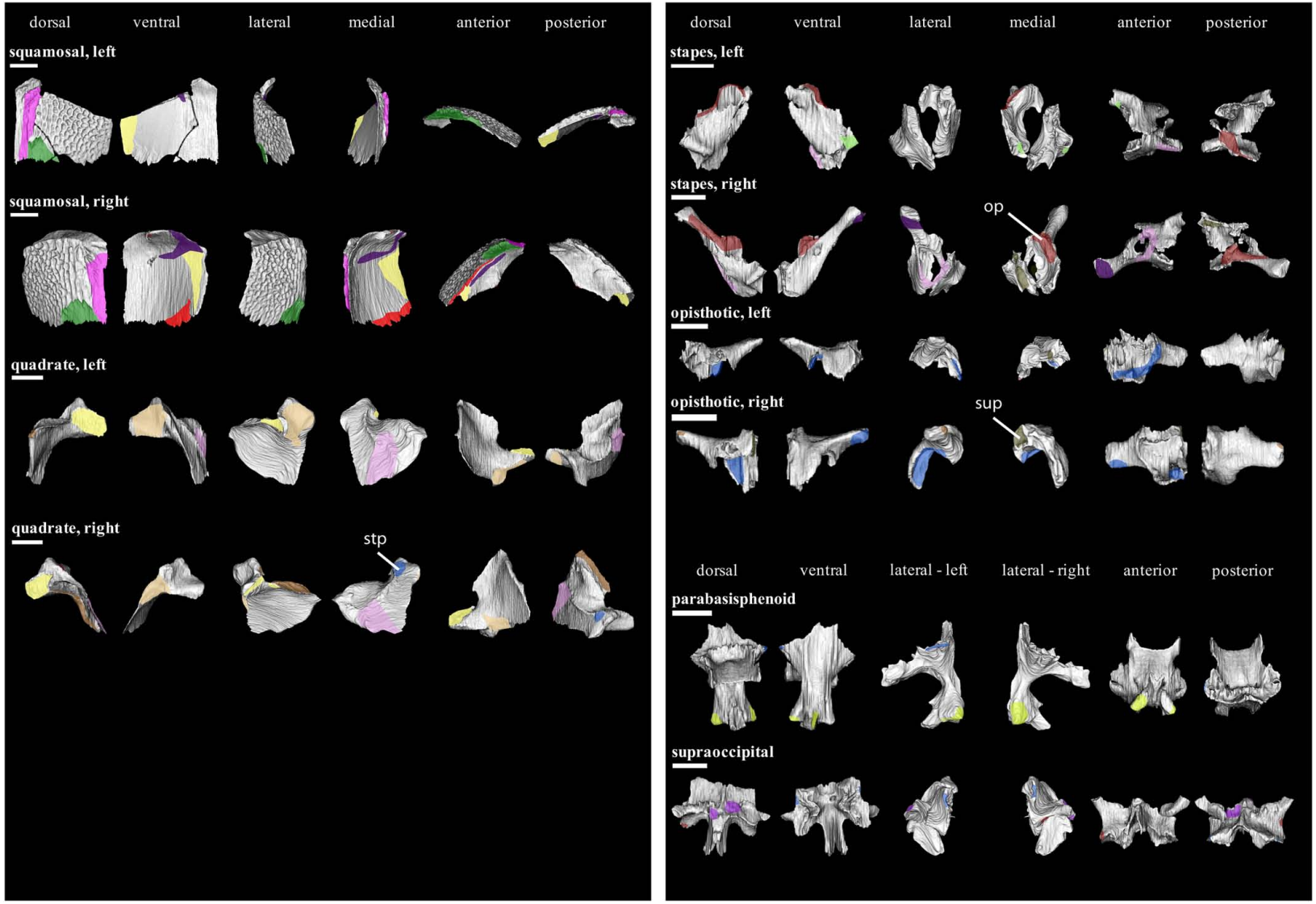

FIGURE 9 | Isolated bones in dorsal, ventral, lateral, medial, anterior and posterior views. Articulation areas with other bones are colored. Left and right squamosal, Left and right quadrate, Left and right stapes, Left and right opisthotic, parabasisphenoid, and supraoccipital are shown. Scale bar = 10 mm. For abbreviations see caption to **Figure 1**.

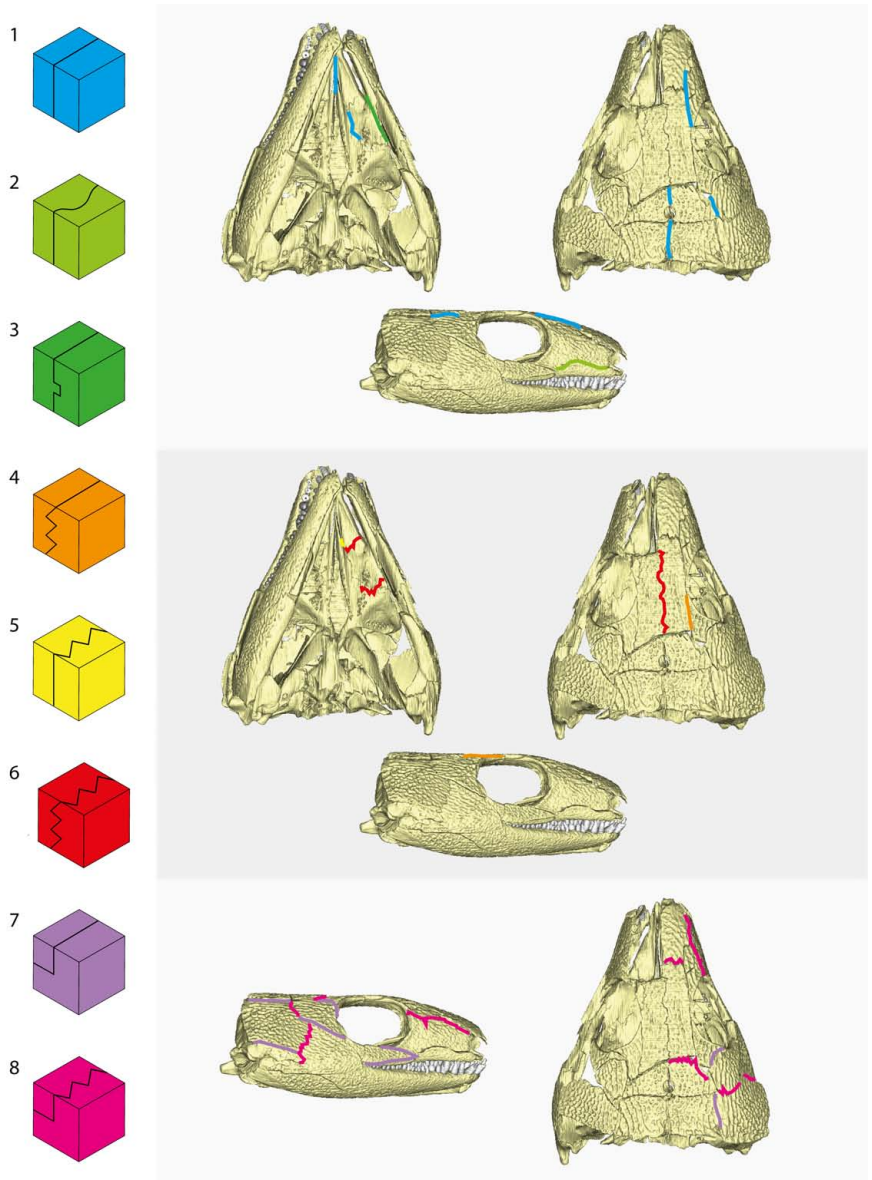

FIGURE 10 | Suture types observed in the dermatocranium of OMNH 44816 and their position in the skull. 1, butt joint; 2, tongue-and-groove joint; 3, slot joint; 4, Type-A interdigitation; 5, Type-B interdigitation; 6, Type-C interdigitation; 7, stepped joint; 8, stepped interdigitation. Terminology mostly after Jones et al. (2011).

The postorbital (**Figure 8**) anterodorsally underlies the postfrontal (stepped joint). Dorsally, the postorbital is simply contacted by the parietal (butt joint; 1 in **Figure 10**). Posteriorly, the postorbital is underlain by the squamosal, and like between the squamosal and the jugal, both contacts interdigitate externally (stepped interdigitation).

Next to its sutures with the postorbital and frontal, the postfrontal (**Figure 8**) likewise contacts the parietal posteriorly by a stepped interdigitation.

The squamosal (**Figure 9**) underlies the parietal dorsally, forming together another stepped joint. Ventrally, the squamosal itself is underlain by the quadratojugal in a similar manner. Posterodorsally, it would have also sutured to the supratemporal; however, we were not able to reconstruct the latter for OMNH 44816. Similarly, both postparietals are too badly preserved to make any judgment about their contact to the squamosal. Medially, the squamosal is contacted by the quadrate. At the medial margin of its occipital flange, the squamosal forms a short contact with the opisthotic. We are not able to unambiguously confirm a contact with the supraoccipital.

In addition to the contacts with the squamosal and jugal, the quadratojugal (**Figure 7**) is underlain posteriorly by the quadrate.

Other sutures with the parietal (**Figure 8**) include the contact with the postparietal, which it overlaps posteriorly (stepped joint). Posterolaterally, it would have contacted the

supratemporal. Both parietals suture each other medially by a butt joint. The supraoccipital would have sutured with the parietals posteroventrally.

The left and right postparietal (**Figure 8**) are sutured to each other medially by a thin Type-C interdigitation (6 in **Figure 10**). Ventrally, they overlap the supraoccipital.

Palatal Region

The dermal palate consists of three bones: the vomer, palatine, and pterygoid. All three bones are rigidly connected by interdigitating sutures.

Both vomers (**Figure 4**) contact each other medially at their anterior end by a butt joint (1 in **Figure 10**). Posteriorly, the vomer interdigitates with the palatine by a Type-C interdigitation (6 in **Figure 10**). A shorter interdigitation with the pterygoid can be observed at its posteromedial edge ("Type-B interdigitation"; 5 in **Figure 10**). Additionally, the rod-shaped anterior extension of the pterygoid is on much of its lateral margin contacted with the vomer by a butt joint. Anteriorly, the vomer would have contacted the premaxilla.

The palatine (**Figure 7**) interdigitates further with the pterygoid at its posterior and medial margins (Type-C interdigitation). Anteromedially, the palatine-pterygoid contact develops into simple a butt joint. As described above for the preorbital region, the palatine is laterally contacts the maxilla and lacrimal.

At their anterior extremity, both pterygoids (**Figure 7**) contact each other medially by a short butt joint. In the anteromedial section of the quadrate process, the pterygoid is overlapped by the epipterygoid. The pterygoid does not contact the parabasisphenoid. Posterolaterally, the quadrate broadly contacts the quadrate process of the pterygoid. Posteromedially, the same process is abutted by the stapes.

Mandible

The bones of the mandible comprise the dentary, angular, surangular, coronoid, splenial, prearticular, and articular. The mandibular symphysis is restricted to the anterior tip of the mandible. In most cases, the bones of the lower jaw have simple contacts with each other. Interdigitating sutures appear only on the external surface.

Both dentaries (**Figure 3**) are sutured to each other on their anteromedial end by a butt joint (1 in **Figure 10**). On its external surface, the dentary interdigitates posteriorly with the angular by a Type-B interdigitation (5 in **Figure 10**). Medially, the two bones contact each other along the posterior half of the dentary by what may be referred to as a butt joint. A similar arrangement exists between dentary and surangular; the latter borders the dentary posterodorsally. Medially, the splenial also contacts the dentary both dorsally and ventrally to the Meckelian groove. The dorsal contact is similar to the medial contacts with the angular and surangular described above, however, ventrally, the splenial slightly underlies the dentary by a stepped joint (7 in **Figure 10**). Posterior to the dorsal dentary-splenial suture, the dentary contacts the anterior end of the prearticular by another butt joint. The medial portion of the dentary, dorsally to the other mandibular bones, is mostly covered by the coronoid.

Next to its already described contact with the dentary, the midsection of the coronoid (**Figure 3**) overlaps the anterior prearticular by a butt joint. Anteriorly, the coronoid tapers between the dentary and splenial. Posteriorly, a large wedge of the surangular protrudes to the coronoid, forming a short interdigitating sequence.

At their anterior ends, both splenials (**Figure 4**) contact each other medially by a butt joint as part of the mandibular symphysis. Posterodorsally, the prearticular tapers in-between the dentary-splenial contact. Posterolaterally, the angular contacts the splenial by a butt joint; posteroventrally, it also overlies the splenial by a stepped joint.

Like described above, the surangular interdigitates anteriorly with the dentary and coronoid by a Type-B interdigitation. On its external surface, it is ventrally overlapped by the angular by a stepped joint. On their internal surface, both bones exhibit a Type-B interdigitation. The prearticular simply sutures the surangular by a butt joint at its posteroventral extremity. Posteromedially, the surangular is wedged into the articular.

Apart from its sutures mentioned above, the angular (**Figure 3**) is dorsally overlain by the prearticular medially to the Meckelian groove. The latter widens medially at its posterior end to surround the ventral portion of the articular.

Suture Thickness

The thickness of bones at their sutures varies greatly in the dermatocranium of OMNH 44816 (**Supplementary Table 2** and **Figure 11**). Overall, the thinnest sutural areas in the skull are the anterior palate (0.52–0.79 mm), the intersection of jugal, squamosal, and postorbital (0.46–1.33 mm), the interparietal contact (0.36–1.34 mm) as well as the dorsolateral rostrum (0.78–1.12 mm). The thickest areas are located close to the maxilla (max. 2.93 mm), in the anterior "cheek" (max. 3.56 mm), at the lacrimal-palatine contact (max. 3.55 mm), and between both pterygoids (max. 2.32 mm). Noteworthy trends include a thinning of the jugal-squamosal, jugal-postorbital, and squamosal-postorbital sutures toward the jugal-squamosal-postorbital intersection, as well as a thinning in anterior direction along the sutures between parietal and "cheek."

DISCUSSION

Suture Morphology and Strain Transmission in OMNH 44816

Sutures connect neighboring skull bones by differently arranged viscoelastic fibers (Herring, 2008). In addition to providing sites for bone growth, the main function of sutures is likely the absorption and transmission of strain (e.g., Herring et al., 1996; Herring and Teng, 2000; Herring, 2008; Moazen et al., 2009; Curtis et al., 2013; even though some theoretical approaches showed only little effect of sutures on strain distribution: see Ferreira et al., 2020). Moreover, soft- and hard-tissue suture morphology is dependent on the presence and, probably, also on the type of strain (e.g., Moss, 1957; Herring, 1972, 2008; Herring and Mucci, 1991). However, osteological evidence alone is not suitable to unambiguously determine the main type of strain

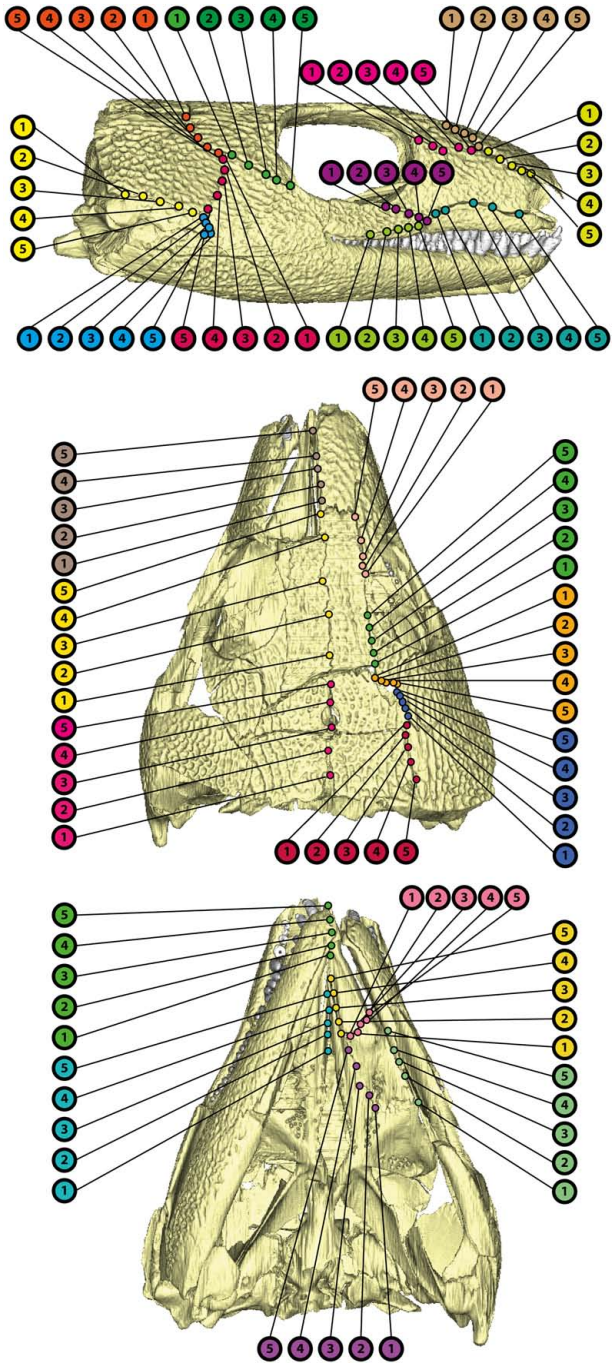

FIGURE 11 | Points of measurements for suture thickness in OMNH 44816 as indicated in **Supplementary Table 2**.

affecting a suture (Herring and Mucci, 1991; Rayfield, 2005). Overall, suture morphology may be used to roughly infer the distribution of strain within the skull and jaw adductor action even when *in vivo* observations are not possible (Herring, 1972).

The eight identified suture types can be broadly subdivided based on their complexity and, hence, their assumed robustness (Herring, 2008). Simple butt joints (1 in **Figure 10**) like they occur especially in the anterior palate, but also at the prefrontal-nasal and postorbital-parietal contacts, as well as between the parietals, could be interpreted as regions little affected by mechanical stimuli (Moss, 1957). Butt joints have been associated with both compressional and tensile strain (Herring and Mucci, 1991; Rayfield, 2005; Porro et al., 2015), making a more detailed interpretation for OMNH 44816 difficult. Compared to other suture morphotypes, butt joints might be least resistant toward stress and strain due to less available attachment area for the fibers (Jones et al., 2011). The slot and tongue-and-groove joints (2 and 3 in **Figure 10**) only occur in the preorbital region and adjacent palatal contacts. Tongue-and-groove joints had been previously interpreted as an adaptation toward tensile strains (Herring and Mucci, 1991; Porro et al., 2015; Rawson et al., 2021). Based on their horizontally intercalated geometry, we would tentatively argue that slot joints are more resistant to compressive than to tensile strains. The majority of the dermal bones in *C. aguti* are connected by stepped joints or stepped interdigitations [7 and 8 in **Figure 10**; see also Jones and Zikmund (2012)]. Other types of interdigitations (4, 5, and 6 in **Figure 10**) are restricted to the frontal and palatal region. The role of stepped joints appears to be more complex (Rayfield, 2005; Porro et al., 2015; Rawson et al., 2021). They might act as a response to shear (Bolt, 1974), torsion (Busbey, 1995; Clack, 2002), or to a combination of tension and compression (Gans, 1960; Markey et al., 2006). Robustness of stepped joints might have been higher when the respective bones were additionally connected by external interdigitations (8 in **Figure 3**). Generally, interdigitations have been shown to be an adaptation to compression and overall high strains (e.g., Herring, 1972; Rafferty and Herring, 1999; Rayfield, 2005; Markey et al., 2006).

Additionally, suture robustness may be also controlled by interdigitation type. Bones that are only interdigitated at their articulation facet (5 in **Figure 10**) may be less resistant to forces acting longitudinally to the suture than bones that are additionally interdigitated at their external surfaces (6 in **Figure 10**). Comparably, a lack of interdigitations at the articulation facet may also reduce the resistance to vertical forces (4 in **Figure 10**). Overall, a higher degree of interdigitation leads to more available fiber attachment area and thus to a higher resistance toward strain than simpler suture morphotypes (Herring, 1972). Also considering thickness measurements, potentially weak areas might have been at the jugal-squamosal-postorbital intersection, at the parietal-postorbital suture, between both parietals, at the dorsolateral rostrum, and in the anterior palate.

These assumptions also allow direct comparisons with the suture morphology described for several Paleozoic non-amniotes (e.g., Klembara, 1994; Kathe, 1995, 1999; Berman et al., 2010; Porro et al., 2015; Gruntmejer et al., 2019; Rawson et al., 2021), especially when focusing on the temporal region. Interdigitations can be seen in a wide array of taxa, and often developed for more sutures than found in the skull of OMNH 44816 (Porro et al., 2015; Gruntmejer et al., 2019; Rawson et al., 2021); however, there are also numerous examples with less pronounced or absent interdigitations in this part of the skull.

In many cases, morphotypes corresponding to the herein used butt and stepped joints prevail (Klembara, 1994; Kathe, 1995), arguing that compressional strain on the temporal region was comparatively low. This highlights that strain distribution in the temporal region could differ markedly among Paleozoic limbed vertebrates. Considering that the formation of temporal openings is due to specific distributions of strain within the temporal region (Abel and Werneburg, 2021), this might explain why temporal openings occur mainly in amniotes and only in few other clades in which these preconditions are met (see section "Cranial Mechanics and the Evolution of Temporal Openings").

The main source of strain within the temporal region is likely related to the action of the jaw musculature (Jones et al., 2011). Indeed, it has been demonstrated that attachment of the jaw adductors is directly related to suture morphology (Herring and Mucci, 1991; Herring and Teng, 2000). More precisely, forces that are applied onto the cranium by muscle action cause the bony coverage to respond by a strengthening of the affected bones and sutures (e.g., Case, 1924; Herring and Mucci, 1991; Rayfield, 2005; Jones et al., 2011); with stronger sutures inevitably reducing the intracranial mobility in the respective skull areas (Clack, 2002). Such forces are expected to be applied especially by direct or indirect action of the jaw adductors (Herring and Mucci, 1991; Herring et al., 1996; Rafferty et al., 2000); we, hence, focus on this set of muscles herein. We appreciate, however, that also neck muscles, related to the posture and movement of the head and being relevant for feeding biology when pulling food items, play a role for the biomechanics of the temporal region (*sensu* Werneburg, 2015; Werneburg et al., 2015). As no radical differences in neck mobility are expected among most early amniotes, we consider that as a stable condition among clades and do not discuss neck musculature any further.

Jaw Musculature in *Captorhinus aguti*

Challenges of Cranial Muscle Reconstruction

Direct evidence for muscle is usually not preserved in the fossil record. While specific morphological features of bones like processes, ridges, or scars can be used to deduce former muscle attachment sites (e.g., Fox, 1964; Heaton, 1979; Witzmann and Werneburg, 2017), there are also some limitations to a purely osteological approach as muscles may also attach to cartilage or other soft tissue like skin and usually do not leave any trace on the bones (e.g., Romer, 1927; Schumacher, 1973; Werneburg, 2011; Wilken et al., 2019). The development of osteological correlates may be dependent on the type of attaching tissue [fleshy or tendinous; Bryant and Seymour (1990) and references therein; Werneburg, 2011, 2013a,b] and may vary within a species or even between both sides of the skull (Poglayen-Neuwall, 1953; Witzmann and Werneburg, 2017). Such uncertainties could be met by taking the known myology of comparable taxa into account.

Analogs to Reconstruct Fossil Musculature

Comparative anatomical studies show that in tetrapods the jaw adductors generally can be subdivided into an external, internal, and posterior compartment based on their respective position relative to the divisions of the trigeminal nerve (e.g., Luther, 1914; Barghusen, 1973; Holliday and Witmer, 2007; Diogo et al., 2008; Witzmann and Werneburg, 2017; Ferreira and Werneburg, 2019). Within reptiles, the external jaw adductors ["adductor mandibulae externus" (AME)] usually originate from the dermal bones of the skull roof and "cheek," and sometimes also from the quadrate or neurocranium. The internal adductors ["adductor mandibulae internus" (AMI)] originate mostly from the palate and the lateral braincase wall. The posterior jaw adductor ["adductor mandibulae posterior" (AMP)] arises from the quadrate. All jaw adductors insert onto the posterior portion of the mandible (Holliday and Witmer, 2007; Diogo and Abdala, 2010; Werneburg, 2011, 2013a; Ziermann et al., 2018; Ferreira and Werneburg, 2019).

In reptiles, the external adductor (AME) can be usually further subdivided into a lateral ["adductor mandibulae externus superficialis" (AMES)], a deep ["adductor mandibulae externus profundus" (AMEP)], and a medial muscle portion ["adductor mandibulae externus medialis" (AMEM)]; the internal adductors can be subdivided into the pterygoideus (PT), pseudotemporalis (PST), and constrictor internus dorsalis (CID) muscles (Holliday and Witmer, 2007; Werneburg, 2011; Ferreira and Werneburg, 2019; and references in these works). However, variation to this pattern can be observed widely across various taxa (Holliday and Witmer, 2007; Daza et al., 2011; Werneburg, 2013a). Nevertheless, assuming these subdivisions to represent the plesiomorphic condition of extant reptiles, it may be inferred that it also represented the condition in an early-diverging taxon like *C. aguti*. The condition found in mammals is highly derived with a masseter muscle first evolving in Cynodontia (Barghusen, 1973; Abdala and Damiani, 2004; Werneburg, 2013b). Homologizations of reptilian to lissamphibian muscles are possible (Diogo and Abdala, 2010). Therefore, we consider the ancestral reptilian condition as also ancestral to Amniota as a whole.

Most extant amniotes possess temporal fenestrae, and at least the external jaw adductors are usually associated with the surrounding temporal bars (e.g., Holliday and Witmer, 2007; Jones et al., 2009; Werneburg, 2019). Consequently, the muscle attachment sites for an extinct taxon with a scutal temporal region like *C. aguti* may not be fully predictable based on these taxa. Considering the shared trait of a skull without temporal fenestrae, turtles instead might be an intuitively fitting extant analog for *C. aguti*. Whereas the majority of extant turtles also possess a distinctly reduced dermal armor in the form of a highly emarginated temporal region (Gaffney, 1979; Jones et al., 2012; Werneburg, 2012; Abel and Werneburg, 2021), some groups like sea turtles as well as the earliest known Testudinata exhibit, like *C. aguti*, a scutal morphology without distinct temporal openings (Gaffney, 1990; Jones et al., 2012). However, most current phylogenetic placements of turtles (e.g., Rieppel and deBraga, 1996; deBraga and Rieppel, 1997; Crawford et al., 2012, 2015; Lyson et al., 2012; Field et al., 2014; Schoch and Sues, 2015; Irisarri et al., 2017; Li et al., 2018; Gemmell et al., 2020; but see also Lichtig and Lucas, 2021) indicate that they are deeply nested within Diapsida and the scutal morphology in early Testudinata likely derived from a fenestrated ancestor due to selective pressures specific to the turtle skull

(Zdansky, 1923–1925; Kilias, 1957; Werneburg, 2015), which also involved a comprehensive rearrangement of soft tissue (Werneburg, 2013a,b) and the suturing of the quadrate to the braincase (Werneburg and Maier, 2019). Additionally, the scutal sea turtle skull likely represents a secondary evolution within Testudines and its jaw muscle arrangement is probably different from the one in early Testudinata (Jones et al., 2012; Werneburg, 2013a; Ferreira and Werneburg, 2019; Werneburg et al., 2019). Hence, while extant turtles can help to predict how the jaw adductors would attach in a scutal skull in general, their derived morphology would limit their applicability for the reconstruction of the jaw musculature in an ancestral "anapsid."

Yet, comparisons with taxa outside of Reptilia might be even less adequate. As mentioned above, mammalian jaw adductors are distinctly derived from the assumed condition in their early synapsid ancestors and cannot be directly homologized with the reptilian condition (Barghusen, 1973; Diogo et al., 2008). Likewise, the specifics of lissamphibian anatomy are largely influenced by metamorphotic developmental events (Haas, 2001, 2003; Iordansky, 2010; Kleinteich and Haas, 2011; Ziermann, 2019), and the nearest extant non-tetrapod relatives, Dipnoi, are argumentatively too distantly related to reptiles to provide a good bracketing taxon (but see Werneburg, 2019). Taking all into account, the jaw adductors of *C. aguti* may be best inferred from the assumed myology in the last common ancestor of all extant reptiles in the context of a scutal temporal region with respect to the osteological peculiarities of *C. aguti*.

Previous Reconstructions of Captorhinid Jaw Musculature

Reconstructions and suggestions regarding the jaw musculature of *C. aguti* and other captorhinids have been already provided by previous authors (Adams, 1919; Fox, 1964; Fox and Bowman, 1966; Heaton, 1979; Dodick and Modesto, 1995). Fox (1964) subdivided the external adductors of *Captorhinus* ["capitimandibularis" in Fox (1964)] into two main sections, the lateral "masseter" (i.e., AMES) and the medial "temporal" (i.e., AMEP) section. Additionally, he discussed also the presence of a third section between the AMES and AMEP, which would likely correspond to the AMEM of diapsids. Fox (1964) argued that the AMEP would have been the largest section and attached to the parietal, postfrontal, postorbital, and squamosal. The AMES would have been sheet-like and originated from the jugal, quadratojugal, and squamosal from where it inserted onto the coronoid process (Fox, 1964; Fox and Bowman, 1966). If the AMEM was present, Fox (1964) argued it would have been sheet-like and extend from the skull roof onto a bony "knob" anterodorsally to the Meckelian fossa, as observed for extant tuatara [however, this is likely more complicated, see Jones et al. (2009), given also the fact that tuatara has a diapsid skull morphotype with specifically derived muscle arrangements]. In regard of the internal jaw adductors ["pterygoideus" in Fox (1964)], he suggested a subdivision into an anterior (i.e., PT) and a posterior section (i.e., AMP). Fox (1964) let the PT occupy large portions of the dorsal pterygoid surface as well as the lateral surface of the pterygoid flange. He argued it would have extended in a posteroventral direction, medially to the AMEP, and inserted medially inside the Meckelian fossa. The AMP would have been of limited size and attached to the quadrate from where it would have inserted onto the mandible between the jaw joint and Meckelian fossa. Lastly, Fox (1964) also discussed the presence of a pseudotemporalis muscle (i.e., PST), but he argued that if it would have been present, the relative position of the pterygoid would prohibit an arrangement as observed for extant taxa.

Fox (1964) and Fox and Bowman (1966) partly provided osteological arguments for their suggested muscle arrangements. However, in some cases they also argued for particular muscle attachment sites without describing a clear reasoning, or despite the lack of osteological evidence like muscle scars. Nevertheless, the latter is *per se* legitimated as discussed above as the authors indeed highlighted the impact of different attaching tissues on the presence of osteological correlates.

Fox and Bowman (1966) described distinct striae on the medial portion of the parietals close to the suture between these bones, which would likely indicate a tendinous attachment of the AMEP there [however, see Heaton (1979) below for a different interpretation]. Likewise, they interpreted distinct concavities occupying most of the medial parietal surface as likely fleshy attachment sites of the AMEP, because no structures were visible on the internal bone surface. A bony ridge which ran close to the squamosal-parietal suture probably separated the AMEP from the AMES (Fox, 1964; Fox and Bowman, 1966). Apparently, Fox (1964) also assumed the attachment of the AMES onto the jugal and quadratojugal to be fleshy as he highlighted the smooth medial surfaces of these bones. In the mandible, the AMES would insert onto the surangular portion of the coronoid process at a vertical flange of the surangular that bore two concavities (Fox, 1964; Fox and Bowman, 1966).

Fox (1964) further argued for a tendinous attachment of the PT onto the lateral pterygoid flange as evident by its size, which he also compared to the condition in crocodiles. According to him, too, the attachment to the dorsal pterygoid surface was likely fleshy. The PT could have inserted onto the ventral and medial surfaces of the angular. A medial groove on the prearticular, bearing pits and striae, might have been another insertion site of the PT (Fox and Bowman, 1966). These latter authors suggested that the AMP could have inserted onto a medial ridge formed by the articular and prearticular and a small concavity dorsal to that ridge as indicated by probable muscle scars on both structures. Lastly, based on comparison with tuatara, Fox (1964) suggested that an AMEM with uncertain origin on the skull roof (see above) might have inserted onto a "knob" anterior to the Meckelian fossa.

Heaton (1979) discussed the cranial musculature in the related species *Captorhinus laticeps* ["*Eocaptorhinus*" in Heaton (1979)] and other material referred to the genus. In fact, some of the material described by Heaton (1979) and used for his illustrations might be actually referable to *C. aguti*, namely the specimens found at the Dolese Brothers Quarry (Robert Reisz, personal communication, 2021).

Heaton (1979) disagreed with Fox and Bowman (1966) on the interpretation of the medial striae in the parietals of *Captorhinus* being remnants of a tendinous attachment of the jaw adductors.

Instead, he argued they were due to attachment of meninx and taenia marginalis. The bony ridge that runs parallel to the parietosquamosal suture identified by Fox (1964) and Fox and Bowman (1966) as the border between AMES and AMEP was recognized by Heaton (1979) as an attachment site solely for the AMES. Other sections of the AMES might have attached to the mediodorsal portion of the squamosal. Also, the ventral concavities of the parietals already reported by Fox and Bowman (1966) as likely attachment sites for the AMEP are, according to Heaton (1979), muscle scars from the AMEM. He argued that the AMEM was further divided into an "adductor mandibulae externus 2 c (pars media C)" and "adductor mandibulae externus 2 a (pars media A)" muscle head (*sensu* Lakjer, 1926). The two muscle heads would have been subdivided by the temporal artery, evident by a distinct foramen in the proximity of the mentioned parietal concavity. The "adductor mandibulae externus 2 b (pars media B)" is said to have been attached anteriorly to the concavity, where it left an additional number of muscle scars. A more posterior section of the AMEM would have attached to the quadrate, together with the AMP. Heaton (1979) considered the AMEP to be present; however, he only stated that it would have inserted ventrally to the coronoid like in Fox (1964). For the AMES and AMEM, Heaton (1979) argued that they would have inserted by a joint tendon onto the lateral surface of the surangular.

In addition to the already mentioned AMP, Heaton (1979) identified the PT and PST for the internal jaw adductors. He distinguished between an "anterior" and "posterior" muscle head of the PT [apparently synonymous with "pterygoideus lateralis" and "pterygoideus medius" of Heaton (1979, Figure 24)]. Overall, the PT originated, according to Heaton (1979), from the mediodorsal surface of the pterygoid, including the anterior section of the quadrate process. The PST, subdivided into "pseudotemporalis superficialis" and "pseudotemporalis profundus" after Heaton (1979), originated from the epipterygoid. Heaton (1979) reconstructed a mostly tendinous insertion of the internal jaw adductors onto the mandibular fossa, coronoid, medioposterior prearticular, and onto the medial articular.

The reconstructions of Fox (1964) and Heaton (1979) differ markedly from an earlier proposal of Adams (1919) on the jaw muscles of the captorhinid *Labidosaurus*. Like Fox (1964), Adams (1919) argued that the AMES would attach to the jugal and squamosal, but also to the quadrate instead of the quadratojugal. The AMEP instead would have not been attached to the skull roof, but only to the pterygoid and epipterygoid ["alisphenoid" in Adams (1919)]. He further reconstructed the AMEM as attaching mostly to the parietal and squamosal, which resembles the reconstruction by Heaton (1979) and effectively may be the attachment sites Fox (1964) suggested for the AMEP in *Captorhinus*. Adams (1919) suggested that the external adductors would insert onto the suprameckelian fossa, the PT ventrally onto the retroarticular process. The cranial attachment sites proposed by Adams (1919) for the PT are similar to the ones by Fox (1964) and Heaton (1979); i.e., attaching to the pterygoid]. Adams (1919) did not discuss the AMP and PST. None of the cited references discussed the CID.

Reassessment of the Jaw Adductors in *Captorhinus aguti*

Based on our observations on bone structure and comparisons with published extant amniote jaw muscle anatomy (e.g., Diogo et al., 2008; Daza et al., 2011; Ziermann et al., 2018), we would modify and expand the models of Fox (1964) and Heaton (1979) as follows: In our model, the external section consists of a medial (AMEP) and lateral muscle portion. In lateral view, the lateral portion occupies most of the "cheek" region (**Figure 12A**). It attaches to the jugal and quadratojugal, and it extends dorsally to the squamosal until it meets the ventral bony ridge of the parietal that runs roughly parallel to the parietosquamosal suture (**Figure 12C**).

It is known for marine turtles that the AMES may separate a distinct lateral muscle portion inserting to the broadly armored "cheek" region (Werneburg, 2011; Jones et al., 2012). When present, AMEM is known to attach anterolaterally to the quadrate and medially to the quadratojugal in many turtles (Schumacher, 1973). As highlighted by Werneburg (2011, 2013a), jaw musculature is highly plastic in its anatomy and basically "follows" the arrangements of the temporal skull bones. In this regard, AMEM, which is relatively well-defined in reptiles with temporal fenestration and placed between AMEP and AMES (Holliday and Witmer, 2007; Jones et al., 2009), is considered to exhibit a more fluent nature in non-fenestrated forms. That said, the homology of particular muscle portions and muscle heads among reptiles is debatable (Rieppel, 1987; Werneburg, 2013a). By positional criteria, AMES of turtles might be homologous to AMEM in other reptiles, and the AMEM of turtles might be identical with AMES of other reptiles. However, as musculature develops from a consistent cell mass in early ontogeny and differentiates based on perinatal requirements of the respective animal (Werneburg, 2019), the developmental fate and differentiation of muscle portions might actually be unique to each individual taxon. Medially to the AMES, in our assessment, the AMEP would attach to the postfrontal, postorbital, and parietal (**Figure 12C**). Both external adductors would fuse at the height of the squamosal and insert onto the coronoid process of the mandible (**Figure 12B**).

The internal adductor section would comprise an anterior (PT) and posterior (AMP) muscle portion, an intercalated pseudotemporalis (PST), and a constrictor internus dorsalis (CID) part. The PT would cover the dorsal face of the dermal palate and reach anteriorly to the palatine as indicated by the smooth transition between palatine and pterygoid (**Figures 12D,E**). The PST would attach to the lateral face of the posterior process of the pterygoid, to the (mainly cartilaginous) lateral braincase wall, and maybe with a few fibers to the epipterygoid (*sensu* Heaton, 1979; **Figure 12E**). The AMP would attach to the anterolateral surface of the quadrate (**Figure 12A**). All three muscle portions of the internal adductor section would insert onto the posterior part of the mandibular fossa (**Figure 12B**). The CID is here considered to have been present around the epipterygoid, with an anterior and a posterior part, and attach to the pterygoid dorsally (**Figure 12E**). It is difficult to reconstruct levator arcus palatini, which would dorsally connect to the skull roof and/or the

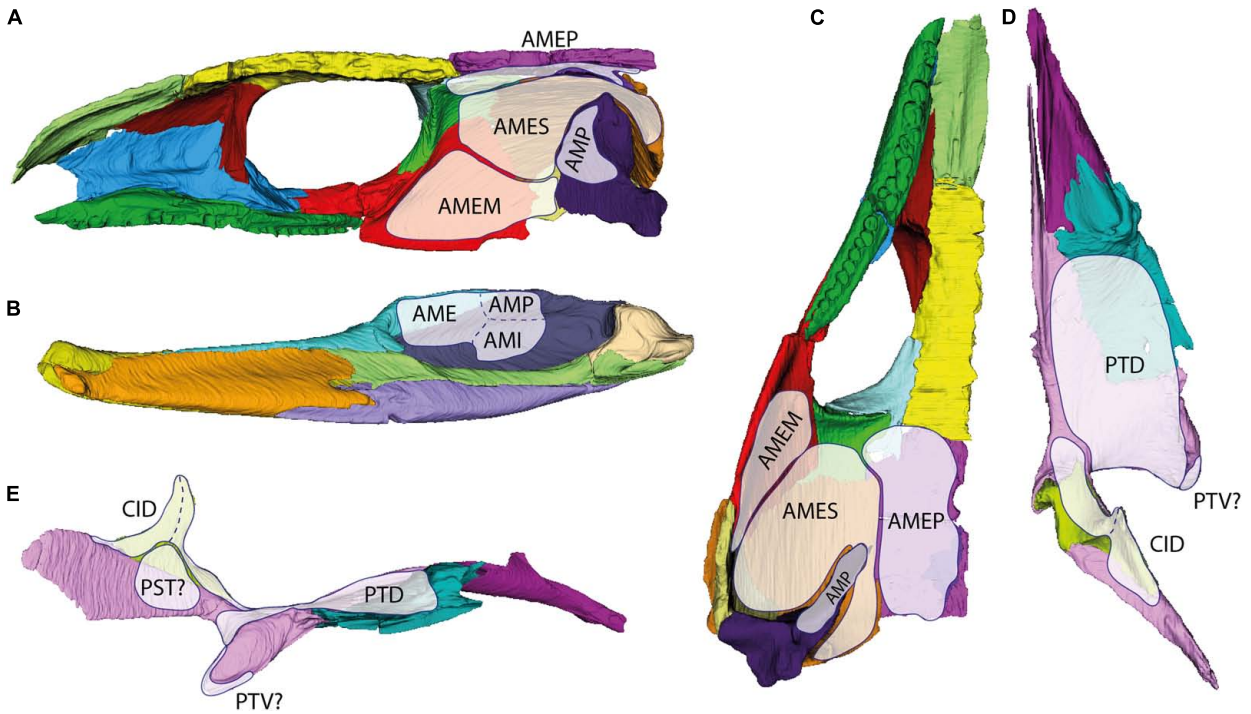

FIGURE 12 | Rough position of the jaw adductor musculature in the temporal dermatocranium of OMNH 44816 in medial **(A)** and ventral view **(C)**; as well as of the internal adductor and constrictor musculature in the palate and epipterygoid in dorsal **(D)** and lateral view **(E)**, and the insertion of all named muscles onto the mandible in medial view **(B)**. AME, adductor mandibulae externus; AMEM, adductor mandibulae externus medialis; AMEP, adductor mandibulae externus profundus; AMES, adductor mandibulae externus superficialis; AMI, adductor mandibulae internus; AMP, adductor mandibulae posterior; CID, constrictor internus dorsalis; PST, pseudotemporalis; PTD, pterygoideus dorsalis; PTV, pterygoideus ventralis.

lateral wall of the braincase and might help to position the palate. Other muscles of the head were not considered for our assessment. Heaton (1979) provided reconstructions of several muscle heads for different muscles, which we think are much too speculative to discern given the rather unspecific osteological correlates in this fossil.

Cranial Kinesis and Elasticity in *Captorhinus aguti*

Our assessments on suture morphology and jaw adductors allow further inferences on cranial kinesis and elasticity. Cranial kinesis describes the movement of one or more bones relative to other bones or set of bones along intracranial sutures. Among extant tetrapods, it is present in various squamates, birds, and lissamphibians, but effectively absent in mammals, crocodylians, turtles, and tuatara (e.g., Versluys, 1910; Frazzetta, 1962; Bock, 1964; Iordansky, 1990; Metzger, 2002; Holliday and Witmer, 2008; Jones et al., 2011; Natchev et al., 2016; Werneburg and Maier, 2019; Yaryhin and Werneburg, 2019). The presence and evolution of cranial kinesis has been also discussed for various extinct clades (e.g., Versluys, 1910, 1912; Carroll, 1969a; Bramble and Wake, 1985; Iordansky, 1990; Clack, 2002; Holliday and Witmer, 2008; Cost et al., 2020), even though the inapplicability of *in vivo* studies represents a considerable limitation. In fact, intracranial mobility observed in prepared specimens does not necessarily correspond to movements actually exhibited by the living animal [Evans, 2008; Holliday and Witmer, 2008; however, see also Iordansky (2011)]. Cranial kinesis proper, which describes active movements of skull parts due to muscle action, should further be distinguished from passive elastic/flexible movements of bone and cartilage due to applied strain (Fracasso, 1983; Rayfield, 2005; Moazen et al., 2009). Indeed, all skulls require at least some degree of elasticity/flexibility to avoid breakage; hence, "passive kinesis" is also present in skulls that might usually be considered akinetic in terms of cranial kinesis proper (Thomson, 1967; Beaumont, 1977; Kathe, 1999; Herring, 2008; Natchev et al., 2016). It is expected that even "stepped joints" and distinctly interdigitated sutures still react elastically to mechanical stimuli, especially when the respective bones are thin in the sutural area (Beaumont, 1977; Clack, 2002; Natchev et al., 2016). The relationship between elasticity at intracranial sutures and the evolution of cranial kinesis proper is uncertain (Moazen et al., 2009).

Using the examples of lepidosaurs and bird-line archosaurs, Holliday and Witmer (2008) provided a list of criteria that need to be fulfilled to allow cranial kinesis proper. In the following, we will discuss these criteria based on our observations on OMNH 44816 and whether previously defined types of cranial kinesis (i.e., at the basicranial joint; otic joint; pleurokinesis; metakinesis; mesokinesis; prokinesis; rhynchokinesis) were present in *C. aguti*.

For the condylar basicranial joint (i.e., between the palate and neurocranium), we can confirm previous observations in *Captorhinus* specimens (Warren, 1961; Heaton, 1979; however, see also Olson, 1951; Fox and Bowman, 1966) that the pterygoid does not directly contact the parabasisphenoid. Instead, the joint is formed only between parabasisphenoid and epipterygoid (see Werneburg and Maier, 2019). The basicranial joint is plesiomorphic in tetrapods (Thomson, 1967; Beaumont, 1977; Iordansky, 1990; Porro et al., 2015) and notably immobilized in extant turtles (e.g., Gaffney, 1979; Werneburg and Maier, 2019; Ferreira et al., 2020), further highlighting their more derived state relative to early scutal reptiles. Presence of a synovial basicranial joint is the first criterion defined for cranial kinesis ("basipterygopterygoid joint" in Holliday and Witmer, 2008); however, whether a condylar joint was indeed synovial is hard to determine for fossil specimens (Bailleul and Holliday, 2017) and even if present, it might not necessarily imply any form of cranial kinesis proper (Holliday and Witmer, 2008; Johnston, 2010; Payne et al., 2011). Nevertheless, using a modularity approach of skull network integrity, Werneburg and Abel (2022) reconstructed a clear distinction between the palate and epipterygoid on one side and the braincase on the other side suggesting the presence of ancestral basicranial mobility in *C. aguti*. The anatomical network approach (AnNA) uded by the authors does not consider suture anatomy but only the presence and absence of bone contact with bones contacting many other bones being more integrated and, hence, less labile or mobile in a functional sense. This methodology might be understood as additional line of evidence to understand intracranial mobility (Werneburg and Abel, 2022).

Iordansky (1990, 2011, 2015) considered pleurokinesis (i.e., mediolateral movement of the quadrate together with other "maxillobuccal" segments relative to the axial parts of the skull) to be present in the earliest amniotes ["reptiles" in Iordansky (1990, 2011, 2015)]. Indeed, the butting contact of the quadrate with the quadrate wing of the pterygoid as well as the probable attachment site of the AMP suggest that some degree of mediolateral movement could have been possible in the quadrate of *C. aguti*. Yet, this was certainly restricted by the contact of the quadrate with the quadratojugal and squamosal. In fact, a condylar and, therefore, potentially synovial otic joint like it can be observed in many later diverging taxa is not observable in OMNH 44816, *C. aguti* thereby lacked an important criterion for cranial kinesis *sensu* Holliday and Witmer (2008). Similar to the basicranial joint, pleurokinesis has been considered to be the plesiomorphic condition in tetrapods (Iordansky, 1990) and proposed for various extant and extinct taxa like lissamphibians (e.g., Iordansky, 2000; Natchev et al., 2016), squamates (e.g., Iordansky, 2004, 2015), or ornithopod dinosaurs (e.g., Norman and Weishampel, 1985); however, unambiguous evidence for active pleurokinesis in any of these taxa is rare at best, if present at all (Evans, 2008; Holliday and Witmer, 2008; Cuthbertson et al., 2012; Heiss and Grell, 2019; but see also Werneburg and Abel, 2022).

A metakinetic joint (i.e., movement of the temporal dermatocranium, together with the snout, relative to the occiput; Frazzetta, 1962) has been repeatedly described for early amniotes (e.g., Versluys, 1912; Carroll, 1969a; Gow, 1972; Bramble and Wake, 1985; Iordansky, 1990), even though its nature in extant taxa has remained barely understood until recently (Mezzasalma et al., 2014; Handschuh et al., 2019), where it is mainly present in squamates (Evans, 2008; Jones et al., 2011), but maybe also in some other tetrapods (Natchev et al., 2016). In OMNH 44816, bony contacts between the temporal dermatocranium and the braincase are only present between the postparietal and supraoccipital, as well as between squamosal and opisthotic. Based on other *Captorhinus* specimens, the supraoccipital was also dorsally sutured to the parietal by a bony process (Fox and Bowman, 1966; Heaton, 1979) and might have been also sutured to the squamosals (Price, 1935). Even though captorhinids shared with later-diverging taxa the loss of the tabulars (e.g., Modesto et al., 2007), especially the retained contact between postparietals and supraoccipital argues against any major mobility in the metakinetic axis of *C. aguti* (Evans, 2008). Werneburg and Abel (2022) found the braincase to form a separate functional module in *C. aguti*, which would argue for some form of metakinesis or for a weaker connection at the metakinetic axis at least that could serve as a precondition to establish metakinesis later in evolution.

Mesokinesis (*sensu* Frazzetta, 1962; i.e., active movements of the parietals relative to the frontals) can be excluded for *C. aguti* based on the stepped interdigitation between the respective bones. In fact, mesokinesis can be considered a highly derived condition mostly restricted to squamates and some caudates (Frazzetta, 1962; Bramble and Wake, 1985; Natchev et al., 2016). However, this does not necessarily exclude any form of elasticity in the frontoparietal region (Natchev et al., 2016; Werneburg and Abel, 2022). When the jaw was closed in *C. aguti*, the AMEP probably exerted a pulling force on the parietals relative to the frontals, distributing force onto the frontoparietal suture, eventually triggering the development of a more complexly stepped interdigitation there. Nevertheless, the comparatively high thickness in the sutures of the frontal region in *C. aguti* (**Supplementary Table 2**) as well as the external bony ridges might additionally have decreased the degree of elastic movements. Werneburg and Abel (2022) found a modular distinction between frontals and parietals, but based on the results presented herein, they basically refuted mesokinesis in *C. aguti*. The distinction between two modules in this area of the skull might hint at functionally differentiated skull parts in *C. aguti*—that moved against each other by elasticity as assumed herein—or to an ancestral differentiation of the skull inherited from more rootward tetrapods.

Likewise, action of AMEM (of our reconstruction) and AMES onto the "cheek" might have also exerted pulling forces on the jugal, squamosal, and postorbital. Being overall thinner than the parietal, elasticity was probably generally higher in the "cheek" than in the skull roof. Like in the frontoparietal suture, the pulling force on the "cheek" likely selected for a similarly stepped interdigitation between these bones (**Figure 13C**, sutures II, III, V). Yet, the contact of the parietals with the "cheek" is less complex and might even be considered "weak" (Frazzetta, 1968). However, this area seems to be more stabilized against

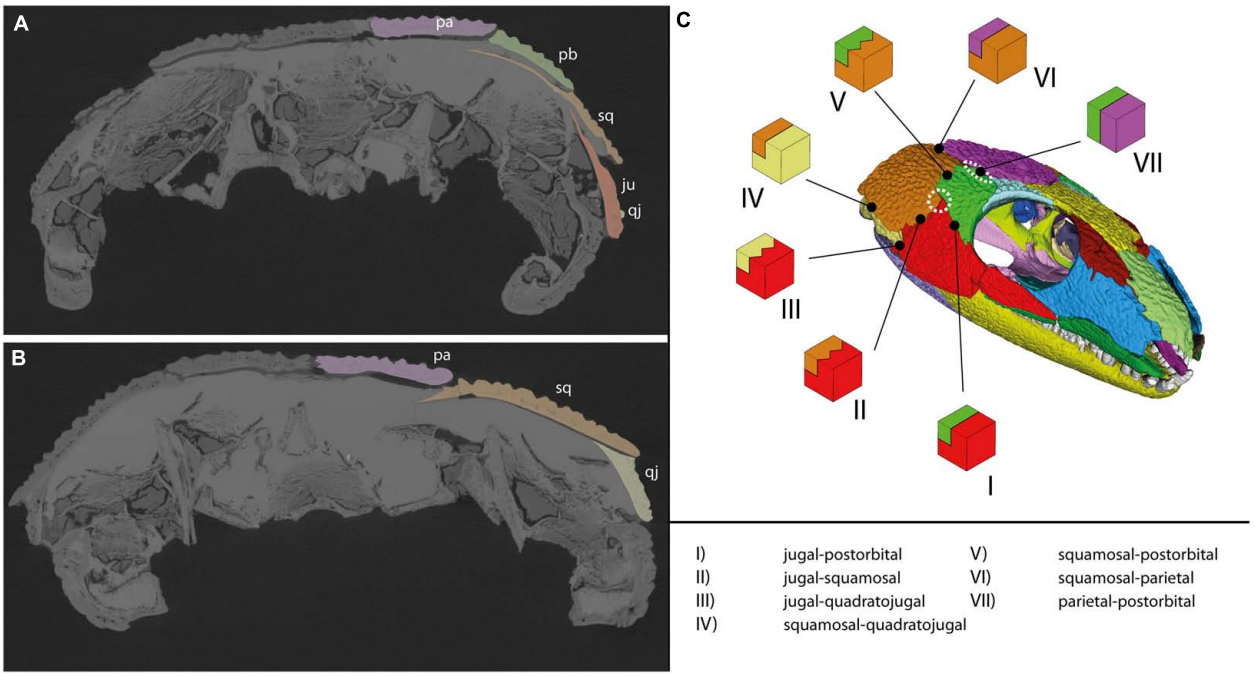

FIGURE 13 | Cross section through the temporal region of OMNH 44816 in posterior view highlighting the internal contacts of the dermal bones. **(A)** Anterior temporal region; **(B)** posterior temporal region. **(C)** 3D view on the dermal sutures in the temporal region of OMNH 44816. Dashed lines indicate potentially weak areas that could correspond to temporal openings in other early amniotes.

torsion due to the lamina extruding from the squamosal medially to meet a medioventral ridge of the parietal (**Figure 13B**). Only the parietal-postorbital contact still appears to be simple (**Figure 13A**). Nevertheless, the high modular integrity of the postorbital within the dermatocranium and the more complex sutures to its neighboring bones, as well as the parietal-squamosal contact, likely restricted further mobility (Werneburg and Abel, 2022). Yet, the simple nature of the parietal-postorbital suture could indicate that it was less affected by compressional forces than the other sutures in the temporal region (**Figure 13C**).

A joint between the snout and more posterior parts of the skull, as it occurs in most batrachians, snakes, and birds (prokinesis, rhynchokinesis; Bock, 1964; Iordansky, 1990), can be excluded for *C. aguti*. The frequently stepped interdigitations in the snout likely evolved to withstand the forces generated from the interaction between the tooth-bearing maxilla and food items (Jones and Zikmund, 2012). This is further evident by the relatively thick sutures between the maxilla, lacrimal, and jugal. The force was probably absorbed by the thinner and, hence, more elastic sutures in more dorsal areas of the snout (between lacrimal, nasal, and prefrontal). Analogous to the parietal-postorbital suture, the simple frontal-prefrontal suture might indicate that this skull area was less affected by compressional forces generated during biting (see also Werneburg and Abel, 2022), but again the high integrity of the prefrontal, as well as the thicker suture, argues against any major mobility.

The derived condition and possible mobility of the palate in *Captorhinus* and other early amniotes has been highlighted by previous authors (Fox, 1964; Carroll, 1969a; Bramble and Wake, 1985; however, see also Heaton, 1979, for an opposing view). At the anterior end of the palate, both vomers as well as both pterygoids were likely only loosely connected to each other. Likewise, the articulation between vomer and premaxilla was likely rather simple (Fox and Bowman, 1966). As described by Fox (1964) and Fox and Bowman (1966), and confirmed by our observations herein, there was a joint between the palatine and maxilla that could, on its own, have allowed some rotational movement of the palate. Yet, we agree with Bolt (1974) that in *C. aguti* the palatine also sutured to the lacrimal, which would have restricted rotational motion. Further restriction was likely caused by the anterolateral contact of the pterygoid with the jugal. We were not able to confirm a contact between palatine and the ventral process of the prefrontal (see Williston, 1925; Bolt, 1974). While there was no true kinetic joint between the palatine, vomer, and pterygoid, the relatively thin palatines suggest that the middle palate was quite elastic and would have bent dorsally by action of the dorsally attaching PT when the jaw was closed. The epipterygoid is ancestrally not fused to the braincase (as in mammals, turtles, and crocodylians) in *C. aguti*, suggesting the presence of the epipterygoid-associated CID musculature. Together, they might have permitted a certain pro- and retraction of the palate relative to the rest of the skull. The differentiation of CID into a "protractor pterygoidei," another criterion for cranial kinesis proper in lepidosaurs and bird-line archosaurs (Holliday and Witmer, 2008), cannot be confirmed for *C. aguti*.

In summary, none of the traditionally defined types of cranial kinesis can be unambiguously confirmed for *C. aguti*. While we do not exclude that at least some of the criteria by Holliday and Witmer (2008) could have been fulfilled by *C. aguti* (i.e., synovial basicranial joint, m. protractor pterygoideus), we conclude that *C. aguti*, and likely also other early scutal reptiles, were functionally akinetic in terms of cranial kinesis proper. Nevertheless, due to observed differences in suture morphology and thickness, we expect the degree of passive elastic movements to differ depending on the respective skull part and, also, between different parts of the temporal dermatocranium. We wish to highlight that the criteria of Holliday and Witmer (2008) were erected for and nicely apply to extant diapsids, but our discussion might motivate future studies on intracranial mobility beyond traditional perceptions and categorizations.

Cranial Mechanics and the Evolution of Temporal Openings

Taking our morphological considerations, as well as comparisons with other taxa into account, we were able to roughly reconstruct the cranial mechanics in *C. aguti* that likely applies also to other early scutal reptiles. We argue that this offers new insights into the evolution of the amniote temporal region and allows us to infer how temporal openings might have formed in early amniotes.

It can be debated whether *C. aguti* actually represents a suitable model for this approach. As stated previously, the presence of several derived traits in the skull of *C. aguti* as well as its geological age urge to caution in using it as an analog for the condition in the hypothetical ancestral amniote. To complicate things further, interrelationships at the base of Amniota are still widely discussed (e.g., Laurin and Piñeiro, 2017; MacDougall et al., 2018; Klembara et al., 2019; Mann et al., 2019, 2021; Ford and Benson, 2020). Hence, the ancestral morphology of the amniote skull, and especially the point of when as well as how often temporal openings appeared, is difficult to reconstruct (Laurin and Piñeiro, 2017; Ford and Benson, 2020; Abel and Werneburg, 2021). However, due to reasons mentioned in the Introduction section, we think *Captorhinus aguti* may well be, for now, an acceptable representative to investigate the origins of temporal fenestration in ancestral amniotes (see also Maier, 1993, 1999). We will also further discuss in this chapter differences and similarities between *C. aguti* and other taxa, notably earlier captorhinids, "protorothyrididś", and some other early potential amniotes.

In case of the "cheek," the cranial mechanics of *C. aguti* can be generally described as outlined by Fox (1964). Contraction of the AMES/AMEM (in our reconstruction) would have exerted a ventromedial bending of the bones in the "cheek" region. Additionally, the quadrate would have directed force from posterior onto the squamosal and quadratojugal. This might explain the more stabilized squamosal-quadratojugal contact by the distinctly extruding bony lamina from the quadratojugal medial to the squamosal (**Figure 13B**). We can confirm the observation of Fox (1964) that there is a thin area at the intersection of jugal, squamosal, and postorbital (**Supplementary Table 2**), suggesting that it was less affected by muscle forces. Appropriately, the interdigitation that runs dorsoventrally to form most of the anterior contact of the squamosal with jugal and postorbital becomes a less complex suture in the intersection area of the three bones. Fox (1964) reports further that the marginal areas of the "cheek" were strengthened in *Captorhinus* by medially aligned ridges that might have also served as muscle attachment sites (at least for the stronger tendinous attachments, see above). This is also backed up by our own observations. According to the latter, these would also correspond to the external patterns of bone ornamentation, probably another response to force distribution. Such a "network of lines of stress" (Olson, 1961) on its own might select against ossification in lesser loaded areas of the "cheek," eventually forming an opening (e.g., Case, 1924; Olson, 1961; Fox, 1964). Intersections between more than two bones like they occur in the "cheek" of *C. aguti* (**Figure 13C**) might be especially prone to forming a temporal opening (Frazzetta, 1968; Kuhn-Schnyder, 1980; Werneburg and Abel, 2022).

Indeed, there is more evidence for this scenario in other taxa. Next to their typical infratemporal fenestra between jugal, squamosal, and postorbital, some specimens of the early synapsids *Ophiacodon retroversus* Cope (1878) and *Varanosaurus acutirostris* Broili 1904 also exhibit an "accessory temporal fenestra" at their thinned jugal-squamosal-quadratojugal intersection; sometimes even restricted to only one side of the skull (Romer and Price, 1940; Frazzetta, 1968; Berman et al., 1995; Ford, 2018). In the usually non-fenestrated parareptile *Procolophon trigoniceps* Owen 1876, small infratemporal fenestrae can appear in-between different sets of three to four bones (Cisneros, 2008). Moving more rootward, Jaekel (1902) reported for the possible amniote-line tetrapod *Gephyrostegus bohemicus* Jaekel, 1902 thin regions in the "cheek" and parietal area, presumably fitting to the position of temporal openings in later amniotes. These traits have not been mentioned in a recent reassessment of the species (Klembara et al., 2014) and until now, we were not able to study the fossils in person to confirm or refute Jaekel's (1902) observation. Conclusively, it might be nevertheless rather easy to form small temporal openings within thin bone intersections, with their occasional presence representing no major disadvantage for the animal (Romer and Price, 1940; Cisneros, 2008).

While we currently do not possess data on relative suture thickness in other early scutal tetrapods, a jugal-squamosal-postorbital intersection like observed in *C. aguti* is widespread among scutal taxa close to the amniote base (e.g., Clark and Carroll, 1973; Berman et al., 1988; Boy and Martens, 1991; Modesto et al., 2007; Kissel, 2010). Like infratemporal fenestrae (e.g., Abel and Werneburg, 2021), these intersections vary in their relative position in the "cheek," probably related to differences in muscle force distribution. In fact, the latter is thought to play a significant role for the formation of temporal openings during early ontogeny (Werneburg, 2019). Such variation in jaw adductor arrangement might also explain why in many parareptiles the infratemporal fenestra is located within the jugal-squamosal-quadratojugal intersection instead

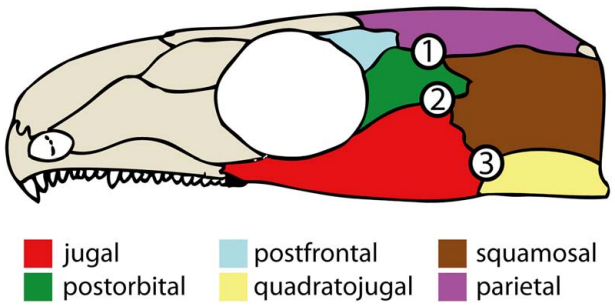

FIGURE 14 | Drawing of the skull of *Captorhinus aguti* after Fox and Bowman (1966) with possible origin sites for temporal openings in the hypothetical ancestral amniote. 1, squamosal-postorbital-parietal intersection; 2, jugal-squamosal-postorbital intersection; 3, jugal-squamosal-quadratojugal intersection. Sites 1 and 2 are the most likely origin sites for a taxon similar to *Captorhinus*. Site 3 occurs especially in Parareptilia. Temporal openings in early Synapsida and Diapsida formed probably by fusion of two of such origin sites (see also Werneburg and Abel, 2022).

(MacDougall and Reisz, 2014; 3 in **Figure 14**), whereas in many non-sphenacodontian synapsids as well as in some early diapsids, jugal, squamosal, postorbital, and quadratojugal form the margin of the infratemporal fenestra (Romer and Price, 1940; Ford and Benson, 2020). In regard of the condition in non-sphenacodontian synapsids and early diapsids, the formation of the fenestra may be explained by a larger weak area in the "cheek" incorporating both discussed three-bone-intersections. Alternatively, the formation of "accessory temporal fenestrae" like observed for some ophiacodontids as mentioned above could have led to a later fusion of two separate temporal openings (see also Werneburg and Abel, 2022).

In fact, this is congruent with our own observations on *Protorothyris archeri* Price (1937) (MCZ 1532, 2148; Museum of Comparative Zoology, Harvard, United States), a close relative of Diapsida, which still possessed a scutal morphology (e.g., Müller and Reisz, 2006; MacDougall et al., 2018; Ford and Benson, 2020). *P. archeri* is similar to *C. aguti* in regards of the jugal interdigitating with the squamosal posteriorly. Likewise, the parietal overlaps the squamosal, and there also seems to be a butt joint between parietal and postorbital. However, it differs from *C. aguti* by the lack of interdigitation in the postorbital-squamosal suture and the simpler contact between jugal and quadratojugal. These might be suitable preconditions for the formation of two pairs of temporal fenestrae in the diapsid ancestor. Yet, as we currently have no information on relative suture thickness in *P. archeri*, segmentation of a μCT-scan like herein applied to OMNH 44816 would be needed to further elaborate on this hypothesis.

There are more reasons to assume that as a model captorhinids alone might not be able to explain the whole morphological diversity of the temporal region in early amniotes. An infratemporal fenestra corresponding to the weak area in *C. aguti* (i.e., within the jugal-squamosal-postorbital intersection; 2 in **Figure 14**) occurs mostly, likely as a derived trait, in taxa with a reduced quadratojugal (e.g., Romer and Price, 1940; Modesto and Reisz, 1990), sometimes by also involving the parietal (Modesto, 1995; Lucas et al., 2018). In fact, while especially moradisaurine captorhinids likely evolved larger external jaw adductors in context of their derived herbivorous lifestyle, neither they or any other known captorhinid evolved an infratemporal fenestra like it can be observed in coeval herbivorous synapsids, but enlarged their adductor chamber instead (Dodick and Modesto, 1995; Sues and Reisz, 1998). This might be due to other constraints like skull flattening during ontogeny, especially in more deeply nested captorhinids (Heaton, 1979). Indeed, skull doming and accompanying changes in jaw adductor orientation has been repeatedly argued to be necessary for the initial evolution of temporal openings (Olson, 1961; Frazzetta, 1968; Tarsitano et al., 2001; Abel and Werneburg, 2021), even though it might have been the opposite in lissamphibians (Schoch, 2014). There might be also a phylogenetic signal due to herbivorous synapsids retaining their fenestrae from their fenestrated non-herbivorous ancestors. Considering this and other peculiarities of the captorhinid temporal region, notably the loss of the tabular and the distinctly reduced supratemporal (e.g., Fox and Bowman, 1966; Dodick and Modesto, 1995), it emphasizes that even early scutal radiations like captorhinids might not offer a "perfect" analog for the ancestral amniote.

Lastly, the probably weak connection between the parietal and "cheek" (i.e., postorbital and, to a lesser degree, squamosal) could have been related to what Kemp (1980) called the "crossopterygian hinge line," a mobile joint presumably inherited from tetrapodomorph fishes and retained as a loose contact between squamosal and supratemporal in probable amniote-line tetrapods and other early limbed vertebrates (Panchen, 1964; Thomson, 1967; Frazzetta, 1968; Kemp, 1980; Klembara et al., 2014).

In this regard, Kemp (1980) highlighted that the temporal region of early synapsids plesiomorphically bears large supratemporals and tabulars; thus, they differ from *C. aguti* and other early non-diapsid reptiles. The author suggested that the synapsid fenestra originated between postorbital, squamosal, and supratemporal by attaching the jaw adductors around the former "crossopterygian hinge line." The postorbital would have later extended posteriorly along the lateroventral margin of the supratemporal. The argumentation of Kemp (1980) implies that the synapsid fenestra would have subsequently expanded to also incorporate the jugal and quadratojugal into its border. The possible role of the "crossopterygian hinge line" has been also discussed by others (Frazzetta, 1968; Gow, 1972; Werneburg and Abel, 2022). In regard of the parareptile *Milleretta rubidgei* Broom 1938, which possessed a small opening between the jugal, squamosal, and postorbital that was presumably closed in adult specimens, Gow (1972) argued that a firm suture between squamosal and skull roof was present. This would have led to the formation of a "line of weakness" between the squamosal, jugal, and quadratojugal in *M. rubidgei* at whose dorsal end the opening formed. A similar case might have been also present in the embolomere *Anthracosaurus russelli* Huxley 1863, which differs from other embolomeres by interdigitation of the suture between skull roof and "cheek" as well as the formation of an infratemporal fenestra between jugal and squamosal, adjacent to

the jugal-squamosal-quadratojugal intersection (Panchen, 1977; Clack, 1987a).

It is worth noting that there are several other interpretations of this presumed "hinge line," which either has been argued to represent a taphonomic phenomenon (Reisz and Heaton, 1980), a misinterpretation of the sutures (Berman et al., 2010) or, if present, to be of little functional relevance (Clack, 1987b). Also, given that the jugal seems to be always involved in the infratemporal fenestra of early synapsids, we consider it more parsimonious that the fenestra would form within one of the three-bone intersections discussed above. This would also apply to other taxa like diapsids or especially to those in which the postorbital does not contribute to the infratemporal fenestra like in *A. russelli* or many parareptiles. Moreover, an infratemporal fenestra bordered by the jugal might still develop if there is a weaker contact between the skull roof and "cheek" (Frazzetta, 1968). Nonetheless, a contact as observed for *C. aguti* and probably other scutal non-diapsid reptiles might have implications for the formation of the diapsid supratemporal fenestra (Werneburg and Abel, 2022).

When the jaw was closed in *C. aguti*, contraction of the AMEP would have exerted a pulling force with the parietals bending in ventral direction, concentrating the main forces onto the anterior and posterior ends of the parietals, while their lateral contacts to the "cheeks" would have been less affected. Like discussed in the previous section, this could have maintained the plesiomorphically interdigitated suture found between parietals and frontals. Indeed, such an interdigitated frontoparietal suture can be also observed in many other species close to the amniote base, including other captorhinids even though with varying degree of complexity (e.g., Clark and Carroll, 1973; Gaffney and McKenna, 1979; Heaton, 1979; Dodick and Modesto, 1995; Kissel et al., 2002; Müller and Reisz, 2005; Modesto et al., 2007; Kissel, 2010).

The simpler contacts of the parietal to the squamosals and postorbitals fit their interpretation as less affected areas. Analogous to the formation of the infratemporal fenestra, the less loaded parietal-postorbital and parietal-squamosal contacts could be selected to form a temporal opening. Especially the simple parietal-postorbital contact would be affected by this. In moradisaurine captorhinids with their enlarged adductor chamber, the sutures between skull roof and "cheek" appear to be more strengthened than in *C. aguti* (Dodick and Modesto, 1995), whereas in other early non-diapsid reptiles, including the ones closest to diapsids (e.g., *Protorothyris* Price, 1937), the parietal simply overlapped the postorbital and squamosal (Carroll, 1969b; Carroll and Baird, 1972; Clark and Carroll, 1973), indicating that the ancestor of diapsids still possessed a comparatively weak suture there and, hence, the suggested precondition to form a supratemporal fenestra (1 in **Figure 14**). The question remains why an amniote supratemporal fenestra has only evolved in diapsids. Observation of a weaker contact between skull roof and "cheek" in some early synapsids (Frazzetta, 1968) might suggest that the potential to evolve a more dorsal fenestra was also present in synapsids. Indeed, expansion of the infratemporal fenestra toward the parietals in early therapsids and other sphenacomorph synapsids (Boonstra, 1936; Romer and Price, 1940; Modesto, 1995; Kammerer, 2011) could have been enabled by a still rather weak connection in that region of the skull.

There might be other factors involved for the lack of temporal openings in most other early limbed vertebrates. These include a less mobile head-neck joint (Panchen, 1964; Kuhn-Schnyder, 1980), differing jaw mechanics (Olson, 1961; Clack, 1987b) with a, hence, different role of the external jaw adductors, eventually affected by differences in ontogenetic strategies (Werneburg, 2019). Studies on fenestrated lissamphibians (e.g., Paluh et al., 2020) could also provide more insights into morphological patterns underlying tetrapod temporal openings. However, more detailed data on the suture morphology of lissamphibians and other non-amniotes is needed to comprehend the biomechanical differences between fenestrated and non-fenestrated taxa.

CONCLUSION

Our reconstruction of the likely arrangement of jaw adductors and cranial mechanics in *Captorhinus aguti* highlighted the biomechanical differences between the non-fenestrated skull of an early reptile with equally non-fenestrated skulls in extant turtles and possible extinct amniote-line tetrapods. We confirm previous observations of a comparatively thin area in the jugal-squamosal-postorbital intersection (2 in **Figure 14**) but also report another thin area for the parietal-postorbital contact (1 in **Figure 14**). These correspond to the position of temporal fenestrae in other early amniotes, corroborating the hypothesis that such openings formed due to the reduction of less loaded areas. Yet, consideration of captorhinid evolution also emphasizes that an increasing role of the external jaw adductors does not necessarily lead to the formation of temporal openings. Hence, even a generalist captorhinid like *C. aguti* might not be the best analog for the ancestor of fenestrated amniotes. Future studies on taxa closer to early fenestrated amniotes (e.g., "protorothyridids") or of different early diverging taxa (e.g., embolomeres, *Gephyrostegus*, seymouriamorphs, "lepospondyls", diadectomorphs), as well as quantitative approaches, might further deepen our understanding of the early evolution of temporal openings.

DATA AVAILABILITY STATEMENT

The original contributions presented in the study are included in the article/**Supplementary Material**, further inquiries can be directed to the corresponding author/s.

AUTHOR CONTRIBUTIONS

PA and IW: manuscript writing and conceptualization. PA, YP, and IW: analyses and illustrations. DF: material providing. IW and DK: fund raising. All authors critically revised the manuscript.

FUNDING

This study was funded by DFG grant WE 5440/6-1 (to IW).

ACKNOWLEDGMENTS

Gabriel Ferreira (University of Tübingen) supported the segmentation process in Avizo. Richard Cifelli (Sam Noble Oklahoma Museum of Natural History) and Nicholas Czaplewski (Sam Noble Oklahoma Museum of Natural History) kindly provided access to OMNH 44816. The scan was created by Matthew Colbert (University of Texas at Austin) and prepared by Jessica Maisano (University of Texas at Austin). We thank JF and DM for their valuable comments that enhanced our manuscript. Lastly, we thank Robert Reisz, Sean Modesto, and two reviewers for comments/support with a former version of this manuscript.

SUPPLEMENTARY MATERIAL

The Supplementary Material for this article can be found online at: https://www.frontiersin.org/articles/10.3389/fevo.2022.841784/full#supplementary-material

REFERENCES

Abdala, F., and Damiani, R. (2004). Early development of the mammalian superficial masseter muscle in cynodonts. *Palaeontologica Africana* 40, 23–29.

Abel, P., Pommery, Y., Ford, D. P., Koyabu, D., and Werneburg, I. (in press). 3D models related to the publication: Skull sutures and cranial mechanics in the Permian reptile *Captorhinus aguti* and the evolution of the temporal region in early amniotes. *MorphoMuseuM*. doi: 10.18563/m3.167

Abel, P., and Werneburg, I. (2021). Morphology of the temporal skull region in tetrapods: research history, functional explanations, and a new comprehensive classification scheme. *Biolog. Rev.* 96, 2229–2257. doi: 10.1111/brv.12751

Adams, L. A. (1919). A memoir on the phylogeny of the jaw muscles in recent and fossil vertebrates. *Ann. N Y Acad. Sci.* 28, 51–166. doi: 10.1111/j.1749-6632.1918.tb55350.x

Bailleul, A. M., and Holliday, C. M. (2017). Joint histology in *Alligator mississippiensis* challenges the identification of synovial joints in fossil archosaurs and inferences of cranial kinesis. *Proc. R. Soc. B* 284:20170038. doi: 10.1098/rspb.2017.0038

Barghusen, H. R. (1973). The adductor jaw musculature of *Dimetrodon* (Reptilia. Pelycosauria). *J. Paleontol.* 47, 823–834.

Beaumont, E. H. (1977). Cranial morphology of the Loxommatidae (Amphibia: Labyrinthodontia). *Philosoph. Trans. R. Soc. Lond.* 280, 29–101. doi: 10.1098/rstb.1977.0099

Berman, D. S., Eberth, D. A., and Brinkman, D. B. (1988). *Stegotretus agyrus* a new genus and species of microsaur (amphibian) from the Permo-Pennsylvanian of New Mexico. *Ann. Carn. Mus.* 57, 293–323.

Berman, D. S., Reisz, R. R., Bolt, J. R., and Scott, D. (1995). The cranial anatomy and relationships of the synapsid *Varanosaurus* (Eupelycosauria: Ophiacodontidae) from the Early Permian of Texas and Oklahoma. *Ann. Carn. Mus.* 64, 99–133.

Berman, D. S., Reisz, R. R., and Scott, D. (2010). Redescription of the skull of *Limmoscelis paludis* Williston (Diadectomorpha: Limnoscelidae) from the Pennsylvanian of Cañon del Cobre, Northern New Mexico. *New Mex. Mus. Nat. Hist. Sci. Bull.* 49, 185–210.

Blackburn, D. G., and Stewart, J. R. (2021). Morphological research on amniote eggs and embryos: an introduction and historical retrospective. *J. Morphol.* 282, 1–23. doi: 10.1002/jmor.21320

Bock, W. J. (1964). Kinetics of the avian skull. *J. Morphol.* 114, 1–42. doi: 10.1002/jmor.1051140102

Bolt, J. R. (1974). Evolution and functional interpretation of some suture patterns in Paleozoic labyrinthodont amphibians and other lower tetrapods. *J. Paleontol.* 48, 434–458.

Boonstra, L. D. (1936). On some features of the cranial morphology of the tapinocephalid deinocephalians. *Bull. Am. Mus. Nat. Hist.* 72, 75–98.

Boy, J. A., and Martens, T. (1991). Ein neues captorhinomorphes Reptil aus dem thüringischen Rotliegend (Unter-Perm; Ost-Deutschland). *Paläontol. Zeitschrift* 65, 363–389. doi: 10.1007/BF02989852

Bramble, D. M., and Wake, D. B. (1985). "Feeding Mechanisms of Lower *Tetrapods*," in *Functional Vertebrate Morphology*, eds M. Hildebrand, D. Bramble, K. Liem, and D. Wake (Cambridge, MA: Harvard University Press), 230–261. doi: 10.4159/harvard.9780674184404.c13

Branson, E. B. (1911). Notes on the osteology of the skull of *Pariotichus*. *J. Geol.* 19, 135–139. doi: 10.1086/621823

Bryant, H. N., and Seymour, K. L. (1990). Observations and comments on the reliability of muscle reconstruction in fossil vertebrates. *J. Morphol.* 206, 109–117. doi: 10.1002/jmor.1052060111

Buchwitz, M., Jansen, M., Renaudie, J., Marchetti, L., and Voigt, S. (2021). Evolutionary change in locomotion close to the origin of amniotes inferred from trackway data in an ancestral state reconstruction approach. *Front. Ecol. Evol.* 9, 1–24. doi: 10.3389/fevo.2021.674779

Busbey, A. B. (1995). "The structural consequences of skull flattening in crocodiles," in *Functional Morphology in Vertebrate Paleontology*, ed. J. J. Thomason (Cambridge, MA: Cambridge University Press), 173–192.

Carroll, R. L. (1969a). Problems of the origins of reptiles. *Biolog. Rev.* 44, 393–432. doi: 10.1111/j.1469-185X.1969.tb01218.x

Carroll, R. L. (1969b). A Middle Pennsylvanian captorhinomorph, and the interrelationships of primitive reptiles. *J. Paleontol.* 43, 151–170.

Carroll, R. L., and Baird, D. (1972). Carboniferous stem-reptiles of the family Romeriidae. *Bull. Mus. Comp. Zool.* 143, 321–363.

Case, E. C. (1911). *A Revision of the Cotylosauria of North America*. Washington, D. C.: Carnegie Institution of Washington.

Case, E. C. (1924). A possible explanation of fenestration in the primitive reptilian skull, with notes on the temporal region of the genus *Dimetrodon*. *Contrib. Mus. Geol. Univ.* 2, 1–12. doi: 10.15625/2615-9023/15888

Cisneros, J. C. (2008). Taxonomic status of the reptile genus *Procolophon* from the Gondwanan Triassic. *Palaeontol. Afr.* 43, 7–17.

Clack, J. A. (1987a). Two new specimens of *Anthracosaurus* (Amphibia: Anthracosauria) from the Northumberland Coal Measures. *Palaeontology* 30, 15–26.

Clack, J. A. (1987b). *Pholiderpeton scutigerum* Huxley, an amphibian from the Yorkshire coal measures. *Philosoph. Trans. R. Soc. Lond.* 318, 1–107. doi: 10.1098/rstb.1987.0082

Clack, J. A. (2002). The dermal skull roof of *Acanthostega gunnari*, an early tetrapod from the Late Devonian. *Trans. R. So. Edinb.* 93, 17–33. doi: 10.1017/S0263593300000304

Clark, J., and Carroll, R. L. (1973). Romeriid reptiles from the Lower Permian. *Bull. Mus. Comp. Zool.* 144, 353–407.

Cope, E. D. (1878). Descriptions of extinct Batrachia and Reptilia from the Permian formation of Texas. *Proc. Am. Philos. Soc.* 17, 505–530.

Cope, E. D. (1882). Third contribution to the history of the Vertebrata of the Permian formation of Texas. *Proc. Am. Philosoph. Soc.* 20, 447–461.

Cope, E. D. (1895). The reptilian order Cotylosauria. *Proc. Am. Philos. Soc.* 34, 436–457.

Cost, I. N., Middleton, K. M., Sellers, K. C., Echols, M. S., Witmer, L. M., Davis, J. L., et al. (2020). Palatal biomechanics and its significance for cranial kinesis in *Tyrannosaurus rex*. *Anat. Rec.* 303, 999–1017. doi: 10.1002/ar.24219

Crawford, N. G., Faircloth, B. C., McCormack, J. E., Brumfield, R. T., Winker, K., and Glenn, T. C. (2012). More than 1000 ultraconserved elements provide evidence that turtles are the sister group of archosaurs. *Biol. Lett.* 8, 783–786. doi: 10.1098/rsbl.2012.0331

Crawford, N. G., Parham, J. F., Sellas, A. B., Faircloth, B. C., Glenn, T. C., Papenfuss, T. J., et al. (2015). A phylogenomic analysis of turtles. *Mole. Phylogenet. Evol.* 83, 250–257. doi: 10.1016/j.ympev.2014.10.021

Curtis, N., Jones, M. E. H., Evans, S. E., O'Higgins, P., and Fagan, M. (2013). Cranial sutures work collectively to distribute strain throughout the reptile skull. *J. R. Soc. Interf.* 10, 1–8. doi: 10.1098/rsif.2013.0442

Cuthbertson, R. S., Tirabasso, A., Rybczynski, N., and Holmes, R. B. (2012). Kinetic limitations of intracranial joints in *Brachylophosaurus canadensis* and *Edmontosaurus regalis* (Dinosauria: Hadrosauridae), and their implications for the chewing mechanics of hadrosaurids. *Anat. Rec.* 295, 968–979. doi: 10.1002/ar.22458

Dawson, J. W. (1860). On a terrestrial mollusk, a chilognathous myriapod, and some new species of reptiles, from the Coal-Formation of Nova Scotia. *Q. J. Geol. Soc. Lond.* 16, 268–277. doi: 10.1144/GSL.JGS.1860.016.01-02.37

Daza, J. D., Diogo, R., Johnston, P., and Abdala, V. (2011). Jaw adductor muscles across lepidosaurs: a reappraisal. *Anat. Rec.* 294, 1765–1782. doi: 10.1002/ar.21467

deBraga, M., and Rieppel, O. (1997). Reptile phylogeny and the interrelationships of turtles. *Zool. J. Linn. Soc.* 120, 281–354. doi: 10.1111/j.1096-3642.1997.tb01280.x

Diogo, R., and Abdala, F. (2010). "The Head Muscles of Dipnoans – a Review on the Homologies and Evolution of these Muscles within Vertebrates," in *Biology of Lungfishes*, eds J. Joss and J. M. Jorgensen (Boca Raton: CRC Press), 169–218.

Diogo, R., Abdala, V., Lonergan, N., and Wood, B. A. (2008). From fish to modern humans – comparative anatomy, homologies and evolution of the head and neck musculature. *J. Anat.* 213, 391–424. doi: 10.1111/j.1469-7580.2008.00953.x

Dodick, J. T., and Modesto, S. P. (1995). The cranial anatomy of the captorhinid reptile *Labidosaurikos meachami* from the Lower Permian of Oklahoma. *Palaeontology* 38, 687–711.

Egberts, S. (2008). A morphological study of *Captorhinus aguti* using X-ray computed tomography: new insights on a well-studied species. *J. Paleont.* 28:74A.

Evans, S. E. (2008). "The skull of lizards and tuatara," in *Biology of the Reptilia*, eds C. Gans, A. S. Gaunt, and K. Adler (New York, NY: Society for the Study of Amphibians and Reptiles), 1–347.

Ferreira, G. S., Lautenschlager, S., Evers, S. W., Pfaff, C., Kriwet, J., Raselli, I., et al. (2020). Feeding biomechanics suggests progressive correlation of skull architecture and neck evolution in turtles. *Sci. Rep.* 10, 1–11. doi: 10.1038/s41598-020-62179-5

Ferreira, G. S., and Werneburg, I. (2019). "Evolution, Diversity, and Development of the Craniocervical System in Turtles with Special Reference to Jaw Musculature," in *Heads, Jaws, and Muscles - Anatomical, Functional, and Developmental Diversity in Chordate Evolution*, eds J. M. Ziermann, R. E. Diaz Jr., and R. Diogo (New York, NY: Springer), 171–206. doi: 10.1007/978-3-319-93560-7_8

Field, D. J., Gauthier, J. A., King, B. L., Pisani, D., Lyson, T. R., and Peterson, K. J. (2014). Toward consilience in reptile phylogeny: miRNAs support an archosaur, not lepidosaur, affinity for turtles. *Evol. Dev.* 16, 189–196. doi: 10.1111/ede.12081

Ford, D. P. (2018). *The Evolution and Phylogeny of Early Amniotes.* Dissertation. Oxford: University of Oxford.

Ford, D. P., and Benson, R. B. J. (2020). The phylogeny of early amniotes and the affinities of Parareptilia and Varanopidae. *Nat. Ecol. Evol.* 4, 57–65. doi: 10.1038/s41559-019-1047-3

Fox, R. C. (1964). The adductor muscles of the jaw in some primitive reptiles. *Univ. Kan. Publ.* 12, 657–680.

Fox, R. C., and Bowman, M. C. (1966). Osteology and relationships of *Captorhinus aguti* (Cope) (Reptilia: Captorhinomorpha). *Univ. Kans. Paleont. Contrib. Vert.* 11, 1–79.

Fracasso, M. A. (1983). *Cranial osteology, functional morphology, systematics and paleoenvironment of* Limnoscelis paludis *Williston.* Dissertation. New Haven: Yale University.

Frazzetta, T. H. (1962). A functional consideration of cranial kinesis in lizards. *J. Morphol.* 111, 287–319. doi: 10.1002/jmor.1051110306

Frazzetta, T. H. (1968). Adaptive problems and possibilities in the temporal fenestration of tetrapod skulls. *J. Morphol.* 125, 145–157. doi: 10.1002/jmor.1051250203

Gaffney, E. S. (1979). Comparative cranial morphology of recent and fossil turtles. *Bull. Am. Mus. Hist.* 164, 65–376. doi: 10.7717/peerj.5964

Gaffney, E. S. (1990). The comparative osteology of the Triassic turtle *Proganochelys*. *Bull. Am. Mus. Nat. Hist.* 194, 1–263. doi: 10.1127/0077-7749/2007/0246-0001

Gaffney, E. S., and McKenna, M. C. (1979). A Late Permian captorhinid from Rhodesia. *Am. Mus. Novit.* 2688, 1–15.

Gans, C. (1960). Studies on amphisbaenids (Amphisbaenia, Reptilia) – 1. A taxonomic revision of the Trogonophinae, and a functional interpretation of the amphisbaenid adaptive pattern. *Bull. Am. Mus. Nat. Hist.* 119, 133–204.

Gaupp, E. (1895). Ueber die Jochbogen-Bildungen am Schädel der Wirbelthiere. *Jahres-Bericht der Schlesischen Gesellschaft für vaterländische Cultur* 72, 56–63.

Gemmell, N. J., Rutherford, K., Prost, S., Tollis, M., and Winter, D. (2020). The tuatara genome reveals ancient features of amniote evolution. *Nature* 584, 403–409. doi: 10.1038/s41586-020-2561-9

Gervais, P. (1865). Description du *Mesosaurus tenuidens*, reptile fossile de l'Afrique australe. *Académie des Sciences et Lettres de Montpellier, Mémoires de la Section des Sciences* 6, 169–175.

Gow, C. E. (1972). The osteology and relationships of the Millerettidae (Reptilia: Cotylosauria). *J. Zool.* 167, 219–264. doi: 10.1111/j.1469-7998.1972.tb01731.x

Gruntmejer, K., Konietzko-Meier, D., Marcé-Nogué, J., Bodzioch, A., and Fortuny, J. (2019). Cranial suture biomechanics in *Metoposaurus krasiejowensis* (Temnospondyli, Stereospondyli) from the Upper Triassic of Poland. *J. Morph.* 280, 1850–1864. doi: 10.1002/jmor.21070

Haas, A. (2001). Mandibular arch musculature of anuran tadpoles; with comments on homologies of amphibian jaw muscles. *J. Morph.* 247, 1–33. doi: 10.1002/1097-4687(200101)247:1<1::AID-JMOR1000<3.0.CO;2-3

Haas, A. (2003). Phylogeny of frogs as inferred from primarily larval characters (Amphibia: Anura). *Cladistics* 19, 23–89. doi: 10.1111/j.1096-0031.2003.tb00405.x

Handschuh, S., Natchev, N., Kummer, S., Beisser, C. J., Lemell, P., Herrel, A., et al. (2019). Cranial kinesis in the miniaturised lizard *Ablepharus kitaibelii* (Squamata: Scincidae). *J. Exp. Biol.* 222:jeb198291. doi: 10.1242/jeb.198291

Heaton, M. J. (1979). Cranial anatomy of primitive captorhinid reptiles from the Late Pennsylvanian and Early Permian Oklahoma and Texas. *Oklah. Geolog. Surv.* 127, 1–84. doi: 10.1130/spe152-p1

Heiss, E., and Grell, J. (2019). Same but different: aquatic prey capture in paedomorphic and metamorphic Alpine newts. *Zoolog. Lett.* 5, 1–12. doi: 10.1186/s40851-019-0140-4

Herring, S. W. (1972). Sutures – a tool in functional cranial analysis. *Acta Anatom.* 83, 222–247. doi: 10.1159/000143860

Herring, S. W. (2008). "Mechanical Influences on Suture Development and Patency," in *Craniofacial Sut*ures. *Development, Disease and Treatment*, ed. D. P. Rice (Basel: Karger), 41–56. doi: 10.1159/000115031

Herring, S. W., and Mucci, R. J. (1991). In vivo strain in cranial sutures: the zygomatic arch. *J. Morph.* 207, 225–239. doi: 10.1002/jmor.1052070302

Herring, S. W., and Teng, S. (2000). Strain in the braincase and its sutures during function. *Am. J. Phys. Anthrop.* 112, 575–593. doi: 10.1002/1096-8644(200008)112:4<575::AID-AJPA10<3.0.CO;2-0

Herring, S. W., Teng, S., Huang, X., Mucci, R. J., and Freeman, J. (1996). Patterns of bone strain in the zygomatic arch. *Anat. Rec.* 246, 446–457. doi: 10.1002/(SICI)1097-0185(199612)246:4<446::AID-AR4<3.0.CO;2-T

Holliday, C. M., and Witmer, L. M. (2007). Archosaur adductor evolution: integration of musculoskeletal and topological criteria in jaw muscle homology. *J. Morphol.* 268, 457–484. doi: 10.1002/jmor.10524

Holliday, C. M., and Witmer, L. M. (2008). Cranial kinesis in dinosaurs: intracranial joints, protractor muscles, and their significance for cranial evolution and function in diapsids. *J. Verteb. Paleont.* 28, 1073–1088. doi: 10.1671/0272-4634-28.4.1073

Hotton, N., Olson, E. C., and Beerbower, R. (1997). "The Amniote Transition and the Discovery of Herbivory," in *Amniote Origins – Completing the Transition to Land*, eds S. Sumida and K. L. M. Martin (San Diego: Academic Press), 207–264. doi: 10.1016/b978-012676460-4/50008-1

Iordansky, N. N. (1990). Evolution of cranial kinesis in lower tetrapods. *Netherl. J. Zool.* 40, 32–54. doi: 10.1163/156854289x00174

Iordansky, N. N. (2000). Cranial kinesis in the Amphibia: a review. *Zhurnal Obshchei Biologii* 61, 102–118.

Iordansky, N. N. (2004). The jaw apparatus of *Lialis* (Lacertilia, Pygopodidae): patterns of intensification of cranial kinesis and the problem of the origin of snakes. *Entomol. Rev.* 84(Suppl. 1), S99–S109.

Iordansky, N. N. (2010). Pterygoideus muscles and other jaw adductors in amphibians and reptiles. *Biol. Bull.* 37, 905–914. doi: 10.1134/S1062359010090050

Iordansky, N. N. (2011). Cranial kinesis in lizards (Lacertilia): origin, biomechanics, and evolution. *Biol. Bull.* 38, 868–877. doi: 10.1134/S1062359011090032

Iordansky, N. N. (2015). Streptostyly and biological coordinations in the jaw apparatus of lizards (Lacertilia). *Biol. Bull.* 42, 784–792. doi: 10.1134/S1062359015090046

Irisarri, I., Baurain, D., Brinkmann, H., Delsuc, F., Sire, J.-Y., Kupfer, A., et al. (2017). Phylotranscriptomic consolidation of the jawed vertebrate timetree. *Nat. Ecol. Evol.* 1, 1370–1378. doi: 10.1038/s41559-017-0240-5

Jaekel, O. (1902). Ueber *Gephyrostegus bohemicus*. *Z. Dtsch. Geol. Ges.* 54, 127–133.

Johnston, P. (2010). The constrictor dorsalis musculature and basipterygoid articulation in *Sphenodon*. *J. Morph.* 271, 280–292. doi: 10.1002/jmor.10797

Jones, M. E. H., Curtis, N., Fagan, M. J., O'Higgins, P., and Evans, S. E. (2011). Hard tissue anatomy of the cranial joints in *Sphenodon* (Rhynchocephalia): sutures, kinesis, and skull mechanics. *Palaeontol. Electr.* 14, 1–92.

Jones, M. E. H., Curtis, N., O'Higgins, P., Fagan, M., and Evans, S. E. (2009). The head and neck muscles associated with feeding in *Sphenodon* (Reptilia: Lepidosauria: Rhynchocephalia). *Palaeontol. Electr.* 12, 1–56.

Jones, M. E. H., Werneburg, I., Curtis, N., Penrose, R., O'Higgins, P., Fagan, M. J., et al. (2012). The head and neck anatomy of sea turtles (Cryptodira: Chelonioidea) and skull shape in Testudines. *PLoS One* 7:e47852. doi: 10.1371/journal.pone.0047852

Jones, M. E. H., and Zikmund, T. (2012). A functional interpretation of the cranial suture morphology in *Captorhinus aguti* (Reptilia). *J. Paleont.* 32:118. doi: 10.1080/02724634.2012.10635175

Kammerer, C. F. (2011). Systematics of the Anteosauria (Therapsida: Dinocephalia). *J. Syst. Palaeont.* 9, 261–304. doi: 10.1080/14772019.2010.492645

Kathe, W. (1995). Morphology and function of the sutures in the dermal skull roof of *Discosauriscus austriacus* Makowsky, 1876 (Seymouriamorpha; Lower Permian of Moravia) and *Onchiodon labyrinthicus* Geinitz, 1861 (Temnospondyli; Lower Permian of Germany). *Geobios* 19, 255–261. doi: 10.1016/S0016-6995(95)80123-5

Kathe, W. (1999). Comparative morphology and functional interpretation of the sutures in the dermal skull roof of temnospondyl amphibians. *Zool. J. Lin. Soc.* 126, 1–39. doi: 10.1111/j.1096-3642.1999.tb00605.x

Kemp, T. S. (1980). Origin of the mammal-like reptiles. *Nature* 283, 378–380. doi: 10.1038/283378a0

Kilias, R. (1957). Die funktionell-anatomische und systematische Bedeutung der Schläfenreduktionen bei Schildkröten. *Mitteilungen aus dem Museum für Naturkunde in Berlin* 33, 307–354. doi: 10.1002/mmnz.19570330203

Kissel, R. A. (2010). *Morphology, Phylogeny, and Evolution of Diadectidae (Cotylosauria: Diadectomorpha)*. Dissertation. Toronto: University of Toronto.

Kissel, R. A., Dilkes, D. W., and Reisz, R. R. (2002). *Captorhinus magnus*, a new captorhinid (Amniota: Eureptilia) from the Lower Permian of Oklahoma, with new evidence on the homology of the astragalus. *Can. J. Earth Sci.* 39, 1363–1372. doi: 10.1139/e02-040

Kleinteich, T., and Haas, A. (2011). The hyal and ventral branchial muscles in caecilian and salamander larvae: Homologies and evolution. *J. Morphol.* 272, 598–613. doi: 10.1002/jmor.10940

Klembara, J. (1994). The sutural pattern of skull-roof bones in Lower Permian *Discosauriscus austriacus* from Moravia. *Lethaia* 27, 85–95. doi: 10.1111/j.1502-3931.1994.tb01560.x

Klembara, J., Clack, J. A., Milner, A. R., and Ruta, M. (2014). Cranial anatomy, ontogeny, and relationships of the Late Carboniferous tetrapod *Gephyrostegus bohemicus* Jaekel, 1902. *J. Verteb. Paleont.* 34, 774–792. doi: 10.1080/02724634.2014.837055

Klembara, J., Hain, M., Ruta, M., Berman, D. S., Pierce, S. E., and Henrici, A. C. (2019). Inner ear morphology of diadectomorphs and seymouriamorphs (Tetrapoda) uncovered by high-resolution X-ray microcomputed tomography, and the origin of the amniote crown group. *Palaeontology* 63, 131–154. doi: 10.1111/pala.12448

Koyabu, D., Maier, W., and Sánchez-Villagra, M. R. (2012). Paleontological and developmental evidence resolve the homology and dual embryonic origin of a mammalian skull bone, the interparietal. *Proc. Natl. Acad. Sci. U S A* 109, 14075–14080. doi: 10.1073/pnas.1208693109

Koyabu, D., Werneburg, I., Morimoto, N., Zollikofer, C. P. E., Forasiepi, A. M., Endo, H., et al. (2014). Mammalian skull heterochrony reveals modular evolution and a link between cranial development and brain size. *Nat. Comm.* 5, 1–9. doi: 10.1038/ncomms4625

Kuhn-Schnyder, E. (1980). "Observations on Temporal Openings of Reptilian Skulls and the Classification of Reptiles," in *Aspects of Vertebrate History, Essays in Honor of Edwin Harris Colbert*, ed. L. L. Jacobs (Flagstaff: Museum of Northern Arizona), 153–175.

Lakjer, T. (1926). *Studien über die Trigeminus-versorgte Kaumuskulatur der Sauropsiden*. Kopenhagen: CA Reitzel, Buchandlung.

Lauder, G. V., and Gillis, G. B. (1997). "Origin of the amniote feeding mechanism: experimental analyses of outgroup clades," in *Amniote Origins - Completing the Transition to Land*, eds S. Sumida and K. L. M. Martin (San Diego: Academic Press), 169–206. doi: 10.1016/b978-012676460-4/50007-x

Laurin, M. (2010). *How Vertebrates Left the Water*. Berkeley: University of California Press, doi: 10.1525/9780520947986

Laurin, M., and Piñeiro, G. H. (2017). A reassessment of the taxonomic position of mesosaurs, and a surprising phylogeny of early amniotes. *Front. Earth Sci.* 5, 1–13. doi: 10.3389/feart.2017.00088

Lebrun, R. (2018). "MorphoDig, an open-source 3D freeware dedicated to biology," in *The 5th International Palaeontological Congress, abstract volume*, (Paris).

Li, C., Fraser, N. C., Rieppel, O., and Wu, X.-C. (2018). A Triassic stem turtle with an edentulous beak. *Nature* 560, 476–479. doi: 10.1038/s41586-018-0419-1

Lichtig, A. J., and Lucas, S. G. (2021). *Chinlechelys* from the Upper Triassic of New Mexico, USA, and the origin of turtles. *Palaeont. Electr.* 24, 1–49. doi: 10.26879/886

Lucas, S. G., Rinehart, L. F., and Celeskey, M. D. (2018). The oldest specialized tetrapod herbivore: a new eupelycosaur from the Permian of New Mexico, USA. *Palaeontol. Electr.* 21, 1–42. doi: 10.26879/899

Luther, A. (1914). Über die vom N. trigeminus versorgte Muskulatur der Amphibien, mit einem vergleichenden Ausblick über den Adductor mandibulae der Gnathostomen, und einem Beitrag zum Verständnis der Organisation der Anurenlarven. *Acta Societ. Sci. Fennicae* 7, 1–151.

Lyson, T. R., Sperling, E. A., Heimberg, A. M., Gauthier, J. A., King, B. L., and Peterson, K. J. (2012). MicroRNAs support a turtle + lizard clade. *Biol. Lett.* 8, 104–107. doi: 10.1098/rsbl.2011.0477

MacDougall, M. J., Modesto, S. P., Brocklehurst, N., Verrière, A., Reisz, R. R., and Fröbisch, J. (2018). Commentary: a reassessment of the taxonomic position of mesosaurs, and a surprising phylogeny of early amniotes. *Front. Earth Sci.* 6, 1–5. doi: 10.3389/feart.2018.00099

MacDougall, M. J., and Reisz, R. R. (2014). The first record of a nyctiphruretid parareptile from the Early Permian of North America, with a discussion of parareptilian temporal fenestration. *Zoolog. J. Linn. So.* 172, 616–630. doi: 10.1111/zoj.12180

Maier, W. (1993). "Cranial Morphology of the Therian Common Ancestor, as Suggested by the Adaptation of Neonate Marsupials," in *Mesozoic Differentiation, Multituberculates, Monotremes and Early Marsupials*, eds F. S. Szalay, M. J. Novacek, and M. C. McKenna (New York, NY: Springer Verlag), 165–181. doi: 10.1007/978-1-4613-9249-1_12

Maier, W. (1999). On the evolutionary biology of early mammals – with methodological remarks on the interaction between ontogenetic adaptation and phylogenetic transformation. *Zoologischer Anzeiger* 238, 55–74.

Mann, A., Calthorpe, A. S., and Maddin, H. C. (2021). *Joermungandr bolti*, an exceptionally preserved 'microsaur' from the Mazon Creek Lagerstätte reveals patterns of integumentary evolution in Recumbirostra. *R. Soc. Open Sci.* 8:210319. doi: 10.1098/rsos.210319

Mann, A., Pardo, J. D., and Maddin, H. C. (2019). *Infernovenator steenae*, a new serpentine recumbirostran from the 'Mazon Creek' Lagerstätte further clarifies lysorophian origins. *Zoolog. J. Linn. Soc.* 187, 506–517. doi: 10.1093/zoolinnean/zlz130

Markey, M. J., Main, R. P., and Marshall, C. D. (2006). *In vivo* cranial suture function and suture morphology in the extant fish *Polypterus*: implications for inferring skull function in living and fossil fish. *J. Exp. Biol.* 209, 2085–2102. doi: 10.1242/jeb.02266

Metzger, K. (2002). "Cranial Kinesis in Lepidosaurs: Skulls in Motion," in *Topics in Functional and Ecological Vertebrate Morphology*, eds P. Aerts, K. D'Août, A. Herrel, and R. Van Damme (Düren: Shaker Publishing), 15–46.

Mezzasalma, M., Maio, N., and Guarino, F. M. (2014). To move or not to move: cranial joints in European gekkotans and lacertids, an osteological and histological perspective. *Anat. Rec.* 297, 463–472. doi: 10.1002/ar.22827

Moazen, M., Curtis, N., O'Higgins, P., Jones, M. E. H., Evans, S. E., and Fagan, M. (2009). Assessment of the role of sutures in a lizard skull: a computer modelling study. *Proc. R. Soc. B* 276, 39–46. doi: 10.1098/rspb.2008.0863

Modesto, S. P. (1995). The skull of the herbivorous synapsid *Edaphosaurus boanerges* from the Lower Permian of Texas. *Palaeontology* 38, 213–239.

Modesto, S. P. (1998). New information on the skull of the Early Permian reptile *Captorhinus aguti*. *Paleobios* 18, 21–35.

Modesto, S. P. (2006). The cranial skeleton of the Early Permian aquatic reptile *Mesosaurus tenuidens*: implications for relationships and palaeobiology. *Zool. J. Linn. Soc.* 146, 345–368. doi: 10.1111/j.1096-3642.2006.00205.x

Modesto, S. P., and Anderson, J. S. (2004). The phylogenetic defintion of Reptilia. *System. Biol.* 53, 815–821. doi: 10.1080/10635150490503026

Modesto, S. P., and Reisz, R. R. (1990). A new skeleton of *Ianthasaurus hardestii*, a primitive edaphosaur (Synapsida: Pelycosauria) from the Upper Pennsylvanian of Kansas. *Can. J. Earth Sci.* 27, 834–844. doi: 10.1139/e90-086

Modesto, S. P., Scott, D. M., Berman, D. S., Müller, J., and Reisz, R. R. (2007). The skull and palaeoecological significance of *Labidosaurus hamatus*, a captorhinid reptile from the Lower Permian of Texas. *Zoolog. J. Linn. Soc.* 149, 237–262. doi: 10.1111/j.1096-3642.2007.00242.x

Moss, M. L. (1957). Experimental alteration of sutural area morphology. *Anat. Rec.* 127, 569–589. doi: 10.1002/ar.1091270307

Müller, J., and Reisz, R. R. (2005). An early captorhinid reptile (Amniota, Eureptilia) from the Upper Carboniferous of Hamilton, Kansas. *J. Verteb. Paleont.* 25, 561–568. doi: 10.1671/0272-46342005025[0561:AECRAE]2.0.CO;2

Müller, J., and Reisz, R. R. (2006). The phylogeny of early eureptiles: comparing parsimony and Bayesian approaches in the investigation of a basal fossil clade. *Syst. Biol.* 55, 503–511. doi: 10.1080/10635150600755396

Natchev, N., Handschuh, S., Lukanov, S., Tzankov, N., Naumov, B., and Werneburg, I. (2016). Contributions to the functional morphology of caudate skulls: kinetic and akinetic forms. *PeerJ* 4, 1–15. doi: 10.7717/peerj.2392

Norman, D. B., and Weishampel, D. B. (1985). Ornithopod feeding mechanisms: their bearing on the evolution of herbivory. *Am. Natur.* 126, 154–164. doi: 10.1086/284406

Nyakatura, J. A., Melo, K., Horvat, T., Karakasiliotis, K., Allen, V. R., Andikfar, A., et al. (2019). Reverse-engineering the locomotion of a stem amniote. *Nature* 565, 351–355. doi: 10.1038/s41586-018-0851-2

Olson, E. C. (1951). Fauna of Upper Vale and Choza: 1–5. *Fieldiana Geol.* 10, 89–128.

Olson, E. C. (1961). Jaw mechanisms: rhipidistians, amphibians, reptiles. *Am. Zool.* 1, 205–215. doi: 10.1093/icb/1.2.205

Packard, M. J., and Seymour, R. S. (1997). "Evolution of the amniote egg," in *Amniote Origins - Completing the Transition to Land*, eds S. S. Sumida and K. L. M. Martin (San Diego: Academic Press), 265–290. doi: 10.1016/b978-012676460-4/50009-3

Paluh, D. J., Stanley, E. L., and Blackburn, D. C. (2020). Evolution of hyperossification expands skull diversity in frogs. *Proc. Natl. Acad. Sci. U S A* 117, 8554–8562. doi: 10.1073/pnas.2000872117

Panchen, A. L. (1964). The cranial anatomy of two Coal Measure anthracosaurs. *Philosoph. Trans. R. Soc.* 247, 593–637. doi: 10.1098/rstb.1964.0006

Panchen, A. L. (1977). On *Anthracosaurus russelli* Huxley (Amphibia: Labyrinthodontia) and the family Anthracosauridae. *Philosoph. Trans. R. Soc. Lond.* 279, 447–512. doi: 10.1098/rstb.1977.0096

Payne, S. L., Holliday, C. M., and Vickaryous, M. K. (2011). An osteological and histological investigation of cranial joints in geckos. *Anat. Rec.* 294, 399–405. doi: 10.1002/ar.21329

Poglayen-Neuwall, I. (1953). Untersuchungen der Kiefermuskulatur und deren Innervation bei Schildkröten. *Acta Zool.* 34, 241–292. doi: 10.1111/j.1463-6395.1953.tb00472.x

Porro, L. B., Rayfield, E. J., and Clack, J. A. (2015). Descriptive anatomy and three-dimensional reconstruction of the skull of the early tetrapod *Acanthostega gunnari* Jarvik, 1952. *PLoS One* 10:e0118882. doi: 10.1371/journal.pone.0118882

Price, L. I. (1935). Notes on the brain case of *Captorhinus*. *Proc. Bost. Soc. Natur. Hist.* 40, 377–386.

Price, L. I. (1937). Two new cotylosaurs from the Permian of Texas. *N. Engl. Zool. Club* 16, 97–102.

Rafferty, K. L., and Herring, S. W. (1999). Craniofacial sutures: morphology, growth, and in vivo masticatory strains. *J. Morphol.* 242, 167–179. doi: 10.1002/(SICI)1097-4687(199911)242:2<167::AID-JMOR8<3.0.CO;2-1

Rafferty, K. L., Herring, S. W., and Artese, F. (2000). Three-dimensional loading and growth of the zygomatic arch. *J. Exp. Biol.* 203, 2093–3004. doi: 10.1242/jeb.203.14.2093

Rawson, J. R. G., Porro, L. B., Martin-Silverstone, E., and Rayfield, E. J. (2021). Osteology and digital reconstruction of the skull of the early tetrapod *Whatcheeria deltae*. *J. Vert. Paleontol.* 2021, 1–16. doi: 10.1080/02724634.2021.1927749

Rayfield, E. J. (2005). Using finite-element analysis to investigate suture morphology: a case study using large carnivorous dinosaurs. *Anat. Rec.* 283, 349–365. doi: 10.1002/ar.a.20168

Reisz, R. R., and Heaton, M. J. (1980). Matters arising: origin of mammal-like reptiles. *Nature* 288:193. doi: 10.1038/288193b0

Rieppel, O. (1987). The development of the trigeminal jaw adductor musculature and associated skull elements in the lizard *Podarcis sicula*. *J. Zool.* 212, 131–150. doi: 10.1111/j.1469-7998.1987.tb05120.x

Rieppel, O., and deBraga, M. (1996). Turtles as diapsid reptiles. *Nature* 384, 453–455. doi: 10.1038/384453a0

Romer, A. S. (1927). The pelvic musculature of ornithischian dinosaurs. *Acta Zool.* 8, 225–275. doi: 10.1111/j.1463-6395.1927.tb00653.x

Romer, A. S. (1956). *A Typical Reptilian Skull Pattern – the Captorhinomorph Skull in Osteology of the Reptiles*. Malabar: Krieger Publishing Company, 69–73.

Romer, A. S., and Price, L. I. (1940). Review of the Pelycosauria. *Special Paper Geol. Soc. Am.* 28, 1–538. doi: 10.1130/spe28-p1

Schoch, R. R. (2014). Amphibian skull evolution: The developmental and functional context of simplification, bone loss and heterotopy. *Journal of Experimental Zoology (Molecular and Dev. Evol.* 322B, 619–630. doi: 10.1002/jez.b.22599

Schoch, R. R., and Sues, H.-D. (2015). A Middle Triassic stem-turtle and the evolution of the turtle body plan. *Nature* 523, 584–587. doi: 10.1038/nature14472

Schumacher, G. (1973). "The Head Muscles and Hyolaryngeal Skeleton of Turtles and Crocodilians," in *Biology of the Reptilia*, eds C. Gans and T. S. Parsons (New York, NY: Academic Press), 101–199.

Sues, H.-D., and Reisz, R. R. (1998). Origins and early evolution of herbivory in tetrapods. *Trends Ecol. Evol.* 13, 141–145. doi: 10.1016/S0169-5347(97)01257-3

Sumida, S. S. (1997). "Locomotor features of taxa spanning the origin of amniotes," in *Amniote Origins - Completing the Transition to Land*, eds S. Sumida and K. L. M. Martin (San Diego: Academic Press), 353–398. doi: 10.1016/b978-012676460-4/50012-3

Sushkin, P. P. (1928). Contributions to the cranial morphology of *Captorhinus* Cope (Reptilia, Cotylosauria, Captorhinidae). *Palaeobiologica* 1, 263–280.

Tarsitano, S. F., Oelofsen, B., Frey, E., and Riess, J. (2001). The origin of temporal fenestrae. *South Afr. J. Sci.* 97, 334–336.

Thomson, K. S. (1967). Mechanisms of intracranial kinetics in fossil rhipidistian fishes (Crossopterygii) and their relatives. *Zool. J. Linn. Soc.* 46, 223–253. doi: 10.1111/j.1096-3642.1967.tb00505.x

Versluys, J. (1910). Streptostylie bei Dinosauriern, nebst Bemerkungen über die Verwandtschaft der Vögel und Dinosaurier. *Zoologische Jahrbücher, Abteilung für Anatomie und Ontogenie der Tiere* 30, 177–260.

Versluys, J. (1912). Das Streptostylie-Problem und die Bewegungen im Schädel der Sauropsiden. *Zoologische Jahrbücher* 15(Suppl. pt. 2), 545–702.

Versluys, J. (1919). Über die Phylogenie der Schläfengruben und Jochbogen bei den Reptilia. *Sitzungsberichte der Heidelberger Akademie der Wissenschaften, Stiftung Heinrich Lanz, Mathematisch-naturwissenschaftliche Klasse Abteilung B. Biologische Wissenschaften* 13, 3–29.

Warren, J. W. (1961). The basicranial articulation of the Early Permian cotylosaur, *Captorhinus*. *J. Paleont.* 35, 561–563.

Werneburg, I. (2011). The cranial musculature of turtles. *Palaeontol. Electr.* 14, 1–99.

Werneburg, I. (2012). Temporal bone arrangements in turtles: an overview. *J. Exp. Zool.* 318, 235–249. doi: 10.1002/jez.b.22450

Werneburg, I. (2013a). Jaw musculature during the dawn of turtle evolution. *Org. Div. Evol.* 13, 225–254. doi: 10.1007/s13127-012-0103-5

Werneburg, I. (2013b). The tendinous framework in the temporal skull region of turtles and considerations about its morphological implications in amniotes: a review. *Zool. Sci.* 30, 141–153. doi: 10.2108/zsj.30.141

Werneburg, I. (2015). Neck motion in turtles and its relation to the shape of the temporal skull region. *Comptes Rendus Palevol* 14, 527–548. doi: 10.1016/j.crpv.2015.01.007

Werneburg, I. (2019). Morphofunctional categories and ontogenetic origin of temporal skull openings in amniotes. *Front. Earth Sci.* 7, 1–7. doi: 10.3389/feart.2019.00013

Werneburg, I., and Abel, P. (2022). Modeling skull network integrity at the dawn of amniote diversification with considerations on functional morphology and fossil jaw muscle reconstructions. *Front. Ecol. Evol.* 9:799637. doi: 10.3389/fevo.2021.799637

Werneburg, I., Esteve-Altava, B., Bruno, J., Torres Ladeira, M., and Diogo, R. (2019). Unique skull network complexity of *Tyrannosaurus rex* among land vertebrates. *Scient. Rep.* 9:1520. doi: 10.1038/s41598-018-37976-8

Werneburg, I., and Maier, W. (2019). Diverging development of akinetic skulls in cryptodire and pleurodire turtles: an ontogenetic and phylogenetic study. *Verteb. Zool.* 69, 113–143. doi: 10.26049/VZ69-2-2019-01

Werneburg, I., Wilson, L. A. B., Parr, W. C. H., and Joyce, W. G. (2015). Evolution of neck vertebral shape and neck retraction at the transition to modern turtles: an integrated geometric morphometric approach. *Syst. Biol.* 64, 187–204. doi: 10.1093/sysbio/syu072

Wilken, A. T., Middleton, K. M., Sellers, K. C., Cost, I. N., and Holliday, C. M. (2019). The roles of joint tissues and jaw muscles in palatal biomechanics of the savannah monitor (*Varanus exanthematicus*) and their significance for cranial kinesis. *J. Exp. Biol.* 222:jeb201459. doi: 10.1242/jeb.201459

Williston, S. W. (1925). *The Osteology of the Reptiles*. Cambridge, MA: Harvard University Press.

Witzmann, F., and Werneburg, I. (2017). The palatal interpterygoid vacuities of temnospondyls and the implications for the associated eye-and jaw musculature. *Anat. Rec.* 300, 1240–1269. doi: 10.1002/ar.23582

Woodhead, J., Reisz, R. R., Fox, D., Drysdale, R., Hellstrom, J., Maas, R., et al. (2010). Speleothem climate records from deep time? Exploring the potential with an example from the Permian. *Geology* 38, 455–458. doi: 10.1130/G30354.1

Yaryhin, O., and Werneburg, I. (2019). The origin of orbitotemporal diversity in lepidosaurs: insights from tuatara chondrocranial anatomy. *Verteb. Zool.* 69, 169–181. doi: 10.26049/VZ69-2-2019-04

Zdansky, O. (1923–1925). Über die Temporalregion des Schildkrötenschädels. *Bull. Geolog. Instit. Univ. Upasala* 19, 89–114.

Ziermann, J. M. (2019). "Diversity of Heads, Jaws, and Cephalic Muscles in Amphibians," in *Heads, Jaws, and Muscles - Anatomical, Functional, and Developmental Diversity in Chordate Evolution*, eds J. M. Ziermann, R. E. Diaz Jr., and R. Diogo (New York, NY: Springer), 143–170. doi: 10.1007/978-3-319-93560-7_7

Ziermann, J. M., Clement, A. M., Ericsson, R., and Olsson, L. (2018). Cephalic muscle development in the Australian lungfish, *Neoceratodus forsteri*. *J. Morphol.* 279, 494–516. doi: 10.1002/jmor.20784

Conflict of Interest: The authors declare that the research was conducted in the absence of any commercial or financial relationships that could be construed as a potential conflict of interest.

Publisher's Note: All claims expressed in this article are solely those of the authors and do not necessarily represent those of their affiliated organizations, or those of the publisher, the editors and the reviewers. Any product that may be evaluated in this article, or claim that may be made by its manufacturer, is not guaranteed or endorsed by the publisher.

frontiers | Frontiers in Ecology and Evolution

ORIGINAL RESEARCH
published: 19 May 2022
doi: 10.3389/fevo.2022.887172

The Evolution of the Spiracular Region From Jawless Fishes to Tetrapods

Zhikun Gai[1,2,3], Min Zhu[1,2,3], Per E. Ahlberg[4] and Philip C. J. Donoghue[5]**

[1] Key Laboratory of Vertebrate Evolution and Human Origins of Chinese Academy of Sciences, Institute of Vertebrate Paleontology and Paleoanthropology, Chinese Academy of Sciences, Beijing, China, [2] Center for Excellence in Life and Paleoenvironment, Beijing, China, [3] College of Earth and Planetary Sciences, University of Chinese Academy of Sciences, Beijing, China, [4] Department of Organismal Biology, Uppsala University, Uppsala, Sweden, [5] Bristol Palaeobiology Group, School of Earth Sciences, University of Bristol, Bristol, United Kingdom

The spiracular region, comprising the hyomandibular pouch together with the mandibular and hyoid arches, has a complex evolutionary history. In living vertebrates, the embryonic hyomandibular pouch may disappear in the adult, develop into a small opening between the palatoquadrate and hyomandibula containing a single gill-like pseudobranch, or create a middle ear cavity, but it never develops into a fully formed gill with two hemibranchs. The belief that a complete spiracular gill must be the ancestral condition led some 20th century researchers to search for such a gill between the mandibular and hyoid arches in early jawed vertebrates. This hypothesized ancestral state was named the aphetohyoidean condition, but so far it has not been verified in any fossil; supposed examples, such as in the acanthodian *Acanthodes* and symmoriid chondrichthyans, have been reinterpreted and discounted. Here we present the first confirmed example of a complete spiracular gill in any vertebrate, in the galeaspid (jawless stem gnathostome) *Shuyu*. Comparisons with two other groups of jawless stem gnathostomes, osteostracans and heterostracans, indicate that they also probably possessed full-sized spiracular gills and that this condition may thus be primitive for the gnathostome stem group. This contrasts with the living jawless cyclostomes, in which the mandibular and hyoid arches are strongly modified and the hyomandibular pouch is lost in the adult. While no truly aphetohyoidean spiracular gill has been found in any jawed vertebrate, the recently reported presence in acanthodians of two pseudobranchs suggests a two-step evolutionary process whereby initial miniaturization of the spiracular gill was followed, independently in chondrichthyans and osteichthyans, by the loss of the anterior pseudobranch. On the basis of these findings we present an overview of spiracular evolution among vertebrates.

Keywords: spiracle, mandibular arch, hyoid arch, Galeaspida, stem-gnathostome, *Shuyu*

OPEN ACCESS

Edited by:
Ingmar Werneburg,
University of Tübingen, Germany

Reviewed by:
Shigeru Kuratani,
Riken Center for Biosystems Dynamics Research (BDR), Japan
Philippe Janvier,
Centre National de la Recherche Scientifique (CNRS), France

****Correspondence:***
Per E. Ahlberg
Per.Ahlberg@ebc.uu.se
Philip C. J. Donoghue
Phil.Donoghue@bristol.ac.uk

Specialty section:
This article was submitted to Paleontology, a section of the journal Frontiers in Ecology and Evolution

Received: *01 March 2022*
Accepted: *13 April 2022*
Published: *19 May 2022*

Citation:
Gai Z, Zhu M, Ahlberg PE and Donoghue PCJ (2022) The Evolution of the Spiracular Region From Jawless Fishes to Tetrapods. Front. Ecol. Evol. 10:887172. doi: 10.3389/fevo.2022.887172

INTRODUCTION

The origin of the vertebrate spiracle is a major 100-year-old unresolved mystery in vertebrate evolution since the German morphologist Carl Gegenbaur proposed the classic segmentation theory of the vertebrate head (Gegenbaur, 1872). An external dorsal opening with a tube extending to the oro-pharyngeal cavity, known as the spiracle, exists between the mandibular and hyoid arches

in most extant sharks (**Figure 1B**), all rays except mantas (**Figures 1C,D**), and in some primitive bony fishes (sturgeons, paddlefishes and bichirs) (**Figures 1E–H**; Bone and Moore, 2008; Holland and Long, 2009; Kardong, 2012; Graham et al., 2014; Ziermann et al., 2019). It originates in the embryo as a pharyngeal pouch (the hyomandibular pouch) between two visceral arches, very much like the more posterior gill slits, but the adult condition is distinctively different from the normal gills. The spiracle is restricted to the dorsal half of the arches, lodged between the palatoquadrate (mandibular arch) and hyomandibula (hyoid arch), and never extends ventral to the jaw joint. It contains a small gill-like structure known as the pseudobranch, which differs from a normal gill in two respects. Firstly, while a normal gill slit between two gill arches contains two half-gills or hemibranchs, one attached to the anterior gill arch and one to the posterior gill arch, the spiracle contains only a single pseudobranch attached to the posterior wall. Secondly, while the normal gills all receive deoxygenated blood, the pseudobranch receives already oxygenated blood from the anteriormost normal gill. The function of the pseudobranch has been debated extensively but somewhat inconclusively; it may have a role in supplementing the oxygen supply to the eye (Möhlich et al., 2009; Perry et al., 2011; Waser, 2011). Although the spiracle has vanished altogether in some sharks (great whites, makos, hammerheads) and in most living ray-finned bony fishes, they still retain the pseudobranch.

Compared with the posterior gill slits, the morphology and function of the spiracle are highly specialized. It is an inhalant opening for the influx of water in chondrichthyans (Hughes, 1960; Summers and Ferry-Graham, 2001) and air in *Polypterus* (Allis, 1922; Graham et al., 2014). In tetrapods, the spiracular pouch of the embryo gives rise to the middle ear cavity and the Eustachian tube, while the dorsal part of the embryonic hyoid arch gives rise to the stapes, which is either the sole ear ossicle of the middle ear (in amphibians, reptiles and birds) or the innermost of three ossicles (in mammals). This suggests that the middle ear arose as a modification of the spiracle plus hyomandibula, but the relationship between the two is complicated and there is evidence that a middle ear adapted for amplifying airborne sound has evolved more than once (Clack, 1993, 2002; Liem et al., 2001; Clack et al., 2003; Brazeau and Ahlberg, 2006).

The origin of the spiracle is a major evolutionary puzzle and cannot be fully resolved on the basis of evidence from living vertebrates. Spiracular pouches are present in all vertebrate embryos. However, in the jawless cyclostomes (hagfishes and lampreys)—which, as the sister group of total-group gnathostomes, might be expected to show an informative and potentially ancestral outgroup condition—the adult morphology never includes a spiracular gill slit. Although a hyomandibular pouch exists between the mandibular and hyoid arches in the lamprey embryo, it disappears early in development and never develops into a normal gill pouch (Janvier, 1996b; Miyashita and Diogo, 2016). In adult lampreys, the hyoid arch is closely associated with the mandibular arch (velar skeleton) without a gill slit between them (**Figure 1A**; Gaskell, 1908; Janvier, 1996b). The glossopharyngeal nerve is thought to innervate the gill muscles of the first branchial arch, and the vagus nerve innervates those of the remaining arches and viscera (Johnston, 1905), whereas the facial nerve (VII) has no branchial component (Johnston, 1905; Jefferies, 1986; Kuratani et al., 1997). In hagfishes, the hyomandibular pouch and the following two gill pouches, degenerate during embryonic development (Stockard, 1906; Holmgren, 1946). In adult hagfishes, the facial nerve is rather small and does not participate in the sensory innervation, but innervates several muscles associated with the basal cartilage (Wicht and Tusch, 1998). Therefore, none of the cyclostome gill pouches can be regarded as homologous with the gnathostome spiracle.

The adult condition of the anterior pharyngeal region of gnathostomes is arguably less modified from its embryonic beginnings than that of cyclostomes, insofar as the mandibular and (especially) the hyoid arches somewhat resemble branchial arches in shape, and the spiracular pouch often persists in some form, whether as a spiracle or a middle ear. The fact that the mandibular and hyoid arches, and the spiracular pouch between them, appear modified relative to the iterative pattern of the more posterior branchial arches and pouches, led researchers to propose that the ancestral condition for the pharynx was a complete series of gill arches separated by gill slits. The so-called "aphetohyoidean" theory speculated that the hyoid arch did not initially attach to or support the mandibular arch, and that a fully open (i.e., gill-like) cleft existed between the mandibular and hyoid arches in early gnathostomes (Gegenbaur, 1872; Watson, 1937; Janvier, 1996b). However, after a century of careful scrutiny, the search for a prehyoidean gill cleft (aphetohyoidean condition) in early jawed vertebrates such as placoderms, acanthodians, and Chondrichthyes has so far been unsuccessful (Watson, 1937; Zangerl and Williams, 1975; Maisey, 1986; Johanson, 1998; Frey et al., 2020).

In recent years, the impact of molecular phylogenies has resulted in a robust phylogenetic consensus that cyclostomes are a clade (Heimberg et al., 2010), not paraphyletic with hagfishes as the sister group to lampreys plus gnathostomes (Forey, 1995; Janvier, 1996a, 2001; Donoghue et al., 2000; Donoghue and Smith, 2001). This new consensus also places all of the extinct bony jawless vertebrates, or "ostracoderms," with the possible exception of some anaspids, in the jawed vertebrate stem group (Miyashita et al., 2021). This gives them potential to be uniquely informative about the origin of the jawed vertebrate spiracle, as they can be expected not to possess the confusing autapomorphies of cyclostomes. Galeaspids, a 435–370-million-year-old "ostracoderm" group from China and Vietnam, are regarded as the sister group of osteostracans plus jawed vertebrates. Osteostracans have a highly specialized cranial anatomy with an anteriorized pharynx (Kuratani and Ahlberg, 2018), but galeaspids lack these specializations and appear to provide key insights into the reorganization of the vertebrate head before the evolutionary origin of jaws (Gai et al., 2011, 2019; Gai and Zhu, 2012).

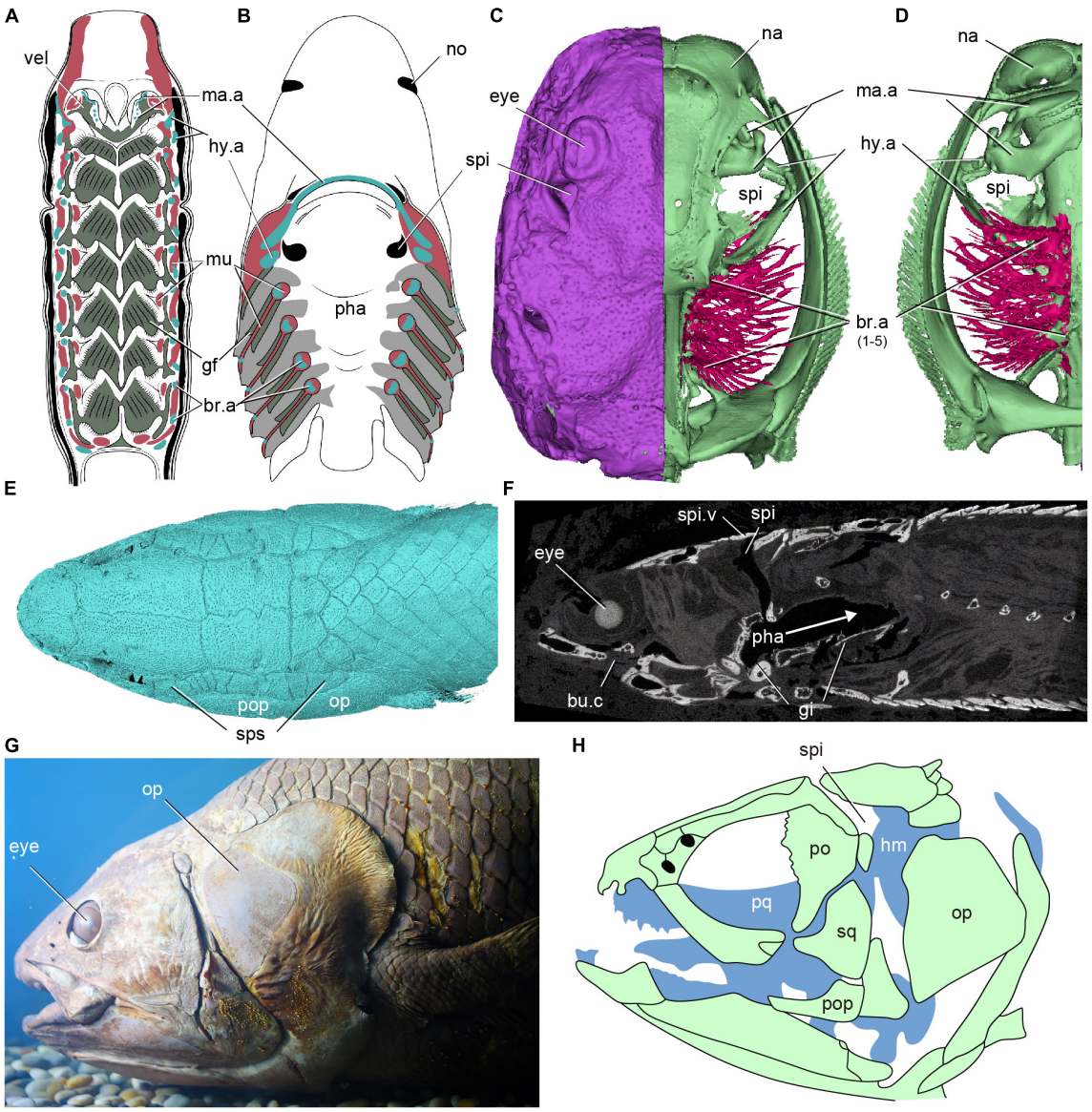

FIGURE 1 | The distribution of spiracles in extant fishes. **(A)** Dorsal half of a horizontally sectioned lamprey (*Petromyzon marinus*) ammocoete larva, in ventral view, showing no branchial chambers between mandibular (velum) and hyoid arch. **(B)** Dorsal half of a horizontally sectioned dogfish (*Squalus acanthias*), in ventral view, showing a ventral opening of the spiracular tube on the palate between mandibular (jaw) and hyoid arch. **(C,D)** The 3D reconstruction of a modern ray, showing a spiracle between the mandibular and hyoid arches, **(C)** in dorsal view, panel **(D)** in ventral view. **(E,F)** 3D reconstruction **(E)** and a sagittal Micro CT image **(F)** of a polypterid fish *Erpetoichthys calabaricus,* showing the path (arrows) of air through the spiracles to the buccopharyngeal chamber and lungs. **(G,H)** Photo **(G)** and skeleton **(H)** of the head of an African coelacanth *Latimeria chalumnae*, in lateral view, showing a non-functional internal spiracular cavity but no external opening. [**(A)** redraw from Gaskell (1908), **(B)** redraw from Mallatt (1984), **(G)** photo from the specimen IVPP OP392, **(H)** redraw from Forey (1998)] br.a, branchial arch; bu.c, buccal chamber; gi, gill; gf, gill filaments; hy.a, hyoid arch; hm, hyomandubular; ma.a, mandibular arch; mu, muscle; na, nasal sacs; no, nostril; op, opercle; pha, pharynx; po, postorbital; pop, preopercle; pq, palatoquadrate; spi, spiracle; spi.v, spiracle valve; sps, spiracular series; vel, velum.

Using synchrotron radiation X-ray tomographic microscopy of *Shuyu* and new material of gill filaments in galeaspids, here, we provide the first fossil evidence for a complete gill-functional hyomandibular pouch (aphetohyoidean condition) in stem-gnathostomes, an observation that sheds new light on the origin of the spiracle of jawed vertebrates. Based on our new findings, the evolution of the vertebrate spiracular region is reviewed.

MATERIALS AND METHODS

The material of *Shuyu zhejiangensis* investigated in this study includes a total of 28 specimens (IVPP V14334.1-28) collected from the Silurian of Zhejiang Province. Among these specimens, specimens V14334.1-7 are preserved with three-dimensional neurocrania suitable for Synchrotron X-ray Tomographic Microscopy (SRXTM) from which virtual endocasts may be

derived, whereas specimens V14334.8-27 represent incomplete headshields or natural endocasts which are suitable for simple visual and optic microscopic examination, illustrated by digital photographs. These specimens are used to complement the description of the SRXTM data. In addition, the specimen of *Polybranchiaspis liaojiaoshanensis* IVPP V3027 and the new material of *Laxaspis*-like galeaspids from the Xishancun Formation of the Lower Devonian of Yunnan Province, were also investigated to illustrate the dorsal roof of the oralobranchial chamber and gill filaments in the hyomandibular branchial pouch for the first time. All specimens are housed in the collections of the Institute of Vertebrate Paleontology and Paleoanthropology (IVPP), Chinese Academy of Sciences, Beijing, China.

Our SRXTM investigations were performed at the X02DA TOMCAT beamline of the Swiss Light Source at the Paul Scherrer Institute (Villigen, Switzerland). Slice data derived from the scans were then analyzed and manipulated using AVIZO software[1] for computed tomography on a Hewlett Packard Workstation with a 2-GHz Intel processor and 16 GB of RAM. For further details of the materials and methods refer to Gai (2018), Gai et al. (2019, 2011). Following best practice (Davies et al., 2017), the tomographic slice data, AVIZO models, and a stereolithographic model of virtual endocast of *Shuyu zhejiangensis* have been made openly available from the University of Bristol Data Repository: https://data.bris.ac.uk/data/dataset/p34vnx48p4772ouez5a1sfoqh, published as (Gai et al., 2019). Photographs and micrographs were obtained using a Canon EOS 5D Mark III camera coupled with a Canon EF 100 mm 1:2.8 L macro photo lens for the general morphology as well as a Canon MP-E 65 mm 1:2.8 1–5 × macro photo lens for close-up images of gill filaments in the hyomandibular branchial pouch.

RESULTS

Our new evidence indicates that the so-called interbranchial ridges of galeaspids are actually the dorsal portion of branchial arches (Gai, 2011; Gai et al., 2011; **Figures 2A–F**, **3A–C**, **4A**). They are incorporated into the neurocranium to form a massive skull as assumed in osteostracans by Stensiö (Stensiö, 1927, 1964). Compared to osteostracans, the entire branchial apparatus in *Shuyu* retains a general vertebrate condition, thus, it is easy to identify the mandibular and hyoid arches according to their topological position and nerve innervation (**Figures 2A–F**, **3A–C**, **4A**). Like most of gnathostomes, galeaspids primitively possess a mandibular, hyoid, and five gill arches (ma.a, hy.a, br.a$_{1-5}$, **Figure 4A**). Topologically, the mandibular arch (*ma.a*, **Figures 2A–F**, **3A–C**, **4A**) is located directly behind the orbital cavity and formed the posterior wall of orbital cavity. There is a broad and shallow fossa (*vel.f*, **Figures 2A,C,E**, **3B**, **4A**) rostral to the mandibular arch. The fossa slants anteriorly in a bigger angle than the posterior six branchial fossae and is obviously differentiated from the posterior six branchial fossae. Gai et al. (2011) interpreted this fossa as containing a velum like that of lampreys, since it is supported by the mandibular arch. The identification of the mandibular arch and velar fossa is also corroborated by its nerve innervation. In specimens V14334.13B (**Figure 3A**) and V14334.3, 4 (**Figures 2B–D**), the whole path of trigeminal nerve canal can be traced continuously. The canals for the maxillo-mandibular branch or nasopalatine component of the trigeminal nerve ($V_{2,3}$) arises from the junction of the mesencephalic and metencephalic division anteroventrally (**Figure 2D**). It extends forward into a large cavity for the trigeminal chamber and leads to the velar fossa. The presence of a velum in galeaspids is also supported by a large canal separates from the marginal artery and penetrates the roof of velar fossa (vj.v, **Figures 2G,H**; Gai, 2011; Gai et al., 2019). This indicates that a strong muscle probably for the velum was attached in this fossa. In addition, the whole oralobranchial chamber of galeaspids is closed posteriorly by a complete postbranchial wall (Wang, 1991; Janvier et al., 2009; Gai et al., 2022), which precludes tidal ventilation by the hypobranchial muscle. Therefore, a velum must have been present in galeaspids to provide ventilation from the oronasal cavity to the gill pouches as in osteostracans (Janvier, 1996b).

The hyoid arch, which is located just between the mandibular arch and labyrinth cavity (hy.a, **Figures 2C**, **3A**, **4A**), did not initially attach to or support the mandibular arch (aphetohyoidean condition). In specimens V1433.13B (**Figure 3A**), V14334.2 (**Figure 2A**), V14334.3 (**Figures 2D,F**), and V14334.4 (**Figure 2B**), the canal for the facial nerve (*VII*, **Figures 2A,B,D,F**, **3A**), which can be traced continuously, leaves the myelencephalic cavity through an individual canal ventral to the labyrinth cavity and extends anteroventrally to the hyoid arch. Therefore, the first branchial chamber just posterior to the orbital opening can be interpreted as the hyomandibular pouch (*hm.f*, **Figures 2A–H**, **3A–D**, **4A**) in galeaspids. The dorsal aortic canals collected the oxygenated blood from the branchial chambers through five successive short transverse canals for the efferent branchial arteries (ehy.a, ebr.a$_{1-4}$, **Figures 2C,E,F**, **3A,C**, **4A**), which is just located between the two adjacent branchial fossae (Gai et al., 2019). The first efferent branchial canal is relatively large and leads to the hyomandibular pouch at an anteriorly inclined angle, thus probably contains the efferent hyoid artery (ehy.a, **Figures 2C,E,F**, **4A**). The remaining four efferent branchial canals (ebr.a $_{1-4}$, **Figures 2C,E,F**, **3A,C**, **4A**) extend transversely to their respective branchial fossae. No canal for the pseudobranchial artery is observed. Our new data indicates that the hyomandibular pouch is complete and indistinguishable from the other five branchial pouches, and probably serves as a normal branchial chamber, which housed the posterior hemibranch of the mandibular arch and the anterior hemibranch of the hyoid arch. This observation has been corroborated by the impressions of the gill filaments (gf, **Figures 3C–E**) in the first branchial chamber for the hyomandibular pouch (hm.f, **Figures 3C–E**) just posterior to the orbital opening in our new material of *Laxaspis*-like galeaspids from the Xishancun Formation of the Lower Devonian of Yunnan Province. So it is apparent that

[1]https://www.fei.com/software/amira-avizo/

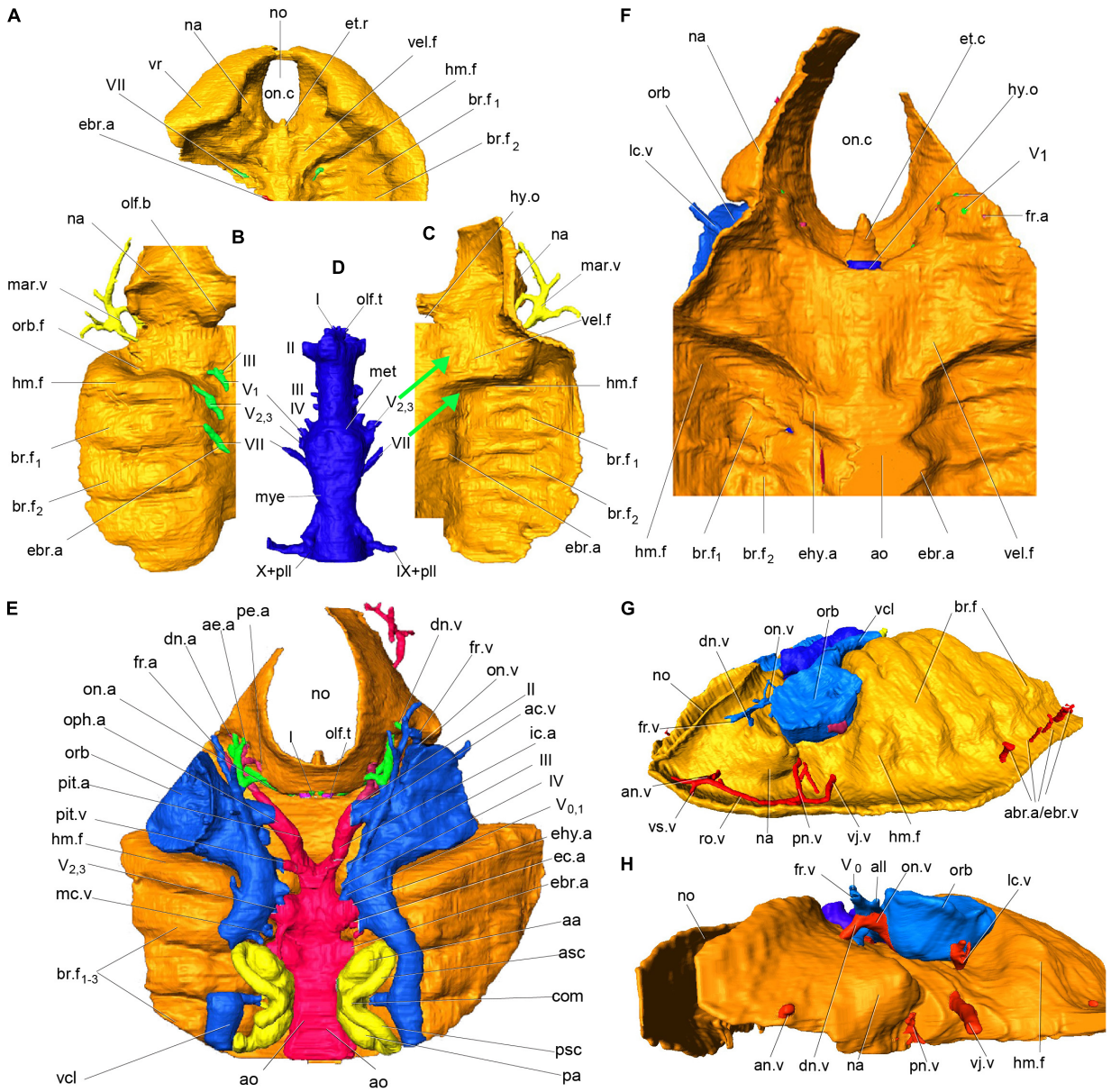

FIGURE 2 | Virtual endocast and oralobranchial chamber of *Shuyu zhejiangensis* and its associated cranial nerve and blood vessels. **(A)** 3D reconstruction of oralobranchial chamber, anterior part, in ventral view, V 14334.2. **(B,C)** 3D reconstruction of an incomplete oralobranchial chamber, left half part, V 14334.4, in dorsal view, showing the nasopalatine component of trigeminal nerve ($V_{2,3}$) innervates the first interbranchial ridge for the mandibular arch and the facial nerve (VII) innervates the second interbranchial ridge for the hyoid arch, **(C)** in ventral view, showing a large shallow fossa probably for a velum (vel.f) beneath the orbital cavity which obviously differentiates for the posterior six branchial fossae (br.f). **(D–F)** Endocast of skull reconstructed from the specimen V14334.3 **(E)** after removing the brain cavity and cranial nerve **(D)**, in dorsal view; and anterior part of the oralobranchial chamber **(F)**, in ventral view, showing a large shallow fossa probably for a velum (vel.f) beneath the orbital cavity which obviously differentiates for the posterior six branchial fossae (br.f). **(G)** Virtual endocast of specimen V14334.2, in antero-lateral view from the left side. **(H)** Virtual endocast of specimen V14334.1, in antero-lateral view from the left side. **(A–H)** The thickness of golden material is meaningless. aa, anterior ampulla; abr.a, afferent branchial artery; ac.v, anterior cerebral vein; ae.a, anterior ethmoidal artery; al.a, anterior labyrinth artery; all, anterior lateral line nerve; al.v, anterior labyrinth vein; an.v, anterior nasal vein; ao, dorsal aorta; asc, anterior semicircular canal; br.f, branchial fossae; com, commissural division of two vertical semicircular canals; dn.a, dorsal nasal artery; dn.v, dorsal nasal vein; ebr.a, efferent branchial artery; ec.a, external carotid artery; ehy.a, efferent hyoid artery; et.r, ethmoid rod; fr.a, frontal artery; fr.v, frontal vein; hm.f, hyomandibular fossa; hy.o, hypophysial opening; ic.a, internal carotid artery; mar.v, marginal vein; mc.a, middle cerebral artery; mc.v, middle cerebral vein; met, metencephalic division; mye, myelencephalic division; na, nasal sacs; no, nostril; lab.v, labyrinth vein; lc.v, lateral capitis vein; olf.t, olfactory tract; on.a, orbitonasal artery; oph.a, ophthalmic artery; orb, orbital opening; orb.f, orbital fossa; olf.b, olfactory bulb; on.c, oronasal chamber; on.v, orbitonasal vein; pa, posterior ampulla; pe.a, posterior ethmoidal artery; pll, posterior lateral line nerve; pl.v, posterior labyrinth vein; pi, pineal organ; pit.a, pituitary artery; pit.v, pituitary vein; pn.v, posterior nasal vein; psc, posterior semicircular canals; ro.v, rostral vein; vcl, lateral head vein; vel.f, velar fossa; vj.v, ventral jugular vein; vr, ventral rim; I, olfactory nerve; II, optic nerve; III, oculomotor nerve; IV, trochlear nerve; V_0, superficial ophthalmic branch of trigeminal nerve; V_1, deep ophthalmic or profundus branch of trigeminal nerve; $V_{2,3}$, nasopalatine component or maxillo-mandibular nerve; VII, facial nerve; VIII, auditory nerve; IX, glossopharyngeal nerve; X, vagus nerve.

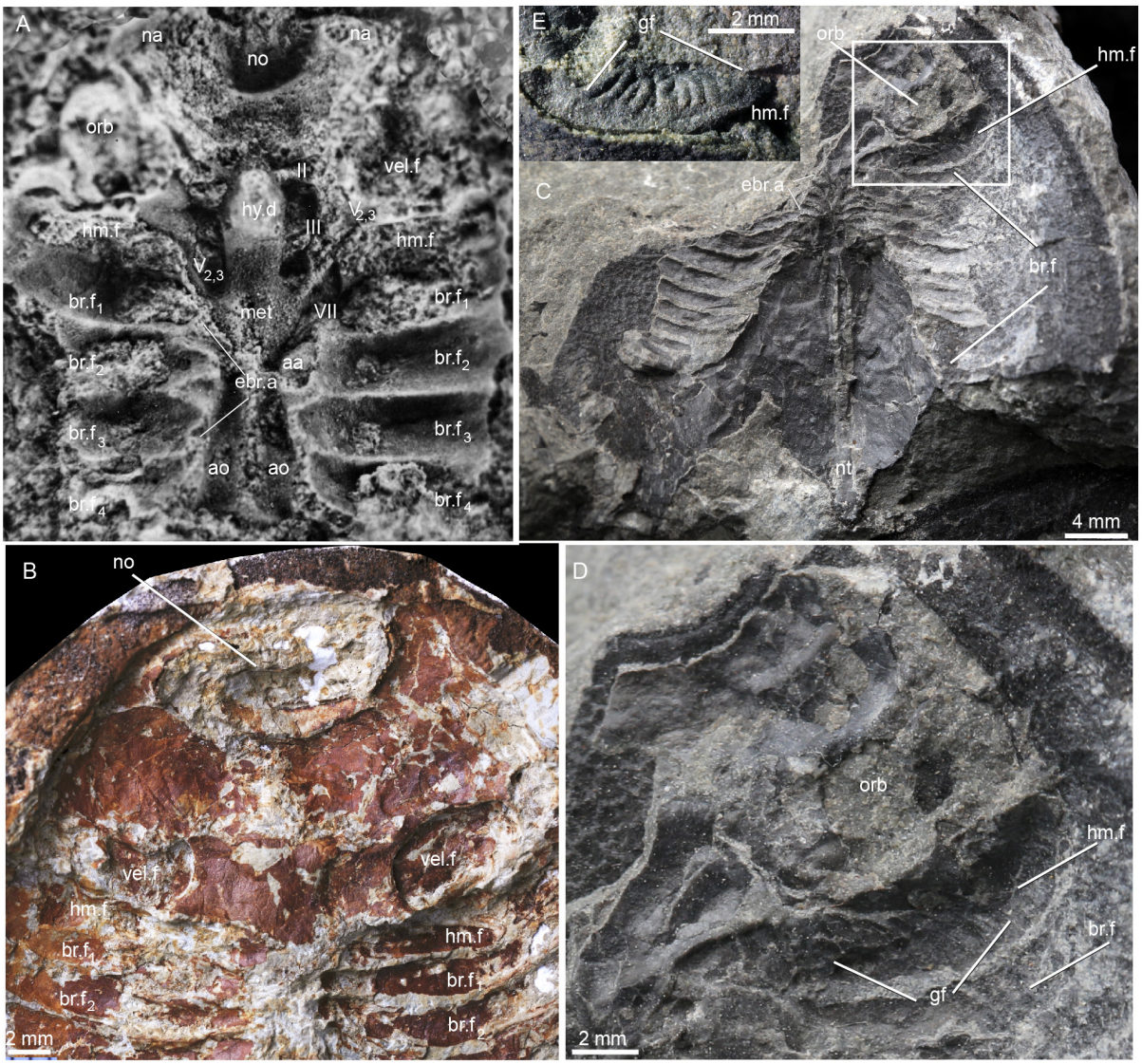

FIGURE 3 | Natural casts of oralobranchial chamber in galeaspids. **(A)** Natural cast of oralobranchial chamber of *Shuyu zhejiangensis*, specimen V14334.13B, showing a complete hyomandibular fossa (*hm.f*), four branchial fossae (*br.f*), paired grooves for dorsal aorta (*ao*), a middle ridge for the notochord (*nt*), the nasopalatine component of trigeminal nerve ($V_{2,3}$) innervates the first interbranchial ridge for the mandibular arch (*ma.a*) and the facial nerve (*VII*) innervates the second interbranchial ridge for the hyoid arch. **(B)** Natural cast of oralobranchial chamber of *Polybranchiaspis liaojiaoshanensis*, specimen V3027, in ventral view, showing a large shallow differentiated fossa (vel.f) probably for a velum anterior to the first branchial fossa. **(C–E)** Natural cast of oralobranchial chamber **(C)** of a *Laxaspis*-like galeasids from the Lower Devonian of Qujing showing the impression of gill filaments **(D,E)** in the hyomandibular pouch **(D)**. abbreviations as in **Figures 1**, **2**.

galeaspids possess a fully gill-functioned hyomandibular pouch (aphetohyoidean condition), rather than a reduced spiracle of jawed vertebrates.

DISCUSSION

The Origin of a Functional Spiracular Gill in "Ostracoderms"

The presence of the hyomandibular pouch in other "ostracoderms" still remains controversial (Stensiö, 1927, 1964; Halstead, 1971; Janvier, 1996b, 2004; Mallatt, 1996). In heterostracans, the foremost gill compartment impression is always situated behind the eye, and is classically interpreted as the hyomandibular pouch (**Figure 4E**) (Stensiö, 1964; Novitskaya, 1983, 2015; Mallatt, 1996), though only on the basis of a topological argument (Janvier, 2004). By contrast, Halstead (Halstead, 1971, 1973) thought that a true spiracle has been present in some amphiaspid heterostracans, a group of cyathaspidiforms from the Lower Devonian of Siberia, which possess a pair of bean-shaped openings in the carapace immediately lateral to the eyes (**Figures 4G,H**), a position

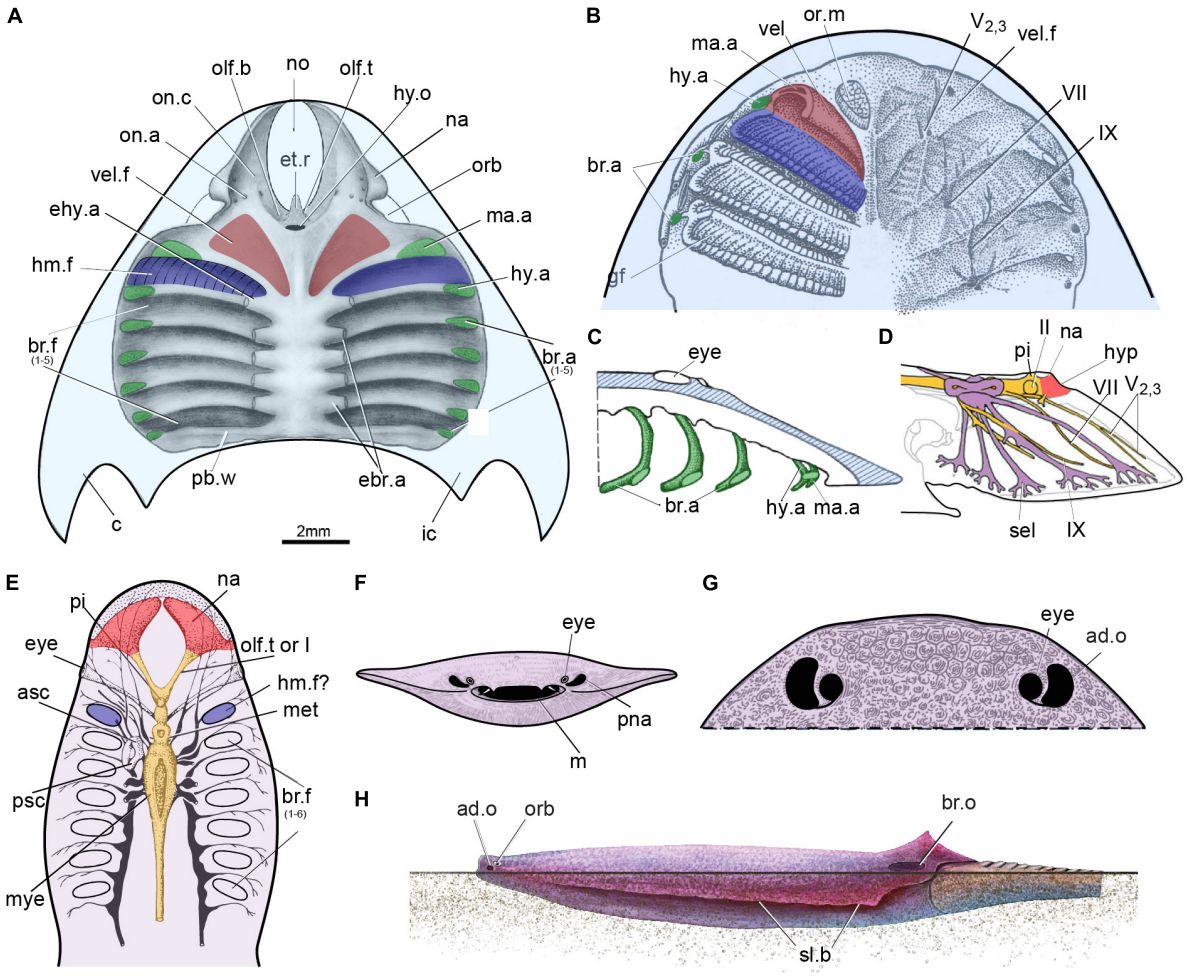

FIGURE 4 | The possible hyomandibular pouch in the stem-gnathostomes. **(A)** Roof of the oralobranchial cavity of *Shuyu* from the Silurian of China. **(B–D)** Roof of the oralobranchial cavity of *Scolenaspis* from the Early Devonian of Spitsbergen, with velum, gill arch, and gills reconstructed on left-hand side, panel **(B)** in ventral view, panel **(C)** in sagittal view with attempted restoration of gill-arch elements; **(D)** cranial anatomy of osteostracan *Norselaspis*, composite reconstruction based on Janvier (1985), showing the mandibular branch of trigeminal nerve passed through the foremost canal, together with the maxillary branch. **(E)** Reconstruction of the internal structure of the heterostracan *Poraspis pompeckji* Brotzen (redrawn after Novitskaya, 1983). **(F,G)** An infraorbital opening in a infraorbital position in an amphiaspid heterostracan *Gabreyaspis* from the Early Devonian of Siberia, was interpreted as a displaced opening of the prenasal sinus **(F)** (Janvier, 1974), or an adorbital opening **(G)** (Janvier, 1996b) probably with an inhalent function for intake of clear water. **(H)** Amphiaspid heterostracan *Kureykaspis* using its adorbital opening for the intake of respiratory water when buried in sand. ad.o, adorbital opening; br.o, branchial opening; hyp, hypophysis; m, mouth; or.m, oral musculure; pna, prenasal sina; "sel" canal to the lateral field; sl.b, serrated lateral brim; other abbreviations as in **Figures 1**, **2**.

moreover exactly as in the living benthonic elasmobranchs. However, most authors think it unlikely that these paired openings are equivalent to the spiracles of gnathostomes (Burrow et al., 2020). They were later interpreted as either displaced openings of the prenasal sina (**Figure 4F**; Janvier, 1974), or adorbital openings (**Figure 4G**; Janvier, 1996b), probably with an inhalent function for intake of clear water since these amphiaspids were benthic animals (Janvier, 1996b). As the neurocranial anatomy of heterostracans cannot be reconstructed in detail, they will not be considered further here.

In osteostracans, the entire branchial apparatus uniquely shifted forward so that the first two branchial gill pouches lie anterior to the eyes (**Figures 4B,C**; Stensiö, 1927, 1964; Jarvik, 1980; Kuratani and Ahlberg, 2018). Therefore, it is difficult to determine the hierarchy of the branchial arches according to their topological positions. Mallatt (1996) considered that the foremost gill compartment was the hyomandibular pouch, whereas Janvier (Janvier, 1985, 1996b, 2007) thought that there is no reason to assume that they possessed a prespiracular or even a spiracular gill-pouch (**Figures 4B,C**) since the mandibular arch bore a velum as in lampreys. In osteostracans, the canal for the facial nerve fused with the trigeminal chamber in the postero-ventral part of orbital cavity (Janvier, 1981; *trig*, Figures 13–17). Thus, it still cannot be determined whether the mandibular branch of trigeminal nerve passed through the foremost canal, together with the maxillary branch (**Figure 4D**), or passed through the second canal, together with the facial nerve (**Figure 4B**). Janvier preferred the latter interpretation, thus the mandibular

arch and the hyoid arch of osteostracans are probably closely associated or perhaps fused into a single arch (**Figures 4B,C**), and a hyomandibular pouch is absent in osteostracans as that of adult lampreys (Janvier, 1981, 1996b). However, Kuratani and Ahlberg (2018) preferred the first interpretation and the hyomandibular pouch of osteostracans appears to have been developed into a normal full-size gill as in galeaspids. In *Shuyu*, the canals for the facial nerve and trigeminal nerve have entirely separate courses and there is no evidence for the trigeminal nerve bifurcating into the maxillary and mandibular branches. The condition in *Shuyu* suggests that the mandibular and the maxillary branch of osteostracans probably always united as the nasopalatine component of trigeminal nerve ($V_{2,3}$, **Figure 4D**) and passed through the foremost canal together since there are no differentiated upper and lower jaws developed in these stem groups of gnathostomes. Therefore, osteostracans, probably like galeaspids, possess both the velum and a full-size hyomandibular pouch as well.

Various types of water intake device have evolved with the same function as the spiracles of modern rays in jawless fishes, e.g., the prenasal sinus and nasopharyngeal duct in hagfishes, thelodonts and heterostracans, the adorbital openings in amphiaspid heterostracans and pituriaspids (**Figure 4H**), and the median dorsal opening in galeaspids. These have been considered analogous, but not homologous, to the gnathostome spiracle (Gai et al., 2018). Thus, the hyomandibular pouch probably has been developed as a normal full-size gill pouch (aphetohyoidean condition) in ostracoderms. It has secondarily been lost in cyclostomes because of the evolution of the rasping tongue, which greatly modifies the mandibular arch. In sum, galeaspids provide the first definitive evidence for the presence of a full-size gill pouch between the hyoid and mandibular arches before it was reduced to a spiracle in jawed vertebrates. This observation is not only based on the number and topology of gill arches compared with that of jawed vertebrates, but also on the innervation of the cranial nerve and the impressions of the gill filaments in the first branchial chamber.

The Evolution of the Spiracle in Early Jawed Vertebrates

While the condition in galeaspids (and probably other ostracoderms) can be described as aphetohyoidean in the sense that a fully developed gill is present between the mandibular and hyoid arches, this does not quite correspond to the "classic" idea of an aphetohyoidean condition in jawed vertebrates, where a fully developed spiracular gill is combined with a mandibular arch developed into jaws. The galeaspid condition would make a perfect evolutionary precursor to the "classic aphetohyoidean" condition, but this would require the retention of the spiracular gill while the mandibular arch was transformed into jaws. Great efforts at finding the aphetohyoidean condition have been made in placoderms, acanthodians and chondrichthyans. Watson (1937) believed that this condition existed in acanthodians (e.g., *Acanthodes,* **Figure 5A**), and in placoderms such as arthrodires, petalichthyids and rhenanids, mainly based on the mistaken assumption that their operculum was attached to the mandibular arch, rather than to the hyoid arch as in bony fishes. As the endoskeletal neurocranium and visceral skeleton remain poorly known in early fossil jawed vertebrates, the presence of spiracles has typically been inferred from the spiracular grooves or notches on the cranial bones, as in actinopterygians (Gardiner, 1984; Graham et al., 2014) and sarcopterygians (Jarvik, 1980).

Among acanthodians, the visceral skeleton is only adequately known in *Acanthodes* from the Lower Permian of Lebach, Germany, a late representative of this derived genus that had to serve as an endoskeletal proxy for all acanthodians. However, the "aphetohyoidean" condition has been doubted by several authors (Holmgren, 1942; Stensiö, 1947; Denison, 1961). Miles (1964, 1965, 1968, 1973) has studied a large number of well-prepared specimens of *Acanthodes bronni* and *Climatius reticulatus*, but found no evidence for such an "aphetohyoidean" condition. By contrast, he found the spiracular grooves on the neurocranium in *Acanthodes* probably containing the spiracular tube. However, as there is no external spiracle opening observed from these tubes, such openings were presumed to be lacking in *Acanthodes*, rendering the spiracles non-functional. Recently, a very small external spiracular opening was described from the Middle Devonian acanthodiforms *Cheiracanthus* (**Figure 5B**) and *Mesacanthus* in northern Scotland (Burrow et al., 2020). Remarkably, unlike all living jawed vertebrates, these acanthodians prove to have not one but two spiracular pseudobranchs, represented in the fossils by their cartilage supports (**Figure 5B**). In addition to the posterior, forward-facing, hyoid arch pseudobranch shared with sharks, rays and bony fishes, there is an anterior, backward-facing pseudobranch that must belong to the mandibular arch (Burrow et al., 2020). The spiracle thus contained a complete, albeit miniaturized, gill. Acanthodians are now generally considered to be a group of stem chondrichthyans (Zhu et al., 2013, 2016; Dupret et al., 2014; Burrow et al., 2016; Maisey et al., 2019), which carries the implication that the mandibular-arch spiracular pseudobranch must have been lost independently in osteichthyans and crown-group chondrichthyans. Nevertheless, this is not a fully aphetohyoidean condition, as the gill is miniaturized and restricted to the dorsal space between the palatoquadrate and hyomandibula.

As for the aphetohyoidean condition in placoderms, fossil evidence since the time of Watson (1937) has convincingly demonstrated that the hyoid arch has been strongly modified in many placoderms, e.g., a larger hyomandibula in the Rhenanida (Stensiö, 1963), and suggests that they did not have a complete spiracular gill-slit. One of the evidences in support of Watson's aphetohyoidean theory is that the postsuborbital plate in placoderms has been interpreted as a mandibular operculum guarding a spiracular slit, because of its relations to the quadrate (Watson, 1937). However, the discovery of *Entelognathus*, and new phylogenetic frameworks, indicate that the posterior mobile submarginal plate in non-*Entelognathus* placoderms should be considered homologous with the opercular cover of osteichthyans (Zhu et al., 2013; Gai et al., 2017). The submarginal is primitively free in ptyctodontids and primitive arthrodires, but it is enclosed in the cheek and sutured with surrounding bones in advanced arthrodires (Schultze, 1993). A reduced spiracle has

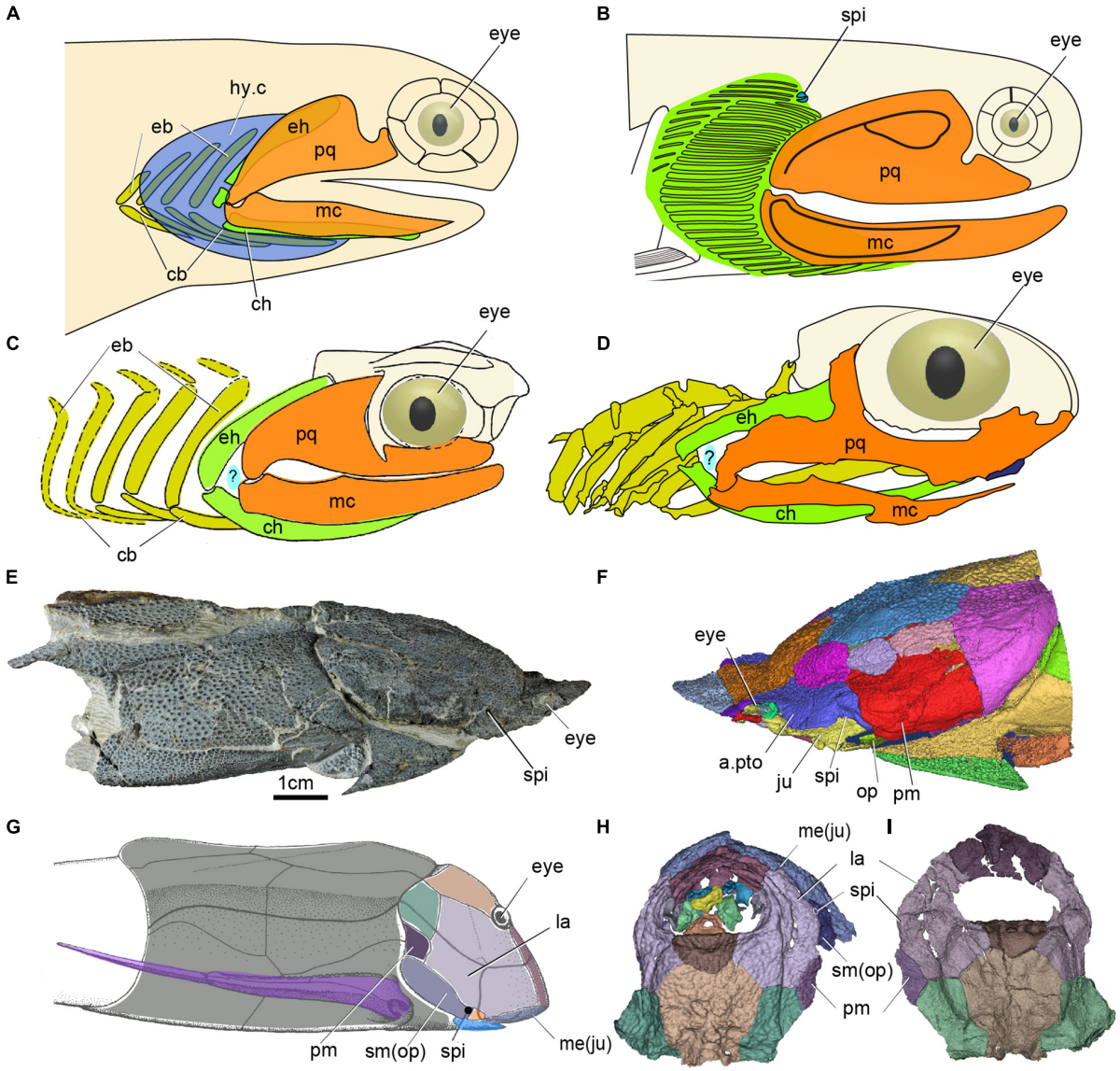

FIGURE 5 | The spiracle in early jawed vertebrates. **(A)** Head and branchial region of *Acanthodes* redraw after (DeLaurier, 2018). **(B)** Head and branchial region of *Cheiracanthus* showing position of spiracle, redraw after (Burrow et al., 2020). **(C)** Head and branchial region of *Cobelodus*, redraw after (Zangerl and Case, 1976). **(D)** Head and branchial region of *Ozarcus*, redraw after (Pradel et al., 2014), panels **(C,D)** showing the possible aphetohyoidean condition, but a respiratory gill pore between its mandibular and hyoid arches is hypothetical (indicated by a question mark). **(E,F)** Photo **(E)** and 3D reconstruction **(F)** of the dermal skeleton of *Qilinyu*. **(G)** Dermal skeleton of *Bothriolepis* redraw after (Arsenault et al., 2004). **(H,I)** 3D reconstruction of the dermal skeleton of *Parayunnanolepis*, **(E–I)** showing a spiracle in placoderms, **(A–G)** in lateral view, **(H)** in dorsal view, **(I)** in ventral view. a.pto, anterior postorbital plate; cb, ceratobranchial; ch, ceratohyal; eb, epibranchial; eh, epihyal; hy.c, hyoid gill cove; hm, hyomandibular; ju, jugal; la, lateral plate; mc, Meckel's cartilage; me, mental; op, opercular; pm, postmarginal plate; sm, submarginal plate, other abbreviations as in **Figures 1**, **2**.

been identified in a hyomandibular position in antiarchs (spi, **Figures 5G–I**; Stensiö, 1947; Johanson, 1998; Arsenault et al., 2004; Young, 2008; Wang and Zhu, 2020) —the most stemward jawed vertebrate group, and in the maxillate placoderm *Qilinyu* (spi, **Figures 5E,F**) — representing the most crownward stem gnathostome group (Zhu et al., 2016). Therefore, a restricted spiracular opening may well have existed in all placoderms, but it would be difficult to distinguish it from a gap between dermal elements in most of them (Miyashita, 2016).

The aphetohyoidean theory was later revived for some symmoriiform chondrichthyans, e.g., *Cobelodus* from Upper Carboniferous black shales of North America (Zangerl and Williams, 1975; Zangerl and Case, 1976), and *Ozarcus* from the Lower Carboniferous of Arkansas (Pradel et al., 2014). The Symmoriiformes, which were widely distributed from the Late Devonian through to the early Permian, have been regarded as exemplifying early chondrichthyan, and even generalized gnathostome, conditions (Pradel et al., 2011). The

hyoid arch of *Ozarcus* and *Cobelodus* gives no support to the jaw, and there appears to be a rather wide space between the mandibular and hyoid arches (**Figures 5C,D**), which suggests that the prehyoidean gill slit had not been reduced to a spiracle in these sharks (Zangerl and Williams, 1975; Zangerl and Case, 1976; Pradel et al., 2014). However, in the earlier symmoriiform shark *Ferromirum* from the Late Devonian of the Anti-Atlas in Morocco, the three-dimensionally preserved mandibular and hyoid arches leave no room for a prehyoidean gill slit, implying that the apparent gap between mandibular and hyoid arches in *Ozarcus* and *Cobelodus* is most probably a post-mortem artifact (Frey et al., 2020). Recent phylogenetic analyses have resolved symmoriiforms as stem holocephalans (Coates et al., 2017, 2018; Frey et al., 2019, 2020), which suggest that they are too derived to represent the primitive jawed vertebrate condition.

In summary, no placoderm or chondrichthyan has yet been shown convincingly to possess a full, aphetohyoidean, spiracular gill slit. Given that osteichthyans also lack such a gill slit (see below), it seems likely that it had been reduced to a dorsally positioned spiracle in the last common ancestor of living jawed vertebrates, i.e., at the gnathostome crown group node. However, the presence of two pseudobranchs in acanthodians, which are believed to be stem chondrichthyans, suggests that full reduction to the modern spiracular condition was a two-step process: an initial size reduction and shift to a dorsal position in the common ancestor of crown gnathostomes was followed, independently in chondrichthyans and osteichthyans, by the loss of the anterior (mandibular arch) pseudobranch. This interpretation implies that two pseudobranchs were also present in placoderms, where no evidence of their attachment survives.

The Evolution of the Spiracle From Bony Fishes to Tetropods

Among bony fishes, the hyomandibular pouch and its derivatives can be observed directly in extant actinopterygians (polypterids, sturgeons and paddlefishes, gar and bowfin, and teleosts) and sarcoptergian fishes (coelacanths and lungfishes). In addition, reasonably robust inferences about its condition in the adult of extinct groups such as tetrapodomorph fishes can be drawn from the morphology of the surrounding skeletal structures of the fossils. Among actinopterygians, an open spiracle broadly similar to that of sharks is found in polypterids, sturgeons and paddlefishes. In *Polypterus* (**Figure 6A**), which has a functional lung and is heavily dependent on air-beathing, the large and dorsally positioned spiracle plays an important role in lung ventilation (Graham et al., 2014). Up to 93% of air inhalation occurs through the spiracle. This has important implications for the interpretation of the morphologically similar spiracular region in tetrapodomorph fishes (see below). By contrast, the small spiracles of sturgeons and paddlefishes seem to have no respiratory function (Burggren, 1978; Burggren and Bemis, 1991). In neopterygians (gars, bowfins and teleosts) the spiracles are vestigial or absent, although the pseudobranch often persists inside the gill chamber. Its function is uncertain; it seems not to regulate the hypoxia response (Perry et al., 2011), but may have a role in supplying oxygen to the retina of the eye (Möhlich et al., 2009; Waser, 2011).

Neither of the two living groups of sarcopterygian fishes has a functional spiracle. In the coelacanth *Latimeria* there is a spiracular chamber (**Figure 1H**), but this does not open to the outside (**Figure 1G**) and the pseudobranch is absent (Forey, 1998). In lungfishes, both spiracle and pseudobranch are lost. The spiracular rudiment consists largely of a solid endodermal cellular strand, which never (or only for short time in ontogeny) opens to the outside and the pharyngeal endoderm, respectively (Bartsch, 1994). By contrast, the early bony fishes such as *Cheirolepis* (stem actinopterygians, **Figure 6B**; Pearson and Westoll, 1979), *Guiyu* (stem sarcopterygian, **Figure 6D**; Zhu et al., 2009), *Ligulalepis* (stem osteichthyan, **Figure 6C**; Basden and Young, 2001), *Onychodus* (Onychodontiformes, **Figure 7C**; Long, 2001), *Porolepis* (porolepiformes, **Figure 7B**) and tetrapodomorph fishes (fossil fishes belonging to the tetrapod stem group) such as *Eusthenopteron* (**Figures 7A**, **8A**; Jarvik, 1980) and *Gogonasus* (**Figure 6E**; Long et al., 2006) always have an open spiracle (spi, **Figures 6**, **7**), judging by the surrounding skeletal anatomy. In *Gogonasus* the dorsally positioned spiracle is strikingly large (**Figure 6E**), suggesting an important respiratory role similar to that of *Polypterus*.

Essentially the same spiracular morphology as in these tetrapodomorphs, but accompanied by a shorter and wider space for the spiracular canal, is found in the elpistostegids *Panderichthys* (**Figure 7D**) and *Tiktaalik* (**Figure 6F**; Brazeau and Ahlberg, 2006; Downs et al., 2008). *Elpistostege* is probably similar, though the internal part of the spiracular region is currently unknown (Cloutier et al., 2020). Given the shape of the elpistostegid skull, which suggests a surface-skimming lifestyle, it seems likely that the spiracle was used for air-breathing in a manner similar to *Polypterus*. This conclusion is further supported by the fact that the external nostril was low on the face, near the upper lip, and would have been submerged in a crocodile-like surface-skimming pose. Interestingly, in both *Panderichthys* and *Tiktaalik* the distal part of the hyomandibula has been lost, so that the bone no longer reaches down toward the jaw joint (Brazeau and Ahlberg, 2006; Downs et al., 2008). The corresponding portion of the hyomandibula in *Polypterus* is the part that lies ventral to the internal opening of the spiracular canal (Datovo and Rizzato, 2018), so it seems highly likely that this truncation of the elpistostegid hyomandibula reflects a change in its relationship to the spiracle, but the exact nature of this change cannot be determined.

Beginning in tetrapods, the hyomandibula ceases to be involved in jaw suspension and instead becomes dedicated eventually to hearing as the stapes (or columella) within the middle ear. Among the earliest Devonian tetrapods, we find the same combination of large, dorsally placed spiracles and small, ventrally facing external nostrils in *Parmastega*, *Ventastega* (**Figure 6G**) and *Acanthostega* (**Figure 8B**; Clack, 2003; Ahlberg et al., 2008; Beznosov et al., 2019). This suggests a conserved air-breathing function for the spiracle across the fish-tetrapod transition (Brazeau and Ahlberg, 2006). However, the skeletal morphology of the hyomandibula (henceforth termed "stapes") and braincase have changed

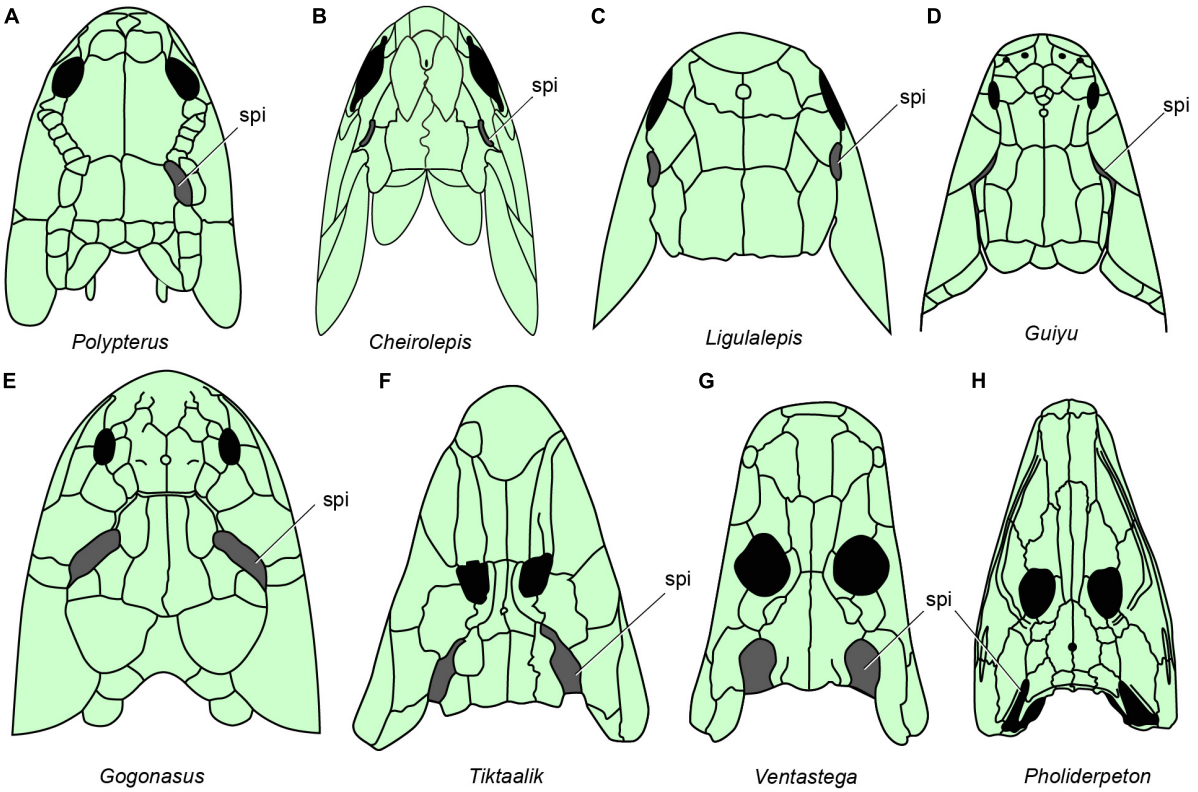

FIGURE 6 | The distribution of spiracles in bony fishes and tetrapods. **(A)** *Polypterus* redraw after (Graham et al., 2014). **(B)** *Cheirolepis* redraw after (Pearson and Westoll, 1979). **(C)** *Ligulalepis* redraw after (Basden and Young, 2001). **(D)** *Guiyu* redraw after (Zhu et al., 2009). **(E)** *Gogonasus* redraw after (Long et al., 2006). **(F)** *Tiktaalik* redraw after (Daeschler et al., 2006). **(G)** *Ventastega* redraw after (Ahlberg et al., 2008). **(H)** *Pholiderpeton* redraw after (Clack, 2012), **(A–H)**, in dorsal view.

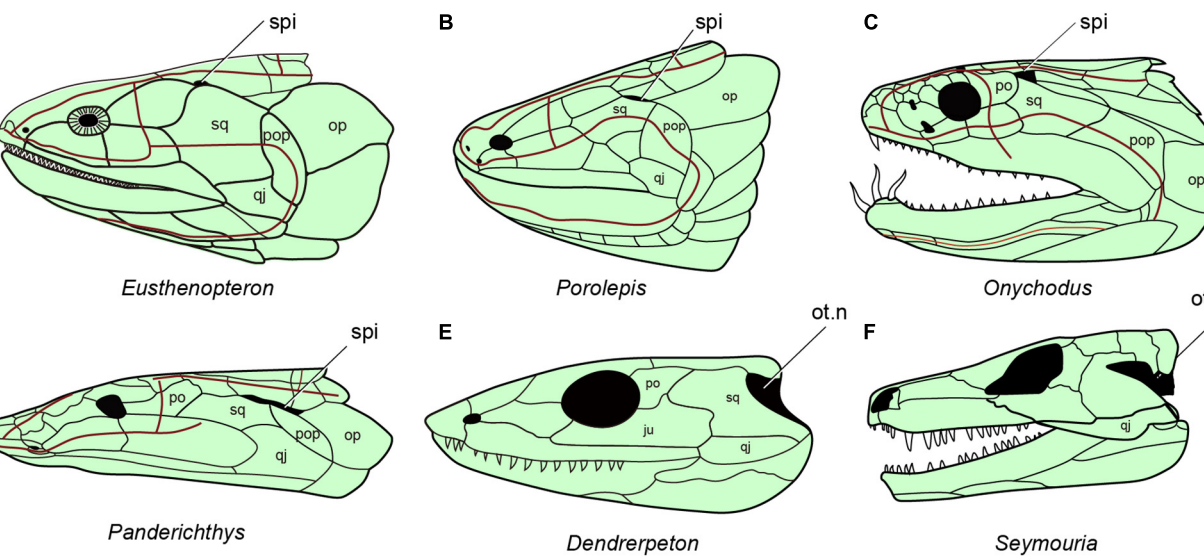

FIGURE 7 | The distribution of spiracles in bony fishes and tetrapods. **(A)** *Eusthenopteron*, redraw after (Jarvik, 1980). **(B)** *Porolepis* redraw after (Janvier, 1996b). **(C)** *Onychodus* redraw after (Long, 2001). **(D)** *Panderichthys* redraw after (Vorobyeva and Schultze, 1991). **(E)** Carboniferous tetrapod *Dendrerpeton* redraw after (Carroll, 1967). **(F)** *Seymouria* redraw after (White, 1939), **(A–F)**, in lateral view.

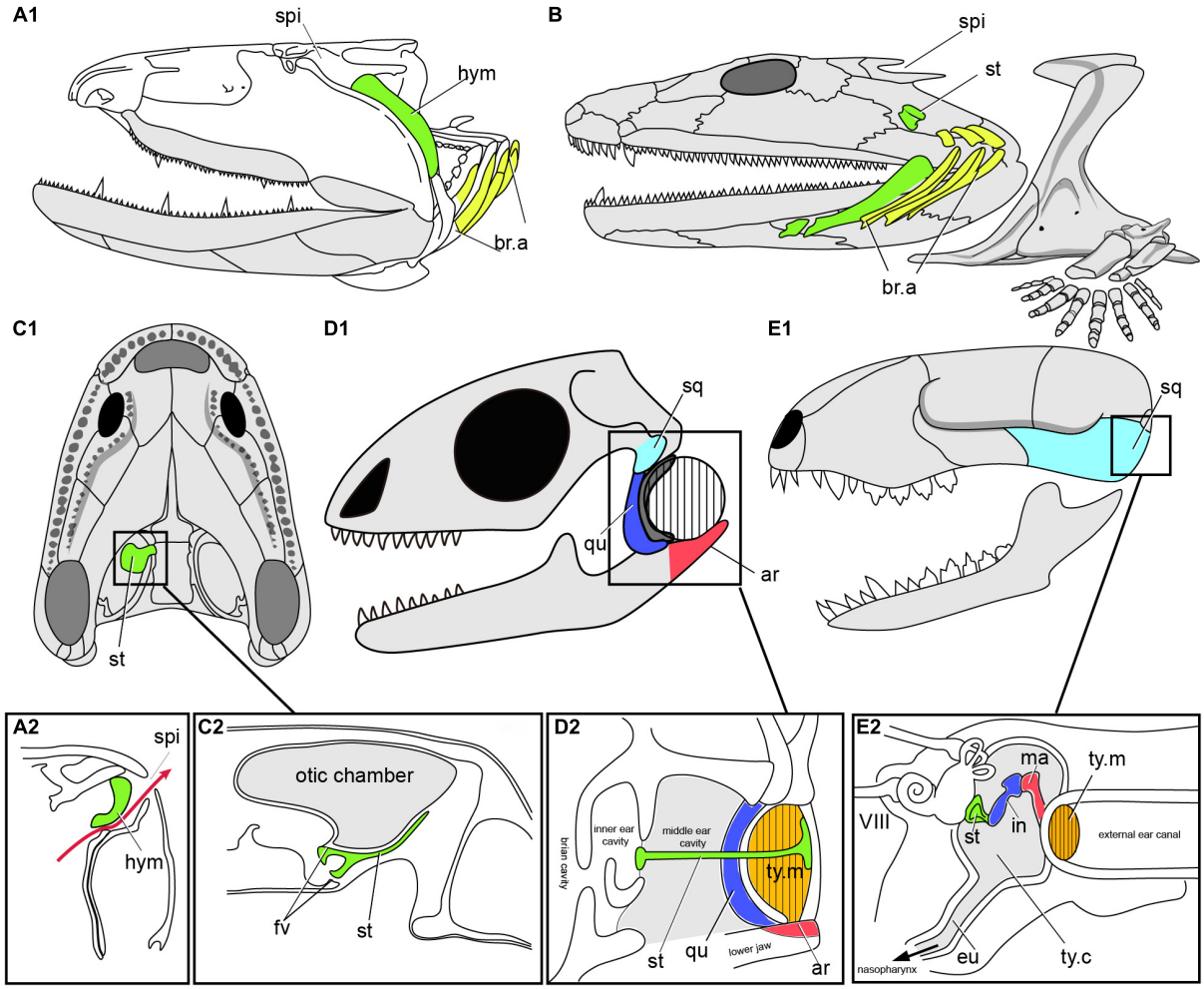

FIGURE 8 | The transition from spiracular pouch of fishes to the middle ear cavity of tetrapods. **(A)** Fossil osteolepiform *Eusthenopteron* **(A1)**, Late Devonian, showing the hyomadibular in the spiracular pouch **(A2)**, in lateral view, redrawn after (Janvier, 1996b; Brazeau and Ahlberg, 2006). **(B)** Early tetrapod *Acanthostega*, Late Devonian of Greenland, showing stapes and the presumed position of the gill arches, in lateral view, redrawn after (Clack et al., 2003; Clack, 2012). **(C)** Early tetrapod *Ichthyostega* **(C1)**, Late Devonian of Greenland, and the reconstructed section **(C2)** through the air chamber showing its relation to the otic capsule and stapes. **(D)** Skull of Lizard **(D1)**, showing the section of middle ear cavity, and the tympanic ear **(D2)** in reptiles, redrawn after (Clack, 2012). **(E)** Skull of mammals **(E1)**, showing the section of middle ear cavity, and the tympanic ear **(E2)**, redraw after (Farooq et al., 2020). ar, articular; eu, eustachian tube; fv, fenestra vestibuli; hym, hyomandibuar; in, incus; ma. malleus; qu, quadrate; sq, squamosal; st, stapes (columella), ty.c, tympanic cavity; ty.m, tympanic membrane (ear drum); other abbreviations as in **Figures 1**, **2**.

substantially compared to the elpistostegid condition. The most complete example of the earliest tetrapod condition is given by *Acanthostega* (**Figure 6B**; Clack, 1998; Clack et al., 2003); the stapes is unknown in *Parmastega* and *Ventastega*, though the braincase of *Ventastega* appears very similar to that of *Acanthostega* (Ahlberg et al., 2008). In contrast to the fish hyomandibula, which articulates proximally with the lateral commissure (a bony bridge that straddles the jugular vein), the footplate of the tetrapod stapes is lodged in a large opening in the braincase side wall, known as the fenestra vestibuli (fv, **Figure 8C2**). This puts it in direct contact with the inner ear and suggests that it may have acquired a sound-transducing function even at this very early stage in its evolution. The stapes is also shorter than even the elpistostegid hyomandibula, and is oriented transversely to the long axis of the head.

The stapes of *Acanthostega* is large, butterfly-shaped and evidently not associated with a tympanum (**Figure 8B**; Clack, 1998; Clack et al., 2003). Its precise function is difficult to determine, but it was presumably embedded in the posterior wall of the spiracular tract. An essentially similar non-tympanic stapes, usually but not invariably associated with a spiracular notch, is also found in a number of Carboniferous tetrapods including *Pederpes*, *Greererpeton* and *Pholiderpeton* (**Figure 6H**; Clack et al., 2003). This is thus almost certainly the primitive condition for the tetrapod middle ear. A distinctive variant on the same theme is found in *Ichthyostega* (**Figure 8C1**), where the stapes is thin and plate-like, and seems to have formed the floor

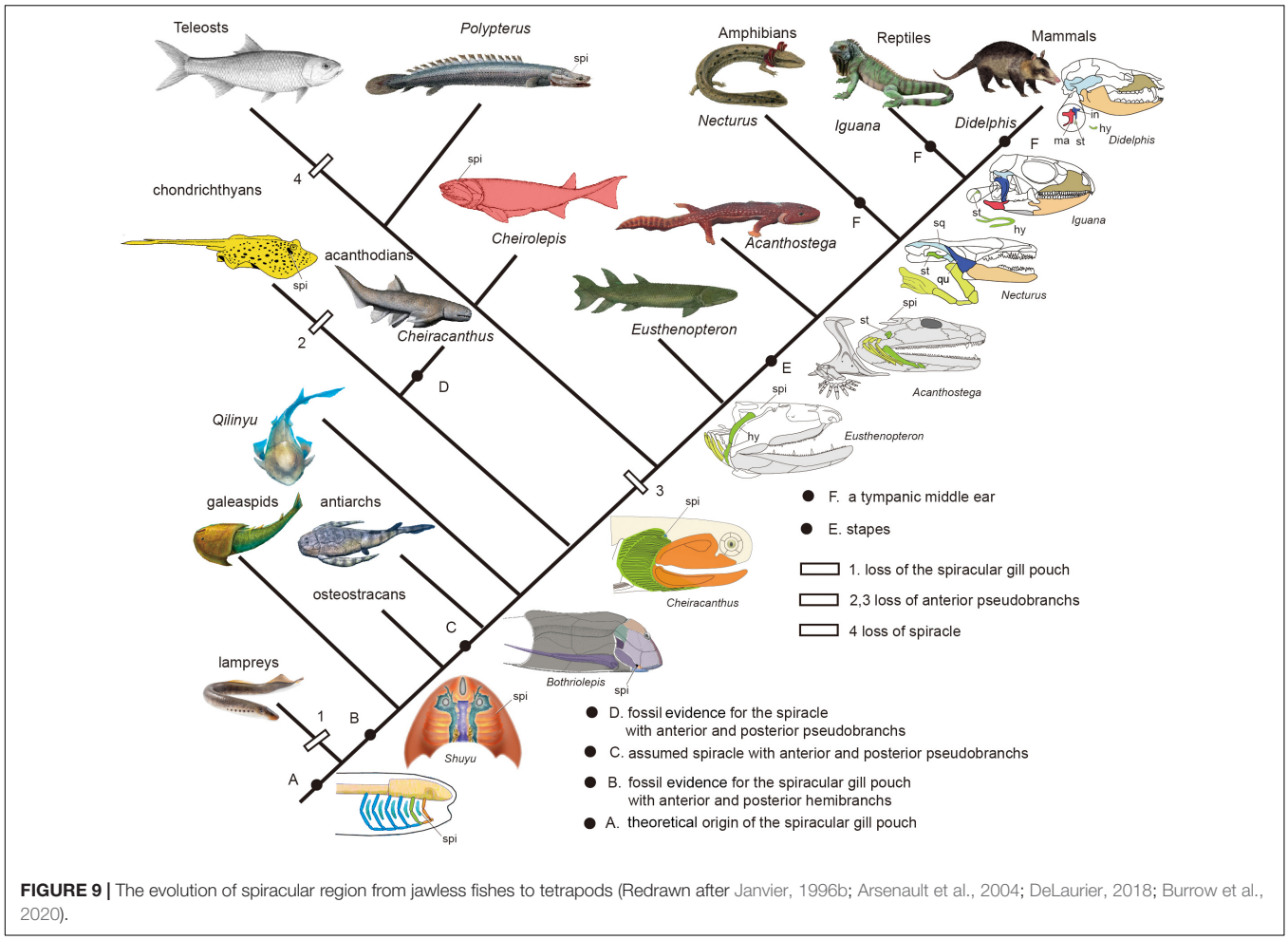

FIGURE 9 | The evolution of spiracular region from jawless fishes to tetrapods (Redrawn after Janvier, 1996b; Arsenault et al., 2004; DeLaurier, 2018; Burrow et al., 2020).

of a large diverticulum of the spiracular tract (**Figure 8C2**; Clack et al., 2003). Although it is impossible to fully understand this structure in the absence of the all-important soft tissues, it seems probable that it combined a retained air-breathing function with an aquatic auditory function based on sound waves being picked up by the density contrast between body tissues and the enclosed air space, similar to the use of the swim bladder and Weberian ossicles in ostariophysian teleosts.

Turning to the tetrapod crown group, we find some puzzling patterns that point to multiple origins of the tympanic ear (**Figures 8D,E**; Clack, 2012). In the temnospondyls, which form the stem group of the extant amphibians, a tympanic ear develops in the same position as the spiracular notch; the transition is documented by the stapes developing a rod-like morphology and the notch acquiring a distinct attachment rim. Unlike Devonian tetrapods, temnospondyls with crocodile-like skulls also have large, dorsally facing external nostrils, which appear to have taken over the air-breathing function previously performed by the spiracles. The earliest well-preserved example of a temnospondyl stapes is that of *Dendrerpeton* (**Figure 7E**) from the Late Carboniferous of Canada (Robinson et al., 2005). This type of ear is retained essentially unchanged by modern anurans, whereas urodeles and caecilians have lost the tympanum.

Among crown amniotes, we find that early reptiles such as *Captorhinus* and early synapsids (stem mammals) such as *Ophiacodon* lack a tympanic notch and have a large stapes that braces between the quadrate and the braincase. This strongly suggests that the primitive condition for the amniote crown group was non-tympanic, a conclusion that is further supported by the different construction of the middle ears (one ear ossicle or three), and their different position (above the jaw joint or below it), in reptiles (including birds) on the one hand and mammals on the other. The evolution of the mammalian middle ear is well documented in the fossil record (**Figure 8E**), which shows how it originates at the posteroventral margin of the lower jaw; this is also supported by developmental data (Maier and Ruf, 2016).

Somewhat surprisingly, the stem amniotes *Seymouria* (**Figure 7F**) and *Diadectes* both have tympanic notches that seem to have contained ear drums, and the stapes points toward this notch rather than toward the quadrate; in *Diadectes*, the tympanum is at least partly ossified (Romer, 1928; Klembara et al., 2020). This type of ear is most similar to that of the temnospondyls, raising the intriguing possibility that a tympanic ear may be primitive for the tetrapod crown group and subsequently lost at the base of the amniote crown group, only to be re-evolved independently in mammals (**Figures 8E**, **9**)

on the one hand and reptiles including birds on the other. Critical to answering this question is the phylogenetic position of the anthracosaurs, a Carboniferous to Permian group that includes such genera as *Archeria* and *Pholiderpeton* (**Figure 6H**; Clack, 2012). Anthracosaurs, which are sometimes recovered as stem amniotes and sometimes as stem tetrapods, have a butterfly-shaped stapes and probably had an open spiracle. If they are stem tetrapods, the tympanic ears of stem amniotes and temnospondyls may be homologous, but if anthracosaurs also belong in the amniote stem group these ears are probably convergent. In any case it is clear that tympanic ears evolved at least three times in parallel among the ancestors of the living tetrapods. The persistence of the hyomandibular pouch as an organizing structure in the embryo, coupled with its ability in later development to either break through to the exterior (creating a spiracle), fail to break through but remain separated from the outside world by a thin membrane (creating a tympanum), or recede altogether (creating a non-tympanic ear), provides a mechanistic basis for this remarkable sequence of evolutionary changes.

CONCLUSION

The anatomical triad of mandibular arch, hyomandibular pouch and hyoid arch has had a much more adventurous evolutionary history than the more posterior branchial arches and pouches, reflecting its role as the interface between the mouth and the gill region. While it has been obvious for more than a century that the two arches and intervening pouch may have evolved as modifications of the branchial system, it is only very recently that the combination of a stable phylogeny and new data from fossils have allowed us to begin to understand their early evolution. Critically important has been the recognition that the extant cyclostomes form a clade, not a paraphyletic grade, and that their peculiar adult morphology with a mandibular-arch rasping tongue and an obliterated hyomandibular pouch is thus likely to be a specialization rather than a reflection of the ancestral vertebrate condition.

In contrast to this, the pharyngeal region of jawless stem gnathostomes, the fossil "ostracoderms," shows conditions likely to be much closer to the ancestral state of crown vertebrates. Most informative among the ostracoderms are the galeaspids, which combine well-preserved three-dimensional anatomy with an absence of the confounding autapomorphies of the other anatomically informative ostracoderm group, the osteostracans. In this paper we present evidence that the galeaspids, exemplified principally by the genus *Shuyu*, had a fully developed spiracular gill pouch. Less conclusive evidence from osteostracans and heterostracans suggests that these groups also had complete spiracular gills, leading to the conclusion that this condition may be characteristic for the gnathostome total group as a whole.

The discovery of a spiracular gill in galeaspids leads unavoidably to a reconsideration of the "aphetohyoidean" hypothesis of primitive jawed vertebrate anatomy, according to which a complete spiracular gill separated the mandibular and hyoid arches in the earliest jawed vertebrates. In essence, the galeaspid condition would form a plausible evolutionary precursor to this condition, if the gill was retained across the jawless-to-jawed transition. However, at present there is no convincing evidence for a fully aphetohyoidean condition in any group of fossil or living jawed vertebrates. The spiracle, if present, is always a small and dorsally placed opening rather than a complete gill slit. However, in the acanthodians, an extinct group of probable stem chondrichthyans, there is evidence for the presence of a miniaturized but complete spiracular gill, comprising anterior and posterior pseudobranchs (corresponding to the hemibranchs of a normal gill), rather than the single posterior pseudobranch of living jawed vertebrates. The phylogenetic position of acanthodians suggests that the anterior pseudobranch was lost independently in chondrichthyans and osteichthyans.

Among osteichthyans and chondrichthyans, the primitive condition of the spiracle appears to be a small opening as seen in many sharks, but in many representatives of these groups it has undergone one of three modifications: loss, enlargement into an important inhalatory opening, or conversion into a tympanic middle ear for the amplification of airborne sound. Interestingly, all three modifications have happened several times in parallel. The spiracle has been lost in manta rays, requiem sharks, hammerhead sharks, chimaeras, lungfishes, coelacanths and neopterygian ray-finned fishes (bowfins, gars and teleosts). It has become an important inhalatory opening in rays, where it is used for water, and the primitive actinopterygian *Polypterus*, where it is used for air. A similar spiracular morphology and probable air-breathing function can be inferred for the tetrapod stem group, including tetrapodomorph fishes such as *Eusthenopteron*, transitionals such as *Tiktaalik* and stem tetrapods such as *Acanthostega*. Only in the tetrapod crown group did the spiracle lose this inhalatory function and evolve into a middle ear capped with a tympanum; remarkably, this happened at least three times in parallel, in amphibians, reptiles including birds, and mammals. This extraordinary series of evolutionary transformations bears testimony to the flexibility and potential of the triad of mandibular arch, hyomandibular pouch and hyoid arch, which appears early in the development of every vertebrate embryo.

DATA AVAILABILITY STATEMENT

The original contributions presented in the study are included in the article/supplementary material, further inquiries can be directed to the corresponding author/s.

AUTHOR CONTRIBUTIONS

ZG, PA, and PD conceived and designed the study. ZG, PD, and MZ performed the 3D segmentation. ZG and PA wrote the first draft of the manuscript. All authors contributed to the

interpretation of results, editing of the manuscript, and have approved this final version for re-submission.

FUNDING

This work was supported by Strategic Priority Research Program of CAS (XDB26000000), the National Natural Science Foundation of China (41972006 and 42072026), National Program for Support of Topnotch Young Professionals, and Key Research Program of Frontier Sciences, CAS (QYZDB-SSW-DQC040). PA acknowledges the support of a Wallenberg Scholarship from the Knut & Alice Wallenberg Foundation. PD was funded by the Natural Environment Research Council (NE/G016623/1 and NE/P013678/1), the Biotechnology and Biological Sciences Research Council (BB/T012773/1) and the Leverhulme Trust (RF-2022-167).

ACKNOWLEDGMENTS

We would like to thank Philippe Janvier and Yajing Wang for constructive discussion and their courtesies allowing us to modify their figures. We thank Neil Gostling, Yemao Hou, Xianghong Lin and Xingdong Cui for assistance in retrieving microCT data, and Mingzhi Kong for assistance in photoing *Latimeria*. We are especially grateful to Aijuan Shi, Xianghong Lin, Dinghua Yang, Brian Choo, and Nobu Tamura for drawing illustrations.

REFERENCES

Ahlberg, P. E., Clack, J. A., Lukševičs, E., Blom, H., and Zupiņš, I. (2008). Ventastega curonica and the origin of tetrapod morphology. *Nature* 453, 1199–1204. doi: 10.1038/nature06991

Allis, E. P. (1922). The cranial anatomy of Polypterus, with special reference to Polypterus bichir. *J. Anat.* 56, 190–294.

Arsenault, M., Desbiens, S., Janvier, P., and Kerr, J. (2004). "New data on the soft tissues and external morphology of the antiarch *Bothriolepis canadensis* (Whiteaves, 1880) from the Upper Devonian of Miguasha, Quebec," in *Recent Advances in the Origin and Early Radiation of Vertebrates*, eds G. Arratia, M. V. H. Wilson, and R. Cloutier (München: Verlag), 439–454.

Bartsch, P. (1994). Development of the cranium of *Neoceratodus forsteri*, with a discussion of the suspensorium and the opercular apparatus in Dipnoi. *Zoomorphology* 114, 1–31. doi: 10.1007/bf00574911

Basden, A. M., and Young, G. C. (2001). A primitive actinopterygian neurocranium from the Early Devonian of southeastern Australia. *J. Vertebr. Paleontol.* 21, 754–766. doi: 10.1671/0272-4634(2001)021[0754:apanft]2.0.co;2

Beznosov, P. A., Clack, J. A., Luksevics, E., Ruta, M., and Ahlberg, P. E. (2019). Morphology of the earliest reconstructable tetrapod Parmastega aelidae. *Nature* 574, 527–531. doi: 10.1038/s41586-019-1636-y

Bone, Q., and Moore, R. H. (2008). *Biology of Fishes*, 3rd Edn. New York, NY: Taylor & Francis.

Brazeau, M. D., and Ahlberg, P. E. (2006). Tetrapod-like middle ear architecture in a Devonian fish. *Nature* 439, 318–321. doi: 10.1038/nature04196

Burggren, W. W. (1978). Gill ventilation in the sturgeon, Acipenser transmontanus: unusual adaptations for bottom dwelling. *Respir. Physiol.* 34, 153–170. doi: 10.1016/0034-5687(78)90025-7

Burggren, W. W., and Bemis, W. E. (1991). Metabolism and ram gill ventilation in juvenile paddlefish, Polyodon spathula (Chondrostei: Polyodontidae). *Physiol. Zool.* 65, 515–539.

Burrow, C. J., den Blaauwen, J., Newman, M., and Davidson, R. (2016). The diplacanthid fishes (Acanthodii, Diplacanthiformes, Diplacanthidae) from the Middle Devonian of Scotland. *Palaeontol. Electron.* 19, 1–83.

Burrow, C. J., Newman, M. J., and den Blaauwen, J. L. (2020). First evidence of a functional spiracle in stem chondrichthyan acanthodians, with the oldest known elastic cartilage. *J. Anat.* 236, 1154–1159. doi: 10.1111/joa.13170

Carroll, R. L. (1967). Labyrinthodonts from the Joggins fauna. *J. Paleontol.* 41, 111–142.

Clack, J. A. (1993). Homologies in the fossil record: the middle ear as a test case. *Acta Biotheor.* 41, 391–409. doi: 10.1007/BF00709373

Clack, J. A. (1998). The neurocranium of *Acanthostega gunnari* Jarvik and the evolution of the otic region in tetrapods. *Zool. J. Linn. Soc.* 122, 61–97. doi: 10.1111/j.1096-3642.1998.tb02525.x

Clack, J. A. (2002). Patterns and processes in the early evolution of the tetrapod ear. *J. Neurobiol.* 53, 251–264. doi: 10.1002/neu.10129

Clack, J. A. (2003). A revised reconstruction of the dermal skull roof of Acanthostega gunneri, an early tetrapod from the Late Devonian. *Trans. R. Soc. Edinburgh* 93, 163–165. doi: 10.1017/s0263593302000111

Clack, J. A. (2012). *Gaining Ground: The Origin and Evolution of Tetrapods*. Bloomington: Indiana University Press, 1–523.

Clack, J. A., Ahlberg, P. E., Finney, S. M., Alonso, P. D., Robinson, J., and Ketcham, R. A. (2003). A uniquely specialized ear in a very early tetrapod. *Nature* 425, 65–69. doi: 10.1038/nature01904

Cloutier, R., Clement, A. M., Lee, M. S. Y., Noël, R., Béchard, I., Roy, V., et al. (2020). Elpistostege and the origin of the vertebrate hand. *Nature* 579, 549–554. doi: 10.1038/s41586-020-2100-8

Coates, M. I., Finarelli, J. A. I, Sansom, J., Andreev, P. S., Criswell, K. E., Tietjen, K., et al. (2018). An early chondrichthyan and the evolutionary assembly of a shark body plan. *Proc. R. Soc. B* 285:20172418. doi: 10.1098/rspb.2017.2418

Coates, M. I., Gess, R. W., Finarelli, J. A., Criswell, K. E., and Tietjen, K. (2017). A symmoriiform chondrichthyan braincase and the origin of chimaeroid fishes. *Nature* 541, 208–211. doi: 10.1038/nature20806

Daeschler, E. B., Shubin, N. H., and Jenkins, F. A. (2006). A Devonian tetrapod-like fish and the evolution of the tetrapod body plan. *Nature* 440, 757–763. doi: 10.1038/nature04639

Datovo, A., and Rizzato, P. P. (2018). Evolution of the facial musculature in basal ray-finned fishes. *Front. Zool.* 15:40. doi: 10.1186/s12983-018-0285-6

Davies, T. G. I, Rahman, A., Lautenschlager, S., Cunningham, J. A., Asher, R. J., Barrett, P. M., et al. (2017). Open data and digital morphology. *Proc. R. Soc. B* 284, 1852. doi: 10.1098/rspb.2017.0194

DeLaurier, A. (2018). Evolution and development of the fish jaw skeleton. *Wiley Interdiscip. Rev.* 8:e337. doi: 10.1002/wdev.337

Denison, R. H. (1961). Feeding mechanisms of agnatha and early gnathostomes. *Am. Zool.* 1, 177–181. doi: 10.1093/icb/1.2.177

Donoghue, P. C. J., Forey, P. L., and Aldridge, R. J. (2000). Conodont affinity and chordate phylogeny. *Biol. Rev.* 75, 191–251. doi: 10.1017/s0006323199005472

Donoghue, P. C. J., and Smith, M. P. (2001). The anatomy of *Turinia pagei* (Powrie), and the phylogenetic status of the Thelodonti. *Trans. R. Soc.* 92, 15–37. doi: 10.1017/s0263593301000025

Downs, J. P., Daeschler, E. B., Jenkins, F. A., and Shubin, N. H. (2008). The cranial endoskeleton of *Tiktaalik roseae*. *Nature* 455, 925–929. doi: 10.1038/nature07189

Dupret, V., Sanchez, S., Goujet, D., Tafforeau, P., and Ahlberg, P. E. (2014). A primitive placoderm sheds light on the origin of the jawed vertebrate face. *Nature* 507, 500–503. doi: 10.1038/nature12980

Farooq, R., Hussain, K., Tariq, M., Farooq, A., and Mustafa, M. (2020). CRISPR/Cas9: targeted genome editing for the treatment of hereditary hearing loss. *J. Appl. Genet.* 61, 51–65. doi: 10.1007/s13353-019-00535-6

Forey, P. L. (1995). Agnathans recent and fossil, and the origin of jawed vertebrates. *Rev. Fish Biol. Fish.* 5, 267–303. doi: 10.1007/bf00043003

Forey, P. L. (1998). *History of the Coelacanth Fishes*. London: Chapman&Hall.

Frey, L., Coates, M., Ginter, M., Hairapetian, V., Rucklin, M., Jerjen, I., et al. (2019). The early elasmobranch Phoebodus: phylogenetic relationships,

ecomorphology and a new time-scale for shark evolution. *Proc. Biol. Sci.* 286:20191336.

Frey, L., Coates, M. I., Tietjen, K., Rucklin, M., and Klug, C. (2020). A symmoriiform from the Late Devonian of Morocco demonstrates a derived jaw function in ancient chondrichthyans. *Commun. Biol.* 3:681. doi: 10.1038/s42003-020-01394-2

Gai, Z., Lu, L., Zhao, W., and Zhu, M. (2018). New polybranchiaspiform fishes (Agnatha: Galeaspida) from the Middle Palaeozoic of China and their ecomorphological implications. *PLoS One* 13, e0202217. doi: 10.1371/journal.pone.0202217

Gai, Z., and Zhu, M. (2012). The origin of the vertebrate jaw: intersection between developmental biology-based model and fossil evidence. *Chin. Sci. Bull.* 57, 3819–3828. doi: 10.1007/s11434-012-5372-z

Gai, Z. K. (2011). *The Cranial Anatomy of Galeaspida (Agnatha) and the Origin of Jawed Vertebrates*. Doctoral dessertation. Bristol: University of Bristol.

Gai, Z. K. (2018). Synchrotron X-ray tomographic microscopy reveals histology and internal structure of Galeaspida (Agnatha). *Vert. PalAs.* 56, 93–105.

Gai, Z.-K., Donoghue, P. C. J., Zhu, M., Janvier, P., and Stampanoni, M. (2011). Fossil jawless fish from China foreshadows early jawed vertebrate anatomy. *Nature* 476, 324–327. doi: 10.1038/nature10276

Gai, Z. K., Jiang, W. Y., Zhao, W. J., Li, Q., Shi, X. D., and Zhu, M. (2022). Redescription of the Sanqiaspidae (Galeaspida) from the Lower Devonian of South China and its biostratigraphic significance. *Palaeobiodiversity and Palaeoenvironments* 102, 173–191. doi: 10.1007/s12549-021-00486-z

Gai, Z. K., Yu, X. B., and Zhu, M. (2017). The evolution of the zygomatic bone from Agnatha to Tetrapoda. *Anatom. Rec.*300, 16–29. doi: 10.1002/ar.23512

Gai, Z. K., Zhu, M., and Donoghue, C. J. P. (2019). The circulatory system of Galeaspida (Vertebrata; stem-Gnathostomata) revealed by synchrotron X-ray tomographic microscopy. *Palaeoworld* 28, 441–460. doi: 10.1016/j.palwor.2019.04.005

Gardiner, B. G. (1984). The relationships of the palaeoniscid fishes, a review based on new specimens of *Mimia* and *Moythomasia* from the Upper Devonian of Western Australia. *Bull. Br. Museum Geol.* 37, 173–428.

Gaskell, W. H. (1908). *On the Origin of Vertebrates*. London: Longmans.

Gegenbaur, C. (1872). *Untersuchungen zur Vergleichenden Anatomie der Wirbeltiere. 3: Das Kopfskelett der Selachier*. Leipzig: Englemann.

Graham, J. B., Wegner, N. C., Miller, L. A., Jew, C. J., Lai, N. C., Berquist, R. M., et al. (2014). Spiracular air breathing in polypterid fishes and its implications for aerial respiration in stem tetrapods. *Nat. Commun.* 5:3022. doi: 10.1038/ncomms4022

Halstead, L. B. (1971). The presence of a spiracle in the Heterostraci (Agnatha). *Zool. J. Linn. Soc.* 50, 195–197. doi: 10.1111/j.1096-3642.1971.tb00760.x

Halstead, L. B. (1973). The heterostracan fishes. *Biol. Rev.* 48, 279–332. doi: 10.1111/j.1469-185x.1973.tb01005.x

Heimberg, A. M., Cowper-Sallari, R., Semon, M., Donoghue, P. C. J., and Peterson, K. J. (2010). MicroRNAs reveal the interrelationships of hagfish, lampreys, and gnathostomes and the nature of the ancestral vertebrate. *Proc. Natl. Acad. Sci. U.S.A.* 107, 19379–19383. doi: 10.1073/pnas.1010350107

Holland, T., and Long, J. A. (2009). On the phylogenetic position of *Gogonasus andrewsae* Long 1985, within the Tetrapodomorpha. *Acta Zool.* 90, 285–296. doi: 10.1111/j.1463-6395.2008.00377.x

Holmgren, N. (1942). Studies on the head of fishes. Part III. *Acta Zool.* 23, 129–261. doi: 10.1111/j.1463-6395.1942.tb00012.x

Holmgren, N. (1946). On two embryos of *Myxine glutinosa*. *Acta Zool.* 27, 1–90. doi: 10.1111/j.1463-6395.1946.tb00019.x

Hughes, G. M. (1960). The mechanism of gill ventilation in the Dogfish and Skate. *J. Exp. Biol.* 37, 11–27. doi: 10.1016/j.zool.2015.09.002

Janvier, P. (1974). The structure of the naso-hypophysial complex and the mouth in fossil and extant cyclostomes, with remaks on amphiaspiforms. *Zool. Scr.* 3, 193–200. doi: 10.1111/j.1463-6409.1974.tb00816.x

Janvier, P. (1981). Norselaspis glacialis n.g., n.sp. et les relations phylogénétiques entre les Kiaeraspidiens (Osteostraci) du Dévonien Inférieur du Spitsberg. *Palaeovertebrata* 11, 19–131.

Janvier, P. (1985). *Les Céphalaspides du Spitsberg: Anatomie, Phylogénie et Systématique des Ostéostracés Siluro-Dévoniens; Revisions des Ostéostracés de la Formation de Wood Bay (Dévonien inférieur du Spitsberg)*. Paris: Centre national de la Recherche scientifique.

Janvier, P. (1996b). The dawn of the vertebrates: characters versus common ascent in the rise of current vertebrate phylogenies. *Palaeontology* 39, 259–287.

Janvier, P. (1996a). *Early Vertebrates*. Oxford: Clarendon Press.

Janvier, P. (2001). "Ostracoderms and the shaping of the gnathostome characters," in *Major Events in Early Vertebrate Evolution: Palaeontology, Phylogeny, Genetics and Development*, ed. P. Ahlberg (London: Taylor Francis), 172–186. doi: 10.7717/peerj.5249

Janvier, P. (2004). "Early specializations in the branchial apparatus of jawless vertebrates: a consideration of gill number and size," in *Recent Advances in the Origin and Early Radiation of Vertebrates*, eds G. Arratia, M. V. H. Wilson, and R. Cloutier (München: Verlag), 29–52.

Janvier, P. (2007). "Homologies and evolutionary transitions in early vertebrate history," in *Major Transitions in Vertebrate Evolution*, eds J. S. Anderson and H.-D. Sues (Bloomington: Indiana University Press), 57–121.

Janvier, P., Thanh, T.-D., Phuong, T. H., Clément, G., and Phong, N. D. (2009). Occurrence of Sanqiaspis, Liu, 1975 (Vertebrata, Galeaspida) in the Lower Devonian of Vietnam, with remarks on the anatomy and systematics of the Sanqiaspididae. *C. R. Palevol* 8, 59–65. doi: 10.1016/j.crpv.2008.10.008

Jarvik, E. (1980). *Basic Structure and Evolution of Vertebrates*, Vol. 1. London: Academic Press.

Jefferies, R. P. S. (1986). *The Ancestry of the Vertebrates*. London: British Museum.

Johanson, Z. (1998). The upper devonian fish bothriolepis (Placodermi: Antiarchi) from near Canowindra, New South Wales, Australia. *Rec. Aust. Museum* 50, 315–348. doi: 10.3853/j.0067-1975.50.1998.1289

Johnston, J. B. (1905). The cranial nerve components of Petromyzon. *Gegenbaurs Morphol. Jahrb.* 34, 149–203.

Kardong, K. V. (2012). *Vertebrates: Comparative Anatomy, Function, Evolution*. Dubuque: McGraw-Hill.

Klembara, J., Hain, M., Cernansky, A., Berman, D. S., and Henrici, A. C. (2020). Anatomy of the neural endocranium, parasphenoid and stapes of Diadectes absitus (Diadectomorpha) from the early Permian of Germany based on the high-resolution X-ray microcomputed tomography. *Anat. Rec.* 303, 2977–2999. doi: 10.1002/ar.24376

Kuratani, S., and Ahlberg, P. E. (2018). Evolution of the vertebrate neurocranium: problems of the premandibular domain and the origin of the trabecula. *Zool. Lett.* 4:1. doi: 10.1186/s40851-017-0083-6

Kuratani, S., Ueki, T., Aizawa, S., and Hirano, S. (1997). Peripheral development of cranial nerves in a cyclostome, *Lampetra japonica*: morphological distribution of nerve branches and the vertebrate body plan. *J. Comp. Neurol.* 384, 483–500. doi: 10.1002/(sici)1096-9861(19970811)384:4<483::aid-cne1>3.0.co;2-z

Liem, K., Bemis, W., Walker, W. F. Jr., and Grande, L. (2001). *Functional Anatomy of the Vertebrates: an Evolutionary Perspective*, 3rd Edn. Philadelphia: Thomson Brooks/Cole.

Long, J. A. (2001). On the relationships of *Psarolepis* and the onychodontiform fishes. *J. Vertebr. Paleontol.* 21, 815–820. doi: 10.1671/0272-4634(2001)021[0815:otropa]2.0.co;2

Long, J. A., Young, G. C., Holland, T., Senden, T. J., and Fitzgerald, E. M. G. (2006). An exceptional Devonian fish from Australia sheds light on tetrapod origins. *Nature* 444, 199–202. doi: 10.1038/nature05243

Maier, W., and Ruf, I. (2016). Evolution of the mammalian middle ear: a historical review. *J. Anat.* 228, 270–283. doi: 10.1111/joa.12379

Maisey, J. G. (1986). Heads and tails: a chordate phylogeny. *Cladistics* 2, 201–256. doi: 10.1111/j.1096-0031.1986.tb00462.x

Maisey, J. G., Janvier, P., Pradel, A., Denton, J. S. S., Bronson, A., Miller, R., et al. (2019). "Doliodus and pucapampellids: contrasting perspectives on stem chondrichthyan morphology," in *Evolution and Development of Fishes*, eds Z. Johanson, C. Underwood, and M. Richter (Cambridge: Cambridge University Press), 87–109. doi: 10.1017/9781316832172.006

Mallatt, J. (1984). Early vertebrate evolution: pharyngeal structure and the origin of gnathostomes. *J. Zool.* 204, 169–183. doi: 10.1111/j.1469-7998.1984.tb02368.x

Mallatt, J. (1996). Ventilation and the origin of jawed vertebrates: a new mouth. *Zool. J. Linn. Soc.* 117, 329–404. doi: 10.1111/j.1096-3642.1996.tb01658.x

Miles, R. S. (1964). A reinterpretation of the visceral skeleton of Acanthodes. *Nature* 204, 457–459. doi: 10.1038/204457a0

Miles, R. S. (1965). Some features in the cranial morphology of acanthodians and the relationships of the Acanthodii. *Acta Zool.* 46, 233–255. doi: 10.1111/j.1463-6395.1965.tb00733.x

Miles, R. S. (1968). "Jaw articulation and suspension in *Acanthodes* and their significance," in *Current Problems of Lower Vertebrate Phylogeney. Nobel Symposium 4*, ed. T. Ørvig (Stockholm: Almqvist & Wiksell), 109–127.

Miles, R. S. (1973). Articulated acanthodian fishes from the Old Red Sandstone of England, with a review of the structure and evolution of the acanthodian shoulder-girdle. *Bull. Br. Museum Geol.* 24, 111–213. doi: 10.5962/p.313823

Miyashita, T. (2016). Fishing for jaws in early vertebrate evolution: a new hypothesis of mandibular confinement. *Biol. Rev.* 91, 611–657. doi: 10.1111/brv.12187

Miyashita, T., and Diogo, R. (2016). Evolution of serial patterns in the vertebrate pharyngeal apparatus and paired appendages via assimilation of dissimilar units. *Front. Ecol. Evol.* 4:71. doi: 10.3389/fevo.2016.00071

Miyashita, T., Gess, R. W., and Tietjen, K. E. A. (2021). Non-ammocoete larvae of Palaeozoic stem lampreys. *Nature* 591, 408–412. doi: 10.1038/s41586-021-03305-9

Möhlich, A., Waser, W., and Heisler, N. (2009). The teleost pseudobranch: a role for preconditioning of ocular blood supply? *Fish Physiol. Biochem.* 35, 273–286. doi: 10.1007/s10695-008-9207-4

Novitskaya, L. I. (1983). *Morfologiya Drevnikh Beschelyustnykh (Heterostraci i problema Svyazi Beschelyustnykh i Chelyustnorotykh Pozvonochnykh*. Moscow: Trudi Palaeontologicheskogo Instituta.

Novitskaya, L. I. (2015). Brain of the most ancient vertebrates (Agnatha: Heterostraci) and man: comparison and inferences. *Paleontol. J.* 49, 79–88. doi: 10.1134/s0031030115010086

Pearson, D. M., and Westoll, T. S. (1979). The Devonian actinopterygian *Cheirolepis* Agassiz. *Trans. R. Soc. Edinburgh* 70, 337–399. doi: 10.1017/s0080456800012850

Perry, C. T., Salter, M. A., Harborn, A. R., Crowley, S. F., Jelks, H. L., and Wilson, R. W. (2011). Fish as major carbonate mud producers and missing components of the tropical carbonate factory. *Proc. Natl. Acad. Sci. U.S.A.* 108, 3865–3869. doi: 10.1073/pnas.1015895108

Pradel, A., Maisey, J. G., Tafforeau, P., Mapes, R. H., and Mallatt, J. (2014). A Palaeozoic shark with osteichthyan-like branchial arches. *Nature* 509, 608–611. doi: 10.1038/nature13195

Pradel, A., Tafforeau, P., Maisey, J. G., and Janvier, P. (2011). A new paleozoic Symmoriiformes (Chondrichthyes) from the Late Carboniferous of Kansas (USA) and cladistic analysis of early chondrichthyans. *PLoS One* 6:e24938. doi: 10.1371/journal.pone.0024938

Robinson, J., Ahlberg, P. E., and Koentges, G. (2005). The braincase and middle ear region of *Dendrerpeton acadianum* (Tetrapoda: Temnospondyli). *Zool. J. Linn. Soc.* 143, 577–597. doi: 10.1111/j.1096-3642.2005.00156.x

Romer, A. S. (1928). A skeletal model of the primitive reptile Seymouria, and the phylogenetic position of that type. *J. Geol.* 36, 248–260. doi: 10.1086/623510

Schultze, H.-P. (1993). "Patterns of diversity in the skull of jawed fishes," in *The Skull*, Vol. 2, eds J. Janke and B. K. Hall (Chicago: University of Chicago Press), 189–254.

Stensiö, E. A. (1927). The downtonian and devonian vertebrates of spitsbergen. part i. family cephalaspidae. *Skrifter Svalbard Nordishavet* 12, 1–391.

Stensiö, E. A. (1947). The sensory lines and dermal bones of the cheek in fishes and amphibians. *Kungliga Svenska Vetenskapsakademiens Handlingar* 24, 1–195.

Stensiö, E. A. (1963). Anatomical studies on the arthrodiran head. Part 1. Preface, geological and geographical distribution, the organization of the head in the Dolichothoraci, Coccosteomorphi and Pachyosteomorphi. Taxonomic appendix. *Kungliga Svenska Vetenskapsakademiens Handlingar* 9, 1–419. doi: 10.1007/s12105-017-0785-2

Stensiö, E. (1964). "Les Cyclostomes fossiles ou Ostracodermes," in *Traité de Paléontologie*, ed. J. Piveteau (Paris: Masson), 96–382.

Stockard, C. R. (1906). The development of the mouth and gills in Bdellostoma stouti. *Am. J. Anat.* 5, 481–517. doi: 10.1002/aja.1000050405

Summers, A. P., and Ferry-Graham, L. A. (2001). Ventilatory modes and mechanics of the hedgehog skate (*Leucoraja erinacea*): testing the continuous ?ow model. *J. Exp. Biol.* 204, 1577–1587. doi: 10.1242/jeb.204.9.1577

Vorobyeva, E. I., and Schultze, H.-P. (1991). "Description and systematics of panderichthyid fishes with comments on their relationship to tetrapods," in *Origins of the Higher Groups of Tetrapods: Controversy and Consensus*, eds H.-P. Schultze and L. Trueb (Ithaca: Cornell Publishing Associates), 68–109. doi: 10.7591/9781501718335-005

Wang, N.-Z. (1991). "Two new Silurian galeaspids (jawless craniates) from Zhejiang Province, China, with a discussion of galeaspid-gnathostome relationships," in *Early Vertebrates and Related Problems of Evolutionary Biology*, eds M. M. Chang, Y. H. Liu, and G. R. Zhang (Beijing: Science Press), 41–66.

Wang, Y. J., and Zhu, M. (2020). New data on the headshield of *Parayunnanolepis xitunensis* (Placodermi, Antiarcha), with comments on nasal capsules in antiarchs. *J. Vertebr. Paleontol.* 40:e1855189. doi: 10.1080/02724634.2020.1855189

Waser, W. (2011). "Transport and exchange of respiratory gases in the blood | root effect: root effect definition, functional role in oxygen delivery to the eye and swimbladder," in *Encyclopedia of Fish Physiology*, ed. A. P. Farrell (Cambrige, MA: academic Press).

Watson, D. M. S. (1937). The acanthodian fishes. *Philos. Trans. R. Soc. Lond. Ser. B* 228, 49–146. doi: 10.1098/rstb.1937.0009

White, T. E. (1939). Osteology of Seymouria baylorensis Broili. *Bull. Museum Comp. Zool.* 85, 325–409.

Wicht, H., and Tusch, U. (1998). "Ontogeny of the head and nervous system of myxinoids," in *The Biology of Hagfishes*, eds J. M. Jørgensen, J. P. Lomholt, R. E. Weber, and H. Malte (London: Chapman & Hall), 431–451. doi: 10.1007/978-94-011-5834-3_28

Young, G. C. (2008). The relationships of antiarchs (Devonian Placoderm Fishes)—evidence supporting placoderm monophyly. *J. Vertebr. Paleontol.* 28, 626–636. doi: 10.1671/0272-4634(2008)28[626:troadp]2.0.co;2

Zangerl, R., and Case, G. R. (1976). *Cobelodus aculeatus* (Cope), an snacanthous shark from Pennsylvanian black shales of North America. *Palaeontogr. Abt. A* 154, 107–157.

Zangerl, R., and Williams, M. E. (1975). New evidence on the nature of the jaw suspension in Palaeozoic anacanthous sharks. *Palaeontology* 18, 333–341.

Zhu, M., Ahlberg, P. E., Pan, Z., Zhu, Y., Qiao, T., Zhao, W., et al. (2016). A Silurian maxillate placoderm illuminates jaw evolution. *Science* 354, 334–336. doi: 10.1126/science.aah3764

Zhu, M., Yu, X., Ahlberg, P. E., Choo, B., Lu, J., Qiao, T., et al. (2013). A Silurian placoderm with osteichthyan-like marginal jaw bones. *Nature* 502, 188–193. doi: 10.1038/nature12617

Zhu, M., Zhao, W.-J., Jia, L.-T., Lu, J., Qiao, T., and Qu, Q.-M. (2009). The oldest articulated osteichthyan reveals mosaic gnathostome characters. *Nature* 458, 469–474. doi: 10.1038/nature07855

Ziermann, J. M., Diaz, R. E. Jr., and Diogo, R. (2019). *Heads, Jaws, and Muscles: Anatomical, Functional, and Developmental Diversity in Chordate Evolution*. Berlin: Springer.

Conflict of Interest: The authors declare that the research was conducted in the absence of any commercial or financial relationships that could be construed as a potential conflict of interest.

Publisher's Note: All claims expressed in this article are solely those of the authors and do not necessarily represent those of their affiliated organizations, or those of the publisher, the editors and the reviewers. Any product that may be evaluated in this article, or claim that may be made by its manufacturer, is not guaranteed or endorsed by the publisher.

Advantages of publishing in Frontiers

OPEN ACCESS
Articles are free to read for greatest visibility and readership

FAST PUBLICATION
Around 90 days from submission to decision

HIGH QUALITY PEER-REVIEW
Rigorous, collaborative, and constructive peer-review

TRANSPARENT PEER-REVIEW
Editors and reviewers acknowledged by name on published articles

Frontiers
Avenue du Tribunal-Fédéral 34
1005 Lausanne | Switzerland

Visit us: www.frontiersin.org
Contact us: frontiersin.org/about/contact

REPRODUCIBILITY OF RESEARCH
Support open data and methods to enhance research reproducibility

DIGITAL PUBLISHING
Articles designed for optimal readership across devices

FOLLOW US
@frontiersin

IMPACT METRICS
Advanced article metrics track visibility across digital media

EXTENSIVE PROMOTION
Marketing and promotion of impactful research

LOOP RESEARCH NETWORK
Our network increases your article's readership